P

Volu

PHYSICAL REVIEW

A journal [illegible] *established by E. L. Nichols in 1893*

Published by the American [illegible]
for the
AMERICAN PHYSICAL [illegible]

Officers

President

C. C. LAURITSEN
California Institute [illegible]
Pasadena, California

Vice-President

J. H. VAN VLECK
Harvard University
Cambridge, Mass.

Secretary

K. K. DARROW
Bell Telephone Laboratories
Office:
Columbia University
New York 27, New York

Treasurer

G. B. PEGRAM
Columbia University
New York 27, New York

Local Secretary for the Pacific Coast

J. KAPLAN
University of California at Los Angeles
Los Angeles, California

Managing Editor

S. A. GOUDSMIT
Brookhaven National Laboratory
Upton, Long Island
New York

BOARD OF EDITORS

Editor

[illegible]

Associate Editors

HARVEY BROOKS
R. F. CHRISTY
C. L. CRITCHFIELD
M. DEUTSCH
T. H. JOHNSON
SIGURD ROSEN

The Physical Review is published [illegible] Ann Street, Lancaster, Pennsylvania.
Entered as second-class matter [illegible] at the Post Office at Lancaster, Pennsylvania, under the Act of March 3, 1879.
Acceptance for mailing at special rate of postage provided for in paragraph (d-2), Section 34.40, P. L. & R., of 1948, authorized [illegible]

THE
PHYSICAL REVIEW

A journal of experimental and theoretical physics established by E. L. Nichols in 1893

SECOND SERIES, VOL. 83, NO. 4 AUGUST 15, 1951

Angular Distribution of Neutrons from Targets Bombarded by 20-Mev Deuterons*†

L. SCHECTER
Radiation Laboratory, Department of Physics, University of California, Berkeley, California
(Received April 10, 1951)

The angular distribution of neutrons from deuteron-bombarded targets has been investigated, using various threshold detectors. The distributions are found to have a structure which is characteristic of the particular process which produces the neutrons. In some cases, small angle structure appears, and these cases have been analyzed by applying the theory due to S. T. Butler. Parities and possible spin values have been assigned to the states of the final nuclei which are produced in the reactions.

I. INTRODUCTION

RECENT determinations[1–5] of the spatial distribution of fast neutrons produced by the bombardment of various targets by deuterons of energy less than 20 Mev indicate that there is a group of neutrons emitted in a forward direction in addition to a roughly isotropic background. Serber's theory of stripping[6] has satisfactorily explained the high energy (190 Mev) results of Helmholtz, McMillan, and Sewell;[7] but the application to the low energy results is not so satisfactory.[4,5] The present work establishes information about the neutron distributions from deuterons of maximum energy 20 Mev, which show that several different processes operate in the production of these neutrons, and that the neutron energies are characteristic of the processes producing them.

II. EXPERIMENTAL DETAILS

This set of measurements was carried out using the 60-inch cyclotron of the Crocker Laboratory, which produces an external deuteron beam of energy about 20 Mev. This has the advantage that no corrections need be made for the scattering of the neutrons before their detection. The targets bombarded include Be, Al, Cu, Sn, Pb, and U, and were of sufficient thickness to stop all the deuterons. Thick targets were necessary in order to minimize the effect of neutrons due to deuterons bombarding parts of the cyclotron tank and dee system other than the external target. The bombarding currents were all of the order of 15 microamperes.

The neutrons were detected by the beta-activities, induced by exposure, in arrays of C, Cu, and Al foils. The foils, 1″×1¼″×maximum beta-range, were enclosed in $\frac{1}{32}$″ Cd and placed in a circular arc of 10½″ radius, with the target as center. This arc covered an angular range from −16 degrees to +66 degrees, relative to the incident deuteron beam direction, and was limited by the cyclotron tank wall on one side, and the target cooling lines on the other. This method was chosen for the following reasons: (1) all foils receive exactly the same exposure, so that no monitor is necessary; (2) by choosing foil materials with suitable activation thresholds, a selection of energy ranges can be made, and, in addition, neutrons which have lost a certain amount of energy by inelastic scattering from nearby matter are not detected; (3) Falk has shown[5] that this simple scheme gives substantially the same results as those from detection by a proportional counter telescope.

The activities induced in every foil were each measured two or three times in a standard Geiger tube and lead chamber arrangement, and then extrapolated back to some convenient time so that they could be compared. The activities consisted of the 20.5-minute activity of C^{11}, the 10.5-minute activity of Cu^{62}, the 10.2-minute activity of Mg^{27}, and the 14.8-hour activity of Na^{24}. The

* Reported at the Los Angeles Meeting of the American Physical Society, December 28–30, 1950 [Phys. Rev. **81**, 652 (1951)].
† This work was performed under the auspices of the AEC.
[1] R. B. Roberts and P. H. Abelson, Phys. Rev. **72**, 76 (1947).
[2] Falk, Creutz, and Seitz, Phys. Rev. **74**, 1226 (1948).
[3] Falk, Creutz, and Seitz, Phys. Rev. **76**, 322 (1949).
[4] P. Ammiraju, Phys. Rev. **76**, 1421 (1949).
[5] C. E. Falk, Carnegie Institute of Technology Report No. 5, July 1, 1950 (unpublished).
[6] R. Serber, Phys. Rev. **72**, 1008 (1947).
[7] Helmholz, McMillan, and Sewell, Phys. Rev. **72**, 1003 (1947).

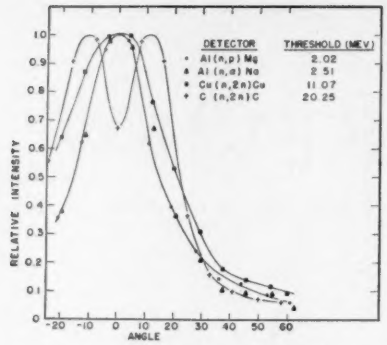

FIG. 1. Angular distribution of neutrons from deuterons on beryllium.

reactions and their thresholds are shown in Fig. 1. Independent determinations were made of the half-life of each activity in order to identify the activity for accurate extrapolation purposes, and also to define the time interval in which the desired activity could be counted before other activities became important. The high bombarding currents resulted in large activity yields, so that the counting error (in the forward direction) was less than 1 percent for points determined by the Cu^{62} and Mg^{27} activities, and less than 5 percent for points determined by the C^{11} and Na^{24} activities.

III. RESULTS AND DISCUSSION

The characteristics of the neutron distributions are conveniently described in terms of the forward-to-isotropic yield ratio, the width at half-maximum, and the angular position of the maximum with respect to the incident beam direction. A typical set of distributions is shown in Fig. 1. In each case there is a maximum in the forward direction superimposed on what appears to be an isotropic background. This was measured only out to about 65 degrees and has been assumed constant beyond that. The ratio of the number of neutrons emitted in the forward peak to the number emitted isotropically is shown in Table I. While the numbers are rough because of the uncertainty in the isotropic component, they indicate a relative increase in this component as the atomic number of the target increases. The isotropic background is presumably due in part to the formation of a compound nucleus by the addition of a deuteron with the subsequent boiling off of a neutron. In addition, there is an irregularity at Sn, which also appears in the discussion of the half-widths below.

TABLE I. Ratio of forward-to-isotropic neutrons in the observed angular distribution.

Target	Detector $Al^{27}(n,p)Mg^{27}$	$Al^{27}(n,\alpha)Na^{24}$	$Cu^{63}(n,2n)Cu^{62}$	$C^{12}(n,2n)C^{11}$
Be	2.4	4.8	1.8	2.4
Al	2.0	3.7	2.0	1.5
Cu	1.4	1.8	0.48	0.61
Sn	1.6	2.3	0.52	2.1
Pb	2.5	1.1	0.38	0.33
U	0.47	0.66	0.14	0.34

Table II, which lists the half-widths of the forward peaks for the elements investigated, shows a nonregular variation in the shapes of the distributions. However, there is a tendency for higher energy neutrons to be concentrated in the forward direction, as evidenced by narrowing of the forward peak as the detector threshold increases, particularly for the data on Al and Pb. Weisskopf has pointed out[4] that for heavy elements the deuteron loses so much energy in climbing the potential barrier that the neutron can obtain sufficient momentum to cause, say, the $Cu(n,2n)$ reaction only by adding its internal momentum in the deuteron parallel to the center-of-mass momentum. This will cause a sharpening of the peak for essentially energetic reasons, the neutrons at wide angles being of lower energy. It is to be noted that in the case of Sn, the distribution is somewhat wider than all the others for neutrons above 11 Mev.

TABLE II. Full width at half-maximum, in degrees, of the observed angular distributions.

Target	Detector $Al^{27}(n,p)Mg^{27}$	$Al^{27}(n,\alpha)Na^{24}$	$Cu^{63}(n,2n)Cu^{62}$	$C^{12}(n,2n)C^{11}$
Be	34	34	42	Double±11 32% dip
Al	30	28	28	22
Cu	44	40	36	Double±7 13% dip
Sn	44	38	48	30
Pb	40	34	36	24
U	38	38	40	30

Table II also shows that in the cases of Be and Cu, neutrons are emitted, which, above 20 Mev, have their spatial maximum displaced from the direction of the incident deuteron beam. Similar results have been reported by Falk.[5] At lower energies, this apparent "double peak" is washed out, indicating that the distributions result from several different nuclear processes of comparable magnitude. This feature is clearly shown in Fig. 1 for the case of Be and is to be compared with the distributions found[7] for high energy deuteron impacts. The latter show "single peaks" exclusively, whose half-widths increase in a regular way with atomic number, and which agree quantitatively with the Serber process of stripping.[6] Electric separation[8] of the deuteron, to be sure, does predict a double-peaked distribution of neutrons from the action of the coulomb field of the target nucleus upon the proton in the deuteron. However, field separation of a deuteron of 20 Mev can produce a neutron of maximum energy only 18 Mev, which is insufficient to cause the $C(n,2n)$ reaction. The

[8] S. M. Dancoff, Phys. Rev. **72**, 1017 (1947).

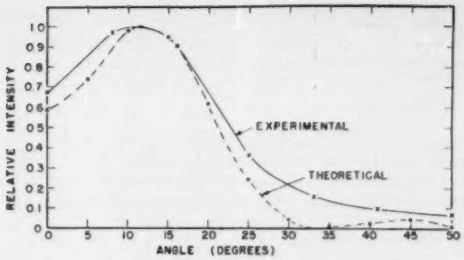

FIG. 2. Angular distribution of neutrons from deuterons on beryllium detected by the carbon foils.

further observation that double peaked distributions results from Be and Cu targets only would seem to rule out these usual theories as the sole mechanisms involved. The same reasons rule out the possibility that the double peaks may be due simply to the coulomb field action on the deuteron before stripping or electric separation occurs.

The collision times for deuterons of less than 20 Mev are, of course, longer than those for the high energy case. This suggests a mechanism by which some neutrons can gain energy in sufficient amount for them to be detected in the carbon foils. The mechanism consists in keeping the deuteron together long enough so that the binding energy given up when the proton sticks, forming a compound nucleus, can be wholly or partly communicated to the neutron.

Since the present data were collected, a quantitative examination of this process has been made by Butler.[9] The model used by him has been applied to the small-angle structure observed in (d,p) angular distributions[10,11] with considerable success, and the calculations reveal significant information concerning the parities and possible spin states of the nuclei formed in this way. It seemed worthwhile, therefore, to apply the theoretical considerations to the information collected here. The theoretical curves of Butler depend on (1) the radius of the target nucleus; (2) the incident deuteron energy; (3) the outgoing neutron energy; (4) the angular momentum carried by the proton, which sticks. These have been suitably modified to fit the conditions of the experiment. The circumstance that the 60-inch cyclotron produces 20-Mev deuterons, while the threshold for the carbon reaction is 20.25 Mev, results in the fact that neutron distributions from collisions of the type described above can be examined separately, without having superimposed upon them neutrons due solely to the other processes of stripping, electric disintegration, and compound nucleus formation.

[9] S. T. Butler, Phys. Rev. **80**, 1095 (1950).
[10] Burrows, Gibson, and Rotblat, Phys. Rev. **80**, 1095 (1950).
[11] J. R. Holt and C. T. Young, Proc. Phys. Soc. (London) **78**, 833 (1950).

TABLE III. Results of analysis: l_p is the angular momentum transferred to the target nucleus.

Reaction	Ground state of initial nucleus		l_p	State of final nucleus	
$Be^9(d,n)B^{10}$	$3/2, 5/2, 7/2, 9/2$	−	1	3	+
$Al^{27}(d,n)Si^{28}$	$5/2$	+	0	2, 3	+
$Cu^{63}(d,n)Zn^{64}$	$3/2, 5/2$	+	2	0	+

However, the use of threshold detectors does not allow the outgoing neutron energy, and consequently the states of excitation of the final nucleus, to be determined. In fact, the observed distributions from carbon detectors are themselves the superposition of contributions from the various final nuclear states, so that with this method, unambiguous spin and parity values cannot be assigned in general.

But in the cases of Be^9, Al^{27}, and Cu^{63} targets, the distribution structure is definite enough so that it can be safely assumed that probably only one of the final states enters in determining the angular distribution. By comparing the theoretical and experimentally observed angular distributions, an example of which is shown in Fig. 2, it has been possible to find agreement good enough to assign parity and possible spin values to either the initial or final state, the other being assumed known. The results are given in Table III.

For the Be^9 reaction, it has been assumed that only the ground state of B^{10} has been produced. Taking the spin value 3 and the shell model prediction of even parity for this state, the necessary spin assignments for Be^9 include the known value of 3/2, while the parity must be different from that of B^{10}. For the Al^{27} reaction, the initial state has been assumed to be 5/2, even, and the resulting Si^{28} state must be assigned a rather large spin and like parity. Since the ground state of Si^{28} is expected to have spin zero, it is thus shown that the capture of a proton by Al^{27} to form the ground state of Si^{28} is forbidden; rather, an excited state is formed which has the properties listed above. For the Cu^{63} reaction, transition to the ground state of Zn^{64} is assumed, which leads to possible spins for Cu^{63} which include the value 3/2. However, in this case, the ground state of the Cu^{63} must be of even parity, which is in disagreement with the prediction from the shell model of Mayer.

An expression of appreciation is due to Professor A. C. Helmholz for his continued interest, advice, and encouragement during the course of this work. The criticisms and discussions of Professor R. Serber and Mr. Warren Heckrotte were of great value. Mr. Heckrotte also aided in making the necessary calculations. The author is greatly indebted to Dr. S. T. Butler for making his analysis available before publication. Finally, thanks are due to Mr. Thomas M. Putnam and the crews of the 60-inch cyclotron for their aid in making the bombardments.

Radiations from F^{18}, Mo^{93}, and Cl^{34}

LAWRENCE RUBY* AND J. REGINALD RICHARDSON
Department of Physics, University of California,† Los Angeles, California
(Received April 16, 1951)

The positron spectrum of F^{18} was investigated with a magnetic lens spectrometer and found to be of the allowed type with an upper limit at 649±9 kev. The gamma-radiation from Mo^{93} was found to consist of three lines at 262±2 kev, 692±11 kev, and 1.51±0.035 Mev. The K to L conversion ratio for the low energy line indicates 2^8 pole electric radiation. The positron spectrum of Cl^{34} consists of three components with upper limits at 4.45 Mev, 2.6 Mev, and 1.3 Mev. Gamma-ray lines were found at 3.3 Mev and 2.1 Mev and at 0.145±0.003 Mev. The latter line gives rise to internal conversion electrons.

I. INTRODUCTION

THE radiations of F^{18}, Mo^{93}, and Cl^{34} have been investigated on a large magnetic lens spectrometer, similar in dimensions and internal design to one already described.[1] The chamber is 48″ long and 10″ i.d. Internal baffles include a set of helical fins to separate positive and negative electrons, and a variable ring focus aperture to minimize spherical aberration. The coils are wound of insulated copper ribbon, 1536 turns of which have been combined to form two thick magnetic lenses, placed one at the source and one at the detector position. This produces a field form which has been found to give minimum lens aberration.[2] Iron bands spaced along the spectrometer chamber provide magnetic shielding to stray fields.[3] Current regulation of better than 0.1 percent is accomplished through the use of grid-controlled rectifiers. Using internal conversion electrons from the 661.4-kev gamma-ray of Ba^{137}, the spectrometer has been calibrated at resolutions of 1.75 and 4.11 percent. The calibration was checked with photoelectrons from the gamma-rays of Ni^{60}.

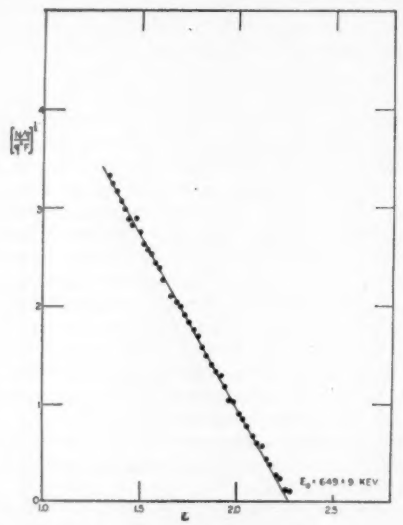

FIG. 1. Kurie plot of positron spectrum of F^{18}.

II. FLUORINE 18

As a preliminary to the measurement of the spectrum of F^{18}, our apparatus was checked by a measurement of the well known spectrum of N^{13}.

The spectrum of 112-min F^{18} has been studied in a spectrometer by Blaser *et al.*[4] The activity was produced in mica by $O^{18}(p,n)F^{18}$. Blaser obtained a position spectrum which gave a straight line Kurie plot with intercept at 635±15 kev. No gamma-rays were mentioned. Knox has also searched with negative result for gamma-rays from F^{18}.

The activity was produced here in Al_2F_6 by $F^{19}(p,pn)$

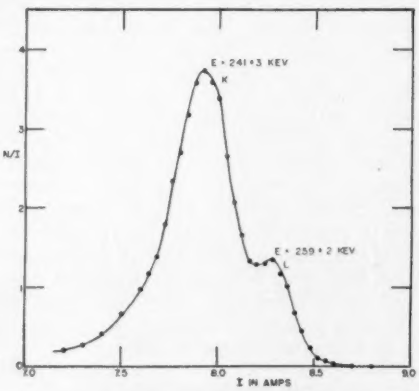

FIG. 2. Conversion electrons from Mo^{93}.

* Now with the Radiation Laboratory, University of California, Berkeley, California.

† Part of the work reported here was submitted as a thesis by one of us (L.R.) in partial fulfillment of the requirements for the Ph.D. degree at the University of California, Los Angeles. The work was supported in part by the joint program of the ONR and AEC.

[1] Hornyak, Lauritsen, and Rasmussen, Phys. Rev. **76**, 731 (1949).

[2] W. Glaser, Z. Physik **116**, 19 (1940).

[3] L. M. Langer, Phys. Rev. **77**, 50 (1950).

[4] Blaser, Boehm, and Marmier, Phys. Rev. **75**, 1953 (1949).

F^{18}. No gamma-rays were found. The Kurie plot is a straight line with intercept at 649±9 kev (see Fig. 1). Below 100 kev the plot becomes distorted, principally because of window absorption. The maximum energy corresponds to a mass difference $M(F^{18})-M(O^{18})=1.795\pm0.0097$ milli-mass units. The value of ft is about 5×10^3, indicating an allowed transition. Since the ground state of O^{18} is assumed to be $^1S_0$, G.-T. selection rules require that the ground state of F^{18} is $^3S_1$.

III. MOLYBDENUM 93

The 6.7-hour activity of Mo^{93} has been investigated by Kundu and Pool.[5] The latest report describes the activity as an isomer decaying by the emission of three gamma-rays in tandem, followed by a beta-decay of long half-life. The gamma-ray energies are 0.3 and 0.7 Mev, identified by conversion electrons, and 1.6 Mev, identified by Compton electrons.

The activity was produced here in columbium (niobium) foil by $Cb^{93}(p,n)Mo^{93}$. Internal conversion electrons at 241±3 kev for K and 259±2 kev for L conversion were found (Fig. 2). This corresponds to a gamma-ray of 262±2 kev. With the spectrometer adjusted for high transmission, conversion electrons at 672±11 kev were observed, corresponding to a gamma-ray of 692±11 kev. The ratio of intensity for the internal conversion lines from the two gamma-rays is 3.2×10^2/1. Photoelectrons from a 2-mil thorium converter occur with maxima at 547±6 kev and 1.37±0.03 Mev (Fig. 3). The peak shift correction, 30±5 kev, has been obtained at the lower energy from measuring the shift in the same converter of the 661.4-kev Ba^{137} gamma-ray. The correction at the higher energy is estimated to be essentially the same.[1] Taking into account peak shift and K binding corrections gives for the gamma-ray energies 687±11 kev and 1.51±0.035 Mev.

From N_K/N_L for the 262-kev gamma-ray, an estimate of the character and multipolarity of the radiation can be made and the K shell partial internal conversion coefficient calculated. Separation of the composite spectrum (Fig. 2) gives $N_K/N_L=2.9\pm0.2$. This value is in agreement with the results of Alburger *et al.*,[6] who obtained a ratio of 2.8±0.3. The theoretically predicted value of N_K/N_L for a 2^5 pole electric transition is 3.0.

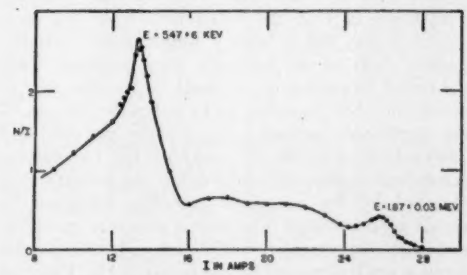

FIG. 3. Photoelectrons produced by Mo^{93} in a 2-mil Th foil.

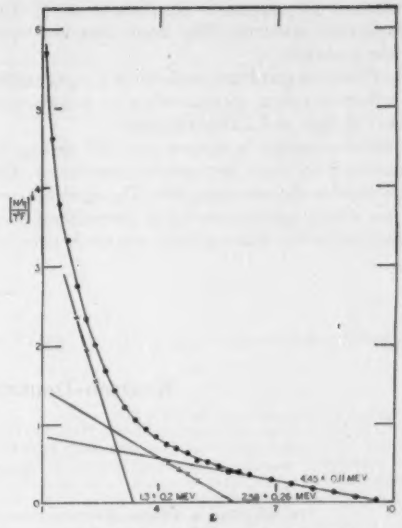

FIG. 4. Kurie plot of positron spectrum of Cl^{34}.

IV. CHLORINE 34

The spectrum of 35-min Cl^{34} has been investigated by Zah Wei-Ho using a cloud chamber.[7] A gamma-ray of 3.4 Mev and two groups of positrons were found. Analysis by means of a modified Kurie plot, involving a Konopinski-Uhlenbeck correction, gave end points at 5.1 and 2.4 Mev.

A preliminary report on this isotope has already been made by the present authors.[8] The activity was produced by $S^{34}(p,n)Cl^{34}$ and by $Cl^{35}(p,pn)Cl^{34}$. For practical reasons, spectroscopic measurements were made by bombarding NaCl, thus making use of the latter mode. Three groups of positrons are indicated. This is evident both from the positron spectrum[8] and the fact that the Kurie plot cannot be resolved into two components (Fig. 4). The maximum energies are 4.45±0.11 Mev, 2.58±0.26 Mev, and 1.3±0.2 Mev.

Conversion electrons at 142±3 kev, corresponding to a 145±3 kev gamma-ray, have been found.[8] The decay of this line has been followed for three half-lives in the spectrometer to verify its origin in Cl^{34}. The ratio

[5] D. N. Kundu and M. L. Pool, Phys. Rev. **70**, 111 (1946), and Phys. Rev. **76**, 183 (1949); M. L. Pool, Helv. Phys. Acta, Supplement III (1950).

[6] D. Alburger, *et al.*, Brookhaven National Laboratory Quarterly Progress Report, July 1–September 30, 1950 (unpublished).

[7] Zah Wei-Ho, Phys. Rev. **70**, 782 (1946).

[8] L. Ruby and J. R. Richardson, Phys. Rev. **80**, 760 (1950).

of positrons to conversion electrons is 17/1. The L photoelectron spectrum has been observed with a thorium converter.

The Compton spectrum produced in a copper radiator has inflection points corresponding to gamma-rays of 3.30±0.14 Mev and 2.13±0.12 Mev.

It seems plausible to assume that Cl^{34} decays to S^{34} alternatively by three beta-gamma transitions. This is summarized in the following table. The figures involving the low energy gamma-ray are in parentheses because its position in the disintegration scheme is uncertain.

Beta-energy	Branching ratio	fl	Gamma-energy	Total energy
4.45±0.11 Mev	0.46	1.2×10^7	(0.145±0.003 Mev)	(4.6±0.11 Mev)
2.58±0.26 Mev	0.28	1.7×10^8	2.13±0.12 Mev	4.7±0.3 Mev
1.3 ±0.2 Mev	0.26	8.9×10^8	3.30±0.14 Mev	4.6±0.2 Mev

The portion of the Kurie plot due exclusively to the high energy positron component has been examined more extensively in this laboratory.[9] However, using the allowed Fermi function, no evidence of any divergence from linearity was found in the resulting plot.

[9] David Green (private communication).

PHYSICAL REVIEW VOLUME 83, NUMBER 4 AUGUST 15, 1951

Neutron-Deuteron Scattering Amplitudes

E. O. Wollan, C. G. Shull, and W. C. Koehler
Oak Ridge National Laboratory, Oak Ridge, Tennessee

(Received May 3, 1951)

The diffraction of neutrons from deuterium containing compounds gives the coherent scattering section of deuterium which can be used to determine the spin dependent scattering amplitudes. Studies have been made on a number of deuterium containing compounds but the results reported here are concerned primarily with recent measurements on NaD. X-ray measurements have been used in interpreting the thermal vibration effects in the crystal and use has been made of Na scattering cross-section data obtained from various sodium containing compounds. This experiment gives $\sigma_{coh}=5.2\pm0.3$ barns. This value can be combined with the results of other deuterium cross-section measurements to give pairs of values for the individual quartet and doublet spin amplitudes for n-d scattering. Various experimental results bearing on this point are summarized. Recent theoretical work seems to have eliminated the ambiguity in the experiments with regard to which of two sets of values of the spin amplitudes is to be chosen.

THE first measurements of the coherent scattering cross section for neutrons on deuterium were made by studying the powder diffraction pattern of NaD.[1] These measurements showed the coherent scattering amplitude to have a positive sign and although the accuracy of the cross-section measurements suffered from uncertainty in the sample purity, they definitely indicated that the coherent scattering cross section is smaller than the total scattering cross section and hence that the scattering is spin dependent.

Since the time of these early experiments a number of other measurements involving the deuterium scattering amplitudes have been made. Powder diffraction patterns have been obtained at this Laboratory on several deuterium containing compounds; Fermi and Marshall[2] have studied the transmission of neutrons by deuterium gas, and Hurst and Alcock[3] have measured the angular dependence of the scattering by the gas.

Compounds studied by the powder technique include heavy ice,[4] ThD_2 and UD_3,[5] and more recent measurements on NaD and LiD, and in addition, a study by Levy and Peterson[6] has been made on ND_4Br. Most of these compounds have been studied for the primary purpose of determining the hydrogen positions in the respective crystal lattices. Pure compounds have, however, been used in every case and each experiment can be considered as a separate determination of the coherent scattering cross section of deuterium. The recent measurements with NaD and LiD* have, however, been made for this express purpose and these compounds have the advantage over the more complex compounds in that the determination of the cross section is not tied in with a simultaneous crystallographic study of the hydrogen atom locations. Only the recent measurements on NaD will be discussed in detail; the large absorption by Li makes the LiD results less significant. Samples were carefully prepared and analyzed for us by Mr. D. Lavalle of this Laboratory. A sufficient number of powder diffraction patterns were obtained by the automatic recording technique to obtain good statistics. The crystal structure scattering amplitudes calculated from the pattern by the powder formula are represented by the points in Fig. 1 plotted on semilog scale against $\sin^2\theta/\lambda^2$. The ordinate scale of

[1] Shull, Wollan, Morton, and Davidson, Phys. Rev. **73**, 842 (1948).
[2] E. Fermi and L. Marshall, Phys. Rev. **75**, 578 (1949).
[3] D. G. Hurst and N. Z. Alcock, Can. J. Phys. **29**, 36 (1951).
[4] Wollan, Davidson, and Shull, Phys. Rev. **75**, 1348 (1949).
[5] Unpublished data by R. E. Rundle and the present authors.
[6] H. Levy and S. W. Peterson, private communication.
* The sample of LiD was kindly supplied by Metal Hydrides, Inc., Beverly, Massachusetts.

scattering amplitudes has been put on an absolute basis by our usual method of comparing the powder peak intensities in the pattern with the peaks from a standard scatterer. The standardization was based primarily on measurements with powdered samples of Ni^{58}, Th, and $Ni^{58}O$ which involve only zero spin nuclei.

The peak intensities were corrected for a small amount of second-order ($\lambda/2$) scattering, the amount of which has been determined from second-order reflections from the (200) planes of powdered crystals having strong (200) peaks. The total amount of second-order scattering is less than two percent of the corresponding first-order scattering. Correction was also made for the presence of about 3 percent by weight of NaOH. Patterns for NaOH samples have been obtained and the small effect of NaOH contaminant on the NaD pattern and also on the effective weight of sample have been taken into account. The data in Fig. 1 have been corrected for both these effects.

To obtain the deuterium scattering amplitude from the measured points it is necessary to take into account the effects of thermal vibration of the atoms in the crystal. The Debye-Waller temperature factor, which was derived for the x-ray case, has been shown by Weinstock[7] to apply also to the case of neutron scattering. This factor is strictly applicable only to a monatomic cubic crystal for which the true scattering amplitude, f_0, for an atom at rest is related to the value f_T measured in a crystal at a given temperature T and at a given $(\sin\theta)/\lambda$ by

$$f_T = f_0 \exp[-W(\Theta, m, T)(\sin^2\theta)/\lambda^2], \qquad (1)$$

where Θ is the characteristic temperature, and m is the mass of the atoms which make up the crystal. It has been found in practice[8] that the factor holds for diatomic crystalline compounds if the masses of the constituent atoms are not too different in which case a single factor involving the average mass in the function W applies to the amplitudes of both atoms.

If this condition could be assumed to hold also for a compound such as NaD where the ratio of the masses of the constituent atoms is large, then the best straight lines through the experimental points in curves A and D of Fig. 1 would represent the effect of lattice vibrations, and the intercept at $(\sin^2\theta)/\lambda^2 = 0$ would give the values of the sum and difference of the deuterium and sodium scattering amplitudes.

In related studies (unpublished) which we have made on the scattering of neutrons by NaH, this point has been investigated by a method which depends on the characteristic differences between x-ray and neutron diffraction for just such a case. With x-rays the diffraction by NaH arises almost wholly from the scattering by the Na atoms, and hence the lattice vibration effects in the pattern will also be due primarily to Na atoms. The slope of the dashed curve C in Fig. 1 represents this lattice vibration effect on the sodium scattering amplitude as determined from x-ray intensity measurements on NaH. Although similar measurements were not made with NaD, it would be expected that the sodium amplitude would be very nearly the same for the two compounds.

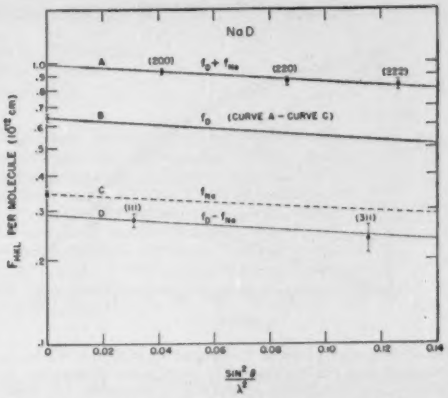

FIG. 1. Crystal structure scattering amplitudes as determined in NaD. Curves A and D represent the experimental data for a series of all-even and all-odd reflections respectively. Curve C corresponds to the scattering amplitude in this crystal for sodium only, making use of x-ray data on NaD and sodium scattering in other compounds. Curve B is obtained by subtracting C from A and corresponds to deuterium scattering only.

It is to be noted also that the curve for Na atoms alone is almost parallel within experimental error to the lines through the sum and difference reflections for NaD, and hence one can conclude that the thermal motion effects for the Na and D atoms in this crystal are very nearly equal. The NaD data could then be used directly for determining the deuterium scattering amplitude. If one were to proceed in this way, however, the accuracy of the results would depend strongly on the relatively weak and hence less accurately determined odd index reflections represented by the points on curve D. The deuterium amplitude can, however, be more accurately determined by making use of data on the sodium scattering amplitude obtained with compounds better suited to give accurate results. In line with this procedure, the intercept at $(\sin^2\theta)/\lambda^2 = 0$ of the dashed curve whose slope has been taken from x-ray measurements has been normalized to the average value of the sodium cross section ($\sigma = 1.50 \pm 0.04$ barns) obtained from several sodium-containing compounds.[9] Subtracting this curve C from the experimental data in curve A gives curve B, which then represents the case for the scattering by deuterium atoms alone. With this procedure the accuracy of the scattering amplitude for deuterium determined from curve B depends primarily on the accuracy of the present measurements of the strong (200) reflection and on the accuracy with which

[7] R. Weinstock, Phys. Rev. **65**, 1 (1944).
[8] Kathleen Lonsdale, Acta Cryst. **1**, 142 (1948).
[9] C. G. Shull and E. O. Wollan, Phys. Rev. **81**, 527 (1951).

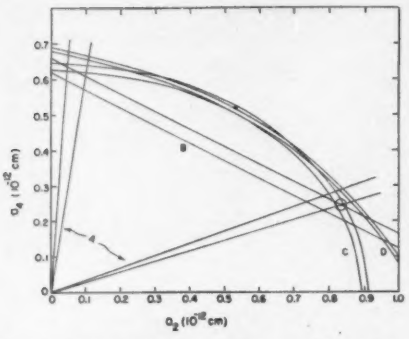

FIG. 2. Summary graph of the various experimental results for the quartet and doublet scattering amplitudes of neutrons on deuterons. The experiment designation is as follows: (A) Hurst and Alcock angular distribution of scattering by D_2 gas, (B) coherent scattering amplitude evaluation from crystal diffraction, (C) free scattering cross section by transmission at epi-thermal neutron energy and (D) Fermi-Marshall transmission at very low neutron energy. Theory suggests that the amplitude assignment should follow $a_2 > a_4$, and the circled point corresponds to mean values of the amplitudes as suggested by all of the experiment data.

the sodium cross section was determined from the study of other sodium-containing compounds. The results obtained from curves *A* and *D* or from curve *B* lead to the same value for the deuterium scattering amplitude, the latter, however, being the more accurate. The deuterium scattering amplitude obtained from this experiment is

$$f_D = +(0.64 \pm 0.02) \times 10^{-12} \text{ cm}$$

and the corresponding cross section

$$\sigma_{\text{coh}} = 5.2 \pm 0.3 \text{ barns.}$$

The experiments with heavy ice, ThD_2, and LiD are less accurate than those with NaD, but they are all consistent with the above value of σ_{coh}.

On the basis of measurements on ND_4Br, Levy and Peterson give the same value ($\sigma = 5.2 \pm 0.3$ barns) as that obtained with NaD. This value has then been taken as representing the crystal diffraction data.

SPIN SCATTERING AMPLITUDES

The coherent scattering cross section can be expressed in terms of the individual scattering amplitudes for the two spin states, $i+\frac{1}{2}$ and $i-\frac{1}{2}$, of the compound nucleus

$$\sigma_{\text{coh}} = 4\pi f_{\text{coh}}^2 = \frac{4\pi}{(2i+1)^2}[(i+1)f_{i+\frac{1}{2}} + i f_{i-\frac{1}{2}}]^2, \quad (2)$$

where the f's refer to bound scattering amplitudes, which are related to the free amplitudes a for a nucleus of mass number A by $f = [(A+1)/A]a$. For the case of *n-d* scattering, Eq. (2) can be written as:

$$f_{\text{coh}} = \pm\tfrac{1}{3}(2a_4 + a_2), \quad (3)$$

where a_4 and a_2 are the free amplitudes for scattering in the quartet and doublet states of the compound nucleus, the triton.

The total free scattering cross section is given by

$$\sigma_s{}^f = \tfrac{4}{3}\pi(2a_4{}^2 + a_2{}^2). \quad (4)$$

These two equations give solutions for the scattering amplitudes a_4 and a_2. Since f_{coh} has already been determined to be positive there will be only two sets of values for these scattering amplitudes.

Hurst and Alcock have made measurements of the angular distribution of the scattering by deuterium gas and these experiments can be expressed in terms of the ratio a_2/a_4, but again the quadratic character of the cross-section relation leads to two roots for this ratio. Fermi and Marshall have measured the transmission by deuterium gas with long wavelength neutrons and this leads to still another relation between a_4 and a_2.

These results are all represented graphically in Fig. 2. The total scattering cross section of deuterium is taken from transmission measurements[2,10] on D_2O for epithermal neutrons with the contribution from the oxygen cross section subtracted. A value of $\sigma_{\text{total}} = 3.4 \pm 0.1$ barns seems consistent with these measurements. The errors in the other data are those given by the experimenters.

As seen in Fig. 1, there exist two regions of common intersection among the four independent sets of amplitudes. The experiments are not capable of resolving the selection ambiguity, but recent theoretical work[11–13] on neutron-deuteron scattering indicates that the only acceptable pair of values for the scattering amplitudes is that for which $a_2 > a_4$. This case is represented in Fig. 2 by the circle, which might be considered as a reasonable mean value for the over-all experimental results. The corresponding mean values for the various amplitudes and cross sections according to this selection are given as

$$a_2 = +0.83 \pm 0.015 \times 10^{-12} \text{ cm}$$

$$a_4 = +0.24 \pm 0.015 \times 10^{-12} \text{ cm}$$

$$\sigma_{\text{coh}} = 5.4 \pm 0.4 \text{ barns}$$

and

$$\sigma_s{}^f = 3.40 \pm 0.15 \text{ barns.}$$

The algebraic signs associated with these scattering amplitudes follow the convention of assigning a positive sign to potential scattering amplitudes.

[10] Rainwater, Havens, Dunning, and Wu, Phys. Rev. **73**, 733 (1948).
[11] M. M. Gordon, Phys. Rev. **80**, 1111 (1950).
[12] A. Troesch and M. Verde, Helv. Phys. Acta **24**, 39 (1951).
[13] F. G. Prohammer and T. A. Welton, Quarterly Report ORNL-1005.

Gamma-Rays from Deuteron Bombardment of B^{10}, B^{11}, N^{14}, and F^{19}

JAMES TERRELL* AND G. C. PHILLIPS
Rice Institute,† Houston, Texas

(Received April 30, 1951)

A pair spectrometer has been used to analyze the high energy gamma-ray spectra produced by bombarding thick targets of natural boron, enriched boron, nitrogen, and fluorine with 1.56-Mev deuterons from a Van de Graaff generator. The $B^{10}+d$ spectrum shows gamma-rays of energy 4.52±0.10, 6.71±0.13, and 9.04±0.18 Mev; the spectrum from $B^{11}+d$, partially masked by the strong $B^{10}+d$ gamma-rays, shows a single 4.5±0.1-Mev gamma-ray. The nitrogen target produced strong gamma-rays of energy 5.33±0.11, 7.40±0.15, and 8.46±0.17 Mev, with some indication of unresolved lines at 4.4 and 6.4 Mev. The $F^{19}+d$ spectrum shows weak high energy gamma-rays, not previously observed, of energy 8.1±0.4, 9.3±0.3, and 11.5±0.4 Mev; a level in Ne^{20} at 11.5±0.4 Mev is indicated. In any of these spectra lower energy gamma-rays may be present though undetected, because of the large variation of spectrometer sensitivity with energy. Absolute yield values are estimated for each of these gamma-rays.

I. INTRODUCTION

HIGH energy gamma-ray spectra produced by a number of light-element nuclear reactions have not been fully clarified; the earlier cloud-chamber and absorption techniques did not, in general, have the resolution and statistical accuracy needed to resolve these spectra fully. The reasonably high counting rates and good resolution now available in pair spectrometers have made reinvestigations desirable.

The investigation reported here was undertaken with a pair spectrometer designed specifically for high counting rate, at the expense of some resolution. This spectrometer has been previously used with success on the low intensity gamma-rays produced by a polonium-beryllium mixture.[1] The reactions investigated were produced by deuteron bombardment of thick targets of natural boron, enriched boron, nitrogen, and fluorine.

The gamma-rays from $B+d$ have been analyzed by Gaerttner, Fowler, and Lauritsen,[2] and by Halpern and Crane,[3] both groups using cloud chambers and the natural isotopic mixture of B^{10} and B^{11}; Hudspeth and Swann[4] have investigated the low energy gamma-rays by coincidence absorption methods. Very recently, Rutherglen[5,6] has observed the gamma-ray spectrum using separated isotopes and a pair spectrometer, obtaining results similar to those reported here.

The $N^{14}+d$ gamma-ray spectrum has been analyzed only by means of cloud-chambers; results have been reported by Gaerttner and Pardue,[7] and by Crane, Halpern, and Oleson.[8]

The only report on the $F^{19}+d$ high energy gamma-ray spectrum seems to be that of Bennett, Bonner, and Watt,[9] who used absorption methods. Jelley[10] and Littauer[11] have published investigations of the low energy gamma-rays from the beta-disintegration of F^{20}, produced by this reaction.

In addition to these direct measurements of the gamma-ray spectra there is much indirect information on the gamma-ray energies from Q-value measurements and from α-γ, β-γ, and p-γ coincidence measurements. Many references to this literature may be found in the review article by Hornyak, Lauritsen, Morrison, and Fowler.[6]

II. PROCEDURE

The 180°-focusing magnetic pair spectrometer used in this work is similar to that of Walker and McDaniel[12] and has been described in a previous paper.[1] High energy gamma-rays were produced by bombarding thick targets of natural boron (about 18.8 percent B^{10}), enriched boron (96 percent B^{10}, obtained from the Oak Ridge National Laboratories), nitrogen, and fluorine with 1.56-Mev deuterons from the Rice Institute pressure Van de Graaff generator. The boron targets were in the form of B_2O_3, fused onto silver disks; the nitrogen and fluorine targets were the respective calcium compounds. (The calcium nitride was obtained from Metal Hydrides, Inc.) The calcium nitride target was scraped to a fresh surface immediately before it was placed in vacuum to remove the calcium hydroxide film which forms rapidly in the presence of water vapor. The deuterons were magnetically analyzed; the deuteron beam current, measured by a current integrator, was generally about 0.25 microampere. The geometry of the pair spectrometer and

* AEC Predoctoral Fellow during part of this work. Now at Los Alamos Scientific Laboratory, Los Alamos, New Mexico.

† This paper is based in part on a Ph.D. thesis submitted by the first-named author to the faculty of the Rice Institute in May, 1950. A preliminary report of this work was presented at the February, 1951, meeting of the American Physical Society [J. Terrell, Phys. Rev. **82**, 300(A) (1951)]. This work was supported by the joint program of the ONR and AEC, and by the Research Corporation.

[1] J. Terrell, Phys. Rev. **80**, 1076 (1950).
[2] Gaerttner, Fowler, and Lauritsen, Phys. Rev. **55**, 27 (1939).
[3] J. Halpern and H. R. Crane, Phys. Rev. **55**, 415 (1939).
[4] E. L. Hudspeth and C. P. Swann, Phys. Rev. **76**, 1150 (1949).
[5] Proceedings of the Harwell Nuclear Physics Conference, September, 1950.
[6] Hornyak, Lauritsen, Morrison, and Fowler, Revs. Modern Phys. **22**, 291 (1950).
[7] E. R. Gaerttner and L. A. Pardue, Phys. Rev. **57**, 386 (1940).
[8] Crane, Halpern, and Oleson, Phys. Rev. **57**, 13 (1940).
[9] Bennett, Bonner, and Watt, Phys. Rev. **59**, 793 (1941).
[10] J. V. Jelley, Phil. Mag. **41**, 1199 (1950).
[11] R. M. Littauer, Phil. Mag. **41**, 1214 (1950).
[12] R. L. Walker and B. D. McDaniel, Phys. Rev. **74**, 315 (1948)

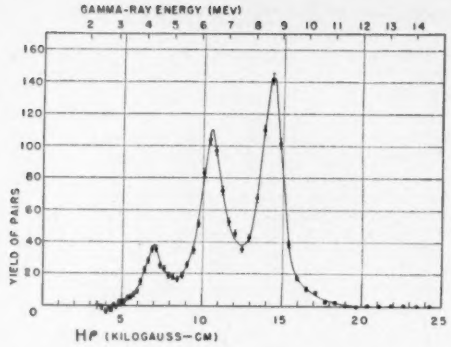

FIG. 1. Pair spectrum from deuteron bombardment of B_2O_3 (96 percent B^{10}). Ordinate scale is pair counts per 80 microcoulombs of deuterons.

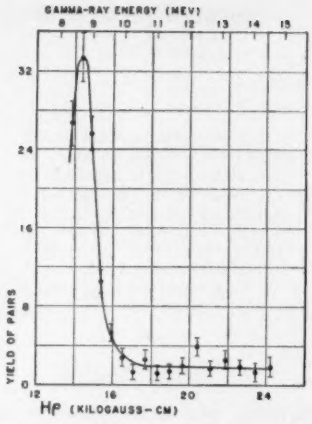

FIG. 3. Pair spectrum (high energy end) from deuteron bombardment of B_2O_3 (81 percent B^{11}). Ordinate scale is pair counts per 80 microcoulombs of deuterons.

the radiator thickness (31.0 mg/cm² tin) were the same as in the work with ThC″ and polonium-beryllium,[1] simplifying yield comparisons.

III. RESULTS

The results obtained are shown in Figs. 1 through 5, in which the yield of pairs is plotted as a function of $H\rho$ for either positron or electron in the case of equally shared energy. The ordinate units are the same for all figures and represent pair counts per 80 microcoulombs of deuterons for a single pair of counters. Small corrections have been made for nonradiator background and for accidental coincidences. Standard deviations are shown for each point, unless the deviation is covered by the area of the point. Each point on the graphs, except for a few on the ends, represents the weighted average of four determinations, one in each channel used; each determination was for 80 microcoulombs of deuterons, except for the main portions of the spectra from N^{14} and F^{19}, where each determination was for 160 microcoulombs. Each of these curves except Fig. 3 took about ten hours of running time, not including the shorter time needed to measure the nonradiator counting rate as a function of $H\rho$. The highest point in the $N^{14}+d$ curve represents about 2400 pair counts.

The gamma-ray spectra obtained with boron targets are shown in Figs. 1, 2, and 3. Figures 1 and 2 show the spectra from enriched and natural boron, respectively; Fig. 3 shows a more precise analysis of the high energy end of Fig. 2, indicating that the high energy fluctuations above the main peak are largely, if not entirely, statistical in nature. In each of these two spectra the same three lines appear; the two highest energy lines are five times stronger from B^{10} than from natural boron, indicating that they come from B^{10} only. The lowest energy line is of the same order of intensity in both spectra, so that it must come from both isotopes. Because of the overlapping of the lines, the width at half-maximum can be measured with some accuracy

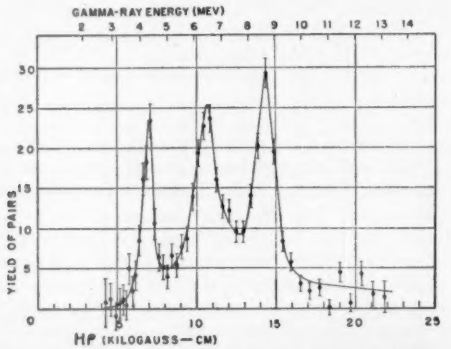

FIG. 2. Pair spectrum from deuteron bombardment of B_2O_3 (81 percent B^{11}). Ordinate scale is pair counts per 80 microcoulombs of deuterons.

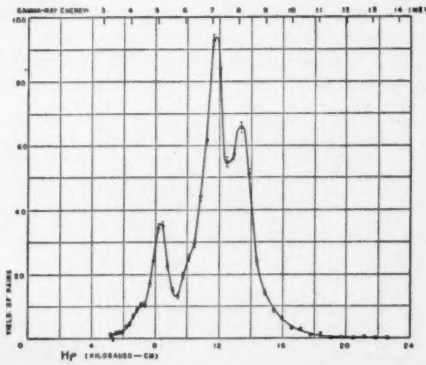

FIG. 4. Pair spectrum from deuteron bombardment of Ca_3N_2. Ordinate scale is pair counts per 80 microcoulombs of deuterons.

only for the line of highest energy from the enriched target, which has a width of 11.1 percent. The method of difference of squares used in the earlier work[1] then indicates a peak shift of 4.4 percent in momentum, if a single gamma-ray is responsible for the peak, which is doubtful (see below). Theoretical calculations of the effects of angular distribution of pairs leaving the radiator and of energy loss in the radiator lead to a peak shift of about 3 percent; a peak shift of 4.0 percent has been adopted as a compromise. No other peak width in any of the work reported here can be measured with equal accuracy. Therefore, the peak shift for other gamma-ray energies has been estimated by plotting a smooth curve through this value (4.0 percent at 9 Mev) and through the peak shifts used at lower energies[1] (4.9 percent at 4.45 Mev; 6.0 percent at 2.62 Mev).

Using these peak shifts to correct the energies, we find that the gamma-rays from $B^{10}+d$ have energies of 4.52, 6.71, and 9.04 Mev. The lines from natural boron have apparently identical energies, though the peaks cannot be located as accurately as for the separated isotope. The results are summarized in Table I.

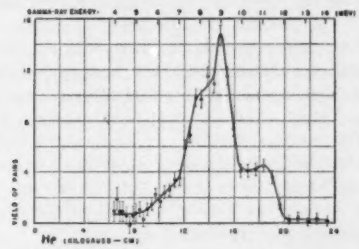

FIG. 5. Pair spectrum from deuteron bombardment of CaF_2. Ordinate scale is pair counts per 80 microcoulombs of deuterons.

The ratios of the yields from separated B^{10} to those from natural boron for the 6.7- and 9.0-Mev gamma-rays are respectively 4.6 and 5.2, which are equal to the ratio of 96 percent to 19 percent of B^{10} within statistical error. There is thus no doubt that these two gamma-rays are due to the B^{10} isotope. Any radiation from the heavier isotope in this range is very weak, if present, and is completely obscured by the strong high energy quanta from $B^{10}+d$. The calculated yield which would have been obtained from 100 percent separated boron isotopes is given in Table II. The 6.7-Mev gamma-ray peak appears to have too much width for a single gamma-ray, particularly on the high energy side. The results indicate that there is no appreciable gamma-radiation above 10 Mev from deuteron bombardment of B^{10}. In the region from 11.5- to 15-Mev statistical fluctuations are of the order of 0.5 percent of the peak counting rate. Allowing for the increased pair-production cross section in this energy range, we estimate the upper limit of possible gamma-radiation in this range as a few tenths of 1 percent of the intensity at 9 Mev. For the case of $B^{11}+d$ we estimate that there is no gamma-radiation in this high energy range of the order of 1 or 2 percent of the intensity of the 4.5-Mev gamma-ray produced by this reaction.

TABLE I. Gamma-rays from $B+d$.

Target	$H\rho$ at peak (gauss-cm)	Gamma-ray energy (Mev)	Pair counts (per 80 microcoulombs)
B_2O_3 (96% B^{10})	7000	4.52±0.10	38
	10,600	6.71±0.13	110
	14,400	9.04±0.18	141
B_2O_3 (81% B^{11})	7000	4.5 ±0.1	23
	10,600	6.7 ±0.2	24
	14,400	9.0 ±0.2	27

In order to make sure that the 4.5-Mev gamma-ray actually came from both boron isotopes and not from another element, a check was made on the pair spectrum from a thick target of boron carbide. Because of considerable background, the spectrum was not observed with great accuracy, but it appeared to be identical with that from normal boron oxide, except that the yield was roughly 1.6 times as large. This difference is to be expected because of the larger percentage of boron atoms in boron carbide.

The pair spectrum produced by deuteron bombardment of the calcium nitride target is shown in Fig. 4. The high energy gamma-radiation is nearly as intense as that from $B^{10}+d$, with correspondingly good statistics. There are three well-defined peaks, corresponding to gamma-ray energies of 5.33, 7.40, and 8.46 Mev. There is some indication of unresolved lines at 4.4 and 6.4 Mev, of lower intensity.

The results obtained with a calcium fluoride target are plotted in Fig. 5. The pair yield is lower than in any of the other cases, with correspondingly larger statistical fluctuations. It is apparent that there are at least three high energy gamma-rays present, since the main peak is much too wide for a single gamma-ray. If we assume that there are three gamma-rays in this

TABLE II. Summary for gamma-rays produced by deuteron bombardment.

Target	$H\rho$ at peak (gauss-cm)	Gamma-ray energy (Mev)	Pair counts (per 80 microcoulombs)	Gamma-ray yield (quanta/microcoulomb)
B_2O_3 (100% B^{10})	7000	4.52±0.10	39	34×10^6
	10,600	6.71±0.13	115	19×10^6
	14,400	9.04±0.18	147	12×10^6
B_2O_3 (100% B^{11})	7000	4.5 ±0.1	19	17×10^6
Ca_3N_2	(6800)	(4.4 ±0.3)	(4)	(4×10^6)
	8330	5.33±0.11	37	15×10^6
	(10,200)	(6.4 ±0.5)	(9)	(2×10^6)
	11,720	7.40±0.15	91	11×10^6
	13,450	8.46±0.17	57	5×10^6
CaF_2	12,800	8.1 ±0.4	5	0.5×10^6
	14,900	9.3 ±0.3	14	1.1×10^6
	18,500	11.5 ±0.4	3	0.2×10^6

spectrum, we obtain gamma-ray energies of 8.1, 9.3, and 11.5 Mev. It was not possible to obtain good statistics below 6 Mev, because of high nonradiator background in this range.

All of the experimental results reported in this paper are summarized in Table II. The pair counting rates have been converted roughly to absolute yield values by interpolating between spectrometer sensitivities found at lower energies and the theoretically calculated value at 9 Mev. It has been found[1] that, with this same geometry and radiator, this spectrometer counts one pair for each 8×10^9 quanta at 2.62 Mev, and one pair for each 7×10^7 quanta at 4.45 Mev. It becomes possible to calculate the sensitivity at higher energies with fair accuracy; the value obtained at 9.0 Mev is 6.5×10^6 quanta per pair count. This value takes into account only the geometry of the apparatus, the theoretical pair-production cross section, and an estimated 30 percent loss of counts due to angular distribution effects at this energy. Although the absolute yield values obtained in this way are not very accurate, they are probably not in error by much more than a factor of two.

Rough measurements of the intensity of gamma-radiation from deuteron bombardment of the boron targets, by comparison with radium gamma-radiation, using a small Geiger counter sheathed in $\frac{1}{2}$ inch of lead, indicated that the $B^{10}+d$ radiation was equivalent to 8 mg of radium per microampere of deuterons, and the normal boron target was equivalent to 5 mg per microampere. Making a rough estimate as to the counter efficiency at the various energies involved, we find that about 8×10^7 quanta/microcoulomb are obtained from the B^{10} target and about 6×10^7 from the normal isotopic mixture. These values are not inconsistent with the intensity values estimated in Table II, which indicates that the total high energy intensity is about 6.4×10^7 quanta/microcoulomb from the 96 percent B^{10} target, and about 2.6×10^7 from normal boron oxide. This includes only gamma-rays of more than 4-Mev energy, as the sensitivity of the spectrometer drops rapidly below this energy. To the extent that these intensity estimates are correct, most of the $B^{10}+d$ radiation is of energy greater than 4 Mev, while more than half of the weaker $B^{11}+d$ radiation is of lower energy. It is possible that an appreciable amount of low energy radiation comes from $O^{16}+d$ in each case.

IV. DISCUSSION

A. $B^{11}+d$

The high energy gamma-rays produced by bombardment of natural boron with deuterons have been observed in earlier cloud-chamber work. Gaerttner, Fowler, and Lauritsen,[2] bombarding with 550 to 850 kilovolts peak voltage, found gamma-rays of 1.5, 2.2±0.3, 4.4±0.3, 6.9±0.4, and 9.1±0.4 Mev, with relative intensities of >2.5, 2.5, 1.0, 0.3, and 0.1. Halpern and Crane[3] found lines of 1.4, 2.4, 4.2, 6.0, and 9.1 Mev, with relative intensities of 1, 1, 6, 2, and 1 (with 700-kev maximum deuteron energy). The present work does not give greatly different results for the natural boron target; the relative intensities of the 4.5-, 6.7-, and 9.0-Mev gamma-rays are approximately given (see Table II) by 10, 2, and 1. Because no work had been done with separated isotopes, the two highest energy lines were generally assigned[13] until very recently to the reaction $B^{11}(d,n)C^{12}$. As the present work and that of Rutherglen[5,6] show, these gamma-rays should have been assigned to $B^{10}+d$, only the 4.5-Mev quanta coming in part from $B^{11}+d$. Rutherglen has reported 4.5, 6.5, 6.7, and 8.94 Mev gamma-rays from $B^{10}+d$, and 4.45 Mev from $B^{11}+d$.

There are several reactions which might account for the 4.5-Mev gamma-ray observed from $B^{11}+d$. These are the following (Q-values taken from Hornyak, Lauritsen, Morrison, and Fowler[6]):

(1) $B^{11}(d,\alpha)Be^9$, $Q=8.03$ Mev.
(2) $B^{11}(d,p)B^{12}$, $Q=1.1$ Mev; $B^{12}(\beta^-)C^{12}$, $Q=13.4$ Mev.
(3) $B^{11}(d,n)C^{12}$, $Q=13.78$ Mev.

None of the high energy gamma-rays could come from $O^{16}+d$, because of insufficient Q-values. As to reaction (1), alpha-particle studies by Van Patter *et al.*[14] indicate a level in Be^9 at 2.42 Mev, but give no evidence of other levels up to 5.0-Mev excitation energy. Their estimated yield values at 1.51-Mev deuteron energy (1.6 millibarns/steradian for transitions to the 2.42-Mev level in Be^9, with transitions to other levels at least six times less intense) seem to rule out this reaction as the 4.5-Mev gamma-ray source, or even as the origin of much of the low energy radiation.

The second and third reactions lead to the same levels in C^{12}. At a deuteron bombarding energy of 1.47 Mev, Hudspeth and Swann[4] estimated the thick target yield from (2) to be about 10^7 beta-particles/microcoulomb. Hornyak and Lauritsen[15] found deviations in the beta-spectrum which suggest that about 5 percent of the beta-transitions are to excited levels of C^{12}. Thus, the high energy gamma-ray yield may be of the order or 5×10^5 quanta/microcoulomb, which seems entirely too small to account for the results reported in the present paper. The yield of 1-Mev gamma-rays from an excited level in B^{12} is reported as about 20 percent[16] of the yield of B^{12} (there is some conflicting data[4]), which might indicate 2×10^6 quanta/microcoulomb. If so, this reaction could not account for much of the low energy gamma-radiation from $B^{11}+d$.

Gibson[17] investigated reaction (3), using a separated B^{11} target 120 kev thick and deuterons of 930-kev

[13] W. F. Hornyak and T. Lauritsen, Revs. Modern Phys. **20**, 191 (1948).
[14] Van Patter, Sperduto, Huang, Strait, and Buechner, Phys. Rev. **81**, 233 (1951).
[15] W. F. Hornyak and T. Lauritsen, Phys. Rev. **77**, 160 (1950).
[16] Buechner, Van Patter, Strait, and Sperduto, Phys. Rev. **79**, 262 (1950).
[17] W. M. Gibson, Proc. Phys. Soc. (London) **62A**, 586 (1949).

energy, and found strong neutron groups of roughly equal intensity from 4.47- and 9.72-Mev levels in C^{12}, as well as a weak group corresponding to a 7-Mev level. Similar groups were found by Bonner and Brubaker[18] using unseparated isotopes and 0.9-Mev deuterons. The weak group in Gibson's work could be assigned to B^{10} contamination, as 5 percent contamination would account for its intensity. The main reason Gibson did not do this seems to be that the observed neutron energy was slightly too low; however, he observed a similar lowering of energy for neutrons from B^{11} contamination of the B^{10} target. There seems to be little strong evidence for a 7-Mev level in C^{12} in other recent work.[1,17,19–23]

The most reasonable explanation of the observed 4.5-Mev gamma-ray seems to be that it is from reaction (3), involving the well-verified[6] 4.5-Mev level in C^{12}. The absence of higher energy gamma-radiation is probably accounted for by the fact that the 9.7-Mev level in C^{12} is unstable to alpha-particle emission, the dissociation level being at 7.39 Mev. The lower energy gamma-radiation apparently present may come from a number of possible reactions, and may involve $O^{16}+d$.

B. $B^{10}+d$

Considering next the gamma-rays produced by $B^{10}+d$, we have the following possible reactions:

(1) $B^{10}(d,n)C^{11}$, $Q=6.53$ Mev;

$C^{11}(\beta^+)B^{11}$, $Q=0.98+1.02$ Mev.

(2) $B^{10}(d,\alpha)Be^8$, $Q=17.81$ Mev;

$Be^8\rightarrow 2He^4$, $Q=0.1$ Mev.

(3) $B^{10}(d,p)B^{11}$, $Q=9.24$ Mev.

Reaction (1) might account for the 4.5- and 6.7-Mev gamma-rays, as Swann and Hudspeth,[24] as well as Johnson,[25] have found evidence of levels in C^{11} at about these energies from studies of the neutron groups. Reaction (2) could account for all the gamma-rays on the basis of energy available. However, Thirion[26] has found no evidence for gamma-alpha-coincidences from $B^{10}+d$, at 600-kev deuteron energy. It is of interest to note that the 17.60-Mev state of Be^8 is evidently not excited by (2), since the known[12] 14- and 17-Mev gamma-rays from this state are not observed. The excitation of this level is improbable because of the low energy available for alpha-particle emission; but is not forbidden by selection rules, as C^{12} can apparently be formed in states of either parity[27] at the bombarding energy used here.

The most probable source of the gamma-rays seems to be reaction (3), the protons from which have been investigated by several observers. Bateson[28] observed levels in B^{11} at 2.15, 4.48, 5.03, 6.92, 7.82, 8.48, and 8.86 Mev, using separated B^{10} and 3.76-Mev deuterons. Van Patter and Buechner,[29,30] using 96 percent B^{10} and 1.5 Mev deuterons, have found levels, in B^{11} at 2.138, 4.459, 5.034, 6.758, 6.808, 7.298, 8.568, 8.926, 9.190, and 9.276 Mev. The weakest proton groups were those corresponding to the 2.138-, 6.808-, and 8.568-Mev levels.[30] This level structure fits the observed gamma-ray spectrum quite well; thus, the asymmetry of the 6.7-Mev gamma-ray peak may be due to the presence of a 7.3-Mev gamma-ray. Obviously, gamma-rays of 8.926, 9.190, and 9.276 Mev would not be resolved by this spectrometer. Curling and Newton[31] have observed proton-gamma-coincidences from (3). At their bombarding energy of 430 kev the lower energy proton group, to the 4.5-Mev level in B^{11}, was 3.5 times as intense as the group to the 2.1-Mev level, whether or not coincidence with gamma-rays was required. This evidence is consistent with the small amount of low energy radiation produced by $B^{10}+d$, as observed in the present work.

C. $N^{14}+d$

The gamma-ray spectrum from $N^{14}+d$ has been reported in earlier cloud-chamber work. Gaerttner and Pardue,[7] bombarding at 700 kev, found gamma-rays of energy 2.2, 4.2, 5.3±0.4, 7.2±0.4, and up to 11 Mev; Crane, Halpern, and Oleson[8] measured the energies as 2.5, 4.1, 5.1±0.3, 6.6±0.3, and 8.2±0.5 (deuteron energy 0.6 Mev). The values found with this pair spectrometer are (4.4±0.3), 5.33±0.11, (6.4±0.5), 7.40±0.15, and 8.46±0.17, which agree reasonably well with the earlier results. Reactions which must be considered include the following:

(1) $N^{14}(d,\alpha)C^{12}$, $Q=13.50$ Mev.

(2) $N^{14}(d,n)O^{15}$, $Q=5.1$ Mev;

$O^{15}(\beta^+)N^{15}$, $Q=1.68+1.02$ Mev.

(3) $N^{14}(d,p)N^{15}$, $Q=8.57$ Mev.

Reaction (1) has been observed in various laboratories. Holloway and Moore,[32] bombarding enriched mixtures of nitrogen isotopes with 1-Mev deuterons, observed alpha-groups from N^{14} leading to C^{12} levels at 4.37 and 7.62 Mev, the latter group being weak. Guggenheimer, Heitler, and Powell,[23] bombarding gase-

[18] T. W. Bonner and W. M. Brubaker, Phys. Rev. **50**, 308 (1936).
[19] Levinthal, Martinelli, and Silverman, Phys. Rev. **78**, 199 (1950).
[20] R. Malm and W. W. Buechner, Phys. Rev. **81**, 519 (1951).
[21] W. H. Guier and J. H. Roberts, Phys. Rev. **79**, 719 (1950).
[22] Pringle, Roulston, and Standil, Phys. Rev. **78**, 627 (1950).
[23] Guggenheimer, Heitler, and Powell, Proc. Roy. Soc. (London) **190A**, 196 (1947).
[24] C. P. Swann and E. L. Hudspeth, Phys. Rev. **76**, 168 (1949).
[25] V. R. Johnson, Phys. Rev. **81**, 316 (1951).
[26] J. Thirion, Compt. rend. **229**, 1007 (1949).
[27] G. C. Phillips, Phys. Rev. **79**, 240 (1950).
[28] W. O. Bateson, Phys. Rev. **80**, 982 (1951).
[29] W. W. Buechner and D. M. Van Patter, Phys. Rev. **79**, 240 (1950).
[30] Van Patter, Buechner, and Sperduto, Phys. Rev. **82**, 248 (1951).
[31] C. D. Curling and J. O. Newton, Nature **166**, 339 (1950).
[32] M. G. Holloway and B. L. Moore, Phys. Rev. **58**, 847 (1940).

ous nitrogen with 6.5-Mev deuterons, observed these same groups with less statistical accuracy. However, Malm and Buechner,[30] using 1.4-Mev deuterons, performed a magnetic analysis of the alpha-particles from (1) and found evidence of excited C^{12} levels only at 4.438 and 9.620 Mev, with no group from a 7-Mev level to about 10 percent of the intensity. They also observed that the 9.620-Mev level was unusually wide, presumably due to dissociation into Be^8+He^4. Thus, it seems certain only that a 4.5-Mev gamma-ray should be produced by this reaction.

Reaction (2) does not produce enough energy to account for the highest energy gamma-rays. There is evidence that two neutron groups are present,[33,34] the less energetic group involving a 4.0-Mev level in O^{16}, which could account for some of the 4.4-Mev gamma-radiation.

Reaction (3) is the probable source of all of the gamma-rays of energy higher than 4.4 Mev. The recent work of Malm and Buechner[35] on magnetic analysis of the proton groups (1.42-Mev bombarding energy) gives evidence of levels in N^{15} at 5.276, 5.305, 6.328, 7.164, 7.309, and 8.315 Mev. Wyly[36] has found, by absorption methods, levels at 5.32, 6.31, and 7.21 Mev, and some evidence of an 8.2-Mev level (deuteron energy 3.32 Mev). Kinsey, Bartholomew, and Walker[37] found levels in N^{15}, from the reaction $N^{14}(n,\gamma)N^{15}$, at 5.29, 6.32, 7.16, 7.36, 8.28, and 9.16 Mev. All of these energy level values are consistent with the gamma-ray energies greater than 4.4 Mev from $N^{14}+d$.

D. $F^{19}+d$

The gamma-rays observed with this spectrometer from $F^{19}+d$ have not previously been reported. Earlier work by Bennett, Bonner, and Watt,[9] using absorption methods, indicated a complex gamma-ray spectrum with a maximum of 6.7 Mev. The following reactions can take place for $F^{19}+d$:

(1) $F^{19}(d,\alpha)O^{17}$, $Q=10.07$ Mev.

(2) $F^{19}(d,p)F^{20}$, $Q=4.3$ Mev; $F^{20}(\beta^-)Ne^{20}$, $Q=7.2$ Mev.

(3) $F^{19}(d,n)Ne^{20}$, $Q=10.72$ Mev.

Energy levels in O^{17} have been found at 7.60 and 8.23 Mev by Rotblat,[5,6] from a study of the alpha-particle groups of (1), at 7.8-Mev bombarding energy. Thus, the 8.1-Mev gamma-ray may be produced by (1); as to the 9.3- and 11.5-Mev gamma-rays, penetrability considerations make (1) improbable and impossible, respectively, as the source. It is, of course, possible that there are more than three high energy gamma-rays from $F^{19}+d$, as they are not fully resolved in the present work. We can rule out reaction (2) in any case, as not releasing enough energy.

Reaction (3) is certainly responsible for the 11.5-Mev gamma-ray, indicating a level in Ne^{20} at 11.5 ± 0.4 Mev, and may be responsible for all the high energy quanta. Neutron groups from (3) have been observed by Bonner[38] and by Powell[39] at energies corresponding to levels of Ne^{20} at 7.8, 9.0, and 10.1 Mev, as well as at lower energies. The uppermost of these levels can decay into $O^{16}+He^4$, as observed by French, Meyer, and Treacy,[40] who found 9.7 Mev as the energy of the level. The levels at 7.8 and 9.0 Mev may be responsible for the 8.1 ± 0.4- and 9.3 ± 0.3-Mev gamma-rays.

There seems to be no previous direct evidence for a level in Ne^{20} at 11.5 ± 0.4 Mev, but this level may be involved in the high energy capture radiation produced at the 669-kev resonance for $F^{19}(p,\gamma)Ne^{20}$. Rae, Rutherglen, and Smyth,[41] using a pair spectrometer, have recently observed 12.0 ± 0.2-Mev gamma-radiation at this resonance; Carver and Wilkinson[42] have found the energy to be 12.09 ± 0.28 Mev, by measuring the energy of photoprotons from deuterium. This capture radiation has been interpreted as a transition between the 13.4-Mev resonance level in Ne^{20} and a known 1.4-Mev level,[6,10,11] but may be due to a cascade transition between the levels of Ne^{20} at 13.4 Mev, 11.5 ± 0.4 Mev, and the ground state.

We wish to thank Dr. T. W. Bonner for guidance of this work, and to express our appreciation to S. J. Bame and L. M. Baggett for construction of an improved magnet current regulator, to W. H. Burke for assistance in the preparation of boron targets, and to other graduate students at Rice Institute for their invaluable help in operating the Van de Graaff generator.

[30] E. L. Hudspeth and C. P. Swann, Phys. Rev. **76**, 464 (1949).
[34] Stephens, Djanab, and Bonner, Phys. Rev. **52**, 1079 (1937).
[35] R. Malm and W. W. Buechner, Phys. Rev. **80**, 771 (1950).
[36] L. D. Wyly, Phys. Rev. **76**, 316 (1949).
[37] Kinsey, Bartholomew, and Walker, Phys. Rev. **77**, 723 (1950).
[38] T. W. Bonner, Proc. Roy. Soc. (London) **174A**, 339 (1940).
[39] C. F. Powell, Proc. Roy. Soc. (London) **181A**, 344 (1942).
[40] French, Meyer, and Treacy, Proc. Phys. Soc. (London) **63A**, 666 (1950).
[41] Rae, Rutherglen, and Smyth, Proc. Phys. Soc. (London) **63A**, 775 (1950).
[42] J. H. Carver and D. H. Wilkinson, Proc. Phys. Soc. (London) **64A**, 199 (1951).

Precipitation of Carbon and Nitrogen in Cold-Worked Alpha-Iron

S. HARPER
Institute for the Study of Metals, University of Chicago, Chicago, Illinois
(Received March 27, 1951)

The strain-induced precipitation of carbon and nitrogen from supersaturated solution in alpha-iron is shown to be in agreement with a dislocation mechanism and estimates of the dislocation density required to produce the observed precipitation rates are in agreement with dislocation theory. The activation energies involved in the process are found to be 20,000 cal/mole for carbon and 17,200 for nitrogen, in agreement with published data for the activation energies of diffusion of the two solutes.

INTRODUCTION

PREVIOUS work by Griffis, Kenyon, and Burns, Davenport and Bain,[1] and Cottrell and Churchman[2] has shown that the precipitation of carbon and nitrogen from supersaturated solution in alpha-iron can be greatly accelerated by the presence of lattice distortions due to cold work, giving rise to the well-known strain aging phenomena. These experiments, however, have depended on the measurement of such factors as the change in hardness, electrical resistivity or the appearance of Luders bands on re-straining, factors which cannot be simply related to the rate of precipitation of the solute atoms.

By measuring the internal friction arising from the stress-induced interstitial diffusion of the solute atoms it is possible to measure the amount of dissolved solute at any time and thus conveniently and quantitatively study the precipitation process. This internal friction has been studied exhaustively by Snoek[3] and Dijkstra[4] and the technique well established for the study of normal precipitation from supersaturated solution by Wert.[5]

A recent analysis by Cottrell and Bilby[6] of the dislocation theory of "strain aging," deduces a quantitative estimate of the rate of precipitation in a strained material. The present paper describes a series of experiments which permit us to estimate the accuracy of such a dislocation mechanism.

EXPERIMENTAL PROCEDURE

Puron iron of purity 99.95 percent was used in these experiments. The iron was in the form of wires 0.03 in. in diameter and 12 in. in length. The carbon and nitrogen content of the iron was first reduced to less than 0.0005 wt percent by heating for a period of a few hours at 720°C in an atmosphere of wet hydrogen. Carbon or nitrogen was then introduced into the wire in controlled amounts. The carbon was dissolved by heating to 720°C, for a period of an hour or so, in an atmosphere of dry hydrogen and *n* heptane, the nitrogen by heating to 590°C in an atmosphere of dry hydrogen with a small amount of ammonia gas present. These alloys, on quenching to the aging temperatures used, showed no decrease in the amount of material in solution even after a period of some days. We are thus justified in assuming that the precipitation studied was due solely to the presence of cold work.

The wires were cold-worked by small extensions in a rigid frame apparatus and were then placed in the aging furnace. This furnace was required to control temperature in the range of room temperature. A forced air circulation furnace which could be water-cooled on the outside was used, the temperature being controlled by a de Khotinsky mercury regulator, the apparatus permitting control to 0.1°C within the range 15–60°C. The specimen attained the aging temperature within three minutes of straining, a negligible period with the rates of precipitation encountered.

The internal friction of the specimen was measured directly by means of a torsion pendulum, which was set oscillating and the friction measured by the decay of the free vibrations. The frequency corresponding to the internal friction peak at the temperature of aging was used in each case. This method has been already described in some detail by Kê.[7]

DISLOCATION MODEL OF STRAIN AGING

Cottrell and Bilby in considering this problem show that the aggregation of solute atoms, in *substitutional* solution, around a simple edge dislocation would lower the strain energy of the system. Thus the interaction energy between an atom and a positive edge dislocation is equal to

$$V=-\frac{4}{3}G\epsilon r_0^3\lambda\frac{1+\nu}{1-\nu}\frac{\sin\alpha}{r}=A\frac{\sin\alpha}{r}, \qquad (1)$$

where G is the rigidity modulus, ν Poisson's ratio, r_0 and $r_0(1+\epsilon)$ are the atomic radii of solvent and solute. r and α are the polar coordinates of the position of the atom with the dislocation at the origin, and λ is the slip distance.

[1] E. W. Davenport and E. C. Bain, Trans. Am. Soc. Metals **23**, 1047 (1935).
[2] A. H. Cottrell and A. T. Churchman, J. Iron Steel Inst. (July, 1949).
[3] J. L. Snoek, Physica **8**, 711 (1941).
[4] L. J. Dijkstra, Philips Research Repts. **2**, 357 (1947).
[5] C. Wert, Am. Soc. Metals Symposium on Thermodynamics in Physical Metallurgy, Cleveland (1949).
[6] A. H. Cottrell and B. Bilby, Proc. Phys. Soc. (London) Series A, **62**, 49 (1949).
[7] T. S. Kê, Phys. Rev. **71**, 533 (1947).

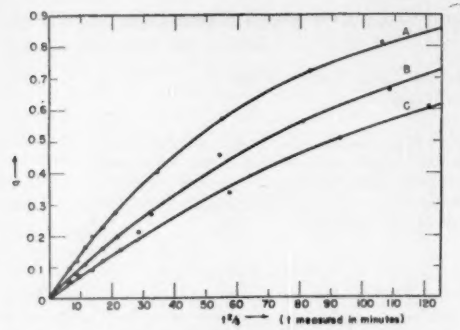

FIG. 1. Variation of strain aging with the degree of cold work (carbon in alpha-iron).

From this basis they estimate the rate at which solute atoms should migrate towards such a dislocation, and obtain:

$$N_t = 2n_0 L(\tfrac{1}{2}\pi)^{\frac{1}{3}}(ADt/kT)^{\frac{1}{3}} \qquad (2)$$

where N_t is the number of atoms precipitated, per unit volume of material in time t, L is the total length of edge dislocation per unit volume, n_0 is number of solute atoms per unit volume, and D is the diffusion coefficient at the absolute temperature T. Or we have

$$q = 2L(\tfrac{1}{2}\pi)^{\frac{1}{3}}(ADt/kT)^{\frac{1}{3}} \qquad (3)$$

where q is the fraction of the original amount of solute material which has precipitated during the time t. This law will only be applicable during the early stages of the precipitation, as the rate of precipitation will decrease more rapidly with time than Eq. (3) would indicate because of the mutual interference of the growing precipitates, continually reducing the value of n_0. It seems reasonable to assume that the decrease in the precipitation rate will be proportional to the fraction already precipitated (Johnson and Mehl[8]). The equation governing the precipitation will then be

$$\partial q/\partial t = (1-q)f(t). \qquad (4)$$

Solving this with the boundary condition $t \doteq 0$ defined by Eq. (3) we have

$$q = 1-\exp[-2L(\tfrac{1}{2}\pi)^{\frac{1}{3}}(ADt/kT)^{\frac{1}{3}}]. \qquad (5)$$

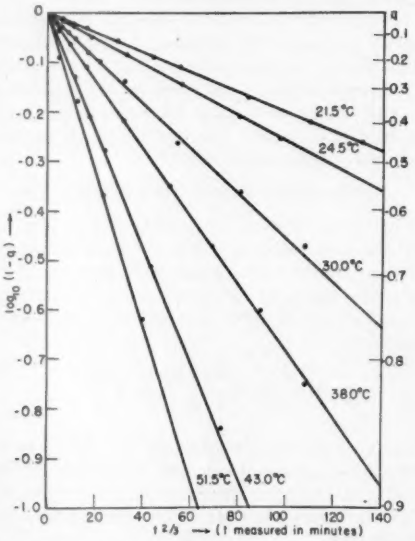

FIG. 2. The effect of temperature on the rate of strain aging (carbon in alpha-iron).

PRECIPITATION OF CARBON

The magnitude of the internal friction peak is linearly proportional to the amount of material in solution.

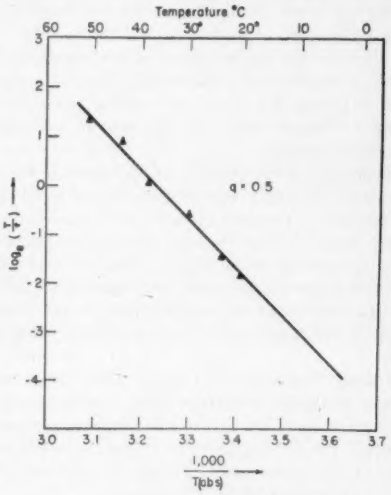

FIG. 3. The activation energy for strain aging (carbon in alpha-iron).

We can thus measure the quantity

$$1-q = Q_t^{-1}/Q_0^{-1}, \qquad (6)$$

where Q_0^{-1} and Q_t^{-1} are the values of the maximum of the internal friction peak at the beginning of aging and after aging has proceeded for a period of time t, respectively. Three specimens were taken with carbon contents of 0.015, 0.009, and 0.013 wt percent and were strained by approximately 5, 10, and 15 percent extensions, respectively, and aged at 30°C. Figure 1 shows the parameter (q) plotted against $t^{\frac{1}{3}}$, the full lines being equations of the type of Eq. (5). The parameter A has been estimated, for this case of

[8] W. A. Johnson and R. F. Mehl, Trans. Am. Inst. Mining Engrs. 135, 416 (1939).

interstitial solution, from the volume change produced when a carbon atom enters a unit cell of the iron lattice, this data being taken from the x-ray work of Lipson and Parker[9] on martensite. The value of D at the temperature in question was taken from the work of Wert and Zener.[10] These three specimens gave values of L as follows:

A. 15 percent extension	$L=3.72\times10^{11}$ lines cm^{-2}
B. 10 percent extension	2.46×10^{11} lines cm^{-2}
C. 5 percent extension	1.86×10^{11} lines cm^{-2}.

These values of dislocation density are compatible with previous estimates.[11]

Because of some uncertainty in estimating the constants in Eq. (5), the absolute values of L obtained are subject to some error and are only valuable as an order of magnitude estimate. Much greater reliance can be placed, however, on their relative values.

ACTIVATION ENERGY FOR STRAIN PRECIPITATION

We should expect the activation energy for this process to be identical with that for the diffusion of carbon in alpha-iron. Indeed, Nabarro[12] has analyzed data published by Davenport and Bain and shown that the activation energy involved is of this magnitude. To obtain further confirmation of this, 6 specimens were loaded with carbon and each strained as nearly as possible by the same amount (about 10 percent extension). They were then stored in liquid nitrogen until required and were then aged at the following temperatures: 21.5°, 24.5°, 30°, 38°, 43°, and 51.5° C. Figure 2 shows the aging curves for these specimens, while Fig. 3 shows the plot of $\log_e(T/t)$ against the inverse of the absolute temperature for the case of 50 percent precipitation ($q=0.5$). The slope of this line gives an energy of 20,000 cal/mole in good agreement with the published values of Snoek[13] and Polder[14] (18,000 cal/mole) and Wert and Zener[10] (19,800 cal/mole).

PRECIPITATION OF NITROGEN

Nitrogen behaves in an exactly similar manner as carbon in this matter, giving the same shaped aging curve. Figure 4 shows the results obtained from four specimens given identical strains and aged at 19.5°, 26°, 31.5°, and 34.5°C, respectively. Values taken from these curves at $q=0.5$ are plotted in Fig. 5, giving an activation energy of 17,200 cal/mole, again in agreement with published values for the diffusion of nitrogen in

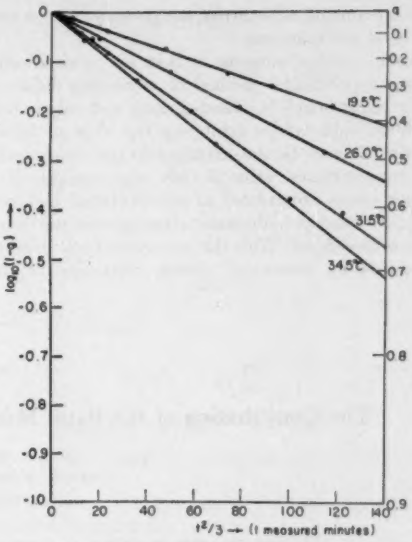

FIG. 4. The effect of temperature on the rate of strain aging (nitrogen in alpha-iron).

α-Fe (Snoek[13] (16,400 cal/mole) and Wert[10] (17,700 cal/mole)).

CONCLUSIONS

The experimental results obtained are in agreement with the dislocation model of the process. Equation (3) was closely obeyed up to about 25 percent of the total precipitation, whereas Eq. (5) was applicable as far as

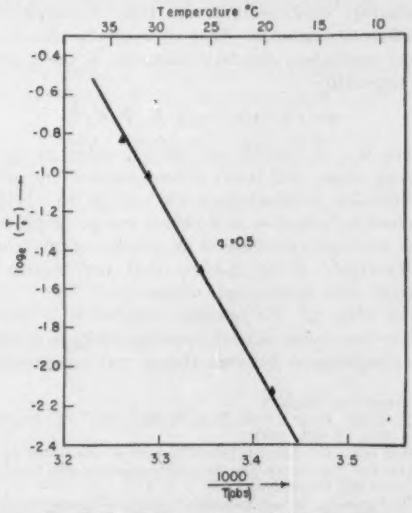

FIG. 5. The activation energy for strain aging (nitrogen in alpha-iron).

[9] H. Lipson and A. M. B. Parker, J. Iron Steel Inst. **149**, 123 (1944).
[10] C. Wert and C. Zener, Phys. Rev. **76**, 1169 (1949).
[11] J. S. Koehler, Phys. Rev. **60**, 397 (1941). F. Seitz and T. A. Read, J. Appl. Phys. **12** (1941). W. L. Bragg, Trans. North East Coast Inst. Eng. & Shipbuilders **62**, 25 (1945). G. I. Taylor and H. Quinney, Proc. Roy. Soc. (London), Series A, **143**, 307 (1934); **163**, 157 (1937). W. F. Brown, Phys. Rev. **60**, 139 (1941).
[12] F. R. N. Nabarro, Report of Bristol Conference, Phys. Soc. (London) **38** (1948).
[13] J. Snoek, Physica **6**, 591 (1939).
[14] D. Polder, Philips Research Repts. **1**, 1 (1945).

the experiments were carried out (to about 90 percent of the total precipitation).

An interesting outcome is that the work affords a simple experimental method of measuring dislocation densities, although in a limited range and only in body-centered cubic alloys exhibiting this type of internal friction. It must be realized also that the theory leading to this estimated value is only approximate, as the solute atoms are treated as substitutional and hence only the relief of hydrostatic stress around the dislocation is considered. With the nonsymmetrical distortion produced by interstitial atoms, relaxation of shear stresses can also occur (Nabarro[12]), and thus there will be a tendency for such atoms to migrate to the Burgers type component of the dislocations.

Nevertheless the method may be of use in studying problems involving the amount of internal strain in a material.

Finally, by studying the case of carbon and nitrogen separately it has been possible to show that the temperature dependence of the process is identical with that of the diffusion of the elements in the mother metal.

The author wishes to thank Professor C. Zener for many helpful discussions during the course of this work.

PHYSICAL REVIEW VOLUME 83, NUMBER 4 AUGUST 15, 1951

The Contribution of the Pauli Moment to π-Meson Production by Photons*

M. F. KAPLON
University of Rochester, Rochester, New York

(Received February 26, 1951)

The photon-nucleon production of π-mesons has been calculated incorporating in the interaction a Pauli-type term representing the interaction of the photon with the anomalous magnetic moments of the nucleons. The effect of the added interaction for the scalar theory is to increase somewhat the charged meson production while leaving the neutral production virtually unchanged. For the pseudoscalar theory the charged meson production is relatively unaffected while the neutral meson production is greatly enhanced. Comparison with the neutral meson experiments in hydrogen therefore favors the pseudoscalar theory.

I. INTRODUCTION

WEAK coupling calculations of the production of neutral π-mesons by photons[1] yield cross sections which are much smaller than the charged π-meson production cross sections for both the scalar and pseudoscalar theories.[2] That is, it can be shown that if the anomalous magnetic moments of the nucleons are neglected,

$$d\sigma(\pi^0)/d\sigma(\pi^+)=(\boldsymbol{q}\cdot\boldsymbol{K}_0/\boldsymbol{P}\cdot\boldsymbol{K}_0)^2,$$

where ($K_{0\mu}$, q_μ, and P_μ are the four-momenta for the photon, meson, and recoil nucleon respectively) which, for instance, decreases from $\sim 1/5$ at 180° to $\sim 1/500$ in the forward direction at a photon energy of 250 Mev. This small ratio contradicts recent experimental results in hydrogen[3] which indicate that the neutral and charged cross sections are comparable.

One may ask the question whether it is possible within the context of weak coupling theory to eliminate the disagreement between theory and experiment by including a Pauli-type term in the hamiltonian to represent the interaction of the electromagnetic field with the anomalous magnetic moments of the nucleons. It turns out that such a phenomenological approach markedly improves the agreement for the pseudoscalar theory, whereas it actually increases the discrepancy for the scalar theory. At the same time it must be shown that the good qualitative agreement between the pseudoscalar theory[4] and experiment for charged π-meson production is not affected by taking into account the anomalous magnetic moments. We here report the results of calculations on the effect of the anomalous magnetic moments on meson production by photons, treating them in the Pauli fashion and assuming that the static values can be used at photon energies of several hundred Mev.

The calculations have been performed with the Feynman[5] techniques. The notation is that of Feynman with the exception $(\gamma^5)^2=-1$. The interaction of the electromagnetic field with the anomalous magnetic moment[6] of the nucleon $(1/2)F_{\mu\nu}\gamma^\mu\gamma^\nu$, when transformed to momentum space, is $(\mu/2M)(\mathfrak{K}_0\mathfrak{A})$, where[7] $\mathfrak{A}=\epsilon_\mu\gamma^\mu$ (ϵ_μ is the 4-polarization of the photon), $\mathfrak{K}_0=K_{0\mu}\gamma^\mu$ ($K_{0\mu}$

* Assisted by the AEC.

[1] G. Araki, Prog. Theor. Phys. **5**, 507 (1951). K. Brueckner, Phys. Rev. **79**, 641 (1950).

[2] The neutral π-meson is known to possess spin 0 and we shall assume that the charged π-meson also possesses spin 0 although this must still be demonstrated.

[3] W. Panofsky, private communication; preliminary results are $(d\sigma_{\pi^0}/d\Omega)(90°)\approx 3\times 10^{-30}$ cm²/sterad compared to $(d\sigma_{\pi^+}/d\Omega)(90°)\approx 8\times 10^{-30}$ cm²/sterad. Panofsky also finds $d\sigma_{\pi^0}(45°)\approx 2d\sigma_{\pi^0}(90°)$.

[4] Bishop, Steinberger, and Cook, Phys. Rev. **80**, 291 (1950); see Brueckner, reference 1.

[5] R. P. Feynman, Phys. Rev. **76**, 749, 769 (1949).

[6] W. Pauli, Handbuch d. Physik **24**, I (233).

[7] We use $\mathfrak{A}=A_\mu\gamma^\mu$; $A\cdot B=A_4B_4-\mathbf{A}\cdot\mathbf{B}$; and A is the length of the three vector $\mathbf{A}$; thus $\mathfrak{A}$ is a 4-vector associated with a 4-matrix.

is the 4-momentum of the photon), γ_μ are the Dirac matrices defined by Feynman and $\mu_p = 1.789, \mu_n = -1.91$ nuclear magnetons. We shall consider the scalar theory with scalar coupling (S, S), the pseudoscalar theory with direct coupling (PS, PS) and with derivative coupling (PS, PV).

For these theories with the inclusion of the Pauli term there are the 6 Feynman diagrams of Fig. 1, where $P_{0\mu}(E_0; \mathbf{P}_0)$, $P_\mu(E; \mathbf{P})$ are the initial and recoil nucleon 4-momenta, $K_{0\mu}(K_0; \mathbf{K}_0)$ is the photon 4-momentum and $q_\mu(\omega; \mathbf{q})$ is the meson 4-momentum. Diagrams 4 and 5 represent the anomalous moment interaction and diagram 6 represents the triple term required for gauge invariance in the (PS, PV) theory. The conservation laws require $(K_0 + P_0 = q + P)$. The matrix elements are:

$$\mathbf{M}_1 = -iC_1(\mathbf{P}|I(2\mathbf{A}\cdot\mathbf{P}_0 + \mathfrak{K}_0\mathfrak{A})|\mathbf{P}_0)\varphi/2\mathbf{P}_0\cdot\mathbf{K}_0$$

$$\mathbf{M}_2 = iC_2(\mathbf{P}|(2\mathbf{A}\cdot\mathbf{P} + \mathfrak{K}_0\mathfrak{A})I|\mathbf{P}_0)\varphi/2\mathbf{P}\cdot\mathbf{K}_0$$

$$\mathbf{M}_3 = iC_3\mathbf{A}\cdot\mathbf{q}(\mathbf{P}|I|\mathbf{P}_0)\varphi/\mathbf{q}\cdot\mathbf{K}_0$$

$$\mathbf{M}_4 = -iC_4(\mathbf{P}|I\{M\mathfrak{K}_0\mathfrak{A} - (\mathbf{A}\cdot\mathbf{P}_0)\mathfrak{K}_0 + (\mathbf{P}_0\cdot\mathbf{K}_0)\mathfrak{A}\}|\mathbf{P}_0)\varphi/2M\mathbf{P}_0\cdot\mathbf{K}_0$$

$$\mathbf{M}_5 = iC_5(\mathbf{P}|\{M\mathfrak{K}_0\mathfrak{A} + (\mathbf{A}\cdot\mathbf{P})\mathfrak{K}_0 - (\mathbf{P}\cdot\mathbf{K}_0)\mathfrak{A}\}I|\mathbf{P}_0)\varphi/2M\mathbf{P}\cdot\mathbf{K}_0$$

$$\mathbf{M}_6 = -iC_6(\mathbf{P}|\gamma^5\mathfrak{A}|\mathbf{P}_0)\varphi$$

with

$$I = 1 \qquad (S, S)$$

$$= \gamma^5 \qquad (PS, PS)$$

$$= \gamma^5 \begin{cases} \mathfrak{q} & \text{Diagrams 1, 2, 4, 5} \\ (\mathfrak{P}_0 - \mathfrak{P}) & \text{Diagram 3} \end{cases} \qquad (PS, PV)$$

and the normalizations $\varphi^*\varphi = 2\pi/\omega$, $(\mathbf{P}/P) = M/E$ (M is the nucleon mass taken to be equal for neutron and proton).

Table I gives the coefficients C_1 to C_6 corresponding to the Feynman diagrams 1 to 6 for the various production possibilities, where e is the charge of the proton and C_i is to be multiplied by g', g, f/μ; g_P', g_P, f_P/μ; g_N', g_N, f_N/μ (μ is the meson mass taken to be equal for π^+ and π^0), for processes (I, II), (III), and (IV) respectively where g', g, f are the coupling constants for the (S, S), (PS, PS), and (PS, PV) theories, respectively.

One can demonstrate a partial equivalence between the direct and derivative couplings of the pseudoscalar theory:

$$\sum_i \mathbf{M}_i^{(PS,PV)} = \sum_i[2M\mathbf{M}_i^{(PS,PS)} + a_i(\mathbf{P}|\gamma^5\mathfrak{K}_0\mathfrak{A}|\mathbf{P}_0)\varphi]$$

$$\sum a_i = \mu_P + \mu_N \quad \text{for I, II}$$

$$= 2\mu_P, 2\mu_N \quad \text{for III, IV, respectively.}$$

$\mathfrak{A}\mathfrak{B} = (A_\mu\gamma^\mu)(B_\nu\gamma^\nu)$ is the product of $\mathfrak{A}$ and $\mathfrak{B}$, while $\mathbf{A}\cdot\mathbf{B}$ is a scalar.

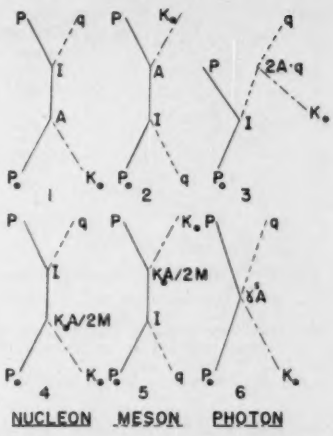

FIG. 1. Feynman diagrams for photonucleon production of mesons.

That is to say, the equivalence theorem holds if the Pauli term is omitted.

The following identities hold and are convenient for computational purposes:

$$\sum_{i=\mathrm{II}} \mathbf{M}_i(\mu_{P,N} = 0) = -(\mathbf{P}_0\cdot\mathbf{K}_0/\mathbf{P}\cdot\mathbf{K}_0)\sum_{i=1}\mathbf{M}_i(\mu_{P,N} = 0)$$

$$\sum_{i=\mathrm{III}} \mathbf{M}_i(\mu_{P,N} = 0) = -(\mathbf{K}_0\cdot\mathbf{q}/\mathbf{P}\cdot\mathbf{K}_0)\sum_{i=1}\mathbf{M}_i(\mu_{P,N} = 0).$$

One demonstrates gauge invariance for any process by the condition:

$$\sum_i \mathbf{M}_i(\mathfrak{A} \to \mathfrak{K}_0) = 0.$$

The cross section in the laboratory system is

$$d\sigma = (2\pi)^4\langle|\textstyle\sum_i \mathbf{M}_i|^2\rangle_{\mathrm{Av}}\rho_f/K_0,$$

where the symbol $\langle\ \rangle_{\mathrm{Av}}$ signifies an average over photon polarizations and initial nucleon spin and a sum over

TABLE I. Coefficients for matrix elements.

	C_1	C_2	C_3	C_4	C_5	C_6(PS, PV) only
I. $\gamma+p\to\pi^++n$	e	0	e	$\mu_P e$	$\mu_N e$	$-e$
II. $\gamma+n\to\pi^-+p$	0	e	$-e$	$\mu_N e$	$\mu_P e$	e
III. $\gamma+p\to\pi^0+p$	e	e	0	$\mu_P e$	$\mu_P e$	0
IV. $\gamma+n\to\pi^0+n$	0	0	0	$\mu_N e$	$\mu_N e$	0

TABLE II. Coefficients for Eqs. (1) and (2).

	G	A	μ_1	μ_2	α	β
I. $\frac{(S,S);}{(PS,PV)}$	$\frac{g';}{f/\mu}$ g	1	μ_P	μ_N	$\frac{1}{2M}$	0 1
II. $\frac{(S,S);}{(PS,PV)}$	$\frac{g';}{f/\mu}$ g	$-(P_0\cdot K_0/P\cdot K_0)$	μ_N	μ_P	$\frac{1}{2M}$	0 1
III. $\frac{(S,S);}{(PS,PV)}$	$\frac{g_P';}{f_P/\mu}$ g_P	$-(K_0\cdot q/P\cdot K_0)$	μ_P	μ_P	$\frac{1}{2M}$	0 1
IV. $\frac{(S,S);}{(PS,PV)}$	$\frac{g_N';}{f_N/\mu}$ g_N	0	μ_N	μ_N	$\frac{1}{2M}$	0 1

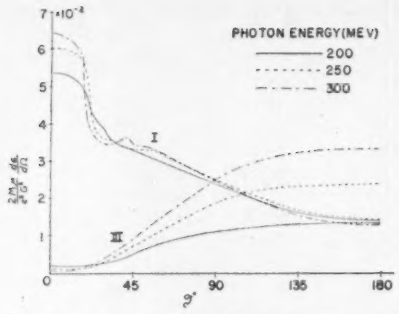

FIG. 2. Differential cross section in the laboratory system for production of π^+ mesons (curves I, anomalous magnetic moment not included) and π^0 mesons (curves III) in photon-proton collisions for the (PS, PS) theory.

final nucleon spin, ρ_f is the density of final states per unit energy, and the factor $2\pi/K_0$ arises from the expansion of the photon field.

The cross sections in the laboratory system become

$$(S,S)\quad d\sigma/d\Omega$$

$$=\frac{q^3e^2G^2}{2MK_0[\omega(K_0M+\mu^2/2)-\mu^2(M+K_0)]}$$

$$\times\left\{A^2\left[\boldsymbol{P}\cdot\boldsymbol{K}_0/2\boldsymbol{P}_0\cdot\boldsymbol{K}_0+\frac{M^2q^2\sin^2\vartheta}{(\boldsymbol{K}_0\cdot\boldsymbol{q})^2}(1-\mu^2/4M^2)\right]\right.$$

$$+A(\mu_1-\mu_2)\boldsymbol{K}_0\cdot\boldsymbol{q}/4\boldsymbol{P}_0\cdot\boldsymbol{K}_0$$

$$-(\mu_1\mu_2/4M^2)(q^2\sin^2\vartheta\boldsymbol{P}_0\cdot\boldsymbol{K}_0/\boldsymbol{P}\cdot\boldsymbol{K}_0)$$

$$+1/2[(\mu_1-\mu_2)^2-\mu_1\mu_2(\boldsymbol{K}_0\cdot\boldsymbol{q})^2/((\boldsymbol{P}_0\cdot\boldsymbol{K}_0)(\boldsymbol{P}\cdot\boldsymbol{K}_0))]$$

$$\left.+(\mu_1+\mu_2)^2(\boldsymbol{K}_0\cdot\boldsymbol{q}-\mu^2/2)/4M^2\right\}\quad(1)$$

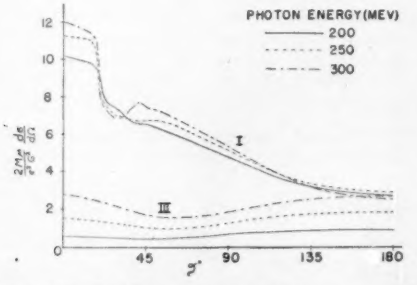

FIG. 3. Differential cross section in the laboratory system for production of π^+ mesons (curves I) and π^0 mesons (curves III) in photon-proton collisions for the (PS, PV) theory.

$$\left.\begin{matrix}(PS,\ PS)\\(PS,\ PV)\end{matrix}\right\}\quad d\sigma/d\Omega$$

$$=\frac{q^3e^2G^2}{2MK_0[\omega(K_0M+\mu^2/2)-\mu^2(M+K_0)]}$$

$$\times\{\alpha^2[A^2(\boldsymbol{P}\cdot\boldsymbol{K}_0/2\boldsymbol{P}_0\cdot\boldsymbol{K}_0-\mu^2q^2\sin^2\vartheta/4(\boldsymbol{q}\cdot\boldsymbol{K}_0)^2)$$

$$-A(\mu_1+\mu_2)\boldsymbol{K}_0\cdot\boldsymbol{q}/2\boldsymbol{P}_0\cdot\boldsymbol{K}_0$$

$$+(\mu_1^2+\mu_2^2)(\boldsymbol{K}_0\cdot\boldsymbol{q}-\mu^2/2)/4M^2$$

$$+\mu_1\mu_2(\boldsymbol{K}_0\cdot\boldsymbol{q})^2/(4(\boldsymbol{P}_0\cdot\boldsymbol{K}_0)(\boldsymbol{P}\cdot\boldsymbol{K}_0))]$$

$$+\beta[((\mu_1+\mu_2)^2/2)((\boldsymbol{P}\cdot\boldsymbol{K}_0)(\boldsymbol{P}_0\cdot\boldsymbol{K}_0)/M^2-2\boldsymbol{K}_0\cdot\boldsymbol{q})$$

$$+A(\mu_1+\mu_2)(2\boldsymbol{P}\cdot\boldsymbol{K}_0-q^2\sin^2\vartheta\boldsymbol{P}_0\cdot\boldsymbol{K}_0/\boldsymbol{q}\cdot\boldsymbol{K}_0)]\},\quad(2)$$

where ϑ is the angle between $\mathbf{q}$ and $\mathbf{K}_0$ and the coefficients are given in Table II.

Examination of Eq. (1) shows that for the scalar theory the π^+ production in hydrogen is strongly enhanced relative to the π^0 production by the introduction of the Pauli moment so that the ratio of the π^+ to the π^0 cross sections is increased even more. The Pauli moments contribute an approximately constant term to $\langle|\mathbf{M}(\pi^+)|^2\rangle_{Av}$, yielding a net angular distribution that still has a dipole character though less exaggerated. The contribution of the Pauli term to the π^0 production is $\sim 1/10$ that due to the charge of the proton.[8] This coupled with the fact that the π^0 angular distribution (which has its maximum at $\sim 90°$ and decreases in both the forward and backward directions) is in complete disagreement with experiment (see reference 3) makes it unlikely that the π^0 is scalar.

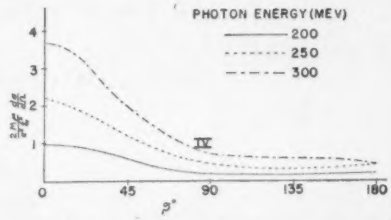

FIG. 4. Differential cross section in the laboratory system for production of π^0 mesons in photon-neutron collisions for the (PS, PV) theory.

Figure 2 gives the (PS, PS) angular distribution in the laboratory system at 3 photon energies including the Pauli term only in the π^0 case. The angular distributions of (PS, PS) π^0 mesons produced in photon-proton collisions without the inclusion of the Pauli term

[8] This can be seen by considering in the nonrelativistic approximation the matrix-elements for meson production by those diagrams representing the interaction of the photon with the anomalous moments of the nucleons: $(F|\boldsymbol{\sigma}\cdot\mathbf{H}|I)(\mu_1-\mu_2)/2MK_0$ which yields $|\mu_P|+|\mu_N|$ for charged meson production and 0 for neutral meson production.

TABLE III. Total cross sections$\times 10^{28}$ cm^2.

Photon energy (Mev)	200	250	300
I. (PS, PS)[a]	0.033	0.034	$0.034\times g^2$
I. (PS, PV)	6.6	6.9	$7.1\times f^2$
III. (PS, PS)	0.013	0.023	$0.031\times g_P^2$
III. (PS, PV)	0.52	1.9	$3.0\times f_P^2$
IV. (PS, PV)	0.16	0.85	$1.55\times f_N^2$

[a] Does not include anomalous moment.

are similar to those in Fig. 2, though of much smaller magnitude. Figure 3 gives the (PS, PV) angular distributions for hydrogen including the anomalous moment interaction for both π^+ and π^0 production. To a good approximation ($\sim$3 percent),

$$d\sigma(+)^{(PS,PS)}/d\Omega=(\mu/2M)^2 d\sigma(+)^{(PS,PV)}/d\Omega$$

even when the Pauli term is included. Figure 4 gives the (PS, PV) angular distribution for π^0 meson production in photon-neutron collisions;[9] these curves will be useful for calculations of π^0 production in photon-deuteron collisions. Table III lists the total cross sections for the pseudoscalar theories at 3 different photon energies.

Since the angular distribution of the π^0 production for the direct coupling cases (with or without inclusion of the Pauli term) is in poor agreement with experiment (see reference 3), we consider further only the derivative coupling of the pseudoscalar theory. Figure 5 gives the excitation functions at 90° for π^+ and π^0 production, normalized so that $d\sigma(+)/d\Omega\approx d\sigma(0)/d\Omega$ when integrated over the experimental bremsstrahlung spectrum[10] (the experimental ratio of $\pi^0/\pi^+\sim\frac{1}{3}$ at 90° requires $f_P\sim f$). The included experimental points[3, 4] are normalized in the same way. The agreement is fair and indeed the qualitative features of the excitation functions at 90° agree well with the experimental points.

It is interesting to note that the π^-/π^+ ratio, which is given for the spin 0 theories without the inclusion of the Pauli moment by

$$\pi^-/\pi^+=(\boldsymbol{P}_0\cdot\boldsymbol{K}_0/\boldsymbol{P}\cdot\boldsymbol{K}_0)^2=(K_0/(\omega-\mu^2/2M))^2,$$

is only slightly changed by the inclusion of the anomalous magnetic moment interaction. It is, however, somewhat energy sensitive; for example at 90° to the beam it varies from $\sim$5 to 12 percent less than the ratio given above for photon energies in the range 200 to 300 Mev.

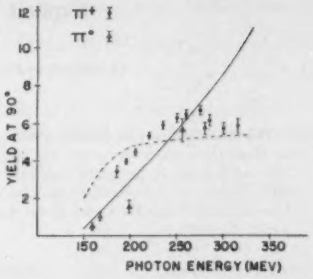

FIG. 5. Excitation functions at 90° to the photon beam for π^+ (dotted curve) and π^0 (solid curve) production in photon-proton collisions for the (PS, PV) theory.

Although the inclusion of the Pauli term can only be justified on an *ad hoc* basis,[11] it seems to us significant that in the pseudoscalar theory, the π^0 production can be raised by a large factor (for the energy region considered) without affecting the π^+ production to any appreciable extent. In addition, the fact that the same qualitatively correct excitation function and angular distribution are predicted by the weak coupling and classical (PS, PV) theories is evidence for a magnetic origin of the π^0 mesons in photon-proton collisions. Further evidence for the magnetic moment explanation of π^0 production can be obtained from experiments on π^0 production in deuterium since the neutron can interact only through its anomalous magnetic moment.[12]

I should like to thank Professor R. E. Marshak for suggesting this calculation and for many valuable discussions. I am indebted to Professor W. Panofsky for a discussion of the experimental data and to Professor R. P. Feynman and Dr. K. Brueckner for helpful discussion.

[9] For the (PS, PV) theory in nonrelativistic approximation, the matrix elements involving the interaction of the photon with the anomalous magnetic moments are

$$[\mu_1(F|(\boldsymbol{\sigma}\cdot\mathbf{q})(\boldsymbol{\sigma}\cdot\mathbf{H})|I)-\mu_2(F|(\boldsymbol{\sigma}\cdot\mathbf{H})(\boldsymbol{\sigma}\cdot\mathbf{q})|I)]/2MK_0$$

which yield $d\sigma/d\Omega=(e^2f^2/K_0)(\mu_N^2/2M^2)(q^2/\mu^2)\sin^2\vartheta$ for the photo-neutron production of charged π^- mesons ($|\mu_P|\approx|\mu_N|$) and $d\sigma/d\Omega=(e^2f_N^2/K_0)(\mu_N^2/2M^2)(q^3/\mu^3)(1+\cos^2\vartheta)$ for the photo-neutron production of neutral π^0 mesons. The latter result is identical with the classical cross section given by Serber (Summer lectures, University of Michigan, 1950) if one sets $\sigma_0^2=3$ in the latter formula. The formula given in Serber's notes is too low by a factor of 4 due to an incorrect spin equation of motion; I am indebted to Dr. K. M. Watson for confirmation of this point.

[10] Hartsough, Hill, and Powell (to be published).

[11] It is fully realized that a consistent theory of the meson nucleon interaction should lead to an explanation of the anomalous magnetic moments of the nucleons in higher order; however, such a theory does not exist and this is the justification for attempting a phenomonological approach.

[12] The spin zero π^0 meson cannot possess an anomalous magnetic moment; however, it should be remembered that the π^0 meson may be directly coupled to the electromagnetic field plus the (bilinear) nucleon field so that a large photon-neutron cross section would not necessarily imply a large anomalous moment interaction.

Explicit γ-γ Angular Correlations

STUART P. LLOYD
Department of Physics, University of Illinois, Urbana, Illinois
(Received April 26, 1951)

The theoretical γ-γ directional correlation function is given as a Legendre series: $W(\theta)=1+\Sigma A_L P_L(\cos\theta)$, for those cases where the γ-rays are emitted with the lowest angular momentum allowed by selection rules. The coefficients A_L are given algebraically and are also tabulated as four-place decimals for all cascades up to 2^4-pole—2^6-pole in which the largest nuclear spin does not exceed nine. Rules are given for obtaining from the tables: (a) the lowest order multipole mixture interference terms, (b) certain α-γ and α-α directional correlations.

1. GUIDE TO THE TABLES

THE general γ-γ directional correlation function[1] has been obtained by the author,[2] and independently by Racah,[3] in the form of a Legendre series in the cosine of the angle θ between the successive γ-rays:

$$W(\theta)=1+\sum A_L P_L(\cos\theta), \qquad (1)$$

normalized to unit average. The sum is over even values of L: $L=2, 4, 6, \cdots, L_m$, where L_m will be given presently. In general, the coefficients A_L are functions of the initial, intermediate, and final nuclear angular momenta j_1, j, and j_2, respectively, and of the multipole orders and relative amplitudes of the various multipole fields describing the emitted γ-rays. We simplify the formula by assuming that the γ-rays are emitted with the lowest angular momentum allowed by angular momentum selection rules, so that if l_1 and l_2 are the multipole orders of the γ-rays emitted in the first and second transitions (respectively) of the cascade $j_1\to j\to j_2$, then $l_1=1$ if $j_1=j$, $l_1=|j_1-j|$ if $j_1\neq j$, and $l_2=1$ if $j_2=j_2$, $l_2=|j_2-j|$ if $j_2\neq j$. We denote this cascade by $j_1(l_1)j(l_2)j_2$, or by $j_1(\gamma, l_1)j(\gamma, l_2)j_2$ if necessary. The maximum value L_m of L in the sum, Eq. (1), is then the largest even integer satisfying each of $L_m\leq 2l_1$, $L_m\leq 2l_2$ and $L_m\leq 2j$.[4] There is no correlation if $j=\frac{1}{2}$. In Sec. II we give rules for obtaining the lowest order multipole mixture interference terms from the tabulated A_L.

We reproduce the formula used to obtain the tables,[5] in case points beyond the range of the tables are needed, or in case more accurate values of the coefficients are desired. The coefficients A_L are the same for both of the 2^{l_1}-pole–2^{l_2}-pole cascades $j-l_1(l_1)j(l_2)j+l_2$ and $j+l_1(l_1)j(l_2)j-l_2$; furthermore, the coefficients A_L for these particular cascades are independent of the value of j. We will refer to this correlation as the "basic" 2^{l_1}-pole–2^{l_2}-pole γ-γ correlation, and will denote the coefficients by $A_L{}^{(b)}$. Explicitly:

$$W(\theta)\doteq 1+\sum A_L{}^{(b)}P_L(\cos\theta) \quad \text{for} \quad j\pm l_1(l_1)j(l_2)j\mp l_2,$$

where

$$A_L{}^{(b)}=(2L+1)b_L(l_1)b_L(l_2),$$

with

$$b_L(l)=\left[1-\frac{L(L+1)}{2l(l+1)}\right]\frac{(2l+1)!L!(l+(L/2))!}{(2l+L+1)!((L/2)!)^2(l-(L/2))!}.$$

The other 2^{l_1}-pole–2^{l_2}-pole correlations are given by

$$W(\theta)=1+\sum w_L A_L{}^{(b)}P_L(\cos\theta),$$

where

$$w_L=\frac{(2j-L)!(2j+L+1)!}{(2j)!(2j+1)!} \quad \text{for} \quad j-l_1(l_1)j(l_2)j-l_2,$$

$$w_L=\frac{(2j)!(2j+1)!}{(2j-L)!(2j+L+1)!} \quad \text{for} \quad j+l_1(l_1)j(l_2)j+l_2,$$

$$w_2=-(2j+3)/j \quad \text{for} \quad j(1)j(l_2)j-l_2,$$

$$w_2=-(2j-1)/(j+1) \quad \text{for} \quad j(1)j(l_2)j+l_2,$$

$$w_2=(2j-1)(2j+3)/(j(j+1)) \quad \text{for} \quad j(1)j(1)j.$$

These "pure multipole" correlations do not depend on the parities of the γ-rays, so that "2^l-pole" means either an electric 2^l-pole or a magnetic 2^l-pole γ-ray.[6]

One important symmetry property of the pure multipole correlation function is that the correlation for $j_2(l_2)j(l_1)j_1$ is the same as the one for $j_1(l_1)j(l_2)j_2$; this was shown by Hamilton in his original paper on γ-γ correlations,[7] and cuts the size of the tables roughly in half. In Tables I–IX the numerically smallest multipole in the cascade is supposed to occur in the first transition, so that, e.g., the $9/2\to 3/2\to 3/2$ octupole-dipole correlation is to be found as the $3/2\to 3/2\to 9/2$ dipole-octupole entry in the tables. The second symmetry is the equality of the basic correlation for the two cascades $j\pm l_1(l_1)j(l_2)j\mp l_2$, and the nondependence of this corre-

[1] D. L. Falkoff and G. E. Uhlenbeck, Phys. Rev. **79**, 323 (1950).
[2] S. P. Lloyd, Phys. Rev. **81**, 307 (1951).
[3] G. Racah, Phys. Rev. **82**, 309 (1951).
[4] These become Yang's rules when the Legendre polynomials are written out as polynomials in $\cos\theta$. C. N. Yang, Phys. Rev. **74**, 764 (1948).
[5] The derivation of a general two-step cascade angular correlation formula is part of the material to be submitted by the author as his inaugural dissertation (University of Illinois, 1951), under the sponsorship of Professor S. M. Dancoff. The results stated without proof in this article are special cases from the general formula. Complete publication will appear subsequently; it was felt that this interim presentation of some of the results would be of use to the experimentalist.
[6] D. S. Ling, Jr., and D. L. Falkoff, Phys. Rev. **76**, 1639 (1949).
[7] D. R. Hamilton, Phys. Rev. **58**, 122 (1940).

lation on the value of j. The coefficients A_L[(b)] of the basic correlation are to be found at the top of the columns in the tables. Thus in Tables II–III in the columns marked "2^1-2^2," one finds in the row marked "Basic" the entry: $A_2=-0.1250$, so that the correlation for all of the transitions: 0(1)1(3)4, 1/2(1)3/2(3)9/2, 1(1)2(3)5, ···, 4(1)3(3)0, 9/2(1)7/2(3)1/2, 5(1)4(3)1, ···, and also, from the first symmetry property, 4(3)1(1)0, 9/2(3)3/2(1)1/2, ···, 0(3)3(1)4, 1/2(3)7/2(1)9/2, ···, is $W(\theta)=1-0.1250P_2(\cos\theta)$.

When the sequence of nuclear angular momenta is not definitely monotonic, the coefficients A are functions of the nuclear angular momenta, and are tabulated as functions of the intermediate nuclear angular momentum j. The initial and final nuclear angular momenta are to be obtained from the column markings; e.g., in Table III, the column "2^1-2^4," in the bottom half of the column under "$j-1\to j\to j-4$," one finds $A_2=-0.2833$ at $j=9/2$, so that the 7/2(1)9/2(4)1/2 correlation is $W(\theta)=1-0.2833P_2(\cos\theta)$. In the top half of the same column, under "$j+1\to j\to j+4$," one finds $A_2=-0.0843$ at $j=9/2$, so that the 11/2(1)9/2(4)17/2 correlation is $W(\theta)=1-0.0843P_2(\cos\theta)$.

2. MULTIPOLE MIXTURE INTERFERENCE TERMS[8]

Recent theoretical estimates of Weisskopf of the ratios of matrix elements[8] indicate that in parity forbidden γ-ray transitions (where magnetic 2^l-pole and electric 2^{l+1}-pole multipoles are the lowest and next lowest multipoles, respectively, allowed by both angular momentum and parity selection rules), the intensity of the electric 2^{l+1}-pole is a small fraction of the intensity of the magnetic 2^l-pole. Most of the γ-rays are emitted as the lowest allowed magnetic 2^l-pole, so that correlations from the tables are applicable as they stand. Reinterpretation of experimental data as well as new data support this conclusion. Nevertheless, we give the rules for obtaining the lowest order "multipole mixture" interference terms in the correlation from the tabulated "pure multipole" correlation.

Let the real[9] quantity δ be such that its square is the ratio of the electric 2^{l+1}-pole intensity to the intensity of the (lowest allowed) magnetic 2^l-pole in a given parity forbidden transition; the sign of δ is the relative sign of the reduced (magnetic quantum number independent) nuclear matrix elements for the emission of the two multipoles, i.e., δ is the ratio of these matrix elements. If both transitions in the cascade $j_1(l_1)j(l_2)j_2$ are parity forbidden, and δ_1 and δ_2 are the matrix element ratios for the first and second transitions, respectively, then, neglecting terms in δ_1^2, δ_2^2 and $\delta_1\delta_2$, the directional correlation of the two γ-rays is

$$W(\theta)=1+\sum A_L P_L(\cos\theta)+x_1\delta_1\sum y_L(l_1)A_L P_L(\cos\theta) -x_2\delta_2\sum y_L(l_2)A_L P_L(\cos\theta). \quad (2)$$

The coefficients A_L are those tabulated; the coefficients $y_L(l)$ are independent of nuclear angular momenta and are explicitly

$$y_L(l)=2\left(\frac{l(2l+3)}{l+2}\right)^{\frac{1}{2}}\cdot\frac{L(L+1)}{2l(l+1)-L(L+1)}. \quad (3)$$

The coefficients x_1 and x_2 depend only on the quantities describing the first and second transitions, respectively; for either transition:

$$x=((j-l)/(j+1))^{\frac{1}{2}} \text{ if } j'=j-l,$$

$$x=-((j+l+1)/j)^{\frac{1}{2}} \text{ if } j'=j+l,$$

$$x=-((2j-1)(2j+3)/3)^{-\frac{1}{2}} \text{ if } j'=j \text{ (dipole only)}, \quad (4)$$

where $(j', l)=(j_1, l_1)$ or (j_2, l_2).

These rules are quite general and give the multipole mixture terms in any correlation involving a γ-ray. Suppose that

$$W(\theta)=1+\sum B_L P_L(\cos\theta)$$

is the directional correlation between a γ-ray emitted in the first transition of the cascade $j_1(l_1)j(X)j_2$ and some other nuclear radiation X (such as an α-particle, β-ray, etc.) emitted in the second transition. The (first) γ-ray is supposed to be emitted as the lowest allowed 2^{l_1}-pole multipole. If the first transition is parity forbidden and the matrix element ratio δ_1 is not negligible (assume that δ_1^2 *is* negligible), then the correlation is modified by multipole mixture to

$$W(\theta)=1+\sum B_L P_L(\cos\theta)+x_1\delta_1\sum y_L(l_1)B_L P_L(\cos\theta),$$

where the quantities x_1, $y_L(l_1)$ are those defined in Eqs. (3)–(4). If the γ-ray transition is second, the X–γ correlation for $j_1(X)j(l_2)j_2$,

$$W(\theta)=1+\sum B_L' P_L(\cos\theta),$$

becomes

$$W(\theta)=1+\sum B_L' P_L(\cos\theta)-x_2\delta_2\sum y_L(l_2)B_L' P_L(\cos\theta)$$

when multipole mixture effects in the second transition are taken into account to order δ_2.

3. CORRELATIONS INVOLVING α-PARTICLES

We describe here a method whereby certain correlations involving α-particles can be obtained from the γ-γ tables given. Suppose that an α-particle is emitted in the first transition of $j_1(\alpha)j(X)j_2$, and that the nuclear parity changes in the first transition is $(-1)^{j_1-j}$ if $j_1\neq j$, and (-1) if $j_1=j$. Suppose also that the corresponding γ-X correlation for $j_1(\gamma, l_1)j(X)j_2$ is available and has the value

$$W(\theta)=1+\sum C_L P_L(\cos\theta),$$

[8] Unpublished; the formulas are given by R. D. Hill, Phys. Rev. **81**, 470 (1951). See also A. W. Sunyar and M. Goldhaber, Phys. Rev. **83**, 216(A) (1951).

[9] S. P. Lloyd, Phys. Rev. **81**, 161 (1951). With the author's choice of phase for the reduced matrix elements, the matrix δ is antihermitian. This leads to the difference in sign of the interference terms in Eq. (2), following.

where l_1 is the lowest allowed γ-ray multipole order in the first transition. If all the α-particles are emitted with angular momentum l_1, the α-X correlation is

$$W(\theta)=1+\sum z_L(l_1)C_L P_L(\cos\theta),$$

where

$$z_L(l)=\frac{2l(l+1)}{2l(l+1)-L(L+1)}.$$

For α-particles emitted in the second transition the formula is essentially the same. If the X-γ lowest γ-multipole correlation for $j_1(X)j(\gamma, l_2)j_2$ is

$$W(\theta)=1+\sum C_L' P_L(\cos\theta),$$

the corresponding X-α correlation for $j_1(X)j(\alpha, l_2)j_2$ is

$$W(\theta)=1+\sum z_L(l_2)C_L' P_L(\cos\theta).$$

Double application of the rule gives the $j_1(\alpha, l_1)j(\alpha, l_2)j_2$ correlation

$$W(\theta)=1+\sum z_L(l_1)z_L(l_2)A_L P_L(\cos\theta)$$

from the coefficients A_L of the $j_1(\gamma, l_1)j(\gamma, l_2)j_2$ correlation.

The results of this section apply to any scalar particle emitted in a nuclear transition; α-particles, for example, and also conversion electrons, if the electron is from an atomic s-shell (e.g., K or L_I shell) and the converted γ-ray is an electric multipole. In this case the angular momentum of the electron is to be taken as the multipole order of the γ-ray.[10,*]

4. POWER SERIES AND LEGENDRE SERIES

That the Legendre series is the theoretically natural form for the directional correlation function is clearly indicated in Secs. II–III, preceding. The rule for obtaining the multipole mixture terms from the pure multipole γ-γ correlation, for instance, would become quite unwieldy if both were to be presented in the familiar form as a power series in $\cos^2\theta$. One might also argue that the orthogonality properties of the Legendre polynomials on the unit sphere makes them an intuitively more natural set with which to describe the non-isotropy of the relative angular distribution of the emitted particles. Angular correlations have been previously computed and reported as power series in $\cos^2\theta$, however, so we reproduce the following reversion formulas, obtained from formulas in MacRobert's *Spherical Harmonics*.[11]

$$Q+R\cos^2\theta+S\cos^4\theta+T\cos^6\theta+U\cos^8\theta$$
$$=A_0+A_2P_2(\cos\theta)+A_4P_4(\cos\theta)$$
$$+A_6P_6(\cos\theta)+A_8P_8(\cos\theta),$$

then

$$A_0=Q+\tfrac{1}{3}R+\tfrac{1}{5}S+(1/7)T+(1/9)U,$$
$$A_2=\tfrac{2}{3}R+(4/7)S+(10/21)T+(40/99)U,$$
$$A_4=(8/35)S+(24/77)T+(48/143)U,$$
$$A_6(16/231)T+(64/495)U,$$
$$A_8+(128/5435)U,$$

and

$$Q=A_0-\tfrac{1}{3}A_2+\tfrac{3}{35}A_4-\tfrac{5}{143}A_6+(35/128)A_8,$$
$$R=\tfrac{2}{3}A_2-(30/8)A_4+(105/16)A_6-(1260/128)A_8,$$
$$S=(35/8)A_4-(315/16)A_6+(6930/128)A_8,$$
$$T=(231/16)A_6-(12012/128)A_8,$$
$$U=(6435/128)A_8.$$

5. TABLES[12]

TABLE I. Dipole-dipole correlations: $W(\theta)=1+A_2P_2(\cos\theta)$. Basic: $A_2=0.05$.

	A_2				
j	$\frac{j\to j}{-j}$	$\frac{j\to j}{-j-1}$	$\frac{j\to j}{-j+1}$	$\frac{j-1\to j}{-j-1}$	$\frac{j+1\to j}{-j+1}$
1	0.1250	−0.2500	−0.0250	0.5000	0.0050
3/2	0.1600	−0.2000	−0.0400	0.2500	0.0100
2	0.1750	−0.1750	−0.0500	0.1750	0.0143
5/2	0.1829	−0.1600	−0.0571	0.1400	0.0179
3	0.1875	−0.1500	−0.0625	0.1200	0.0208
7/2	0.1905	−0.1429	−0.0667	0.1071	0.0233
4	0.1925	−0.1375	−0.0700	0.0982	0.0255
9/2	0.1939	−0.1333	−0.0727	0.0917	0.0273
5	0.1950	−0.1300	−0.0750	0.0867	0.0288
11/2	0.1958	−0.1273	−0.0769	0.0827	0.0302
6	0.1964	−0.1250	−0.0786	0.0795	0.0314
13/2	0.1969	−0.1231	−0.0800	0.0769	0.0325
7	0.1973	−0.1214	−0.0813	0.0747	0.0335
15/2	0.1976	−0.1200	−0.0824	0.0729	0.0343
8	0.1979	−0.1188	−0.0833	0.0713	0.0351
17/2	0.1981	−0.1176		0.0699	
9	0.1983	−0.1167		0.0686	

TABLE II. Certain dipole–2^l-pole correlations: $W(\theta)=1+A_2P_2(\cos\theta)$.

			$j\to j-j\pm l$		
	2^1-2^3	2^1-2^2	2^1-2^4	2^1-2^5	2^1-2^6
			A_2		
Basic	−0.0714	−0.1250	−0.1545	−0.1731	−0.1857
j	$\frac{j\to j}{-j+2}$	$\frac{j\to j}{-j+3}$	$\frac{j\to j}{-j+4}$	$\frac{j\to j}{-j+5}$	$\frac{j\to j}{-j+6}$
1	0.0357	0.0625	0.0773	0.0865	0.0929
3/2	0.0571	0.1000	0.1236	0.1385	0.1486
2	0.0714	0.1250	0.1545	0.1731	0.1857
5/2	0.0816	0.1429	0.1766	0.1978	0.2122
3	0.0893	0.1563	0.1932	0.2163	0.2321
7/2	0.0952	0.1667	0.2061	0.2308	
4	0.1000	0.1750	0.2164	0.2423	
9/2	0.1039	0.1818	0.2248		
5	0.1071	0.1875	0.2318		
11/2	0.1099	0.1923			
6	0.1122	0.1964			
13/2	0.1143				
7	0.1161				

[10] J. W. Gardner, Proc. Phys. Soc. (London) **62A**, 763 (1949).

[*] *Note added in proof:*—This holds only when the electrons are treated nonrelativistically.

[11] T. MacRobert, *Spherical Harmonics* (Methuen and Company, Ltd., London, 1928), first edition.

[12] These tables are a corrected version of a set circulated privately.

TABLE II.—*Continued*

	$j\to j$ $\to j-2$	$j\to j$ $\to j-3$	$j\to j$ $\to j-4$	$j\to j$ $\to j-5$	$j\to j$ $\to j-6$
2	0.2500				
5/2	0.2286				
3	0.2143	0.3750			
7/2	0.2041	0.3571			
4	0.1964	0.3438	0.4250		
9/2	0.1905	0.3333	0.4121		
5	0.1857	0.3250	0.4018	0.4500	
11/2	0.1818	0.3182	0.3934	0.4406	
6	0.1786	0.3125	0.3864	0.4327	0.4643
13/2	0.1758	0.3077	0.3804	0.4260	0.4571
7	0.1735	0.3036	0.3753	0.4203	0.4510
15/2	0.1714	0.3000	0.3709	0.4154	0.4457
8	0.1696	0.2969	0.3670	0.4111	0.4411
17/2	0.1681	0.2941	0.3636	0.4072	0.4370
9	0.1667	0.2917	0.3606	0.4038	0.4333

TABLE III. Certain dipole–2^L-pole correlations: $W(\theta)=1+A_2P_2(\cos\theta)$.

	2^1-2^2	2^1-2^3	$j\pm1\to j\to j\pm1$ 2^1-2^4	2^1-2^5	2^1-2^6
			A_2		
Basic	−0.0714	−0.1250	−0.1545	−0.1731	−0.1857
j	$j+1\to j$ $\to j+2$	$j+1\to j$ $\to j+3$	$j+1\to j$ $\to j+4$	$j+1\to j$ $\to j+5$	$j+1\to j$ $\to j+6$
1	−0.0071	−0.0125	−0.0155	−0.0173	−0.0186
3/2	−0.0143	−0.0250	−0.0309	−0.0346	−0.0371
2	−0.0204	−0.0357	−0.0442	−0.0495	−0.0531
5/2	−0.0255	−0.0446	−0.0552	−0.0618	−0.0663
3	−0.0298	−0.0521	−0.0644	−0.0721	−0.0774
7/2	−0.0333	−0.0583	−0.0721	−0.0808	
4	−0.0364	−0.0636	−0.0787	−0.0881	
9/2	−0.0390	−0.0682	−0.0843		
5	−0.0412	−0.0721	−0.0892		
11/2	−0.0432	−0.0755			
6	−0.0449	−0.0786			
13/2	−0.0464				
7	−0.0478				
	$j-1\to j$ $\to j-2$	$j-1\to j$ $\to j-3$	$j-1\to j$ $\to j-4$	$j-1\to j$ $\to j-5$	$j-1\to j$ $\to j-6$
2	−0.2500				
5/2	−0.2000				
3	−0.1714	−0.3000			
7/2	−0.1531	−0.2679			
4	−0.1403	−0.2455	−0.3036		
9/2	−0.1310	−0.2292	−0.2833		
5	−0.1238	−0.2167	−0.2679	−0.3000	
11/2	−0.1182	−0.2068	−0.2557	−0.2864	
6	−0.1136	−0.1989	−0.2459	−0.2753	−0.2955
13/2	−0.1099	−0.1923	−0.2378	−0.2663	−0.2857
7	−0.1068	−0.1868	−0.2310	−0.2587	−0.2776
15/2	−0.1041	−0.1821	−0.2252	−0.2522	−0.2706
8	−0.1018	−0.1781	−0.2202	−0.2466	−0.2646
17/2	−0.0998	−0.1746	−0.2159	−0.2418	−0.2595
9	−0.0980	−0.1716	−0.2121	−0.2376	−0.2549

TABLE IV. Quadrupole–2^2-, 2^3-, and 2^4-pole correlations: $W(\theta)=1+A_2P_2(\cos\theta)+A_4P_4(\cos\theta)$.

	2^2-2^2		2^2-2^3		2^2-2^4	
	A_2	A_4	A_2	A_4	A_2	A_4
Basic	0.1020	0.0091	0.1786	−0.0043	0.2208	−0.0018
j	$j+2\to j\to j+2$		$j+2\to j\to j+3$		$j+2\to j\to j+4$	
1	0.0102	0	0.0179	0	0.0221	0
3/2	0.0204	0	0.0357	0	0.0442	0
2	0.0292	0.0001	0.0510	−0.0000	0.0631	−0.0000
5/2	0.0364	0.0002	0.0638	−0.0001	0.0788	−0.0000
3	0.0425	0.0004	0.0744	−0.0002	0.0920	−0.0001
7/2	0.0476	0.0006	0.0833	−0.0003	0.1030	−0.0001
4	0.0519	0.0009	0.0909	−0.0004	0.1124	−0.0002
9/2	0.0557	0.0011	0.0974	−0.0005	0.1204	−0.0002
5	0.0589	0.0014	0.1030	−0.0007	0.1274	−0.0003
11/2	0.0617	0.0016	0.1079	−0.0008		
6	0.0641	0.0019	0.1122	−0.0009		
13/2	0.0663	0.0021				
7	0.0683	0.0023				
	$j-2\to j\to j-2$		$j+2\to j\to j-3$		$j-2\to j\to j-4$	
2	0.3571	1.1429				
5/2	0.2857	0.3810				
3	0.2449	0.1995	0.4286	−0.0952		
7/2	0.2187	0.1283	0.3827	−0.0612		
4	0.2004	0.0926	0.3508	−0.0442	0.4337	−0.0184
9/2	0.1871	0.0721	0.3274	−0.0344	0.4048	−0.0143
5	0.1769	0.0590	0.3095	−0.0281	0.3827	−0.0117
11/2	0.1688	0.0500	0.2955	−0.0239	0.3653	−0.0099
6	0.1623	0.0436	0.2841	−0.0208	0.3512	−0.0086
13/2	0.1570	0.0388	0.2747	−0.0185	0.3397	−0.0077
7	0.1525	0.0351	0.2669	−0.0168	0.3300	−0.0070
15/2	0.1487	0.0322	0.2602	−0.0154	0.3217	−0.0064
8	0.1454	0.0298	0.2545	−0.0142	0.3146	−0.0059
17/2	0.1426	0.0279	0.2495	−0.0133	0.3084	−0.0055
9	0.1401	0.0262	0.2451	−0.0125	0.3030	−0.0052

TABLE V. Quadrupole–2^5- and 2^6-pole correlations: $W(\theta)=1+A_2P_2(\cos\theta)+A_4P_4(\cos\theta)$.

	2^5-2^5		2^5-2^6	
	A_2	A_4	A_2	A_4
Basic	0.2473	−0.0293	0.2653	−0.0384
j	$j+2\to j\to j+5$		$j+2\to j\to j+6$	
1	0.0247	0	0.0265	0
3/2	0.0495	0	0.0531	0
2	0.0706	−0.0002	0.0758	−0.0003
5/2	0.0883	−0.0007	0.0948	−0.0009
3	0.1030	−0.0013	0.1105	−0.0017
7/2	0.1154	−0.0021		
4	0.1259	−0.0029		
	$j-2\to j\to j-5$		$j-2\to j\to j-6$	
5	0.4286	−0.1905		
11/2	0.4091	−0.1616		
6	0.3934	−0.1409	0.4221	−0.1847
13/2	0.3804	−0.1254	0.4082	−0.1644
7	0.3695	−0.1135	0.3965	−0.1487
15/2	0.3603	−0.1040	0.3866	−0.1364
8	0.3523	−0.0964	0.3781	−0.1263
17/2	0.3454	−0.0901	0.3706	−0.1181
9	0.3394	−0.0848	0.3641	−0.1112

TABLE VI. Octuple–2^3- and 2^4-pole correlations: $W(\theta)=1+A_2P_2(\cos\theta)+A_4P_4(\cos\theta)+A_8P_8(\cos\theta)$.

	2^3-2^3			2^3-2^4		
	A_2	A_4	A_8	A_2	A_4	A_8
Basic	0.3125	0.0021	0.0010	0.3864	0.0086	0.0002
j	$j+3\to j\to j+3$			$j+3\to j\to j+4$		
1	0.0313	0	0	0.0386	0	0
3/2	0.0625	0	0	0.0773	0	0
2	0.0893	0.0000	0	0.1104	0.0001	0
5/2	0.1116	0.0000	0	0.1380	0.0002	0
3	0.1302	0.0001	0.0000	0.1610	0.0004	0.0000
7/2	0.1458	0.0001	0.0000	0.1803	0.0006	0.0000
4	0.1591	0.0002	0.0000	0.1967	0.0008	0.0000
9/2	0.1705	0.0003	0.0000	0.2107	0.0011	0.0000
5	0.1803	0.0003	0.0000	0.2229	0.0013	0.0000
11/2	0.1889	0.0004	0.0000			
6	0.1964	0.0004	0.0000			
	$j-3\to j\to j-3$			$j-3\to j\to j-4$		
3	0.7500	0.0455	1.7045			
7/2	0.6696	0.0292	0.4261			
4	0.6138	0.0211	0.1776	0.7589	0.0877	0.0284
9/2	0.5729	0.0164	0.0947	0.7083	0.0682	0.0152
5	0.5417	0.0134	0.0585	0.6697	0.0558	0.0094
11/2	0.5170	0.0114	0.0399	0.6393	0.0473	0.0064
6	0.4972	0.0099	0.0292	0.6147	0.0413	0.0047
13/2	0.4808	0.0088	0.0224	0.5944	0.0367	0.0036
7	0.4670	0.0080	0.0179	0.5774	0.0332	0.0029
15/2	0.4554	0.0073	0.0148	0.5630	0.0305	0.0024
8	0.4453	0.0068	0.0125	0.5506	0.0282	0.0020
17/2	0.4366	0.0064	0.0108	0.5398	0.0264	0.0017
9	0.4289	0.0060	0.0095	0.5303	0.0248	0.0015

TABLE VII. Octuple–2^5- and 2^4-pole correlations: $W(\theta)=1+A_2P_2(\cos\theta)+A_4P_4(\cos\theta)+A_8P_8(\cos\theta)$.

	2^3-2^5			2^3-2^4		
	A_2	A_4	A_8	A_2	A_4	A_8
Basic	0.4327	0.0140	−0.0015	0.4643	0.0183	−0.0035
j	$j+3\to j\to j+5$			$j+3\to j\to j+6$		
1	0.0433	0	0	0.0464	0	0
3/2	0.0865	0	0	0.0929	0	0
2	0.1236	0.0001	0	0.1327	0.0001	0
5/2	0.1545	0.0003	0	0.1658	0.0004	0
3	0.1803	0.0006	−0.0000	0.1935	0.0008	−0.0000
7/2	0.2019	0.0010	−0.0000			
4	0.2203	0.0014	−0.0000			
	$j-3\to j\to j-5$			$j-3\to j\to j-6$		
5	0.7500	0.0909	−0.0909			
11/2	0.7159	0.0771	−0.0620			
6	0.6884	0.0672	−0.0453	0.7386	0.0882	−0.1033
13/2	0.6657	0.0599	−0.0348	0.7143	0.0785	−0.0795
7	0.6467	0.0542	−0.0279	0.6939	0.0710	−0.0636
15/2	0.6305	0.0496	−0.0230	0.6765	0.0651	−0.0524
8	0.6166	0.0460	−0.0194	0.6616	0.0603	−0.0443
17/2	0.6045	0.0430	−0.0168	0.6486	0.0564	−0.0383
9	0.5939	0.0405	−0.0147	0.6373	0.0531	−0.0336

TABLE VIII. 2^4-pole–2^4-pole and 2^4-pole–2^5-pole correlations: $W(\theta)=1+A_2P_2(\cos\theta)+A_4P_4(\cos\theta)+A_6P_6(\cos\theta)+A_8P_8(\cos\theta)$.

	2^4-2^4				2^4-2^5			
	A_2	A_4	A_6	A_8	A_2	A_4	A_6	A_8
Basic	0.4777	0.0356	0.0000	0.0001	0.5350	0.0581	−0.0002	0.0001
j		$j+4\to j\to j+4$				$j+4\to j\to j+5$		
1	0.0478	0	0	0	0.0535	0	0	0
3/2	0.0955	0	0	0	0.1070	0	0	0
2	0.1365	0.0003	0	0	0.1528	0.0005	0	0
5/2	0.1706	0.0008	0	0	0.1911	0.0014	0	0
3	0.1990	0.0016	0.0000	0	0.2229	0.0026	−0.0000	0
7/2	0.2229	0.0025	0.0000	0	0.2497	0.0041	−0.0000	0
4	0.2432	0.0035	0.0000	0.0000	0.2723	0.0057	−0.0000	0.0000
9/2	0.2606	0.0045	0.0000	0.0000				
5	0.2756	0.0055	0.0000	0.0000				
		$j-4\to j\to j-4$				$j-4\to j\to j-5$		
4	0.9383	0.3641	0.0045	2.1930				
9/2	0.8758	0.2832	0.0024	0.4386				
5	0.8280	0.2317	0.0015	0.1515	0.9273	0.3776	−0.0145	0.1097
11/2	0.7904	0.1966	0.0010	0.0689	0.8851	0.3204	−0.0099	0.0498
6	0.7600	0.1714	0.0007	0.0371	0.8511	0.2793	−0.0072	0.0268
13/2	0.7349	0.1526	0.0006	0.0224	0.8230	0.2486	−0.0056	0.0162
7	0.7139	0.1380	0.0005	0.0147	0.7995	0.2250	−0.0045	0.0107
15/2	0.6961	0.1265	0.0004	0.0103	0.7795	0.2062	−0.0037	0.0075
8	0.6807	0.1172	0.0003	0.0076	0.7623	0.1910	−0.0031	0.0055
17/2	0.6674	0.1096	0.0003	0.0058	0.7474	0.1786	−0.0027	0.0042
9	0.6556	0.1032	0.0002	0.0046	0.7343	0.1681	−0.0024	0.0033

TABLE IX. 2^4-pole–2^6-pole correlations: $W(\theta)=1+A_2P_2(\cos\theta)+A_4P_4(\cos\theta)+A_6P_6(\cos\theta)+A_8P_8(\cos\theta)$.

	2^4-2^6			
	A_2	A_4	A_6	A_8
Basic	0.5740	0.0762	−0.0006	−0.0001
j			$j+4\to j\to j+6$	
1	0.0574	0	0	0
3/2	0.1148	0	0	0
2	0.1640	0.0006	0	0
5/2	0.2050	0.0018	0	0
3	0.2392	0.0035	−0.0000	0
			$j-4\to j\to j-6$	
6	0.9132	0.3662	−0.0165	−0.0356
13/2	0.8831	0.3259	−0.0127	−0.0215
7	0.8579	0.2949	−0.0102	−0.0141
15/2	0.8364	0.2703	−0.0084	−0.0099
8	0.8180	0.2504	−0.0071	−0.0073
17/2	0.8019	0.2341	−0.0061	−0.0056
9	0.7879	0.2204	−0.0054	−0.0044

Multiple Elastic Scattering and Radiation Damping. I*

H. EKSTEIN
Armour Research Foundation of Illinois Institute of Technology, Chicago, Illinois
(Received April 23, 1951)

The problem of potential scattering by a number of similar scatterers is reformulated so that the potential is eliminated from the equations and replaced by a function which characterizes the scattering properties of the individual scatterer. The resulting equations can be used for the more general case where the single-scattering process is not describable by a potential, e.g., absorption or—to a certain extent—inelastic scattering. A solution of the equations by iteration is considered and compared with Born's approximation. As an application, the second approximation for the scattering of thermal neutron by a small crystal is calculated.

I. INTRODUCTION

MOST papers on multiple scattering deal with the case where the coherence between individual scattering processes can be disregarded. This is true either when the wavelength is small in comparison with the distance between scatterers or when the individual scattering is essentially incoherent. The subject of this paper is the opposite end of the range, where elastic scattering and wave interference are of prime importance.

Most problems involving scattering of an incident particle by a scatterer are complicated many-body problems, in which often not even the correct form of the hamiltonian is known. To describe elastic scattering, an "effective potential" is usually introduced which is chosen so that it gives the observed scattering amplitudes. For the study of multiple scattering, the effective potentials of the scatterers are introduced into the Schrödinger equation. This paper formulates the multiple-scattering problem so that it contains not the effective potential but the scattering properties of the individual scatterers. Once the problem of potential scattering is restated in terms of the scattering properties of the individual scatterers, it is plausible that the equations remain approximately correct if the individual scattering problem is not really a potential problem. This is similar to the idea underlying the S-matrix theory. But since in our problem the scatterers are held at fixed finite distances, the S-matrix alone does not give sufficient information about the scatterer; it is necessary to know its behavior when the stream of incident particles issues from a source at a finite distance rather than from infinity, as well as the scattered amplitude at finite distances.

Another reason for this investigation is that the solution of the multiple scattering problem is often simplified by eliminating the potential from the equations, even if the potential is definitely known.

Most calculating methods are based on the smallness of the interaction. If the scatterers are, for instance, nearly impenetrable objects, the potential is very large so that the usual approximation methods fail. However, the scattering cross section of a single scatterer may be small, so that the problem in its restated form may be solved by expansion in terms of the single-scatterer cross section. The case of point-scatterers has been the subject of extensive work, first in the classical dispersion theory, and later in Ewald's rigorous lattice theory. Goldberger and Seitz[1] treated the refraction and diffraction of slow neutrons by nuclei in an analogous way. Foldy[2] studied the case of random atomic positions of point scatterers. The present paper generalizes these results for scatterers of finite size.

In Part I the general equations are derived, and the solution by iteration is investigated and compared with Born's approximation. The two methods are shown to be complementary. The results are applied to the calculation of the second approximation of the intensity of a thermal neutron beam scattered by a small crystal.

In Part II, the propagation of waves in an infinite medium is treated. It is found that the effect of radiation damping on multiple scattering is different from that assumed in previous work; in particular, for an infinite crystal the individual scattering amplitudes must be corrected for the lack of radiation damping, since no particles are lost by scattering to infinity in an indefinitely extended medium.

II. SINGLE SCATTERING IN MOMENTUM REPRESENTATION

The general formalism of scattering in momentum representation has been presented by Møller.[3] For the simplest case of nonrelativistic scalar particles, the Schrödinger equation is

$$[(-\hbar^2/2m)\nabla^2+v-E]\psi=0, \tag{1}$$

with the additional requirement that the asymptotic form of the wave function be

$$\psi\sim e^{ikz}+F(\theta,\phi)e^{ikr}/r. \tag{2}$$

* Work supported in part by the ONR.

[1] M. L. Goldberger and F. Seitz, Phys. Rev. **71**, 294 (1947).
[2] L. L. Foldy, Phys. Rev. **67**, 107 (1945).
[3] C. Møller, Kgl. Danske Videnskab. Selskab. Mat.-fys. Medd. **23**, No. 1 (1945); **22**, No. 19 (1946).

Let

$$u(\mathbf{k})=\frac{-2m}{\hbar^2(2\pi)^3}\int v(\mathbf{x})\exp(-i\mathbf{k}\cdot\mathbf{x})d\mathbf{x}, \quad (3)$$

$$f(\mathbf{k})=\frac{-2m}{\hbar^2(2\pi)^3}\int v\psi(\mathbf{x})\exp(-i\mathbf{k}\cdot\mathbf{x})d\mathbf{x}, \quad (4)$$

$$k_0^2=2m/\hbar^2=E. \quad (5)$$

Then the equivalent of Eqs. (1) and (2) is

$$f(\mathbf{k})-\int_h \frac{u(\mathbf{k}-\mathbf{k}')}{k'^2-k_0^2}f(\mathbf{k}')d\mathbf{k}'=u(\mathbf{k}-\mathbf{k}_0), \quad (6)$$

where $\mathbf{k}_0$ is the propagation vector of the incident wave. The symbol h (for hook-integral) below the integral sign has the following meaning: in polar coordinates k', θ', ϕ', the path of integration with respect to k' is to be indented at $k'=k_0$ and deviated into the lower half of the complex k' plane. Explicitly,

$$\int_h \frac{u(\mathbf{k}-\mathbf{k}')}{k'^2-k_0^2}f(\mathbf{k}')d\mathbf{k}'$$

$$=\frac{i\pi k_0}{2}\int_s u(\mathbf{k}-\mathbf{k}')f(\mathbf{k}')d\Omega+P\int\frac{u(\mathbf{k}-\mathbf{k}')}{k'^2-k_0^2}f(\mathbf{k}')d\mathbf{k}', \quad (7)$$

where the first integral or the right-hand side extends only over the sphere $\mathbf{k}'^2=k_0^2$ and P stands for the principal value of the second integral. The direct significance of $f(\mathbf{k})$ is given by

$$\psi_{sc}(\mathbf{r})\sim(2\pi^2/r)\exp(ik_0r)f(k_0\mathbf{r}/|r|), \quad (8)$$

which states that the asymptotic value of the scattered wave ψ_{sc} is proportional to the value of f at the point where the vector $\mathbf{r}$ intersects the sphere $\mathbf{k}^2=k_0^2$. To exhibit the meaning of Eq. (6) in coordinate space, it can be re-transformed, giving term by term

$$-\frac{2m}{\hbar^2}v\psi-\frac{(2m)^2}{4\pi\hbar^4}v\int\frac{\exp(ik_0r_{12})}{r_{12}}v(\mathbf{r}_2)\psi(\mathbf{r}_2)d\mathbf{r}_2$$

$$=-\frac{2m}{\hbar^2}v\exp(i\mathbf{k}_0\cdot\mathbf{r}), \quad (9)$$

i.e., the well-known integral equation of scattering,[4] multiplied by $(-2mv/\hbar^2)$.

When the potential has spherical symmetry, the introduction of polar coordinates k, θ, ϕ makes possible a separation of variables. With the usual notation, let

$$f(\mathbf{k})=\sum_l f_l(k)P_l(\cos\theta) \quad (10)$$

and one obtains the set of one-dimensional integral equations[5]

$$f_l(x)-2\pi\int_h\frac{y^2dy}{y^2-k_0^2}f_l(y)K_l(x,y)=\frac{2l+1}{2}K_l(x,k_0), \quad (11)$$

where

$$K_l(x,y)=\int_{-1}^{+1}P_l(t)u[(x^2+y^2-2xyt)^{\frac{1}{2}}]dt. \quad (12)$$

To exhibit the connection between the kernels K_l and the potential v, one can substitute the definition (3) for u, which reduces to

$$u(k)=\frac{1}{2\pi^2k}\int_0^\infty v(r)\sin krdr \quad (13)$$

and use the expansion theorem[6]

$$\frac{\sin r(x^2+y^2-2xyt)^{\frac{1}{2}}}{(x^2+y^2-2xyt)^{\frac{1}{2}}}=\pi\sum_0^\infty\frac{(m+\frac{1}{2})}{(xy)^{\frac{1}{2}}}J_{m+\frac{1}{2}}(rx)J_{m+\frac{1}{2}}(ry)P_m(t) \quad (14)$$

to obtain

$$K_l(x,y)=\frac{-m}{\pi\hbar^2(xy)^{\frac{1}{2}}}\int_0^\infty rv(r)J_{l+\frac{1}{2}}(rx)J_{l+\frac{1}{2}}(ry)dr. \quad (15)$$

It is possible to separate the influence of radiation damping as follows:[7] by the definition (7) of the symbol h, one can write instead of Eq. (11):

$$f_l(x)-2\pi P\int_0^\infty\frac{y^2dy}{y^2-k_0^2}f_l(y)K_l(x,y)$$

$$=K_l(x,k_0)\left[\frac{2l+1}{2}+i\pi^2k_0f_l(k_0)\right]. \quad (16)$$

Now consider the auxiliary equation

$$g_l(x)-2\pi P\int_0^\infty\frac{y^2dy}{y^2-k_0^2}g_l(y)K_l(x,y)=\frac{2l+1}{2}K_l(x,y), \quad (17)$$

which involves only real quantities; hence, g_l is real. Then,

$$f_l(x)=g_l(x)\left(1+\frac{2}{2l+1}i\pi^2k_0f_l(k_0)\right) \quad (18)$$

and in particular, for $x=k_0$

$$f_l(k_0)=\frac{g_l(k_0)}{1-i\pi^2k_0g_l(k_0)2/(2l+1)}. \quad (19)$$

Equation (17) can be thought as having been derived

[4] N. F. Mott and H. S. W. Massey, *The Theory of Atomic Collisions* (Oxford University Press, London, 1949), p. 116.

[5] V. Fock, Z. Physik **98**, 145 (1935); M. Lévy, Proc. Roy. Soc. (London) **A204**, 145 (1950).

[6] G. N. Watson, *Bessel Functions* (Cambridge University Press, London, 1944), p. 366.

[7] H. Ekstein, Phys. Rev. **75**, 1322 (1949).

by separating a three-dimensional equation similar to Eq. (6) but containing the principal value instead of the hook-integral. This equation may be considered as describing a scattering problem in which radiation damping is absent. Equation (19) then is the degenerate one-dimensional form of Heitler's integral equation[8] which shows the influence of radiation damping on the actual solution.

The connection with the usual formula

$$\psi_{sc}(r)\sim\frac{\exp(ik_0r)}{2ik_0r}\sum P_l(\cos\theta)(2l+1)[\exp(2i\delta_l)-1] \quad (20)$$

is established by comparing with Eqs. (8), (10), and (18). One finds

$$f_l(k_0)=\frac{2l+1}{4\pi^2ik_0}[\exp(2i\delta_l)-1], \quad (21)$$

$$g_l(k_0)=\frac{2l+1}{2\pi^2k_0}\tan\delta_l. \quad (22)$$

$g_l(k_0)$ is unbounded, because the homogeneous equation corresponding to Eq. (17) may have solutions. This is understood by the observation that a system without radiation damping can have nonvanishing solutions without a source at infinity.

For the study of multiple scattering, we will have to consider the case where the source of incident particles is at a finite distance R. The solution of this problem is the Green's function $G(\mathbf{r}, \mathbf{R})$ which satisfies the differential equation:

$$\left(\frac{-\hbar^2}{2m}\nabla^2+v-E\right)G(\mathbf{r}, \mathbf{R})=\delta(\mathbf{r}-\mathbf{R}) \quad (23)$$

and if the required asymptotic form represents outgoing waves only, the integral equation

$$G(\mathbf{r}, \mathbf{R})+\frac{2m}{4\pi\hbar^2}\int\frac{\exp[ik_0|\mathbf{r}-\mathbf{r}'|]}{|\mathbf{r}-\mathbf{r}'|}v(\mathbf{r}')G(\mathbf{r}', \mathbf{R})d\mathbf{r}'=-\frac{2m}{4\pi\hbar^2}\frac{\exp(ik_0|\mathbf{r}-\mathbf{R}|)}{|\mathbf{r}-\mathbf{R}|}. \quad (24)$$

For calculations in momentum representation, it is more convenient to use the solution of the related equation

$$\chi(\mathbf{r}, \boldsymbol{\kappa})+\frac{2m}{4\pi\hbar^2}\int\frac{\exp(ik_0|\mathbf{r}-\mathbf{r}'|)}{|\mathbf{r}-\mathbf{r}'|}v(\mathbf{r}')\chi(\mathbf{r}', \boldsymbol{\kappa})d\mathbf{r}'=\exp(i\boldsymbol{\kappa}\cdot\mathbf{r}). \quad (25)$$

The connection between G and χ is established by noticing that

$$\int\frac{\exp(ik_0|\mathbf{r}-\mathbf{R}|)}{|\mathbf{r}-\mathbf{R}|}\exp(i\boldsymbol{\kappa}\cdot\mathbf{R})d\mathbf{R}=\exp(i\boldsymbol{\kappa}\cdot\mathbf{r})\frac{4\pi}{\kappa^2-k_0^2}. \quad (26)$$

Hence, by multiplying Eq. (24) by $\exp(i\boldsymbol{\kappa}\cdot\mathbf{R})$ and integrating with respect to the parameter $\mathbf{R}$, it is shown that

$$\chi(\mathbf{r}, \boldsymbol{\kappa})=-\frac{\hbar^2(\kappa^2-k_0^2)}{2m}\int G(\mathbf{r}, \mathbf{R})\exp(i\boldsymbol{\kappa}\cdot\mathbf{R})d\mathbf{R}. \quad (27)$$

If G is considered known, χ is also known. In momentum representation, we consider the equation

$$\alpha(\mathbf{k}, \boldsymbol{\kappa})-\int_A\frac{u(\mathbf{k}-\mathbf{k}')}{k'^2-k_0^2}\alpha(\mathbf{k}', \boldsymbol{\kappa})d\mathbf{k}'=u(\mathbf{k}-\boldsymbol{\kappa}) \quad (28)$$

of which Eq. (6) is a special case. The transformation of Eq. (25) into momentum space (after multiplication by $(-2mv/\hbar^2)$) leads directly to Eq. (28) if

$$\alpha(\mathbf{k}, \boldsymbol{\kappa})=\frac{-2m}{\hbar^2(2\pi)^3}\int v\chi(\mathbf{r}, \boldsymbol{\kappa})\exp(-i\mathbf{k}\cdot\mathbf{r})d\mathbf{r}. \quad (29)$$

In the theory of multiple scattering (Part II) we will have to consider an analog of Eq. (28) from which radiation damping has been eliminated:

$$\beta(\mathbf{k}, \boldsymbol{\kappa})-P\int\frac{u(\mathbf{k}-\mathbf{k}')\beta(\mathbf{k}', \boldsymbol{\kappa})}{k'^2-k_0^2}d\mathbf{k}'=u(\mathbf{k}-\boldsymbol{\kappa}). \quad (30)$$

If the potential has spherical symmetry, separation of variables is again possible, leading to the set of one-dimensional integral equations

$$\alpha_l(k)-2\pi\int_A^\infty\frac{y^2dy}{y^2-k_0^2}\alpha_l(y)K_l(k, y)=\frac{2l+1}{2}K_l(k, \kappa) \quad (31)$$

and

$$\beta_l(k)-2\pi P\int_0^\infty\frac{y^2dy}{y^2-k_0^2}\beta_l(y)K_l(k, y)=\frac{2l+1}{2}K_l(k, \kappa). \quad (32)$$

In the case where the wave function has several components, the scattering problem can be treated in a similar manner. In particular, for the scattering of electromagnetic waves by an object of dielectric constant $\epsilon(\mathbf{r})$ we have[9]

$$\mathbf{f}(\mathbf{k})+\mathbf{k}\times\mathbf{k}\times\int_A\frac{u(\mathbf{k}-\mathbf{k}')}{k'^2-k_0^2}\mathbf{f}(\mathbf{k}')d\mathbf{k}'=-\mathbf{k}\times\mathbf{k}\times\mathbf{E}_0u(\mathbf{k}-\mathbf{k}_0) \quad (33)$$

[8] W. Pauli, *Meson Theory of Nuclear Forces* (Interscience Publishers, Inc., New York, 1948), p. 45.

[9] H. Ekstein, Phys. Rev. **62**, 255 (1942).

analogous to Eq. (7). The asymptotic value of the scattered field is connected to $\mathbf{f}$ by

$$\mathbf{E}_{sc}\sim(1/r)\exp(ik_0r)2\pi^2\mathbf{f}(k_0\mathbf{r}/|\mathbf{r}|) \quad (34)$$

similar to Eq. (8). The potential u is defined by

$$u(\mathbf{k})=\frac{1}{(2\pi)^3}\int\frac{\epsilon-1}{\epsilon}\exp(-i\mathbf{k}\cdot\mathbf{r})d\mathbf{r} \quad (35)$$

similar to Eq. (3). In Eq. (33), $k_0^2=\omega^2/c^2$ and $\mathbf{E}_0$ is the field intensity of the incident wave. The variable $\mathbf{f}$ is connected to the polarization $\mathbf{P}$ by

$$\mathbf{f}=(2\pi)^{-3}\int\exp(-i\mathbf{k}\cdot\mathbf{r})\nabla\times\nabla\times\mathbf{P}dr. \quad (36)$$

Most of the results obtained for the scalar case can be generalized for the case of many components, but this paper will mainly be concerned with the scalar case.

III. MULTIPLE SCATTERING: GENERAL EQUATIONS

We consider N similar scatterers at positions $\mathbf{r}=\mathbf{r}_n$. The total potential V is

$$V=\sum_n^N v(\mathbf{r}-\mathbf{r}_n). \quad (37)$$

To obtain the generalization of Eq. (3) we form

$$\int\sum v(\mathbf{r}-\mathbf{r}_n)\exp(-i\mathbf{k}\cdot\mathbf{r})d\mathbf{r}$$
$$=\sum\exp(-i\mathbf{k}\cdot\mathbf{r}_n)\int v(\mathbf{r})\exp(-i\mathbf{k}\cdot\mathbf{r})d\mathbf{r}, \quad (38)$$

so that the quantity $U(\mathbf{k})$ to use instead of $u(\mathbf{k})$ for multiple scattering is

$$U=u\sum\exp(-i\mathbf{k}\cdot\mathbf{r}_n). \quad (39)$$

If we designate by $F(\mathbf{k})$ the equivalent of $f(\mathbf{k})$ in multiple scattering, Eq. (6) becomes

$$F(\mathbf{k})-\int_h\frac{d\mathbf{k}'}{k'^2-k_0^2}\sum\exp[-i\mathbf{r}_n\cdot(\mathbf{k}-\mathbf{k}')]u(\mathbf{k}-\mathbf{k}')F(\mathbf{k}')$$
$$=u(\mathbf{k}-\mathbf{k}_0)\sum\exp[-i\mathbf{r}_n\cdot(\mathbf{k}-\mathbf{k}_0)]. \quad (40)$$

We define a set of functions $F_n(\mathbf{k})$ by the equations

$$F_n(\mathbf{k})-\int_h\frac{d\mathbf{k}'}{k'^2-k_0^2}\exp[-i\mathbf{r}_n\cdot(\mathbf{k}-\mathbf{k}')]u(\mathbf{k}-\mathbf{k}')F(\mathbf{k}')$$
$$=u(\mathbf{k}-\mathbf{k}_0)\exp[-i\mathbf{r}_n\cdot(\mathbf{k}-\mathbf{k}_0)]. \quad (41)$$

By summing Eq. (41) with respect to n, one sees that

$$F=\sum_n^N F_n. \quad (42)$$

Substitution of Eq. (42) into the second term of (41) gives

$$F_n(\mathbf{k})-\int_h\frac{d\mathbf{k}'}{k'^2-k_0^2}\exp[-i\mathbf{r}_n\cdot(\mathbf{k}-\mathbf{k}')]u(\mathbf{k}-\mathbf{k}')F_n(\mathbf{k}')$$
$$=u(\mathbf{k}-\mathbf{k}_0)\exp[-i\mathbf{r}_n\cdot(\mathbf{k}-\mathbf{k}_0)]+\sum_{m\neq n}\int\frac{d\mathbf{k}'}{k'^2-k_0^2}$$
$$\times\exp[-i\mathbf{r}_n\cdot(\mathbf{k}-\mathbf{k}')]u(\mathbf{k}-\mathbf{k}')F_m(\mathbf{k}'). \quad (43)$$

If, for the moment, the quantities on the right-hand side are considered as known, Eq. (43) is an inhomogeneous integral equation which can be solved in terms of the function $\alpha(\mathbf{k},\boldsymbol{\kappa})$ as follows: Let

$$G_n=\exp(i\mathbf{r}_n\cdot\mathbf{k})F_n, \quad (44)$$

so that

$$G_n(\mathbf{k})-\int_h\frac{d\mathbf{k}'}{k'^2-k_0^2}u(\mathbf{k}-\mathbf{k}')G_n(\mathbf{k}')$$
$$=u(\mathbf{k}-\mathbf{k}_0)\exp(i\mathbf{r}_n\cdot\mathbf{k}_0)+\sum_{m\neq n}\int_h\frac{d\mathbf{k}'}{k'^2-k_0^2}$$
$$\times\exp[i(\mathbf{r}_n-\mathbf{r}_m)\cdot\mathbf{k}']u(\mathbf{k}-\mathbf{k}')G_m(\mathbf{k}'). \quad (45)$$

Let $G_n^{(m)}$ be defined as the formal solution of

$$G_n^{(m)}(\mathbf{k})-\int_h\frac{d\mathbf{k}'}{k'^2-k_0^2}u(\mathbf{k}-\mathbf{k}')G_n^{(m)}(\mathbf{k}')$$
$$=\int_h\frac{d\mathbf{k}'}{k'^2-k_0^2}\exp[i(\mathbf{r}_n-\mathbf{r}_m)\cdot\mathbf{k}']u(\mathbf{k}-\mathbf{k}')G_m(\mathbf{k}') \quad (46)$$

and

$$G_n^{inc}-\int_h\frac{d\mathbf{k}'}{k'^2-k_0^2}u(\mathbf{k}-\mathbf{k}')G_n^{inc}(\mathbf{k}')$$
$$=u(\mathbf{k}-\mathbf{k}_0)\exp(i\mathbf{r}_n\cdot\mathbf{k}_0), \quad (47)$$

so that

$$G_n=\sum_m G_n^{(m)}+G_n^{inc}. \quad (48)$$

By multiplying Eq. (28) by

$$\frac{\exp[i(\mathbf{r}_n-\mathbf{r}_m)\cdot\boldsymbol{\kappa}]G_m(\boldsymbol{\kappa})}{\kappa^2-k_0^2} \quad (49)$$

and integrating with respect to the parameter $\boldsymbol{\kappa}$, one obtains

$$G_n^{(m)}(\mathbf{k})=\int_h\frac{d\boldsymbol{\kappa}}{\kappa^2-k_0^2}\exp[i(\mathbf{r}_n-\mathbf{r}_m)\cdot\boldsymbol{\kappa}]G_m(\boldsymbol{\kappa})\alpha(\mathbf{k},\boldsymbol{\kappa})d\boldsymbol{\kappa}, \quad (50)$$

so that

$$G_n(\mathbf{k})=\alpha(\mathbf{k},\mathbf{k}_0)\exp(i\mathbf{r}_n\cdot\mathbf{k}_0)$$
$$+\sum_{m\neq n}\int_h\frac{d\boldsymbol{\kappa}}{\kappa^2-k_0^2}\exp[i(\mathbf{r}_n-\mathbf{r}_m)\cdot\boldsymbol{\kappa}]G_m(\boldsymbol{\kappa})\alpha(\mathbf{k},\boldsymbol{\kappa}) \quad (51)$$

or, returning to the original notation,

$$F_n(\mathbf{k})=\alpha(\mathbf{k},\mathbf{k}_0)\exp[-i\mathbf{r}_n(\mathbf{k}-\mathbf{k}_0)]$$
$$+\sum_{m\neq n}\int_k \frac{d\kappa}{\kappa^2-k_0^2}\exp[-i\mathbf{r}_n(\mathbf{k}-\kappa)]\alpha(\mathbf{k},\kappa)F_m(\kappa). \quad (52)$$

Equation (52) together with Eq. (42) is a restatement of the multiple scattering problem from which the original potential has been eliminated, and only the function α characterizing the properties of the individual scatterer has been left. It is now possible to drop the restriction to potential scattering and consider α as solution of a much more general problem. For instance, the original interaction hamiltonian may not be diagonal in coordinate representation, or it may be non-hermitian so that it describes particle absorption. Inelastic scattering processes may be described in part by this formalism, by considering all inelastically scattered particles as lost, so that the elastic phase δ_s becomes complex. Of course, the present equations do not account for the particles which have been inelastically scattered at least once. This generalization is clearly approximate also in another respect; every inelastic process changes the state of the scatterer, whereas in our formalism the scatterers have definite time-independent properties. One can assume that the present approximation will be adequate as long as only a small part of the scatterers has been excited. Clearly, the present approximation does not cover such cases as Compton-scattering, which is essentially inelastic.

From the viewpoint of mathematical convenience, if a definite potential is either known or assumed, Eq. (52) is useful when the potential is very large. One may think of impenetrable spheres or very deep potential holes where the large numerical values of U prevents the usual approximation methods, whereas $\alpha(\mathbf{k},\kappa)$ may be quite small.

To illustrate the physical meaning of Eq. (52), the equivalent of the preceding calculation in coordinate representation will be given.

If the potential is given by Eq. (37), the integral equation for scattering, multiplied by V is

$$V\psi+\frac{2m}{\hbar^2 4\pi}V\int\frac{\exp(ik_0r_{12})}{r_{12}}V(\mathbf{r}_2)\psi(\mathbf{r}_2)d\mathbf{r}_2=V\exp(i\mathbf{k}_0\cdot\mathbf{r}). \quad (53)$$

Let

$$V\psi=P \quad (54)$$

and define a set of functions $P_n=\psi(\mathbf{r})v(\mathbf{r}-\mathbf{r}_n)$:

$$P_n+\frac{2m}{4\pi\hbar^2}v(\mathbf{r}-\mathbf{r}_n)\int\frac{\exp(ik_0r_{12})}{r_{12}}P(\mathbf{r}_2)d\mathbf{r}_2$$
$$=v(\mathbf{r}-\mathbf{r}_n)\exp(i\mathbf{k}_0\cdot\mathbf{r}). \quad (55)$$

Summation with respect to n shows that

$$\textstyle\sum_n P_n=P. \quad (56)$$

On the other hand, if Eq. (24) is multiplied by v and the notation

$$p(\mathbf{r},\mathbf{R})=v(\mathbf{r})G(\mathbf{r},\mathbf{R}) \quad (57)$$

is used, we have

$$p(\mathbf{r},\mathbf{R})+\frac{2m}{4\pi\hbar^2}v(\mathbf{r})\int\frac{\exp(ik_0r_{12})}{r_{12}}p(\mathbf{r}_2,\mathbf{R})d\mathbf{r}_2$$
$$=-\frac{2m}{4\pi\hbar^2}v(\mathbf{r})\frac{\exp(ik_0|(\mathbf{r}-\mathbf{R}|)}{|\mathbf{r}-\mathbf{R}|}. \quad (58)$$

By the procedure used in the preceding calculation in momentum space, one shows by comparison of Eqs. (55) and (58) that

$$P_n=\sum_{m\neq n}\int p(\mathbf{r}-\mathbf{r}_n,\mathbf{R})P_m(\mathbf{R}+\mathbf{r}_n)d\mathbf{R}+p(\mathbf{r}-\mathbf{r}_n,\mathbf{k}_0). \quad (59)$$

Here, $p(\mathbf{r},k_0)$ means the solution of Eq. (58) if the source is removed to infinity; i.e., $\exp(ik_0\cdot\mathbf{r})$ is substituted for $1/|\mathbf{r}-\mathbf{R}|[\exp(ik_0|\mathbf{r}-\mathbf{R}|)]$. Equation (59) restates the multiple scattering problem in terms of $p(\mathbf{r},\mathbf{R})$ which is essentially the Green's function of the individual scattering problem. The meaning of Eq. (59) can be seen more clearly if, after summation over n, the original notation is used:

$$v(\mathbf{r}-\mathbf{r}_n)\psi(\mathbf{r})=v(\mathbf{r}-\mathbf{r}_n)\sum_{m\neq n}\int G(\mathbf{r}-\mathbf{r}_n,\mathbf{R})v(\mathbf{R}+\mathbf{r}_n-\mathbf{r}_m)$$
$$\times\psi(\mathbf{R}+\mathbf{r}_n)d\mathbf{R}+v(\mathbf{r}-\mathbf{r}_n)G(\mathbf{r}-\mathbf{r}_n,\mathbf{k}_0). \quad (60)$$

IV. SOLUTION BY ITERATION

The most obvious method for solving Eq. (52) is iteration. In the first approximation, we disregard all integrals on the right-hand side. In the second approximation, the values of F_n so obtained are substituted into the integrals and so forth. It is usually more convenient to consider this solution as a power series in terms of a parameter. For this purpose, let α_0 be a number representative of the order of magnitude of $\alpha(\mathbf{k},\kappa)$. For instance,

$$\alpha_0=\alpha(\mathbf{k}_0,\mathbf{k}_0) \quad (61)$$

or

$$\alpha_0=\left[(1/4\pi)\int\alpha^2(\mathbf{k},\mathbf{k}_0)d\Omega\right]^{\frac{1}{2}}, \quad (62)$$

where the integration extends over a sphere $k^2=k_0^2$. Then we can define a dimensionless function $\bar{\alpha}$ by

$$\alpha=\alpha_0\bar{\alpha}. \quad (63)$$

α_0 has the dimension of a length. If the solution of Eq.

(52) is written as a power series in α_0,

$$F_n=\sum_{l=1}\alpha_0{}^l F_n{}^{(l)}, \tag{64}$$

substitution into Eq. (52) and comparison of coefficients shows that

$$F_n{}^{(1)}=\bar{\alpha}(\mathbf{k},\mathbf{k}_0)\exp[-i\mathbf{r}_n\cdot(\mathbf{k}-\mathbf{k}_0)] \tag{65}$$

and, for $l\neq 1$,

$$F_n{}^{(l)}=\sum_{m\neq n}\int_h\frac{d\boldsymbol{\kappa}}{\kappa^2-k_0{}^2}\exp[-i\mathbf{r}_n\cdot(\mathbf{k}-\boldsymbol{\kappa})]\bar{\alpha}(\mathbf{k},\boldsymbol{\kappa})F_m{}^{(l-1)}. \tag{66}$$

In first approximation, we obtain after summation

$$F^{(1)}(\mathbf{k})=\bar{\alpha}(\mathbf{k},\mathbf{k}_0)\sum\exp[-i\mathbf{r}_n(\mathbf{k}-\mathbf{k}_0)] \tag{67}$$

and, for the scattered wave, by Eq. (8)

$$\psi_{sc}\sim(2\pi^2/r)\exp(ik_0r)\alpha(k_0\mathbf{r}/r,\mathbf{k}_0)\sum\exp[-i\mathbf{r}_n\cdot(\mathbf{k}-\mathbf{k}_0)], \tag{68}$$

i.e., the sum of all waves scattered by the individual scatterers under the influence of the primary wave alone. This is, of course, what one has to expect in the first approximation. It is clear now that our expansion is just the usual expansion into primary, secondary, tertiary, etc., waves, which is usually made for infinitely small scatterers. The expansion (64) is not restricted in this respect. This expansion can be expected to be useful when the number of scattering units is small. Actually, it will be shown that its first term is, under certain practical conditions, sufficient even when N exceeds 10^{15}. However, for extended media other methods must be used which will be discussed in the second part of this paper.

The expansions (64, 65, 66) can be compared to Born's approximation, which is obtained by direct iteration of Eq. (40). Let us again define a parameter such that

$$u=u_0\tilde{u}, \tag{69}$$

where $\tilde{u}$ is dimensionless, and u_0 has the dimension of a length. For instance,

$$u_0=u(0). \tag{70}$$

We have then the expansion

$$F=\sum_{l=1}u_0{}^l F^{(l)} \tag{71}$$

and

$$F^{(1)}=\tilde{u}(\mathbf{k}-\mathbf{k}_0)\sum\exp[-i\mathbf{r}_n(\mathbf{k}-\mathbf{k}_0)], \tag{72}$$

$$(l\neq 1)\quad F^{(l)}=\int_h\frac{d\mathbf{k}'}{k'^2-k_0{}^2}\sum\exp[-i\mathbf{r}_n\cdot(\mathbf{k}-\mathbf{k}')]\times\tilde{u}(\mathbf{k}')F^{(l-1)}(\mathbf{k}'). \tag{73}$$

The convergence of the two series will depend on the value of the parameters α_0 and u_0, respectively, and on the rapidity of decrease of $\bar{\alpha}$ and $\tilde{u}$, respectively, for large values of $\mathbf{k}'$. When the potential is very large, as for impenetrable spheres, u_0 is also very large, whereas α_0 may be quite small. To obtain an idea of the magnitude of α_0, let us consider the case of very small scatterers. If we use the definition (61), then, by Eqs. (28) and (6)

$$\alpha_0=\alpha(\mathbf{k}_0,\mathbf{k}_0)=f(\mathbf{k}_0) \tag{74}$$

and since for small scatterers only S-scattering is important,

$$f(\mathbf{k}_0)=f_0(k_0)=\frac{1}{4\pi^2ik_0}[\exp(2i\delta_0)-1] \tag{75}$$

by Eqs. (10) and (21). If, in addition, δ_0 is small, we have

$$\alpha_0\approx\frac{\delta_0}{2\pi^2k_0}, \tag{76}$$

so that α_0 is of the order of $(1/2\pi^2)$ times the scattering length. Thus, where the potential is large but the individual scattering length is small, the expansion (64–66) is preferable to the Born approximation.

To discuss the second element mentioned above, we may consider the extreme case where the scatterers are represented by delta-functions. Then, the second Born approximation diverges already for the single scatterer; it is easy to verify that this holds for $F^{(2)}$ in Eq. (73). However, Eq. (66) gives

$$F_n{}^{(2)}=\int_h\frac{d\boldsymbol{\kappa}}{\kappa^2-k_0{}^2}\bar{\alpha}(\boldsymbol{\kappa},\mathbf{k}_0)\bar{\alpha}(\mathbf{k},\boldsymbol{\kappa})\exp[-i\mathbf{r}_n\cdot(\mathbf{k}-\boldsymbol{\kappa})]\times\sum_m\exp[-i\mathbf{r}_m\cdot(\boldsymbol{\kappa}-\mathbf{k}_0)]-\exp[-i\mathbf{r}_n(\mathbf{k}-\mathbf{k}_0)] \tag{77}$$

and by summation

$$F^{(2)}=\int_h\frac{d\boldsymbol{\kappa}}{\kappa^2-k_0{}^2}\bar{\alpha}(\boldsymbol{\kappa},\mathbf{k}_0)\bar{\alpha}(\mathbf{k},\boldsymbol{\kappa})\times[S(\mathbf{k}-\boldsymbol{\kappa})S(\boldsymbol{\kappa}-\mathbf{k}_0)-S(\mathbf{k}-\mathbf{k}_0)], \tag{78}$$

where

$$S(\mathbf{k})=\textstyle\sum_n\exp(-i\mathbf{r}_n\cdot\mathbf{k}). \tag{79}$$

This equation holds in general; if, in particular, the scatterer becomes vanishingly small, $\bar{\alpha}$ becomes a constant (equal to one, if α_0 is chosen as in Eqs. (61) or (62)). But $F^{(2)}$ still converges, because

$$S(\mathbf{k}-\boldsymbol{\kappa})S(\boldsymbol{\kappa}-\mathbf{k}_0)-S(\mathbf{k}-\mathbf{k}_0)=\sum_{m\neq n}\exp[-i\mathbf{r}_n(\mathbf{k}-\boldsymbol{\kappa})+i\mathbf{r}_m(\mathbf{k}_0-\boldsymbol{\kappa})] \tag{80}$$

has oscillating terms only. This oscillating behavior is sufficient to make the integral converge, as one can easily verify. The corresponding formula in Born's

approximation is

$$F^{(2)}=\int_h \frac{d\boldsymbol{\kappa}}{\kappa^2-k_0^2}\bar{u}(\boldsymbol{\kappa}-\mathbf{k}_0)\bar{u}(\mathbf{k}-\boldsymbol{\kappa})S(\mathbf{k}-\boldsymbol{\kappa})S(\boldsymbol{\kappa}-\mathbf{k}_0), \quad (81)$$

which is divergent when $\bar{u}$ becomes a constant. We may conclude, in general, that the expansion (64–66) is preferable when the potential is large or the scatterers small.

On the other hand, one can see intuitively that in the case of largely overlapping scatterers the Born approximation will be preferable; in this case, the interaction of scatterers, disregarded in Eq. (67), is of major importance. Therefore, it would be probably impractical to subdivide the total potential into a sum of individual terms and proceed according to Eqs. (64–66) in the case of electron scattering by a small metal crystal. To illustrate the point by an extreme example: if the scattering by a small homogeneous body is to be calculated, one could arbitrarily subdivide the body into smaller homogeneous cubes, calculate their individual scattering amplitudes α and use the expansion (64), but this would clearly be impractical, even though the expansion finally may converge to the correct result.

Comparison of first approximation (67) with the first Born approximation (72) admits the following simple interpretation: given a number of scatterers with potential v, one defines an "effective potential" $\alpha(\mathbf{k}, \boldsymbol{\kappa})$ in momentum space, and proceeds by iteration of the scattering equation (40) [where $\alpha(\mathbf{k}, \mathbf{k}')$ has been substituted for $u(\mathbf{k}-\mathbf{k}')$]. In particular, for very small scatterers, the effective potential is the constant α_0. In the latter case, one can even define a potential in coordinate space which is a delta-function, whereas in general the transformation into coordinate space of an equation of the type (40) with $\alpha(\mathbf{k}, \mathbf{k}')$ substituted for $u(\mathbf{k}-\mathbf{k}')$ would lead to an integro-differential equation; in other words, the interaction matrix $\alpha(\mathbf{k}, \mathbf{k}')$ is no longer diagonal in coordinate representation.

For the case of slow neutron scattering by nuclei, the above interpretation is widely used in scattering calculations: when more than one kind of nucleus exists, one can make the obvious generalization and replace each nucleus by a delta-function with appropriate constant factor, essentially the scattering length.

However, this interpretation holds only for the first approximation; the higher terms are different, as shown for instance by comparison between Eqs. (78) and (81) (where $\bar{\alpha}$ is to be substituted for $\bar{u}$). A similar result was obtained by Breit[10] in connection with the scattering of a neutron by a bound proton: Fermi's replacement of the actual interaction by an effective delta-function is correct only if one uses Born's *first* approximation with the effective potentials.

However, a somewhat modified rule for the equivalent potential for small scatterers can be stated as follows:

[10] G. Breit, Phys. Rev. **71**, 215 (1947).

The integrand (78) consists of terms

$$\frac{1}{\kappa^2-k_0^2}\exp(-i\mathbf{r}_{mn}\cdot\boldsymbol{\kappa}),$$

which contribute very little beyond a limit $|\boldsymbol{\kappa}_m|\gg k_0$, $|\boldsymbol{\kappa}_m|\gg 1/r_{mn}$, since the denominator has become almost constant, and a large number of periods of the oscillatory function cancel each other. Hence, the integral can be cut off at this limit. On the other hand, the constant term $S(\mathbf{k}-\mathbf{k}_0)$ contributes only N terms as against the first term in brackets which contributes N^2 terms. Thus, if the number of scatterers is not too small, the second term is negligible in the domain where all terms contribute about evenly. Therefore, $F^{(2)}$ can be written

$$F^{(2)}\approx\alpha_0^2\int_h^{|\kappa_m|}\frac{d\boldsymbol{\kappa}}{\kappa^2-k_0^2}S(\mathbf{k}-\boldsymbol{\kappa})S(\boldsymbol{\kappa}-k_0); \quad (82)$$

and this has the same form as Born's second approximation, with a cutoff $|\boldsymbol{\kappa}_m|\gg k_0, 1/r_{mn}$. It can be shown similarly that the higher approximations can be written formally like terms of the Born approximation with a cutoff of the same order.

Thus we can formulate the following heuristic rule: replace the actual potential by the "effective potential" α_0 and proceed by Born's approximation, cutting off all integrals at some value $\kappa\gg 1/r_{mn}, k_0$. In many cases, as in the following application, the result is quite insensitive toward the exact point of cutoff.

V. SCATTERING OF THERMAL NEUTRONS BY SMALL CRYSTALS (SECOND APPROXIMATION)

The nuclear scattering of neutrons by crystals is well understood in the two extreme ranges of very small and very large crystals.[1,11] In addition, the theory of an infinitely extended plane-parallel plate of finite thickness has been adapted from the dynamical theory of x-rays.[1] No results for three-dimensional crystals of intermediate size are available. In this section, the preceding results will be used to calculate in second approximation the intensity scattered by a spherical crystal, for a special orientation of the primary ray with respect to the crystal.

Because of the small size of the nuclei, $\bar{\alpha}$ can be set equal to one. We shall consider a simple Bravais lattice; a generalization for a composite lattice would be obvious. The function $S(\mathbf{k})$ can be written

$$S=\sum c_n\exp(-i\mathbf{a}_n\cdot\mathbf{k}), \quad (83)$$

where $\mathbf{a}_n$ are the lattice vectors and c_n is unity inside, and zero outside the sphere of radius ρ. By Poisson's sum formula[12]

$$S=\sum_m s(\mathbf{k}-2\pi\mathbf{A}_m), \quad (84)$$

[11] G. C. Wick, Physik. Z. **38**, 403, 689 (1937).

[12] S. Bochner, *Vorlesungen über Fouriersche Integrale* (Leipzig, 1932), p. 203.

where $\mathbf{A}_m$ are the reciprocal lattice vectors, and s is the fourier transform of the function $c(\mathbf{r})$ which interpolates the discrete values c_n:

$$s(\mathbf{k})=(1/v)\int c(\mathbf{r})\exp(-i\mathbf{k}\cdot\mathbf{r})d\mathbf{r}$$

$$=(1/v)\int_0^\rho r^2\exp(-i\mathbf{k}\cdot\mathbf{r})drd\Omega$$

$$=\frac{4\pi}{k^3v}(\sin k\rho-k\rho\cos k\rho)=\frac{-4\pi}{vk}\frac{d}{dk}\left(\frac{\sin k\rho}{k}\right), \qquad (85)$$

v being the volume of the unit cell.[13]

We consider the value of the second approximation for a direction close to the incident beam ($\mathbf{k}=\mathbf{k}_0+\mathbf{p}$) in the case when the crystal is exactly in reflecting position; i.e., one reciprocal lattice point satisfies the condition

$$(\mathbf{k}_0+2\pi\mathbf{A}_1)^2-k_0^2=0. \qquad (86)$$

We have

$$S(\mathbf{k}-\boldsymbol{\kappa})=S(\mathbf{k}_0-\boldsymbol{\kappa})+\mathbf{p}\cdot\nabla S(\mathbf{k}_0-\boldsymbol{\kappa})$$
$$=\sum s(\mathbf{k}_0-\boldsymbol{\kappa}-2\pi\mathbf{A}_m)+\mathbf{p}\cdot\sum\nabla s(\mathbf{k}_0-\boldsymbol{\kappa}-2\pi\mathbf{A}_m). \qquad (87)$$

In the integral (78) this is multiplied by $S(\boldsymbol{\kappa}-\mathbf{k}_0)=\sum s(\mathbf{k}_0-\boldsymbol{\kappa}-2\pi\mathbf{A}_m)$. Since the function s decreases rapidly from its maximum value at the origin, only the immediate neighborhood of those points $\boldsymbol{\kappa}$ will be of importance which make the argument of one of the terms vanish. But the gradient of s at that point vanishes by Eq. (85), so that the second term in (87) is negligible. Thus, the value of $F^{(2)}$ in the neighborhood of the forward direction is approximately constant, and we have

$$F^{(2)}=\int_h\frac{d\boldsymbol{\kappa}}{\kappa^2-k_0^2}[|S(\mathbf{k}-\boldsymbol{\kappa})|^2-S(0)]. \qquad (88)$$

The range of values $|\mathbf{p}|$ for which $F^{(2)}$ is constant can be estimated by determining the point at which $s(k)$ begins to decrease noticeably from its peak value. By Eq. (85), the first zero is the first root of

$$\tan k\rho=k\rho.$$

Thus, Eq. (88) may be considered correct for a range of the order of $|\mathbf{p}|\rho\leq 2$.

We consider now $F^{(2)}$ for values of $\mathbf{k}$ close to the reflecting point, i.e., $\mathbf{k}=\mathbf{k}_0+2\pi\mathbf{A}_1+\mathbf{p}$. From the geometry it can be seen that this case is symmetric to the previous one, so that Eq. (88) holds also for the neighborhood of the reflecting direction, and for the same range. Of the terms in the sum (84), only the two with $m=0$ and $m=1$ are important, because the corresponding reciprocal points are on the Laue sphere $\kappa^2=k_0^2$. All other contributions are much smaller, and we shall take them into account in a summary manner, by using the average value of $|S|^2$ over a cell of the reciprocal lattice, rather than the exact function. Since, by Eq. (83), S is periodic in momentum space, we can use Parseval's theorem to obtain

$$\langle|S|^2\rangle=v\int_{\text{cell}}|S|^2d\mathbf{k}=\sum|c_n|^2=N. \qquad (89)$$

By inspection of Eq. (83) this can be seen to be also the value of $S(0)$, so that the contributions of the two terms in the integrand cancel for the more remote reciprocal lattice points. This example illustrates the general theory of the preceding section: we would have obtained the same result by cutting off the integral and disregarding the contributions of all points $\mathbf{A}_m$, $m\neq 0, 1$. However, the naive use of Born's approximation would have led to a divergent integral. It is true that taking into account the finite nuclear radius one would obtain a function $\bar{\alpha}$ decreasing asymptotically so that the integral would converge; but then, the Born approximation would be incorrect (in most cases far too large) although finite.

To evaluate the contribution of the two remaining reciprocal lattice points, we set

$$\mathbf{k}_0+2\pi\mathbf{A}_1=\boldsymbol{\kappa}_1, \qquad (90)$$

and remember that the point $\boldsymbol{\kappa}=\boldsymbol{\kappa}_1$ is exactly on the Laue sphere. By Eq. (84)

$$|S(\mathbf{k}_0-\boldsymbol{\kappa})|^2=|s(\boldsymbol{\kappa}-\mathbf{k}_0)+s(\boldsymbol{\kappa}-\boldsymbol{\kappa}_1)|^2$$
$$\approx|s(\boldsymbol{\kappa}-\mathbf{k}_0)|^2+|s(\boldsymbol{\kappa}-\boldsymbol{\kappa}_1)|^2, \qquad (91)$$

since, owing to the rapid decrease of s, the overlap is negligible. In carrying out the integration, the sphere $\kappa^2=k_0^2$ can be replaced by its tangent plane, because the range of s is small against the radius k_0. The two contributions to $|S|^2$ have spherical symmetry with respect to the two points $\mathbf{k}_0$ and $\boldsymbol{\kappa}_1$, respectively, which are both situated on the sphere. Hence, the principal value contributes nothing to the integral (88), and we are left with

$$F^{(2)}=\frac{\pi i}{2k_0}\int d\sigma[|s(\boldsymbol{\kappa}-\mathbf{k}_0)|^2+|s(\boldsymbol{\kappa}-\boldsymbol{\kappa}_1)|^2-S(0)], \qquad (92)$$

the integral being extended over the sphere of radius k_0. In using the tangent plane approximation for the second term, we choose as new origin for a system of plane polar coordinates r, ϕ the point $\boldsymbol{\kappa}=\boldsymbol{\kappa}_1$, so that

$$\int d\sigma|s(\boldsymbol{\kappa}-\boldsymbol{\kappa}_1)|^2=2\pi\int_0^\infty rdrs^2(r)$$
$$=2\pi\left(\frac{4\pi}{v}\right)^2\int_0^\infty\frac{dr}{r}\left[\frac{d}{dr}\left(\frac{\sin\rho r}{r}\right)\right]^2. \qquad (93)$$

[13] This is a simplified derivation of a result obtained previously by A. L. Patterson, Phys. Rev. **56**, 972 (1939), and H. Ekstein, Cahiers phys. **B**, 33 (1942).

This integral can be calculated by differentiation with respect to the parameter ρ, giving

$$\int d\sigma |s(\kappa-\kappa_1)|^2 = 2\pi(4\pi/v)^2(\rho^4/4). \tag{94}$$

The first term gives obviously the same contribution, so that

$$F^{(2)} = 2i(2\pi^2/v)^2(\rho^4/k_0) - i2\pi^2 k_0 N. \tag{95}$$

The second term is entirely negligible; this illustrates the rule of the preceding section; we would have obtained the same result by merely cutting off and dropping the term $S(0)$.

The second approximation is here entirely due to radiation damping. As a consequence, the second term in the expansion of $|\psi_{ee}|^2$, proportional to α_0^3, vanishes for real α_0, as one sees immediately by forming the square modulus of $\alpha_0 F^{(1)} + \alpha_0^2 F^{(2)}$. Therefore, it is necessary to calculate the third approximation $F^{(3)}$ in order to obtain the first nonvanishing correction to the scattered intensity.

For this calculation, we use the rule stated in Sec. IV to limit the integration to the neighborhood of the sphere $\kappa^2 = k_0^2$. We have

$$F^{(3)} = \int_k \frac{d\kappa}{\kappa^2 - k_0^2} S(\kappa_1 - \kappa) F^{(2)}(\kappa), \tag{96}$$

where we consider only the exact Laue reflecting direction. Again, we have only the contributions of the neighborhood of κ_1 and $\mathbf{k}_0$; and again, because of the symmetry with respect to the tangent plane of the Laue sphere, the principal value is negligible. According to the previous result, $F^{(2)}$ is approximately constant for a distance $r\rho \approx 2$ from either $\kappa = \kappa_1$ or $\mathbf{k}_0$. For this range, we can use the peak value

$$s(0) = 4\pi\rho^3/3v$$

to approximate S. Hence, by analogy to Eq. (92)

$$F^{(3)} \approx \frac{2\pi i}{2k_0} F^{(2)} \frac{4\pi}{v} \frac{\rho^3}{3} \int_0^{2/\rho} 2\pi r dr = -\frac{2^6\pi^7\rho^5}{k_0^2 v^3}, \tag{97}$$

the factor 2 being due to the contribution of the two lattice points. For the absolute square of the amplitude, the argument of the complex number α_0 is of importance. According to Eqs. (74) and (75), α_0 is, strictly speaking, never real, not even in the case of pure potential scattering, because of radiation damping, and even less when absorption is present. However, for small absorption and small phase δ_0, the imaginary part is small, of second order. In this case, according to Eqs. (64), (67), (95), and (97)

$$|F|^2 = \alpha_0^2 \frac{(4\pi)^2\rho^6}{9v^2} - \alpha_0^4 \frac{7\cdot 2^6\pi^8\rho^8}{9v^4 k_0^2}. \tag{98}$$

By introducing the number of atoms per cm^3

$$n = 1/v, \tag{99}$$

the scattering length

$$a = 2\pi^2\alpha_0, \tag{100}$$

and the wavelength

$$\lambda = 2\pi/k_0, \tag{101}$$

Eq. (98) simplifies:

$$|F|^2 = \left(\frac{2an\rho^3}{3\pi}\right)^2 [1 - (7/4)(an\lambda\rho)^2]. \tag{102}$$

In a typical case, $n = 3\times 10^{22}$, $\lambda = 1.5\times 10^{-8}$, $a = 10^{-12}$, with a particle diameter $2\rho = 10\mu$, the second term amounts only to 9 percent. Thus, the range of validity of the first approximation is larger than is frequently assumed in cautious estimates.[14] This fact is caused by the vanishing of the term proportional to α_0^3. It is true that our calculation concerns only the intensity in exact Laue position, whereas for comparison with experiment an integration over all crystal orientations would be necessary. However, it is probable that the exact Laue orientation is the "worst" case with respect to the importance of higher order terms.

That the corrective term is negative is what one would expect: for sufficiently large crystals the intensity must become proportional to ρ^2 rather than to ρ^6. Hence, if the crystal is large enough so that the second term matters, the intensity must be smaller than if this term had been omitted.

[14] Fermi, Sturm, and Sachs, Phys. Rev. **71**, 589 (1947).

A Remark on the Conventional Perturbation Theory

SHI-SHU WU
Department of Physics, University of Illinois, Urbana, Illinois
(Received January 22, 1951)

It is shown that Dyson's S-matrix theory can also be attained by the perturbation method used in the conventional field theory formalism.

I. INTRODUCTION

ONE can show explicitly in a step-by-step way that the conventional perturbation theory is just Dyson's S-matrix theory[1] and that the Feynman[2]-Dyson rules are the rules which have been used conventionally. Recently, Yang and Feldman[3] and Källen[4] have succeeded in formulating the S-matrix theory directly in the Heisenberg representation; our arguments have then the same advantages as theirs because we start from the Schrödinger representation.

II. RÉSUMÉ OF THE CONVENTIONAL PERTURBATION METHOD

The Schrödinger representation will be used; the hamiltonian density $H(\mathbf{x})$ and the hamiltonian

$$\bar{H}=\int d^3x H(\mathbf{x})$$

are all time-independent. The expression $\Phi(t)$ denotes the Schrödinger time-dependent functional; $\{\Phi_n^0(q)\}$ is a complete orthonormal set of solutions of the stationary Schrödinger eigenvalue problem $\bar{H}_0\Phi_n^0(q)=E_n\Phi_n^0(q)$. The index n indicates the set of quantum numbers which characterize the state $\Phi_n^0(q)$. Further, we shall always use the subscripts 0 and 1 to refer, respectively, to free fields and interaction terms.

Instead of putting the initial time $t_0=0$ as is usually done, we shall take $t_0=-\infty$. Certain precautions are then to be taken concerning the indeterminacy of $\exp(-i\hbar^{-1}E_nt)$ at $t=\pm\infty$. However, they are conventional; on some occasions one multiplies the integrand by a factor $\exp(-\epsilon|t|)$ with $\epsilon>0$ and one then takes the limit $\epsilon\to+0$ after the integration, while in other cases one may simply imagine that $\pm\infty$ is $\pm T$, because the value of T will not appear in the final results or $\exp(\pm i/\hbar E_nT)$ will merely be a constant phase factor.

The following Eqs. (1) and (2) are well known.[5] Let

$$\Phi(t)=\textstyle\sum_n A_n(t)\exp(-i/\hbar E_nt)\Phi_n^0(q).$$

From the Schrödinger equation

$$i\hbar\partial\Phi(t)/\partial t=(\bar{H}_0+\bar{H}_1)\Phi(t),$$

we have

$$i\hbar\dot{A}_f(t)=\textstyle\sum_i A_i(t)\exp(i/\hbar(E_f-E_i)t)\bar{H}_{fi}{}^1, \qquad (1)$$

where

$$\bar{H}_{fi}{}^1=(\Phi_f{}^0,\bar{H}_1\Phi_i{}^0).$$

Let us define

$$\bar{H}_{fi}{}^1=\lim_{\epsilon\to1-0}(\epsilon\bar{H}_{fi}{}^1)=\bar{H}_{fi}{}^1$$

and

$$A_i(t)=\lim_{\epsilon\to1-0}[A_i{}^{(0)}(t)+\epsilon A_i{}^{(1)}(t)+\epsilon^2A_i{}^{(2)}(t)+\cdots]$$
$$=A_i{}^{(0)}(t)+A_i{}^{(1)}(t)+A_i{}^{(2)}(t)+\cdots.$$

We obtain as a solution of (1):

$$A_f{}^{(0)}(t)=A_f{}^{(0)}(-\infty)=\text{const.},$$

$$A_f{}^{(k)}(t)=(1/i\hbar)^k\textstyle\sum_i\Big\{\sum_{\phi(k-1)}\sum_{\phi(k-2)}\cdots\sum_{\phi(1)}\int_{-\infty}^{t}d\tau_k\bar{H}^1{}_{f\phi(k-1)}\exp[i\hbar^{-1}(E_f-E_{\phi(k-1)})\tau_k]$$
$$\times\int_{-\infty}^{\tau_k}d\tau_{k-1}\bar{H}^1{}_{\phi(k-1)\phi(k-2)}\exp[i\hbar^{-1}(E_{\phi(k-1)}-E_{\phi(k-2)})\tau_{k-1}]\cdots$$
$$\times\int_{-\infty}^{\tau_2}d\tau_1\bar{H}^1{}_{\phi(1)i}\exp[i\hbar^{-1}(E_{\phi(1)}-E_i)\tau_1]\Big\}A_i{}^{(0)}(-\infty), \qquad (2)$$

where the superscripts $k=1, 2, \cdots$ indicate the order of approximation. One may also write

$$A_m(t)=\textstyle\sum_n\bar{S}_{mn}'(t)A_n{}^{(0)}(-\infty), \qquad (3)$$

which at the same time serves to define the matrix

$$\bar{S}'(t)=\{\bar{S}_{mn}'(t)\}.$$

We note that $\bar{S}'(-\infty)=1$, and since in the S-matrix theory only stationary problems are considered, $\bar{S}'(\infty)$ (with a slight change as will be mentioned later) can be

[1] F. J. Dyson, Phys. Rev. **75**, 486 (1949); **75**, 1736 (1949).
[2] R. P. Feynman, Phys. Rev. **76**, 749 and 769 (1949).
[3] C. N. Yang and D. Feldman, Phys. Rev. **79**, 972 (1950).
[4] G. Källen, Arkiv f. Fysik **19**, 187 (1950).
[5] W. Pauli, Handbuch der Physik Bd. **24** (2te Auflage), p. 158.

shown to be equivalent to Dyson's S-matrix $U(\infty)$. Since $\bar{H}_1=\int d^3x H_1(\mathbf{x})$ is time-independent and

$$\int_{-\infty}^{\infty} d\tau_k \exp[ih^{-1}(E_f-E_{\phi(k-1)})\tau_k]\int_{-\infty}^{\tau_k} d\tau_{k-1}\exp[ih^{-1}(E_{\phi(k-1)}-E_{\phi(k-2)})\tau_{k-1}]\cdots\int_{-\infty}^{\tau_2} d\tau_1\exp[ih^{-1}(E_{\phi(1)}-E_i)\tau_1]$$

$$=\frac{\int_{-\infty}^{\infty} d\tau_k \exp[ih^{-1}(E_f-E_i)\tau_k]}{(ih^{-1})^{k-1}(E_{\phi(k-1)}-E_i)(E_{\phi(k-2)}-E_i)\cdots(E_{\phi(1)}-E_i)}=\frac{2\pi}{(ih^{-1})^{k-1}}\cdot\frac{h\delta(E_f-E_i)}{(E_{\phi(k-1)}-E_i)\cdots(E_{\phi(1)}-E_i)}$$

where, in doing the integration, we have made use of the device

$$\lim_{\epsilon\to+0}[\exp(-\epsilon|t|)].$$

In essence, this just corresponds to throwing away the transients in the customary procedure. We observe that the so-called matrix element of kth order in the conventional perturbation theory, multiplied by the δ-function between the energies of the initial and final state, can be also written as follows:

$$ME^{(k)}\delta(E_f-E_i)=\sum_{\phi(k-1)}\sum_{\phi(k-2)}\cdots\sum_{\phi(1)}\frac{\bar{H}^1{}_{f\phi(k-1)}\bar{H}^1{}_{\phi(k-1)\phi(k-2)}\cdots\bar{H}^1{}_{\phi(1)i}\delta(E_f-E_i)}{(E_i-E_{\phi(k-1)})\cdots(E_i-E_{\phi(1)})}$$

$$=(1/(ih)^{k-1}2\pi h)\sum_{\phi(k-1)}\cdots\sum_{\phi(1)}\int_{-\infty}^{\infty}d\tau_k\bar{H}^1{}_{f\phi(k-1)}\exp[ih^{-1}(E_f-E_{\phi(k-1)})\tau_k]\cdots$$

$$\times\int_{-\infty}^{\tau_2}d\tau_1 P^1{}_{\phi(1)i}\exp[ih^{-1}(E_{\phi(1)}-E_i)\tau_1]. \quad (4)$$

Our program is first to show that the customary method of calculation leads exactly to Feynman-Dyson's rules, and then to point out that the S-matrix attained in our way is in full agreement with Dyson's.

III. EQUIVALENCE OF THE CONVENTIONAL METHOD OF CALCULATION AND FEYNMAN-DYSON'S RULES

We will restrict our discussion to quantum electrodynamics. We shall use Heaviside and natural ($h=c=1$) units, and a repeated Greek index is to be summed over 1 to 4, while a repeated Latin index is to be summed only over 1 to 3. Since we follow the conventional formulation of field theory, the groundwork is well known.[6] The total hamiltonian density may be written in the form

$$H(\mathbf{x})=H_0(\mathbf{x})+H_1(\mathbf{x})$$

where, with $\bar{\psi}=\psi^*\beta$, we have

$$H_1(\mathbf{x})=ie\bar{\psi}(\mathbf{x})\gamma_\mu\psi(\mathbf{x})A_\mu(\mathbf{x});\quad(\mathbf{x}=(x,y,z)).^7 \quad (5)$$

The quantization of the electron field is the ordinary one according to Pauli's exclusion principle.[7] For the electromagnetic field we shall follow a treatment by Gupta,[8] where an indefinite metric has been introduced for the scalar photon part. Let us introduce the following fourier expansions:

$$\psi(\mathbf{x})=(2\pi)^{-\frac{3}{2}}\int d^3p\sum_{s=1}^{4}f(\mathbf{p},s)u(\mathbf{p},s)\exp(i\mathbf{p}\cdot\mathbf{x}),$$

$$\psi^*(\mathbf{x})=(2\pi)^{-\frac{3}{2}}\int d^3p\sum_{s=1}^{4}f^*(\mathbf{p},s)u^*(\mathbf{p},s)\exp(-i\mathbf{p}\cdot\mathbf{x}),$$

$$A_i(\mathbf{x})=(2\pi)^{-\frac{3}{2}}\int d^3q[2|\mathbf{q}|]^{-\frac{1}{2}}\times\{C_i(\mathbf{q})\exp(i\mathbf{q}\cdot\mathbf{x})+C_i^+(\mathbf{q})\exp(-i\mathbf{q}\cdot\mathbf{x})\},$$

$$A_0(\mathbf{x})=i^{-1}A_4(\mathbf{x})=(2\pi)^{-\frac{3}{2}}\int d^3q[2|\mathbf{q}|]^{-\frac{1}{2}}\times\{C(\mathbf{q})\exp(i\mathbf{q}\cdot\mathbf{x})+C_0^+(\mathbf{q})\exp(-i\mathbf{q}\cdot\mathbf{x})\},$$

where $u^*(p,s)$ and $u(p,s)$ are the Dirac plane wave spinors, and an asterisk will always be used to denote a hermitian conjugate, while a dagger denotes an adjoint. $f^*(p,s)$ and $f(p,s)$ are, respectively, the creation and annihilation operators for the electron field, $f^*(p,s)f(p,s)$ represents the number of electrons of momentum $\mathbf{p}$ at the spin state s (due to our fourier expansions this number is to be understood, here as well as for the electromagnetic field, as the number per unit volume in wave number space), and $[f(p,s),f^*(p',s')]_+=\delta_{pp'}\delta_{ss'}$ etc. For the photon field, C_μ and $C_\mu{}^+$ are still annihilation and creation operators ($\mu=1,2,3,$ and 4), while $C_i{}^+C_i$ ($i=1,2,$ or 3) represents the number of photons associated with the ith component; the number of scalar photons is now given by $-C_0{}^+C_0$. The com-

[6] G. Wentzel, *Quantum Theory of Fields* (Interscience Publishers, Inc., New York, 1949).

[7] Following Dyson (reference 1) we have deliberately not chosen the charge conjugate expression.

[8] S. N. Gupta, Proc. Phys. Soc. (London) **63**, 681 (1950); also K. Bleuler, Helv. Phys. Acta **23**, 567 (1950). Note: Our intention is only to obtain $(\bar{P}(A_\mu(x)A_\nu(y)))_0=\frac{1}{2}\delta_{\mu\nu}D_F(x-y)$ in a simple and more satisfactory way; that this can be equally well accomplished for our purpose without introducing any indefinite metric, see S. T. Ma, Phys. Rev. **80**, 729 (1950) and other literature quoted by him.

mutation relations are

$$[C_1(q), C_1^+(q)]_-=[C_2(q), C_2^+(q)]_- =[C_3(q), C_3^+(q)]_-=1,$$
$$[C_0(q), C_0^+(q)]_-=-1,$$

with all other commutators being zero. As far as the perturbation calculation is concerned, no complications are involved.[8]

Before proceeding, we would like to make the following remarks:

$$\bar{H}^1{}_{\phi(j)\phi(j-1)} \exp[i(E_j-E_{j-1})t]$$
$$=(\Phi_j^0, \bar{H}_1 \exp[i(E_j-E_{j-1})t]\Phi_{j-1}^0)=(\Phi_j^0, \bar{H}_1(t)\Phi_{j-1}^0),$$

where $\bar{H}_1(t)=\int d^3x H_1(\mathbf{x}, t)$ and $H_1(\mathbf{x}, t)$ is obtained from $H_1(x)$ by the substitution that replaces every $\exp(i\mathbf{k}\cdot\mathbf{x})$ by $\exp(ik_\mu x_\mu)$ and every $\exp(-i\mathbf{k}\cdot\mathbf{x})$ by $\exp(-ik_\mu x_\mu)$, with $x_\mu=(\mathbf{x}, it)$, $k_\mu=(\mathbf{k}, ik_0)$ and $\mathbf{k}$ standing either for $\mathbf{p}$ or for $\mathbf{q}$. It is clear that this is true. For instance, if Φ_{j-1}^0 goes to Φ_j^0 by the transition in which a positive energy electron (p_1, $s_1=1$ or 2) absorbs a transverse photon (q, $i=1$ or 2, say) and goes to a new positive energy state (p_2, $s_2=1$ or 2), then

$$E_j-E_{j-1}=(p_2^2+K^2)^{\frac{1}{2}}-\{(p_1^2+K^2)^{\frac{1}{2}}+|q|\}.$$

We also have

$$(\Phi_j^0, \bar{H}_1 \exp[i(E_j-E_{j-1})t]\Phi_{j-1}^0)$$
$$=\Big(\Phi_j^0, (2\pi)^{-9/2}ie\int d^3x f^*(\mathbf{p}_2, s_2)f(\mathbf{p}_1, s_1)$$
$$\times\bar{u}(\mathbf{p}_2, s_2)\gamma_\epsilon u(\mathbf{p}_1, s_1)C_\epsilon(\mathbf{q})[2|\mathbf{q}|]^{-\frac{1}{2}}$$
$$\times\exp[-i\mathbf{p}_2\cdot\mathbf{x}+i(p_2^2+K^2)^{\frac{1}{2}}t+i\mathbf{p}_1\cdot\mathbf{x}$$
$$-i(p_1^2+K^2)^{\frac{1}{2}}t+i\mathbf{q}\cdot\mathbf{x}-i|q|t]\Phi_{j-1}^0\Big)$$
$$=\Big(\Phi_j^0, \int d^3x ie\bar{\psi}(\mathbf{x}, t)\gamma_\mu\psi(\mathbf{x}, t)A_\mu(\mathbf{x}, t)\Phi_{j-1}^0\Big),$$

because the other terms in the corresponding fourier expansions of $\bar{\psi}(\mathbf{x})$, $\psi(\mathbf{x})$ and $A_\mu(\mathbf{x})$ contribute nothing by the orthogonality of $\{\Phi_n^0(q)\}$. K is the mass of electron and i is either 1 or 2 and not to be summed.

$$\delta_+(a)=(2\pi)^{-1}\int_0^\infty dt\exp(-iat)=1/2\delta(a)+1/2\pi ia$$
$$\times\int_{-\infty}^{\infty}dk_0\exp(\pm ik_0t)\delta_+(k_\mu^2+K^2)$$
$$=\begin{cases}\exp(-i|E|t)/2|E| & \text{if } t>0\\ \exp(+i|E|t)/2|E| & t<0\end{cases} \quad (6_1)$$
$$\times\int_{-\infty}^{\infty}dk_0\exp(\pm ik_0t)\delta_+(k_\mu^2+K^2)k_0$$
$$=\begin{cases}\mp(1/2)\exp(-i|E|t) & \text{if } t>0\\ \pm(1/2)\exp(+i|E|t) & t<0,\end{cases} \quad (6_2)$$

where $E=+(|\mathbf{k}|^2+K^2)^{\frac{1}{2}}$. The derivation of the above equations is trivial.

In the conventional perturbation calculation we observe that in order to accomplish the transition from the initial state (i) to the final state (f), we must have in our matrix element (ME) enough operators to annihilate i and enough operators to create f. Following Dyson, we shall call them free operators. The rest of the operators in ME just cause the so-called virtual effects; in order to yield a nonzero contribution to ME and so to the physical problem under consideration, these operators should occur in pairs, each of which refers to a virtual particle. Customarily, one calculates ME by listing schemes which take account of all the possible ways belonging to the same order of approximation to reach f from i *via* virtual states. Because of momentum conservation ensured by the δ-function contained in $\int d^3x H_1(\mathbf{x})$, some momentum sums reduce to a single term and the calculation becomes easier. We shall keep these δ-functions explicitly, not carrying out the sums over momenta in which they occur. Virtual particles are those that did not exist in the initial state and therefore must have been created first in order to be annihilated (this just corresponds to Dyson's order "P").[1] This statement involves no ambiguity concerning the photon field, because we have followed Gupta's method of quantization.[8,9] However, we can first annihilate one of the negative energy electrons which are always available and fill up the hole again, but then the other way around is prohibited (exclusion principle); in this case the intermediate holes will be thought of as virtual particles. By Eq. (6_1) the contribution to ME due to a virtual photon operator pair (summed over all intermediate states of the virtual photon) can be collected as follows:

$$A_\mu(x)A_\nu(y)\to\delta_{\mu\nu}\int d^3q[(2\pi)^{-1}(2|q|)^{-1}]^2$$
$$\times\exp(iq_\mu x_\mu)\exp(-iq_\mu y_\mu)$$
$$=\delta_{\mu\nu}(2\pi)^{-3}\int d^3q\exp[i\mathbf{q}\cdot(\mathbf{x}-\mathbf{y})](2|\mathbf{q}|)^{-1}$$
$$\times\exp[-i|\mathbf{q}|(t_x-t_y)]$$
$$=\delta_{\mu\nu}(2\pi)^{-3}\int d^3q\exp[i\mathbf{q}\cdot(\mathbf{x}-\mathbf{y})]$$
$$\times\int_{-\infty}^{\infty}dq_0\exp[-iq_0(t_x-t_y)]\delta_+(q_\mu^2)$$
$$=\delta_{\mu\nu}(2\pi)^{-3}\int d^4q\exp[iq_\mu(x_\mu-y_\mu)]\delta_+(q_\mu^2)$$
$$=1/2\delta_{\mu\nu}D_F(x-y), \quad (7)$$

[9] See a discussion by F. J. Belinfante, Phys. Rev. **76**, 226 (1949).

where $t_x > t_y$, because the virtual photon must be created first in order to be annihilated; and $\rightarrow$ means that, so far as the contribution to ME is concerned, a pair $A_\mu(x)A_\nu(y)$ referring to the same virtual photon may be replaced by the right-hand side, which is just Dyson's $\langle P(A_\mu(x)A_\nu(y))\rangle_0$[1]. It should be clear that this is correct and is what one obtains according to the conventional rules, except that one has usually used up the momentum δ-functions earlier and we now keep them there. The contribution to ME from a free photon operator is obvious. In the final result no photon operators will remain in ME. The contribution to ME due to a virtual electron operator pair (summed over all intermediate states of the virtual electron) according to the conventional method of calculation can be rewritten in a similar manner; however, because of the negative energy electrons we need to distinguish two cases:

(a) A Virtual Electron of Positive Energy ($s=1$ and 2) First Created and Then Annihilated

The $\bar{\psi}$ and ψ in ME either are free operators or they just cause virtual effects. The contribution to ME from a free electron operator is simply:

$$(2\pi)^{-\frac{3}{2}}u(p, s)\exp(ip_\mu x_\mu)$$

and

$$(2\pi)^{-\frac{3}{2}}\bar{u}(p, s)\exp(-ip_\mu x_\mu),$$

where $s=1$, 2, 3, or 4. Since the virtual electron of positive energy must be created first in order to be annihilated, the corresponding operator pair must occur in ME in the order $\cdots\psi(x)\cdots\bar{\psi}(y)\cdots$ with $t_x > t_y$; according to the fourier transform and the meaning of $f(p, s)$ and $f^*(p', s')$, only the combination $\cdots f(p, s)\cdots \times f^*(p, s)\cdots$ with the same p and s (here $s=1$ and 2) can give a nonzero contribution. Further, we observe that in the final result all the creation and annihilation operators will be used up and none will remain in ME. Hence the contribution due to the virtual pair can be first indicated as follows:

$$\cdots(2\pi)^{-3}\int d^3p\sum_{s=1}^{2}\exp[ip_\mu(x_\mu-y_\mu)]$$
$$\times\{(\bar{\psi}(x)\gamma_\mu u(p, s))\cdots(\bar{u}(p, s)\gamma_\nu\psi(y))\}\cdots;$$

in this way all the operators $\bar{\psi}$ and ψ will be replaced by the ordinary Dirac plane wave spinors

$$\bar{u}(p', s')=u^*(p', s')\beta$$

and $u(p', s')$ multiplied by $\exp(\pm ip_\mu' x_\mu')$, respectively, and with the corresponding momentum integrals and $\sum_{s'}$ summed over 1 and 2 or over 3 and 4 before them. Let P and Q be two arbitrary matrix operators, and introduce the ordinary projection operator

$$\Lambda^{\pm}(k)=\tfrac{1}{2}[1\pm(\boldsymbol{\alpha}\cdot\mathbf{k}+K\beta)/|E|],$$

where K is mass of electron and $E=+(|\mathbf{k}|^2+K^2)^{\frac{1}{2}}$. We have the well-known relations:

$$\sum_{s=1}^{2}(\bar{u}(p', s')Pu(p, s))(\bar{u}(p, s)Qu(p'', s''))$$
$$=\sum_{s=1}^{2}(\bar{u}_\alpha(p', s')P_{\alpha\gamma}u_\gamma(p, s)\bar{u}_\delta(p, s)Q_{\delta\epsilon}u_\epsilon(p'', s''))$$
$$=\bar{u}_\alpha(p', s')P_{\alpha\gamma}(\Lambda^+(p)\beta)_{\gamma\delta}Q_{\delta\epsilon}u_\epsilon(p'', s'')$$

and

$$\sum_{s=3}^{4}(\bar{u}(p, s)Pu(p', s'))(\bar{u}(p'', s'')Qu(p, s))$$
$$=\sum_{s=1}^{4}(\bar{u}(p, s)Pu(p', s'))(\bar{u}(p'', s'')Q\Lambda^-(p)u(p, s))$$
$$=\sum_{s=3}^{4}(\bar{u}_\alpha(p, s)P_{\alpha\gamma}u_\gamma(p', s')\bar{u}_\delta(p'', s'')Q_{\delta\epsilon}u_\epsilon(p, s))$$
$$=P_{\alpha\gamma}u_\gamma(p', s')\bar{u}_\delta(p'', s'')Q_{\delta\epsilon}(\Lambda^-(p)\beta)_{\epsilon\alpha}.$$

Since, finally, there are no field operators in ME, we can, instead of following the customary procedure, evaluate ME according to the above equations by making the following replacement for each associated pair $\psi_\alpha(x)\bar{\psi}_\beta(y)$ when $t_x > t_y$:

$$\psi_\alpha(x)\bar{\psi}_\beta(y)\rightarrow(2\pi)^{-3}\int d^3p\exp[ip_\mu(x_\mu-y_\mu)](\Lambda^+(p)\beta)_{\alpha\beta}$$
$$=(2\pi)^{-3}\int d^3p\exp[i\mathbf{p}\cdot(\mathbf{x}-\mathbf{y})]\exp[-i|E|(t_x-t_y)]$$
$$\times\tfrac{1}{2}(\beta+(\boldsymbol{\alpha}\cdot\mathbf{p}+K\beta)\beta/|E|)_{\alpha\beta}$$
$$=(2\pi)^{-3}\int d^3p\exp[i\mathbf{p}\cdot(\mathbf{x}-\mathbf{y})]\int_{-\infty}^{\infty}dp_0$$
$$\times\exp[-ip_0(t_x-t_y)]\delta_+(p_\mu^2+K^2)$$
$$\times[p_0\beta+\boldsymbol{\alpha}\cdot\mathbf{p}\beta+K]_{\alpha\beta}$$
$$=-(2\pi)^{-3}\int d^4p\exp[ip_\mu(x_\mu-y_\mu)]\delta_+(p_\mu^2+K^2)$$
$$\times(ip_\mu\gamma_\mu-K)_{\alpha\beta},\quad(8_1)$$

where we have made use of Eqs. (6_1) and (6_2).

(b) A Virtual Hole First Created, Then Annihilated

The corresponding operator pair in ME must now occur in the order $\cdots\bar{\psi}(x)\cdots\psi(y)\cdots$ with $t_x > t_y$, and only the combination $\cdots f^*(p, s)\cdots f(p, s)\cdots$ with the same p and s (here $s=3$ and 4) will yield a nonzero contribution. Following the same procedure as in (a), it is immediately seen that this contribution to ME is equivalent to the following substitution:

$$\bar{\psi}_\alpha(x)\psi_\beta(y)\rightarrow(2\pi)^{-3}\int d^3p\exp[-ip_\mu(x_\mu-y_\mu)](\Lambda^-(p)\beta)_{\beta\alpha}$$
$$=+(2\pi)^{-3}\int d^4p\exp[-ip_\mu(x_\mu-y_\mu)]$$
$$\times\delta_+(p_\mu^2+K^2)(ip_\mu\gamma_\mu-K)_{\beta\alpha}.\quad(8_2)$$

By (8_1) and (8_2), and remembering Dyson's definition and interpretation of the order "P", we observe that Dyson's rule:[3] "replacing each ordered pair $P(\bar{\psi}_\alpha(x)\psi_\beta(y))$ by $\langle P(\bar{\psi}_\alpha(x)\psi_\beta(y))\rangle_0 = 1/2\eta(x,y)S_{F\beta\alpha}(x-y)$" is just what has been done in the conventional method of calculation.

In our discussion above we have left out the sign factor θ_k resulting from

$$f_k\Phi^0_{\text{electron}}(n_1, \cdots, n_k, \cdots) = \theta_k n_k \Phi^0_{\text{electron}}(n_1, \cdots, 1-n_k, \cdots)$$

and

$$f_k^*\Phi^0_{\text{electron}}(n_1, \cdots, n_k, \cdots) = \theta_k(1-n_k)\Phi^0_{\text{electron}}(n_1, \cdots, 1-n_k, \cdots),$$

where $\theta_k = (-1)^{\nu_k}$,

$$\nu_k = \sum_{j=1}^{k=1} n_j,$$

and $k \equiv (p, s)$. However, we notice that if f_k and f_k^* referring to the same virtual particle were adjacent to each other, the resulting sign would be $\theta_k^2 = +1$, while the sign factor resulting from bringing each associated operator pair together and then arranging the order of the pairs in a suitable way for the purpose of calculation can be obtained obviously in the same way as has been amply discussed by Dyson.[1] By the closure theorem we have

$$\sum_j(\Phi_{j+1}{}^0, \bar{H}_1(t)\Phi_j{}^0)(\Phi_j{}^0, \bar{H}_1(t')\Phi_{j-1}{}^0) = (\Phi_{j+1}{}^0, \bar{H}_1(t)\bar{H}_1(t')\Phi_{j-1}{}^0).$$

Hence, if we define the order "P" according to Dyson, we obtain immediately

$$\begin{aligned}
&\sum_{\phi(k-1)}\sum_{\phi(k-2)}\cdots\sum_{\phi(1)}\int_{-\infty}^{\infty} d\tau_k \bar{H}^1{}_{f\phi(k-)}(\tau_k) \\
&\quad\times\int_{-\infty}^{\tau_k} d\tau_{k-1}\bar{H}^1{}_{\phi(k-1)\phi(k-2)}(\tau_{k-1})\cdots \\
&\quad\times\int_{-\infty}^{\tau_2} d\tau_1 \bar{H}^1{}_{\phi(1)i}(\tau_1) \\
&= \left(\Phi_f{}^0, \int_{-\infty}^{\infty} d\tau_k \bar{H}_1(\tau_k)\int_{\infty}^{\tau_k} d\tau_{k-1}\bar{H}_1(\tau_{k-1})\cdots\right. \\
&\quad\left.\times\int_{-\infty}^{\tau_2} d\tau_1 \bar{H}_1(\tau_1)\Phi_i{}^0\right) \\
&= \left(\Phi_f{}^0, \frac{1}{k!}\int_{-\infty}^{\infty} d^4x_1\int_{-\infty}^{\infty} d^4x_2\cdots\int_{-\infty}^{\infty} d^4x_k\right. \\
&\quad\left.\times P(H_1(x_1), H_1(x_2), \cdots, H_1(x_k))\Phi_i{}^0\right) \quad (9)
\end{aligned}$$

and

$$\begin{aligned}
&ME^{(k)}\delta(E_f - E_i) \\
&= (2\pi)^{-1}i^{k-1}\left(\Phi_f{}^0, \frac{(-1)^{k-1}}{k!}\int d^4x_1\cdots\int d^4x_k\right. \\
&\quad\left.\times P(H_1(x_1), \cdots, H_1(x_k))\Phi_i{}^0\right) \quad (10)
\end{aligned}$$

which is an immediate consequence of (4) and (9).

It has been shown by Dyson, purely on the basis of the S-matrix, that the self-energy effects can be formally cancelled in all orders by a constant, independent of the physical situation in which the effects occur. It is clear that his argument can be directly applied to (10), so that the idea of mass renormalization is also formally justified on the basis of the conventional formulation of field theory. According to (2) and (3), we have

$$\begin{aligned}
\bar{S}_{fi}'(\infty) &= \left(\Phi_f{}^0, \sum_{n=0}^{\infty}\frac{(-i)^n}{n!}\int d^4x_1\cdots\int d^4x_n\right. \\
&\quad\left.\times P(H_1(x_1), \cdots, H_1(x_n))\Phi_i{}^0\right). \quad (11)
\end{aligned}$$

Since the self-energy effects merely produce a renormalization of the electron mass which, though infinite, has no observable consequences, we may now cancel it formally in the following way by writing

$$\begin{aligned}
H(\mathbf{x}) &= H_0(\mathbf{x}) + \delta m\bar{\psi}(\mathbf{x})\psi(\mathbf{x}) + H_1(\mathbf{x}) - \delta m\bar{\psi}(\mathbf{x})\psi(\mathbf{x}) \\
&= H_0(x) + \delta m\bar{\psi}(\mathbf{x})\psi(\mathbf{x}) + H^I(\mathbf{x}),
\end{aligned}$$

and substituting $H^I(x)$, in place of $H_1(x)$, in (10) and (11), while understanding the mass of the electron to be $m+\delta m$ instead of m. It is interesting to note that all this can be based also on the conventional field theory formalism. From (11) we then obtain

$$\begin{aligned}
\bar{S}_{fi}(\infty) &= \left(\Phi_f{}^0, \sum_{n=0}^{\infty}\frac{(-i)^n}{n!}\int d^4x_1\cdots\int d^4x_n\right. \\
&\quad\left.\times P(H^I(x_1), \cdots, H^I(x_n))\Phi_i{}^0\right) \\
&= (\Phi_f{}^0, s(\infty)\Phi_i{}^0), \quad (x=(\mathbf{x}, it)), \quad (12)
\end{aligned}$$

where $S(\infty)$ is just Dyson's $U(\infty)$.

In conclusion, I should like to express my sincere thanks to Professors A. T. Nordsieck and S. M. Dancoff for their encouragement and interest in the work and also for many enlightening discussions. Further, I wish to express my indebtedness to Mr. M. H. Kalos for help in my English. The discussion of this problem came up in the course of an investigation suggested by Professor S. M. Dancoff concerning the neutron-electron interaction.

On the Spin of the μ-Meson

E. R. CAIANIELLO
University of Rochester, Rochester, New York

(Received January 15, 1951)

The behavior of a μ-meson of spin ½ is investigated for the processes $\mu \to e+2\nu$, $\pi \to \mu+\nu$, μ^-+"p"$\to$"n"$+\nu$. These processes have been chosen because they give direct information on the nature of the μ-meson and do not require second quantization of the μ-meson field, which is not feasible for spin values greater than 1 when electromagnetic interactions are present. The theory used to describe the μ-meson is due to Rarita and Schwinger.

The spectra for the $\mu \to e+2\nu$ decay are obtained for the same modes of decay considered by Tiomno and Wheeler for μ-mesons of spin ½. Their most relevant feature is that none of them goes to zero at maximum electron energy. It is to be hoped that more careful measurements of this spectrum will permit a decision on the spin value of the μ-meson.

The μ-capture is studied by assuming the process to happen via an intermediate scalar or pseudoscalar π-meson. Comparison with the lifetime for $\pi \to \mu$-decay and use of experimental data allow an evaluation of the constant coupling the π-meson to nucleons. The plausibility of this value is taken as a test for the plausibility of the assumed spin value of the μ-meson. The results do not appear to contradict present-day evidence, due to the uncertainty of the nuclear matrix elements. The formulas obtained apply of course to any spin ½ particle undergoing similar processes.

I. INTRODUCTION

THE question of the spin of the μ-meson does not have as yet a certain answer; experimental evidence requires the assumption of at least a three-particle decay process:[1]

$$\text{I.}\quad \mu \to \mu_0 + e + \nu,$$

where e and ν denote electron and neutrino respectively and μ_0 denotes the second neutral particle. More information can be obtained from the other known processes:

$$\text{II.}\quad \pi \to \mu + \mu_0.$$

$$\text{III.}\quad \mu^- + \text{"}p\text{"} \to \text{"}n\text{"} + \mu_0.$$

(The quotes denote nucleons bound in a nucleus.) With certainty, we can only conclude that μ and the neutral μ_0 are both bosons or fermions. Tiomno[2] has shown that μ and μ_0 can be assumed to be of spin zero, thus obtaining agreement with experiment for all the processes considered above, if the coupling is properly chosen. A spin 1 for μ is excluded by Christy and Kusaka's study of bursts.[3]

On the other hand, it is well known that a satisfactory agreement is reached by assuming both μ and μ_0 to be Dirac particles. Klein[4] and Tiomno and Wheeler[1] have emphasized the analogy between μ-decay and the β-decay of nucleons, so that it is tempting to identify μ_0 with a neutrino, thereby avoiding the introduction of a new particle. Even if μ_0 is a neutrino, it is possible that the spin of the μ-meson has a value larger than ½, namely ⅜. The object of this investigation is to determine the behavior of a μ-meson of spin ⅜ in the processes I, II, III. The calculations will be presented in some detail, since, apart from their interest for the μ-meson, it is possible that a heavier meson may be found possessing spin ⅜.

The first question which must be decided, when considering particles of spin higher than 1, is that of the theory to use for their description. There is indeed quite a variety of (physically equivalent) formalisms, because the requirements of relativistic covariance do not fix uniquely the form of the equations of motion;[5] these equations must be furthermore accompanied by auxiliary conditions, if we wish to restrict the state of the particle to one of definite mass and spin.

The theory here followed is that of Rarita and Schwinger.[6] It has the advantages of appearing to be the natural extension of the Dirac and Proca theories without the introduction of auxiliary potentials, and of eliminating formal complications as far as possible; it shares with other theories the disadvantage, pointed out by Kusaka and Weinberg,[7] that, due to the auxiliary conditions, second quantization is not feasible in the presence of an electromagnetic field without the introduction of finite distance operators in the expressions for the relativistic commutators. (This last feature prevents its use in a calculation of the type of Christy and Kusaka's, at least without a further theoretical investigation; a study of bremsstrahlung according to the pattern set by Dirac[8] and Bhabha[9] can be carried out in principle, but is prohibitive numerically.)

The essentials of the Rarita-Schwinger theory will be recalled here, with a view to establishing the notation used in this work. For further details, the reader is

[1] Tiomno, Wheeler, and Rau, Revs. Modern Phys. **21**, 144 (1949).
[2] J. Tiomno, Phys. Rev. **76**, 856 (1949).
[3] R. F. Christy and S. Kusaka, Phys. Rev. **59**, 414 (1941).
[4] O. Klein, Nature **161**, 897 (1948).
[5] See for example H. J. Bhabha, Revs. Modern Phys. **21**, 451 (1949).
[6] W. Rarita and J. Schwinger, Phys. Rev. **60**, 61 (1940).
[7] S. Kusaka and J. W. Weinberg, thesis (University of California, June, 1943).
[8] P. A. M. Dirac, Proc. Cambridge Phil. Soc. **26**, 361 (1930).
[9] H. J. Bhabha, Proc. Roy. Soc. (London) **152**, 559 (1935).

referred to the original paper. Natural ($\hbar=c=1$) Heaviside units are used throughout the calculations; final results are restated in ordinary cgs units.

The equations of motion of a spin $\frac{3}{2}$ μ-meson can be derived from the lagrangian:

$$L=\bar{\Psi}_\mu(\gamma_\tau\partial_\tau+m)\Psi_\mu-\tfrac{1}{3}\bar{\Psi}_\mu(\gamma_\mu\partial_\nu+\gamma_\nu\partial_\mu)\Psi_\nu + \tfrac{1}{3}\bar{\Psi}_\mu\gamma_\mu(\gamma_\tau\partial_\tau-m)\gamma_\nu\Psi_\nu, \quad (1)$$

where: $\bar{\Psi}_\mu=\Psi_\mu^*\gamma_4$, $\partial_\mu=\partial/\partial x_\mu-ie\varphi_\mu$, m=mass of μ-meson, φ_μ=4-vector electromagnetic potential, $\{\Psi_\mu\}$ is the 4-vector (each component of which is a spinor) which describes the meson.

From the equations of motion:

$$(\gamma_\tau\partial_\tau+m)\Psi_\mu-\tfrac{1}{3}(\gamma_\mu\partial_\nu+\gamma_\nu\partial_\mu)\Psi_\nu + \tfrac{1}{3}\gamma_\mu(\gamma_\tau\partial_\tau-m)\gamma_\nu\Psi_\nu=0, \quad (2)$$

one obtains immediately

$$2\partial_\mu\Psi_\mu=m\gamma_\mu\Psi_\mu, \quad (3)$$

and from (2) and (3):

$$[m^2+(ie/3)\gamma_\mu\gamma_\tau F_{\tau\mu}]\gamma_\nu\Psi_\nu+2ie\gamma_\tau F_{\tau\mu}\Psi_\mu=0, \quad (4)$$

where $F_{\mu\nu}=\partial\varphi_\nu/\partial x_\mu-\partial\varphi_\mu/\partial x_\nu$. If no electromagnetic field is present, each component Ψ_μ obeys the Dirac equation:

$$(\gamma_\tau\partial_\tau+m)\Psi_\mu=0 \quad (5)$$

with the conditions

$$\gamma_\mu\Psi_\mu=0 \quad (6)$$

$$\partial\Psi_\mu/\partial x_\mu=0. \quad (7)$$

A set of four orthonormal positive energy solutions to (5), (6), (7) has been conveniently determined by Kusaka[10] in the form:

$$\begin{aligned}
&\{\Psi_\mu^{(1)}\}\equiv\{\mathbf{e}_1\psi_{+1},\,0\}\\
&\{\Psi_\mu^{(2)}\}\equiv\{\mathbf{e}_2\psi_{-1},\,0\}\\
&\{\Psi_\mu^{(3)}\}\equiv\{1/\sqrt{3}\mathbf{e}_2\psi_{+1}-\sqrt{2}/\sqrt{3}E/m\mathbf{e}_3\psi_{-1},\\
&\qquad -i\sqrt{2}/\sqrt{3}k/m\psi_{-1}\}\\
&\{\Psi_\mu^{(4)}\}\equiv\{1/\sqrt{3}\mathbf{e}_1\psi_{-1}+\sqrt{2}/\sqrt{3}E/m\mathbf{e}_3\psi_{+1},\\
&\qquad i\sqrt{2}/\sqrt{3}k/m\psi_{+1}\},
\end{aligned} \quad (8)$$

where

$$\mathbf{e}_1\equiv\{1/\sqrt{2},\,i/\sqrt{2},\,0\};\quad \mathbf{e}_2\equiv\{1/\sqrt{2},\,-i/\sqrt{2},\,0\};\quad \mathbf{e}_3=\mathbf{k}/k\equiv\{0,\,0,\,1\},$$

and ψ_{+1}, ψ_{-1} are the positive energy Dirac wave functions for spin parallel and antiparallel to the momentum $\mathbf{k}$ of the μ-meson.

In the general case, in so far as the external field can be considered as a perturbation, one obtains from (4):

$$\gamma_\nu\Psi_\nu\cong-(2ie/m^2)\gamma_\tau F_{\tau\mu}\Psi_\mu, \quad (9)$$

where the right-hand term is extremely small (in ordinary units, for a coulomb field, $\sim(e^2/\hbar c)(\hbar/mc)^2$). Equation (6) is therefore a very good approximation to Eq. (9): this will considerably simplify the study of the μ-capture.

II. DECAY OF THE μ-MESON

We have studied the same modes of decay of the μ-meson which Tiomno and Wheeler[1] have considered in the case of spin $\frac{1}{2}$, with a view to an eventual comparison with experiment. The possible modes of decay reduce to:

SCE (Simple Charge Exchange)

$$\begin{pmatrix}\mu^-\\ \bar{\nu}''\end{pmatrix}\rightarrow\begin{pmatrix}\nu'\\ e\end{pmatrix}$$

CR (Charge Retention)

$$\begin{pmatrix}\mu^-\\ \bar{\nu}''\end{pmatrix}\rightarrow\begin{pmatrix}e\\ \nu'\end{pmatrix}$$

ACE (Antisymmetric Charge Exchange)

$$\begin{pmatrix}\mu^+\\ \bar{e}\end{pmatrix}\rightarrow\begin{pmatrix}\nu'\\ \nu''\end{pmatrix}.$$

The last one requires, of course, antisymmetrization of the wave functions of the two neutrinos. The Dirac theory is used for electrons and neutrinos. If we consider in general a process $\begin{pmatrix}\mu\\ c\end{pmatrix}\rightarrow\begin{pmatrix}a\\ b\end{pmatrix}$ we readily find that the only possible interaction hamiltonians are:

V (Vector)

$$H_V=ig_V\{\bar{\psi}_b(\mathbf{x}_1)\gamma_\mu\psi_c(\mathbf{x}_1)\}\{\bar{\psi}_a(\mathbf{x}_2)\Psi_\mu(\mathbf{x}_2)\}\delta(\mathbf{x}_1-\mathbf{x}_2)$$

PV (Pseudovector)

$$H_{PV}=g_{PV}\{\bar{\psi}_b(\mathbf{x}_1)\gamma_5\gamma_\mu\psi_c(\mathbf{x}_1)\}\{\bar{\psi}_a(\mathbf{x}_2)\gamma_5\Psi_\mu(\mathbf{x}_2)\}\delta(\mathbf{x}_1-\mathbf{x}_2)$$

T (Tensor)

$$\begin{aligned}H_T&=g_T\{\bar{\psi}_b(\mathbf{x}_1)\gamma_\mu\gamma_\nu\psi_c(\mathbf{x}_1)\}\{\bar{\psi}_a(\mathbf{x}_2)\gamma_\mu\Psi_\nu(\mathbf{x}_2)\}\delta(\mathbf{x}_1-\mathbf{x}_2)\\ &\equiv g_T\{\bar{\psi}_b(\mathbf{x}_1)\gamma_\mu\gamma_\nu\psi_c(\mathbf{x}_1)\}\{\bar{\psi}_a(\mathbf{x}_2)\tfrac{1}{2}[\gamma_\mu\Psi_\nu(\mathbf{x}_2)\\ &\qquad -\gamma_\nu\Psi_\mu(\mathbf{x}_2)]\delta(\mathbf{x}_1-\mathbf{x}_2)\}.\end{aligned}$$

The scalar and pseudoscalar couplings vanish because of (6). From (6), it also follows that $\Psi_4=0$ for a μ-meson at rest, as considered here. The summation over spins for the Dirac particles is performed in the customary fashion; the average over-spin for the μ-meson should be done by actual use of the positive energy solutions (8) of the wave equation. It turns out, however, that when all other summations have been performed, the

[10] S. Kusaka, Phys. Rev. **60**, 61 (1940).

relations ($\sigma_1=i\alpha_2\alpha_3$; $\cdots$):

$$(\boldsymbol{\alpha}\cdot\mathbf{u})(\boldsymbol{\alpha}\cdot\mathbf{v})=\mathbf{u}\cdot\mathbf{v}-i\boldsymbol{\sigma}\cdot(\mathbf{u}\times\mathbf{v})$$

$$(\boldsymbol{\sigma}\cdot\mathbf{u})(\boldsymbol{\alpha}\cdot\mathbf{v})=\gamma_5\mathbf{u}\cdot\mathbf{v}-i\boldsymbol{\alpha}\cdot(\mathbf{u}\times\mathbf{v})$$

allow all the terms bracketed between two $\{\Psi_\mu\}$'s to be expressed as a linear combination of 1, β, γ_5, $\boldsymbol{\alpha}\cdot\mathbf{u}$, $i\boldsymbol{\sigma}\cdot\mathbf{v}$. The last three terms are easily seen to give zero over-all contribution, and β, when operating directly on a $\{\Psi_\mu\}$, can be replaced by 1. The final expressions are therefore given in terms of

$$\sum_{\mu\ \text{spin}}\langle\Psi^*\cdot\Psi\rangle=4$$

$$\sum_{\mu\ \text{spin}}\langle\mathbf{u}\cdot\Psi^*\rangle\langle\mathbf{v}\cdot\Psi\rangle+\text{compl. conj.}=(8/3)\mathbf{u}\cdot\mathbf{v}$$

and are evaluated on simple inspection.

The squares of the matrix elements, averaged over the spin of the μ-meson and summed over all other spins, result finally given by the following expressions (nat. units):

SCE

$$I_V=\frac{g_V^2}{g_{PV}^2}I_{PV}=\frac{1}{2}g_V^2\left(1-\frac{1}{3}\frac{\mathbf{k}_e\cdot\mathbf{k}_{\nu''}}{E_eE_{\nu''}}\right)$$

$$I_T=g_T^2\left\{1+\frac{1}{3}\left[\frac{\mathbf{k}_e\cdot\mathbf{k}_{\nu''}}{E_eE_{\nu''}}-\frac{\mathbf{k}_e\cdot\mathbf{k}_{\nu'}}{E_eE_{\nu'}}-\frac{\mathbf{k}_{\nu'}\cdot\mathbf{k}_{\nu''}}{E_{\nu'}E_{\nu''}}\right]\right\}$$

CR

$$I_V=\frac{1}{2}g_V^2\left(1+\frac{m_e}{E_e}\right)\left(1-\frac{1}{3}\frac{\mathbf{k}_{\nu'}\cdot\mathbf{k}_{\nu''}}{E_{\nu'}E_{\nu''}}\right)$$

$$I_{PV}=\frac{1}{2}g_{PV}^2\left(1-\frac{m_e}{E_e}\right)\left(1-\frac{1}{3}\frac{\mathbf{k}_{\nu'}\cdot\mathbf{k}_{\nu''}}{E_{\nu'}E_{\nu''}}\right)$$

$$I_T=g_T^2\left\{1+\frac{1}{3}\left[\frac{\mathbf{k}_{\nu'}\cdot\mathbf{k}_{\nu''}}{E_{\nu'}E_{\nu''}}-\frac{\mathbf{k}_e\cdot\mathbf{k}_{\nu'}}{E_eE_{\nu'}}-\frac{\mathbf{k}_e\cdot\mathbf{k}_{\nu''}}{E_eE_{\nu''}}\right]\right\}$$

ACE

$$I_V=(g_V^2/g_{PV}^2)I_{PV}=\tfrac{1}{2}I_V\quad\text{for CR}$$

$$I_T=g_T^2\left\{1+\frac{m_e}{E_e}-\left(\frac{1}{3}+\frac{m_e}{E_e}\right)\frac{\mathbf{k}_{\nu'}\cdot\mathbf{k}_{\nu''}}{E_{\nu'}E_{\nu''}}\right\}.$$

The μ-decay spectra for electron momentum between p_e and p_e+dp_e (using now ordinary units) are obtained by standard methods (see reference 1, appendix by Rau). They are conveniently expressed in terms of the maximum electron energy

$$E_0=\tfrac{1}{2}m_\mu c^2+(m_e/m_\mu)\cdot\tfrac{1}{2}m_e c^2.$$

Introducing the dimensionless quantities

$$\epsilon=E_e/m_ec^2;\quad \epsilon_0=E_0/m_ec^2;\quad k=p_e/m_ec;\quad r=m_e/m_\mu$$

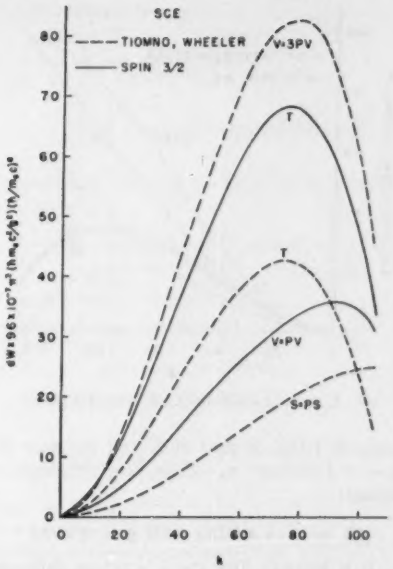

FIG. 1. Decay spectra for simple charge exchange theory. Vector and pseudovector couplings yield the same spectrum. (The ordinate, in this and in the other figures, is actually $1.41\times K$ as given in the text.)

the probabilities for the aforesaid decays become (g in erg cm^3):

$$dW=g^2\frac{m_\mu(m_ec)^4}{144\pi^3\hbar^7}Kdk$$

where the dimensionless factor K is defined as:

SCE

$$K_V=K_{PV}=9k^2(\epsilon_0-\epsilon)+k^4(2r+1/\epsilon)$$

$$K_T=4[6k^2(\epsilon_0-\epsilon)+rk^4]$$

CR

$$K_V=2(1+1/\epsilon)[6k^2(\epsilon_0-\epsilon)+rk^4]$$

$$K_{PV}=2(1-1/\epsilon)[6k^2(\epsilon_0-\epsilon)+rk^4]$$

$$K_T=4[3k^2(\epsilon_0-\epsilon)+k^4(r+1/\epsilon)]$$

ACE

$$K_V=K_{PV}=\tfrac{1}{2}K_V\quad\text{for CR}$$

$$K_T=4[9k^2(\tfrac{2}{3}+1/\epsilon)(\epsilon_0-\epsilon)+rk^4].$$

A common feature of these spectra is that none of them goes to zero when $\epsilon\to\epsilon_0$; this is perhaps the most significant result obtained in this section. Figures 1–3 show how these spectra compare with those given by Tiomno and Wheeler for the case of spin $\frac{1}{2}$ (some of the curves for spin $\frac{1}{2}$ might have been affected by slight errors in numerical computation). The ordinate scale has been chosen so as to coincide with the one used by Tiomno and Wheeler; this simply amounts to plotting

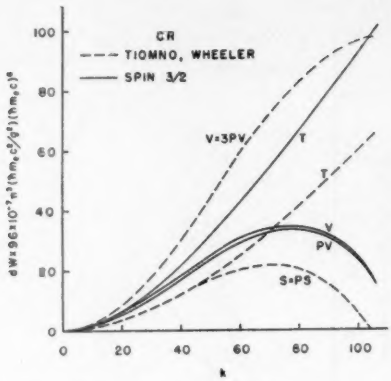

FIG. 2. Decay spectra for charge retention theory.

as ordinate 1.41K instead of K (we use $m_\mu=212m_e$, Tiomno and Wheeler $m_\mu=210m_e$: the difference is not significant).

III. $\pi\to\mu+\nu$ DECAY AND μ^--CAPTURE

(a) It is known[11] that the μ^--capture data can be accounted for by a scheme

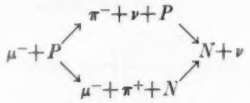

under the assumptions: π-scalar or pseudoscalar, μ of spin $\frac{1}{2}$. This fact is very satisfactory, and leads us to consider the same scheme for a μ^--meson of spin $\frac{3}{2}$. Comparison with the lifetime for the $\pi\to\mu_{\frac{1}{2}}+\nu$ decay and use of experimental data for the μ^- capture allow indeed an indirect determination of the coupling constant g for the μ-meson with the nucleon: the consistency of the assumption of a spin $\frac{3}{2}$ for the μ-meson will be judged from the plausibility of the values found for g.

Simplifying assumptions required to make the above calculation feasible are: use of free waves for the π-meson, use of the equivalence theorems for the couplings of the π-meson with the nucleon, neglect of the energy imparted to the nucleus with respect to the rest energy of the virtual π-meson (this simplifies the energy denominators), use of Eq. (6) instead of Eq. (9) in forming the interaction lagrangians and neglect of the electromagnetic interaction in the derivative couplings. These assumptions are easily justified (see reference 11) to a good approximation. Further approximations will be specifically stated when needed.

Let φ, ψ_P, ψ_N, χ be, respectively, the π-meson, proton, neutron, neutrino-wave functions. Let g, f/m_π refer to the (pseudo) scalar and (pseudo) vector couplings (specified, when needed, by a superscript ^{S} or ^{PS}). The possible interaction lagrangians between the π-meson and the (P, N), (μ, ν) fields reduce, as a consequence of our assumptions, to

$$L'=-g\varphi^*U-(f/m_\pi)\partial_\mu\varphi V_\mu+\text{compl. conj.},$$

where:

$$U=\psi_N{}^*O\psi_P;\quad V_\mu=\chi^*O\Psi_\mu$$

and $O=\gamma_4$ for scalar π-meson, $=i\gamma_4\gamma_5$ for pseudoscalar π-meson. The compl. conj. part does not contribute to the capture process. Quantization of the π-meson field in the customary manner:

$$\varphi=\sum(2\omega_k)^{-\frac{1}{2}}(a_k+b_k{}^*)\exp(i\mathbf{k}\cdot\mathbf{x})$$

$$\pi=\sum i(\omega_k/2)^{\frac{1}{2}}(a_k{}^*-b_k)\exp(-i\mathbf{k}\cdot\mathbf{x})$$

($\omega_k=(m_\pi{}^2+k_\pi{}^2)^{\frac{1}{2}}$, $k=\pm k_{\pi\pm}$; normalization per unit volume) gives the interaction hamiltonian in the form ($V_4=iV_0$)

$$H'=\sum\Big\{g(2\omega_k)^{-\frac{1}{2}}(a_k{}^*+b_k)\int\exp(-i\mathbf{k}\cdot\mathbf{x})U d\mathbf{x}$$

$$+(if/m_\pi)(2\omega_k)^{-\frac{1}{2}}\Big[\omega_k(-a_k+b_k{}^*)\int\exp(i\mathbf{k}\cdot\mathbf{x})V_0 d\mathbf{x}$$

$$+(a_k+b_k{}^*)\int\exp(i\mathbf{k}\cdot\mathbf{x})\mathbf{k}\cdot\mathbf{V}d\mathbf{x}\Big]\Big\}. \quad (10)$$

(b) *Decay of π-meson at rest.* Consideration of the equivalent process $\pi+\bar\nu\to\mu$ and use of (10) yield immediately for the lifetime τ_μ the expression:

$$\frac{1}{\tau_\mu}=\frac{1}{12}\frac{f_{cgs}{}^2}{\hbar c}\frac{m_\pi{}^3}{m_\mu{}^2}\frac{c^2}{\hbar}\Big[1-\Big(\frac{m_\mu}{m_\pi}\Big)^2\Big]^2 \quad (11)$$

(in ordinary cgs units). Equation (11) is valid for both scalar and pseudoscalar π-mesons, as a consequence of the assumption $m_\nu=0$.

(c) *μ^- capture by a nucleus.*

An alternative treatment of the μ^- capture by complex nuclei consists in considering first the capture by a free proton and then using some nuclear model for the study of the actual case.

Since results obtained in this way do not at present give any better accuracy than those above reported, we only state here for possible future reference the relevant formulas, which require some computational work. Taking into account the two possible intermediate states, one obtains for the capture of a free μ^--meson by a free proton (with the neglect of electromagnetic interaction).

$$I=\sum_{\text{spins}}\text{Av}|H''|^2=\frac{1}{12}\Big(\frac{gf}{m_\pi m_\mu}\Big)^2\frac{(E_\mu E_\nu-\mathbf{k}_\mu\cdot\mathbf{k}_\nu)^2}{E_\mu E_\nu[m_\pi{}^2-m_\mu{}^2+2(E_\mu E_\nu-\mathbf{k}_\mu\cdot\mathbf{k}_\nu)]^2}$$

$$\times\Big(1-\frac{\mathbf{k}_P\cdot\mathbf{k}_N}{E_PE_N}\pm\frac{M_PM_N}{E_PE_N}\Big)$$

(strictly relativistic) where the + and − signs refer respectively to the cases of scalar and pseudoscalar π-mesons. The lifetime

[11] R. Latter, thesis (California Institute of Techology, 1949).

for μ^- capture from a K-orbit is then, in ordinary cgs units:

$$\frac{1}{\tau^S}=\frac{1}{24}\frac{(g_{\rm cgs}{}^S)^2}{\hbar c}\frac{(f_{\rm cgs}{}^S)^2}{\hbar c}\left(\frac{e^2}{\hbar c}\right)^3\frac{m_\mu c^2}{\hbar}\frac{m_\mu{}^6[m_\mu{}^2+4M(m_\mu+M)]}{m_\pi{}^2[m_\pi{}^2(M+m_\mu)+Mm_\mu{}^2]^2}\times\left(1+\frac{M}{M+m_\mu}\right)^4$$

$$\frac{1}{\tau^{PS}}=\left(\frac{g^{PS}f^{PS}}{g^Sf^S}\right)_{\rm cgs}{}^2\frac{1}{\tau^S}\frac{m_\mu{}^2}{m_\mu{}^2+4M(m_\mu+M)}.$$

If a Z^4 law is assumed, one can very roughly extrapolate, and obtain from the value $1/\tau$ capt. $=47$/sec for a free proton the values $(g_{\rm cgs}{}^S)^2/\hbar c=0.09$; $(g_{\rm cgs}{}^{PS})^2/\hbar c=30.43$. These values are a poorer approximation than those found above. The adoption of a free particle model for the nucleus[12] would increase them by a factor of about 4.

The nucleus can take up any amount of momentum. From (10) once obtains then easily, remembering the stated assumptions, that the expression for the matrix element of the capture process can be reduced to the form:

$$H''=(gf/m_\pi)\int d\mathbf{x}\int d\mathbf{x}'\times\left[\sum_{\mathbf{k}_\nu}\frac{\sin[\mathbf{k}_\nu\cdot(\mathbf{x}'-\mathbf{x})]}{\omega_\nu{}^2}\mathbf{k}_\nu\cdot\mathbf{V}(\mathbf{x}')\right]U(\mathbf{x})$$

$$=-(gf/4\pi m_\pi)\int d\mathbf{x}\int d\mathbf{x}'U(\mathbf{x})V(\mathbf{x}')\nabla_R\times[\exp(-m_\pi R)/R]\quad(\mathbf{R}=\mathbf{x}'-\mathbf{x}).$$

The main contribution to this integral comes from distances of order $\hbar/mc$ from the nucleus; we approximate $\{\Psi_\mu(\mathbf{x}')\}$ over this range by the constant $\{\Psi_\mu(0)\}$, its value at the center of the nucleus. The gradient operator and the factor $\exp(-m_\pi R)/R$ are eliminated by two further integrations. We find:

$$H''=-\frac{igf}{m_\pi(m_\pi{}^2+k_\nu{}^2)}\langle v^*O\mathbf{k}_\nu\cdot\Psi(0)\rangle\cdot\sum_{\substack{\rm all\\ \rm protons}}\int\exp(-i\mathbf{k}_\nu\cdot\mathbf{x})\langle\psi_N{}^*(\mathbf{x})O\psi_P(\mathbf{x})\rangle d\mathbf{x},\quad(12)$$

where v is the neutrino wave amplitude. The lifetime for μ^- capture is determined by the equation

$$1/\tau_{\rm capt}=2\pi/(2\pi)^3\int Ik_\nu{}^2d\Omega,$$

where I is the average over μ and P spins and the sum over the other spins of $|H''|^2$. The statistical factor is determined by the consideration of the neutrino states only. One obtains, treating the nucleons nonrelativistically:

(1) *Scalar π-meson:* $O=\gamma_4$

$$\frac{1}{\tau^S}=\frac{1}{6\pi}\left(\frac{g^Sf^S}{m_\pi}\right)^2\frac{E_\nu{}^4}{[m_\pi{}^2+E_\nu{}^2]^2}|\Psi(0)|^2\cdot\left|\sum\int\exp(-i\mathbf{k}_\nu\cdot\mathbf{x})\psi_N{}^*(\mathbf{x})\psi_P(\mathbf{x})d\mathbf{x}\right|^2.\quad(13)$$

(2) *Pseudoscalar π-meson:* $O=i\gamma_4\gamma_5$. With our approximation, we get:

$$\langle\psi_N{}^*O\psi_P\rangle\cong-\frac{1}{2M}\nabla\cdot\langle\psi_N{}^*\boldsymbol{\sigma}\psi_P\rangle,$$

($M=$ nucleon mass.) This gives:

$$\sum_{\rm spins}|H''^{PS}|^2=\frac{1}{2}\left[\frac{g^{PS}f^{PS}}{2m_\pi M(m_\pi{}^2+k_\nu{}^2)}\right]^2\times\langle[\mathbf{k}_\nu\cdot\Psi^*(0)][\mathbf{k}_\nu\cdot\Psi(0)]\rangle\times\left|\mathbf{k}_\nu\cdot\sum\int\exp(-i\mathbf{k}_\nu\cdot\mathbf{x})\langle\psi_N{}^*(\mathbf{x})\boldsymbol{\sigma}\psi_P(\mathbf{x})\rangle d\mathbf{x}\right|^2.$$

Taking, then, the z-axis in the direction of $\Psi(0)$, we write $\boldsymbol{\sigma}=\boldsymbol{\sigma}_{||}+\boldsymbol{\sigma}_\perp$ (for each of the terms of the $\sum$ over all protons), where $\boldsymbol{\sigma}_{||}$ is parallel and $\boldsymbol{\sigma}_\perp$ is perpendicular to $\Psi(0)$. Then;

$$\int d\Omega\sum_{N,\nu\,\rm spins}\underset{P\ \rm spin}{\rm Av.}|H''^{PS}|^2=\frac{2\pi}{5}\left[\frac{g^{PS}f^{PS}}{2m_\pi M(m_\pi{}^2+k_\nu{}^2)}\right]^2\cdot k_\nu{}^4|\Psi(0)|^2\left\{\left|\sum\int\exp(-i\mathbf{k}_\nu\cdot\mathbf{x})\psi_N{}^*(\mathbf{x})\sigma_{||}\psi_P(\mathbf{x})d\mathbf{x}\right|^2+\frac{1}{3}\left|\sum\int\exp(-i\mathbf{k}_\nu\cdot\mathbf{x})\psi_N{}^*(\mathbf{x})\sigma_\perp\psi_P(\mathbf{x})d\mathbf{x}\right|^2\right\}.$$

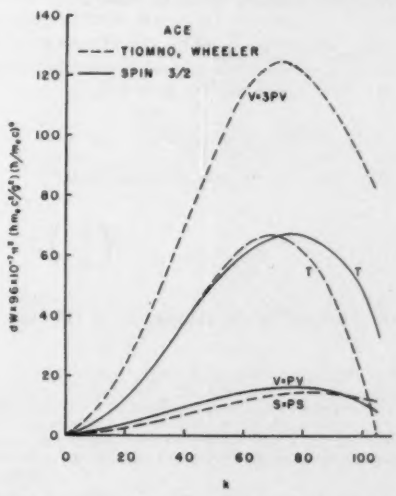

FIG. 3. Decay spectra for antisymmetric charge exchange theory. Vector and pseudovector couplings yield the same spectrum.

[12] J. Tiomno and J. A. Wheeler, Revs. Modern Phys. **21**, 153 (1949).

We must finally average over the μ-spin. Keeping in mind that for the evaluation of $|\Psi(0)|^2$ we shall use the nonrelativistic approximation, i.e., the ground-state hydrogen-like wave functions, for which the vector character is lost, we recognize that such an average will simply reduce a term

$$\left|\sum\int \exp(-i\mathbf{k}_\nu\cdot\mathbf{x})\psi_N^*(\mathbf{x})\sigma_{||}{}^{(r)}\psi_P(\mathbf{x})d\mathbf{x}\right|^2,$$

r denoting the projection of $\boldsymbol{\sigma}$ onto the $\Psi^{*(r)}(0)$ corresponding to the rth spin state, to a sum of such terms divided by their number. As we ultimately cannot evaluate them, but must resort to an approximation, nothing is practically changed by writing the final result in the form:

$$\frac{1}{\tau^{PS}}=\frac{1}{40\pi}\left(\frac{g^{PS}f^{PS}}{m_\pi}\right)^2\frac{E_\nu^4}{[m_\pi{}^2+E_\nu{}^2]^2}\frac{E_\nu^2}{M^2}|\Psi^*(0)|^2$$

$$\cdot\left\{\left|\sum\int \exp(-i\mathbf{k}_\nu\cdot\mathbf{x})\psi_N^*(\mathbf{x})\sigma_{||}\psi_P(\mathbf{x})d\mathbf{x}\right|^2\right.$$

$$\left.+\frac{1}{3}\left|\sum\int \exp(-i\mathbf{k}_\nu\cdot\mathbf{x})\psi_N^*(\mathbf{x})\sigma_\perp\psi_P(\mathbf{x})d\mathbf{x}\right|^2\right\}. \quad (14)$$

(d) We take now in (13) and (14) $|\Psi^*(0)|^2=(Zm_\mu e^2)^3/\pi$ and $Z/3$ for the sums squared of the nuclear matrix elements (see reference 11), and express the final results in ordinary cgs units. They are:

$$\frac{1}{\tau^S}=\frac{8}{9}\frac{(g_{\text{cgs}}{}^S)^2}{\hbar c}\frac{(f_{\text{cgs}}{}^S)^2}{\hbar c}\frac{m_\mu{}^3e^6}{m_\pi{}^2\hbar^4c}\frac{E_\nu^4}{[m_\pi{}^2c^4+E_\nu{}^2]^2}Z^4 \quad (15)$$

$$\frac{1}{\tau^{PS}}=\frac{8}{45}\frac{(g_{\text{cgs}}{}^{PS})^2}{\hbar c}\frac{(f_{\text{cgs}}{}^{PS})^2}{\hbar c}\frac{m_\mu{}^3e^6}{m_\pi{}^2\hbar^4c}\frac{E_\nu^4}{[m_\pi{}^2c^4+E_\nu{}^2]^2}$$

$$\times\left(\frac{E_\nu}{Mc^2}\right)^2Z^4. \quad (16)$$

We are interested in the comparison of (15) and (16) with (11). Denoting by r_μ the ratio m_μ/m_π we obtain:

$$\left(\frac{\tau_\mu}{\tau_{\text{capt}}}\right)^S=\frac{32}{3}\frac{(g_{\text{cgs}}{}^S)^2}{\hbar c}\left(\frac{e^2}{\hbar c}\right)^3\frac{r_\mu{}^5}{(1-r_\mu{}^2)^4}\frac{E_\nu^4}{[m_\pi{}^2c^4+E_\nu{}^2]^2}Z^4$$

$$\left(\frac{\tau_\mu}{\tau_{\text{capt}}}\right)^{PS}=\frac{1}{5}\left(\frac{g_{\text{cgs}}{}^{PS}}{g_{\text{cgs}}{}^S}\right)^2\left(\frac{E_\nu}{Mc^2}\right)^2\left(\frac{\tau_\mu}{\tau_{\text{capt}}}\right)^S.$$

For a numerical determination of $g^2/\hbar c$, we use the values: $m_\pi=280m_e$; $m_\mu=212m_e$; $Z=10$; $\tau_\mu=1.97\times10^{-6}$ sec; $\tau_{\text{capt}}=2.15\times10^{-6}$ sec. We have then:

$$E_\nu=E_\mu-[E_{\text{``}n\text{''}}-E_{\text{``}p\text{''}}]=98\text{ Mev},$$

taking the excitation energy of the nucleus to be 10 Mev (a reasonable estimate from the absence of stars accompanying the μ^--capture). We obtain finally:

$$(g_{\text{cgs}}{}^S)^2/\hbar c=0.29;\quad (g_{\text{cgs}}{}^{PS})^2/\hbar c=136.$$

These values are uncertain chiefly for two reasons: (1) the value assigned to the squares of the nuclear matrix elements, (2) the value of 10 Mev taken for the nuclear excitation energy. Only τ^{PS} is however, sensitive to the second uncertainty: an increased value for the excitation energy would sensibly increase $(g_{\text{cgs}}{}^{PS})^2/\hbar c$.

IV. CONCLUSION

We have investigated the processes

$$\text{I}\quad \mu\to e+2\nu$$

$$\text{II}\quad \pi\to\mu+\nu$$

$$\text{III}\quad \mu^-+\text{``}p\text{''}\to\text{``}n\text{''}+\nu$$

assuming a spin $\frac{3}{2}$ for the μ-meson. Process III has been studied under assumption of an intermediate scalar or pseudoscalar π-meson. The results obtained do not disagree with the experimental information available at present. It may be possible to exclude spin $\frac{3}{2}$ for the μ-meson when the nuclear matrix elements and the nuclear excitation energy are known with greater accuracy. The spectra obtained from the study of process I may be even more decisive when the experimental electron spectrum is known very accurately.

The author wishes to thank Dr. R. E. Marshak for suggesting this research and for invaluable guidance throughout; Dr. J. Ashkin for most helpful and generous advice; Messrs. P. B. Daitch, M. F. Kaplon, A. Simon, and S. Tamor for many interesting discussions.

A Note Concerning *l*-Type Doubling in Axially Symmetric Molecules, in Particular with Reference to Molecules Belonging to the Symmetry Groups C_{4v} and V_d

J. DE HEER
Department of Physics and Astronomy, Ohio State University, Columbus, Ohio
(Received May 7, 1951)

The theory of the *l*-type doubling for axially symmetric polyatomic molecules is applied to molecules belonging to the symmetry groups C_{4v} and V_d. It is shown that here *l*-type doubling may be expected in *both* degenerate Coriolis levels (referring to a positive and a negative product of the quantum numbers K and l, respectively). A detailed analysis of a pyramidal XY_4 model reveals that the doubling in these two levels is of the same order. On the basis of our discussion a microwave absorption pattern is predicted for the transitions $J=1\rightarrow J=2$, $\Delta K=0$, where a molecule of C_{4v} or V_d symmetry is in an excited degenerate vibration state. An interesting example may be provided by IF_5 if this molecule has the C_{4v} structure recently proposed.

I. INTRODUCTION

CERTAIN anomalies in the microwave spectrum of methyl cyanide and methyl iso-cyanide have led to an investigation[1,2] of the *l*-type doubling in axially symmetric polyatomic molecules, belonging to the group C_{3v}. It had been known that when a degenerate vibration is excited each state where $K\neq 0$ suffers a degenerate Coriolis-type splitting,[3] resulting in two levels, one where the product Kl is positive and one where it is negative, separated by a frequency interval $4Kl\zeta C_v$, where $C_v=h/8\pi^2 I_{zz}^{(v)}c$, and ζ is the Coriolis coupling constant. The sign of ζ determines which of the two Coriolis components, each of which is still twofold degenerate, has the higher energy. It has been shown[2] that the hamiltonian contains terms which in principle may further remove, in second order of approximation, this degeneracy. A detailed analysis reveals, however, that in this order of approximation only the Coriolis level $K=l=1$ (taken to be the upper level) splits (Fig. 1(a)). Moreover, a more general argument on the basis of group theory (see Sec. II below) proved that even in higher approximations the degeneracy of the level $K=l=1$ cannot possibly be removed. The microwave absorption pattern thus predicted (Fig. 1(b)) is in agreement with experiment (provided the difference in centrifugal stretching of the two Coriolis components is taken into account).

In the case of linear molecules the Coriolis splitting mentioned above is absent, since always $K=l$. Here too, for $K\neq 0$, *l*-type doubling will occur.[4-6]

It is now tempting to inquire into the question of whether it is generally true for all axially symmetric molecules (the linear ones considered as a limiting case) that only the level $K=l=1$ is subject to *l*-type doubling, while for other K values, in particular $K=-l=1$ (if such a state exists) the degeneracy concerned is not removed. In the present paper we shall show that no general rule can be established and shall investigate for which type of molecule a splitting of both Coriolis components may be expected.

II. GROUP THEORETICAL DISCUSSION

For C_{3v} molecules the following argument was suggested by Dennison and reported by Nielsen.[2] All vibrational states $l=\pm 1$ are characterized by vibrational wave functions belonging to the irreducible representation E of the C_{3v} group. The rotational wave functions will belong to the C_3 subgroup, and those for $K=\pm 1$ will be of the species E. Hence, there will be four complete rotation-vibration wave functions of symmetry $E\times E=2A+E$, out of which we can form four independent linear combinations, two of which are symmetrical with respect to permutations corresponding to rotations, whereas the other two form a degenerate pair.[7] Apparently the levels $K=l=1$, for which the internal angular momentum of the framework spinning

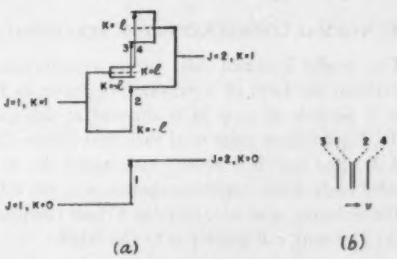

FIG. 1. (a) Rotation levels of an axially symmetric molecule, belonging to the group C_{3v}, for $J=1$ and $J=2$, showing *l*-type doubling, when the molecule is in a vibration state where $l=1$, for $K=l$. (See reference 2.) (b) Microwave absorption pattern predicted on the basis of *l*-type doubling (Fig. 1 (a)) and assuming the centrifugal stretching of both Coriolis components to be alike. (See reference 2.)

[1] H. H. Nielsen, Phys. Rev. **75**, 1961 (1949).
[2] H. H. Nielsen, Phys. Rev. **77**, 130 (1950).
[3] See, for example, E. Teller and L. Tisza, Z. Physik **73**, 791 (1932); M. Johnston and D. M. Dennison, Phys. Rev. **48**, 868 (1935).
[4] G. K. Herzberg, Revs. Modern Phys. **14**, 219 (1942).
[5] H. H. Nielsen and W. H. Shaffer, J. Chem. Phys. **11**, 140 (1943).
[6] H. H. Nielsen, Phys. Rev. **78**, 296 (1950).
[7] E. Bright Wilson, Jr., J. Chem. Phys. **3**, 818 (1935).

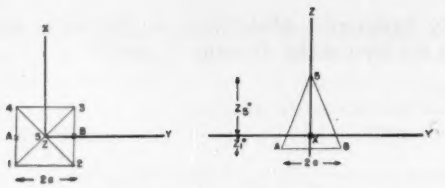

FIG. 2. The XY_4 model (see text).

around its axis, $L=|K-l|$, is zero, have the A symmetry, while the other two ($K=-l=1$, hence $L=\pm 2$) form a degenerate pair. Since this degeneracy cannot be removed by a perturbation which has the same symmetry as the molecule, the level of species E will remain degenerate in any order of approximation and cannot suffer l-type splitting.

For axially symmetric molecules belonging to other symmetry groups, the argument follows essentially along the same lines. A difference will only arise if the direct product of an E irreducible representation of the symmetry group concerned with itself (or with another irreducible representation of species E of the same group) will no longer be equal to $2A+E$ (or $2B+E$). In particular we wish to inquire whether in a given case this direct product might no longer contain an E component; this might, in principle, result in l-type doubling for both levels $K=l=1$ and $K=-l=1$. A quick survey of the character table of the symmetry groups concerned shows that the only important case where such a situation arises presents itself in the C_{4v} group (or V_d group). Here $E\times E=2A+2B$, and hence splitting of both Coriolis levels is possible. It remains of interest to inquire whether the splitting in both levels is of the same order. This question cannot be answered by group theory but necessitates a detailed analysis of a particular molecule. In the next paragraphs we shall report such an analysis for the simplest system with C_{4v} symmetry, the pyramidal XY_4 molecule.

III. NORMAL COORDINATES FOR PYRAMIDAL XY_4

The model assumed has, in its equilibrium configuration, the form of a pyramid as drawn in Fig. 2. The X particle of mass M is situated at the apex (5) and a Y particle of mass m at each base corner (1, 2, 3, and 4). The base is a square with length $2a$. A right-handed body-fixed coordinate system x, y, z is attached to the molecule so as to satisfy the Eckart conditions:[8,9]

(a) The center of gravity is at the origin:

$$\sum_{i=1}^{5}(mx_i^{\circ})+Mx_5^{\circ}=0, \text{ etc.}$$

(b) The angular momentum of vibration vanishes in zeroth approximation:

$$\sum_{i=1}^{5} m(x_i^{\circ}\dot{y}_i-y_i^{\circ}\dot{x}_i)+M(x_5^{\circ}\dot{y}_5-y_5^{\circ}\dot{x}_5)=0, \text{ etc.}$$

It follows from simple geometrical considerations that the moments of inertia in the equilibrium configuration, $I_{\alpha\alpha}^{(e)}$, are given by

$$I_{xx}^{(e)}=I_{yy}^{(e)}=4m\{a^2+(z_1^{e})^2\}+[16m^2(z_1^{e})^2/M], \quad (1a)$$

$$I_{zz}^{(e)}=8ma^2. \quad (1b)$$

Herzberg[10] has drawn schematically the nine normal vibrations which have the symmetry A_1 (twice), B_1 (twice), B_2 (one), and E (four), respectively. In order to relate the normal coordinates to the displacement coordinates (for small displacements), δx_i, δy_i, δz_i, etc., we introduce the following symmetry coordinates:

Symmetry A_1

$$q_1=(x_3+x_4)-(x_1+x_2)+(y_2+y_3)-(y_1+y_4)$$

$$q_2=z_5-\tfrac{1}{4}(z_1+z_2+z_3+z_4),$$

Symmetry B_1

$$q_3=(x_1+x_4)-(x_2+x_3)+(y_1+y_2)-(y_3+y_4)$$

$$q_4=(z_1+z_3)-(z_2+z_4),$$

Symmetry B_2

$$q_5=(x_1+x_2)-(x_3+x_4)+(y_2+y_3)-(y_1+y_4), \quad (2)$$

Symmetry E

$$q_6=x_5-\tfrac{1}{4}(x_1+x_2+x_3+x_4)$$

$$q_7=(y_1-y_2)+(y_3-y_4)$$

$$q_8=y_5-\tfrac{1}{4}(y_1+y_2+y_3+y_4)$$

$$q_9=(x_1-x_2)+(x_3-x_4).$$

With the aid of the Eckart conditions given above, we easily obtain from Eq. (2) the expressions for the instantaneous coordinates of the particles x_i, y_i, z_i, etc., and those for the distance between pairs of particles δS_{ij}, in terms of the symmetry coordinates q_i. The details concerned are irrelevant for our purpose. For the kinetic energy we finally obtain the expression

$$2T=\tfrac{1}{8}m\{q_1^2+q_3^2+2q_4^2+q_5^2+2q_7^2+2q_9^2\}$$
$$+\mu q_2^2+\mu'(q_6^2+q_8^2), \quad (3)$$

where

$$\mu=4mM/(4m+M), \quad (4a)$$

$$\mu'=\mu+[4m(z_1^{e})^2/a^2]. \quad (4b)$$

The quadratic portion of V appears to have cross terms only in those pairs of symmetry coordinates that

[8] C. Eckart, Phys. Rev. **47**, 552 (1935).
[9] E. Bright Wilson, Jr., and J. B. Howard, J. Chem. Phys. **4**, 262 (1936).
[10] G. K. Herzberg, *Infrared and Raman Spectra of Polyatomic Molecules* (Prentice-Hall, Inc., New York, 1945), Vol. 2.

TABLE I. Values of $l^{(\alpha)}_{is''}$ and $l^{(\alpha)}_{iss}$.

	1	2	3	4	5	$s1$	$s'1$	$s2$	$s'2$
x_1	$-\frac{1}{2}\sqrt{2}\alpha_{12}$	$-\frac{1}{2}\sqrt{2}\beta_{12}$	$\frac{1}{2}\sqrt{2}\alpha_{34}$	$\frac{1}{2}\sqrt{2}\beta_{34}$	$\frac{1}{2}\sqrt{2}$	$-\frac{1}{2}\mu(m\mu')^{-\frac{1}{2}}\alpha$	$-\frac{1}{2}\mu(m\mu')^{-\frac{1}{2}}\beta$	$-\frac{1}{2}\beta$	$\frac{1}{2}\alpha$
x_2	$-\frac{1}{2}\sqrt{2}\alpha_{12}$	$-\frac{1}{2}\sqrt{2}\beta_{12}$	$-\frac{1}{2}\sqrt{2}\alpha_{34}$	$-\frac{1}{2}\sqrt{2}\beta_{34}$	$\frac{1}{2}\sqrt{2}$	$-\frac{1}{2}\mu(m\mu')^{-\frac{1}{2}}\alpha$	$-\frac{1}{2}\mu(m\mu')^{-\frac{1}{2}}\beta$	$\frac{1}{2}\beta$	$-\frac{1}{2}\alpha$
x_3	$\frac{1}{2}\sqrt{2}\alpha_{12}$	$\frac{1}{2}\sqrt{2}\beta_{12}$	$-\frac{1}{2}\sqrt{2}\alpha_{34}$	$-\frac{1}{2}\sqrt{2}\beta_{34}$	$-\frac{1}{2}\sqrt{2}$	$-\frac{1}{2}\mu(m\mu')^{-\frac{1}{2}}\alpha$	$-\frac{1}{2}\mu(m\mu')^{-\frac{1}{2}}\beta$	$-\frac{1}{2}\beta$	$\frac{1}{2}\alpha$
x_4	$\frac{1}{2}\sqrt{2}\alpha_{12}$	$\frac{1}{2}\sqrt{2}\beta_{12}$	$\frac{1}{2}\sqrt{2}\alpha_{34}$	$\frac{1}{2}\sqrt{2}\beta_{34}$	$-\frac{1}{2}\sqrt{2}$	$-\frac{1}{2}\mu(m\mu')^{-\frac{1}{2}}\alpha$	$-\frac{1}{2}\mu(m\mu')^{-\frac{1}{2}}\beta$	$\frac{1}{2}\beta$	$-\frac{1}{2}\alpha$
x_5	0	0	0	0	0	$\mu(M\mu')^{-\frac{1}{2}}\alpha$	$\mu(M\mu')^{-\frac{1}{2}}\beta$	0	0
y_1	$-\frac{1}{2}\sqrt{2}\alpha_{12}$	$-\frac{1}{2}\sqrt{2}\beta_{12}$	$\frac{1}{2}\sqrt{2}\alpha_{34}$	$\frac{1}{2}\sqrt{2}\beta_{34}$	$-\frac{1}{2}\sqrt{2}$	$-\frac{1}{2}\beta$	$\frac{1}{2}\alpha$	$-\frac{1}{2}\mu(m\mu')^{-\frac{1}{2}}\alpha$	$-\frac{1}{2}\mu(m\mu')^{-\frac{1}{2}}\beta$
y_2	$\frac{1}{2}\sqrt{2}\alpha_{12}$	$\frac{1}{2}\sqrt{2}\beta_{12}$	$\frac{1}{2}\sqrt{2}\alpha_{34}$	$\frac{1}{2}\sqrt{2}\beta_{34}$	$\frac{1}{2}\sqrt{2}$	$\frac{1}{2}\beta$	$-\frac{1}{2}\alpha$	$-\frac{1}{2}\mu(m\mu')^{-\frac{1}{2}}\alpha$	$-\frac{1}{2}\mu(m\mu')^{-\frac{1}{2}}\beta$
y_3	$\frac{1}{2}\sqrt{2}\alpha_{12}$	$\frac{1}{2}\sqrt{2}\beta_{12}$	$-\frac{1}{2}\sqrt{2}\alpha_{34}$	$-\frac{1}{2}\sqrt{2}\beta_{34}$	$\frac{1}{2}\sqrt{2}$	$-\frac{1}{2}\beta$	$\frac{1}{2}\alpha$	$-\frac{1}{2}\mu(m\mu')^{-\frac{1}{2}}\alpha$	$-\frac{1}{2}\mu(m\mu')^{-\frac{1}{2}}\beta$
y_4	$-\frac{1}{2}\sqrt{2}\alpha_{12}$	$-\frac{1}{2}\sqrt{2}\beta_{12}$	$-\frac{1}{2}\sqrt{2}\alpha_{34}$	$-\frac{1}{2}\sqrt{2}\beta_{34}$	$-\frac{1}{2}\sqrt{2}$	$\frac{1}{2}\beta$	$-\frac{1}{2}\alpha$	$-\frac{1}{2}\mu(m\mu')^{-\frac{1}{2}}\alpha$	$-\frac{1}{2}\mu(m\mu')^{-\frac{1}{2}}\beta$
y_5	0	0	0	0	0	0	0	$\mu(M\mu')^{-\frac{1}{2}}\alpha$	$\mu(M\mu')^{-\frac{1}{2}}\beta$
z_1	$\frac{1}{2}(\mu/m)^{\frac{1}{2}}\beta_{12}$	$-\frac{1}{2}(\mu/m)^{\frac{1}{2}}\alpha_{12}$	$-\frac{1}{2}\beta_{34}$	$\frac{1}{2}\alpha_{34}$	0	$(z_1^e/a)(m/\mu')^{\frac{1}{2}}\alpha$	$(z_1^e/a)(m/\mu')^{\frac{1}{2}}\beta$	$(z_1^e/a)(m/\mu')^{\frac{1}{2}}\alpha$	$(z_1^e/a)(m/\mu')^{\frac{1}{2}}\beta$
z_2	$\frac{1}{2}(\mu/m)^{\frac{1}{2}}\beta_{12}$	$-\frac{1}{2}(\mu/m)^{\frac{1}{2}}\alpha_{12}$	$\frac{1}{2}\beta_{34}$	$-\frac{1}{2}\alpha_{34}$	0	$(z_1^e/a)(m/\mu')^{\frac{1}{2}}\alpha$	$(z_1^e/a)(m/\mu')^{\frac{1}{2}}\beta$	$-(z_1^e/a)(m/\mu')^{\frac{1}{2}}\alpha$	$-(z_1^e/a)(m/\mu')^{\frac{1}{2}}\beta$
z_3	$\frac{1}{2}(\mu/m)^{\frac{1}{2}}\beta_{12}$	$-\frac{1}{2}(\mu/m)^{\frac{1}{2}}\alpha_{12}$	$-\frac{1}{2}\beta_{34}$	$\frac{1}{2}\alpha_{34}$	0	$-(z_1^e/a)(m/\mu')^{\frac{1}{2}}\alpha$	$-(z_1^e/a)(m/\mu')^{\frac{1}{2}}\beta$	$-(z_1^e/a)(m/\mu')^{\frac{1}{2}}\alpha$	$-(z_1^e/a)(m/\mu')^{\frac{1}{2}}\beta$
z_4	$\frac{1}{2}(\mu/m)^{\frac{1}{2}}\beta_{12}$	$-\frac{1}{2}(\mu/m)^{\frac{1}{2}}\alpha_{12}$	$\frac{1}{2}\beta_{34}$	$-\frac{1}{2}\alpha_{34}$	0	$-(z_1^e/a)(m/\mu')^{\frac{1}{2}}\alpha$	$-(z_1^e/a)(m/\mu')^{\frac{1}{2}}\beta$	$(z_1^e/a)(m/\mu')^{\frac{1}{2}}\alpha$	$(z_1^e/a)(m/\mu')^{\frac{1}{2}}\beta$
z_5	$-(\mu/M)^{\frac{1}{2}}\beta_{12}$	$(\mu/M)^{\frac{1}{2}}\alpha_{12}$	0	0	0	0	0	0	0

belong to the same species. This confirms that our choice of symmetry coordinates (2) was a suitable one and that we may introduce a set of normal coordinates $Q_1, \cdots, Q_9$ satisfying the relations

$$\begin{aligned} q_1&=2(2/m)^{\frac{1}{2}}(\alpha_{12}Q_1+\beta_{12}Q_2),\\ q_2&=\mu^{-\frac{1}{2}}(-\beta_{12}Q_1+\alpha_{12}Q_2),\\ q_3&=2(2/m)^{\frac{1}{2}}(\alpha_{34}Q_3+\beta_{34}Q_4),\\ q_4&=2m^{-\frac{1}{2}}(-\beta_{34}Q_3+\alpha_{34}Q_4),\\ q_5&=2(2/m)^{\frac{1}{2}}Q_5, \end{aligned} \tag{5a}$$

$$\begin{aligned} q_6&=(\mu')^{-\frac{1}{2}}(\alpha_{67}Q_6+\beta_{67}Q_7),\\ q_7&=2m^{-\frac{1}{2}}(-\beta_{67}Q_6+\alpha_{67}Q_7),\\ q_8&=(\mu')^{-\frac{1}{2}}(\alpha_{67}Q_8+\beta_{67}Q_9),\\ q_9&=2m^{-\frac{1}{2}}(-\beta_{67}Q_8+\alpha_{67}Q_9). \end{aligned} \tag{5b}$$

The α_{ij} and β_{ij} are related in a complicated way to the constants determining both the geometry and the force field of the molecule. For our purpose the explicit expressions need not be written down. For each ij, we have the normalizing condition

$$\alpha_{ij}^2+\beta_{ij}^2=1. \tag{6}$$

Within the scope of the present investigation, we are mainly interested in the degenerate modes of vibration. In order that our notation may conform to common usage, we rewrite Eqs. (5b) as follows (put $\alpha_{67}=\alpha$ and $\beta_{67}=\beta$):

$$\begin{aligned} q_6&=(\mu')^{-\frac{1}{2}}(\alpha Q_{s1}+\beta Q_{s'1}),\\ q_7&=2m^{-\frac{1}{2}}(-\beta Q_{s1}+\alpha Q_{s'1}),\\ q_8&=(\mu')^{-\frac{1}{2}}(\alpha Q_{s2}+\beta Q_{s'2}),\\ q_9&=2m^{-\frac{1}{2}}(-\beta Q_{s2}+\alpha Q_{s'2}). \end{aligned} \tag{7}$$

Here Q_{s1} and Q_{s2} denote the degenerate vibrations with frequency ω_s, and $Q_{s'1}$ and $Q_{s'2}$ those associated with $\omega_{s'}$.

From Eqs. (2), (5a), and (7), we finally obtain the constants $l^{(\alpha)}_{iss}$, giving the displacement coordinates (x_i, y_i, z_i) in terms of the normal coordinates Q_i, according to

$$m_i^{\frac{1}{2}}\dot{\alpha}_i=\sum_{s''=1}^{5} l^{(\alpha)}_{is''}\dot{Q}_{s''}+\sum_{ss's'} l^{(\alpha)}_{iss'}\dot{Q}_{ss'}. \tag{8}$$

Values of the $l^{(\alpha)}_{is''}$ and $l^{(\alpha)}_{iss}$ are given in Table I.

IV. l-TYPE DOUBLING IN PYRAMIDAL XY_4

The general form of that part of the hamiltonian for an axially symmetric polyatomic molecule which gives rise to l-type doubling in second-order approximation has been given by Nielsen:[11]

$$\begin{aligned} H^{(2)'}=&-\sum_{\alpha}\sum_{ss}\sum_{s's'}(\hbar/2\lambda_s^{\frac{1}{2}}\lambda_{s'}^{\frac{1}{2}}(I^{(e)}_{\alpha\alpha})^2)\\ &\cdot\{[A^{(\alpha\alpha)}_{sss's'}-\sum_{\beta}(a^{(\alpha\beta)}_{ss}\,a^{(\alpha\beta)}_{s's'}/I^{(e)}_{\beta\beta})\\ &-2\sum_{s''s''}\zeta^{(\alpha)}_{sss''s''}\zeta^{(\alpha)}_{s's's''s''}\cdot\lambda_s/(\lambda_s-\lambda_{s''})]q_{ss}q_{s's'}\\ &-2\sum_{s''s''}[\zeta^{(\alpha)}_{sss''s''}\zeta^{(\alpha)}_{s's's''s''}\cdot\lambda_s^{\frac{1}{2}}\lambda_{s'}^{\frac{1}{2}}/(\lambda_s-\lambda_{s''})]\\ &\times(p_{ss}p_{s's'}/\hbar^2)\}P_\alpha^2+\sum_{\alpha,\beta,\gamma}'\sum_{ss}\sum_{s's'}(\hbar/2\lambda_s^{\frac{1}{2}}\lambda_{s'}^{\frac{1}{2}}\\ &\times I^{(e)}_{\alpha\alpha}I^{(e)}_{\beta\beta})\cdot\{[A^{(\alpha\beta)}_{sss's'}-(a^{(\alpha\alpha)}_{ss}\,a^{(\alpha\beta)}_{s's'}/I^{(e)}_{\alpha\alpha}\\ &-(a^{(\beta\beta)}_{ss}\,a^{(\alpha\beta)}_{s's'}/I^{(e)}_{\beta\beta})+(a^{(\alpha\gamma)}_{ss}\,a^{(\gamma\beta)}_{s's'}/I^{(e)}_{\gamma\gamma})\\ &-2\sum_{s''s''}\zeta^{(\alpha)}_{sss''s''}\zeta^{(\beta)}_{s's's''s''}\cdot\lambda_s/(\lambda_s-\lambda_{s''})]q_{ss}q_{s's'}\\ &-2\sum_{s''s''}[\zeta^{(\alpha)}_{sss''s''}\zeta^{(\beta)}_{s's's''s''}\cdot\lambda_s^{\frac{1}{2}}\lambda_{s'}^{\frac{1}{2}}/(\lambda_s-\lambda_{s''})]\\ &\times p_{ss}p_{s's'}/\hbar^2\}P_\alpha P_\beta+\cdots, \end{aligned} \tag{9}$$

[11] See reference 2. Some errors of sign and a few obvious misprints occur in Eqs. (2) and (3) of that paper. These have been corrected in Eq. (9) of the present publication.

where

$$\lambda_s=(2\pi c\omega_s)^2, \tag{10}$$

$$q_{s\sigma}=(h^2/\lambda_s)^{-\frac{1}{4}}Q_{s\sigma}, \tag{11}$$

$$A^{(\alpha\alpha)}_{s\sigma s''\sigma''}=\sum_i (l^{(\beta)}_{is\sigma}l^{(\beta)}_{is''\sigma''}+l^{(\gamma)}_{is\sigma}l^{(\gamma)}_{is''\sigma''}), \tag{12}$$

$$A^{(\alpha\beta)}_{s\sigma s''\sigma''}=-\sum_i l^{(\alpha)}_{is\sigma}l^{(\beta)}_{is''\sigma''}, \tag{13}$$

$$a^{(\alpha\alpha)}_{s\sigma}=2\sum_i m_i^{\frac{1}{2}}(\beta_i{}^o l^{(\beta)}_{is\sigma}+\gamma_i{}^o l^{(\gamma)}_{is\sigma}), \tag{14}$$

$$a^{(\alpha\beta)}_{s\sigma}=-\sum_i m_i^{\frac{1}{2}}(\alpha_i{}^o l^{(\beta)}_{is\sigma}+\beta_i{}^o l^{(\alpha)}_{is\sigma}), \tag{15}$$

$$\zeta^{(\alpha)}_{s\sigma s'\sigma'}=\sum_i (l^{(\beta)}_{is\sigma}l^{(\gamma)}_{is'\sigma'}-l^{(\beta)}_{is'\sigma'}l^{(\gamma)}_{is\sigma}). \tag{16}$$

In Eq. (9) P_α is the α-component of the total angular momentum, and $p_{s\sigma}$ is the momentum conjugate to $q_{s\sigma}$; the $q_{s\sigma}$ and $p_{s\sigma}$ can be replaced by their equivalents in cylindrical polar coordinates r, χ:

$$q_{s,1}=r_s\cos\chi_s, \quad p_{s,1}=-ih\left[\cos\chi_s\frac{\partial}{\partial r_s}-\frac{\sin\chi_s}{r_s}\frac{\partial}{\partial\chi_s}\right],$$

$$q_{s,2}=r_s\sin\chi_s, \quad p_{s,2}=-ih\left[\sin\chi_s\frac{\partial}{\partial r_s}+\frac{\cos\chi_s}{r_s}\frac{\partial}{\partial\chi_s}\right]. \tag{17}$$

In our case, s can have two values, s and s'; σ takes on the values 1 and 2. In Eq. (9) $\sum'_{\alpha\beta\gamma}$ means that the summation is to be extended over α, β, and γ, where the three indexes may not all be identical. The s'', in our case, refer to the vibrations $Q_1, \cdots, Q_b$, all of which are nondegenerate, so that the subscript σ'' is superfluous.

Of all constants A, a, and ζ, only the following do not vanish (specific values calculated with the l's of Table I):

$$\begin{aligned}
A^{(xx)}_{s1s1}&=\beta^2+4(z_1{}^o/a)^2(m/\mu')\alpha^2,\\
A^{(xx)}_{s2s2}&=\alpha^2,\\
A^{(xy)}_{s1s2}&=-\alpha^2(\mu/\mu'),\\
A^{(xy)}_{s2s1}&=-\beta^2,\\
a^{(xx)}_{s1}&=a^{(xy)}_{s2}=8m(\mu')^{-\frac{1}{2}}z_1{}^o\alpha.
\end{aligned} \tag{18}$$

To obtain the corresponding constants for s', we merely have to interchange α and β

$$\begin{aligned}
\zeta^{(x)}_{s21'}&=-\zeta^{(y)}_{s11'}=\alpha(\mu')^{-\frac{1}{2}}\{\beta_{12}\mu^{\frac{1}{2}}-\alpha_{12}(z_1{}^o/a)(2m)^{\frac{1}{2}}\},\\
\zeta^{(x)}_{s22'}&=-\zeta^{(y)}_{s12'}=-\alpha(\mu')^{-\frac{1}{2}}\{\alpha_{12}\mu^{\frac{1}{2}}+\beta_{12}(z_1{}^o/a)(2m)^{\frac{1}{2}}\},\\
\zeta^{(x)}_{s13'}&=-\zeta^{(y)}_{s23'}=-\beta\cdot\beta_{34}+\alpha\cdot\alpha_{34}(z_1{}^o/a)(2m/\mu')^{\frac{1}{2}},\\
\zeta^{(x)}_{s14'}&=-\zeta^{(y)}_{s24'}=\beta\cdot\alpha_{34}+\alpha\cdot\beta_{34}(z_1{}^o/a)(2m/\mu')^{\frac{1}{2}},\\
\zeta^{(x)}_{s25'}&=-\zeta^{(y)}_{s15'}=-\alpha(z_1{}^o/a)(2m/\mu')^{\frac{1}{2}},\\
\zeta^{(x)}_{s1s2}&=\alpha^2(\mu/\mu')-\beta^2.
\end{aligned} \tag{19}$$

Again, if s is replaced by s', we have to interchange α and β.

Substitution of Eqs. (12)–(19) in the expression for the hamiltonian, (9), yields

$$\begin{aligned}
H^{(2)'}=\cdots&-\bar{\sum_{+}}\sum_s(B_e/4\omega_s)\\
&\times[\{1-\alpha^2[1+64(mz_1{}^o)^2/(\mu' I^{(e)}_{xx})]\}(e^{\pm i\chi_s}\pi_s)^2\\
&-\sum_{s''}(\zeta^{(x)}_{ss''})^2[\lambda_s/(\lambda_s-\lambda_{s''})](e^{\pm i\chi_s})^2\\
&\times\{r_s{}^2+[(p_{r_s}\pm ip\chi_s/r_s)/h]^2\}]\cdot\{P_x\mp iP_y\}^2/I^{(e)}_{xx}\\
&-\bar{\sum_{+}}\sum_s(B_e/4\omega_s)\{-\alpha^2\mu/\mu'\}(e^{\pm i\chi_s}\pi_s)^2\\
&\cdot\{P_x\pm iP_y\}^2/I^{(e)}_{xx}.
\end{aligned} \tag{20}$$

The matrix components of (20) can be evaluated with the aid of the relations given by Shaffer,[12] along the lines indicated by Nielsen.[2] Assume first that the vibration s is excited. Then for the first term in (20) the only nonvanishing components which are diagonal in V_s are $(V_s, l_s, K|H^{(2)'}|V_s, l_s\pm2, K\pm2)$, whereas for the second term only $(V_s, l_s, K|H^{(2)'}|V_s, l_s\pm2, K\mp2)$ will not be equal to zero. Hence, the following nondiagonal matrix elements will be responsible for the l-type

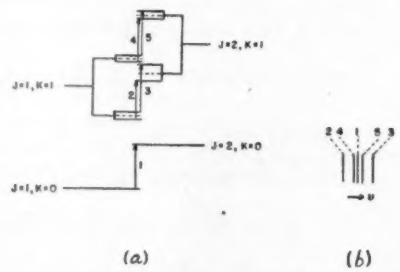

FIG. 3. (a) Rotation levels of an axially symmetric molecule, belonging to the group C_{4v}, for $J=1$ and $J=2$, showing l-type doubling, when the molecule is in a vibration state when $l=1$, both for $K=l$ and $K=-l$. (b) Microwave absorption pattern predicted on the basis of l-type doubling (Fig. 2 (a)) and assuming the centrifugal stretching of both Coriolis components to be alike.

[12] W. H. Shaffer, Revs. Modern Phys. **16**, 235 (1944).

doubling:

(a) For the level $K=l$:

$$(V_s, l_s, K|H^{(2)'}|V_s, l_s\pm 2, K\pm 2)$$
$$=hcB_e(B_e/2\omega_s)$$
$$\cdot\{1-\alpha^2[\mu a^2+12m(z_1^o)^2]/[\mu a^2+4m(z_1^o)^2]$$
$$+4\sum_{s''}{}^{(x)}[\{\zeta_{ss''}^{(z)}\}^2\lambda_s/(\lambda_s-\lambda_{s''})]\}$$
$$\cdot\{[J(J+1)-K(K\pm 1)]\cdot[(J(J+1)$$
$$-(K\pm 1)(K\pm 2)][(V_s\mp l_s)(V_s\pm l_s+2)]\}^{\frac{1}{2}}, \quad (21a)$$

where, making use of Eqs. (1b) and (4b), we have replaced $[1+64(mz_1^o)^2/(\mu' I_{zz}^{(e)})]$ by $[\mu a^2+12m(z_1^o)^2]/[\mu a^2+4m(z_1^o)^2]$.

(b) For the level $K=-l$:

$$(V_s, l_s, K|H^{(2)'}|V_s, l_s\pm 2, K\mp 2)$$
$$=-hcB_e(B_e/2\omega_s)\alpha^2 I_{zz}^{(e)}/(I_{xx}^{(e)}+I_{yy}^{(e)})$$
$$\times\{[J(J+1)-K(K\pm 1)][J(J+1)$$
$$-(K\pm 1)(K\pm 2)]\cdot[(V_s\pm l_s)(V_s\mp l_s+2)]\}^{\frac{1}{2}}, \quad (21b)$$

where, using Eqs. (1a), (1b), (4a), and (4b), we have replaced (μ/μ') by $I_{zz}^{(e)}/(I_{xx}^{(e)}+I_{yy}^{(e)})$.

If the vibration s' is excited, then in Eqs. (21a), and (21b) we have to replace s by s' and interchange α and β.

V. DISCUSSION

The result, embodied in Eqs. (21a) and (21b), is that for the simple XY_4 model chosen, the l-type splitting of both Coriolis components, $K=l=1$ and $K=-l=1$, is of the same order. The actual magnitude of this splitting still depends on both the geometry and the force field (influencing our equations through the constants α and β) of the molecule under consideration. In particular, Eq. (21b) shows that the splitting of the level $K=-l=1$ would be a maximum in the case of planar XY_4 molecules (when $I_{zz}^{(e)}/(I_{xx}^{(e)}+I_{yy}^{(e)})=1$), and that this splitting goes to zero as $I_{zz}^{(e)}$ approaches zero (linear model!). There is no reason to expect the situation for other molecules belonging to the C_{4v} (and V_d) group to be essentially different. A possible sequence of rotational levels is drawn in Fig. 3(a) and a possible microwave absorption pattern in Fig. 3(b). Actually, the relative position of the lines 2 and 4 (or 5 and 3) is still uncertain, since it is undetermined which of the two Coriolis levels will suffer the largest splitting. The sign of $\zeta_{s1s2}^{(z)}$ will determine which of the two Coriolis components is the lower and which is the higher level; subsequently, the l-type doubling will be given by equations of the type (21a) and (21b).

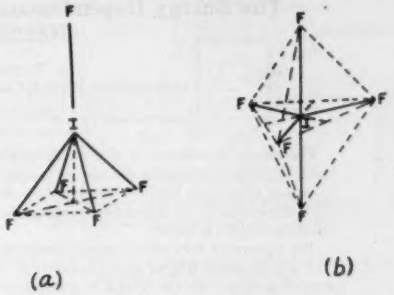

FIG. 4. (a) C_{4v} structure for IF_5. (b) Bipyramidal structure for IF_5.

Recently, Lord *et al.*[13] have proposed a structure for IF_5, which has C_{4v} symmetry (Fig. 4(a)). Their evidence is not quite conclusive, and at present it is not sure whether this molecule has, indeed, this structure or whether it should be represented by a bipyramidal model (Fig. 4(b)). If it has the C_{4v} symmetry as indicated, then IF_5 should show the "twofold l-type doubling," which we have discussed in this paper. Since the bipyramidal structure has no dipole moment around the z axis, it might show no microwave absorption at all. However, if two degenerate frequencies, s and s', lie close enough together, we might get a transition from a rotational level associated with frequency s to one associated with frequency s', a transition that might involve a transition moment around the z axis.[14] If such a microwave spectrum could be observed, only half of the levels (those for $K=l$) will undergo l-type doubling (D_{2h} symmetry!). If no microwave spectrum can be detected at all, the model proposed by Lord *et al.*[13] must be rejected.[15]

Allene, C_3H_4, belonging to the group V_d, should also show the "twofold l-type doubling" discussed in this paper. Again, this can only be detected in the microwave spectrum if a transition from an s rotational sublevel to an s' rotational sublevel is associated with a transition moment along the molecular axis.

The author wishes to acknowledge the award of a post doctoral scholarship from the Graduate School of the Ohio State University, which has enabled him to carry out the investigation reported in this paper. He also wishes to express his gratitude to Professor Harald H. Nielsen for his continuous assistance and stimulating discussions during the course of this investigation.

[13] Lord, Lynch, Schumb, and Slowinsky, J. Am. Chem. Soc. 72, 522 (1950).

[14] A. H. Nielsen and R. M. Talley, J. Chem. Phys. (to be published).

[15] As far as we know, no direct dipole moment investigation on IF_5 has been reported.

The Energy Dependence of the Resonant Scattering of Slow Neutrons from Gold*

JAY TITTMAN AND CHARLES SHEER
Department of Physics, Columbia University, New York, New York

(Received January 31, 1951)

The energy dependence of slow neutrons scattered from a thick gold target has been measured using a newly developed scattering chamber in conjunction with the Columbia slow neutron velocity spectrometer. A method of analysis has been developed for determining the ratio of the scattering cross section to the total cross section, σ_s/σ_t, as a function of energy for an "unknown" sample in terms of a calibration target for which $(\sigma_s/\sigma_t)(E)$ is known.

The agreement between the experimental determination of $(\sigma_s/\sigma_t)(E)$ for gold in the energy range 0.7 to 8 ev and the Breit-Wigner theory is excellent. All the level parameters can be evaluated by combining these scattering data with the results of transmission experiments and the cross section for self-indication. The final results for the 4.9-ev gold level are: $J=1$, $\Gamma=0.172$ ev, $\Gamma_N=0.0211$ ev, $R_{J=1}=1.03$ barn$^{\frac{1}{2}}$, $R_{J=2}=0.917$ barn$^{\frac{1}{2}}$.

I. INTRODUCTION

THE Breit-Wigner equations for nuclear resonance phenomena have been derived from several different viewpoints.[1-3] However, the mechanism of excited compound nucleus formation with subsequent decay, as originally suggested by Bohr,[4] remains intact through all the derivations. For slow neutron interactions it is usually necessary to consider only elastic scattering and radiative capture. The one level expressions for these cross sections for a single isotope can be written as

$$\sigma_c(E)=\sigma_{c0}\Gamma^2(E_0/E)^{\frac{1}{2}}/[4(E-E_0)^2+\Gamma^2]$$

and

$$\sigma_s(E)=(G_{\pm}\sigma_{p\pm}+G_{\mp}\sigma_{p\mp})+4\pi G_{\mp}\left[\frac{\lambda_0^2\Gamma_N^2+4\lambda_0\Gamma_N R_{\mp}(E-E_0)}{4(E-E_0)^2+\Gamma^2}\right],$$

where σ_c = capture cross section; $\sigma_{c0}=4\pi\lambda_0^2G_{\mp}\Gamma_N\Gamma_\gamma/\Gamma^2$ = capture cross section at the energy of exact resonance, E_0; $\Gamma=\Gamma_N+\Gamma_\gamma$ = total level width; Γ_N = neutron width at exact resonance; Γ_γ = gamma-ray width; σ_s = scattering cross section; $\lambda_0=(\frac{1}{2}\pi)\times$neutron wavelength at the resonance energy, E_0; $G=(2J+1)/[(2I+1)(2S+1)]$ = statistical weight; R = effective nuclear radius; σ_p = potential scattering cross section $(=4\pi R^2)$. The statistical weight factor G, where $J=I\pm S$, depends upon the relative orientation of the spins of the incident neutron and of the struck nucleus. The subscripts $\pm$ and $\mp$ are included to designate quantities which depend specifically on the total spin quantum number of the system, J, for the collision. For example $(G_{\pm}\sigma_{p\pm})$ is the contribution to the total potential scattering cross section from collisions which do not satisfy the necessary spin condition for resonance (in the case of a mono-isotopic material). Here $(G_{\mp}\sigma_{p\mp})$ is the contribution from collisions which do have the appropriate total spin. Thus, the total potential scattering cross section σ_p is

$$\sigma_p=G_{\pm}\sigma_{p\pm}+G_{\mp}\sigma_{p\mp}=4\pi R_{\text{eff}}^2,$$

where R_{eff} is the effective nuclear radius for the isotope involved and is not necessarily the same as $R_{\mp}$, which is the effective nuclear radius for collisions which have total spin equal to the J of the level at E_0.

The capture cross section has the straightforward damped resonance form, modulated by the $1/v$ factor. Here σ_s shows the addition of potential and resonance scattering and also contains a term arising from the interference[5] between these two effects. This interference results in a depression of σ_s on the low energy side of resonance and an augmentation on the high energy side. It is worthy of note that at the minimum of the depression, $\sigma_s=G_{\pm}\sigma_{p\pm}$.

Although an abundance of data has been collected on epithermal cross sections for the elements,[6-14] detailed measurements of σ_s as a function of energy have been restricted to regions in which the capture process plays

* For preliminary reports see Tittman, Sheer, Rainwater, and Havens, Phys. Rev. **77**, 748(A) (1950); **80**, 903 (1950); **82**, 344 (1951).

[1] G. Breit and E. Wigner, Phys. Rev. **49**, 519 (1936); H. A. Bethe and G. Placzek, Phys. Rev. **51**, 450 (1937); Kalckar, Oppenheimer, and Serber, Phys. Rev. **52**, 273 (1937); Kapur and R. E. Peierls, Proc. Roy. Soc. (London) **A166**, 277 (1938); Arnold J. F. Siegert, Phys. Rev. **56**, 750 (1939); G. Breit, Phys. Rev. **69**, 472 (1946); E. Wigner, Phys. Rev. **70**, 15, 606 (1946); E. P. Wigner and L. Eisenbud, Phys. Rev. **72**, 29 (1947).

[2] H. A. Bethe, Revs. Modern Phys. **9**, 69 (1937).

[3] Feshbach, Peaslee, and Weisskopf, Phys. Rev. **71**, 145, 564 (1947).

[4] N. Bohr, Nature **137**, 344 (1936).

[5] For curves illustrating this effect in In see reference 3.

[6] Goldsmith, Ibser, and Feld, Revs. Modern Phys. **19**, 259 (1947).

[7] L. J. Rainwater and W. W. Havens, Phys. Rev. **70**, 136 (1946).

[8] W. W. Havens and L. J. Rainwater, Phys. Rev. **70**, 154 (1946).

[9] Rainwater, Havens, Wu, and Dunning, Phys. Rev. **71**, 65 (1947).

[10] Havens, Wu, Rainwater, and Meaker, Phys. Rev. **71**, 165 (1947).

[11] Wu, Rainwater, and Havens, Phys. Rev. **71**, 174 (1947).

[12] Rainwater, Havens, Dunning, and Wu, Phys. Rev. **73**, 733 (1948).

[13] Havens, Rainwater, Wu, and Dunning, Phys. Rev. **73**, 963 (1948).

[14] References 6 through 13 contain additional bibliographies.

a negligible role. At these higher energies the potential-resonance interference has been observed in the case of S-wave scattering from sulfur.[15] At lower energies the Cd resonance has been investigated in detail by transmission measurements.[7,9] However, the only information on scattering in the low energy resonance region has been obtained through the use of resonance scattering detectors or other methods involving the determination of level parameters by means of the measurement of integrals of $\sigma_s(E)$ and/or $\sigma_c(E)$ over relatively broad energy regions.[16–22]

The present paper describes the development of a method for the measurement of the energy dependence of neutron scattering from thick targets and the conversion of this measurement into $(\sigma_s/\sigma_t)(E)$, the ratio of the scattering cross section to the total cross section. Of course, measurements of this type will be of value only in cases where some capture is present. The method consists essentially of the use of the Columbia slow neutron velocity spectrometer[7,9] (NVS) for the energy sorting of neutrons scattered by a thick target. The counting rates are then compared with those due to standard targets of known σ_s/σ_t. Gold has been chosen as the first element to be studied for a number of reasons. It possesses a strong, isolated resonance in an energy region in which the cyclotron intensity is sufficiently high to enable the use of good resolution with the NVS.[8,10] It is a mono-isotopic element of small spin ($I=\frac{3}{2}$) so that the effect of whether $J=I+\frac{1}{2}$ or $I-\frac{1}{2}$ is relatively large. Furthermore, Au has been used in several other experiments as a standard,[22,23] using approximate values for the level parameters, and it was thought desirable to determine these parameters with greater precision than has been done heretofore.

The measurement of $(\sigma_s/\sigma_t)(E)$ does not uniquely determine all the level parameters. However, as will be indicated later, other techniques can be used to fix the remaining unknown ones.

In the remainder of this paper the subscripts t, s, and c refer to total, scattering, and capture, respectively. The subscript 0 refers to a value at exact resonance; for example, $(\sigma_{t0})_{Au}$ is the total cross section for Au at exact resonance. All cross sections are expressed in barns, b ($1\ \text{b}=10^{-24}\ \text{cm}^2$).

II. APPARATUS DESCRIPTION

The Columbia NVS has already been described in detail.[7,9] The present application differs essentially from former ones in that the path of flight of the neutrons now consists of the distance from the paraffin source slab, near the Be cyclotron target, to the scattering target, plus the distance from the scattering target to the BF_3 counter banks. The scattering chamber, a horizontal section of which is illustrated in Fig. 1, is placed in position relative to the cyclotron in a manner similar to that used in the collimating system shown in Fig. 2, reference 7. The neutron beam passes through a hole in the water tanks forming the cyclotron enclosure, is collimated, and strikes the thick scatterer; and the scattered neutrons are detected by the BF_3 proportional counters.

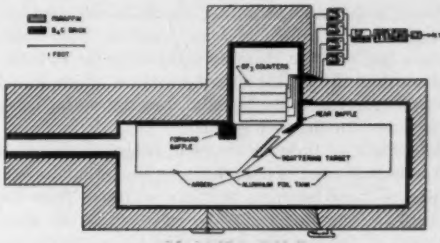

FIG. 1. Schematic drawing of a horizontal section of the neutron scattering chamber.

The inside walls of the scattering chamber are completely lined with B_4C bricks to reduce as much as possible the scattering of neutrons from the walls into the counters. At least 3 inches of paraffin surrounds the B_4C liner to prevent stray fast neutrons outside the cyclotron enclosure from entering the chamber.

The collimator is 3 inches square in cross section, also lined with B_4C bricks to decrease as much as possible "inscattering" to the target and the counters. The principle of design, insofar as the collimator and forward baffle are concerned, requires that no line of sight exist from any point on the collimator wall lining, exposed to the main neutron flux, to the counters. This prevents even the relatively small number of neutrons singly scattered from the collimator walls from contributing to the background. The forward baffle allows the counter banks to be moved close to the scattering target, thus subtending from it a large solid angle, without exposing them to an increased background. By using a thin aluminum target holder, very little extraneous material is exposed to the direct neutron beam to contribute unwanted scattered neutrons to the counting rate to be measured.

The B_4C bricks on the rear wall of the chamber serve as a sink for those neutrons which are either transmitted through the scattering target or pass by its sides. Since even B_4C, however, is not a perfect neutron sink material, some neutrons are backscattered from the backstop, particularly at high energies. Although many of these are captured by the thick scattering target on their way to the counters, some could pass between the

[15] Adair, Bockelman, and Peterson, Phys. Rev. **76**, 308 (1949); Peterson, Barschall, and Bockelman, Phys. Rev. **79**, 593 (1950).
[16] Harris, Seidl, and Langsdorf, Phys. Rev. **72**, 866 (1947).
[17] F. G. P. Seidl, Phys. Rev. **75**, 1508 (1949).
[18] C. T. Hibdon and C. O. Muehlhause, Phys. Rev. **76**, 100 (1949).
[19] C. O. Muehlhause, Phys. Rev. **77**, 739(A) (1950).
[20] Hibdon, Muehlhause, Selove, and Woolf, Phys. Rev. **77**, 730 (1950).
[21] M. Hamermesh and C. O. Muehlhause, Phys. Rev. **78**, 175 (1950).
[22] Harris, Muehlhause, and Thomas, Phys. Rev. **79**, 11 (1950).
[23] H. Pomerance, Phys. Rev. **77**, 747(A) (1950).

scatterer and the upper wall of Fig. 1. To intercept the latter, the rear baffle has been inserted. This baffle extends out into the chamber sufficiently far to intercept most of the backscattered neutrons which would have contributed to background, but not so far as to project into the primary beam.

As a result of these measures in regard to materials and geometry, most of the remaining background would be due to those neutrons multiply scattered from the walls of the chamber and those scattered by air along the path of the incident beam. The air scattering has been eliminated to a large extent by utilizing the very small scattering cross section (0.68 b) of argon.[24] Since it is not feasible to evacuate the chamber, most of the air path has been replaced by an argon path at atmospheric pressure. The argon is contained in the aluminum tanks, shown schematically in Fig. 1. The sides of the tanks are made of 0.004-inch aluminum foil, and the front and back ends, through which the beam passes, are of 0.002-inch foil. Despite the air space remaining between the two tanks and the two aluminum walls before and after the target, it was found that the use of argon to replace air effected an improvement of a factor of two in reduction of background.

The BF_3 proportional counters are stacked in four vertical banks of five counters each, and supported by a thin aluminum framework. The counters all have essentially the same characteristics insofar as pulse height and plateau region are concerned.[25] The outputs of the five counters in each bank are connected in parallel, each bank feeding into its own low input impedance preamplifier. The four preamplifiers then feed their output pulses in parallel onto the grid of a cathode follower and thence to a conventional pulse amplifier (Fig. 1). The pulse amplifier sends approximately 5-volt output pulses to the NVS. Each counter output passes through a plug panel before entering the parallel feed connection into the preamplifier for the bank in which the counter rests. This allows the output of each counter individually to be viewed on an oscilloscope for test purposes. The negative high voltage for the counters, supplied by a radiofrequency high voltage supply, is applied to all the counters in parallel. The $\frac{1}{32}$-inch brass counter cathodes and aluminum frame are contiguous so that the whole assembly is at negative high voltage. The frame stands on 1-inch quartz legs. The gains of the preamplifiers are equalized so that the output pulse height is independent of the counter bank in which the pulse originates. The amplifier output pulses fed to the NVS have a rise time of approximately 0.1 microsecond and width at half-maximum of less than 1 microsecond. The counter voltage, amplifier gain, and NVS level setter are adjusted to give as large a counting rate as possible consistent with the condition that no γ-rays be counted, as determined by tests using strong γ-ray sources.

The time of flight resolution of this system is slightly broadened over that which is encountered in the case of transmission experiments using the NVS. Principally, this is due to the relatively large size (4×6 inches) of the scattering target, depth (8 inches) of the detection volume, and large (~15 percent of total) solid angle subtended by the counters at the target. However, as will be shown later, high resolution is not necessary for the present scattering measurements, and in all cases resolution effects were negligible.

Since the various neutron rays traverse slightly different distances before being counted, it is difficult to assign a measured path length to the path of flight. To fix this value, however, since it is necessary for the determination of the velocity of the scattered neutrons, the following procedure was used. With a thick carbon scatterer in position, to provide high counting rates, the system was used as a scattering detector of slow neutrons, and transmission measurements *vs* time of flight were made for thin Au, In, and Co filters placed before the collimator. Since all of these materials have sharp resonances at well-determined neutron energies, it is possible to determine[7] the effective over-all delay time, t_d', and the effective source-detector distance d with good accuracy from the measured timings for these resonance dips. Use of the three filters mentioned above produced values of t_d' between 8.25 and 9.25 microseconds, which agree well with the independently and more directly measured value of Rainwater and Havens.[26] In this fashion, a mean value of 5.67 meters was measured for the total path of flight.

The background counting rate was about 2 percent of the counting rate due to scattering from a thick carbon target between about 1 and 100 ev.

A test to determine the geometrical width of the beam at the position of the scatterer was made by comparing the scattered neutron counting rates from carbon scatterers of the same thickness and varying widths. This test showed the beam intensity to be constant out to 1.5 inches from the beam axis, dropping to 50 percent of maximum at 2.0 inches, and to 1 percent at 3.5 inches. Thus, the target size was chosen to be 4 inches ×6 inches. Since the target is at 45° to the neutron beam, approximately a projected 4 inch×4 inch square target faces the beam, and an equal projected area faces the counters. This geometry provided a maximum counting rate for a given scatterer, consistent with reasonable resolution.

III. EXPERIMENT ANALYSIS

For a very thin target the number of neutrons scattered should be proportional to the scattering cross section; therefore, by comparing the counting rate due to an "unknown" sample with the counting rate due to

[24] Edward Melkonian, Phys. Rev. **76**, 1750 (1949).

[25] These excellently uniform counters were obtained from the Oak Ridge National Laboratory.

[26] L. J. Rainwater and W. W. Havens, Jr., private communication.

a thin standard such as carbon, the value of $\sigma_s(E)$ could be obtained. Because in many cases this requires inordinately small geometric target thickness and results in extremely low counting rates, a thick target approach has been used for the present measurements. Furthermore, the thin target technique would require far greater cyclotron intensity than is now available for the investigation of resonances, as complete resolution of the level would be necessary unless an integration method of analysis were used.

In order to analyze the significance of the number of scattered neutrons counted with an infinitely thick scatterer, assume the target nucleus to be infinitely heavy so that the neutron suffers no energy loss in the collision. Since only neutron energies well above the thermal region are considered and the solid angle subtended by the detector is fairly large, only free cross sections need be considered. We temporarily neglect the background counting rate. Then, using Fig. 2, which indicates the geometry of the scattering, it can be shown by the method outlined in Appendix A, that the ratio of the counting rate due to neutrons scattered from an *infinitely thick* target of material x to that from a thick carbon target C, is

$$N_x/N_C=\sum_{j=1}^{\infty} g_j(\sigma_s/\sigma_t)^j{}_x\equiv F(\sigma_s/\sigma_t)_x, \qquad (1)$$

where g_j are coefficients depending only on the geometry of the experiment, and j represents the multiplicity of the scattering; i.e., the jth term represents the contribution to the counting rate made by neutrons scattered j times. Note that in Eq. (1) the energy dependence of the ratio N_x/N_C arises solely through the quantity σ_s/σ_t.

The criterion that a target be thick enough to use the "infinite thickness" approximation depends upon the value of σ_s/σ_t. If $(\sigma_s/\sigma_t)<\sim 0.5$, for our geometry, the requirement that the transmission, T, be less than 0.1 is satisfactory to within about 1 percent (see Appendix A). If $(\sigma_s/\sigma_t)>\sim 0.5$, so that more than the first few terms in Eq. (1) contribute appreciably to the scattered neutron counting rate, the appropriate criterion for thickness is that the ratio of geometrical target slant thickness, a, to diffusion length shall be large. All the scatterers used in the present measurements had $T<0.1$ over the range of energy in which they were used. Hence, the results are accurate for measured values of $(\sigma_s/\sigma_t)<\sim 0.5$.

The theoretical evaluation of the g_j with any degree of accuracy for the present "poor geometry" experiment (see Figs. 1 and 2) is extremely difficult. However, by using a standard calibration scatterer, x_0, and measuring $F(\sigma_s/\sigma_t)_{x_0}$, the apparatus can be calibrated experimentally. Subsequent measurement of $F(\sigma_s/\sigma_t)_x$, as a function of E, where x represents the "unknown" scatterer, and comparison with the calibration curve, then yields $(\sigma_s/\sigma_t)_x(E)$. As long as the standard target

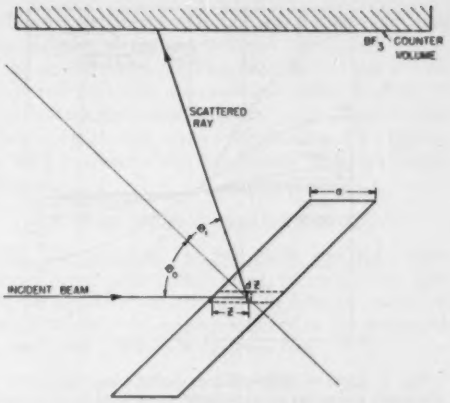

FIG. 2. Horizontal section of target and counters showing the geometry for single scattering analysis.

x_0 and the target x have nearly the same geometrical thickness and not too low atomic weight, the geometry of scattering is essentially the same for both. Therefore, the edge effects occurring for x are nearly identical with those occurring for x_0, and, since both effects are small, the difference between them has been neglected within the accuracy of the present measurements.

The standard targets, x_0's, used were Ni_2B and B_2O_3. By using two standard targets having widely different atomic weights, and overlapping ranges of σ_s/σ_t, two independent determinations of the calibration function were made. Since these were mutually consistent, Eq. (1) was verified. The choice of these compounds for standards was based upon the appropriateness of the range of variation of their σ_s/σ_t values in setting up the calibration function for the apparatus.

IV. APPROXIMATIONS AND CORRECTIONS

The neglect of background counting rate and neutron energy loss on collision (finite nuclear mass effect) necessitates correction of the scattering data.

Since all the scatterers used had very small transmission, the background depended upon whether or not a target was in position. The ideal method of background determination would have been the replacement of the scattering target by a target of infinite thickness and zero scattering cross section. This target would then have contributed no scattered neutrons to the background counting rate and at the same time would have carried out the absorbing function because of its infinite thickness. For this purpose a target of B^{10} was used. Although B^{10} does not have $\sigma_s=0$, it does have $(\sigma_s/\sigma_t)\ll 1$.[27] The method of correcting for the B^{10} scattering contribution to the background is discussed in Appendix B.

The assumption that the struck nucleus is of infinite

[27] The relevant properties of B^{10} are given in Sec. VII.

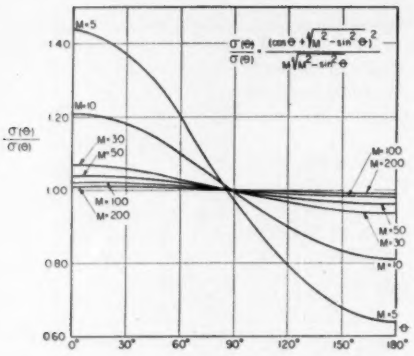

FIG. 3. Ratio of differential scattering cross sections in the laboratory and center-of-mass systems as a function of laboratory scattering angle, varying the parameter M.

mass, used in arriving at Eq. (1), is obviously not exactly satisfied by any of the targets used in this experiment. The corrections which must be considered because of this occur in the conversion of the center-of-mass system of coordinates into the laboratory system. In nearly all cases they are quite small. The following effects are taken into account:

A. Asymmetry of the angular distribution of scattered neutrons in the laboratory system.

B. Dependence of counter sensitivity on the neutron energy after collision rather than on the energy before the collision.

C. Difference between total cross section of the target before and after collision, resulting from the change in energy of the neutron during collision and the energy dependence of the σ_t of the target material.

The corrections for these effects have been applied considering only singly scattered neutrons.

A. Since only S-wave scattering occurs at low energies, $\sigma_s(\Theta)$, the differential scattering cross section in center-of-mass coordinates is spherically symmetric. Thus, the angular dependence of scattering, in the laboratory system, is determined by[28]

$$\frac{\sigma_s(\theta)}{\sigma_s(\Theta)}=\frac{[\cos\theta+(M^2-\sin^2\theta)^{\frac{1}{2}}]^2}{[M(M^2-\sin^2\theta)^{\frac{1}{2}}]}, \tag{2}$$

where θ is the scattering angle in the laboratory system, and M is the ratio of the mass of the struck nucleus to the mass of the incident particle. In the present case the latter is merely the atomic weight of the scattering nucleus. A plot of Eq. (2) is shown in Fig. 3 for various M. Reference to the geometry of Figs. 1 and 2 indicates that the probability of counting a scattered neutron is, on the average, approximately symmetrical about the scattering angle $\theta=90°$. From the form of $\sigma_s(\theta)/\sigma_s(\Theta)$ the deficiency of scattered neutrons in the backward direction is approximately compensated by the excess in the forward direction. Even for moderately low M the unbalance about 90° is small, and for the larger values of M used throughout most of this experiment it is quite negligible.

B. Since the BF_3 counters used have very low detection efficiency in the energy range covered in this experiment, the detection sensitivity can be written as $S\propto 1/v'$, where v' is the neutron velocity in the counter. In the laboratory system the neutron velocity after collision, v', is related to the velocity before collision, v, by[28]

$$v'/v=[1-[2M/(M+1)^2](1-\cos\Theta)]^{\frac{1}{2}}. \tag{3}$$

Setting $\Theta=\theta$ and using $\langle\Theta\rangle_{Av}=90°$, Eq. (3) was applied as a correction factor to all measured counting rates after correction for background (see Appendix B).

C. Since the neutron loses energy on collision and σ_t of the target varies with energy, the mean free path for interaction of the neutron while directed out of the target after collision is different from that while directed into the target prior to collision. In the derivation of Eq. (1) it was assumed that these two were identical (see Appendix A). The approximate, energy dependent correction factor applied to counting rates to take cognizance of this effect is $(\sigma_t+\sigma_t')/2\sigma_t$, where σ_t is the total cross section of the target material before collision, and σ_t' is the total cross section for neutrons of energy $E'<E$ after collision (see Appendix B). With Θ again set equal to $\langle\Theta\rangle_{Av}=90°$, E' was determined from Eq. (3). For all targets which have $\sigma_t(E)$ a slowly varying function, such as Ni_2B and B_2O_3, this factor varies slowly and monotonically with E. In the vicinity of a resonance, however, as in the case of Au, it takes the shape indicated in Fig. 4. Here, even though the energy loss is only 1 percent, $(\sigma_t)_{Au}$ is varying rapidly and σ_t' is appreciably different from σ_t. Although the correction appears quite large near resonance, the smearing action of the NVS resolution

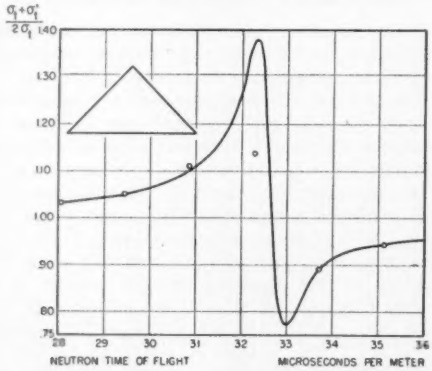

FIG. 4. The correction factor $(\sigma_t+\sigma_t')/2\sigma_t$ for Au, calculated using the parameters for $J=1$, Table II, and $E'=0.99E$. Solid curve is calculated; open circles are the actual correction factors used, determined by numerical integration of the resolution triangle over the calculated curve.

[28] See reference 2, p. 171.

reduces the effect on the counting rate. Thus, in applying the correction in the immediate vicinity of resonance, the integral of $(\sigma_t+\sigma_t')/2\sigma_t$ over the resolution function was used. The effect of this is seen in Fig. 4, where the circles indicate the correction factors actually used with the scattering data taken at the same neutron times of flight.

The net effect of the corrections discussed above, because of compensation, amounts to less than 2.2 percent in the case of B_2O_3 and to less than 0.2 percent for Ni_2B. For Au the only appreciable one is correction C, which is less than 2.5 percent over most of the energy range covered. The few points immediately near resonance have larger corrections, as indicated in Fig. 4.

From Fig. 7 it is seen that the region of principal interest is that of $(\sigma_s/\sigma_t)<\sim 0.5$. Since multiple scattering effects are of the order $(\sigma_s/\sigma_t)^2$, corrections to higher order scattering have been neglected.

It is estimated that $F(\sigma_s/\sigma_t)$, the calibration function shown in Fig. 6, is accurate to within 2 percent for $(\sigma_s/\sigma_t)<\sim 0.5$, apart from errors occurring in the values of the measured quantities used in the correction factors. Here $F(\sigma_s/\sigma_t)_{Au}$ is estimated to be accurate to within 1 percent over most of the time of flight range used in its measurement, with the exception of those points lying within about 4 microseconds/meter on either side of exact resonance; these latter are probably accurate to about 4 percent. In all cases errors due to counting statistics are larger than those discussed above; thus, errors in the level parameters come principally from this source.

V. THE SCATTERING TARGETS

All targets used in the present experiment were in the form of solid slabs or canned powders having the shape indicated in Fig. 2. Since the targets were thick, the vertical edges were cut at 45° so that all portions of the target presented the same thickness to the neutron beam. Table I indicates the pertinent properties of the targets used.

VI. SCATTERING MEASUREMENTS

The targets were inserted in the neutron beam in cyclic fashion, the number of monitor counts being adjusted to require a change of target about every half-hour. For the measurements of the calibration function $F(\sigma_s/\sigma_t)$, for example, the cycle was run as follows: Ni_2B, B_2O_3, B^{10}, C; and for the measurement of $F(\sigma_s/\sigma_t)_{Au}$: Au, Ni_2B, B^{10}, C. The purpose of cycling the targets is to average out slow drifts in counter voltage, amplier gain, level set height, and cyclotron monitor detection efficiency.

X-ray analysis of the Ni_2B target[29] indicated strong Bragg reflection planes with spacings of from 0.775A to 0.923A. Since first- and second-order scattering from these planes, for the geometry used, would affect the calibration curve, the only scattering data used were taken at neutron energies >1 ev.

The excellent agreement between the two sets of data (Ni_2B and B_2O_3) for measurements taken at $E>1$ ev substantiates the corrections made. The three lowest points in Fig. 6 were taken between 0.2 and 1 ev using the B_2O_3 scatterer which has, unlike Ni_2B, a vitreous structure.

VII. TRANSMISSION MEASUREMENTS[7,8]

The $1/v$ regions of the B^{10}, Ni_2B, and B_2O_3 cross sections were investigated using the apparatus and methods previously described[7–13] in order to determine their σ_s/σ_t values. Least-squares fits to the measured transmissions yielded for these samples

$$(\sigma_t)_{B^{10}}=(0.94\pm 1)+(646\pm 22)E^{-\frac{1}{2}}\text{ b},$$
$$(\sigma_t)_{Ni_2B}=(40.2\pm 1)+(133\pm 3)E^{-\frac{1}{2}}\text{ b},$$
$$(\sigma_t)_{B_2O_3}=(20.9\pm 1.5)+(218\pm 3.5)E^{-\frac{1}{2}}\text{ b}.$$

Using the constant terms as the respective σ_s, these become

$$(\sigma_s/\sigma_t)_{B^{10}}=(1+690E^{-\frac{1}{2}})^{-1},$$
$$(\sigma_s/\sigma_t)_{Ni_2B}=(1+3.31E^{-\frac{1}{2}})^{-1},$$
$$(\sigma_s/\sigma_t)_{B_2O_3}=(1+10.4E^{-\frac{1}{2}})^{-1}.$$

These were the values used in the determination of $F(\sigma_s/\sigma_t)$.

TABLE I. Scattering target properties.

Scattering target	Molecule (or atom) equivalent	Maximum transmission in energy range used	Purity	Geometrical slant thickness (inches)	Physical form
Au	Au	0.03	99.9+% Au	1.41	Solid
Ni_2B[a]	$Ni_2B_{1.09}$	0.01	99.8% $Ni_2B_{1.09}$	1.4	Solid
B_2O_3	B_2O_3	0.11	99.9% B_2O_3	1.17	Solid
B^{10}	B^{10}	<0.005	94% B^{10} 4% B^{11} 2% Fe, Mg and Si	0.7	Powder

[a] The Ni_2B was prepared by Cooper Metallurgical Associates, Cleveland, Ohio, and hot pressed by the Norton Company, Niagara Falls, Ontario.

The B^{10} sample for transmission consisted of 0.698 g/cm² of the same powder used in the scattering measurements. Since thin samples of uniform density are difficult to prepare, it was decided to use a sample of fairly large geometrical thickness and to investigate it in the high energy region where its transmission could be measured easily.

The Ni_2B transmission sample was prepared using the powder from which the solid slab for the scattering measurements was made; and the same general considerations concerning thickness applied here. For the measurements of $(\sigma_t)_{Ni_2B}$, four independent sets of data were taken. The sample thickness was 3.90 g/cm².

For the B_2O_3 transmission measurements the sample

[29] Performed by Dr. John P. Nielsen, New York University.

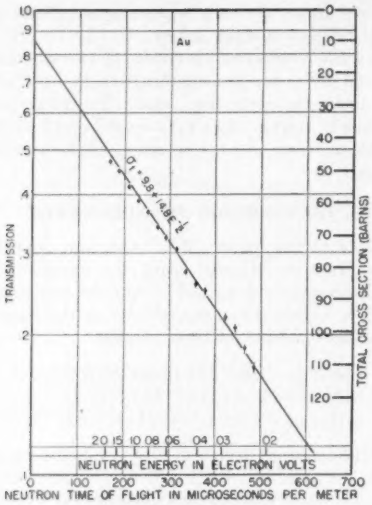

FIG. 5. Slow neutron transmission of 5.21 g/cm² of Au. The higher energy points fall below the linear $1/v$ curve as a result of the increasing importance of E relative to E_0 in the resonance denominator.

used was the solid slab used for the scattering investigations. The sample consisted of 4.03 g/cm².

In order to acquire as much data on the Au resonance as possible, using established techniques, the low energy region transmission for Au was investigated also. A 5.21 g/cm² sample was used in the region where

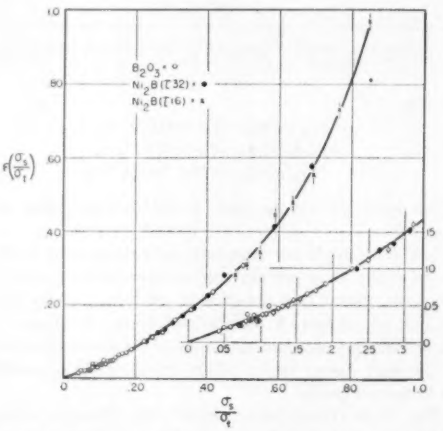

FIG. 6. The calibration function, $F(\sigma_s/\sigma_t)$. Open circles are points taken using B_2O_3 with arc-on (τ_a) and detection $(\tau_{dt})_e$ times of 32 microseconds; solid circles are points taken using Ni_2B with $\tau_a=\tau_{det}=32$ microseconds; crosses are points taken using Ni_2B with $\tau_a=\tau_{det}=16$ microseconds. Note excellent agreement of Ni_2B and B_2O_3 data for $0.23<\sigma_s/\sigma_t<0.5$. Insert shows ower portion of curve on expanded scale.

$\Gamma^2 \ll 4(E-E_0)^2$. A least-squares fit of

$$\sigma_t=[\sigma_{c0}\Gamma^2(E_0/E)^{\frac{1}{2}}/4(E-E_0)^2]+\sigma_s(\text{const})$$

to the results of this measurement yielded

$\sigma_{c0}\Gamma^2=(638\pm16)$ b-ev², and $\sigma_s(\text{const})=(9.8\pm2)$ b.[30]

Here we have used $E_0=(4.87\pm0.07)$ ev, the most recent NVS value. These results are shown in Fig. 5. Since these Au measurements were taken at low neutron energy and transmission ~0.3, a $\frac{1}{3}$ standard filter[31] was used.

In addition, the transmission of 0.02745 g/cm² of Au was measured in the immediate vicinity of resonance. Since instrumental resolution does not allow the direct measurement of total cross section in this region, maximum information on the values of σ_{t0} and Γ can be obtained only by using the area[8] over the transmission dip, $\int_{-\infty}^{+\infty}[1-T(E)]dE$, neglecting σ_y and the $1/v$ dependence of σ_c. The area measured between 28.76- and 37.76-microseconds/meter neutron time of flight was (1.22 ± 0.07) microseconds/meter.

Evaluation of the area integral by series expansion yields $A=(\Gamma/2)F(\alpha)$, where $F(\alpha)$ is a tabulated function and $\alpha=n\sigma_{t0}$, n being the number of Au atoms/cm² in the transmission sample. Correcting the value of the limited area to represent the area between the energy limits $-\infty$ and $+\infty$ allows direct comparison between measured and calculated areas.

VIII. TREATMENT OF DATA AND RESULTS

The measured calibration curve is shown in Fig. 6, where the points determined by Ni_2B and those determined by B_2O_3 are plotted together. The consistency between the two sets of measurements is readily apparent. If the scattering data for the B_2O_3 target were followed to higher energies (thus larger σ_s/σ_t values), we would expect the two sets of data to disagree somewhat, since the ratio of target thickness, a, to effective diffusion length for the two targets would be different. The fact that they do agree in the range of overlap, where they have small but somewhat different transmissions, substantiates the statement that the diffusion length criterion for thickness mentioned in Sec. III need not be invoked for $\sigma_s/\sigma_t<\sim0.5$ and $T<0.1$.

The rapid rise of $F(\sigma_s/\sigma_t)$ for large σ_s/σ_t and its approach to a value greater than unity for $\sigma_s/\sigma_t=1$ result from the following effect. For large values of σ_s/σ_t, multiple scattering becomes large, and this contributes to increased neutron density at greater depths in the scattering target. The subsequent "leakage" of neutrons out through the back of the target makes the total scattered neutron counting rate, which consists to a large extent of multiply scattered neutrons, dependent

[30] These results are essentially in agreement with earlier measurements by McDaniel, Sutton, Lavatelli, and Anderson, Phys. Rev. **72**, 729 (1947), who arrived at $\sigma_{c0}\Gamma^2=625$ b-ev², $\sigma_s(\text{const})=9.0$ b.

[31] Edward Melkonian, Phys. Rev. **76**, 1744 (1949).

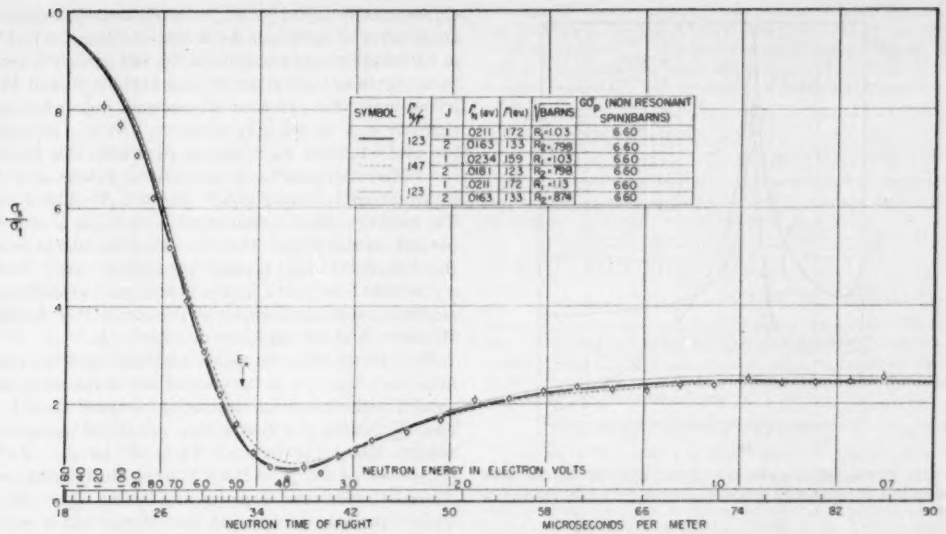

FIG. 7. The ratio $(\sigma_s/\sigma_t)_{Au}$ as a function of neutron time of flight. Heavy solid curve is best theoretical fit, calculated using Breit-Wigner one level formulas of Sec. I, with the level parameters indicated in the table. Effect of increasing Γ_N/Γ and $\sigma_{p\mp}$ by 20 percent are indicated by the dashed and thin solid curves, respectively. Discrepancy at large σ_s/σ_t values is explained by diffusion effect.

upon the ratio of target thickness to diffusion length. In effect, then, a larger fraction of the neutrons which would otherwise have been ultimately scattered to the counters "leaks" out the back of the C target than the Ni_2B target. Hence, the ratio $N_{x_0}/N_C=F(\sigma_s/\sigma_t)_{Ni_2B}$ approaches a value >1 as $(\sigma_s/\sigma_t)_{x_0}\to 1$. For values of $\sigma_s/\sigma_t<\sim 0.5$, where only the singly, doubly, and triply scattered neutrons contribute appreciably to the total counting rate, the use of Eq. (1) is quite valid (see Appendix A).

This line of reasoning is borne out still further by noting that the "best fit" curve of Fig. 7 indicates that the measured values of $(\sigma_s/\sigma_t)_{Au}$ for $\sigma_s/\sigma_t>0.5$ are too small by a relative amount which increases with increasing σ_s/σ_t. This is due to the fact that for large σ_s/σ_t the ratio of slant thickness to diffusion length was not sufficiently great to use the infinite thickness approximation. As a result of this effect, the criterion that the experimental points for $(\sigma_s/\sigma_t)_{Au}<\sim 0.5$ be matched by a theoretical curve has been used in determining a best fit to the data.

Figure 7 contains the final experimental results in the form of $(\sigma_s/\sigma_t)_{Au}$ *vs* neutron time of flight. The method of determining the best group of parameters was as follows. Preliminary calculations of $\sigma_s(E)$, using very approximate values for the level parameters, indicated that σ_s has its minimum in the vicinity of 2 to 3 ev and that the dip is rather broad. At the minimum, $\sigma_s=G_\pm\sigma_{p\pm}$, the potential scattering contribution from the nonresonant spin state, and $(E_{min}-E_0)/(\Gamma/2)^2\gg 1$ so that σ_c is determined by $\sigma_{c0}\Gamma^2$, the value of which was already known. Thus, one of the scattering parameters was fixed. In the immediate vicinity of resonance, σ_s/σ_t is determined almost entirely by Γ_N/Γ, and somewhat farther away it is most sensitive to variations in $R_\mp$, the nuclear radius for the resonant spin condition. Successive approximations were made in Γ_N/Γ and $R_\mp$, using the relations

$$\Gamma^2=(\sigma_{c0}\Gamma^2/4\pi\lambda_0^2G_\mp)/[(\Gamma_N/\Gamma)-(\Gamma_N/\Gamma)^2]$$

and $\sigma_{p\mp}=4\pi R_\mp^2$, choosing one of the possible values of $G_\mp$. Since $(\sigma_s/\sigma_t)_{Au}$ is insensitive to the value of Γ (except in the combination $\sigma_{c0}\Gamma^2$), the above procedure allows one to choose one value for $G_\mp$ and calculate σ_s/σ_t; to this same curve, however, there corresponds another set of values for Γ, Γ_N, and R. In this fashion it was found that the data are fit (heavy solid curve of

TABLE II. Measured and derived parameters for the 4.9-ev Au level.[a] (The correct choice of J is 1.)

E_0	4.87 ±0.07	
Γ_N/Γ	0.123±0.013	
$G_\pm\sigma_{p\pm}$	6.60±0.33	
J	1	2
$R_\mp$	1.03±0.09	0.798±0.06
Γ	0.172±0.01	0.133±0.009
Γ_N	0.0211±0.0018	0.0163±0.0015
$\sigma_{p\pm}$	10.6	17.6
$\sigma_{p\mp}$	13.3	8.0
σ_{t0}	24,600	41,100

[a] Energies are measured in electron volts, cross sections in barns, and $R_\mp$ in barns$^{\frac{1}{2}}$; precisions are estimated; and E_0 is the most recent NVS value of Rainwater and Havens.

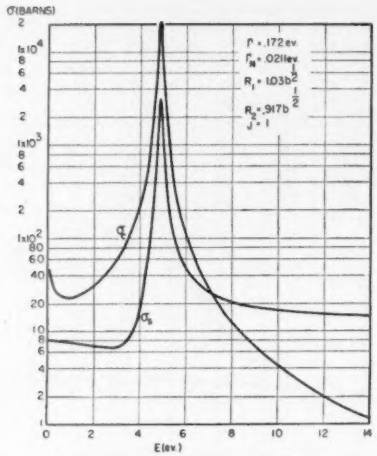

FIG. 8. Theoretical curves of $\sigma_c(E)$ and $\sigma_s(E)$ for Au, calculated using best fit parameters indicated, assuming $J=1$ for the 4.87-ev level.

Fig. 7) by using

$$4\pi\lambda_0^2(G\Gamma_N^2)=89.3 \text{ b-ev}^2,$$
$$16\pi\lambda_0(G\Gamma_N R)=84.5 \text{ b-ev}^2,$$
$$\sigma_p(\text{total})=11.6 \text{ b}.$$

The level parameters corresponding to each of the two possible values of J are presented with estimates of precision in Table II.

To indicate the sensitivity of various parts of the theoretical form of σ_s/σ_t *vs* E, we have, in Fig. 7, presented the curves calculated for Γ_N/Γ larger than optimum by 20 percent and for $\sigma_{p\mp}$ larger than optimum by 20 percent. In Fig. 8 are shown the theoretical curves for $(\sigma_c)_{\text{Au}}$ and $(\sigma_s)_{\text{Au}}$, individually, calculated using the parameters indicated by the choice $J=1$.

In an attempt to decide upon the value of J, the following information may be considered.

A. The experimental value of $\int_{-\infty}^{+\infty}[1-T(E)]dE$, discussed in Sec. VII, is (0.382 ± 0.027) ev. The calculated area, using the parameters of Table II for $J=1$, is 0.372 ev, and the area calculated for $J=2$ is 0.404 ev. Although the experimental area agrees better with the choice $J=1$, the possibility that $J=2$ cannot be ruled out because of the 7 percent uncertainty in the experimental area.

B. Since $G_{\pm}\sigma_{p\pm}$ is found to be 6.60 b, and two distinct possible values for R are indicated, $\sigma_{p\pm}$ and $\sigma_{p\mp}$ are determined for each possible value of J.

As indicated in Table II, the partial potential scattering cross section, $\sigma_{p\pm}$, takes the values of 10.6 b and 17.6 b for $J=1$ and $J=2$, respectively. Since this cross section is far from a resonance with the spin state in question, it is to be expected that it will take a value fairly close to the geometric cross section of Au, i.e., approximately $4\pi(0.15A^{\frac{1}{3}})^2=9.6$ b. These considerations are in favor of the choice $J=1$. The values $\sigma_{p\mp}=13.3$ b or 8.0 b fall on opposite sides of 9.6, but neither is very far away from the values 9.0 and 11.0 for Bi and Pb, for example. The precision is somewhat poorer for $\sigma_{p\mp}$ than for $\sigma_{p\pm}$, so we may conclude that $\sigma_{p\pm}$ strongly favors $J=1$, while $\sigma_{p\mp}$ does not contradict this result.

C. The activation[32] measurement of Coster *et al.*,[33] as corrected by Groendijk,[34] yields $\sigma_{c0}\Gamma=4290$ b-ev. The present authors estimate accuracy limits of $\sim\pm30$ percent on this figure. The two values calculated from the results of the present experiment are: $J=1$, $\sigma_{c0}\Gamma=3690$ b-ev; $J=2$, $\sigma_{c0}\Gamma=4800$ b-ev. Certainly, no positive conclusion can be drawn from this datum. However, it is not inconsistent with $J=1$.

D. A fourth criterion which might be used to determine the value of J is the comparison of the measured value for the resonance scattering integral[22] in a $1/E$ flux, $\sum_s$, with the two values calculated using our results. Using the data of Table II we get: $J=1$, $\sum_s=168$ b; $J=2$, $\sum_s=218$ b. Harris, Muehlhause, and Thomas[22] give the experimental value $\sum_s\sim210$ b. This is the only evidence we have found which might be construed to contradict the choice $J=1$. However, Muehlhause[35] states that this value is expected to be too large, perhaps by as much as ~50 percent, since it includes the effects due to higher levels with large scattering. From these considerations we conclude that this evidence leans in favor of $J=1$, although $J=2$ is not definitely ruled out.

E. The possible values of $(\sigma_{t0})_{\text{Au}}$ calculated from the results of the present experiment, listed in Table II, are: $J=1$, $\sigma_{t0}=24{,}600$ b; $J=2$, $\sigma_{t0}=41{,}100$ b. Since these two values are quite different, it would seem that even a relatively rough experimental determination of σ_{c0} (or σ_{t0}) should strongly indicate the choice of J. By measurement of the cross section for self-indication,[36] neglecting resonance scattering effects, Frisch[37] gives the value $\sigma_0=26{,}000$ b. Although the agreement with $J=1$ seems quite good, this may be somewhat fortuitous in view of the large errors which were later found to be associated with early self-indication experiments. However, a more recent self-indication experiment by Goldhaber,[38] using several thicknesses of Au, yielded the value $\sigma_0=25{,}000$ b with a maximum uncertainty of ±5000 b.

In view of the affirmative data presented in A, B, D, and particularly E, and the lack of contradiction in C, one can conclude that $J=1$ for the resonance level.

[32] Reference 2, pp. 141–143.
[33] Coster, De Vries, and Diemer, Physica **10**, 281 (1943).
[34] H. Groendijk, thesis, Groningen (1949).
[35] C. O. Muehlhause, private communication.
[36] Reference 2, pp. 140, 141, 147, 148.
[37] O. Frisch, K. Danske Vidensk. Selsk. **14**, No. 12 (1937).
[38] M. Goldhaber (private communication). This measurement does not include a correction for scattering, nor for Doppler effect. Neither correction, however, would be large enough to invalidate the conclusion drawn.

The value of $\Gamma_N/\Gamma=\sum_e/(\sum_e+\sum_a)=0.14$ (to be compared with the result of the present experiment, $\Gamma_N/\Gamma=0.123$) has been calculated by Harris *et al.*[22] on the basis of their measurement of $\sum_e$ and a calculated value for $\sum_a$, the resonance capture integral in a $1/E$ flux. The value they used for $\sum_a$, 1296 b, however, is based upon earlier Columbia NVS measurements and is somewhat in error according to calculations based on the results of Table II. Thus, even if their measured value of $\sum_e$ agreed with that calculated from the present measurements, one would expect some disagreement in Γ_N/Γ. We get for $J=1$, $\sum_a=1180$ b. Furthermore, their measured value $\sum_e\sim 210$ b includes the effects of higher levels, as mentioned previously. In view of these considerations and the large probable error allowed their measurements, their result is essentially in agreement with ours.

Our total potential scattering cross section, $(G_\pm\sigma_{p\pm}+G_\mp\sigma_{p\mp})$, is (11.6±1) b. Hibdon and Muehlhause,[18] using Co and Mn scattering detectors, measured the values 10.6 and 10.8 b. It is to be noted, however, that their values reflect conditions at considerably higher energies than those used in our measurements. If the energies at which their measurements were taken are far from resonances, however, we should compare their results with our measured value of $\sigma_{p\pm}$ and not with $(G_\pm\sigma_{p\pm}+G_\mp\sigma_{p\mp})$ (see B above). In that case, for the choice $J=1$, our value of $\sigma_{p\pm}=10.6$ b is in excellent agreement with theirs.

Figure 9 shows the results of high energy scattering from the Au target. The target, in this energy region, is not in general thick in the sense of Sec. III, and since σ_s/σ_t is large, it was felt that the conversion of the data into σ_s/σ_t values according to the calibration curve would be misleading. Hence, N_{Au}/N_C is plotted *vs* time of flight. The dips in the vicinity of 75 ev and between 300 to 500 ev represent, effectively, rises in the percentage of capture present, i.e., the presence of resonances. Since the resolution is quite poor, no analysis can be made. However, in view of the magnitude of the effect and the relatively broad resolution used, we can assert that in both cases capture plays an appreciable role. The dip at ~75 ev may be the result of one or more resonances, while that at 300 to 500 ev is almost certainly the smeared out effect of a number of levels. This latter is, no doubt, the same group of levels noted by Hibdon and Muehlhause.[18]

The authors wish to express their appreciation to Professors L. J. Rainwater and W. W. Havens, Jr., for their active guidance and invaluable suggestions, and to Dean J. R. Dunning for his constant encouragement and advice during the course of the work.

Thanks also are due the United States Atomic Energy Commission for their support of this research.

APPENDIX A. MULTIPLE SCATTERING ANALYSIS

Consider the single scattering event illustrated in Fig. 2. If n is the number of scattering nuclei per unit volume, $N_0(E)$ the incident flux density, and $\alpha S(E)$ the counter detection sensitivity for neutrons emitted isotropically from the element dz, where $S(E)$ indicates the $1/v$ dependence of the BF_3 counter sensitivity and α is a geometrical factor depending on the position of the element in question, then the number of neutrons singly scattered from the lamina dz is

$$dN_1=\alpha S(E)[N_0(E)\exp(-n\sigma_t z)][n\sigma_s dz]\times[\exp(-n\sigma_t z\cos\theta_0/\cos\theta_1)]. \quad \text{(A-1)}$$

Integrating (A-1) from $z=0$ to $z=a$ gives the number of neutrons counted, arising due to single scattering into unit solid angle about θ_1 from the cylindrical element indicated. It is found

$$N_1=\alpha S(E)N_0(E)(\sigma_s/\sigma_t)\left[\frac{1}{1+(\cos\theta_0/\cos\theta_1)}\right]\times[1-T^{[1+(\cos\theta_0/\cos\theta_1)]}], \quad \text{(A-2)}$$

where we set $T=\exp(-n\sigma_t a)$ as the target transmission. Noting that $\langle\cos\theta_0/\cos\theta_1\rangle_{Av}\approx 1$, we see that the last factor is approximately T^2 and that if $T<0.1$, an error of $<\sim 1$ percent is made in N_1 by neglecting the term in T. Calling the remaining geometrical factor $f_1(\theta_0,\theta_1)$ we can write

$$N_1=\alpha S(E)N_0(E)f_1(\theta_0,\theta_1)(\sigma_s/\sigma_t). \quad \text{(A-3)}$$

Iteration of the above procedure, using the element dz as a source point and neglecting edge effects, then yields similar expressions for successive multiplicities of scattering. Thus, the total counting rate due to neutrons originally scattered in the cylindrical element shown and leaving the target x in the direction θ_1 becomes

$$N_x=\alpha S(E)N_0(E)\sum_{j=1}^{\infty} f_j(\theta_0,\theta_1)(\sigma_s/\sigma_t)^j x^j. \quad \text{(A-4)}$$

It is assumed that T and σ_s/σ_t are sufficiently small so that negligible diffusion out the back of the target occurs. Division of (A-4) by the similar expression for a carbon target, in which energy dependence arises only through the factors $S(E)$ and $N_0(E)$, then yields

$$N_x/N_C=\sum_{j=1}^{\infty} g_j(\sigma_s/\sigma_t)^j x^j, \quad \text{(A-5)}$$

which obviously applies for the total counting rate ratio, where the g_j are factors depending on geometry alone. We define the ratio N_x/N_C as $F(\sigma_s/\sigma_t)x$, the scattering ratio to carbon, for infinitely heavy nuclei. A fit of (A-5) to the curve of Fig. 6 indicates that only the first three terms contribute appreciably for $(\sigma_s/\sigma_t)<\sim 0.5$.

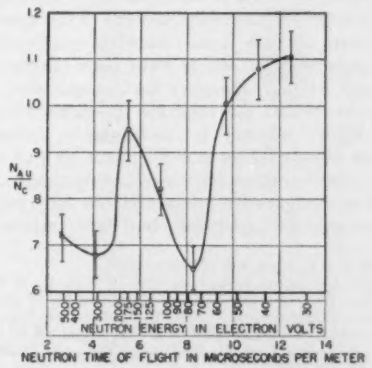

FIG. 9. Ratio of thick target neutron scattering from Au to that from moderately thick graphite. Dips at ~80 ev and >300 ev indicate the presence of levels with appreciable capture.

APPENDIX B. BACKGROUND AND ENERGY LOSS CORRECTIONS

The quantities N_x and N_C in (A-5) represent counting rates *due to scattering* from targets x and C. Then if B represents counting rate due to background when a thick target is in position, $N_x = N_x' - B$, where N_x' is the measured counting rate when x is the scatterer. Letting primes indicate *measured* counting rates generally, we also have $N_{B^{10}} = N_{B^{10}}' - B$ and the left-hand side of (A-5) can be written as

$$\frac{N_x}{N_C} = \frac{N_x' - B}{N_C' - B} = \frac{N_x' - N_{B^{10}}'}{N_C' - N_{B^{10}}'} + \frac{N_{B^{10}}}{N_C' - N_{B^{10}}'}, \tag{A-6}$$

where we have neglected $N_{B^{10}}$ in the denominator since $N_{B^{10}} \ll (N_C' - N_{B^{10}}')$. Since the second term on the right-hand side of (A-6) is small for $x = Ni_2B$ or B_2O_3, we can combine (A-5) and (A-6) to give

$$F(\sigma_x/\sigma_t)_{x_0} = \frac{N_{x_0}' - N_{B^{10}}'}{N_C' - N_{B^{10}}'}\left[1 + \frac{(\sigma_x/\sigma_t)_{B^{10}}}{(\sigma_x/\sigma_t)_{x_0}}\right]. \tag{A-7}$$

The bracketed factor then corrects the background measurement for the small B^{10} scattering contribution. A similar analysis yields for Au

$$F(\sigma_x/\sigma_t)_{Au} = \frac{N_{Au}' - N_{B^{10}}'}{N_C' - N_{B^{10}}'} + F(\sigma_x/\sigma_t)_{B^{10}}. \tag{A-8}$$

Since $F(\sigma_x/\sigma_t)$ has been defined as the scattering ratio to carbon for infinitely heavy nuclei, the right-hand sides of (A-7) and (A-8) must further be multiplied by the factors indicated in Secs. III B and III C to correct at least the "singly scattered" counting rate for the finite mass effect. The latter correction arises in the following manner. In writing (A-1) above, the σ_t appearing in the last bracket is more correctly σ_t', the cross section of the target nuclei for neutrons of energy $E' < E$ after collision. Then using the fact that $(\cos\theta_0/\cos\theta_1)_{Av} \approx 1$, (σ_x/σ_t) in (A-2) becomes $2\sigma_x/(\sigma_t + \sigma_t')$. Thus, multiplication of the right-hand sides of (A-7) and (A-8) by $(\sigma_t + \sigma_t')/2\sigma_t$ corrects for this effect.

PHYSICAL REVIEW VOLUME 83, NUMBER 4 AUGUST 15, 1951

Configuration Interaction in Mn II

R. E. TREES
University of Pennsylvania, Philadelphia, Pennsylvania
(Received May 2, 1951)

The theoretical formulas for d^6 and d^5s are compared with the experimental data of Mn II. The relative positions of these configurations in Mn II allow the magnitude of configuration interaction to be determined accurately without the use of a least-squares calculation. Over-all agreement between theory and experiment is improved by the use of separate parameters in the two configurations and by the introduction of the effects of configuration interaction.

The positions of the terms not yet known experimentally are predicted as a help in further analysis of this spectrum. The positions of terms of the d^5s configuration are believed to be predicted with better than usual accuracy by the use of a correction term proportional to $L(L+1)$.

I. TERM VALUES OF Mn II WITHOUT CONFIGURATION INTERACTION

CURTIS[1] has recently extended the experimental analysis[2] of the $3d^54s$ and $3d^6$ configurations of Mn II to include some of the triplet terms, thus making possible a further theoretical analysis of this spectrum.

The term values in Russell-Saunders coupling for the d^5s configuration of Mn II have been calculated by Bowman[3] without allowance for configuration interaction; his results are valid for the terms which are only slightly affected by configuration interaction (i.e., the majority of terms in d^5s), since his least square fit was based on terms that are probably almost free of effects of configuration interaction. We have repeated his least-squares calculation, but have included the additional experimental values[1] for d^5s. The results are given in part (1) of Table I and are essentially in agreement with Bowman's results (the mean deviation of his data is 447 cm^{-1} compared to 412 cm^{-1} for the d^5s terms in Table I). A comparison of the d^6 data with theory, also neglecting effects of configuration interaction, is given in the same column. The mean deviation between theory and experiment, using separate parameters in d^5s and d^6 and neglecting configuration interaction is 678 cm^{-1}.

The parameters used in the calculation of Table I are those in the formulas of Racah.[4] The d^6 formulas are in the same form as the d^4 formulas with "$6A$" replaced by "A." In the d^5s formulas, "$10A$" (in Racah's formulas for d^5) was replaced by "D" and the proper multiple of G_2 was subtracted.[5] The parameters were evaluated by least squares.

An effort was made to fit the data using the same B and C parameters in d^5s and d^6, again neglecting configuration interaction, with the result shown in part 2

[1] C. W. Curtis, Phys. Rev. **78**, 343 (1950).

[2] Other experimental values were taken from C. W. Curtis, Phys. Rev. **53**, 474 (1938). The ^5D of $3d^6$ and the ^7S and ^5S of $3d^54s$ were found previously by M. A. Catalan, Phil. Trans. Roy. Soc. (London), **A223**, 127 (1922); An. Soc. Espan. **26**, 67 (1928); Russell, Astrophys. J. **66**, 233 (1927); and Black and Duffendack, Science **66**, 402 (1927).

[3] D. S. Bowman, Phys. Rev. **59**, 386 (1941). The term values for d^5 configuration were first calculated by M. A. Catalan and M. T. Antunes, Z. Physik **102**, 432 (1936).

[4] G. Racah, Phys. Rev. **62**, 438 (1942); **63**, 367 (1943). These are referred to as II and III, respectively.

[5] J. H. Van Vleck, Phys. Rev. **45**, 405 (1934).

TABLE I. Term values of Mn II (cm^{-1}). (1) No configuration interactions, separate parameters; (2) No configuration interactions, same B and C in both configurations; (3) With configuration interactions, separate parameters; (4) With configuration interaction and a $L(L+1)$-correction (d^5s configuration only). Terms belong to d^5s or d^6 configuration respectively if they are or are not written with a parent term.

		(1)		(2)		(3)		(4)	
Term	Obs.	Calc.	Diff.	Calc.	Diff.	Calc.	Diff.	Calc.	Diff.
$(^6S)^7S$	0	99	99	693	693	155	155	10	10
$(^6S)^5S$	9473	9732	259	10170	697	9742	269	9578	105
^5D	14584	14928	344	13465	−1119	14844	260		
$(^4G)^6G$	27571	26608	−963	26649	−922	26616	−955	27474	−97
$(^4P)^6P$	29912	30120	208	30291	379	30215	303	29870	−42
^3P	30277	31347	1070	31253	976	31088	811		
^3H	30650	29598	−1052	29476	−1174	29603	−1047		
^3F	31622	31798	176	31870	248	31753	131		
$(^4D)^5D$	32828	33058	230	32757	−71	33000	172	32694	−134
$(^4G)^5G$	33215	33030	−185	32967	−248	32447	−768	33232	17
^3G	34874	33412	−1462	33839	−1035	34147	−727		
$(^4P)^3P$	36321	36541	220	36609	288	36733	412	36363	42
^1I		36933				36954			
^1G		38178				37984			
^3D	37842	38752	910	39947	2105	38215	373		
$(^4D)^3D$	39814	39480	−334	39075	−739	40022	208	39650	164
$(^3I)^3I$		38549				38599		40888	
$(^3I)^1I$		41760				41815		44091	
^1S		42027				41771			
$(^4F)^5F$	43458	43941	483	43380	−78	43814	356	43746	288
$(^2D)^3D$						43720		43461	
$(^2F)^3F$						43960		44160	
^1D						44055			
$(^2F)^1F$						46710		46867	
$(^2D)^1D$						46656		46412	
$(^2H)^3H$						46737		48100	
^1F						49322			
$(^2G)^3G$						48602		49063	
$(^2H)^1H$						49927		51283	
$(^4F)^3F$						50206		50124	
$(^2G)^1G$						51785		52232	
$(^2F')^3F$						52166		51967	
$^3F'$						55450			
$(^2F')^1F$						55582		55380	
$^3P'$						55860			
$(^2S)^3S$						57638		56438	
$^1G'$						60602			
$(^2S)^1S$						61048		59841	
$(^2D')^3D$						63066		62269	
$(^2D')^1D$						66077		65273	
$(^2G')^3G$						69403		69380	
$(^2G')^1G$						72627		72598	
$^1D'$						77121			
$(^2P)^3P$						84855		83117	
$(^2P)^1P$						88005		86258	
$(^2D'')^3D$						90853		89401	
$^1S'$						95127			
$(^2D'')^1D$						94071		92613	
$A(d^6)$		30948.3		31789.4		31734.6		—	
$D(d^5s)$		40375.6		39131.2		39876.5		38744.0	
$B(d^6)$		762.85		872.58		802.57		—	
$B(d^5s)$		921.41		872.58		906.63		878.88	
$C(d^6)$		2904 6		3130.0		2879.6		—	
$C(d^5s)$		3137.9		3130.0		3159.4		3139.3	
G_2		1605.4		1579.5		1597.9		1594.6	
H_2		—		—		99		99	
α		—		—		—		69.2	
Mean deviation		±678 cm^{-1}		±887 cm^{-1}		±551 cm^{-1}		±130 cm^{-1}	

TABLE II. Intervals of experimentally observed ^3D and ^3G terms (cm^{-1}). The d^6 ^3G and the d^5s ^3D are assumed to both have the following percentages of d^6 and d^5s configuration respectively: (*A*) 50 percent–50 percent; (*B*) 64 percent–36 percent; (*C*) 36 percent–64 percent. The d^5s ^3G and the d^6 ^3D have percentages of d^6 and d^5s configuration which are complementary.

Interval		Obs.	Calculated *A*	*B*	*C*
d^6	$^3D_3-{}^3D_2$	3.2	−30	−56	−4
d^6	$^3D_2-{}^3D_1$	36.3	46	47	45
d^5s	$^3D_3-{}^3D_2$	−5.2	5	22	−12
d^5s	$^3D_2-{}^3D_1$	−13.2	34	36	31
d^6	$^3G_5-{}^3G_4$	−148.6	−98	−125	−70
d^6	$^3G_4-{}^3G_3$	−94.0	−78	−100	−56
d^5s	$^3G_5-{}^3G_4$	−100.9	−98	−70	−125
d^5s	$^3G_4-{}^3G_3$	−30.1	−78	− 56	−100

of Table I. The mean deviation of 887 cm^{-1} is much larger than the deviation of the preceding calculation, so that the use of separate parameters in the two configurations is desirable.

II. TERM VALUES OF Mn II WITH CONFIGURATION INTERACTION

The ground configuration $3d^54s$ of Mn II interacts with the configurations $3d^6$ and $3d^44s^2$. The matrix elements of these interactions are given in III.[6]

The ^5D of d^4s^2 is the only term of this configuration found experimentally.[2] From the known position of this ^5D, and the values of the parameters already evaluated for d^5s, the effects of configuration interaction of d^4s^2 with either d^6 or d^5s can be estimated. The mean effect on these levels for which experimental data are available is a depression of 40 cm^{-1}; the lowering of any one of these levels is less than 100 cm^{-1}. Since the mean deviation of the final result is 551 cm^{-1}, the effects of interactions with the d^4s^2 configuration might be expected to be unimportant, and the estimate shows that this is so. Interactions with the d^4s^2 configuration have therefore been neglected to simplify the calculation.

Having eliminated the interactions of d^5s and d^6 with d^4s^2, we now turn to consider their interaction with each other. By consideration of those terms which show the effects of configuration interaction most strongly, the radial parameter H_2 for the interaction between d^5s and d^6 configurations has been evaluated in Sec. III as $H_2=99\pm3$ cm^{-1}. The usual procedure is to evaluate this parameter by least squares adjustment of all the data; this is usually an inaccurate procedure, since large changes of this parameter have small effects relative to the mean deviation between theory and experiment.[7]

The improved agreement produced by introducing the effects of configuration interaction between d^5s and d^6 using $H_2=99$ cm^{-1} can be shown by using the parameters already obtained in part (1) of Table I, and calculating the new theoretical values of the energy. The mean deviation is reduced from 678 cm^{-1} to 577 cm^{-1} when this is done. Slightly better agreement can be obtained by carrying out a least squares adjustment to obtain new values of the other parameters, excluding H_2. The results of this calculation are given in part (3) of Table I. The mean deviation is reduced finally to 551 cm^{-1} when effects of configuration interaction are included.

In getting the eigenvalues of the matrices, we first diagonalized with respect to any pairs of terms that were close together, and then determined the effects of other levels with second-order perturbation theory. The maximum configuration interactions evaluated with perturbation theory were all less than 200 cm^{-1}; the off-diagonal elements of configuration interaction were in all cases less than $\frac{1}{4}$ of the intervals between the levels they connected so that the maximum error in the calculated eigenvalues resulting from the use of perturbation theory is about 15 cm^{-1}.

III. EVALUATION OF THE PARAMETER H_2

The two ^3G terms have an experimentally observed separation of 1659 cm^{-1}, and since the maximum permissible interaction is half of the separation, an upper limit of $H_2\leqslant102$ cm^{-1} can be established in order that the observed separation will not not be exceeded. The separation of the pair of ^3D terms has an experimental value of 1972 cm^{-1} and this sets a slightly higher limit of $H_2\leqslant104$ cm^{-1} on the interaction parameter.

In setting the lower limit on the interaction parameter, it is first assumed that Curtis's assignment of the two ^3G and the two ^3D terms to the d^5s or d^6 configurations is correct, and that interactions with other levels

[6] The $d^6-d^4s^2$ interaction is given by Eq. (75) of III; the $d^4s^2-d^5s$ interaction is obtained from Eq. (81) and Table XXII; the d^6-d^5s interaction is obtained from Table XXII by use of the relation,

$$(d^5\eta'S'L|\Sigma e^2/r_{ij}|d^5(\eta SL)sS'L)$$
$$=(-1)^{S+S'+\frac{1}{2}}\left(\frac{2S+1}{2S'+1}\right)^{\frac{1}{2}}(d^5\eta SL|\Sigma e^2/r_{ij}|d^5(\eta'S'L)sSL).$$

This may be verified by use of (79) of III.

[7] For convenience the theory was assumed to be exact. This is perhaps misleading, since there is such a large error remaining in the final result after effects of configuration interaction with nearby terms is accounted for (i.e., the mean deviation of 551 cm^{-1} in part 4 of Table I has not been identified in the literature with any specific source of error). We were able to consider the theory exact, because the errors in both ^3G and in both ^3D terms are probably nearly the same, as the results in part 4 of Table I seem to indicate. Since only differences between theoretical formulas were compared with experiment, the errors tended to cancel. This line of reasoning is justified generally for Mn II only by the over-all consistency obtained in the results.

Usually one cannot find interacting terms which are sufficiently close together to set an upper limit on the interaction parameters which is small enough to be of any use. It seems rather important to decide how far in error a least-squares determination of the parameters may be, and whether it might not be more accurate to estimate values from neighboring spectra if no better method is available. We might point out, that the separation of a pair of ^3H terms of Cr II sets an upper limit $H_2\leqslant121$ cm^{-1} on the interaction parameter in that spectrum. Since A. A. Schweizer [Phys. Rev. **80**, 1080 (1950)] obtains a value $H_2=150$ cm^{-1} by least squares, the least-squares evaluation would seem to be too high.

not experimentally known will have negligible effect in establishing these assignments. It is then possible to show that the parameter "B" must have a larger value in the d^5s configuration than in the d^6 configuration, since one would otherwise be obliged to interchange the assignments of one or the other pairs of terms. The larger the magnitude of the difference of B-values, the less configuration interaction is needed to account for the observed separations, so that the largest reasonable difference in B-values sets a lower limit on the magnitude of configuration interaction. This lower limit is not very sensitive to the magnitude of the assumed difference in B-values, as long as this difference is not unreasonably large. Using the difference of 160 cm^{-1} from part (1) of Table I, the maximum possible separation of the ^3D and ^3G terms without configuration interaction is about 550 cm^{-1}. In order that configuration interaction cause the remaining part of the observed separation, the parameter H_2 must have a value of about 96 cm^{-1}.

We take the value $H_2 = 99 \pm 3$ cm^{-1} which is the mean of the upper and lower limits.

IV. VERIFICATION OF ASSIGNMENTS FROM INTERVALS

The assignments of the pair of ^3G and the pair of ^3D terms of d^5s and d^6 are the least certain of Curtis's assignments owing to the strong configuration interaction. In this section we obtain additional confirmation of these assignments by consideration of the intervals, and in Sec. V from a consideration of the triplet-quintet separation. The analysis of both these sections also confirms the conclusions of Sec. III in regard to the separation of these pairs of terms in the absence of configuration interaction.

In Table II we have calculated the intervals of the pair of ^3D and the pair of ^3G terms for three possible cases; (A) the terms are a 50–50 mixture of d^5s and d^6 configurations, (B) the term of higher energy (i.e., the d^6s ^3D and the d^6 ^3G according to Curtis's assignments) contains 64 percent of d^6 configuration and 36 percent of d^5s configuration, and (C) the term of higher energy contains 64 percent of d^5s configuration and 36 percent of d^6 configuration. The term of lower energy contains the complementary composition, e.g., 36 percent of d^6 and 64 percent of d^5s in case B. The parameter, ζ_d, which defines the elements of spin-orbit interaction in the d^6 configuration was assumed to have a value 260 cm^{-1} which is the value found in the $3d^6$ ^5D; the corresponding parameter in the $3d^54s$ configuration was taken as 300 cm^{-1}, midway between the value in the $3d^6$ ^5D and the $3d^44s^2$ ^5D. A more accurate interpolation[9] was not considered necessary for these calculations. The matrix elements of spin-orbit interaction were taken from III.[9]

In carrying out the calculations for the pair of ^3G terms it was assumed that the splitting was due solely to the diagonal spin-orbit interaction of the d^6 component of the eigenfunction. Comparison of the calculated results with experiment shows that case B, the choice which agrees with Curtis's assignments, is strongly favored. More extended calculations that include the effects of nondiagonal spin-orbit interaction with other terms, largely explain the remaining deviation between case B and experiment so that there is little doubt about the assignments of the ^3G terms being correct.

For the calculation of the intervals of the pair of ^3D terms it was necessary to include the large effects of nondiagonal spin-orbit interaction with the $d^5(^4P)s^3P$ along with the splitting due to the diagonal spin-orbit interaction of the d^6 component of the eigenfunction. The calculated intervals agree best with experiment for case C, which is the case in agreement with Curtis's assignments. The large error in explaining the d^5s $^3D_3 - ^3D_1$ interval may be partly due to the neglect of effects of configuration interaction with other ^3D terms, since nondiagonal spin-orbit interaction with other levels seems to explain only about half the error.

It would require overly elaborate calculations to explain fully the observed intervals. However, the best ratio of d^6 to d^5s eigenfunction is moderately well defined by the approximate calculation of Table II; i.e., the two ^3G and the two ^3D terms have approximately a 64 percent/36 percent composition, with the dominating configuration the one required by Curtis's assignments. The separation of the terms in the absence of configuration interaction is 7/25 of the experimentally observed separation for this ratio of components, or 464 cm^{-1} for the pair of ^3G terms and 552 cm^{-1} for the pair of ^3D terms. Within the accuracy of the calculations, this is consistent with the upper limit of 550 cm^{-1} placed on the separation in Sec. III.

V. VERIFICATION OF ASSIGNMENTS FROM QUINTET-TRIPLET SEPARATION

We have found[10] that in the d^5s configuration of Fe III the parameter G_2 has very consistent values when determined by subtraction of the experimental values of terms based on the same parent. If this is assumed to be true for all d^5s terms that are free from effects of configuration interaction, then from the experimentally determined positions of the d^5s ^5G and the d^5s ^5D the positions of the corresponding triplets of d^5s, which are based on the same parent, can be determined

[6] H. A. Robinson and G. H. Shortley, Phys. Rev. **52**, 713 (1937).

[9] For the d^6 configuration relation (25) and Table XIII of III are used. For the d^5s configuration, Table XIV is used with the following relation which is derived from II, Eq. (44);

$$(d^n(\nu SL)sS_1LJ|\Sigma\xi(r_i)\mathbf{l}_i\cdot\mathbf{s}_i|d^n(\nu'S'L')sS_1'L'J)$$
$$=(-)^{L'-S'-J-\frac{1}{2}}W(S_1LS_1'L';J1)W(SS_1S'S_1';\tfrac{1}{2}1)$$
$$\times[(2S_1+1)(2S_1'+1)]^{\frac{1}{2}}(d^n\nu SL\|30^{\frac{1}{2}}V^{(11)}\|d^n\nu'S'L')\zeta_d.$$

The nondiagonal elements of the $d^5(^4D)s^3D - d^5(^4P)s^3P$ spin-orbit interaction are found to be $\frac{1}{2}(35)^{\frac{1}{2}}\zeta_d$ and $5/12(7)^{\frac{1}{2}}\zeta_d$ for the elements with $J=2$ and $J=1$ respectively.

[10] (To be published.)

as they would be in the absence of effects of configuration interaction. The relationship of the hypothetical position to the center of gravity of the pair of terms then determines the assignments and the separation in the absence of configuration interaction.

The theoretical separation of quintets and triplets is found to be $4G_2=6310\pm100$ cm^{-1} from the G_2 value of the $^5S-^7S$ separation. To be on the safe side, an error has been assumed which is over three times that needed to include the results of five such determinations in Fe III.[10] In Mn II the $^5P-^3P$ separation leads to a value $4G_2=6409$ cm^{-1}, or if the effects of configuration interaction on the ^3P level are allowed for, $4G_2=6299$ cm^{-1}. This is in close agreement with the value determined from the $^5S-^7S$ separation.

The position of the ^3G of d^5s should be 33881 ± 100 cm^{-1} in the absence of configuration interaction. The center of gravity of the pair of ^3G terms is at 34045 cm^{-1} so that the ^3G of lower energy should be assigned to d^5s in agreement with Curtis's assignments. The separation of the pair of ^3G terms would be 328 ± 200 cm^{-1} in the absence of configuration interaction, which is in agreement with an upper limit of 550 cm^{-1} given in Sec. III and Sec. IV.

The position of the ^3D of d^5s should be 39138 ± 100 cm^{-1} in the absence of configuration interaction. The center of gravity of the pair of ^3D terms is at 38828 cm^{-1} so that the ^3D of higher energy should be assigned to d^5s in agreement with Curtis's assignments. The separation of the pair of ^3D terms would be 620 ± 200 cm^{-1} in the absence of configuration interaction, which is somewhat above the upper limit of 550 cm^{-1}. If a correction is made to account for the effect of the configuration interaction of a ^3D level which is theoretically located at 43720 cm^{-1}, then the separation in the absence of configuration interaction between the two observed ^3D terms is reduced from 620 ± 200 cm^{-1} to 390 ± 200 cm^{-1}.[11]

VI. "CORRECTED" TERM VALUES FOR THE d^5s CONFIGURATION

We have found[10] that a correction of the form

$$\Delta E=\alpha L(L+1)$$

added to the theoretical term values for the d^5s configuration of Fe III reduces the mean deviation (for 21 experimental values) from 857 cm^{-1} to 105 cm^{-1}. We are trying to find a theoretical basis for this correction, but at present it must be accepted on an empirical basis and assumed applicable to all d^5s configurations.

In Mn II, uncertainty in the location of d^6 terms leads to errors in the calculation of the positions of d^5s terms which are important when mean deviations of 100 cm^{-1} are being considered; this is due to the large effects of configuration interaction on the positions of d^5s terms in Mn II. This error was partly overcome by correcting the experimental values of d^6 terms (whenever these values were available) for the effects of configuration interaction to get the diagonal elements of electrostatic interaction for d^6. The error in doing this is considerably less than the error in the theoretically calculated diagonal elements of d^6. The effect of configuration interaction due to d^4s^2 was again neglected, chiefly because it was felt that there was too little experimental data to justify the assumptions necessary for its inclusion; this also could lead to appreciable errors.

The least-squares calculation is carried out for d^5s in a way similar to that used in Sec. I, except that the correction ΔE is first added to each term and the experimental data is corrected for effects of configuration interaction. Using the parameters obtained in this way, the eigenvalues with configuration interaction are then calculated. The result does not depend on the fact that the d^5s experimental data were corrected, as this was only an intermediate step carried out to obtain the best choice of d^5s parameters. The dependence on effects of configuration interaction with d^6 is defined in such a way that the eigenvalues of the matrices for the d^6 terms are required to equal the experimental values for the d^6 terms where such values are available; for other d^6 terms, the diagonal elements for the d^6 parts of the matrix are evaluated with the parameters of part (3) of Table I. The results of this calculation are given in part (4) of Table I; the mean deviation is 130 cm^{-1}.

I wish to thank Dr. C. W. Ufford for suggesting this problem, and for his continued help and encouragement throughout the course of the work. I wish also to thank Dr. C. W. Curtis for making the experimental data available before publication, and for a discussion of his assignments of terms to their configurations.

[11] A small effect of configuration interaction on the ^5D is included.

Zenith Angle and Momentum Spectrum of μ-Mesons at Sea Level*

JACOB L. ZAR†
Physics Department, W. S. College, New York University, New York, New York
(Received April 10, 1951)

The zenith angle dependence of the μ-meson intensity at sea level has been measured for several values of momentum between 280 and 1080 Mev/c. Results were obtained by three methods: the coincidence, anticoincidence, and delayed coincidence methods, and it has been found that the shape of the zenith spectrum depended on which technique was used. The delayed coincidence method was capable of determining meson intensities in the presence of other types of penetrating particles. It suggests the existence of a considerable number of nonmesonic particles in the low energy region of the hard component.

The lifetime of the meson was computed from its anomalous absorption in the atmosphere. It was found to be 2.2 ± 0.3 microseconds.

I. INTRODUCTION

THIS paper reports some measurements of the intensity of sea level mesons in several zenith directions for several momentum intervals. Similar measurements were made in the past, but in the present work a relatively new procedure has been used, making the identification of mesons much more certain. Formerly, it had been assumed that at sea level the number of particles in the hard component besides mesons was negligibly small. In recent years doubt has been cast on this. It has been found or suggested that:

a. A considerable number of protons are in the low energy part of the hard component. For instance, Conversi found an X component (presumably protons) making up sixteen percent of the hard component stopping per g/cm^2 of lead.[1] This is also supported by the cloud chamber experiments of Merkle, Goldwasser, and Brode.[2]

b. A significant number of electrons has been found by Reynolds to penetrate 10 cm of lead.[3]

c. An overestimation of the number of mesons that stop in the apparatus may result from scattering. Kraushaar and Rusk have analyzed this source of error.[4,5]

Two principal types of discrepancies may be found in the preceding work; (1) Coincidence and anticoincidence experiments gave different zenith angle variations of the meson intensity. (2) The lifetime of the meson deduced from its instability in the atmosphere has varied considerably in different experiments. It was usually found to be longer than the directly determined value of 2.2 microseconds. In order to see whether these discrepancies may have arisen from the complete identification of the hard component with mesons, the zenith and momentum spectrum was investigated by the method of delayed coincidences. Counters and electronic circuits were employed to determine the time intervals between the stopping of particles in a graphite absorber and the emission of decay electrons. It was found that the distribution of time intervals agreed with the known mean life of the meson. Hence, there was little doubt that what was measured was the absorption of μ-mesons only and their subsequent decay. This method was first used by Rossi, Sands, and Sard in their measurement of the slow meson intensity as a function of altitude.[6] Shortly afterward Shamos and Levy found the positive excess of mesons in this way.[7] Recently it has been employed by Kraushaar and by others.

Rossi normalized and combined the results of various observers and obtained a single curve representing the best contemporaneous estimate of the differential spectrum of vertical mesons at sea level.[8] This curve is here reproduced in Fig. 6 as the solid line labeled 0°. The momentum spectrum of mesons in inclined zenith directions is not so well known. The variation in intensity is usually expressed by:

$$I(\theta)=I_0\cos^n\theta; \qquad (1)$$

where I_0 is the vertical intensity, θ is the zenith angle, and n is a constant determined from the experiment.

A precise determination of the zenith spectrum was made by Greisen at several altitudes, including near sea level, and with several thicknesses of lead.[9] For the total radiation he found n to be 2.3; for the hard component with momentum greater than about three hundred Mev/c (computed for mesons), n was 2.1; finally for the soft component, n was 3.4.

The most recent determination of n was by Kraushaar who used three techniques: coincidence, anticoincidence, and delayed coincidence.[4] Differences in the zenith variation were found, depending on the type of measurement. With the coincidence technique, n was found to be 2.09 for all particles whose range in lead exceeded that of two hundred Mev/c mesons. In the anticoincidence experiment the momentum range between 200

* Assisted by the joint program of the ONR and AEC.
† This paper is part of a thesis submitted to the Graduate School of Arts and Science of New York University in partial fullfillment of the requirements for the Ph.D. degree.

[1] M. Conversi, Phys. Rev. **76**, 444, 849, 851 (1949).
[2] Merkle, Goldwasser, and Brode, Phys. Rev. **79**, 926 (1950).
[3] G. T. Reynolds, Revs. Modern Phys. **21**, 122 (1949).
[4] W. L. Kraushaar, Phys. Rev. **76**, 1045 (1949).
[5] R. D. Rusk and A. Rosenbaum, Phys. Rev. **76**, 1166 (1949).
[6] Rossi, Sands, and Sard, Phys. Rev. **72**, 120 (1947).
[7] M. H. Shamos and M. G. Levy, Phys. Rev. **73**, 1396 (1948).
[8] B. Rossi, Revs. Modern Phys. **20**, 537 (1948).
[9] K. Greisen, Phys. Rev. **61**, 212 (1942).

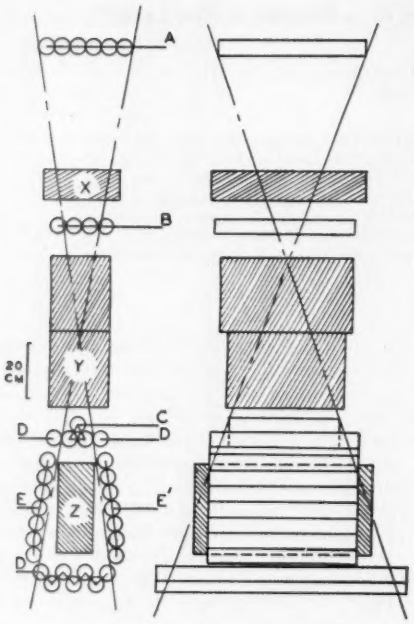

FIG. 1. Telescope for identification of mesons. A, B, and C form a threefold coincidence set with D in anticoincidence. E and E' detect decay electrons. X is lead, Y is iron, and Z is graphite. The whole apparatus may be tilted.

and 330 Mev/c was investigated. The delayed coincidence experiment was on mesons only, with momenta between 25 and 170 Mev/c. In the last two measurements the values obtained for n were both 3.3. The experiments that are here described were, in part, an extension of the work of Kraushaar to higher momentum.

When the intensity of the hard component was compared at different altitudes with allowance for the mass of the intervening column of air, it was found that the intensity lost in the atmosphere greatly exceeded the amount predicted by collision theory. This anomaly resulted from the spontaneous decay of mesons. If a meson is not absorbed, its mean range before decay is:

$$R=vl_0/(1-\beta^2)^{\frac{1}{2}}=pl_0/u_0. \quad (2)$$

Here v, l_0, u_0, and p are, respectively, the velocity, proper lifetime, rest mass, and mean momentum. There are two principal ways by which R may be measured and the lifetime deduced: (a) from the dependence of meson intensity on altitude, (b) from the intensity of mesons at one location but in different zenith directions.

Many observations of the "anomalous" absorption of mesons in the atmosphere have been made and lifetime values ranging from about 1.5 to 7 microseconds have been found. The most recent work in this field was by Cocconi and Tongiorgi.[10] They investigated the relation between the meson lifetime and the assumed mean free path of primaries, and showed that the calculated lifetime did not vary by more than plus or minus ten percent when the origin of the mesons was assumed to be 50, 100, or 200 g/cm² below the top of the atmosphere. Using 100 g/cm² for the mean free path of the primaries and 7.4×10^5 cm for z_0 (see Eq. (5)), they found lifetimes of 2.7 ± 0.4 and 3.1 ± 0.5 microseconds in two series of measurements. It will be shown that a better choice for z_0 would have been 7.0×10^5 cm. With this constant the values become 2.5 ± 0.4 and 2.9 ± 0.5 microseconds.

The delayed coincidence investigations of the present experiment afford an opportunity for measuring the anomalous absorption of mesons without requiring assumptions as to the composition of the hard component. Also, the observations were made sufficiently low in the atmosphere so as to preclude considerable local meson production. Therefore, as a part of this investigation, the estimation of the mean lifetime of the meson was undertaken to see whether an accurate value could be found by this technique.

II. APPARATUS

The apparatus was assembled in a thin-walled penthouse on the roof of the Washington Square College. Figure 1 shows a scale drawing of the essential apparatus. The telescope was mounted in a rigid, angle-iron frame and could be tilited to various zenith directions. Counter trays A, B, and C formed a threefold coincidence set for detecting incoming radiation. The anticoincidence section, D, determined the number of stopped particles. There were two guard counters in this section also for protection against cascade and side showers. Decay electrons were detected by two side trays, E and E'. The soft component was removed by a 116 g/cm² lead filter, X, which was always present. The removable absorbing material was in the form of iron bars, Y, of magnitude 0, 202, and 404 g/cm². These selected the specific region of the momentum spectrum where measurements were to be made. Lastly, a 53-g/cm² block of graphite, Z, was used to absorb mesons and provide a source of decay electrons.

The G-M counters were of the metal type with a diameter of two inches and lengths of fifteen, twenty, and thirty-four inches, as may be seen in Fig. 1. Anodes were four-mil tungsten wire and cathodes were $\frac{1}{32}$-inch brass. A self-quenching filling of 9 cm argon and 1.3 cm ethyl acetate pressure was used. Pulses and counting rates were examined daily. The various counters in a tray were connected to a single preamplifier mounted close by. This contained a cathode follower and a one-shot multivibrator.[11] With this, the pulse rise was so rapid that the number of counts delayed by more than one microsecond (because of the natural time lags of the counters) was quite negligible. Trays A, B, and C

[10] G. Cocconi and V. Tongiorgi, Phys. Rev. **70**, 855 (1946).

[11] W. Y. Chang and J. R. Winckler, Rev. Sci. Instr. **20**, 276 (1949).

were connected to a Rossi type coincidence circuit with a resolving time of about thirty-five microseconds. Its counting rate gave the integral spectrum, that is, the number of particles able to penetrate absorbers X and Y. The anticoincidence circuit received pulses from both the D counters and the coincidence unit, and recorded fourfold coincidences (A, B, C, D). The number of stopped particles was therefore found by subtracting the readings of the anticoincidence from the coincidence registers. The delay circuit counted the decay electrons detected by the E or E' counters in from one to nine microseconds after a particle had stopped in the graphite absorber. It received pulses from the coincidence unit, the anticoincidence unit and the E counters. An output pulse was generated whose height was proportional to the time between the coincidence and the delayed event, provided there was no anticoincidence pulse at that time. The output pulses from the delay circuit were sorted and counted in an eight channel pulse-height discriminator. Calibration was accomplished by introducing artificial pulses with known amounts of delay into the preamplifiers.

The telescope admitted cosmic radiation with a maximum angular divergence in the direction of the zenith of ± 9.2 degrees, and in the direction of the azimuth of ± 19.7 degrees. Not all the rays penetrated the same thickness of absorber, however. In fact, the extreme rays just grazed it. After correction for this, there resulted a mean angular resolution in the zenith direction of ± 8.0 degrees, and in the azimuthal direction of ± 16.1 degrees.

III. EXPERIMENTAL PROCEDURE

The telescope was aligned with its axis of rotation pointing east and west. Observations were taken at zenith angles of thirty-two and fifty-five degrees tilted toward the south, and also vertically upwards. The south was chosen as the direction for measurement because it is in this quarter that the primaries are least disturbed by the magnetic field of the earth.

Before the momenta could be computed from the absorber thicknesses, several corrections were necessary. (1) The thicknesses were multiplied by 1.01 because a portion of the incident beam passed diagonally through the absorbers. (2) The roof above the equipment, the counter walls and the supports contained about 14 g/cm² of material of medium atomic number. This was equivalent to 19 g/cm² of lead in absorbing power, and was included in the computation by adding this amount to the lead. (3) The path of the radiation through the absorbers was increased by multiple scattering. To allow for this, the lead thickness was increased by 9.5 percent, and the iron thickness by 2.5 percent, according to the investigation of Koenig.[12] Multiple scattering in lighter materials was negligible. After including the above three corrections, the equivalent absorber thicknesses that were used in the momentum calculations for the experiment were: (a) 146 g/cm² lead in position X; (b) 146 g/cm² lead in position X and 207 g/cm² iron in position Y; (c) 146 g/cm² lead in position X and 414 g/cm² iron in position Y. The amount of graphite in position Z was 53.3 g/cm². The momentum values that correspond to these ranges were obtained from the curves by Gross.[13] These were slightly corrected to be in accord with a meson mass of 110 Mev/c^2. Since the Gross curves are based on the calculations of Wick, they include some allowance for the polarization of the absorbing medium.[14] The momentum values used in this experiment are given in Table I.

[12] H. P. Koenig, Phys. Rev. **69**, 590 (1946).

TABLE I. Meson momenta corresponding to specified ranges of absorbing material. Corrections have been made for multiple scattering and for divergence of the beam.

Absorber	Momentum
115 g/cm² Pb	283 Mev/c
above+53 g/cm² C	391
115 g/cm² Pb+200 g/cm² Fe	615
above+53 g/cm² C	730
115 g/cm² Pb+400 g/cm² Fe	960
above+53 g/cm² C	1080

Frequent changes were made in the zenith angle and momentum region under observation. With each thickness of lead and iron, the telescope was operated for a day or two, first with the graphite absorber, then without it to obtain the background. On subtracting the background readings from those found with absorber, there were eliminated those disturbing effects which occurred with equal probability in the two cases. These effects included scattering in the metal absorbers, shower or accidental coincidences, the stopping of mesons in counter walls and supports, false delays caused by time lags in the counters, errors caused by dead-time of the counters or anticoincidence circuit, etc. When all the absorber thicknesses had been used, the telescope was tilted to another angle and the series of absorbers again run through.

Although rotation of the experimental conditions tended to smooth out the effects of atmospheric fluctuation, one could not be sure that all measurements represented identical average conditions unless some additional means of correction was employed. Consequently, a second threefold coincidence telescope was operated vertically under ten cm of lead. This continuously monitored the intensity of the hard component. Its readings were used to correct the data of the main zenith telescope in accordance with the day-to-day fluctuations of intensity of the hard component.

IV. MEASUREMENTS OF ZENITH ANGLE SPECTRA

A. Integral Spectrum

The integral spectrum of the hard component is shown as a function of zenith angle in Fig. 2. The ex-

[13] E. P. Gross, *Range, Energy, Ionization Curves*. Distributed by Princeton University (1947).

[14] G. C. Wick, Nuovo cimento, Sec. 9 **1**, 310 (1943).

TABLE II. Data and corrections for the differential spectrum of penetrating particles as a function of momentum and zenith angle.

1	2	3	4	5	6	7	8	9	10
		Data with absorber			Data for background			Difference	
Zen. angle deg.	Mean momentum Mev/c	Hours	Counts per hour	Corr. daily fluc.	Hours	Counts per hour	Corr. daily fluc.	Counts per hour	Corr. for first microsec.
0	337	178	50.4±0.5	51.2±0.5	92	30.4±0.6	30.6±0.6	20.6±0.8	22.2±0.8
0	672	212	30.3±0.4	30.5±0.4	113	15.7±0.4	15.9±0.4	14.6±0.5	16.2±0.5
0	1020	334	27.4±0.3	27.5±0.3	198	14.4±0.3	14.4±0.3	13.1±0.4	14.7±0.4
32	337	232	35.1±0.4	35.0±0.4	125	23.4±0.4	23.2±0.4	11.8±0.6	12.7±0.6
32	672	224	19.4±0.3	19.2±0.3	129	11.0±0.3	10.8±0.3	9.4±0.4	10.3±0.4
32	1020	186	18.2±0.3	18.3±0.3	84	10.7±0.4	10.8±0.3	7.6±0.5	8.5±0.5
55	337	452	16.0±0.2	16.0±0.2	305	11.6±0.2	11.6±0.2	4.4±0.3	4.7±0.3
55	672	243	7.8±0.2	7.8±0.2	137	5.1±0.2	5.1±0.2	2.7±0.3	3.0±0.3
55	1020	223	7.0±0.2	7.0±0.2	155	4.7±0.2	4.7±0.2	2.4±0.3	2.7±0.3

ponent, n, was found to be 2.04, 1.93, and 1.85 for p greater than 283, 615, and 960 Mev/c. This result is in harmony with previous work where exponents between 2.0 and 2.2 were found for the least penetrating portion of the hard component.

B. Differential Spectrum for Penetrating Particles

The number of particles between two momentum limits was found from the readings of the first channel of the delay recorder. This gave the number of particles that failed to set off either the anticoincidence or the delay counters within the first microsecond after a coincidence. Most of the particles that were widely scattered in the graphite were not recorded in this way. On the other hand, the mesons that stopped and decayed within the first microsecond, sending an electron through the E or E' trays of counters, were also not recorded. However, the number of these was found by extrapolation from the measured numbers decaying after one microsecond.

Table II contains the data and corrections for the differential spectrum of penetrating particles. The first correction applied, that given in columns 5 and 8, was for the daily variations of the hard component. The second correction, applied in column 10, was the estimated number of mesons that decayed during the first microsecond. The results are plotted in Fig. 3, where it may be seen that one value of n, 2.97, fits all data obtained for different meson momenta. (The errors shown in the table and in the figure are the standard statistical deviations of the numerical data.) This result is consistent with the measurements by Kraushaar.[4] With a similar method of determining the differential spectrum, he reported a value for n of 3.3 for low momentum mesons. Greisen, who measured the differential zenith spectrum for the soft component, found n to be 3.4.[15]

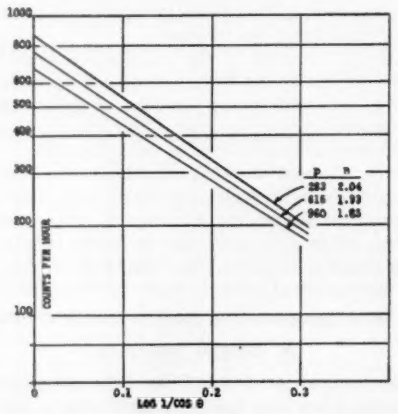

FIG. 2. Integral spectrum of the hard component as a function of zenith angle. This is expressed as a $\cos^n\theta$ law. The values of n decrease with increasing momentum.

C. Differential Spectrum for Mesons

Mesons stopping in the graphite absorber were identified by detection of their decay electrons as already

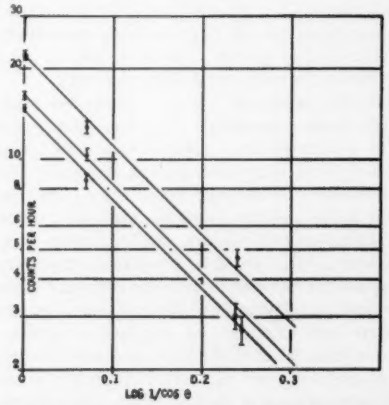

FIG. 3. The differential spectrum of the hard component as a function of zenith angle. The results were obtained with an anticoincidence counter telescope. The exponent n is 2.97 for all momenta.

[15] K. Greisen, Phys. Rev. **61**, 212 (1942).

TABLE III. Data and corrections for the differential spectrum of mesons as a function of momentum and zenith angle.

Zen. angle deg.	Mean momentum Mev/c	Data with absorber Hours	Counts per hour	Corr. for daily fluc.	Data for background Hours	Counts per hour	Corr. for daily fluc.	Difference Counts per hour
0	337	178	3.48±0.14	3.54±0.14	92	1.54±0.13	1.56±0.13	1.98±0.19
0	672	212	3.79±0.13	3.82±0.13	113	1.55±0.12	1.57±0.12	2.25±0.18
0	1020	334	3.62±0.10	3.64±0.10	198	1.42±0.08	1.42±0.08	2.22±0.13
32	337	232	2.31±0.10	2.30±0.10	125	1.07±0.09	1.06±0.09	1.24±0.14
32	672	224	2.30±0.10	2.28±0.10	129	0.98±0.09	0.96±0.09	1.32±0.14
32	1020	186	2.52±0.12	2.53±0.12	84	1.00±0.11	1.01±0.11	1.52±0.16
55	337	452	0.91±0.05	0.91±0.05	305	0.60±0.04	0.60±0.04	0.31±0.06
55	672	243	0.90±0.06	0.90±0.06	137	0.52±0.06	0.52±0.06	0.38±0.09
55	1020	223	0.93±0.06	0.93±0.06	155	0.45±0.05	0.45±0.05	0.48±0.08

explained. The data were corrected for the number of delayed events that would have been observed after 9.0 microseconds had the recorder been sensitive for all time. The corrected integral decay curves for each zenith angle are shown in Fig. 4, where they may be seen to be consistent with the known lifetime of mesons in carbon, namely, 2.15 microseconds. There is one point lying off the curves by about twice the standard deviation. This is expected to occur occasionally as a result of the normal distribution of errors. In Table III are shown the observed intensities of mesons with the background subtracted from the data with absorber. The results are plotted in Fig. 5. The error introduced into the zenith distribution by the finite angular resolution of the telescope was found to be about one percent or less, and was ignored by comparison with the much larger statistical errors.

One may suppose that the exponent for the zenith angle distribution decreases as the meson energy increases. This is suggested by the observation that n for the integral spectrum is approximately two, whereas for the differential spectrum, it is approximately three. This variation of n with energy is consistent with the data in Fig. 5. It should be noted, however, that the meson counting rate was quite low at inclined zenith angles, and so the final numerical results are not known with great accuracy. The spectrum obtained by anticoincidence, as shown in Fig. 3, fails to show this expected variation of n with energy. Two possible explanations may be suggested.

(1) Protons near the end of their range have a greater specific ionization than mesons; and so an absorber in an anticoincidence experiment has a greater stopping power for protons than for mesons. Consequently, if protons of low energy were present in the penetrating component they would have a disproportionate influence on the shape of the anticoincidence differential spectrum.

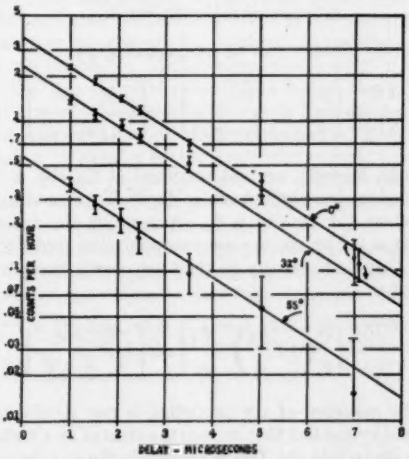

FIG. 4. Meson decay curves. Values are readings of delay discriminator for absorber minus background. They have been corrected to include delays to infinite time. Curves are drawn for a mean life of 2.15 microseconds.

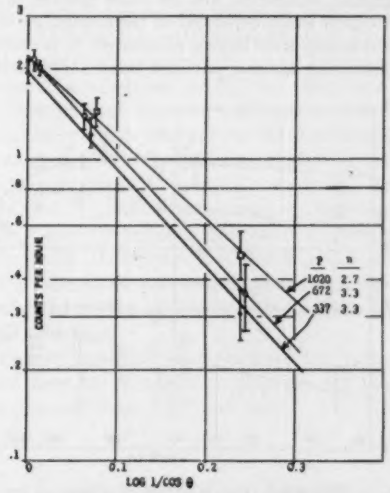

FIG. 5. The zenith angle dependence of mesons at sea level obtained by the method of delayed coincidences. Background intensities have been subtracted from measurements taken with a graphite absorber.

Since there is no *a priori* reason to suppose that the zenith angle distribution for protons is the same as for mesons at sea level, the lack of variation of n in Fig. 3 may in part be attributed to the presence of protons in the low energy region of the hard component.

(2) Kraushaar has pointed out how carefully an anticoincidence telescope must be designed so that errors produced by the scattering of particles in the heavy metal absorbers may be eliminated.[4] The difference between his value of 3.3 and the value obtained here for n may have resulted from different telescope designs.

D. Differential Range Spectrum

A comparison of the zenith and momentum spectra that have been obtained thus far by a number of investigators is shown in Fig. 6. The abscissa is given in terms of the range in air, and the conversion from momentum values to range units was made with the aid of the Gross curves.[12] The solid line graph labeled 0° is the vertical differential range spectrum as given by Rossi.[8] For comparison, the measurements of Kraushaar (K) and of Shamos and Levy (S) are shown plotted along with the delayed coincidence results of the present experiment (circles).[4,7] In order to obtain absolute intensities, the present data were normalized to Rossi's vertical curve at the 280 g/cm² point. The points for the curves at zenith angles of thirty and sixty degrees have been interpolated from Fig. 5 without further normalization.

The anticoincidence data of Fig. 4 were also plotted in Fig. 6 as crosses. For the lowest range, the crosses occur considerably above the meson curves. The anticoincidence measurements were made by subtracting background intensities, and so those sources of systematic error which depended on the momentum of the incident meson were largely eliminated. It is therefore concluded that ionizing particles besides mesons occur with ranges between 100 and 400 g/cm² of air in all zenith directions at sea level. These particles are believed to be protons because: (1) it is unlikely that electrons could penetrate the ten cm of lead absorber in appreciable numbers; (2) an absorber in an anticoincidence experiment has a greater stopping power for low energy heavy particles than for lighter ones of similar range.

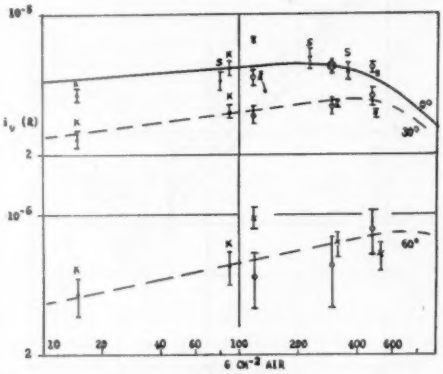

FIG. 6. Differential range spectrum of mesons at sea level. Ordinates are particles per cm² steradian second. Circles are delayed coincidence data; crosses are anticoincidence measurements. Points marked K and S are by Kraushaar and by Shamos and Levy.

The present experimental results extend our knowledge of the meson zenith spectrum. Whenever comparisons can be made with previous work, the agreement appears satisfactory.

V. LIFETIME OF THE μ-MESON

The method of delayed coincidences permits the determination of the lifetime of the μ-meson from its anomalous absorption in the atmosphere. This technique was not affected by the presence of protons in the hard component, and systematic errors were largely eliminated by subtracting background readings. The calculations follow the method given by Janossy.[16]

In a group of $N(t)$ mesons, the number decaying is:

$$-dN=N(z)(\mu_0/t_0)dz/p(z). \tag{3}$$

If $N(0)$ mesons reach sea level with momentum p_1, the number that must have existed at an altitude, z, with momentum $p(z)$ is obtained by integration.

The atmospheric pressure may be approximated by:

$$\theta(z)=\theta_0\exp(-z/z_0), \tag{4}$$

where θ_0 and z_0 are constants.

Let p_A denote the momentum loss of a specified group of mesons in traversing the entire atmosphere.

$$p(z)=p_1+p_A[1-\exp(-z/z_0)]. \tag{5}$$

Equation (3) may now be integrated to give:

$$\frac{N(0)}{N(z)}=\left[\frac{p_A}{p_1}\frac{p(z)}{p_A+p_1-p(z)}\right]\exp\left[\frac{-z_0}{ct_0}\frac{\mu_0 c}{p_1+p_A}\right]. \tag{6}$$

Mesons, however, are not produced at the top of the atmosphere but throughout its depth. Take an altitude z_p, where the density is θ_p, representing the average height at which mesons are produced. The probability that they do not decay on their way down to sea level is then:

$$\frac{N(0)}{N(z_p)}=\left[\frac{\theta_0}{\theta_p}\left(1+\frac{p_A}{p_1}\right)-\frac{p_A}{p_1}\right]\exp\left[\frac{-z_0}{ct_0}\frac{\mu_0 c}{p_1+p_A}\right]. \tag{7}$$

The accuracy of the preceding is not significantly altered by the fact that mesons are created as π's which then decay into μ's. This is because in the π–μ-decay of

[16] L. Janossy, *Cosmic Rays* (Oxford University Press, London, 1950).

energetic particles the momentum of the π is almost entirely transferred to the μ; and, since the lifetime of the π-meson is only about one percent of the μ, the effective value of l_0 that would apply to the whole process is very nearly the lifetime of the μ-meson alone.

The treatment of the problem for travel in an inclined direction, making an angle ϕ with the vertical, is analogous to that which preceded, except that different constants are required, namely: $z_0'=z_0\sec\phi$; $p_A'=p_A\sec\phi$; $\theta_0'=\theta_0\sec\phi$; $z_p'=z_0\ln(\theta_0/\theta_p\cos\phi)$. The probability that these mesons do not decay between the production region and sea level is found in the same way as Eq. (7).

$$\frac{N'(0)}{N'(z_p)}=\left[\frac{\theta_0}{\theta_p\cos\phi}\left(1+\frac{p_A}{p_1\cos\phi}\right)-\frac{p_A}{p_1\cos\phi}\right]\times\exp\left[\frac{-z_0}{cl_0}\,\frac{\mu_0 c}{p_1\cos\phi+p_A}\right]. \quad (8)$$

From the experiments of Winckler and Stroud, it is known that the penetrating cosmic radiation near the top of the atmosphere is uniform in all directions.[17]

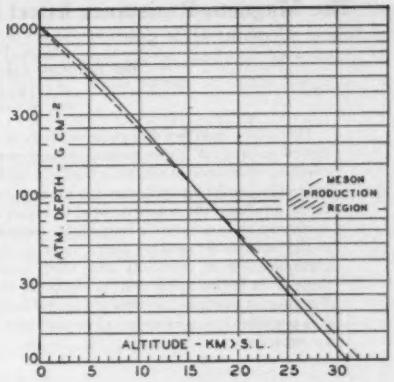

FIG. 7. The standard atmosphere. The solid curve is the atmospheric density variation as given by The National Advisory Committee on Aeronautics. The dashed curve is the exponential approximation used in deriving the probability for meson decay.

Hence,

$$N(z_p)=N'(z_p). \quad (9)$$

Then

$$l_0=\frac{z_0\mu\left\{\ln\left[\dfrac{\theta_0}{\theta_p\cos\phi}\,\dfrac{p_0}{p_1'}-\dfrac{p_A}{p_1'\cos\phi}\right]-\cos\phi\ln\left[\dfrac{\theta_0}{\theta_p}\,\dfrac{p_0}{p_1}-\dfrac{p_A}{p_1}\right]\right\}}{(p_1+p_A)(\cos\phi)\ln[N(0)/N'(0)]}. \quad (10)$$

Former investigators have used values of z_0 of (7.0, 7.5, or even 8.0)$\times10^5$ cm, and have justified their choice by assuming mean temperatures for the atmosphere that were consistent with their selection. Assumptions about the atmospheric temperature, however, are not necessary since all that is required is that the approximate function given in Eq. (4) should fit the atmosphere as well as possible. The "standard atmosphere" is shown in Fig. 7 as the solid curve.[18] The dashed curve is Eq. (4) plotted with $z_0=7.0\times10^5$ cm. It may be seen that this approximation introduces the same path length and change in density as the exact atmospheric function between the region of meson production (approximately 100 g/cm^2) and sea level. This, therefore, gives the same probability for decay.

The mean free path of the primaries, θ_p, was taken as 150 g/cm^2, in keeping with the experimental findings of Conversi and others.[19] (Note that the meson lifetime is not strongly dependent on this quantity.) The values chosen for p_1, p_1', and (p_1+p_A) were 1020, 337, and 3430 Mev/c, respectively. The zenith angle appropriate to these was 39 degrees. For this angle, $N(0)/N'(0)$ was $2.22\pm0.13/0.88\pm0.12$ which was 2.52 ± 0.38. The meson lifetime was then computed to be 2.2 ± 0.3 microseconds. The agreement between the lifetime value found here and 2.15 microseconds is evidence that this experimental technique is effective for the determination of meson intensities in the presence of other particles.

Acknowledgment is greatfully made to the late Professor I. S. Lowen for sponsoring this problem at its outset. Later, the research came under the direction of Professor M. H. Shamos from whom much valuable advice, information and encouragement were received. Thanks and credits are also due Mr. L. Eisen for care of the apparatus.

Financial assistance was tendered the project by grants from the Research Corporation and from the joint program of the ONR and AEC.

[17] J. R. Winckler and W. G. Stroud, Phys. Rev. **76**, 1012 (1949).
[18] W. G. Brombacher, National Committee of Aeronautics, Report No. 538 (1935).
[19] M. Conversi, Phys. Rev. **79**, 749 (1950).

The Magneto-Resistance Effect in Oriented Single Crystals of Germanium

G. L. PEARSON AND H. SUHL
Bell Telephone Laboratories, Murray Hill, New Jersey

(Received May 4, 1951)

This paper describes an extensive study of the magneto-resistance effect in germanium as a function of crystal orientation. Experimental measurements establish the constants involved in the dependence of the effect on orientation of magnetic field and electric current relative to the crystal axes. The measurements are internally consistent with existing phenomenological theory based on cubic crystal symmetry, in which terms involving the magnetic field to higher than the second order are neglected. It is shown that such deviations as do occur arise from higher terms in the field, since an extension of the phenomenological theory to the fourth order predicts their symmetry. Relations are established between the experimentally observed phenomenological constants and those constants appearing in existing magneto-resistance electronic theories. It is concluded that no electronic theory yet worked out is entirely consistent with experiment. The present electronic theories are special cases of a very general theory recently proposed by Shockley, and it is possible that agreement can be obtained as soon as the computational difficulties of the latter theory are overcome.

I. INTRODUCTION

THE effect of magnetic fields on the electrical resistance of semiconductors has been obscure until quite recently. Although simplified theories pertaining to parallel and perpendicular electric and magnetic fields in isotropic media[1] had been formulated, no equations applicable to experimental measurements on allotropic semiconducting materials were available. Adequate experimental data were likewise lacking. Those most often quoted in the literature were obtained by Kapitza[2] on multicrystalline germanium and silicon samples of unknown impurity content.

The phenomenological theory of the magneto-resistance effect in semiconductors has recently been clarified by Seitz,[3] who succeeded in deriving general equations in a closed form relating to semiconducting crystals possessing cubic symmetry. Important contributions on the experimental side have been made by Estermann and Foner,[4] who measured the effect in germanium samples of known impurity content as a function of the temperature and the magnitude and relative directions of the electric and magnetic fields. Their results, however, have limited application to Seitz's theory, since their germanium samples were composed of many small crystals having random orientation.

The present paper reports magneto-resistance measurements on single crystal samples of germanium as a function of the orientation of the electric and magnetic fields with respect to the crystal axes. Other variables studied were strength of magnetic field, temperature, and type of conduction (either by holes or electrons). The numerical results are compared with Seitz's theoretical equations, from which the fundamental magneto-resistance constants of germanium are obtained. Certain discrepancies between theory and experiment lend weight to a more sophisticated model recently treated by Shockley.[5]

II. THEORETICAL DISCUSSION

The theoretical treatment of the effect of magnetic fields on the electrical resistance of semiconductors is simplified over that of metals, in that the concentration of free electrons is usually so low that the electron gas obeys classical statistics. The first study of this problem was made by Ganz,[1] who assumed perfectly free electrons, an isotropic medium, and an energy-independent mean free path. His calculations were limited to the case in which the applied electric and magnetic fields are normal. He carrried the solutions to terms in the current which depend on the first power of the electric field strength and on arbitrary powers of the magnetic field strength, and obtained a solution in closed form for the transverse Hall effect and for the conductivity as a function of the magnetic field.

These calculations have been extended by Harding,[1] Wilson,[1] and Davis[6] to include the case of an allotropic medium. In addition, Davis generalized the treatment to include electric and magnetic fields oriented arbitrarily relative to one another, electrons that are not perfectly free, and a mean free path dependent on the energy in an arbitrary manner. His solution is so general that it cannot be expressed in a closed form but is in terms of series in powers of the magnetic field, the coefficients being integrals which must be evaluated in particular cases.

Seitz[3] has recently established the phenomenological relation between the current density vector $\mathbf{i}$ and the electric and magnetic field $\mathbf{E}$ and $\mathbf{H}$ that must hold in any material having cubic symmetry. His equation, which is perfectly general and subject only to the

[1] R. Ganz, Ann. Physik **20**, 293 (1906). A. Sommerfeld and N. H. Frank, Revs. Modern Phys. **3**, 1 (1931). J. W. Harding, Proc. Roy. Soc. (London) **140**, 205 (1933). A. H. Wilson, *The Theory of Metals* (Cambridge University Press, London, 1936).
[2] P. Kapitza, Proc. Roy. Soc. (London) **123**, 291 (1929).
[3] F. Seitz, Phys. Rev. **79**, 372 (1950)
[4] I. Estermann and A. Foner, Phys. Rev. **79**, 365 (1950).
[5] W. Shockley, Phys. Rev. **78**, 173 (1950); Phys. Rev. **79**, 191 (1950).
[6] Leverett Davis, Jr., Phys. Rev. **56**, 93 (1939).

limitation that terms involving the magnetic field to higher than the second power are neglected, is

$$\mathbf{i}=\sigma_0\mathbf{E}+\alpha(\mathbf{E}\times\mathbf{H})+\beta\mathbf{E}H^2+\gamma\mathbf{H}(\mathbf{E}\cdot\mathbf{H})+\delta T\mathbf{E}, \quad (1)$$

where T is a diagonal tensor with elements H_1^2, H_2^2, and H_3^2 (the coordinate axes 1, 2, and 3 being taken along the crystal axes), σ_0 is the electronic conductivity under zero field conditions, $-\alpha/(\sigma_0)^2$ is the Hall coefficient,[7] and β, γ, δ are the small-field magneto-resistance constants deducible from electronic theory. Any electronic theory must lead to the form of Eq. (1).

All of the magneto-resistance theories mentioned above explicitly determine the current as a function of the magnetic and electric fields applied to the specimen. In magneto-resistance experiments, on the other hand, the change in voltage across the sample due to $\mathbf{H}$ is taken as a measure of the resistance increment due to $\mathbf{H}$. In other words, $\mathbf{i}$ is held constant and $\mathbf{E}$ is permitted to adjust itself accordingly. The experiment is therefore only indirectly related to the constants α, β, γ, and δ. Experiment is more closely related to the constants a, b, c, and d of a reciprocal equation

$$\mathbf{E}=\rho_0[\mathbf{i}+a(\mathbf{i}\times\mathbf{H})+bi H^2+c\mathbf{H}(\mathbf{i}\cdot\mathbf{H})+dT\mathbf{i}] \quad (2)$$

which is also a consequence of cubic symmetry. Straightforward matrix algebra, with neglect of powers of H higher than the second, shows that

$$\left.\begin{aligned} a&=-\alpha\rho_0, \quad b=-(\beta+\rho_0\alpha^2)\rho_0,\\ d&=-\delta\rho_0, \quad c=-(\gamma-\rho_0\alpha^2)\rho_0,\end{aligned}\right\} \quad (3)$$

where $\rho_0=1/\sigma_0$.

In terms of this new set of constants, the resistance increment due to an increase in magnetic field from 0 to H is[8]

$$\frac{\Delta\rho}{\rho H^2}=\frac{(\mathbf{E}-\mathbf{E}_{H=0})\cdot\mathbf{i}}{(\mathbf{E}_{H=0}\cdot\mathbf{i})}=b+c\frac{(\mathbf{i}\cdot\mathbf{H})^2}{i^2H^2}+d\frac{i_1^2H_1^2+i_2^2H_2^2+i_3^2H_3^2}{i^2H^2}. \quad (4)$$

More simply, if ι_1, ι_2, ι_3 and η_1, η_2, η_3 are the direction cosines of $\mathbf{i}$ and $\mathbf{H}$, respectively,

$$\Delta\rho/(\rho_0H^2)=b+c(\Sigma\iota\eta)^2+d\Sigma\iota^2\eta^2. \quad (5)$$

Thus, by measuring the magneto-resistance effect in certain selected directions one can evaluate the constants b, c, and d after which Eq. (5) permits one to calculate the effect for arbitrary directions of $\mathbf{i}$ and $\mathbf{H}$. Likewise, after experimentally determining b, c, and d, one can use Eq. (3) to calculate the constants β, γ, and δ for comparison with electronic theory.

For the simple case of isotropic materials having a mean free path independent of energy, Seitz has shown from electronic theory that $\beta=-\gamma=-9\pi\mu^3ne/16c^2$, where μ is the mobility of the carriers, n is their density, e is the electronic charge, and c is the velocity of light. Substituting these values in Eqs. (3) and (4) it is deduced that

$$\Delta\rho/(\rho H^2)=0, \quad (6)$$

for $\mathbf{i}$ parallel to $\mathbf{H}$, and

$$\Delta\rho/(\rho H^2)=81\times10^4\pi\mu^2(1-\tfrac{1}{4}\pi)/16c^2=3.8\times10^{-17}\mu^2, \quad (7)$$

for $\mathbf{i}$ perpendicular to $\mathbf{H}$. Equations (6) and (7) are in quantitative agreement with the earlier relations[1] for the simple isotropic case at low magnetic field intensities. Harding[1] studied the case of transverse magnetic fields in isotropic semiconductors beyond the quadratic range and predicted that

$$\lim_{H\to\infty}\frac{\Delta\rho}{\rho}=0.13. \quad (8)$$

Seitz[3] has applied an electronic theory of Davis[6] to find the form of α, β, γ, and δ on the hypothesis that the energy-momentum surfaces of the electrons are spheres, whereas the relaxation time τ is an allotropic function of the momentum vector $\mathbf{k}$ such that

$$\tau=\tau_0(k)+\tau_1(k)Y(\theta,\varphi),$$

where $Y(\theta,\varphi)$ is the polar form of the cubically invariant quartic $x^4+y^4+z^4-3(x^2y^2+y^2z^2+z^2x^2)$.* τ_0 and τ_1 depend on the length of $\mathbf{k}$ only and have a constant ratio. His final expressions are

$$\left.\begin{aligned}\beta&=[1+(\tau_1/\tau_0)^2(532/231)]I,\\ \gamma&=-[1+(\tau_1/\tau_0)^2(212/231)]I,\\ \delta&=-(\tau_1/\tau_0)^2(240/231)I,\end{aligned}\right\} \quad (9)$$

where I is a certain integral depending on τ_0 and on the distribution function of $\mathbf{k}$. In order to compare the experimental results described below with this theory we note that

$$b+c+\tfrac{1}{2}d=-(\beta+\gamma+\tfrac{1}{2}\delta)\rho_0=-(\tau_1/\tau_0)^2(200/231)I\rho_0, \quad (10)$$

and

$$b+c+d=-(\beta+\gamma+\delta)\rho_0=-(\tau_1/\tau_0)^2(80/231)I\rho_0. \quad (11)$$

Physically, Eq. (10) is the value of $\Delta\rho/(\rho H^2)$ when $\mathbf{H}$ and $\mathbf{i}$ are parallel and directed along the 110 crystal axis, while Eq. (11) is the value of $\Delta\rho/(\rho H^2)$ when $\mathbf{H}$ and $\mathbf{i}$ are parallel and directed along the 100 crystal axis. The above electronic theory predicts that the ratio of these two magneto-resistance effects should be 2.5.

III. PREPARATION OF SAMPLES

The germanium used in this study was large single crystal ingots prepared by the pulling technique of Teal and Little.[9] As drawn, the conductivity was n-type and

[7] If i is in amp/cm², E in volt/cm, and H in gauss, then $-\alpha/\sigma_0^2$ is in volt cm/amp gauss.

[8] This equation was first called to our attention by J. Bardeen who derived it from symmetry considerations.

* Where $x^2+y^2+z^2=1$.

[9] G. K. Teal and J. B. Little, Phys. Rev. 78, 647 (1950).

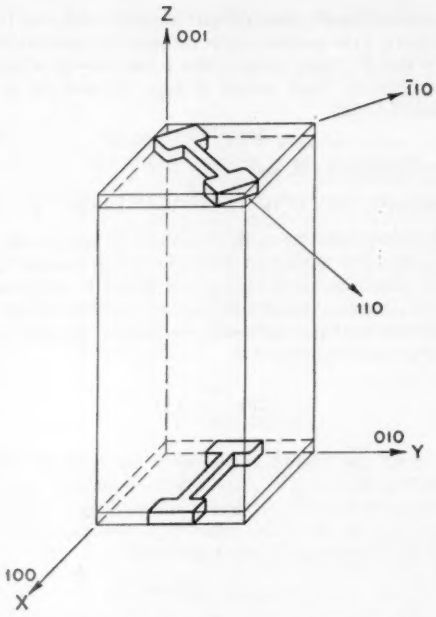

FIG. 1. Orientation of rod samples as cut from a single crystal of germanium.

the purity high as evidenced by a resistivity of 11.5 ohm cm. The crystal structure of germanium is cubic and of the diamond lattice type. The ingots were ground on a carborundum belt grinder into elongated square prisms having their edges parallel to the x, y, and z crystal axes with the help of x-rays as described by Bond.[10] Figure 1 is a sketch of the oriented crystal after grinding. The crystals were then sawed in half along the xy plane and one section of each crystal converted to p-type by heat treating at 900°C for a period of six hours in a helium atmosphere followed by an air quench.[11] The resistivity of the converted sections was 0.38 ohm cm.

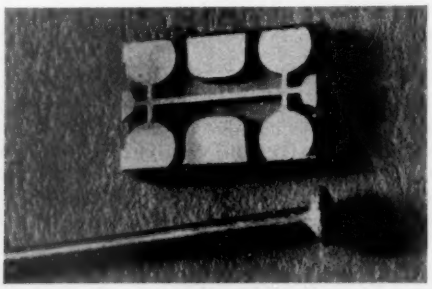

FIG. 2. Photograph of oriented germanium rod for measuring magneto-restistance effect. A common pin is shown for size comparison.

[10] W. L. Bond, Phys. Rev. **78**, 646 (1950).

Samples suitable for making magneto-resistance measurements were prepared by sawing and lapping thin plates as shown in Fig. 1. After etching to clean up the surfaces the plates were cemented to glass substrates and rod samples with intimately attached current, and voltage electrode areas were cut by means of a magnetostrictive driven die as described by Bond.[10] Further steps in the preparation included rhodium electroplating of the electrode surfaces to obtain good ohmic contact and cleaning up of the germanium surfaces by etching. Figure 2 is a photograph of a completed rod sample. The two end electrodes are for current and the four side electrodes for potentiometric measurements. All of the samples were cut with the same die, which resulted in identical dimensions. The length of the rod between potential electrodes is 0.500 cm, the width 0.025 cm, and the thickness 0.025 cm. Several samples from both the n- and p-type sections were made from a number of ingots. They were cut in each of the two different crystal orientations shown in Fig. 1, that is, with the length along either the 100 or the 110 crystal axis and with the thickness always along the 001 axis.

The magneto-resistance measurements were made by passing a fixed current through the sample and measuring the voltage between the potential probes with and without a magnetic field. The voltage drops were measured with a Leeds and Northrup type K2 potentiometer. Since the effect was found to be independent of current magnitude, this was altered for the different samples to always give a convenient maximum of about 1 volt and was usually of the order of 1 ma. Magnetic fields up to 20,000 gauss were furnished by a large electromagnet, and the field strengths were measured by a synchronously driven rotating coil and Ballantine voltmeter. Accurate calibration was obtained by comparison with a permanent magnet which had been calibrated at the U. S. Bureau of Standards. The samples were enclosed in a Dewar flask during the measurements. This eliminated temperature drifts at room temperature, served as a liquid nitrogen and liquid hydrogen container at low temperatures, and eliminated all photoeffects. Temperatures were measured with a Mueller bridge and a platinum resistance thermometer.

IV. EXPERIMENTAL RESULTS

A. Magneto-Resistance Effect *versus* Field Strength

Measurements were first made of $(\rho-\rho_0)/\rho_0=\Delta\rho/\rho$ as a function of $\mathbf{H}$ for given directions of $\mathbf{i}$ and $\mathbf{H}$ with respect to the crystal axes. Since current is always along the length of the rods, the direction of $\mathbf{i}$ is fixed for any given sample and may be either along the 100 or the 110 axis. Runs were made with $\mathbf{H}$ parallel to $\mathbf{i}$ and

[11] H. C. Theuerer and J. H. Scaff, Trans. Am. Inst. Mining Engrs. **189**, 59 (1951).

perpendicular to **i**. The results for p-type rods at both 300°C and 77°C are given in Fig. 3. The general features of these curves include: (1) $\Delta\rho/\rho$ proportional to H^2 at low field strengths with a break in the curve between 5000 and 10,000 gauss and proportional to the first power of H or lower at high fields, (2) at a given field $\Delta\rho/\rho$ increases with decrease in temperature, and (3) the magneto-resistance is much greater for **H** perpendicular to **i** than for **H** parallel to **i**. These features are in agreement with the simplified electronic theory as given by Eqs. (6) and (7). The experiments do not agree with this theory in that they predict a hole mobility three times that measured by other means;[12] also, $\Delta\rho/\rho$ values greater than 0.13 have been achieved at high field strengths without reaching saturation.

The direction of **i** could be reversed without altering the magnitude of $\Delta\rho/\rho$, as could that of **H**. In the sample having **i** along the 100 axis, Fig. 3(A), identical results were obtained with **H** along either the 010 or 001 axis. This is to be expected, since these two axes have complete crystal symmetry. In the sample with **i** along the 110 axis, Fig. 3(B), slightly different results were obtained with **H** along the $1\bar{1}0$ and the 001 unsymmetrical axes.

A corresponding set of measurements on the n-type samples are shown in Fig. 4. The results for **H** perpendicular to **i** are quite similar to those for p-type, and the calculated electron mobility checks that determined by the drift method within 25 percent. In the n-type samples, however, the magneto-resistance effect with **H** parallel to **i** is completely out of line with the simple theory. Instead of being small in comparison with the transverse effect, it is twice as large. Through the cooperation of the Magnetics Laboratory at the Massachusetts Institute of Technology we were able to extend the room temperature measurements on the 100 sample to 100,000 gauss as shown in Fig. 4(a). Notice that saturation has not yet been attained at this high field although $\Delta\rho/\rho$ transverse has reached 1.1 and $\Delta\rho/\rho$ longitudinal has reached 2.2. At 77°K $\Delta\rho/\rho$ longitudinal reached 2.0 for a field of only 20,000 gauss.[12] In the n-type 110 sample, Fig. 4(b), the effect is markedly higher with **H** in the perpendicular 110 direction than in the perpendicular 001 direction. Saturation is fairly complete at $\Delta\rho/\rho$ equal to 0.5 with $H=20{,}000$ gauss, $T=77$°K, and **H** parallel to **i**.

In order to calculate certain fundamental constants to be described in Sec. V it is necessary to determine $\Delta\rho/\rho H^2$ as H approaches zero for the various directions of **i** and **H** shown in Fig. 3 and Fig. 4. These data are given in Fig. 5 and Fig. 6, which are replots of the previous data excepting that $\Delta\rho/\rho H^2$ is plotted along the vertical scale. Notice that at room temperature the curves are horizontal up to 3000 gauss indicating an exact square law relationship between $\Delta\rho/\rho$ and H. At low temperatures the curves do not flatten even at low fields indicating a power of H slightly less than 2.

[12] Pearson, Haynes, and Shockley, Phys. Rev. **78**, 295 (1950). Hole mobility in germanium at room temperature as determined by the drift method is 1700 cm²/volt sec and electron mobility 3600 cm²/volt sec.

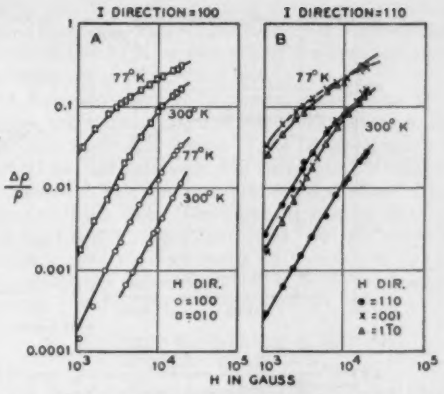

FIG. 3. $\Delta\rho/\rho$ *vs* H in p-type germanium for fixed directions of **I** and **H**; the values of T are as shown.

B. Magneto-Resistance Effect *versus* Temperature

The magneto-resistance effect in an n-type sample with **i** along the 100 direction was measured as a function of temperature for a fixed magnetic field of 4000 gauss in both the 100 longitudinal direction and the 010 transverse direction. These results are shown in Fig. 7, where $\Delta\rho/\rho H^2$ is plotted vertically and the temperature in degrees Kelvin horizontally, both scales being logarithmic. Theory indicates, as shown by Eq. (7) that $\Delta\rho/\rho H^2$ should vary as μ^2. Since μ varies as T^{-1} in the lattice scattering range, $\Delta\rho/\rho G^2$ should vary as T^{-3}. This is verified by the data for temperatures between 150 and 300 degrees Kelvin. At lower temperatures the curves droop as is to be expected because

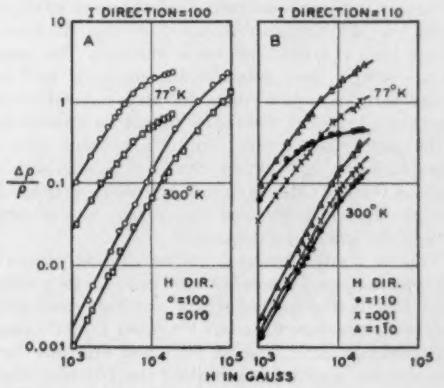

FIG. 4. $\Delta\rho/\rho$ *vs* H in n-type germanium for fixed directions of **I** and **H** and fixed values of T as shown.

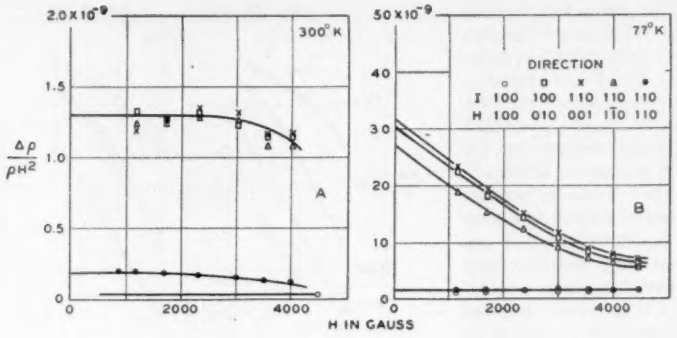

FIG. 5. $\Delta\rho/\rho H^2$ *vs* H in p-type germanium. The fixed directions of **I** and **H** and the values of T are as shown.

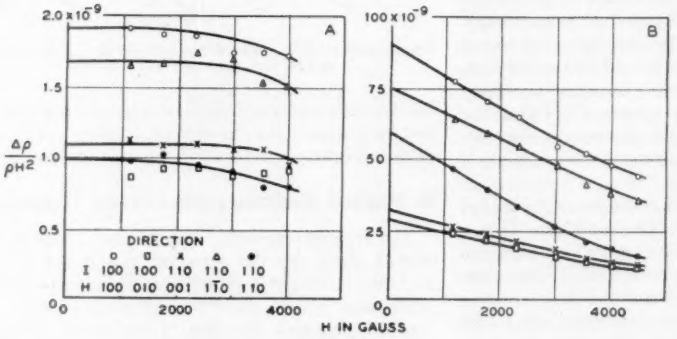

FIG. 6. $\Delta\rho/\rho H^2$ *vs* H in n-type germanium. The fixed directions of **I** and **H** and the values of T are as shown.

of impurity scattering. Results similar to these were obtained for other directions of **i** and **H** and with p-type germanium.

C. Magneto-Resistance Effect *versus* Angle θ

Measurements were next made of $\Delta\rho/\rho$ for fixed values of H and T and a fixed direction of **i** but with varying directions of **H** with respect to the crystal axes. For this purpose the magnetic field was set at 4000 gauss and the electromagnet mounted so that its lines of force were in a fixed horizontal direction. The germanium sample was placed in the magnetic field and attached to a vertically mounted brass rod which could be rotated through 360 degrees about its vertical axis. The germanium sample could be mounted with its length, width, or thickness dimension parallel with the axis of rotation. Measurements were made at either 300 or 77 degrees Kelvin and the current was of course along the lengthwise dimension.

Figure 8 gives the results of such measurements on p-type samples. Figures 8(A) and 8(B) are for a sample cut with its length along the 100 axis, the former giving room temperature data and the latter liquid nitrogen temperature data. Figures 8(C) and 8(D) are for a sample cut with its length along the 110 axis. Figure 8(C) was obtained at room temperature and Fig. 8(D) at liquid nitrogen temperature. In all of these figures $\Delta\rho/\rho$ is plotted vertically and the angle of rotation θ is plotted horizontally. The curves with solid circles apply to the case where the axis of rotation is the sample length, with open circles the axis of rotation is the sample width and with crosses the sample thickness. At θ equal to 0, 90, 180, 270, and 360, the crystal axis parallel to **H** is indicated.

As shown in Fig. 8(A), which applies to a p-type sample at room temperature cut with its length along the 100 axis, $\Delta\rho/\rho$ is constant for all values of θ when the sample length is the axis of rotation. In this experimental arrangement, although **H** rotates through 360 degrees around the 100 crystal axis, it is always perpendicular to **i**. Because of the cubic crystal structure of germanium the experimental result obtained here is to be expected providing H is within the square law range. If the experiment were repeated at 77 degrees Kelvin with the same field strength of 4000 gauss the magneto-resistance effect would be increased by a factor of 6 and the square law range would be exceeded as shown by Fig. 3(A). That such is the case is shown by the upper curve of Fig. 8(B). With **H** parallel to the 001 axis $\Delta\rho/\rho$ has increased from 0.019 to 0.12. Although 90-degree symmetry has been retained, we now have maxima with **H** midway between principal axes.

When the sample was mounted so that its width was along the axis of rotation, the curves designated by

crosses in Fig. 8(A) and Fig. 8(B) were obtained. At θ equal to 0, 180, and 360 degrees **H** is perpendicular to **i** and at θ equal to 90 and 270 **H** is parallel to **i**. As expected from crystal symmetry, rotation with either the width or thickness along the axis of rotation gave identical results.

Figure 8(C) and Fig. 8(D) give the results of similar measurements on a p-type germanium sample cut with its length along the 110 axis. In this case the crystal symmetry is destroyed and $\Delta\rho/\rho$ is no longer constant for rotation about the length axis, the value being greater with **H** along the 001 direction than with **H** along the 110 direction. Although the longitudinal magneto-resistance effect, with **H** and **i** both in the 110 direction, is less than the transverse effect, it does not approach zero as in the 100 cut sample.

Similar rotation measurements on n-type germanium samples are shown in Fig. 9. The more significant features of these curves are: (1) the longitudinal effect is much larger than the transverse effect, (2) in the 110 cut sample the transverse effect with **H** in the 110 direction is larger than in the 001 direction which is opposite to the effect in p-type germanium, and (3) at liquid nitrogen temperatures the same 90-degree symmetry is found as in p-type.

V. CALCULATION OF ANGULAR DEPENDENCE CONSTANTS

The experimentally determined values of $\Delta\rho/\rho H^2$ for selected directions of **i** and **H** as H approaches zero are given in Table I for the n- and p-type germanium samples at 300°K and 77°K. The right-hand column in Table I gives the theoretical values of $\Delta\rho/\rho H^2$ for the selected directions in terms of the phenomenological angular dependence constants b, c, and d obtained by substituting the direction cosines of **i** and **H** in Eq. (5). By taking appropriate combinations of the $\Delta\rho/\rho H^2$ values given in the lower three lines of Table I, the values of b, c, and d shown in Table II are obtained. Using the relations given in Eq. (3) the corresponding phenomenological theory constants β, γ, and δ have been calculated as shown in Table II. The related constants $\alpha=-a\sigma_0=-R_H\sigma_0^2$ are also given in Table II together with the experimentally determined values of zero field conductance (σ_0) and Hall coefficient (R_H in volt cm/amp gauss).

Having obtained the phenomenological constants b, c, and d, it is now possible to calculate the small field magneto-resistance effect in germanium for **i** and **H** oriented in any arbitrary manner. The fact that the experimentally determined curves shown in Fig. 8 and Fig. 9 fit Eq. (5) for most conditions indicates that the phenomenological relationships are in good agreement with experiment.

The particular electronic theory developed by Seitz can be tested by means of Eqs. (9), (10), and (11). The last two predict that $\Delta\rho/\rho H^2$ with **i** and **H** parallel and along 110 should be 2.5 times $\Delta\rho/\rho H^2$ for **i** and **H** along 100. The experimentally determined ratios as found from Table I are 5.2 and 1.4 for p-type germanium at 300°K and 77°K, respectively. For n-type the corresponding ratios are 0.51 and 0.66.

A much more serious discrepancy between the Seitz theory and the experimental results is apparent in the first of Eqs. (9). The integral I can be evaluated for a mean free path independent of energy and is found to be positive.[3] But the experimentally determined β are negative in all cases. Therefore, the first of Eqs. (9) can hold only for imaginary τ_1/τ_0. We are forced to conclude that a theory based on anisotropies in the relaxation time alone does not agree with the observed results.

VI. MAGNETO-RESISTANCE EFFECT OF HIGHER ORDER IN H

The phenomenological theory described above, which extends only to terms of the second order in H, predicts a constant value $\Delta\rho/\rho H^2=b$ when **i** is in the 100 direction and **H** is rotated about the current vector in a plane normal to it. Figures 8(A) and 9(A), which apply to p- and n-type materials respectively at 300°K and 4000 gauss, verify this theory. In Figs. 8(B) and 9(B) the temperature was lowered to 77°K which increased the effect several-fold and induced small modulations in the observed values of $\Delta\rho/\rho$. These have maxima at 45° inclinations (that is with **H** along 011, $0\bar{1}1$, $0\bar{1}\bar{1}$, $01\bar{1}$) and minima at 90° inclinations (010, 001, $0\bar{1}0$, $00\bar{1}$).

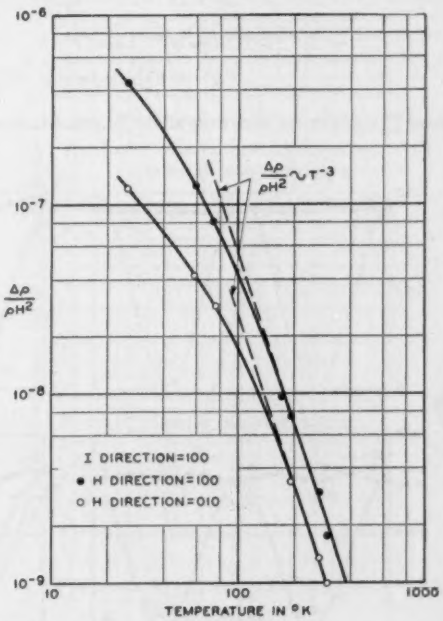

FIG. 7. $\Delta\rho/\rho H^2$ vs temperature. $H=4000$ gauss. Directions of **I** and **H** are as shown.

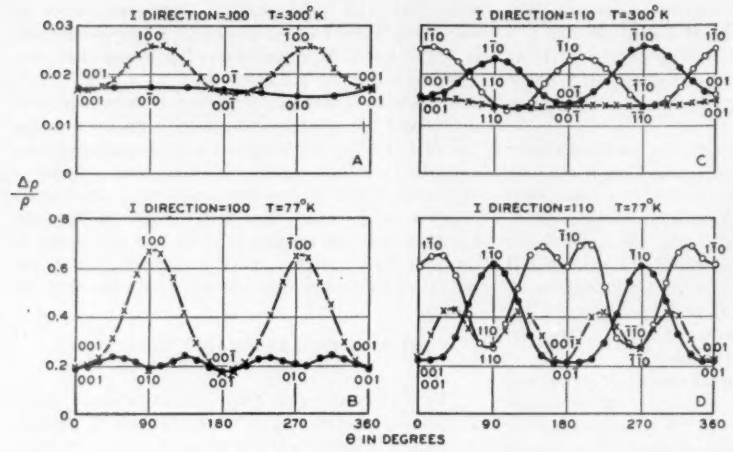

FIG. 8. Variations of $\Delta\rho/\rho$ in p-type germanium as **H** is rotated through an angle θ from 0 to 360 degrees. The magnitude of H is 4000 gauss, and certain cardinal directions of **H** are as indicated. The fixed directions of **I** and the values of T are as shown.

As indicated in Sec. IV above, this new effect arises from exceeding the square law range in H. This may be shown quantitatively by developing the phenomenological expression for $\Delta\rho/\rho$ one stage further, that is to fourth powers in H.

In the same notation as used in Sec. II this extension, obtained from group theory, is

$$\Delta\rho/\rho=H^2[b+c(\sum\iota\eta)^2+d\sum\iota^2\eta^2]+H^4[b'+c'(\sum\iota\eta)^2+d'\sum\iota^2\eta^2+e\sum\eta^4+f\sum\eta_1^2\eta_2^2+g\sum\iota^2\eta^4+h\sum\iota_1\iota_2\eta_1^2\eta_2\eta_3], \quad (12)$$

where $\sum$ signifies the sum over all cyclic permutations of the type indicated. It is seen that the fourth approximation involves the seven additional constants b', c', d', e, f, g, h. This expression is greatly simplified for **i** along the 100 direction and **H** in any direction perpendicular to it. For this condition

$$\left.\begin{aligned}&\iota_1=1, \quad \iota_2=0, \quad \iota_3=0,\\ &\eta_1=0, \quad \eta_2=\cos\theta, \quad \eta_3=\sin\theta,\end{aligned}\right\} \quad (13)$$

and it is easily shown that

$$\Delta\rho/\rho=(b+b'H^2+eH^2)H^2+\tfrac{1}{4}H^4(f-e)\sin^2 2\theta, \quad (14)$$

where θ is the angle between the magnetic vector and the 001 crystal direction. The second term on the right

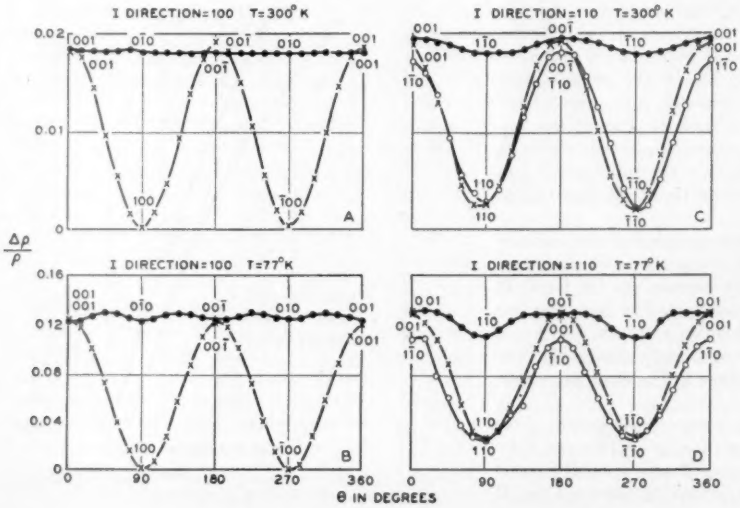

FIG. 9. Variations of $\Delta\rho/\rho$ in n-type germanium as **H** is rotated through an angle θ from 0 to 360 degrees. The magnitude of H is 4000 gauss, and certain cardinal directions of **H** are as indicated. The fixed directions of **I** and the values of T are as shown.

contributes the observed modulations shown in Figs. 8(B) and 9(B), since it has maxima at the 45° inclinations and minima equal to zero at the 90° inclinations.

The explanation of the modulation superposed on the sine curve predicted by second-order theory for the case of **i** parallel to 110 and **H** rotating within the (100, 010) plane is similar. (The experimental result is shown in Fig. 9(D).) In this case

$$\left.\begin{aligned} \iota_1 &= 1/\sqrt{2}, \quad \iota_2 = 1/\sqrt{2}, \quad \iota_3 = 0, \\ \eta_1 &= \cos\theta, \quad \eta_2 = \sin\theta, \quad \eta_3 = 0, \end{aligned}\right\} \quad (15)$$

so that the contribution from fourth-order terms to the angular dependence is $\frac{1}{4}H^4(f-2e-g)\sin^2 2\theta$, where θ is the angle between the magnetic vector and the 100 crystal direction.

In either case the amplitude of the modulation should vary as the fourth power of the magnetic field. Figure 10 shows the experimentally observed power law in the case of n-type germanium at 77°K for the conditions applying in Eq. (14). The discrepancy between the theoretical value of 4.0 and the experimental value of 3.4 could either be due to higher power terms or to the fact that an expansion in ascending powers of H is no longer appropriate at the fields employed in these measurements. Such an expansion is particularly inappropriate when saturation effects are approached as in the case of parallel **i** and **H**, Fig. 4. Measurements in fields up to 170 kilogauss and 77°K carried out at the Bell Telephone Laboratories[13] showed full saturation of $\Delta\rho/\rho$ for all parallel directions of field and current, while saturation was approaching in some perpendicular directions.

TABLE I. Measured values of magneto-resistance in germanium as H approaches zero.

I Direction	H Direction	$\Delta\rho/\rho H^2$ p-type 300°K	p-type 77°K	n-type 300°K	n-type 77°K	Theory Eq. (5)
100	100	0.04×10^{-9}	1.4×10^{-9}	1.92×10^{-9}	88×10^{-9}	$b+c+d$
100	010	1.3	30.4	0.90	28.5	b
110	001	1.3	32.2	1.03	31.5	b
110	$1\bar{1}0$	1.3	27	1.68	75	$b+d/2$
110	110	0.21	2	0.99	58	$b+c+d/2$

VII. CONCLUSIONS

It has been shown that the magneto-resistance in single crystals of germanium conforms with the phenomenological relation. However, the constants characteristic of this relation have experimental values that differ from those calculated on the basis of the two electronic theories so far proposed.

Recently magneto-resistance theory has been formulated in great generality by W. Shockley.[8] His results are not restricted to small magnetic fields, but reduce to the existing theories for small **H**. He suggests that the nonspherical shape of the energy surface may be responsible for magneto-resistance. He shows that for germanium the energy surface for electrons at the bottom of the conduction band may consists of either two or three nonspherical sheets. The parameters specifying these should enter the expression for magneto-resistance and thus be determined from experiment. However, the calculations involved are of considerable algebraic complexity and have so far not been carried out.

TABLE II. The magneto-resistance constants of germanium at low magnetic field strengths.

	p-type 300°K	p-type 77°K	n-type 300°K	n-type 77°K
σ_0	2.6	4.4	0.087	0.59
R_H	8.4×10^{-4}	4.4×10^{-4}	-4.4×10^{-4}	-4.8×10^{-4}
a	2.18×10^{-4}	1.94×10^{-4}	-3.83×10^{-4}	-2.84×10^{-4}
α	-5.7×10^{-5}	-8.5×10^{-4}	3.33×10^{-4}	1.68×10^{-4}
b	1.3×10^{-9}	32.2×10^{-9}	1.03×10^{-9}	31.5×10^{-9}
c	-1.09×10^{-9}	-25.0×10^{-9}	-0.69×10^{-9}	-17.0×10^{-9}
d	0	-10.4×10^{-9}	1.3×10^{-9}	87.0×10^{-9}
β	-4.62×10^{-9}	-307×10^{-9}	-0.205×10^{-9}	-65×10^{-9}
γ	4.07×10^{-9}	274×10^{-9}	0.189×10^{-9}	57×10^{-9}
δ	0	45.7×10^{-9}	-0.113×10^{-9}	-51.4×10^{-9}

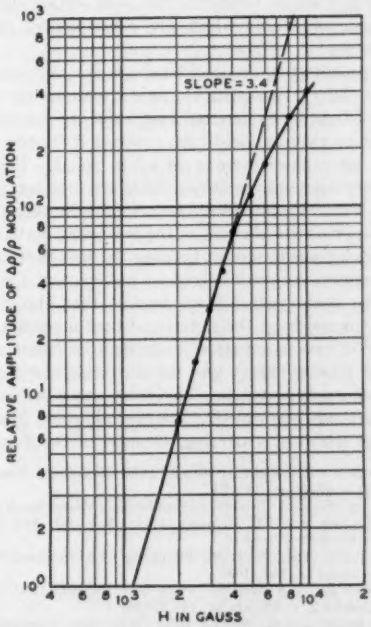

FIG. 10. Amplitude of higher order angular modulation with **i** in the 100 direction and **H** rotating in a plane normal to **i**.

[13] One of the authors has extended these measurements to 170 kilogauss using pulse techniques. H. Suhl, Phys. Rev. **78**, 646 (1950).

VIII. ACKNOWLEDGMENTS

The research described above was carried out under the direction of W. Shockley, to whom the authors are indebted for valuable discussion of the general problem of magneto-resistance. They are also obliged to J. Bardeen, who deduced the second-order dependence of $\Delta\rho/\rho$ as given by Eq. (2) and was frequently consulted as the work progressed, and to C. Herring for help with the group theory involved in the fourth-order expression. Thanks are also due G. K. Teal for supplying the excellent single crystal germanium ingots and to P. W. Foy for assistance with the experimental work.

PHYSICAL REVIEW VOLUME 83, NUMBER 4 AUGUST 15, 1951

The Scattering of Light by Light*

ROBERT KARPLUS† AND MAURICE NEUMAN
Brookhaven National Laboratory, Upton, Long Island, New York
(Received October 6, 1950)

Cross sections for several processes involving electromagnetic fields in a nonlinear manner are derived from the electrodynamic scattering matrix and are expressed in terms of the fourth-order nonlinear vacuum polarization tensor. The differential cross section for the scattering of light by light is calculated as a function of energy and angle. Numerical values are given for scattering at zero and at ninety degrees in the center-of-mass system. Near 1.75 Mev the forward scattering cross section has its largest value of 4.1×10^{-31} cm²/sterad, while the maximum right-angle scattering takes place near 0.7 Mev with a cross section of 2.8×10^{-31} cm²/sterad, all for unpolarized radiation. Numerical results are also given for scattering at the above angles between circularly polarized states. The conclusions in this paper agree with all the results previously calculated for special cases.

IN an earlier paper[1] the nonlinear interactions between electromagnetic fields were expressed in terms of the polarization of the electron-positron vacuum. In this discussion the polarization tensor derived in I will be related to the cross sections for the occurrence of events which are consequences of the nonlinearity.

The processes to be considered are the scattering of light by light,[2] two-quantum pair creation,[3] the scattering of light in an external field,[4] and the creation of pairs in an external field.[5] An expression for the cross section for each of these is set up in Sec. II. The two cases involving only radiation fields are then treated in detail. A certain simplification occurs in the calculation of the appropriate element of the scattering matrix and of the polarization tensor, because the fact that all the 4-momentum vectors involved are null-vectors, together with the conservation laws, implies that the matrix element depends on the initial and final momenta only by way of two parameters; these may be taken as the incident photon energy and the scattering angle in the center-of-gravity system. The total cross section for two-quantum pair creation is easily obtained from the diagonal (forward scattering) element of the S-matrix, as has been described elsewhere;[5b] this relationship follows from the unitary character of the S-matrix.

To obtain the probability for the scattering of a photon by an external field, the electromagnetic potential in the S-matrix is replaced by the potential of a quantized wave (creation or annihilation operator) plus the external potential which causes the scattering. The matrix element of this operator between one-photon states of the appropriate momenta then is the probability amplitude of the scattering process. Here the evaluation of the polarization tensor is much more difficult because the momentum vectors are not null vectors. The forward scattering matrix element again is simply related to the total cross section for pair-creation in the external field.[5b]

Formulas for the differential cross sections for transitions between photon states of definite linear momentum and definite spin angular momentum (circular polarization) are given to summarize the results of the calculation of the scattering of light by light. This choice is convenient because the transitions fall into two groups: the more probable ones conserve spin angular momentum, while the less probable ones do not. In the limiting cases of low and high energy our results agree with the published ones.[2]

I. SCATTERING CROSS SECTION

The total probability W that a transition takes place from an initial state Ψ_i is given in terms of the scattering matrix S by

$$W=(\Psi_i,(S^+-1)(S-1)\Psi_i)$$
$$=-2\,\mathrm{Re}[(\Psi_i,(S-1)\Psi_i)]; \quad (1)$$

* Research carried out at Brookhaven National Laboratory, under the auspices of the AEC.
† Now at Harvard University, Cambridge, Massachusetts.
[1] R. Karplus and M. Neuman, Phys. Rev. **80**, 380 (1950). Henceforth referred to as I.
[2] [a] H. Euler, Ann. Phys. **26**, 398 (1936). [b] A. Achieser, Physik Z. Sowjetunion **11**, 263 (1937).
[3] G. Breit and J. A. Wheeler, Phys. Rev. **46**, 1087 (1934).
[4] M. Delbruck, Z. Physik **84**, 144 (1933).
[5] [a] H. Bethe and W. Heitler, Proc. Roy. Soc. (London) **146**, 83 (1934). [b] Jost, Luttinger, and Slotnick, Phys. Rev. **80**, 189 (1950).

the second part of the identity is a consequence of the unitarity of the S-matrix. If not all transitions from Ψ_i are being considered, then the probability W' for the occurrence of a process that is of interest may be expressed in terms of a part S' of the scattering matrix by

$$W'=(\Psi_i, S'^{+}S'\Psi_i)=\sum_f(\Psi_i, S'^{+}\Psi_f)(\Psi_f, S'\Psi_i), \quad (2)$$

if S' is an operator whose matrix elements are only the relevant scattering amplitudes. S' need no longer be unitary, of course.

A. Two-Photon Scattering

In the calculation of the scattering cross section of photons by photons, the states Ψ_i and Ψ_f refer each to the presence of two light quanta. Hence, to the lowest order in the coupling constant, the operator S' of Eq. (2) is equal to the operator $S^{(4)}$ defined in Eq. (11) of reference I if the quantities $A_\mu(k^{(i)})$ are taken to be the quantized electromagnetic field variables and if the vacuum and single-particle parts are removed. Let the initial state be characterized by the presence of two quanta with momenta $\mathbf{P}_1=\hbar\kappa\mathbf{p}$ and $\mathbf{P}_2=-\hbar\kappa\mathbf{p}$, energies $c|\mathbf{P}_1|=c|\mathbf{P}_2|=\hbar c\kappa\omega=mc^2\omega$, and polarization vectors $e_\mu^{\lambda_1}(-\mathbf{p})$ and $e_\mu^{\lambda_2}(-\mathbf{p})$, respectively, inclosed in a large but finite volume V. The expectation value indicated in Eq. (2) can now be easily evaluated with the help of the usual substitution

$$A_\mu(\mathbf{k}, k_0)\rightarrow V(2|\mathbf{k}|V)^{-\frac{1}{2}}[e_\mu^{\lambda}(\mathbf{k})a^{\lambda}(\mathbf{k})\delta(k_0-|\mathbf{k}|)+e_\mu^{\lambda *}(\mathbf{k})a^{\lambda *}(-\mathbf{k})\delta(k_0+|\mathbf{k}|)], \quad (3)$$

$$\left(\int d\mathbf{k}\rightarrow(1/V)\sum_{\mathbf{k}}\right),$$

where $a^{\lambda}(\mathbf{k})$ annihilates and $a^{\lambda *}(-\mathbf{k})$ creates a photon of momentum $\mathbf{k}$ and polarization $e_\mu^{\lambda}(\mathbf{k})$. The many terms that arise from different identifications of $\mathbf{P}_i$ with the $\mathbf{k}^{(i)}$ all give the same contributions because of the symmetry of the polarization tensor.

The matrix element of the operator part of $S^{(4)}$ to be evaluated is

$$Q=(P_1, \lambda_1; P_2, \lambda_2|(A_{\mu'}{}^{1'}A_{\nu'}{}^{2'}A_{\lambda'}{}^{3'}A_{\sigma'}{}^{4'})_2{}^{+}\times(A_\mu{}^1A_\nu{}^2A_\lambda{}^3A_\sigma{}^4)_2|P_1, \lambda_1; P_2, \lambda_2),$$

where $A_\mu(k^{(i)})$ is abbreviated by $A_\mu{}^i$. The symbol $(\ )_2$ denotes the two-particle part of the enclosed expression: the operator is to be decomposed into products of annihilation and creation operators; then the terms containing two factors of each are taken with the annihilation operators standing on the right. This operator, therefore, annihilates two particles and creates two others; in particular, it transforms a two-particle state into another two-particle state via the vacuum state. The latter fact suggests that Q be factored as follows:

$$Q=\sum_{\text{perm}}(P_1, \lambda_1; P_2, \lambda_2|(A_{\mu'}{}^{1'}A_{\nu'}{}^{2'})^{+}(A_\mu{}^1A_\nu{}^2)|P_1, \lambda_1; P_2, \lambda_2)\times(0|(A_{\lambda'}{}^{3'}A_{\sigma'}{}^{4'})^{+}(A_\lambda{}^3A_\sigma{}^4)|0)$$
$$=\sum_{\text{perm}}(P_1; \lambda_1|A_{\mu'}{}^{1'}{}^{+}A_\mu{}^1|P_1, \lambda_1)(P_2, \lambda_2|A_{\nu'}{}^{2'}{}^{+}A_\nu{}^2|P_2\lambda_2)\times(0|A_{\lambda'}{}^{3'}{}^{+}A_\lambda{}^3|0)(0|A_{\sigma'}{}^{4'}{}^{+}A_\sigma{}^4|0).$$

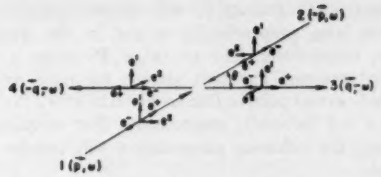

FIG. 1. Definition of the initial and final states in terms of the wave numbers $\mathbf{p}$ and $\mathbf{q}$ and the polarization vectors $\mathbf{e}^{\lambda}$. The directions of the vectors $\mathbf{e}^{\lambda}$ for circular polarization are those of the angular momenta associated with the rotation.

The sums are respectively over the 36 and 288 distinct permutations of the primed and unprimed indices separately. These all make the same contribution, however, because they are multiplied by the symmetrical function $G_{\mu\nu\lambda\sigma}(1234)$. Hence

$$Q\rightarrow 288[e_{\mu'}{}^{\lambda_1 *}e_{\mu}{}^{\lambda_1}\delta(k^{(1')}-P_1)\delta(k^{(1')}-P_1)/2V|P_1|]\times[e_{\nu'}{}^{\lambda_2 *}e_{\nu}{}^{\lambda_2}\delta(k^{(2')}-P_2)\delta(k^{2'}-P_2)/2V|P_2|]\times[\delta_{\lambda\lambda'}\delta(k^{(3)}-k^{(3')})\delta(k_0{}^{(3)}+|\mathbf{k}^{(3)}|)/2(2\pi)^3|\mathbf{k}^{(3)}|]\times[\delta_{\sigma\sigma'}\delta(k^{(4)}-k^{(4')})\delta(k_0{}^{(4)}+|\mathbf{k}^{(4)}|)/2(2\pi)^3|\mathbf{k}^{(4)}|].$$

The probability W' then becomes

$$W_s'=\left[\frac{2}{V^2}\int d^4x\right]\frac{\alpha^4}{128\pi^2}\frac{1}{\omega^2\kappa^2}\int d\Omega(\mathbf{k})\left|e_\mu^{\lambda_1}e_\nu^{\lambda_2}G_{\mu\nu\lambda\sigma}\left(\mathbf{p}, \omega; -\mathbf{p}, \omega; \frac{\mathbf{k}}{\kappa}, -\omega; -\frac{\mathbf{k}}{\kappa}, -\omega\right)\right|^2. \quad (4)$$

Over-all momentum and energy conservation have reduced the number of independent arguments of G, whose space and time components have been written separately for greater clarity; the scale factor κ has been dropped from the arguments because G is dimensionless and, therefore, homogeneous of degree zero in κ. The factor $[(2/V^2)\int d^4x]$ is interpreted as $(2c/V)T$, the incident photon flux multiplied by the time during which transitions have been taking place.[6] The total cross section is, therefore, given by the right side of Eq. (4) with this factor omitted.

The differential cross section for scattering into the state containing one photon with momentum in the solid angle $d\Omega$ around the direction of $\mathbf{P}_3=\hbar\kappa\mathbf{q}$ and polarization $e_\mu^{\lambda_3}$, while the other photon has momentum $-\mathbf{P}_3$ and polarization $e_\mu^{\lambda_4}$, is clearly

$$\sigma_s(\theta, \phi; \omega)=\frac{\alpha^4}{4\pi^2\kappa^2}\frac{1}{16\omega^2}|e_\mu^{\lambda_1}e_\nu^{\lambda_2}e_\lambda^{\lambda_3 *}e_\sigma^{\lambda_4 *}G_{\mu\nu\lambda\sigma}(\mathbf{p}, \omega; -\mathbf{p}, \omega; -\mathbf{q}, -\omega; \mathbf{q}, -\omega)|^2; \quad (5)$$

energy conservation requires that the scattered quanta still have the energy $\hbar c\kappa\omega=\hbar c\kappa|\mathbf{q}|$, as is indicated by the arguments of the polarization tensor in Eqs. (4) and (5).

We now introduce some conventions with regard to the unit vectors specifying states of polarization. The

[6] B. A. Lippmann and J. Schwinger, Phys. Rev. **79**, 469 (1950).

symbols $e_\mu^1(P)$ and $e_\mu^2(P)$ will denote spacelike unit vectors lying perpendicular to and in the scattering plane, respectively. The set $(\mathbf{e}^1, \mathbf{e}^2, \mathbf{P})$ forms a right-handed system. The unit vectors for right and left handed circular polarization are given by $e^+ = 2^{-\frac{1}{2}}(e^1 + ie^2)$ and $e^- = 2^{-\frac{1}{2}}(e^1 - ie^2)$, respectively. For simplicity in writing, the following abbreviation will now be introduced:

$$M_{\lambda_1\lambda_2\lambda_3\lambda_4}(\theta, \omega) = \tfrac{1}{4} e_\mu^{\lambda_1} e_\nu^{\lambda_2} e_\lambda^{\lambda_3 *} e_\sigma^{\lambda_4 *} G_{\mu\nu\lambda\sigma}(\mathbf{p}, \omega; -\mathbf{p}, \omega; -\mathbf{q}, -\omega; \mathbf{q}, -\omega), \quad (6)$$

where

$$\theta = \cos^{-1}(\mathbf{p}\cdot\mathbf{q}/\omega^2)$$

is the angle of scattering in the scattering plane. Figure 1 illustrates the symbols that have been introduced.

An examination of I, Eqs. (21) to (24) indicates the possibility of five distinct scattering configurations in the case of linearly and circularly polarized light. In the former, these correspond to M_{1111}, M_{2222}, M_{1122}, M_{1221} and M_{1212}, with weight factors 1, 1, 2, 2, and 2; in the latter they are M_{++++}, M_{++--}, M_{+-+-}, M_{+--+}, and M_{+++-} with weights 2, 2, 2, 2, and 8. The differential scattering cross section for unpolarized radiation is then given by two alternative formulas

$$\bar{\sigma}_s(\theta, \omega) = \frac{\alpha^4}{4\pi^2\kappa^2}\frac{1}{\omega^2}\langle |M|^2\rangle_{\text{Av}},$$

$$\begin{aligned}\langle |M|^2\rangle_{\text{Av}} &= \tfrac{1}{4}[|M_{1111}|^2 + |M_{2222}|^2 + 2|M_{1122}|^2 \\ &\quad + 2|M_{1221}|^2 + 2|M_{1212}|^2] \\ &= \tfrac{1}{2}[|M_{++++}|^2 + |M_{++--}|^2 + |M_{+-+-}|^2 \\ &\quad + |M_{+--+}|^2 + 4|M_{+++-}|^2].\end{aligned} \quad (7)$$

B. Two-Photon Pair Creation

In the treatment of this process, the states Ψ_i and Ψ_f, Eq. (2) refers to the presence of two photons and of an electron-positron pair, respectively. It is easy to verify[5b] that to the lowest order in the coupling constant the matrix S' appropriate to pair production is equal to S, so that Eq. (1) may be used. The terms of order α^2 in this equation then give

$$W_p = -2\,\text{Re}[(\psi_i, S^{(4)}\psi_i)] = -\left[\frac{2}{V^2}\int d^4x\right]\frac{2\alpha^2}{\kappa^2\omega^2}\,\text{Im}[M_{\lambda_1\lambda_2\lambda_1\lambda_2}(0, \omega)] \quad (8)$$

for the total probability that a pair be produced by two photons of momenta $\mathbf{p}_1 = \hbar\kappa\mathbf{p}$, $\mathbf{p}_2 = -\hbar\kappa\mathbf{p}$, energies $c|\mathbf{p}_1| = c|\mathbf{p}_2| = \hbar c\kappa\omega$, and polarizations $e_\mu^{\lambda_1}$, $e_\mu^{\lambda_2}$. The total cross section is therefore

$$\sigma(\omega) = -2(\alpha^2/\kappa^2\omega^2)\,\text{Im}[M_{\lambda_1\lambda_2\lambda_1\lambda_2}(0, \omega)]. \quad (9)$$

C. Scattering of Photons by an External Static Field

Here again, S' of Eq. (2) is equal to $S^{(4)}$, but now the quantities $A_\mu(k^{(4)})$ must be taken as the sum of a quantized wave amplitude $A_\mu(k^{(4)})$ and a fourier component of the external field $A_\mu{}^e(k^{(4)})$. Only the one-particle part is to be used. The quantized $A_\mu(k^{(4)})$ are again expressed as creation and annihilation operators, Eq. (3), while the three-dimensional fourier transform $\bar{A}_\mu{}^e$ can be introduced by setting

$$A_\mu{}^e(k) = \kappa^{-3}\bar{A}_\mu{}^e(\mathbf{k}/\kappa)\delta(k_0/\kappa). \quad (10)$$

In terms of this quantity, then

$$\begin{aligned}W_s'{}^e &= \left[\frac{\int dx_0}{V}\right]\frac{(2\pi)^4\alpha^4}{4\kappa^2}\int d\Omega(\mathbf{k}_2) \\ &\quad \times\left|\int d\mathbf{k}_3 d\mathbf{k}_4 e_\mu^{\lambda_1}(\mathbf{p})\bar{A}_\lambda{}^e(\mathbf{k}_3)\bar{A}_\sigma{}^e(\mathbf{k}_4)\right. \\ &\quad \times G_{\mu\nu\lambda\sigma}(\mathbf{p}, \omega; \mathbf{k}_2, -\omega; \mathbf{k}_3, 0; \mathbf{k}_4, 0) \\ &\quad \left.\times\delta(\mathbf{p} - \mathbf{k}_2 + \mathbf{k}_3 + \mathbf{k}_4)\right|^2. \quad (11)\end{aligned}$$

Dropping the factor $[\int dx_0/V]$ yields the total cross section, while the differential cross section for scattering into the solid angle $d\Omega$ around the direction $-\mathbf{k}_2 = \mathbf{q}$ and to the polarization $e_\mu^{\lambda_3}(\mathbf{q})$ is

$$\begin{aligned}\sigma_s{}^e(\theta, \omega) &= 4\pi^4\frac{\alpha^4}{\kappa^2}\left|\int d\mathbf{R} e_\mu^{\lambda_1}(\mathbf{p}) e_\nu^{\lambda_2 *}(\mathbf{q})\right. \\ &\quad \times\bar{A}_\tau{}^e\left(-\frac{\mathbf{P}}{2} + \mathbf{R}\right)\bar{A}_\sigma{}^e\left(-\frac{\mathbf{P}}{2} - \mathbf{R}\right) \\ &\quad \left.\times G_{\mu\nu\lambda\sigma}\left(\mathbf{p}, \omega; -\mathbf{q}, -\omega; -\frac{\mathbf{P}}{2} + \mathbf{R}, 0; -\frac{\mathbf{P}}{2} - \mathbf{R}, 0\right)\right|^2,\end{aligned} \quad (12)$$

where $\mathbf{P} = \mathbf{p} - \mathbf{q}$ and $\theta = \cos^{-1}(\mathbf{p}\cdot\mathbf{q}/\omega^2)$ are the momentum transfer and scattering-angle, respectively. The basic polarization vectors are again taken in the scattering plane and perpendicular to it, for convenience.

D. Pair-Creation by Photons in an External Static Field

By an argument corresponding to the one in B, the total cross section for the production of electron-positron pairs by a quantum of energy $\hbar c\kappa\omega$ and polarization e_μ^λ is

$$\begin{aligned}\sigma_p{}^e(\omega) &= -\frac{4\pi^3\alpha^2}{\kappa^2\omega}\,\text{Im}\left[\int d\mathbf{R} e_\mu^\lambda e_\nu^{\lambda *}\bar{A}_\lambda{}^e(\mathbf{R})\bar{A}_\sigma{}^e(-\mathbf{R})\right. \\ &\quad \left.\times G_{\mu\nu\lambda\sigma}(\mathbf{p}, \omega; -\mathbf{p}, -\omega; \mathbf{R}, 0; -\mathbf{R}, 0)\right]. \quad (13)\end{aligned}$$

II. CONSTRUCTION OF THE POLARIZATION TENSOR

In this section we shall evaluate the five distinct invariants that determine the polarization tensor of quantized fields by calculating the eleven quantities $A_1^n(1234)$ (I, Eqs. (30), (31), (33), (34), and (35)) and applying I, Eqs. (36)–(41). The denominator $D(1234)$ (I, Eq. (27)) simplifies greatly when the values of the four momenta from Eq. (5) are introduced. Thus, in terms of the parameters

$$\begin{aligned}\alpha&=-(k^{(1)}k^{(2)})/2\kappa^2=-(k^{(3)}k^{(4)})/2\kappa^2=\omega^2,\\ \beta&=-(k^{(1)}k^{(3)})/2\kappa^2=-(k^{(2)}k^{(4)})/2\kappa^2=-\omega^2\sin^2(\theta/2),\\ \gamma&=-(k^{(1)}k^{(4)})/2\kappa^2=-(k^{(2)}k^{(3)})/2\kappa^2=-\omega^2\cos^2(\theta/2),\\ &\alpha+\beta+\gamma=0,\end{aligned}\tag{14}$$

we have

$$\begin{aligned}&D(1234)=D(3412)=D(2143)=D(4321)=D(\alpha,\gamma),\\ &D(2341)=D(4123)=D(1432)=D(3214)=D(\gamma,\alpha),\\ &D(1243)=D(4312)=D(2134)=D(3421)=D(\alpha,\beta),\\ &D(2431)=D(3124)=D(4213)=D(1342)=D(\beta,\alpha),\\ &D(1324)=D(2413)=D(3142)=D(4231)=D(\beta,\gamma),\\ &D(3241)=D(4132)=D(2314)=D(1423)=D(\gamma,\beta);\\ &D(u,v)=[1-i\epsilon-4(uy_2y_4+vy_1y_3)]^{-1}.\end{aligned}\tag{15}$$

To carry out the integration over the hyperplane defined in I, Eq. (25), it is convenient to introduce three new variables by relations like these:

$$\begin{aligned}y_1&=(1-x)(1-y), & y_3&=(1-z)y,\\ y_2&=x(1-y), & y_4&=zy.\end{aligned}\tag{16}$$

Then integrals of the form

$$\int_{\Sigma y_i=1,\ y_i>0} d\tau P(y)D(u,v)\to\int_0^1 dy\cdot y(1-y)\int_0^1 dx\times\int_0^1 dz P'(x,y,z)D'(u,v),\tag{17}$$

$$D'(u,v)=\{1-i\epsilon-4y(1-y)\times[uxz+v(1-x)(1-z)]\}^{-2},$$

where P and P' are polynomials, must be evaluated. One can deduce useful algebraic relationships among many of these by equating two expressions that contain different functions P' obtained by different permutations of the substitutions Eq. (16) applied to the same function $P(y_i)$ in the integrand.

Straightforward integration, together with the judicious use of the relationships just mentioned, yields lengthy expressions for the $A_1^n(1234)$, and so for the $A^n(1234)$, as functions of α, β, and γ. They are listed in Appendix A. It is useful to give special designations to the three transcendental functions that appear in the A^n in addition to rational functions of α, β, and γ. They are

$$\begin{aligned}B(u)&=\frac{1}{2}\int_0^1 dy\log[1-i\epsilon-4uy(1-y)]\\ &=\left(\frac{u-1}{u}\right)^{\frac{1}{2}}\sinh^{-1}(-u)^{\frac{1}{2}}-1;\quad u<0\\ &=\left(\frac{1-u}{u}\right)^{\frac{1}{2}}\sin^{-1}u^{\frac{1}{2}}-1;\quad 0<u<1\\ &=\left(\frac{u-1}{u}\right)^{\frac{1}{2}}\cosh^{-1}u^{\frac{1}{2}}-1-\frac{\pi i}{2}\left(\frac{u-1}{u}\right)^{\frac{1}{2}};\quad 1<u,\end{aligned}\tag{18}$$

$$\begin{aligned}T(u)&=\int_0^1\frac{dy}{4y(1-y)}\log[1-i\epsilon-4uy(1-y)]\\ &=[\sinh^{-1}(-u)^{\frac{1}{2}}]^2;\quad u<0\\ &=-[\sin^{-1}u^{\frac{1}{2}}]^2;\quad 0<u<1\\ &=[\cosh^{-1}u^{\frac{1}{2}}]^2-\tfrac{1}{4}\pi^2-i\pi\cosh^{-1}u^{\frac{1}{2}};\quad 1<u\end{aligned}\tag{19}$$

and

$$I(u,v)=I(v,u)=\int_0^1\frac{dy}{4y(1-y)-(u+v)/uv}\times\{\log[1-i\epsilon-4uy(1-y)]+\log[1-i\epsilon-4vy(1-y)]\}\tag{20}$$

with the real part

$$\begin{aligned}\mathrm{Re}[I(u,v)]=\frac{1}{2a}\mathrm{Re}\Big[&\phi\left(\frac{a+1}{a+b(u)}\right)+\phi\left(\frac{a+1}{a-b(u)}\right)\\ &-\phi\left(\frac{a-1}{a+b(u)}\right)-\phi\left(\frac{a-1}{a-b(u)}\right)\\ &+\phi\left(\frac{a+1}{a+b(v)}\right)+\phi\left(\frac{a+1}{a-b(v)}\right)\\ &-\phi\left(\frac{a-1}{a+b(v)}\right)-\phi\left(\frac{a-1}{a-b(v)}\right)\Big],\end{aligned}\tag{20'}$$

where

$$\begin{aligned}a&=[1-(u+v)/uv]^{\frac{1}{2}},\\ b(u)&=[(u-1)/u]^{\frac{1}{2}},\quad u<0,\quad u>1\\ &=i[(1-u)/u]^{\frac{1}{2}},\quad 0<u<1\end{aligned}\tag{21}$$

and[7]

$$\phi(z)=\int_0^z\log(1-t)dt/t;\tag{22}$$

[7] The Spence function $\phi(z)$ has been encountered in electrodynamic problems by G. Racah, Nuovo cimento **11**, No. 7 (1939). It is discussed at length by K. Mitchell, Phil. Mag. **40**, 351 (1949), who also gives tables of numerical values.

TABLE I. Expression of the matrix element $M(\pi/2, \omega)$ in terms of the basic invariants A^n for transitions between circularly polarized states.

	$A^{2143}(1234)$	$A^{2143}(1324)$	$A^{2341}(1234)$	$A^{2341}(1324)$	$A^{2111}(1234)$	$A^{2111}(1432)$	$A^{2121}(1234)$	$A^{2121}(1432)$	$A^{2121}(1423)$	$A^{2311}(1234)$
$M_{++++}/\omega^4\kappa^4$	1	$\frac{1}{2}$	2	$-\frac{1}{2}$	0	0	-2	-2	1	-4
$M_{++--}/\omega^4\kappa^4$	1	0	2	1	0	0	-2	0	0	0
$M_{+-+-}/\omega^4\kappa^4$ $=M_{+--+}/\omega^4\kappa^4$	0	$\frac{1}{4}$	$\frac{1}{2}$	$\frac{1}{4}$	0	0	0	-1	$\frac{1}{2}$	0
$M_{+++-}/\omega^4\kappa^4$	0	0	0	0	$-\frac{1}{2}$	2	$\frac{1}{2}$	-1	-1	1

u and v are two distinct members of the triplet (α, β, γ). It should be noted that $(u+v)/uv \leqslant 0$ then follows from the values of α, β, and γ in Eq. (14). Hence care must be taken in the integration only if the logarithms have branch points, only, therefore, if u or v is greater than one. In this case, the imaginary part of $I(u, v)$ is found to be

$$\begin{aligned} \mathrm{Im}[I(u,v)] &= -(\pi/2a)\log[v(a+b(u))^2], \quad u \geqslant 1 \\ &= -(\pi/2a)\log[u(a+b(v))^2], \quad v \geqslant 1. \end{aligned} \tag{20'}$$

Some numerical values of these three functions and their behavior in the limits of large and small arguments are given in Appendix B and Table IV.

It is clear from the discussion of the scattering cross section that the imaginary parts of the functions B, T, and I are connected with the contribution of real intermediate pairs to the cross section. The consistency of this interpretation follows from the fact that the imaginary parts are zero unless $1<u$, $v=\alpha=\omega^2$: the total energy must exceed the rest energy of a pair.

With these results we can obtain the cross section for two-photon scattering and two-photon pair creation by inserting the values of the photon momenta and their polarizations. In the remainder of the paper this is done for several special cases.

IV. LOW ENERGY APPROXIMATION

The result obtained for the polarization tensor in I, Eq. (48) is applicable here. The evaluation of M from Eq. (6) gives the following values for circularly polarized radiation:

$$\begin{aligned} M_{++++}(\theta,\omega) &= (1/15)\omega^4(3+\cos^2\theta), \\ M_{++--}(\theta,\omega) &= -(22/45)\omega^4, \\ M_{+-+-}(\theta,\omega) &= -(11/90)\omega^4(1+\cos\theta)^2, \\ M_{+--+}(\theta,\omega) &= -(11/90)\omega^4(1-\cos\theta)^2, \end{aligned} \tag{23}$$

and finally, for unpolarized radiation,

$$\bar{\sigma}_c(\theta,\omega) = (\alpha^4/4\pi^2\kappa^2)[139/(90)^2]\omega^6(3+\cos^2\theta)^2. \tag{24}$$

These results, of course, are in agreement with those derived from formulas (10, 9)[8] of Euler.[2a]

V. RIGHT-ANGLE SCATTERING

For this scattering angle $\alpha=-2\beta=-2\gamma=\omega^2$. Because β and γ are the same, those permutations of the $A(1234)$ which differ only by the interchange of the variables $k^{(3)}$ and $k^{(4)}$ are numerically equal. Hence the tensor $G_{\mu\nu\lambda\sigma}$ simplifies somewhat to the following form:

$$\begin{aligned} G_{\mu\nu\lambda\sigma}(1234) = \{ & A^{2143}(1234)g^{(1)}(1234) + A^{2143}(1324) \\ & \times[g^{(1)}(1324)+g^{(1)}(2341)] + A^{2341}(1234)[g^{(2)}(1234) \\ & + g^{(2)}(1243)] + A^{2341}(1324)g^{(2)}(1324) \\ & - (1/2\omega^2)A^{2111}(1234)[g^{(3)}(1234)+g^{(3)}(3412) \\ & + g^{(3)}(2143)+g^{(3)}(4321)] + (1/\omega^2)A^{2111}(1432) \\ & \times[g^{(3)}(1432)+g^{(3)}(4123)+g^{(3)}(3214)+g^{(3)}(2341) \\ & + g^{(3)}(1342)+g^{(3)}(4213)+g^{(3)}(3124)+g^{(3)}(2431)] \\ & - (1/2\omega^2)A^{2121}(1234)[g^{(4)}(1234)+g^{(4)}(3412) \\ & + g^{(4)}(3421)+g^{(4)}(2134)] + (1/\omega^2)A^{2121}(1432) \\ & \times[g^{(4)}(1432)+g^{(4)}(3214)+g^{(4)}(3124)+g^{(4)}(2431)] \\ & + (1/\omega^2)A^{2121}(1423)[g^{(4)}(1423)+g^{(4)}(3241) \\ & + g^{(4)}(2413)+g^{(4)}(1324)] + (1/\omega^2)A^{2311}(1234) \\ & + [g^{(5)}(1234)+g^{(5)}(4312)+g^{(5)}(1243) \\ & + g^{(5)}(4321)]\}_{\mu\nu\lambda\sigma}. \end{aligned} \tag{25}$$

The quantity $M_{\lambda_1\lambda_2\lambda_3\lambda_4}$ is a linear combination of the functions A^n. The coefficients depend, of course, on the particular values of λ_i that are being considered. For transitions between states of circular polarization they are listed in Table I. Once the A^n are obtained, they

TABLE II. Expression of the matrix element $M(\pi/2, \omega)$ in terms of the transcendental functions B, T, and I.

	Constant	$(B(\omega^2)-B(-\omega^2/2))$	$T(\omega^2)$	$T(-\omega^2/2)$	$I(\omega^2, -\omega^2/2)$	$I(-\omega^2/2, -\omega^2/2)$
M_{++++}	-1	0	0	0	$-2/\omega^4$	$2/\omega^4$
M_{++--}	1	0	0	$2-4/\omega^2$	$(4/\omega^2)-2/\omega^4$	$-1+2/\omega^2$
M_{+-+-} $=M_{+--+}$	1	-6	$10+4/\omega^2$	$10+4/\omega^2$	$-10-(10/\omega^2)-2/\omega^4$	$(2/\omega^2)+2/\omega^4$
M_{+++-}	-1	0	$3/\omega^2$	$6/\omega^2$	$-(4/\omega^2)-2/\omega^4$	$(1/\omega^2)+2/\omega^4$

[8] This differential cross section gives the number of scattered particles rather than the number of scattering events, so that it is twice as large as the cross section discussed in this paper.

may be combined to give the matrix elements M directly in terms of the three transcendental functions B, T, and I. The coefficients in these expressions are given in Table II. The matrix elements for transitions between states of plane polarized photons can be derived easily from Table II. Since they are more complicated and have no special interest, they are not given here. In Fig. 2 the values of $|M(\pi/2, \omega)|^2/\omega^2$ are plotted as functions of ω; they represent the complete dependence of the cross sections on energy, since they are equal to the cross section when multiplied by the scale factor $\alpha^4/(4\pi^2\kappa^2)$. Although it is the square of the absolute value of M that determines the cross section, separate curves have been drawn for the squares of the real and imaginary parts of M. These represent the contributions to the scattering of virtual and real intermediate pairs, respectively. The latter vanish, of course, at energies below the pair threshold. In Fig. 3 the energy dependence of the cross section for unpolarized radiation is shown. It may be noticed in Fig. 2 that at intermediate energies the cross section for transitions which involve a change in the spin-angular momentum of the system, namely, ${}^{+}_{-}\}\rightarrow\{{}^{+}_{-}$ and ${}^{+}_{+}\}\rightarrow\{{}^{+}_{-}$, are considerably smaller than the other two, and that of these two the one which involves a change in the magnitude of the spin, ${}^{+}_{+}\}\rightarrow\{{}^{+}_{-}$, is smaller than the other, which involves only a change in the direction of the spin. At very high energy, the quantities M approach constant values:

$$M_{++++}(\pi/2, \omega)\sim -1,$$

$$M_{++--}(\pi/2, \omega)\sim 1+\pi^2/4\cong 3.47,$$

$$M_{+--+}(\pi/2, \omega)\sim 1-3\log 2+(5/2)\log^2 2 \qquad (26)$$
$$+\pi i(3-5\log 2)\cong 0.12-0.47\pi i,$$

$$M_{+++-}(\pi/2, \omega)\sim -1.$$

At high energy, therefore, the cross section decreases as ω^{-2}, while it increases as ω^6 for small values of the energy (see preceding section; the same result is obtained by expanding the function $M(\omega)$ in a McLaurin series).

VI. FORWARD SCATTERING

Forward scattering ($\theta=0$) is characterized by $\alpha=-\gamma=\omega^2$, $\beta=0$. To obtain the values of the function $A^n(1234)$, the expansions of $B(u)$, $T(u)$, and $I(u, v)$ given in Appendix B are very useful. The $A^n(1234)$ simplify greatly because the Spence functions disappear on going to the limit $\beta=0$. Another simplification results from the fact that the four collinear space-parts of the momentum vectors are orthogonal to all the space-like polarization vectors. Most terms in the tensors $g_{\mu\nu\lambda\sigma}{}^{(i)}(1234)$ therefore do not contribute to the

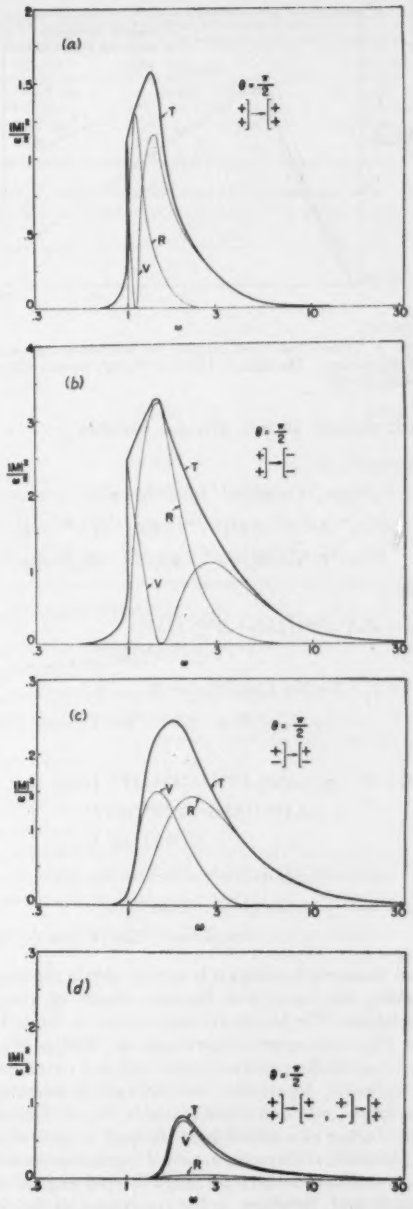

FIG. 2. Differential cross sections for scattering at right angles (cg system) between the indicated states of circular polarization. The unit is 1.07×10^{-31} cm²/sterad; the unit of energy is mc^2. R, V, and T represent the contributions of real intermediate pairs, of virtual intermediate pairs, and their sum, respectively. Note the different scales.

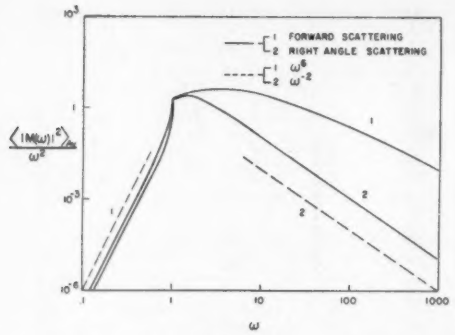

FIG. 3. Differential cross section for scattering unpolarized light (cg system). The unit is 1.07×10^{-21} cm²/sterad; the unit of energy is mc^2.

matrix element. In fact, $M_{\lambda_1\lambda_2\lambda_3\lambda_4}$ becomes

$$\begin{aligned}M_{\lambda_1\lambda_2\lambda_3\lambda_4}(0,\omega)&=(e_\mu^{\lambda_1}(\mathbf{p})e_\mu^{\lambda_3}(-\mathbf{p}))(e_\nu^{\lambda_2*}(\mathbf{p})e_\nu^{\lambda_4*}(-\mathbf{p}))F(\alpha)\\&+(e_\mu^{\lambda_1}(\mathbf{p})e_\mu^{\lambda_4*}(-\mathbf{p}))(e_\nu^{\lambda_2}(-\mathbf{p})e_\nu^{\lambda_3*}(\mathbf{p}))F(-\alpha)\\&+(e_\mu^{\lambda_1}(\mathbf{p})e_\mu^{\lambda_3*}(\mathbf{p}))(e_\nu^{\lambda_2}(-\mathbf{p})e_\nu^{\lambda_4*}(-\mathbf{p}))H(\alpha),\quad(27)\end{aligned}$$

where

$$\begin{aligned}F(\alpha)&=\alpha^2\kappa^4[A^{2143}(1234)+A^{2341}(1234)\\&\qquad-2A^{2121}(1234)]_{\beta=0,\,\gamma=-\alpha}\\&=\tfrac{1}{2}\{-1+(6-1/\alpha)[B(\alpha)-B(-\alpha)]\\&\quad-(2+1/2\alpha^2)T(\alpha)+(2-1/2\alpha^2)T(-\alpha)\},\quad(28)\end{aligned}$$

and

$$\begin{aligned}H(\alpha)=H(-\alpha)&=\alpha^2\kappa^4[A^{2341}(1324)+A^{2341}(1243)\\&\qquad+4A^{2111}(1324)-2A^{2121}(1342)\\&\qquad-2A^{2121}(1324)]_{\beta=0,\,\gamma=-\alpha}\\&=\tfrac{1}{2}\{3-(2+1/\alpha)B(\alpha)-(2-1/\alpha)B(-\alpha)\\&\quad+(2+(1/\alpha)-1/2\alpha^2)T(\alpha)\\&\quad+(2-(1/\alpha)-1/2\alpha^2)T(-\alpha)\}.\quad(29)\end{aligned}$$

From these relationships it is easy to obtain the matrix elements for transitions between states of circular polarization. The results are summarized in Table III.

In Fig. 4 the energy dependence of $|M(0,\omega)|^2/\omega^2$ is shown; again the contributions of real and virtual pairs are indicated separately. The forward scattering of unpolarized radiation is illustrated in Fig. 3. The complete absence of a contribution from $M_{+--+}(0,\omega)$ can be attributed to the conservation of angular momentum: this transition involves a change in spin angular momentum and, therefore, in the component of the total angular momentum along the direction of propagation. Figure 5 is a composition of the two curves in Fig. 3; it shows a plausible angular dependence of the cross section for unpolarized light at a number of energies. Although the cross section changes from being almost independent of angle at intermediate energies to having a strong maximum in the forward direction, this peak does not contribute significantly to the total cross section because the solid angle over which it extends becomes small too rapidly.[2b]

At very high energy the quantities M approach the following values:

$$\begin{aligned}&M_{++++}(0,\omega)\sim\tfrac{1}{2}(\log4\omega^2-1)^2+(5/2)-\pi i(\log4\omega^2-2)\\&M_{++--}(0,\omega)\sim-1\qquad(30)\\&M_{+-+-}(0,\omega)\sim\tfrac{1}{2}(\log4\omega^2-1)^2+(5/2)-\tfrac{1}{2}\pi^2-\pi i.\end{aligned}$$

The cross section, therefore, decreases as $(\alpha^4/\pi^2\kappa^2)\times(\log\omega)^4/\omega^2$, in agreement with the result of Achieser.[2b]

The total cross section for two-quantum pair creation can be deduced by application of Eqs. (9) and (18) and (19). It is

$$\begin{aligned}\sigma_p&=-2(\alpha^2/\kappa^2\omega^2)\,\mathrm{Im}[H(\alpha)+\eta(F(\alpha)+F(-\alpha))]\\&=\pi(\alpha^2/\kappa^2\omega^2)\{2(1+(1/\omega^2)-1/\omega^4)\cosh^{-1}\omega\\&\quad-(1+1/\omega^2)(1-1/\omega^2)^{\frac{1}{2}}+(1-2\eta)[(1/2\omega^2)(1-1/\omega^2)^{\frac{1}{2}}\\&\qquad+(1/4\omega^2)\cosh^{-1}\omega]\},\quad(31)\end{aligned}$$

where $\eta=1$ if the incident photons of energy $mc^2\omega$ have parallel plane polarizations, and $\eta=0$ if they have perpendicular polarizations. This result is identical with that of Breit and Wheeler.[3,9]

Finally, we may discuss the experimental significance of the results. Let us consider two photon beams of equal energy and of intensity n photons/sec colliding with each other; scattered photons are collected from a length L of their common path. Then the number N of collisions occurring per second is

$$N=(n^2/A)L(\sigma/c)\sim10^{-40}n^2(L/A)\ \mathrm{sec}^{-1},\quad(32)$$

where A is the area of the beam in cm², and $\sigma\sim3\times10^{-30}$ cm² was taken as the cross section for scattering into a fair solid angle at an energy of about 1 Mev (see Eq. (7) and Fig. 5). For presently attainable values of the experimental parameters, therefore, it would seem that N is too small to be detected in the presence of the probable background radiation.

We wish to express our appreciation to Dr. Hartland S. Snyder for helpful discussion and criticism. We are grateful to Elizabeth Karplus, Dale Meyer, Rika Sarfaty, and William F. Donoghue for aid with the numerical work.

APPENDIX A

The five invariants appearing in I, Eq. (47) have the general structure

[9] In a recent interesting paper (to be published), Toll and Wheeler essentially reverse the procedure by which Eq. (31) was derived. They start with this result and calculate the entire functions $H(\alpha)$ and $(F(\alpha)+F(-\alpha))$ from their imaginary part by assuming that these functions are analytic over one-half of the α-plane. The present calculation indicates that this assumption is justified.

TABLE III. Expression of the matrix element $M(0, \omega)$ in terms of the transcendental functions B and T.

	Constant	$B(\omega^2)$	$B(-\omega^2)$	$T(\omega^2)$	$T(-\omega^2)$
$M_{++++}(0,\omega)=F(\alpha)+H(\alpha)$	1	$2-1/\omega^2$	$-4+1/\omega^2$	$1/\omega^2-1/2\omega^4$	$2-1/\omega^2-1/2\omega^4$
$M_{++--}(0,\omega)=F(\alpha)+F(-\alpha)$	-1	$-2/\omega^2$	$1/\omega^2$	$-1/2\omega^4$	$-1/2\omega^4$
$M_{+-+-}(0,\omega)=F(-\alpha)+H(\alpha)$	1	$-4-1/\omega^2$	$2+1/\omega^2$	$2+1/\omega^2-1/2\omega^4$	$-1/\omega^2-1/2\omega^4$
$M_{+--+}(0,\omega)=0$	0	0	0	0	0

TABLE IV. Numerical values of the transcendental functions B, T, and I for some values of the arguments.

u	$B(u)$	$T(u)$	$I(u,-u/2)$	$I(u,u)$
-25	1.3583	5.3474		
-12.5	1.0530	3.9024		5.2977
-4	0.6141	2.0841		
-3	0.5207	1.7394		
-2	0.4038	1.3138		0.9286
-1.5	0.3319	1.0644		
-1	0.2465	0.7768		0.3454
-0.5	0.1405	0.4336		0.1176
-0.25	0.0760	0.2315		
0	0.0000	0.0000	0.0000	0.0000
0.25	-0.0933	-0.2741		
0.5	-0.2146	-0.6169		
1	-1.0000	-2.4674	-0.9095	
1.5	$-0.6199-0.2887\pi i$	$-2.0343-0.6581\pi i$		
2	$-0.3768-0.3536\pi i$	$-1.6906-0.8814\pi i$	$-0.2571-0.5376\pi i$	
3	$-0.0634-0.4083\pi i$	$-1.1502-1.1472\pi i$		
4	$0.1405-0.4330\pi i$	$-0.7330-1.3170\pi i$	$0.7675-0.9223\pi i$	
12.5	$0.8564-0.4796\pi i$	$1.2783-1.9354\pi i$		
25	$1.2462-0.4899\pi i$	$2.7878-2.9250\pi i$	$6.5442-1.9178\pi i$	

$$\kappa^4 A(1,2,3,4)=r+b_{+\alpha\beta}[B(\alpha)+B(\beta)]+b_{+\beta\gamma}[B(\beta)+B(\gamma)]+b_{+\gamma\alpha}[B(\gamma)+B(\alpha)]+b_{-\alpha\beta}[B(\alpha)-B(\beta)]+b_{-\beta\gamma}[B(\beta)-B(\gamma)]+b_{-\gamma\alpha}[B(\gamma)-B(\alpha)]+t_{\alpha\beta}[T(\alpha)+T(\beta)]+t_{\beta\gamma}[T(\beta)+T(\gamma)]+t_{\gamma\alpha}[T(\gamma)+T(\alpha)]+i_{\alpha\beta}I(\alpha,\beta)+i_{\beta\gamma}I(\beta,\gamma)+i_{\gamma\alpha}I(\gamma,\alpha). \quad \text{(A1)}$$

The r's, b's, t's, and i's are rational functions of α, β, and γ. A number of these vanish for certain values of the indices. Thus

$$b_{-}{}^{2111}=b_{-}{}^{2111}=b_{-}{}^{2121}=b_{-}{}^{2211}=0, \quad b_{+}{}^{2143}=0. \quad \text{(A2)}$$

In addition,

$$b_{-\beta\gamma}{}^{2143}=0. \quad \text{(A3)}$$

Many others differ only by a permutation of arguments. Thus

$$\begin{aligned} f_{\gamma\alpha}{}^{2143}(\alpha,\beta,\gamma)&=f_{\alpha\beta}{}^{2143}(\alpha,\gamma,\beta),\\ f_{\beta\gamma}{}^{2341}(\alpha,\beta,\gamma)&=f_{\alpha\beta}{}^{2341}(\gamma,\beta,\alpha),\\ f_{\gamma\alpha}{}^{2111}(\alpha,\beta,\gamma)&=f_{\alpha\beta}{}^{2111}(\alpha,\gamma,\beta),\\ f_{\gamma\alpha}{}^{2211}(\alpha,\beta,\gamma)&=-f_{\beta\gamma}{}^{2211}(\beta,\alpha,\gamma), \end{aligned} \quad \text{(A4)}$$

where f stands for b_+, t, and i. For b_- we have the identity

$$b_{-\gamma\alpha}{}^{2143}(\alpha,\beta,\gamma)=-b_{-\alpha\beta}{}^{2143}(\alpha,\gamma,\beta). \quad \text{(A5)}$$

We now list the "irreducible" rational functions:

$$\begin{aligned} r^{2143}&=(3\beta^2\gamma^2)^{-1}(3\alpha^2-10\beta\gamma)\\ r^{2341}&=(3\alpha\beta^2\gamma)^{-1}(3\alpha\gamma-5\beta^2)\\ r^{2111}&=(3\beta\gamma)^{-1}\\ r^{2121}&=-(3\beta^2\gamma)^{-1}(3\alpha+2\beta)\\ r^{2211}&=(3\alpha\beta\gamma)^{-1}(\alpha-\beta) \end{aligned} \quad \text{(A6)}$$

$$\begin{aligned} b_{+\alpha\beta}{}^{2341}&=-(3\alpha\beta\gamma^2)^{-1}(4\alpha^2+21\alpha\beta-12\gamma^2)\\ b_{+\gamma\alpha}{}^{2341}&=(3\alpha^2\gamma^2)^{-1}(4\beta^2+6\alpha\gamma)\\ b_{+\alpha\beta}{}^{2111}&=(3\alpha\beta^2\gamma^2)^{-1}(\alpha^2+\beta^2-\gamma^2)\\ b_{+\beta\gamma}{}^{2111}&=-(3\alpha\beta^2\gamma^2)^{-1}(3\alpha^2+\beta^2+\gamma^2)\\ b_{+\alpha\gamma}{}^{2121}&=-(3\alpha\gamma^2)^{-1}(6\alpha+2\beta)\\ b_{+\alpha\beta}{}^{2121}&=(3\alpha\beta^2\gamma)^{-1}(12\alpha^2\gamma+6\alpha\beta^2-2\beta\gamma^2)\\ b_{+\beta\gamma}{}^{2121}&=-(3\alpha\beta^2\gamma^2)^{-1}(12\alpha^2\gamma^2-6\alpha\beta^3+2\beta^4)\\ b_{+\alpha\beta}{}^{2211}&=(3\alpha^2\beta^2)^{-1}(2\alpha^2-2\beta^2)\\ b_{+\beta\gamma}{}^{2211}&=-(3\alpha\beta^2\gamma^2)^{-1}(2\alpha^3-2\alpha^2\beta+3\beta^2\gamma) \end{aligned} \quad \text{(A7)}$$

$$\begin{aligned} b_{-\alpha\beta}{}^{2143}&=(3\alpha\gamma^2)^{-1}(12\beta^2+2\beta\gamma-6\gamma^2)\\ i_{\alpha\beta}{}^{2143}&=(3\gamma^4)^{-1}(12\beta^2+4\alpha\gamma)+(\alpha\gamma^2)^{-1}2\beta\\ i_{\beta\gamma}{}^{2143}&=(3\alpha^2)^{-1}4\\ i_{\alpha\beta}{}^{2341}&=(3\gamma^2)^{-1}(3\gamma-4\beta)+(2\alpha^2\beta\gamma^2)^{-1}(\beta^3+\gamma^3-\alpha^2)\\ t_{\gamma\alpha}{}^{2341}&=-(3\beta^4)^{-1}(4\beta^2+12\alpha\gamma)\\ &\quad+(2\alpha^2\beta^3\gamma^2)^{-1}(\beta^4+\alpha^2\beta^2+\beta^2\gamma^2-4\alpha^2\gamma^2)\\ t_{\alpha\beta}{}^{2111}&=(3\gamma^2)^{-1}(2\alpha-3\gamma)-(4\beta^2\gamma^2)^{-1}\alpha\\ t_{\beta\gamma}{}^{2111}&=(3\alpha^2)^{-1}2-(4\beta^2\gamma^2)^{-1}\alpha\\ t_{\alpha\beta}{}^{2121}&=-(3\gamma^2)^{-1}(\alpha-3\beta)-(2\alpha\beta\gamma)^{-1}\\ t_{\beta\gamma}{}^{2121}&=(3\alpha^2)^{-1}2+(2\alpha\beta\gamma^2)^{-1}(\alpha-\beta)\\ t_{\gamma\alpha}{}^{2121}&=(3\beta^4)^{-1}(4\alpha^2-8\alpha\beta-3\beta^2)-(2\alpha\gamma^2\beta^2)^{-1}(\alpha^2-\beta^2+3\alpha\gamma^2)\\ t_{\beta\gamma}{}^{2211}&=(3\alpha^2)^{-1}(2\alpha-2\beta)-(4\alpha^2\beta^2\gamma^2)^{-1}(\alpha-\beta)(\alpha^2+\alpha\beta+\beta^2)\\ t_{\alpha\beta}{}^{2211}&=(3\gamma^2)^{-1}(2\alpha-2\beta)-(4\alpha^2\beta^2\gamma^2)^{-1}(\alpha-\beta)(\alpha^2+\alpha\beta+\beta^2) \end{aligned} \quad \text{(A8)}$$

$$\begin{aligned} i_{\alpha\beta}{}^{2143}&=-(3\gamma^4)^{-1}(12\beta^2+4\alpha\gamma)-(3\alpha\beta\gamma^2)^{-1}(12\beta^2+2\alpha\gamma)\\ &\quad+(6\alpha\beta^2\gamma^2)^{-1}(3\alpha^2-8\beta\gamma)\\ i_{\beta\gamma}{}^{2143}&=-(3\alpha^2)^{-1}4-(3\alpha\beta\gamma)^{-1}8+(6\beta^2\gamma^2)^{-1}(3\alpha^2-8\beta\gamma)\\ i_{\alpha\beta}{}^{2341}&=(3\gamma^2)^{-1}(4\beta-3\gamma)+(6\alpha^2\beta^2\gamma^2)^{-1}(6\alpha^2\gamma+7\alpha\beta^2-3\beta^3)\\ &\quad+(6\alpha^2\beta^2\gamma)^{-1}(2\beta^2+3\alpha\gamma)\\ i_{\gamma\alpha}{}^{2341}&=(3\beta^4)^{-1}(4\beta^2+12\alpha\gamma)-(6\alpha^2\beta^2\gamma^2)^{-1}(3\alpha^2\beta^2+3\beta^2\gamma^2\\ &\quad-24\alpha^2\gamma^2-4\alpha\beta^2\gamma)+(6\alpha^2\beta^2\gamma^2)^{-1}(2\beta^2+3\alpha\gamma)\\ i_{\alpha\beta}{}^{2111}&=-(3\gamma^2)^{-1}(2\alpha-3\gamma)-(6\alpha\beta\gamma^2)^{-1}(5\alpha-6\gamma)-(6\alpha\beta^2\gamma)^{-1}\\ i_{\beta\gamma}{}^{2111}&=-(3\alpha^2)^{-1}2-(3\alpha\beta\gamma)^{-1}-(6\beta^2\gamma^2)^{-1}\\ i_{\alpha\beta}{}^{2121}&=+(3\gamma^2)^{-1}(\alpha+3\beta)-(6\alpha\beta^2\gamma^2)^{-1}(3\alpha^2-\alpha\beta+6\beta^2)\\ &\quad-(6\alpha\beta^2\gamma)(3\alpha+\beta)\\ i_{\beta\gamma}{}^{2121}&=-(3\alpha^2)^{-1}2+(6\alpha\beta^2\gamma^2)^{-1}(\alpha^2+4\alpha\beta+2\gamma^2)\\ &\quad-(6\beta^2\gamma^2)^{-1}(3\alpha+\beta)\\ i_{\gamma\alpha}{}^{2121}&=-(3\beta^4)^{-1}(4\alpha^2-8\alpha\gamma-3\beta^2)+(6\alpha\beta^2\gamma^2)^{-1}(24\alpha^2+38\alpha^2\beta\\ &\quad+11\alpha\beta^2-6\beta^2)-(6\alpha\beta^2\gamma^2)^{-1}(3\alpha+\beta)\\ i_{\alpha\beta}{}^{2211}&=-(3\gamma^2)^{-1}(2\alpha-2\beta)-(6\alpha\beta\gamma^2)^{-1}(5\alpha-5\beta)\\ &\quad-(6\alpha^2\beta^2\gamma)^{-1}(\alpha-\beta)\\ i_{\beta\gamma}{}^{2211}&=-(3\alpha^2)^{-1}(2\alpha-2\beta)+(6\alpha^2\beta\gamma^2)^{-1}(2\alpha^2-5\beta^2)\\ &\quad-(6\alpha\beta^2\gamma^2)(\alpha-\beta). \end{aligned} \quad \text{(A9)}$$

(A10)

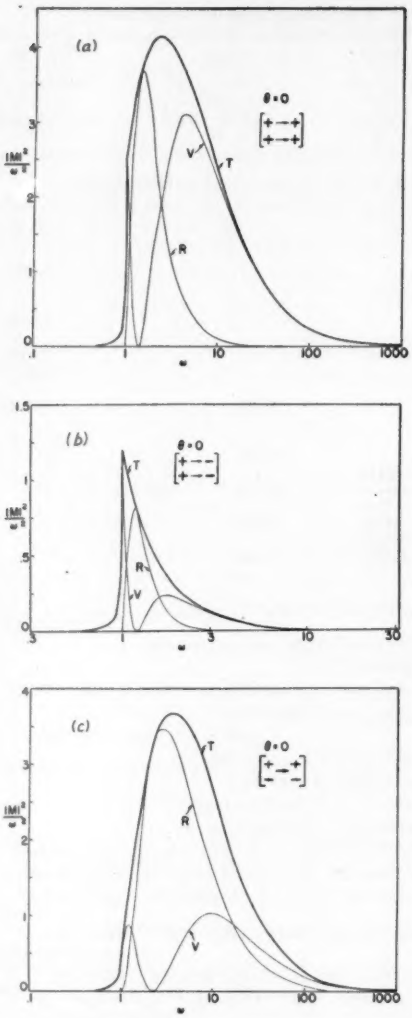

FIG. 4. Differential cross section for forward scattering (cg system) between the indicated states of circular polarization. The unit is 1.07×10^{-31} cm²/sterad; the unit of energy is mc^2. R, V, and T represent the contributions of real intermediate pairs, of virtual intermediate pairs, and their sum, respectively. Note the different scales.

APPENDIX B

Definitions

$$B(u)=\tfrac{1}{2}\int_0^1 dy\,\log[1-i\epsilon-4uy(1-y)]. \tag{B1}$$

$$T(u)=\int_0^1 dy[4y(1-y)]^{-1}\log[1-i\epsilon-4uy(1-y)]. \tag{B2}$$

$$I(u,v)=\int_0^1 dy[4y(1-y)-(uv)^{-1}(u+v)]^{-1}\times\log[1-i\epsilon-4uy(1-y)]. \tag{B3}$$

Approximate Expressions

$$\begin{aligned}&B(u)\sim-(1/3)u-(2/15)u^3-(8/105)u^5;\quad |u|\ll1.\\ &B(u)\sim(1/2)\log|4u|-1-(1/2)i\pi\theta(u)\quad |u|\gg1.\end{aligned} \tag{B4}$$

$$\begin{aligned}&T(u)\sim-u-(1/3)u^3-(8/45)u^5\quad |u|\leqslant1.\\ &T(u)\sim(1/4)\log^2|4u|-((1/4)\pi^2+(1/2)i\pi\log|4u|)\theta(u)\quad |u|\gg1.\end{aligned} \tag{B5}$$

$$\theta(|u|)=1,\quad \theta(-|u|)=0.$$

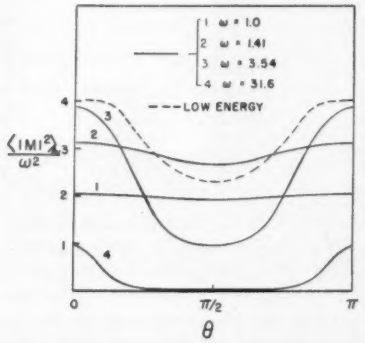

FIG. 5. Angular dependence of the cross section for scattering unpolarized quanta at selected energies (cg system). These curves were interpolated from the values of the cross section at 0°, 90°, and 180°. The shape at low energy is not to scale.

Denoting $(u+v)/uv$ by x we get

$$\begin{aligned}I(u,v)\sim&-[T(u)+T(v)][1+(1/2)x+(3/8)x^2+(5/16)x^3]\\ &+B(u)x[u+(1/4)xf_1(u)+(1/24)x^2f_2(u)]\\ &+B(v)x[v+(1/4)xf_1(v)+(1/24)x^2f_2(v)]\\ &-(1/4)(u+v)x[1+x+(1/24)x^2(45+4uv)]\end{aligned} \tag{B6a}$$

for

$$|x|\ll1,$$

where

$$\begin{aligned}f_1(u)&=3u+2u^3,\\ f_2(u)&=15u+10u^3+8u^5.\end{aligned}$$

$$I(u,v)\sim-(2/x)[B(v)-(4/3)-(4/15)v^2(u+v)^{-2}],\quad |u|\ll1, \tag{B6b}$$

$$\begin{aligned}I(u,v)\sim(1/4)\{&\log^2|4u|+\log^2|4v|-\log^2[|u||v|^{-1}]\\ &-\pi^2-\pi i\theta(u)\log|v|\},\end{aligned} \tag{B6c}$$

$$|u|\gg1,\quad v\ll-1.$$

Properties of a $CaSO_4$: Mn Phosphor under Vacuum Ultraviolet Excitation

K. WATANABE
United States Naval Research Laboratory, Washington, D. C.
(Received January 22, 1951)

The properties of a manganese-activated $CaSO_4$ phosphor were investigated in connection with its use as a detector of extreme ultraviolet solar radiation in upper atmosphere research. The luminescence of particular interest was a long-period phosphorescence which is excited by wavelengths in the range 1350A to gamma-rays. The energy stored in the phosphor after exposure to short ultraviolet was released by heating and measured by means of a photomultiplier. The stored energy was given by the integrated multiplier response and was independent of the form of the heating cycle. It was also nearly independent of the exposure temperature (−30 to +70°C) and humidity. There was a useful exposure range of 10^4 over which the stored energy was directly proportional to the exposure intensity and time; for higher exposures, saturation set in. The excitation spectrum of the stored energy was measured and the maximum quantum efficiency (5 to 10 percent) was found to lie at 1030A. At room temperature, the long-period phosphorescence decay was of the hyperbolic type. Fluorescence in addition to phosphorescence was excited by wavelengths shorter than 1350A, and an additional excitation band of fluorescence only was found in the region 1400–1600A. The emission spectrum extended from 4480 to 5790A.

INTRODUCTION

WIEDEMANN and Schmidt[1] observed that when a $CaSO_4$ phosphor activated with a few percent of $MnSO_4$ was exposed to a condensed spark in air at a distance of a few centimeters and then heated to about 200°C, a green thermoluminescence was given off. Since the interposition of a plate of fluorite prevented the effect, they concluded that the exitation of the phosphor was not due to the ultraviolet component of the spark but to a special radiation, which they named "Entladungsstrahlen." Hoffmann[2] continued the experiment but was not able to establish the nature of this radiation. Later, Laird[3] suggested that the effect was due to x-rays from the spark and not to ultraviolet rays of wavelength longer than 1000A. Lyman[4] prepared the phosphor by Hoffmann's method and showed that its spectral sensitivity began abruptly at 1300A and extended at least to 140A. He also demonstrated that it was radiation in the region of partial transparency of air, 100–1300A, that was Wiedemann's "Entladungsstrahlen." Recently, the phosphor was used by Purcell, Tousey, and Watanabe[5] to detect extreme ultraviolet and x-rays from the sun at high altitudes in the earth's atmosphere by mounting samples on V-2 rockets and exposing them to sunlight during flight.

PREPARATION OF SAMPLES

In our first experiments, the phosphor was prepared by the process described by Hoffmann.[2] A little $MnSO_4$ was mixed thoroughly with a paste of $CaSO_4$ (analytical reagent by Mallinckrodt) and water. The mixture was evaporated to dryness, heated to redness for several minutes, and ground to a fine powder after cooling. The most efficient phosphor was obtained by mixing the sulfates in dilute sulfuric acid, letting the mixture stand for a few hours, evaporating it to dryness, and heating the residue to redness. The powder thus obtained was very nearly white, and its sensitivity was five to ten times that of samples prepared by the method of Hoffmann. Lyman's observation[4] that the exact amount of manganous sulfate is not important was confirmed for samples containing from 0.2 to 17 percent $MnSO_4$. Phosphor strips were prepared by pressing the power into 100 mesh nickel screens.

APPARATUS AND EXPERIMENTAL CONDITIONS

The luminescence of the phosphor was measured with a 1P21 photomultiplier tube. The photocurrent was further amplified by an RCA Ultrasensitive Microammeter, type WV84A; and the amplified current was fed into a recorder. The total emission in arbitrary units was obtained by integrating the recorder trace. Usually, the phosphor strip was clamped between two electrodes at a fixed position 1.8 cm from the surface of the photomultiplier tube and heated by the current from a 2.5-volt filament transformer. The time of heating was between 2 and 5 minutes depending on the setting of a Variac connected to the transformer. For a strip 0.4 inch wide, a current of 8 amperes was required to heat the strip to about 200°C.

The sensitivity of the photomultiplier and amplifier system was checked periodically by use of a self-luminous radium phosphor button as a standard light source. Since each group of measurements extended over only a few days, possible deterioration of the button could be neglected. The sensitivity of the particular tube used when operated at 100 volts per dynode was 4.4×10^4 amp per watt at 5140A; and as ordinarily used, the photomultiplier current ranged from 10^{-5} to 10 microamperes.

For measuring the spectral response of the phosphor to extreme ultraviolet radiation, a vacuum grating

[1] E. Wiedemann and G. C. Schmidt, Wied. Ann. **54**, 604 (1895).
[2] M. W. Hoffmann, Wied. Ann. **60**, 269 (1897).
[3] E. R. Laird, Phys. Rev. **30**, 293 (1910).
[4] T. Lyman, Phys. Rev. **48**, 149 (1935).
[5] Purcell, Tousey, and Watanabe, Phys. Rev. **76**, 165 (1949).

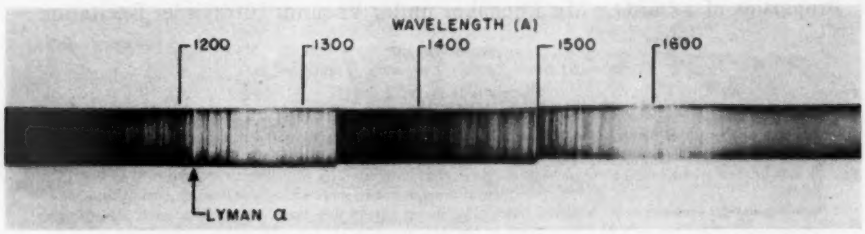

FIG. 1. Composite photograph of the hydrogen spectrum emitted by an Allen-type hydrogen arc with a LiF window. An exposure time of 16 sec was used for the region below 1330A and of one sec for the region above 1330A.

monochromator[6] and a high intensity hydrogen discharge tube source with open window were used. The radiation intensity emerging from the exit slit was known from measurements made with a thermocouple.[7] The wavelength range covered extended from 900 to 2500A.

The study of many of the optical properties of the phosphor did not require monochromatic radiation and was done in the open air with a hydrogen discharge tube with a LiF window. This was possible because of the transparency of air in the region of Lyman alpha, which was first pointed out by Hopfield[8] and later shown by Ladenburg, Van Voorhis, and Boyce[9] to extend from 1100 to 1300A.

The hydrogen discharge tube with a LiF window used as radiation source was of the type described by Allen and Franklin[10] and was constructed by Nestor of the Bartol Foundation. Figure 1 represents a spectrum of the radiation from this source obtained with a vacuum spectrograph. The many-lined spectrum of H_2 extends to 1630A, and the H_2 continuum continues from there to longer wavelengths. Because of the absorption of the LiF window, the intensity falls off rapidly below 1150A.

The region of the spectrum between 1100 and 1300A emerging from the window of the discharge tube penetrated several centimeters of laboratory air with sufficient intensity; however, it was necessary to know something about the dependence of intensity on the air path and on the composition of the air. The wavelengths of the main absorption bands of the common gases in air are fairly well known, but data on their absorption coefficients are meager or inaccurate. Preston[11] has obtained the following values of the absorption coefficients in cm^{-1} at 1216A: oxygen = 0.28, nitrogen <0.0005, carbon dioxide = 2.01, and water vapor about 390 (all values given in base e and reduced to NTP). These values appear to be the most reliable ones in this region.

The dependence of intensity on air path was investigated semiquantitatively in a simple manner. A phosphor sample was placed in front of the hydrogen discharge tube so that the air path between the strip and the window of the tube was x cm, and after a given exposure the stored energy E was measured. The light source within the tube was considered as a point, since its dimensions were small compared with its distance, D, from the phosphor strip. The departure from the inverse square law relation between E and x gave the attenuation of air. Data for air containing water vapor at 10.0–10.8 mm Hg partial pressure are shown in Fig. 2. The "effective absorption coefficients" obtained from the slope of this curve are about 4.2 and 1.8 cm^{-1} at $x=0$ and $x=2$ cm, respectively. Preston's value for the absorption coefficient of water vapor (at 1216A) gives 5.3 cm^{-1} as the absorption coefficient (at 1216A)

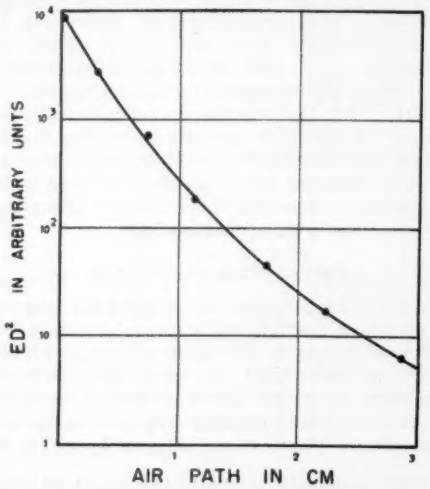

FIG. 2. Attenuation by air of the radiation in the Lyman alpha-region emitted by the Allen-type source. E is the radiation intensity at the phosphor surface, and D is the distance between the "point" source and the phosphor surface.

[6] Tousey, Johnson, Richardson, and Toran, J. Opt. Soc. Am. **40**, 264 (1950).
[7] D. M. Packer and C. Lock, J. Opt. Soc. Am. **40**, 264 (1950).
[8] J. J. Hopfield, Phys. Rev. **20**, 587 (1922).
[9] Ladenburg, Van Voorhis, and Boyce, Phys. Rev. **40**, 1018 (1932).
[10] A. J. Allen and R. G. Franklin, J. Opt. Soc. Am. **29**, 453 (1939).
[11] W. M. Preston, Phys. Rev. **57**, 887 (1940).

of air containing water vapor whose partial pressure is 10 mm Hg. Since other wavelengths were included in the experimental measurement, the agreement was considered good. Similar experiments showed that, when a 2 cm air path was used, the response of the phosphor varied by as much as a factor of two under seemingly identical conditions but at different times. This can be accounted for by variation in absolute humidity. However, by placing the phosphor strip directly in contact with the window during exposure, it was possible to minimize the effect of water vapor.

PROPERTIES OF THE PHOSPHOR

(a) Spectral Sensitivity

To determine the spectral region to which the calcium sulfate phosphor is sensitive, Lyman placed a copper strip coated with the phosphor in a vacuum spectrograph in the place usually occupied by a photographic plate and exposed it to the spectrum from a hydrogen discharge tube for about eight hours. The strip was withdrawn, placed a mm in front of a photographic plate, and heated. The resulting thermoluminescence was thus recorded on the photographic plate. From this experiment and by visual observations, he found that the sensitivity of the phosphor began quite abruptly at 1300A. In order to determine whether our phosphor had the same long wavelength limit of sensitivity, Lyman's experiment was repeated. In addition to the spectrum from 1100 to 1300A, there appeared a trace of response in the region near 1600A. Thus, the phosphor as prepared by us was not completely insensitive to radiation of wavelengths longer than 1300A, but the sensitivity was very low and was estimated at about 10^{-3} of that in the region 1100–1300A.

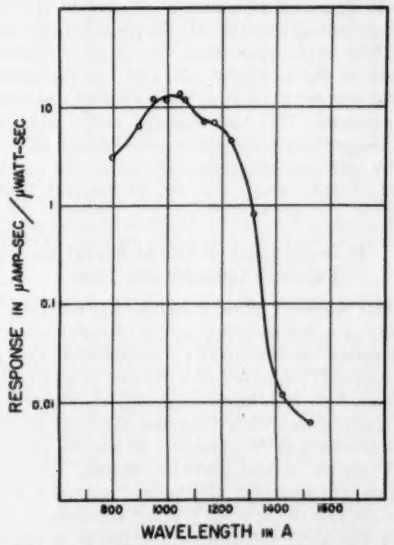

FIG. 3. Spectral sensitivity of the $CaSO_4$:Mn phosphor with respect to thermoluminescent energy. The spectral energy of the radiation producing excitation of the phosphor was measured in microwatt-sec by a thermocouple, and the stored energy was given by the integrated output of a photomultiplier in microamp-sec.

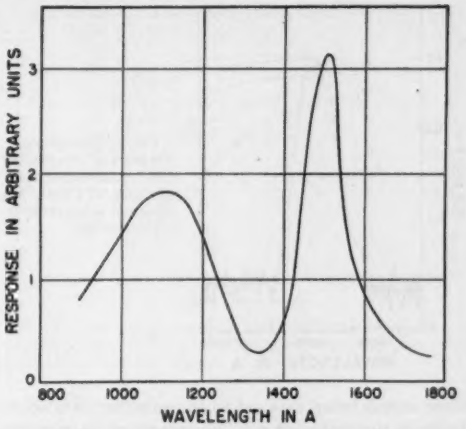

FIG. 4. Response of the $CaSO_4$:Mn phsphor with respect to fluorescence as a function of excitation wavelength.

A direct measurement of the absolute spectral response of the phosphor was made from 900 to 2500A by means of the vacuum monochromator and the high intensity hydrogen discharge tube. The phosphor sample was mounted in vacuum about two millimeters behind the exit slit and exposed to a band width of 14A for 5 to 90 sec, keeping the exposure within the linear portion of the stored energy curve. The exposed strip was removed, and its total thermoluminescence was measured with the photomultiplier-recorder system. The responses of the phosphor for several wavelengths were then compared with the values of the absolute spectral intensity measured by Packer and Lock.[7] Since the energy available below 900A was too small to be measured with the thermocouple, a value for 800A was estimated from the response of a photomultiplier coated with anthracene, making use of the fact that anthracene exhibits constant quantum efficiency[12] at least down to 900A.

The spectral response for one sample is shown in Fig. 3 and is expressed in microamp-sec of integrated photomultiplier current per microwatt-sec of incident radiation. There is a maximum in response at about 1030A and the response drops to 10^{-3} of the peak value at 1422A. The variation in sensitivity at 1050A for five different samples was 13 percent. The quantum efficiency of the phosphor at the peak was estimated to be about 5–10 percent.

An intense fluorescence was emitted by the phosphor

[12] Watanabe, Johnson, and Tousey, Phys. Rev. 79, 217 (1950).

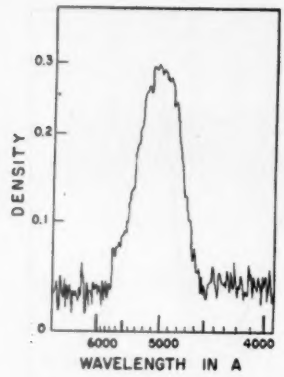

FIG. 5. Microphotometer trace of the emission (thermoluminescence) spectrum of $CaSO_4$:Mn phosphor after extreme-UV excitation.

while it was being exposed to the extreme ultraviolet. To study the dependence of fluorescence on wavelength, a 1P21 coated with the phosphor was placed about an inch behind the exit slit of the monochromator and the spectrum was scanned at the rate of 100A per minute. It was found that the fluorescence was so much stronger than the phosphorescence that the latter could be neglected for the scanning speed used.

Figure 4 represents the relative quantum efficiency of fluorescence response as a function of wavelength. The band at the shorter wavelength is broader than the corresponding thermoluminescence band of Fig. 3 and is displaced a little from it. There is, in addition, a strong excitation band centered at 1500A, and this has not been reported previously.

Laird,[3] and Wick and Slattery[12] have studied the $CaSO_4$:Mn phosphor under x-ray excitation. Preliminary experiments by us indicated that an x-ray tube with a beryllium window using 30 milliamperes at 3 kilovolts was about as effective as the Allen-type hydrogen discharge tube operating at 1.2 amp. It was also found that a one-minute exposure to gamma-rays from a 5-mg radium source at 3 cm produced a barely observable thermoluminescence.

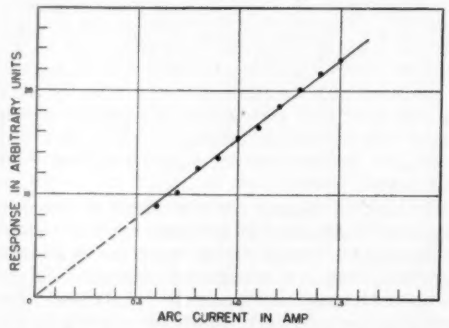

FIG. 6. Total energy stored in the $CaSO_4$:Mn phosphor after a one-minute exposure to the hydrogen arc as a function of the arc current. The intensity of the arc spectrum was known to vary directly with the arc current.

(b) Emission Spectrum

The emission spectrum of the calcium sulfate phosphor excited by wavelengths 1100–1300A was photographed with a Gaertner quartz spectrograph by charging a sample and discharging it thirty times in front of the slit, which was 0.1 mm wide. The band extended over the range 4480 to 5790A, and the microphotometer trace (see Fig. 5) placed the maximum at 5020A.

The emission spectrum of $CaSO_4$ and 0.1 percent $MnSO_4$ excited by cathode rays was studied by Tanaka,[14] who used a Hilger spectrophotometer; and the maximum emission was found to lie at 5050A. Also using cathode-ray excitation, Randall[15] found the maximum at 4975A for the emission band which extended from 4600 to 5800A. A comparison of his microphotometer trace and the one shown in Fig. 5 indicated that the spectral distribution of the band does not appear to vary radically with the mode of excitation.

(c) Thermoluminescence Independent of Heating Cycle

It was hoped that the area under the luminescence trace drawn by the recording photometer would not depend greatly on the way the phosphor was heated and so could be taken as a simple measure of the total ultraviolet energy absorbed by the phosphor. To investigate this, a phosphor strip was given a 30-second exposure to the hydrogen arc, and the thermoluminescence released by heating was measured one minute after exposure. This was repeated with the heating cycle changed in a variety of ways. The area under the recorder trace was found to be constant to within 5 percent of the mean value for 20 different heating cycles.

(d) Dependence of Stored Energy on Exposure Intensity and Time

Several methods were available for reducing the intensity of radiation falling on the phosphor strip: (1) the phosphor could be placed at different distances from the source; (2) plates of LiF with ground surfaces and aluminum foils with many uniformly distributed pinholes could be sandwiched between the window of the discharge tube and the phosphor, leaving no air space; and (3) the arc current could be reduced. Method (1) would require a vacuum. The second method is a very convenient one to use when it is not necessary to know exactly the factor by which the intensity is reduced. The reproducibility of results justified the use of this simple arrangement. The third method was made

[12] F. G. Wick and M. K. Slattery, J. Opt. Soc. Am. **14**, 125 (1927); **16**, 398 (1928).

[14] T. Tanaka, J. Opt. Soc. Am. **8**, 287 (1924).

[15] J. T. Randall, Proc. Roy. Soc. (London) **A170**, 272 (1938).

possible by the fact that thermocouple measurements showed that the radiation intensity in the region 1100–1300A was directly proportional to the arc current. By this method, the intensity could be varied by an accurately known factor up to 3 and the combination of methods (2) and (3) permitted covering a wide range of radiation intensity.

The dependence of the phosphor response on intensity was measured by reducing the intensity by method (3) and is shown in Fig. 6. The intensity level was kept below the point at which saturation was found to commence (30 units—Fig. 6). It is reasonable to believe that linearity is maintained at intensities lower than those used. This could not be checked by this method

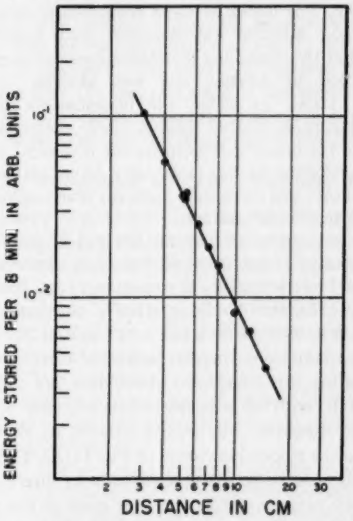

FIG. 7. Linearity of the total stored energy under gamma-ray excitation. The slope of the straight line is -2 in agreement with the intensity reduction according to the inverse square of the distance.

because the arc became unstable for current less than 0.5 amp.

As an additional check, the dependence of response on intensity was investigated using a gamma-ray source consisting of 5 mg of radium placed in a Lucite cylinder. A phosphor sample was placed at distances varying between 3 and 15 cm from the source and the thermoluminescence was measured after an 8 minute exposure. Figure 7 shows that the points fall on a straight line of slope -2, and it was concluded that the stored energy was directly proportional to the intensity over a range of at least 25 for gamma-rays.

To study the amount of stored energy as a function of exposure time, a phosphor sample was pressed against the window of the discharge tube and given different exposures. As summarized in Fig. 8, the total stored

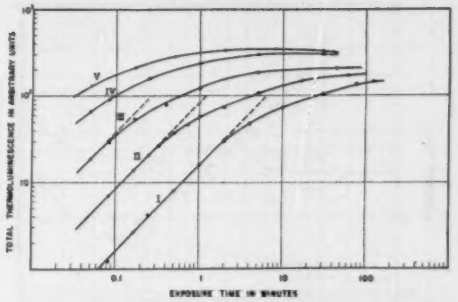

FIG. 8. Total energy stored in the $CaSO_4$:Mn phosphor as a function of exposure time for different exposure intensities. The broken lines have unit slopes.

energy, as measured by the total thermoluminescent emission, at first increased linearly with time and then gradually approached saturation when subjected to constant intensity of radiation. Curve V represents the case when no intensity reducer was used, and for the other curves filters of increasing opacity were interposed. For upper-atmosphere solar-radiation measurements, energies of the order one to two decades less than the lowest value in Fig. 8 were involved. At such low levels, there was no question of saturation effects and the response was strictly linear with exposure time.

(e) Sensitivity Independent of Exposure Temperature and Humidity

A phosphor strip, to which a copper-constantan thermocouple was attached, was pressed against the window of the hydrogen arc and the intensity of radiation was reduced by method 2. To lower the temperature, dry ice was used; and to raise it, electrical current was passed through the strip, which was padded sufficiently to prevent air circulation. When the temperature became constant, the strip received an exposure of one minute, was quickly brought to room temperature, and the thermoluminescence was measured one minute

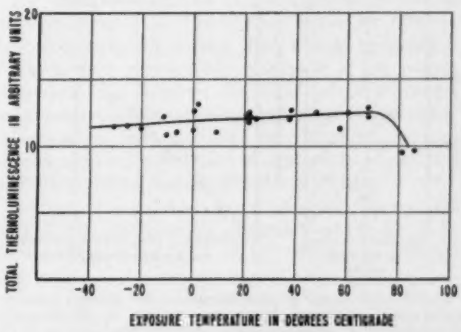

FIG. 9. Sensitivity of the $CaSO_4$:Mn phosphor as a function of the temperature during exposure.

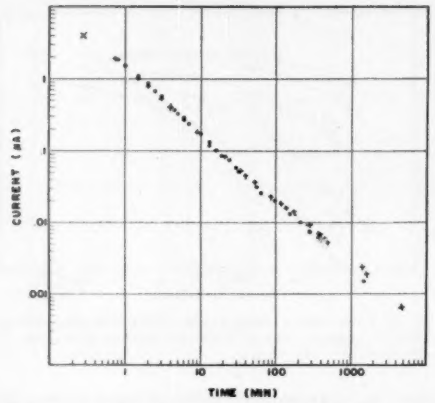

FIG. 10. Decay of phosphorescence of the $CaSO_4$:Mn phosphor at 25°C after extreme-UV excitation.

after exposure. For several reasons, the error was somewhat high; however, the experimental values were consistent and are shown in Fig. 9.

Since calcium sulfate is hygroscopic, tests were also made to study the effect of moisture on its sensitivity. A few samples were dipped in water after they had been irradiated with extreme ultraviolet radiation and allowed to dry at room temperature. Other samples were dipped in water, left standing at room temperature until they appeared dry, and then irradiated. Both sets of samples when discharged showed no appreciable reduction in their sensitivity.

(f) Decay

The energy stored by the phosphor is emitted as visible luminescence at a rate which depends on the temperature. The rate at 0°C is so low as to be unimportant, but at 20°C it is no longer negligible. At 250°C the energy is entirely emitted in two or three minutes under the usual conditions of measurement.

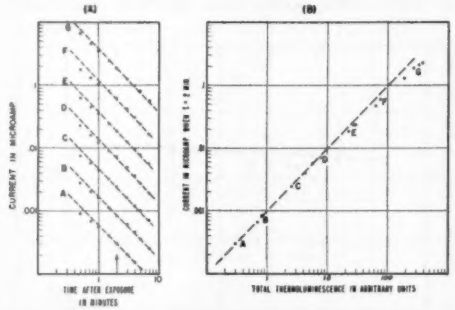

FIG. 11. (A) Decay of phosphorescence for different initially-stored energy, E_0. Slopes of the broken lines are -1. (B) Linearity of brightness of phosphorescence with E_0. The abscissa is E_0 and the ordinate is the brightness as measured by a photomultiplier.

The intensity of phosphorescence at room temperature (25°±1.5°C) as a function of time after exposure is shown in Fig. 10 for two runs with the same sample. It can be seen that the slope of the curve is very nearly minus one for times from 1 to 60 min. The average for eight decay curves was -1.01. For times greater than one hour the absolute value of the slope diminishes gradually.

A portion of the decay curve was studied for different intensities in order to determine whether the slope of the decay curve depended on the total exposure. The arc current, exposure time, and filters were varied so as to subject a given sample to a wide range of exposure intensity. The decay at room temperature during the first eight minutes was recorded, and immediately thereafter the remaining thermoluminescent energy was discharged by heating and was likewise recorded. Figure 11(A), in which the luminescence at room temperature is plotted against time, shows that the slope of the decay curve during the first eight minutes is independent of the exposure. Other experiments showed that this conclusion holds for times considerably greater than eight minutes.

The next question investigated was whether or not the intensity at any point on the decay curve was proportional to the initially stored energy, E_0. The energy E_0 was calculated by integration of the luminescence curves from $t=0$ to $t=8$ min and addition of the total thermoluminescent energies measured directly at $t=8$ by heating the phosphor. These data are plotted in Fig. 11(B) with the intensity of luminescence, I, at $t=2$ min as ordinates. The points lettered A, B, C, etc., refer to the respective curves of Fig. 11(A). The broken line has unit slope and corresponds to direct proportionality between I and E_0. Over most of the range I is directly proportional to E_0, but for large exposures there is a departure.

As a result of these data, it is possible to describe the decay approximately by the empirical equation,

$$I=E_0F(T)/(a+t), \tag{1}$$

where I is the intensity of phosphorescence, E_0 is the total emission (or exposure), $F(T)$ is an unknown function of phosphor temperature during decay, t is the time in minutes after exposure, and a is a constant introduced to fit the decay curve for $t<2$ min and is about 0.22 min.

Equation (1) was found to agree with the individual measurements to within 5 percent for t between 10 sec and 10 min; no measurements were made for $t<10$ sec. Additional data will be required to specialize the form of the function $F(T)$; qualitative experiments showed that $F(T)$ varies faster than T.

The phosphorescence decay law derived theoretically

for a uniform electron trap distribution is given by[16] the equation

$$I = nkT/t(1-e^{-st}), \quad (2)$$

where I = intensity of emission, n = total number of electrons in the trap, k = Boltzmann's constant, T = temperature in degrees Kelvin, t = time in sec, and s is the frequency factor in sec^{-1}. This equation was found unsatisfactory, since constant a is not negligible and $F(T)$ does not appear proportional to T.

The residual thermoluminescent energy E was given approximately by the equation

$$E = E_0 - \int_0^t I dt, \quad (3)$$

provided T was constant during the experiment. This is exemplified by the upper curve in Fig. 12, in which E is plotted against t. That Eq. (3) is true was proved by the fact that the negative slope of the upper curve of Fig. 12, when plotted against time, gave a decay curve (I *versus* t) similar to that plotted in Fig. 10.

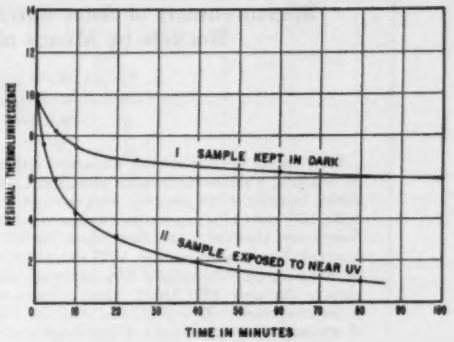

FIG. 12. Effect of near-UV radiation on the decay of energy stored in the $CaSO_4$:Mn phosphor. Both curves were obtained with the same phosphor sample.

(g) Stimulation by Near Ultraviolet

Wiedemann and Schmidt[1] found that the thermoluminescence of the calcium sulfate phosphor, when excited by cathode rays, was "quenched" by exposure to ordinary light and concluded that this was due to infrared radiation. However, for a calcium sulfate phosphor irradiated by x-rays, Wick and Slattery[12] found that the "quenching" was due to the near ultraviolet rays 2000–2400A and not to infrared. According to present usage, the term quenching should be replaced by stimulation. Our experiments confirmed the results of Wick and Slattery.

The effect of stimulation by near ultraviolet is shown in Fig. 12. The residual thermoluminescent energy of a sample which was kept in the dark for different durations after it received a standard exposure from the hydrogen arc was measured and plotted as curve I. In the second run, the same sample and procedure were used except that the phosphor, instead of being kept in the dark after exposure, was allowed to receive the radiation from the hydrogen arc covered with a Corning filter number 791 transmitting no wavelengths below about 2200A. Thus stimulation by near ultraviolet radiation was quite effective (see curve II).

In Fig. 12, let E_0 be the initially stored energy, which is identical for curves I and II, E_1 be the residual energy at time t for curve I, and E_2 be the residual energy at the same t for curve II. Then the ratio $(E_0-E_2)/(E_0-E_1)$ was constant for all values of t within the range measured. For the case shown, the near ultraviolet stimulation hastened the rate of emission by a factor of 2.3.

(h) Effect of Impurities

The calcium sulfate used in preparing our phosphor contained possibly as much as 0.2 percent magnesium and alkali salts and less than 0.005 percent of heavier metals. In order to determine whether the impurities might be contributing to the thermoluminescent property of the material, phosphors of magnesium sulfate, sodium sulfate, and potassium sulfate activated with manganese were prepared and tested for spectral sensitivity and efficiency. Their sensitivity was found to extend to wavelengths longer than 1300A, and the long wavelength limits were in the neighborhood of 2000A. Their efficiencies were considerably less than that of calcium sulfate. The presence of these elements as impurities in the $CaSO_4$:Mn phosphor may account for its feeble response at wavelengths greater than 1300A.

CONCLUSION

The manganese-activated $CaSO_4$ phosphor can be used satisfactorily as a measuring device for extreme ultraviolet radiation. Its lack of sensitivity to radiation of wavelengths above 1350A makes it rather unique among radiation detectors. Its response is linear over a useful range of 10^4 in intensity. The use of the phosphor for measuring from a rocket the intensities in the extreme ultraviolet spectrum of sunlight has been successful and will be described in a later paper.

The author is indebted to Dr. Richard Tousey and Mr. J. D. Purcell for helpful discussions and to Mr. F. S. Johnson for the spectrum of the hydrogen discharge tube.

[16] J. T. Randall and M. H. F. Wilkins, Proc. Roy. Soc. (London) **A184**, 390 (1945).

Measurements of Solar Extreme Ultraviolet and X-Rays from Rockets by Means of a $CaSO_4$:Mn Phosphor

R. Tousey, K. Watanabe, and J. D. Purcell
United States Naval Research Laboratory, Washington, D. C.

(Received March 5, 1951)

The presence of solar extreme ultraviolet and x-rays at high altitudes in the atmosphere was detected by means of a thermoluminescent phosphor, $CaSO_4$:Mn, which was not sensitive to wavelengths above 1340A. Samples of the phosphor were flown in V-2 rockets and exposed to sunlight. By means of filters of Be, LiF, and CaF_2, response was measured in the wavelength bands 0–8A, 1050–1340A, and 1230–1340A. X-rays were observed on one flight which reached 128 km, during which a sudden ionospheric disturbance occurred. Wavelengths between 1050 and 1340A were observed on all four flights and reached as low as 80–90 km. A tentative value of 0.04 microwatt/cm² was calculated for the total intensity in the solar spectrum in the range 1050–1240A, which includes the Lyman alpha-line of hydrogen, at an altitude level somewhere between 82 and 127 km. A similar value for the range 1230–1340A was 0.02 microwatt/cm². A comparison of the responses of the phosphor strips flown without filters and those with filters indicated that radiation between 795 and 1050A reaches the region 82–127 km with an intensity well above that produced by a 6000°K blackbody sun.

INTRODUCTION

SINCE 1946, when V-2 rockets first became available for high altitude research, experimentation has been carried on to observe the solar spectrum to very short wavelengths in the ultraviolet by means of rocket-borne spectrographs. Previously, the limit of the known solar spectrum was 2863A.[1] Shorter wavelengths were prevented from reaching terrestrial or even balloon-carried equipment by the strong absorptions in the high atmosphere caused by the ozone layer and oxygen itself.

The known solar spectrum has now been extended[2,3] to 2100A by means of rocket-borne spectrographs. Despite numerous attempts, this limit has not been exceeded because of insufficient exposure. The time during which a spectrograph is nearly enough directed at the sun to obtain an intense exposure is severely limited by the roll and yaw of the rocket. It is hoped eventually to obtain exposures of a minute or more to full sunlight by means of sun-following stabilizing equipment or stable rockets.

A simple rocket-borne experiment to measure solar extreme ultraviolet-radiation and x-rays in several spectral bands without spectroscopic resolution was devised and carried out as an interim measure. The radiation detecting device used was a thermoluminescent $CaSO_4$:Mn phosphor having the unique property that it is sensitive to wavelengths below, but not above 1340A. After excitation the stored energy can be released as a visible luminescence by heating, and this gives a measure of the ultraviolet to which it was exposed. In order to use the phosphor to measure solar ultraviolet it was necessary to study its properties in detail and this work was reported in a separate paper.[4]

PENETRATION OF SOLAR RADIATION

The nature of the solar spectrum below 2000A is still a subject for much scientific speculation. A great intensity excess in the extreme ultraviolet over that from a blackbody at 6000°K has been proposed for many years and for various reasons. For example, in order to explain terrestrial magnetic storms and aurorae, Maris and Hulburt[5] suggested that solar flares provide an intensity 10^5 greater than that from a 6000°K blackbody in the region 500–1000A. To explain the coronal spectrum Edlen[6] showed that many of the lines can be accounted for by a temperature of the order of 10^6K. This temperature would give rise to significant intensities below 1000A and down to soft x-rays. Martyn and co-workers[7] suggested that radio fadeouts which occur simultaneously with solar flares are due to a sudden increase of ionization of oxygen in the *D* layer (30–80 km), brought about by increased intensity and penetration of solar ultraviolet, particularly the Lyman alpha-line, while others[8,9] suggested x-rays. Finally, the diurnal variation of ionization in the *E* and *F* regions indicates that the solar short wavelengths are present in the radiation from the normal sun in sufficient intensity to cause great changes in the conditions in the ionosphere.

Because of the lack of information on the solar spectrum below 2000A, the scanty knowledge of absorption coefficients, and the scarcity of reliable laboratory data on the various photochemical processes which may

[1] F. W. P. Götz, Strahlentherapie **40**, 690 (1931).
[2] Baum, Johnson, Oberly, Rockwood, Strain, and Tousey, Phys. Rev. **70**, 781 (1946); Naval Research Laboratory Report, No. R-3030, Chapter IV, Sec. A (1946); Durand, Oberly, and Tousey, Phys. Rev. **71**, 827 (1947); Naval Research Laboratory Report No. R-3120, Chapter II, Sec. A (1947); Durand, Oberly, and Tousey, Astrophys. J. **109**, 1 (1949).
[3] J. J. Hopfield and H. E. Clearman, Jr., Phys. Rev. **73**, 877 (1948).
[4] K. Watanabe, Phys. Rev. **77**, 748(A) (1949); Phys. Rev. **83**, 785 (1951).
[5] H. B. Maris and E. O. Hulburt, Phys. Rev. **33**, 412 (1929).
[6] B. Edlen, Arkiv. Mat. Astron. Fysik **28, B**, 1 (1941).
[7] Martyn, Munro, Higgs, and Williams, Nature **140**, 603 (1937).
[8] L. Vegard, Naturwiss. **26**, 639 (1938).
[9] W. M. Preston, Phys. Rev. **57**, 887 (1940).

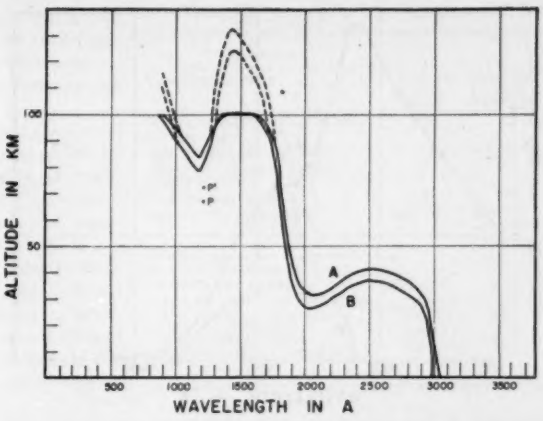

FIG. 1. Calculated altitudes at which the atmosphere above transmits one percent (curve B) and 10 percent (curve A) of the solar radiation for vertical incidence. *P* and *P'* are values for the Lyman alpha-line of hydrogen, based on absorption coefficients obtained by Preston.

occur in the upper atmosphere, there are still no completely acceptable theories of the ionosphere and of other phenomena occurring at altitudes above the ozone layer. It is generally accepted, however, that the process $O_2+h\nu \rightarrow O+O$ due to wavelengths less than 1750A occurs in the region 80–100 km[10,11] and that the various layers of the ionosphere are produced, at least in part, by ionization of nitrogen and oxygen by solar extreme ultraviolet, and that an excess over the radiation from a 6000°K blackbody is required.

Although the detailed processes responsible for creating the various regions of the ionosphere have received a great deal of attention, they are still not well established. For example, Wulf and Deming[10] suggested that the *E* layer is due to the ionization of O_2 by ultraviolet light (1012–910A). Hulburt,[12] on the other hand, proposed that soft x-rays are responsible for *E* layer ionization.

From laboratory data on the absorption spectra of atmospheric gases it is possible to calculate the approximate altitudes at which the various wavelengths in the solar spectrum may be expected to be encountered during the ascent of a rocket. The transmission of the high atmosphere for wavelengths down to about 2100A is now fairly well known. Below 2100A the data are not so well established. The approximate altitudes at which the atmosphere overhead transmits 1 percent and 10 percent of the solar radiation for vertical incidence were calculated and are shown in Fig. 1. Over most of the region the curves for the absorption coefficients are actually quite jagged, and only the mean values were taken for the calculation. In the region 1800–1300A the absorption coefficients for O_2 obtained by Ladenburg and Van Voorhis[13] were used; however, the application of these data to the upper atmosphere is confused by the theory of the dissociation of oxygen. In Fig. 1 the broken curves apply assuming no dissociation, and the solid curves apply if complete dissociation is assumed above 100 km and none below. To still shorter wavelengths there are only the estimates of Schneider,[14] and the curve is extended below 1000A by means of them. Nitrogen absorbs strongly below 795A (15.5 ev), but no quantitative data on its absorption are available. The pressure *versus* altitude data which were used were obtained by Havens, Koll, and LaGow.[15]

The Lyman alpha-line of hydrogen (1216A), which is of great astronomical interest, happens to fall in one of the deepest of the many narrow windows which cover this region. The data for the absorption of Lyman alpha by O_2 are in disagreement; Preston's[9] value differs from that of Williams[16] by a factor of 50. In Fig. 1, the altitudes for 1 percent and 10 percent transmission based on Preston's value for Lyman alpha (which is believed to be the more reliable) are indicated by points *P* and *P'*.

The exact altitudes at which measurable radiation can be detected depend on the radiation intensity present and the sensitivity of the detecting element as well as the atmospheric transmission. In Fig. 1, these factors are not taken into account, and only the transmission of the atmosphere is calculated. However, large changes in solar intensity or in receiver sensitivity produce relatively small changes in altitude, as can be seen from the fact that the displacement between the 10 percent and 1 percent transmission curves is small.

The conclusion from this calculation is that solar wavelengths below 1800A will not be encountered at altitudes below 80 to 100 km. A possible exception is

[10] O. R. Wulf and L. S. Deming, Terr. Mag. Atmos. Elec. **43**, 283 (1938).
[11] R. Penndorf, J. Geophys. Research **54**, 7 (1949).
[12] E. O. Hulburt, Phys. Rev. **53**, 344 (1938).
[13] R. Ladenburg and C. C. Van Voorhis, Phys. Rev. **43**, 315 (1933).
[14] E. G. Schneider, J. Opt. Soc. Am. **30**, 128 (1940).
[15] Havens, Koll, and LaGow, "Pressures and temperatures in the earth's upper atmosphere" (unclassified), Naval Research Laboratory Progress Report (March, 1950).
[16] S. E. Williams, Nature **145**, 68 (1940).

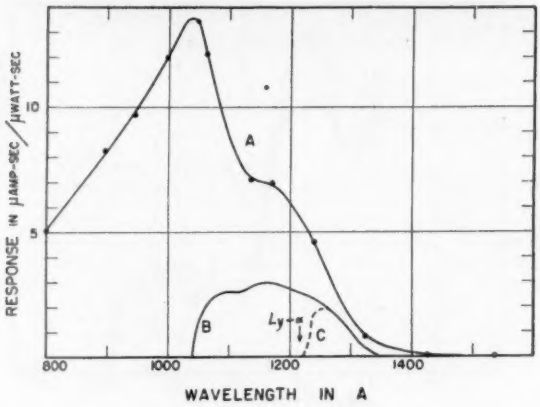

FIG. 2. Curve A is the spectral response of the $CaSO_4$:Mn phosphor calibrated against a thermocouple. Curves B and C are the response curves for the same phosphor with LiF and CaF_2 filters.

Lyman alpha, which, if present in the solar radiation as an emission line, may reach 60 km according to Preston.[9]

EXPERIMENTAL METHOD

Phosphor samples, which were sufficiently rugged to withstand a rocket flight and which could be given controlled heating electrically, were prepared by pressing the powder into nickel screens of 100 per inch mesh. The phosphor powder was bound in place by dipping into dilute Duco cement (5 percent Duco cement and 95 percent acetone). The thin coating of cement reduced the sensitivity of the phosphor to radiation in the region 1100–1300A by only about 10 percent, although Duco cement is quite opaque at these wavelengths in ordinary thin continuous films.

The energy stored in the phosphor, after excitation by short ultraviolet, was quickly released by heating, and the luminescence so produced was measured with a photomultiplier and recorder. Values of response were given in terms of an arbitrary unit, microamperes-sec, of integrated photomultiplier current.

The spectral response of the phosphor is shown in Fig. 2. For most practical purposes the response can be considered zero above 1340A. It was possible to make measurements in several restricted spectral bands in the extreme ultraviolet by placing suitable filters over the phosphor samples. The filters used were CaF_2, LiF, and Be. The curves showing the response of the phosphor through LiF and CaF_2 are also shown in Fig. 2, and were computed from transmission curves of the actual samples flown in flight (4). The bands covered and the filters used are given in Table I.

TABLE I. Wavelength bands obtained by filters.

Filter	Wavelength band
(1) CaF (1–3.4 mm)	1230–1340A
(2) LiF (1–2 mm)	1040–1340A
(3) Be (0.1 mm)	0–8A
(4) None	0–1340A
(5) LiF minus CaF_2	1040–1230A
(6) None minus (Be+LiF)	8–1040A

Bands (5) and (6) were obtained by the filter subtraction method, in which the responses measured through the various filters were subtracted from one another. For exact application, this method requires some knowledge of the relative intensity distribution in the radiation being studied and thus must await a spectrum photograph. It was, however, possible to obtain provisional information by the subtraction method by making certain assumptions concerning the nature of the solar spectrum.

The principal problem in the use of the phosphor was the avoidance of overheating the strips between exposure and measurement. Therefore, the experiment was included only in rockets flown in the winter months, an effort was made to recover the strips from the desert as quickly as possible, and they were shipped to Washington by air, packed in a thermos jug with ice.

As a check on the occurrence of excessive heating during flight and prior to recovery, control strips were included in each flight experiment. These strips were given standard exposures 4 to 12 hours prior to firing. The source used was a hydrogen discharge tube with a LiF window. Some of the control strips were kept in the laboratory at the White Sands Proving Ground and shipped to Washington together with the flight strips. Comparison of the thermoluminescence of the several control strips gave a measure of the loss in stored energy due to heating between flight exposure and shipment. This could be applied in some cases as a correction to the responses to sunlight measured in flight.

DETAILS OF THE SEVERAL ROCKET-BORNE EXPERIMENTS

During the period November, 1948, to February, 1950, six attempts were made with V-2 rockets to detect by means of the phosphor the presence of

extreme ultraviolet and x-rays from the sun in the upper atmosphere. Four experiments were successful, while two failed as the result of severe explosions on impact. Dates of the flights and altitudes reached are given in Tables II and III.

In the first flight four units, each consisting of a steel block with 6 strips and filters, were mounted in the rocket midsection about ½ in. inside the skin, and only partially protected from the windstream. The control strips showed that excessive heating occurred somewhere during the flight.

In flights (2) and (3), the strips were protected from the heating action of the air stream by being mounted on a cylinder which rotated inside a cylindrical cassette. They were exposed from just after fuel burn-out (60 sec) until just before warhead blow-off, a total time of 200 sec. This device solved the problem of excessive heating during flight.

In the fourth flight a phosphor of about 5 times increased sensitivity was used, and this made it possible to use five separate sets of phosphor strips. These were exposed successively during the rocket flight and measured the variation of radiation with altitude. There was only one set of filters and the strips were successively positioned behind them. Starting at 19 km each set of strips was exposed for 50 seconds. The spectral transmission of the LiF and CaF_2 filters was measured, and the absolute spectral sensitivity of the phosphor was known from measurement against a thermocouple.[17] Although the flight was successful, the impact was exceptionally severe and only 10 of the 50 strips flown were recovered. These strips, however, gave quantitative results.

The exposure during flight depended on the roll and yaw of the rocket. On flight (1) this was estimated, and on flights (2) and (3) it was measured by means of a photographic film covered with a dense filter. On the fourth flight good aspect data were available and made possible calculation of the exposure to about 30 percent accuracy.

RESULTS

The numerical response data are presented in Tables II and III. The first experiment, because of the loss in response due to heating, was only qualitative. The fourth flight, however, gave data of sufficient accuracy to warrant energy calculations.

1. X-Rays

The response through beryllium observed on February 17, 1949, is definite evidence of soft x-rays, presumably of solar origin. Since the transmission of the beryllium filter reached a very small value at 10A, the x-rays observed must have been of wavelengths shorter than 10A and most probably were shorter than 8A. Previous to this firing the presence of x-rays was detected by Burnight,[18] who used a Schumann photographic plate covered with Be and flown on August 5, 1948.

Only on our second flight, which reached 128 km, were x-rays definitely detected. It is interesting to note that a sudden ionospheric disturbance occurred during this flight. X-rays were not positively recorded on flight (1), although the maximum altitude reached was 146 km, nor on flight (3), maximum altitude 88 km. On these flights ionospheric conditions were normal.

There were small indications of x-rays on the fourth flight, but they appear contradictory because the value from 19–82 km exceeds that from 82–127 km. It is entirely possible that solar x-rays are emitted from the sun in bursts and may vary during a flight; but until evidence of this sort is repeated, we do not consider it conclusive.

2. Penetration of the Band 1050–1340A

Solar radiation of wavelengths between 1050 and 1340A was observed to reach levels in the atmosphere between 80 and 90 km. This can be seen from Tables

TABLE II. Data obtained from experiments 1, 2, and 3.

Experiment	1	2	3
Time of firing (MST)	November 18, 1948, 3:34 P.M.	February 17, 1949, 10:00 A.M.	April 11, 1949 3:05 P.M.
Maximum height attained in km above sea level	146	128	88
Height during exposure in km	1–146–1	49–128–86	54–88–17
Estimated "effective" exposure time in minutes	1.5	1	0.5
Phosphor area in cm²	1.61	1.61	0.65
Solar activity during flight	Normal	Sudden ionospheric disturbance	Normal
Thermoluminescence of recovered strip in microamp-sec			
with Be filter (<8A)	Doubtful	0.10	0.000
with LiF filter (1040–1340A)	0.01	0.52	0.008
with CaF_2 filter (1230–1340A)	0.005	0.29	0.000
with no filter (<1340A)	0.05	1.14	0.034
Control strip flown ÷control strip grounded	0.014	0.19	0.23

TABLE III. Data obtained from experiment 4.

Time of firing: February 17, 1950, 11:01 A.M. MST
Maximum height attained: 150 km above sea level
Solar activity during flight: No flares or sudden ionospheric disturbance observed
Phosphor area 0.65 cm²

Exposure position	1	2	3
Height during exposure in km above sea level	19–82	82–127	127–148
Effective exposure time in sec	1.5	3	3
Thermoluminescence of recovered strip in microamp-sec			
with Be filter 0.1 mm (<8A)	0.040	0.024	damaged
with LiF filter 1.5 mm (1040–1340A)	0.012	0.126	damaged
with CaF_2 filter 1.6 mm (1230–1340A)	damaged	0.019	damaged
with no filter (<1340A)	0.073	5.84	8.87
Control strip flown ÷control strip grounded	damaged	0.79	0.91

[17] D. M. Packer and C. Lock, J. Opt. Soc. Am. **40**, 264 (1950).

[18] T. R. Burnight, Phys. Rev. **76**, 165 (1949).

II and III. In experiment 3 a positive response was obtained for the LiF-covered strip, and the highest altitude reached was 88 km. In experiment 4, exposure 1, a response was recorded for the LiF-covered strip and the maximum altitude reached during the exposure was 82 km. This result was expected from theoretical grounds; as shown in Fig. 1, one percent of the incident radiation in the wavelength range 1000 to 1300A, on the basis of laboratory measurements of the transmission of air, would penetrate to 90 km or lower.

3. Penetration in the Band 1240–1340A

In the spectral band 1240–1340A considerable intensity was observed in experiment 2 for the altitude range 49–128–86 km, and in experiment 4, for the altitude range 82–127 km. In absolute value the response in experiment 2 was greater than in experiment 4 because the exposure time above 90 km was much greater, owing to the fact that the exposure covered the entire top of the trajectory. For the altitude range below 88 km, covered in experiment 3, no response in this band was recorded. Thus, the penetration altitude for radiation between 1240 and 1340A appears to lie somewhere between 90 and approximately 125 km.

TABLE IV. Comparison of responses observed in experiment 4 with values calculated for a blackbody.

	6000°K BB	5000°K BB	Observed
R with LiF (μa-sec)	3.8	0.082	0.25
R with CaF_2 (μa-sec)	2.1	0.052	0.04
Ratio	1.8	1.6	6.6

This result is reasonable, theoretically, since the absorption data for oxygen, as shown in Fig. 1, indicate that 1340A penetrates (1 percent) to 100 km and 1240A to 82 km.

4. Penetration in the Band 795–1050A

The radiation in the band 795–1050A can be obtained approximately by subtracting from the bare phosphor response (0–1350A), the responses through Be (0–10A) and through LiF (1050–1350A), after making correction for the filter transmission. The radiation below 795 was presumably largely absorbed by N_2 at all altitudes reached in these flights. Furthermore, the phosphor sensitivity, as indicated by Fig. 2, became rapidly decreased below 1050A. Soft x-rays above 10A may have contributed a small amount to the observed response, however.

There is good evidence, from flight (4), exposure 2, that wavelengths from 795 to 1050A were present in considerable intensity in the altitude range 88–127 km, for the response of the bare strip was nearly 50 times that of the strip covered with LiF, and the x-ray response was so small as to be doubtful. From exposure 1 on this flight there is some evidence that radiation in this band penetrates below 88 km; however, the bare strip response was only 6 times the LiF-covered response; this was so close to the 3 times reduction expected because of the transmission of LiF that the conclusion is not regarded as positive.

The response of the bare strips in experiment 4 over the range 127–148 km was 50 percent greater than from 82–127 km, and the effective exposure times were approximately equal. This is compatible with the idea that most of the radiation as seen by the bare phosphor penetrates with little absorption to 127 km, but becomes absorbed in the interval 88 to 127 km. For altitudes above 127 km, it can be seen from Fig. 1 that there is little attenuation by air, especially if the oxygen is dissociated.

CALCULATION OF SOLAR EXTREME ULTRAVIOLET INTENSITIES

Certain numerical values of solar radiation intensity can be calculated from the data obtained in experiment 4 because the phosphor and filters used in this flight were calibrated and a good record of the rocket motion during the exposures was available.

The total measured response of the phosphor, R, may be expressed by the following equation:

$$R=\int_{\lambda_1}^{\lambda_2} H_\lambda S_\lambda T_\lambda d\lambda \int A(\theta,\phi)dt, \qquad (1)$$

where H_λ is the solar spectral intensity. S_λ is the sensitivity of the phosphor and was known. The filter transmittance T_λ was measured for normal incidence, and corrections for departures from normal incidence could be neglected because of the relatively small field of view. The function $A(\theta, \phi)$ is the area of phosphor normal to sunlight, and the second integral gives the total effective exposure and was calculated from data on the rocket aspect during flight. It was possible to solve Eq. (1) approximately for the total energy over the band 1050–1240A. This could be done without knowing the detailed nature of H_λ because $S_\lambda T_\lambda$ is nearly constant over this wavelength interval, as shown in Fig. 2.

The total radiation $\int H_\lambda d\lambda$ for the band 1050–1240A, computed in this way, was 0.04 μw/cm^2. This value applies for the altitude range 82–127 km, and is considered correct within a factor of 2. The value completely above all absorbing gases would be somewhat, but probably not greatly, higher because, as shown in Fig. 1, this wavelength band is transmitted without great attenuation to 90 km.

A calculation was also made for the energy within the band 1230–1340A recorded by the CaF_2 filter and phosphor. In this case $S_\lambda T_\lambda$ cannot be considered constant over the wavelength interval. It is necessary to make some assumption concerning the nature of H_λ. Making the simplest assumption possible, that H_λ is constant over this narrow interval, the result for total

energy was 0.02 μw/cm^2. The accuracy of this result is low because the original datum from which it was computed is small and therefore, subject to considerable error, and because the nature of the spectrum is unknown over this interval.

We shall now consider several possible assumptions concerning the detailed nature of the solar intensity distribution in the neighborhood of Lyman α and see whether the observed data favor one or the other picture of the spectrum. The first assumption is that the spectrum is a blackbody, and that Lyman α is not important either in emission or absorption. The second assumption is that most of the energy in the region 1040–1340A is concentrated in Lyman α in emission. The third assumption is that the spectrum is described by a blackbody, with Lyman α a strong and broad absorption line with a narrow and intense emission line at its center.

The assumption of a pure blackbody distribution can be shown to be in poor agreement with the data over the range 1040–1340A. In Fig. 3, curve A represents a 6000° blackbody distribution, while curves B and C show the response of the phosphor, $H_\lambda S_\lambda T_\lambda$, to this radiation with LiF and CaF_2 filters, respectively. Numerical values of response through the filters and of the response ratio were calculated for 6000°K from these curves, and similarly for 5000°K, and are given in Table IV. The calculated response ratio is below 2 and does not change rapidly with temperature while the observed ratio is between 6 and 7.

The assumption of a pure emission line, on the other hand, does not agree with the experimental data, because, for any reasonable half-width, no energy should be present in the spectral range 1230–1340A. In flights (1), (2), and (4) definite responses were obtained in this spectral range.

Thus the true situation must be more complicated, and it is probable that the spectrum is a continuum upon which Lyman α is superimposed as a wide absorption line with a narrow emission line at its center.

The intensity of solar radiation in the band 795–1050A can be shown, from the data of flight (4), to be well above that produced by a 6000°K blackbody sun. The response in this band was calculated from exposure

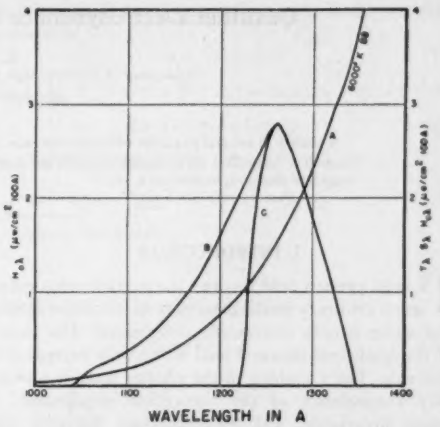

FIG. 3. Curve A is the spectral intensity distribution for a 6000°K blackbody sun. Curves B and C are the calculated response curves for the $CaSO_4$:Mn phosphor with LiF and CaF_2 filters, respectively, when exposed to the 6000°K blackbody spectrum.

2 by subtracting the Be- and LiF-covered strip exposures from the bare strip exposure, after correcting for the filter transmission and the decay of stored energy. The quantum efficiency of the phosphor with respect to thermoluminescence was 5 to 10 percent at 1050A and about half as much at 800A. From these data it was estimated that the flux was between 5×10^{11} and 3×10^{12} quanta per cm^2 per sec. If the sun is taken as a blackbody at 6000°K, the flux for wavelengths below 1050A would be 2.3×10^{19} quanta per cm^2 per sec. Thus, the observed radiant intensity at 82–127 km was one to two orders of magnitude greater than that expected from a blackbody at 6000°K.

Our thanks are due Mr. John R. Pierce of the New Mexico College of Agriculture and Mechanic Arts, who carried out the installation and calibration work at the White Sands Proving Ground. We wish also to express appreciation to Professor Theodore Lyman, who was among the first to suggest flying this phosphor in rockets and who has followed the course of this work with great interest.

Quantum Electrodynamics with Nonvanishing Photon Mass

F. COESTER
Department of Physics, State University of Iowa, Iowa City, Iowa
(Received March 26, 1951)

A theory of neutral particles with spin one and arbitrary mass κ in interaction with electrons is developed in such a form that all observable results go over continuously into the corresponding results of ordinary quantum electrodynamics as $\kappa \to 0$.

I. INTRODUCTION

IN most present field theories the particle mass enters as an arbitrary continuous parameter whose numerical value is only empirically determined. The theory of the quantized maxwell field is the only exception to this rule. The vanishing of the photon mass is a necessary consequence of the theoretical requirement of gauge invariance, and the quantized maxwell field $A_\mu(x)$ cannot be regarded in a straightforward manner as a limiting case of a quantized Proca field $\mathcal{A}_\mu(x)$. The two fields satisfy, respectively, the commutation rules[1]

$$[A_\mu(x), A_\nu(x')] = -ig_{\mu\nu}D(x-x') \tag{1}$$

and

$$[\mathcal{A}_\mu(x), \mathcal{A}_\nu(x')] = -i\left(g_{\mu\nu} - \frac{1}{\kappa^2}\partial_\mu\partial_\nu\right)D(x-x'), \tag{2}$$

where D depends[2] continuously on κ. Equation (2) becomes singular as $\kappa \to 0$. This is related to the fact that $\mathcal{A}_\mu(x)$ satisfies by definition the operator identity

$$\partial_\nu \mathcal{A}^\nu = 0, \tag{3}$$

while no such identity can be imposed on the maxwell field; but a subsidiary condition on the state functionals yields

$$\langle \partial_\nu A^\nu \rangle = 0. \tag{4}$$

Furthermore, the hamiltonian density $-j^\mu(x)\mathcal{A}_\mu(x)$, which would be analogous to the interaction of the maxwell potential with the current, does not satisfy the integrability condition for the Schwinger-Tomanaga equation, since[3]

$$[\mathcal{A}_0(x), \mathcal{A}_k(x')]_{t=t'} = \frac{i}{\kappa^2}\frac{\partial}{\partial x^k}\delta(x-x'). \tag{5}$$

In view of this situation and the common emphasis on the requirement of gauge invariance in quantum electrodynamics, it may be of interest to construct a theory of neutral particles with spin one and arbitrary mass which gives the same observable results as ordinary quantum electrodynamics with any desired accuracy, provided the photon mass is sufficiently small.[4] To achieve this the theory must satisfy the following requirements:

1. The field equations for the expectation values go over continuously into Maxwell's equation.

2. The theory must account for the fact that no longitudinal or scalar photons are observed.

II. THE FREE PHOTON FIELD

Let $A_\mu(x)$ be a vector field satisfying the Klein-Gordon equation

$$(\Box - \kappa^2)A_\mu(x) = 0, \tag{6}$$

and the commutation rules

$$[A_\mu(x), A_\nu(x')] = -ig_{\mu\nu}D(x-x'), \tag{7}$$

where $D(x-x')$ is the same function as in (2) satisfying (6). $A_\mu(x)$ is not restricted by any operator identity.[5]

It is well known that such a field describes particles with both spin one and spin zero. Their contributions to A_μ can be separated by defining a scalar field $B(x)$ by

$$B(x) = (1/\kappa)\partial_\mu A^\mu, \tag{8}$$

and a vector field $\mathcal{A}_\mu(x)$ by

$$A_\mu(x) = \mathcal{A}_\mu(x) + (1/\kappa)\partial_\mu B. \tag{9}$$

As a consequence of Eqs. (7)–(9), $\mathcal{A}_\mu(x)$ satisfies the commutation rules (2) and the identity (3). In addition, we have

$$[\mathcal{A}_\mu(x), B(x')] = 0 \tag{10}$$

and

$$[B(x), B(x')] = iD(x-x'). \tag{11}$$

If $\mathcal{A}_\mu(x)$ is a hermitian operator, its positive and negative frequency[6] parts $\mathcal{A}_\mu^{(+)}$ and $\mathcal{A}_\mu^{(-)}$ contain annihilation and creation operators of the spin-one photons, respectively. For hermitian $B(x)$, however, the roles of $B^{(+)}$ and $B^{(-)}$ are interchanged because of the sign on the right-hand side of (11). $B^{(+)}$ contains the

[1] $\hbar = c = 1$.

[2] For the definition of the D-function see, for instance, W. Pauli, Revs. Modern Phys. **13**, 211 (1941).

[3] This has been pointed out by F. J. Belinfante, Phys. Rev. **76**, 66 (1949), who satisfies the integrability condition by adding a surface dependent term to the interaction. The theory becomes thereby considerably more involved than quantum electrodynamics.

[4] See F. J. Belinfante, Phys. Rev. **75**, 1321(A) (1949), **76**, 66 (1949).

[5] Our formalism is somewhat similar to the vector meson theory proposed by E. C. G. Stueckelberg, Helv. Phys. Acta **11**, 225 (1938). However, our subsidiary condition (24) or (35) is different and does not require the introduction of an additional scalar field.

[6] For the definition of the positive and negative frequency parts of any field operator see J. Schwinger, Phys. Rev. **75**, 651 (1949), Eqs. (1.19) and (1.16).

creation operators, $B^{(-)}$ the annihilation operators. In the S-matrix formalism, where one expands into a sum of "ordered" terms in which all positive frequency parts stand to the right of all negative frequency parts, it may be desirable to have $A_\mu^{(+)}$ contain annihilation operators only. Since the expectation values of $A_\mu(x)$ must be real, this cannot be achieved if they are defined in the usual way. There is, however, a possibility of defining the expectation value of any operator F with the help of an indefinite metric η in Hilbert space:[7]

$$\langle F\rangle=(\Psi,\eta F\Psi), \tag{12}$$

where η is an hermitian operator satisfying $\eta^2=1$. If η commutes with $\mathcal{A}_\mu$ and anticommutes with B, all expectation values are real if $\mathcal{A}_\mu$ is hermitian and B is antihermitian. For antihermitian B, $B^{(+)}$ contains the annihilation operators. The existence of such an η can be proven by pointing out an explicit matrix representation:

$$(N'|\eta|N)=(N'|1|N)(-1)^{N_s}, \tag{13}$$

where N_s is the total number of scalar photons present and N and N' stand for the complete set of all photon numbers. As far as the scope of the present paper is concerned, we shall see that the definitions of the expectation values with or without indefinite metric in Hilbert space are equally satisfactory. In order to make the energy positive definite we must require the absence of scalar photons, which is expressed by the subsidiary condition

$$B^{(-)}(x)\Psi=0 \tag{14a}$$

or

$$B^{(+)}(x)\Psi=0, \tag{14b}$$

in the two alternative cases.

III. THE FIELD EQUATIONS FOR THE EXPECTATION VALUES

If the field is interacting with a current $j^\mu(x)$, the state functional $\Psi(\tau)$ in the interaction representation[8] satisfies the Schrödinger equation

$$i\partial\Psi(\tau)/\partial\tau=H(\tau)\Psi(\tau), \tag{15}$$

with

$$H(\tau)=-\int_{\sigma(\tau)} d\sigma j^\mu(x)A_\mu. \tag{16}$$

Consequently, the expectation values satisfy the equations

$$(\Box-\kappa^2)\langle A_\mu\rangle=-\langle j_\mu\rangle, \tag{17}$$

and

$$\partial\langle j^\mu\rangle/\partial x^\mu=\langle\partial_\mu j^\mu\rangle=0, \tag{18}$$

the equation for the field strengths

$$F_{\mu\nu}=(\partial\langle A_\nu\rangle/\partial x^\mu)-\partial\langle A_\mu\rangle/\partial x^\nu$$

go over into Maxwell's equations as $\kappa\to 0$ if we require in addition

$$\partial\langle A_\mu\rangle/\partial x^\mu=0. \tag{19}$$

Since $[H, A_\mu]=0$ if x lies on the surface $\sigma(\tau)$, we have

$$\partial\langle A^\mu\rangle/\partial x^\mu=\langle\partial^\mu A_\mu\rangle. \tag{20}$$

From (17), (18), and (20) follows

$$(\Box-\kappa^2)\langle\partial^\mu A_\mu\rangle=0. \tag{21}$$

Therefore, the identity,

$$\langle\partial^\mu A_\mu\rangle=0, \tag{22}$$

is equivalent to the initial condition

$$\langle\partial^\mu A_\mu\rangle_{\tau=\tau_0}=0, \tag{23}$$

$$\left(\frac{\partial}{\partial\tau}\langle\partial^\mu A_\mu\rangle\right)_{\tau=\tau_0}=\langle\partial\partial^\mu A_\mu-n^\nu j_\nu\rangle=0, \tag{24}$$

which in turn is equivalent to

$$\langle\Omega(x,\tau_0)\rangle_{\tau_0}=0 \quad \text{for all } x, \tag{25}$$

where the expectation value in (25) is taken with $\Psi(\tau_0)$ and $\Omega(x,\tau_0)$ is defined by

$$\Omega(x,\tau_0)=\partial^\mu A_\mu-\int_{\sigma(\tau_0)} d\sigma' n^\nu j_\nu(x')D(x-x'). \tag{26}$$

The proof of this equivalence is the same as that for the equivalence of (9) and (16) in A. That (25) can always be satisfied is easily seen with the help of a canonical transformation

$$\Phi(\tau)=e^{-i\Sigma(\tau)}\Psi(\tau), \tag{27}$$

where

$$\Sigma(\tau)=-(1/\kappa)\int_{\sigma(\tau)} d\sigma' j^\mu(x')n_\mu B(x'). \tag{28}$$

In the new representation Ω becomes

$$\begin{aligned}\Omega'&=\exp[-i\Sigma(\tau_0)]\Omega(x,\tau_0)\exp[i\Sigma(\tau_0)]\\&=\Omega(x,\tau_0)-i[\Sigma(\tau_0),\Omega(x,\tau_0)]=\partial^\nu A_\nu.\end{aligned} \tag{29}$$

The condition

$$(\Phi(\tau_0), B(x)\Phi(\tau_0))=0, \tag{30a}$$

or for all x

$$(\Phi(\tau_0), \eta B(x)\Phi(\tau_0))=0, \tag{30b}$$

can always be satisfied by requiring

$$B^{(-)}(x)\Phi(\tau_0)=0, \tag{31a}$$

or

$$B^{(+)}(x)\Phi(\tau_0)=0, \tag{31b}$$

which means absence of scalar photons. The corresponding Ψ satisfying (25) is obtained by the transformation (27). $\Phi(\tau)$ satisfies the Schrödinger equation

$$i\partial\Phi/\partial\tau=G(\tau)\Phi, \tag{32}$$

[7] This procedure is analogous to the one introduced into ordinary quantum electrodynamics by S. N. Gupta, Proc. Phys. Soc. (London) **63**, 681 (1950), and K. Bleuler, Helv. Phys. Acta **23**, 567 (1950), in order to secure a normalizable vacuum state.

[8] For definition of the notation see F. Coester and J. M. Jauch, Phys. Rev. **78**, 149 (1950), quoted in the following as A.

where

$$G(\tau)=-\int d\sigma j^\mu \mathcal{A}_\mu-\frac{1}{2\kappa^2}\int_{\sigma(\tau)} d\sigma \int_{\sigma(\tau)} d\sigma' j^\nu(x) \times j^\mu(x')n_\mu\partial_\nu D(x-x'). \quad (33)$$

The scalar field has been eliminated from the hamiltonian.[9]

IV. EVALUATION OF THE S-MATRIX

In order to state the subsidiary condition for the initial state $\Psi(-\infty)$ in the S-matrix formalism, we notice that[10]

$$\lim_{\tau_0\to-\infty}\Omega(x,\tau_0)=\partial^\nu A_\nu. \quad (34)$$

The subsidiary condition is therefore

$$B^{(-)}\Psi(-\infty)=0, \quad (35a)$$

if expectation values are defined in the usual way, or

$$B^{(+)}\Psi(-\infty)=0, \quad (35b)$$

if they are defined with an indefinite metric η. However, B can be eliminated from the S-matrix without using (35). The nth-order term in the S-matrix

$$S^{(n)}=(i^n/n!)\int dx_n\cdots\int dx_1 P(j^{\mu_n}(x_n)\cdots j^{\mu_1}(x_1)) \times P(A_{\mu_n}(x_n)\cdots A_{\mu_1}(x_1)) \quad (36)$$

is expanded into a sum of ordered products in the manner described in A, Sec. V. In the ordered products of the vector-potentials we replace A_μ by the right-hand side of (8) and notice that all terms containing B vanish. This follows from the proof of Eq. (82) of A without the use of (35). If (35) holds for the initial state, it will also hold for the final state.

[9] The details of the calculation are similar to those of the derivation of (34) in A.

[10] See A, Eq. (69).

In order to investigate the behavior of the longitudinal photons, we define a longitudinal field $\Lambda(x)$ by

$$\Lambda(x)=\frac{\partial\partial^\nu-\kappa^2 n^\nu}{\kappa[-(\kappa^2+\partial^2)]^{\frac{1}{2}}}A_\nu(x). \quad (37)$$

This Λ commutes with B and satisfies the commutation rules,

$$[\Lambda(x),\Lambda(x')]=-iD(x-x'). \quad (38)$$

It describes, therefore, creation and annihilation of longitudinal photons in the usual way. The transverse field $\mathfrak{A}_\mu$ satisfying $n^\mu\mathfrak{A}_\mu=0$ and $\partial^\mu\mathfrak{A}_\mu=0$ is defined by

$$\mathcal{A}_\mu(x)=\mathfrak{A}_\mu(x)+\frac{\partial\partial_\mu-\kappa^2 n_\mu}{\kappa[-(\kappa^2+\partial^2)]^{\frac{1}{2}}}\Lambda(x). \quad (39)$$

Terms proportional to $\partial_\mu\Lambda$ do not contribute anything in the S-matrix for the same reason which made it possible to eliminate the scalar field. We may therefore replace finally A_μ in the ordered products in the S-matrix by

$$\mathfrak{A}_\mu-\frac{\kappa(n_\mu+\partial^{-1}\partial_\mu)}{[-(\kappa^2+\partial^2)]^{\frac{1}{2}}}\Lambda.$$

The probability for the emission of a longitudinal photon of momentum k will therefore be $\kappa^2/(\kappa^2+k^2)$ times the probability for the emission of a corresponding transverse photon. For sufficiently small but non-vanishing photon mass one cannot expect to observe any longitudinal photons. The part of S which contains the transverse field $\mathfrak{A}_\mu(x)$ goes over continuously into the corresponding expressions of ordinary quantum electrodynamics only as $\kappa\to 0$.

We have shown that it possible to construct a non-gauge invariant quantum electrodynamics with non-vanishing photon mass in agreement with observation. The requirement of gauge invariance has, of course, a strong aesthetic appeal, but it is not warranted by observations alone.

The Dielectric Constant of Barium Oxide*

RENATE S. BEVER AND ROBERT L. SPROULL
Cornell University, Ithaca, New York

(Received January 15, 1951)

The availability of crystals of BaO made possible an investigation of the low frequency dielectric constant κ of BaO. This has been measured over the frequency range 60 to 6×10^7 cycles per second and the temperature range $-25°$ to 60°C. Over these ranges κ is about 34, which is quite different from the value of 14 frequently quoted. There is some evidence for a rise in κ at the lowest frequencies. Data on dielectric loss is presented.

I. INTRODUCTION

THE purpose of this investigation was to measure the low frequency dielectric constant κ of barium oxide. A knowledge of κ is useful in the interpretation of the relation between optical and thermal excitation processes, since estimates of the energy of lattice relaxation can be made[1] using the values of κ and of κ_0 (the "optical" or "high frequency" dielectric constant).[2] The value of κ of BaO has also been used[3] in attempts to explain the high dielectric constant of barium titanate, but such attempts appear[4] to have been approximations.

κ for BaO does not appear to have been measured,[5] but a value of 14.3 is sometimes quoted.[3] This has its origin in a paper by Højendahl,[6] who extrapolated this number on the basis of immersion-method determinations of the static dielectric constants of BeO, MgO, CaO, and SrO. His immersion liquids were dried with silica gel, which is thought to be a less effective drying agent than CaO.[7] Hence, the values for CaO of 11.8 and SrO of 13.3 may be in error because of contamination by hydroxide.

In the work reported here, the dielectric constant was determined from 60 cycles to 60 Mc to find out whether it was frequency sensitive. In this connection the dissipation factor was also measured, since any dispersion phenomena are often more easily detectable in this quantity than in the dielectric constant.

II. EXPERIMENTAL PROCEDURE

A method for growing crystals of barium oxide from the vapor phase has recently been developed in this laboratory.[8] Thus it was possible to use the plate method of measuring the dielectric constant of single crystals. The same technique of measurement was also used on dense polycrystalline deposits grown directly on circular platinum electrodes, as shown in Fig. 1(a). The use of such deposits allowed a more easily controllable geometry. The plate method is greatly superior to the immersion method in the case of BaO, since this substance is exceedingly hygroscopic,[7] very reactive, and has a conductivity high compared with that of most immersion liquids.

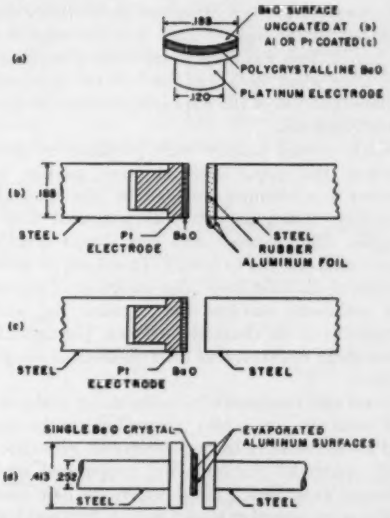

FIG. 1. Parts (a), (b), and (c) illustrate the use of a sample composed of dense, polycrystalline BaO grown on a platinum electrode. (a) shows the electrode with BaO coating. (b) is a cross section of the electrode configuration using a thin aluminum foil contact pressed against the BaO surface. (c) is an arrangement similar to (b) but using an evaporated aluminum or sputtered platinum contact to the BaO. (d) shows the configuration for study of a single crystal with plane parallel faces on which aluminum electrodes have been evaporated. Dimensions are given in inches.

* This work has received support from the ONR and from the Research Corporation.

[1] N. F. Mott and R. W. Gurney, *Electronic Processes in Ionic Crystals* (Oxford University Press, London, 1948), pp. 160 ff.; J. H. Simpson, Proc. Roy. Soc. (London) **197**, 269 (1949).

[2] κ_0 has been found by M. Haase, Z. Kryst. **65**, 534 (1927), to be 4.0.

[3] G. H. Jonker and J. H. van Santen, Chem. Weekblad **43**, 672 (1947); B. T. Matthias, Phys. Rev. **75**, 1771 (1949); S. Roberts, Phys. Rev. **76**, 1215 (1949).

[4] A. von Hippel, Revs. Modern Phys. **22**, 236 (1950).

[5] A preliminary value of 37 was reported from this laboratory in Tech. Rept. No. 2 (unpublished).

[6] K. Højendahl, Kgl. Danske Videnskab. Selskab, Mat.-fys. Medd. **16**, No. 2 (1938).

[7] J. H. Bower, J. Research Natl. Bur. Standards **33**, 199 (1944). From the chemical properties of MgO, CaO, SrO, and BaO it appears likely that SrO is an even better drying agent than CaO.

[8] Sproull, Dash, Tyler, and Moore, Rev. Sci. Instr. **22**, 410 (1951).

TABLE I. Dielectric constant of BaO at 0.5 Mc.

Sample No.	Electrode assembly	Measuring instrument	ΔC $\mu\mu f$	Area cm^2	Thickness cm	κ
3*P*	Fig. 1c	C-meter	24.5±0.2	0.181±0.004	0.0231±0.0005	36±2
4*P*	1c	C-meter	18.3±0.2	0.181	0.0283	33±2
5*P*	1c	C-meter	25.4±0.2	0.181	0.0193	31.5±2
6*P*	1b	C-meter	7.1±0.2	0.172	0.0676	32.5±2
7*P*	1c	Q-meter	13.3±0.5	0.181	0.0393	33.5±2.5
2*S*	1d	C-meter	15.0±0.2	0.226	0.0437	34±1.5
3*S*	1d	C-meter	10.3±0.2	0.106	0.0297	33.5±2.5
4*S*	1d	C-meter	6.0±0.2	0.044	0.0198	32±5
5*S*	1d	Q-meter	14.0±0.5	0.482	0.0940	32±2

(1) Sample Preparation

All samples were prepared in the atmosphere of a dry box, containing porous BaO and a liquid air trap as desiccants.

For polycrystalline BaO, the free surface was polished in a jig so that it was parallel to the platinum-BaO interface, to a tolerance of 0.0004 in. The diameter at the electrode-BaO interfaces was made equal to that of the electrodes, 0.188 in., to within ±0.003 in., as shown in Figs. 1(b) and 1(c). An attempt was made to grind the peripheral surface to a curvature qualitatively like that expected for the lines of force near the edge of an air condenser. This was done to minimize distortion of the field lines when BaO was used as the dielectric and made estimation of the edge effects easier, as discussed in the Appendix.

Single crystal samples were prepared by manually grinding the major surfaces plane parallel to one another to a tolerance of 0.0008 in. The electrode configuration shown in Fig. 1(d) was used with these samples. The electrode area was always considerably larger than the BaO crystals. Therefore, to avoid distortion of the field lines upon insertion of the sample, the peripheral surfaces were ground flat and perpendicular to the electrode surfaces. The crystals were rectangular in shape, and their dimensions are given in Table I.

Good electrical contacts to the major surfaces of the BaO were very important, since all specimens were thin and κ was found to be high compared with that of air. Both sputtered platinum and evaporated aluminum coatings were used, against which the bare steel electrodes were pushed as shown in Figs. 1(c) and 1(d). The samples could be mounted and sealed in the evaporator while it was inside the dry box. The sealed evaporator was then transfered to a pumping station, thus avoiding exposure of the BaO to moist air. The undesirable metallic coating on the peripheral surfaces was later carefully removed with a razor blade under a microscope.

To check whether the above technique caused any penetration of metallic material into the polycrystalline deposits, contact to the BaO surface was also made by pressing aluminum foil against it as shown in detail in Fig. 1(b). Use of this method also permitted rapid changing of the sample thickness.

(2) Measuring Method and Apparatus

The measurements had to be carried out in a dry atmosphere, so a small, 6-inch diameter dry box was constructed which contained porous BaO as desiccant. While the small box was inside the large dry box, the sample was inserted between the electrodes and the small box sealed. One electrode in the small dry box was fixed, the other movable by means of a micrometer screw. A General Radio Type 846 CK variable capacitor (called "C_B" below) was mounted inside the small dry box close to the sample and connected in parallel with it by short leads. Short, wide copper strips were used as leads to outside measuring equipment to minimize lead inductance. All seals in the box were "O-ring" gaskets.

The well-known substitution or compensation method was employed, measurements being made on the entire electrode assembly first with and then without the sample. The dissipation factor, D, and change of parallel capacitance, ΔC, caused by the BaO was then calculated (D is the same as tan δ, which is defined as the ratio of the imaginary part to the real part of the complex dielectric constant). In the case of the polycrystalline BaO the background measurements were made after either replacing the BaO-coated electrode by a dummy platinum electrode, or introducing an air gap of thickness equal to that of the sample between one electrode and the free BaO surface. The latter method causes an error of about 0.1 percent in the measured capacitance change for a substance of dielectric constant about 30. In the case of single crystals, the background measurements could be made after simply removing the sample while leaving the electrode spacing constant.

Several measuring circuits were employed. The most accurate capacitance measurements (to ±0.1 $\mu\mu f$) could be made with a 0.5-Mc heterodyne beat oscillator capacitance meter (called "C-meter" in Table I), developed by Dr. H. S. Sack, which supplied 66 volts across the sample. It was realized that shunting the tank circuit of a feed-back oscillator with a high loss

condenser causes a decrease of voltage output and a frequency change greater than to be expected from the capacitance of the condenser. By calibration with parallel combinations of resistance and capacitance it was found that this effect caused negligible error in this work, the BaO shunt resistance being of the order of several hundred megohms. In order to test the validity of our method, single cleaved crystals of magnesium oxide[9] were measured on this instrument. The dimensions were similar to those of the BaO samples. With the aluminum foil contact on uncoated crystals an average of 9.3 ± 0.1 was obtained for κ. Electrode assembly Fig. 1(d) gave κ as 9.5 ± 0.05. This latter value is in satisfactory agreement with the results cited by Højendahl,[6] which range from 9.25 to 9.93.

The range from 50 kc to 60,000 kc was explored with a Boonton Q-meter, Type 160-A, using the condenser C_B for compensation. C_B was calibrated with a General Radio Type 722N precision condenser, and capacitance increments could be measured to ±0.5 $\mu\mu$f. As a check of possible lead inductance errors at high frequencies, a thin plate of mica was used as the dielectric in the electrodes of Fig. 1(c). The capacitance increments at 500 kc agreed with those measured on the 0.5-Mc capacitance meter to ±2 percent and stayed constant within random errors up to 60 Mc. The accuracy of the D measurements was good to about ±0.002 up to 20 Mc. Above this frequency the inductance of the leads external to the dry box became important and caused greater scattering of the points when different inductors were used.

A General Radio Type 650-A Impedance Bridge served from 0.060 kc to 3 kc. At higher frequencies than this, ground capacitance errors became appreciable. The audiofrequency power for the bridge was supplied through a step-up shielded transformer from a Hewlett-Packard Type 200-B oscillator. The voltage across the crystal was usually about 50 volts. A Hewlett-Packard Type 400-H vacuum tube voltmeter was used as detector. Capacitance increments could be measured to ±0.5 $\mu\mu$f. Dissipation factor measurements were usually better than 10 percent. The direct reading bridge dials gave series capacitance; from this and the dissipation factor the equivalent parallel capacitance could be calculated. The instrument was calibrated with both MgO crystals and artificial dielectrics made up of parallel combinations of carbon resistors and mica condensers. The parallel capacitance of these samples stayed constant to within ±0.3 $\mu\mu$f from 0.06 to 3.0 kc. These measurements agreed with the 0.5-Mc capacitance meter measurements within ±0.5 $\mu\mu$f. The parallel resistance stayed constant from 0.06 to 0.75 kc, but decreased beyond this due to ground capacitance errors, reaching a value 20 percent lower at 3 kc than at 0.75 kc.

The dc resistance of the BaO crystals was estimated by putting 45 volts in series with them and measuring the current. Accurate values could not be obtained, due to a current decay effect with time which is not as yet well understood.

[9] Obtained from the Norton Company, Niagara Falls, Canada.

III. EXPERIMENTAL RESULTS

The results of measurements of κ at 0.5 Mc are summarized in Table I, where ΔC stands for the capacitance increment caused by insertion of the sample, and κ is calculated from the simple formula (later justified in the Appendix):

$$\kappa=1+(4\pi t\Delta C)(1/A).$$

Here t is the sample thickness, and A is the sample area. Samples marked P were polycrystalline, those marked S were single crystals.

From Table I it can be concluded that the average dielectric constant is 34, with an average deviation from the mean due to random errors of ±1. A much more serious uncertainty is caused by hydroxide formation.[10] It is thus felt that κ might be as high as 37, but probably not lower than 33.

Typical results of the measurements of κ and D as a function of frequency from 60 cycles to 60 Mc are shown in Fig. 2 for polycrystalline sample No. 5P, and in Fig. 3 for single crystals Nos. 2S and 5S.

In the region from 50 kc to 60 Mc, κ is constant within random errors. The slight decrease of κ towards 50 Mc for No. 5P is not thought to be significant and did not occur in other samples. The rise of D with frequency, beginning at about 1 Mc may indicate dispersion phenomena in the microwave region. This rise seemed to

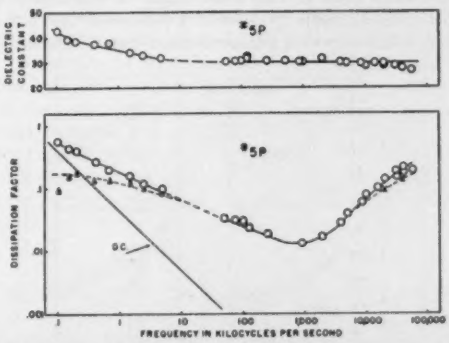

FIG. 2. Dielectric constant and dissipation factor as a function of frequency of a polycrystalline sample, No. 5P, at 25°C. The circles are measured data points. The line marked "dc" shows computed loss due to the measured dc resistance of 120 megohms. The triangles are total loss minus computed dc loss. The crosses represent the dissipation factor corrected approximately for lead inductance.

[10] The measurements summarized in Table I were made immediately after sample preparation. When the same specimens were used to make measurements as a function of frequency several days later, κ had often decreased from 34 to about 32. Bridge measurements and Q-meter measurements as shown in Figs. 2 and 3 did not always join continuously because of this same deterioration with time.

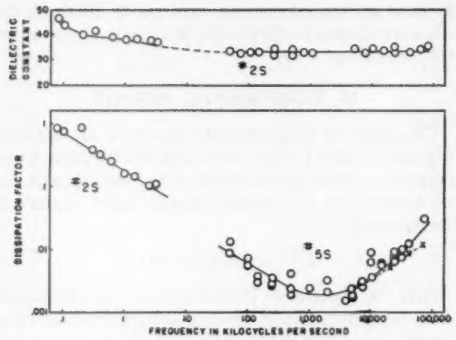

FIG. 3. Dielectric constant and dissipation factor as a function of frequency of single crystals No. 2S and No. 5S, at 25°C. The circles are measured data points. The crosses represent dissipation factor corrected approximately for lead inductance.

start at a somewhat higher frequency in the case of the single crystals than for the polycrystalline material. Above 20 Mc the effect of the inductance of the leads external to the dry box was to make D appear too high. Approximately corrected points are marked by crosses in Figs. 2 and 3 and were obtained using a lead inductance value of 0.15 μhenry as calculated from a lumped circuit theory based on measurements at 40 and 55 Mc.

The behavior with decreasing frequency below 2 kc is somewhat unusual. The dielectric constant apparently increases, as does the dissipation factor, with a slope less steep than 1. This slope might be explainable as being due to a superposition of a nearly constant ac loss and a dc loss having a slope of magnitude 1. The dc loss

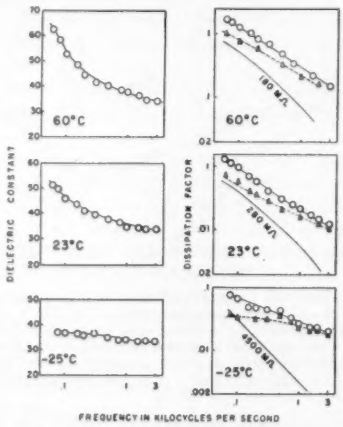

FIG. 4. Dielectric constant and dissipation factor as a function of frequency of a single crystal, No. 3S, at three different temperatures. The circles are measured data points. The line without data points shows computed loss due to the indicated dc resistances, which were measured in a separate experiment. The triangles are total loss minus computed dc loss.

was computed from the estimated values of dc resistance and subtracted from the measured loss to give the "net ac" loss as marked by triangles in Figs. 2 and 4. Typical of results at room temperature, the "net ac" loss curve in Fig. 2 still rises appreciably toward decreasing frequency.

Measurements over the low frequency region from 60 cycles to 3 kc were also made at several temperatures on single crystal No. 3S. Results are shown in Fig. 4 for −25°C, +23°C, and +60°C. At −25°C there was no appreciable change in κ and the "net ac" loss as a function of frequency. At 60°C the changes were more pronounced than at room temperature.

Qualitatively, the audio frequency behavior might be explained in terms of a dispersion peak below 60 cycles, caused by pairs of lattice defects.[11] It might also be due to the formation on the surfaces of a very thin layer of $Ba(OH)_2$ having a much lower conductivity than the BaO. The equivalent circuit representing such a $BaO-Ba(OH)_2$ combination behaves like the actual samples.

The applied voltage with the different instruments could be varied from 0 up to about 150 volts. No changes in κ and D were observed which were greater than expected random variations.

TABLE II. κ as calculated from (2) *versus* crystal thickness.

Thickness in cm	κ	Electrode contact
0.082	32	Fig. 1(b)
0.071	31.5	1(b)
0.054	32	1(b)
0.050	31.5	1(b)
0.042	30	1(b)
0.019	31.5	1(c)

IV. SUMMARY

The low frequency dielectric constant of barium oxide was measured on single crystals while taking substantial precautions to prevent conversion of this substance to barium hydroxide. This value was found to be 34 and remained constant from about 2 kc to 60 Mc, the end of our measuring range. An apparent rise in the dielectric constant accompanied by a rise in the ac loss was observed from 2 kc down to 60 cycles at room temperature, which disappeared upon lowering the temperature to −25°C. A unique explanation for this behavior has not as yet been found.

The authors wish to express their appreciation for the assistance of Professor H. S. Sack, Mr. W. C. Dash, and Mr. S. S. Stevens.

APPENDIX

By means of conformal mapping it is possible to obtain an approximate expression for the capacitance of a condenser such as

[11] R. G. Breckenridge, J. Chem. Phys. **16**, 959 (1948); **18**, 913 (1950).

shown in Figs. 1(b) and (c) with air rather than BaO between the electrodes.[12] In electrostatic units

$$C=(r^2/4t)+(r/2\pi)(1-\ln 2); \quad (t/r)\ll 1,$$

where r is the electrode radius and t is the thickness of the air-gap. The first term is the familiar major term, the second is an end correction term from the charge collected on the flat surface near the intersection of the cylindrical and flat circular surfaces. The end correction from charge on the cylindrical surfaces cannot be correctly obtained by conformal mapping (since this method strictly applies to two-dimensional problems only), and it is omitted here for the following reason: if one introduces a slab of BaO instead of air, its periphery being shaped like the outermost line of force from charge on the intersection between the cylindrical and flat circular surfaces, then the field in the surrounding air remains undistorted. Hence, the difference between the BaO and air condenser capacitance is

$$\Delta C=(\kappa-1)[(r^2/4t)+(r/2\pi)(1-\ln 2)], \quad (1)$$

where κ is the dielectric constant of BaO. By using only the major term,

$$\Delta C=(\kappa-1)(r^2/4t), \quad (2)$$

the calculated κ for a 0.051-cm thick slab of BaO, 0.478 cm in diameter, is 4 percent too high; for a 0.0255-cm thick slab it is 2 percent too high.

Since the shape of the actual periphery of the slab of BaO was far from the ideal, the edge effect was also investigated experimentally. A series of measurements on polycrystalline sample No. 5P of diameter 0.0470 cm gave the results shown in Table II. Electrode contact as in Fig. 1(c) had to be used for thin samples. For these, sufficient pressure to obtain good electrical contact could not be applied with the aluminum foil without shorting the electrodes. The data indicate that random errors in measurement make end effect corrections quite insignificant.

[12] This problem is similar to finding the magnetic field between the magnetic poles of a cyclotron, as discussed by M. E. Rose, Phys. Rev. **53**, 715 (1938).

PHYSICAL REVIEW VOLUME 83, NUMBER 4 AUGUST 15, 1951

Photoconductivity and Photoelectric Emission of Barium Oxide

HENRY B. DEVORE AND JOHN W. DEWDNEY*
RCA Laboratories Division, Radio Corporation of America, Princeton, New Jersey
(Received December 26, 1950)

Barium oxide, in the form of a sprayed coating on a nickel base, was investigated by means of studies of photoconductivity, photoemission, and absorption measurements and the variation of these with temperature. Changes occurring during activation of the oxide were observed. The results are discussed in terms of an energy level structure for barium oxide.

I. INTRODUCTION

THE literature on the oxide cathode is replete with investigations undertaken to establish constants on which to set up a picture of the electron energy band structure for the (Ba, Sr)O emissive coating.[1] Very few of these studies have been concerned with the individual components of these coatings. One of the earliest of these is reported by Nishibori *et al.*,[2] wherein studies of the conductivity and thermionic and photoelectric emissions were combined to derive values for the electron affinity and Fermi level for BaO and SrO, as well as for the combined form.

More recently, Tyler,[3] working with barium oxide single crystals prepared by Sproull, as well as with evaporated films, has studied the optical absorption and photoconductivity. The location of the absorption edge (~3.8 ev) reported by Tyler has been confirmed by Taft and Dickey[4] on the basis of studies of photoelectric emission from thin metallic layers deposited on a base of barium oxide. Apker, Taft, and Dickey[5] have reported studies of the photoelectric emission from BaO which indicate an energy for the top of the filled band 5.0–5.2 ev below vacuum potential.

In the work reported here, photoconductivity, photoelectric emission, and optical reflectivity measurements have been made on barium oxide, as formed, and have been followed through the activation process in order to obtain further information concerning the energy level structure.

II. EXPERIMENTAL

Figure 1 shows the form of the tubes used in this work. Barium carbonate (Mallinckrodt Ultra Pure), dispersed in a nitrocellulose binder, was sprayed on a cathode sleeve of N-81 (pure) nickel to give a coating weight of 10–15 mg/cm². A probe wire of pure platinum, 0.001 in. diameter, was wound over this coating, and a second thin coating of the carbonate was sprayed over the probe wire, primarily to seal it in place. The anode cylinder, also of N-81 nickel, was provided with longitudinal slots to permit irradiation and observation of the oxide surface. The electrode assembly was sealed into an envelope having a fused quartz section sur-

* Now at Sir George Williams College, Montreal, Quebec.

[1] A. S. Eisenstein, Advances in Electronics **1**, 1–64 (1948); J. P. Blewett, J. Appl. Phys. **10**, 668 (1939); **10**, 831 (1939); **17**, 643 (1946).

[2] E. Nishibori and H. Kawamura, Proc. Phys.-Math. Soc. Japan **22**, 378 (1940); Nishibori, Kawamura, and Hirano, Proc. Phys.-Math. Soc. Japan **23**, 37 (1941).

[3] W. W. Tyler, Phys. Rev. **76**, 179(A) (1949); **76**, 1887 (1949); dissertation, Cornell University, Ithaca, New York (1949).

[4] E. A. Taft and J. E. Dickey, Phys. Rev. **78**, 625 (1950).

[5] Apker, Taft, and Dickey, Phys. Rev. **76**, 453(T) (1949).

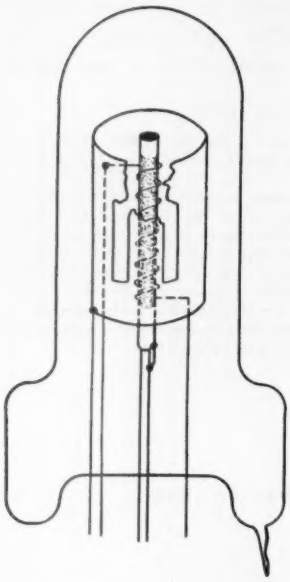

FIG. 1. Experimental tube.

rounding the anode. After exhaust and bakeout, the cathode was converted from carbonate to oxide by heating slowly to approximately 1200°K, the heating being continued until gas evolution has substantially ceased. A small part of the available getter was then flashed, and the tube sealed off.

Temperatures of the oxide coating, in the range in which most of the work was done (300°K–700°K), were measured by using the platinum probe wire as a resistance thermometer.

The arrangement of apparatus used is indicated in Fig. 2. A Perkin-Elmer model 12 infrared spectrometer, with a crystal quartz prism, is used as a monochromator to illuminate the oxide. The light from a high pressure mercury arc, G.E. Type A-H6, is focused on the entrance slit through a sector disk which chops the light at a 23.5-cycles/second rate to give intermittent illumination. This permits separation of photocurrents from any dark current present. After passing through the monochromator, half the light is reflected from the

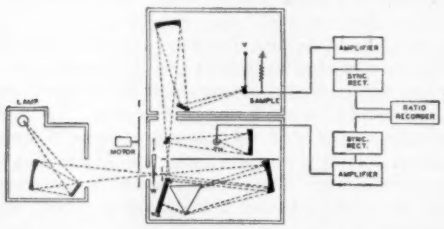

FIG. 2. Arrangement of apparatus.

exit beam and focused on a thermistor bolometer (Western Electric Type V-649) for energy measurement. The remainder of the beam is focused on the oxide cathode in an adjoining shielded and lighttight box. A neutral wedge W, placed just ahead of the entrance slit, has its position servo-controlled from the thermistor output so as to maintain the output of the monochromator nearly constant in power, with 1.5×10^{-5} watt falling on the oxide surface, for all spectral regions. With the H6 lamp source, the system operates satisfactorily over the range from 8200A (1.5 ev) to 2750A (4.5 ev). The lamp output is insufficient to permit measurements at higher photon energies.

For photoelectric emission studies, the cathode and probe are held at a negative potential considerably greater than required for saturation, and the anode is connected through a standard resistor to ground. The photocurrent signal developed across this resistor is taken to an amplifier tuned to the 23.5-cycles/second chopping frequency. The amplified signal is converted to dc by a phase sensitive rectifier, synchronized with

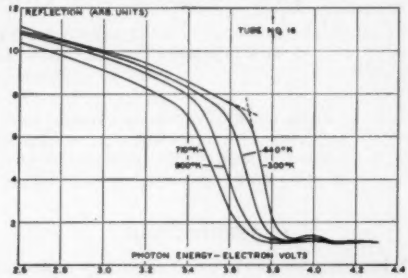

FIG. 3. Reflection from unactivated BaO.

the light chopper, and this is followed by a low pass filter with a cut-off characteristic which can be adjusted to set the over-all band width to values between 1 and 0.1 cycle-second. The thermistor signal is passed through a similar system, and the two signals are fed to a Brown recording potentiometer which has been modified to operate as a ratio recorder. As the spectrum is scanned by the monochromator, the recorder draws a curve showing photocurrent per unit energy through the spectrum.

For photoconduction measurements, in order to reduce polarization phenomena, an alternating voltage at 60 cycles/second is applied to the nickel cathode base and the probe connected through the standard resistor to ground. With the 23.5-cycle/second illumination, this yields photoconduction current signals at the beat frequencies. The current is measured with amplifier and rectifier tuned to 36.5 cycles/second.

In measurements made in this manner, the possibility always exists that photoemission measurements may be affected by the photoconductive effect, since the body of the oxide is effectively in series with the emitting

surface. Conversely, the photoconductivity measurements may be confused by photoelectric emission from the surface above the probe wire to surrounding electrodes and to the rest of the cathode surface, and vice versa. While it is not possible to assert that these effects have been completely eliminated, they are believed to be of negligible importance in these experiments. This is based on the observations that: (1) photoemission currents were always measured under saturation conditions; (2) in one case in which a tube became gassy, so that photoemission could no longer be observed, the photoconduction curve was found to be substantially identical with that observed under high vacuum conditions; and (3) the photoemission and photoconduction curves were, in fact, found to be different in character and to show different behaviors with temperature and with activation.

With the barium oxide in the form of a cathode coating, direct optical absorption measurements are not feasible. However, useful information as to the location of the absorption edge may be inferred from measure-

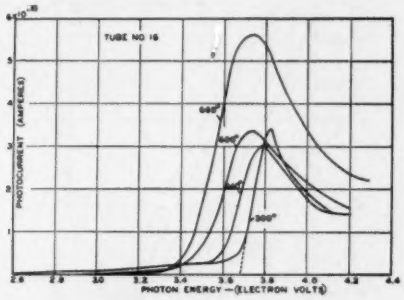

FIG. 4. Photoconductivity in unactivated BaO.

ments of reflectivity. For this purpose, a photomultiplier tube (1P28) is set up to view the cathode surface through an anode slot adjacent to that through which the incident radiation passes. A spectral curve is taken in this way and another made with the radiation falling directly on the multiplier surface. The curves are divided, point by point, to obtain a reflectivity curve.

The barium oxide, after the exhaust and breakdown treatment, has low thermionic activity. Photoconduction, photoemission, and reflection measurements are made at several coating temperatures between 300°K and 700°K. It is then activated by heating the cathode to approximately 1200°K and drawing emission current. After flashing more getter to clean up any additional gas generated during this treatment, the cathode is cooled and the observations repeated. To obtain a measure of the state of activation, the emission current, taken at the point at which it departs 20 percent from the $\frac{3}{2}$ power voltage law,[6] is determined as a function of temperature, before and after activation.

[6] Hannay, McNair, and White, J. Appl. Phys. **20**, 669 (1949).

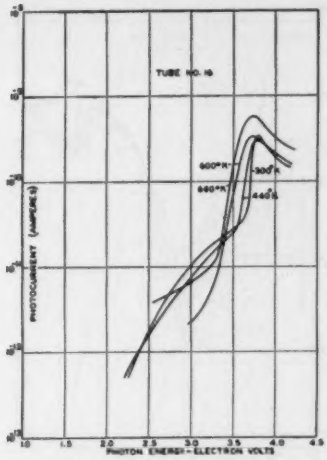

FIG. 5. Photoconductivity in unactivated BaO.

Observations on some twenty tubes have shown good agreement among themselves. The majority of the results presented here were taken on one of these tubes and were selected because a more extensive set of observations was made with this tube than with most of the others. Studies on barium oxide, as observed before any attempt at activation, are described in the following three sections.

III. REFLECTION

Figure 3 shows representative curves of spectral reflection from a barium oxide coating plotted against the quantum energy of the incident radiation. Following a gradual reduction in reflection as the energy increases, there is an abrupt drop corresponding to the characteristic absorption edge. A threshold for this is obtained, as indicated on the curve, by extrapolating the curve from both sides of the knee and finding the intersection of these extrapolated curves. For BaO at room tem-

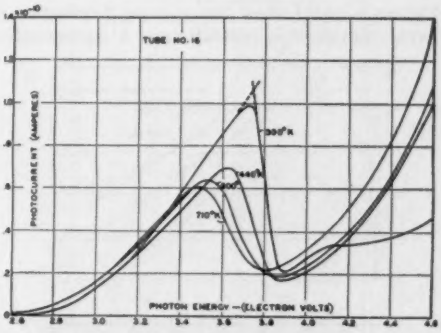

FIG. 6. Photoelectric emission from unactivated BaO.

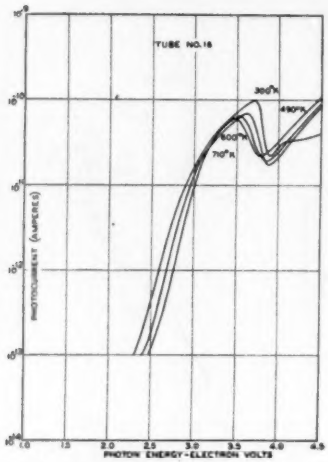

FIG. 7. Photoelectric emission from unactivated BaO.

perature, a threshold value of 3.7 ev is obtained. This is in satisfactory agreement with the value 3.8 ev found by Tyler[3] from absorption measurements on both single crystals and evaporated films of BaO. As the temperature of the oxide is increased, the knee of the curve becomes more rounded and the threshold is displaced towards lower quantum energies.

IV. PHOTOCONDUCTIVITY

Representative curves showing spectral distribution of photoconductivity are shown with the current plotted linearly in Fig. 4 and in a logarithmic form in Fig. 5. The large rise in current, extrapolated as shown in Fig. 4, shows a threshold at the characteristic absorption edge of BaO. As the temperature increases, the photoconduction current shows a small increase in magnitude and at the same time the threshold is displaced towards lower energies, corresponding to the same displacement noted for the reflection curves.

V. PHOTOEMISSION

Figures 6 and 7 show the spectral distribution of external photoelectric emission from a representative BaO specimen. The shape of the curves suggests a continuous rise in emission with increasing quantum energy, on which is superimposed a process which reduces this emission, commencing sharply near the absorption edge and becoming less effective towards higher energies. This appears to be similar to the effect described by Taft and Dickey[4] for the photoemission from thin films of Ba and BaO and to be caused by a reduction of the electric vector of the radiation in the neighborhood of the BaO surface. This electric vector, which is the resultant of the incident and reflected field vectors, suffers a large reduction in the region of an absorption edge, where the index of refraction takes on abnormally large values. If the threshold for this emission reduction is defined as the intersection of the prolongation of the curves before and after the reduction, as indicated in Fig. 6, this is again found to lie close to the characteristic absorption edge for BaO.

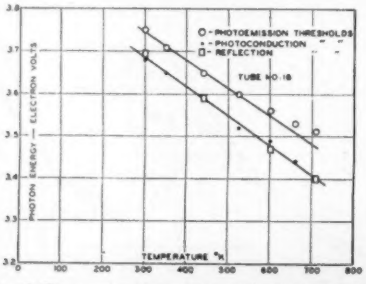

FIG. 8. Temperature dependence of threshold energies.

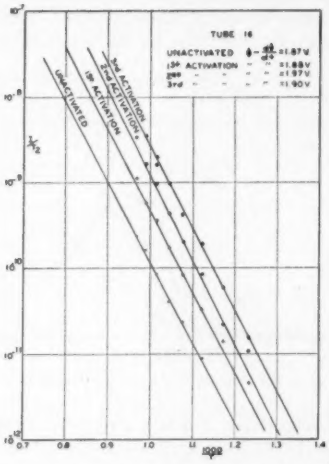

FIG. 9. Richardson plot.

The threshold values of photon energy for reflection, photoconduction, and reduction of photoemission are plotted against temperature in Fig. 8. To a good approximation, these points, over the range from 300°K to 700°K, can be represented by straight lines having a slope corresponding to a threshold displacement of 7×10^{-4} ev per degree.

The low energy tails of photoemission curves have often been fitted to Fowler plots. This was tried for our measurements, but the fit obtained was very poor. This does not seem especially significant, since present semiconductor theory does not lead one to expect such a fit.

VI. ACTIVATION

After observations were made of reflectivity, photoconductivity, and photoelectric emission for the barium

oxide, the cathode was activated by heating and drawing emission current. At each step of the activation, the emission current was measured as a function of the cathode temperature and Richardson plots were made. These plots, for four stages of activation, are shown in Fig. 9. It is notable that the change in slope during the course of the activation is small, as shown by the corresponding values[7] for $(\phi - Td\phi/dT)$, and that the total change in thermionic emission from the initial to the final state of activation is only about a factor of 20. Since the final state gives emission comparable with that for a well-activated BaO cathode, it is indicated that the cathode breakdown treatment used actually produces some activation, as would be expected.

Figures 10 and 11 show photoconductivity and photoemission as measured for the same specimen at the same stages of activation. In both of these a considerable

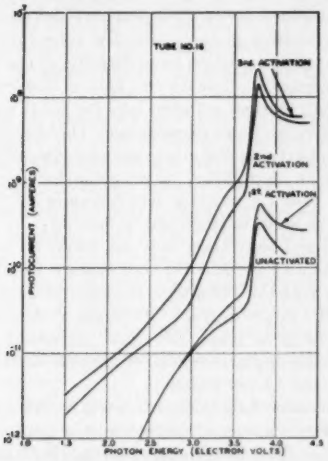

FIG. 10. Dependence of photoconductivity on activation.

change takes place during the second activation treatment, with relatively smaller changes before and after this stage. The thermionic emission data of Fig. 9 do not show a similar progression.

Photoconductivity shows a general increase in magnitude with activation. Photoemission, on the other hand, shows a marked change in spectral distribution when activated. A very large increase is found in the region of high absorption. In the low energy region, the photoemission becomes sensitive to the treatment of the specimen, as is shown in Fig. 12. The currents observed in this region are small if the cathode is heated a few hundred degrees and then cooled in the dark. Irradiation of the cold oxide with light in the region of characteristic absorption (>3.7 ev) causes the photoemission measured subsequently in the low

[7] F. Seitz, *Modern Theory of Solids* (McGraw-Hill Book Company, Inc., New York, 1940), p. 402.

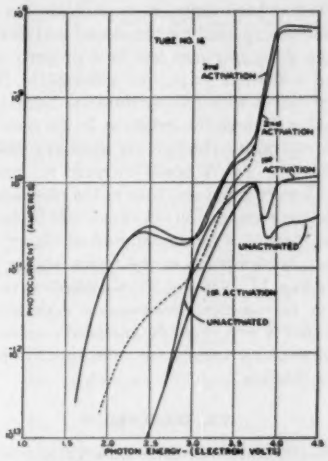

FIG. 11. Dependence of photoelectric emission on activation.

energy region to show a large increase with a peak at 2.5 ev. This high photoemission decays slowly, with a time constant of the order of a day. These changes are reproducible, and the low energy photoemission may be increased by short wavelength irradiation or decreased by annealing, at will. This phenomenon has not been observed in the case of photoemission from the BaO before activation, nor in any of the photoconductivity measurements.

In recording the curves shown in Fig. 11, the BaO surface was in every case exposed to short wavelength illumination before the curves were taken, and the low energy portions correspond to the curve of Fig. 12 for the irradiated oxide. For comparison, the dashed curve

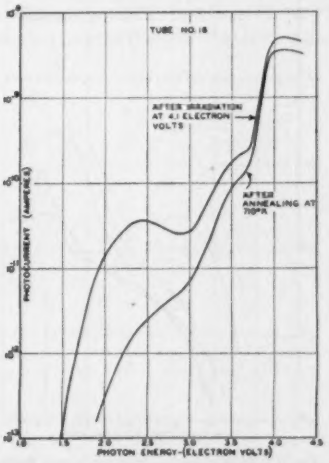

FIG. 12. Effect of irradiation and annealing on photoemission.

in Fig. 11 has been drawn in to indicate the response that would be expected for the second and third activation stages if the specimen had been properly annealed.

In the activated state, the changes in photoconductivity curves with temperature are similar to those observed for the unactivated state. In the case of photoemission, again, the changes are markedly different, as shown in Fig. 13. A small increase in temperature produces a very rapid decrease in the photoemission in the high quantum region. Between 500°K and 600°K, this goes through a minimum, and at higher temperatures the photoemission in the region above 3 ev rises again. In Fig. 13, as in Fig. 11, a dashed curve has been drawn in to indicate the response expected for the oxide at 300°K in a properly annealed condition.

The reflectivity curves are substantially unchanged by the activation.

VII. DISCUSSION

The interpretation of these observations in terms of an energy level diagram for barium oxide is not yet wholly satisfactory, but a number of inferences may be drawn. A representation of such an energy level diagram is given in Fig. 14. It is assumed that a number of both donor and acceptor levels are located in the gap between the bottom of the conduction band and the top of the filled band.

It may be assumed that in the inactive state, the number of donor sites is considerably less than the number of acceptor sites. The Fermi level appropriate to this condition should be comparatively low and the thermionic emission very small. The activation process is regarded as forming a large number of donor sites. When the number of these begins to exceed the number of acceptors, the number of occupied donors will become appreciable, and the Fermi level will rise to a position in the neighborhood of the donors. Further activation will increase rapidly the number of occupied donor sites, but the Fermi level will rise only slowly. The Richardson plots indicate that, in the case of our specimens, the "unactivated" state already corresponds to a density of donors somewhat in excess of the density of acceptors present.

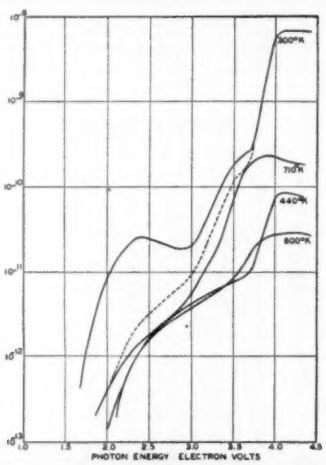

FIG. 13. Photoemission from activated BaO—temperature variation.

Apker, Taft, and Dickey[5] have found that the photoemission from BaO shows a large increase setting in around 5.0–5.2 ev, and it appears probably that this represents the depth V_f of the top of the filled band below vacuum potential. Our light source did not permit measurements for confirmation of these observations.

The large absorption setting in at about 3.7 ev must be ascribed to transitions in which electrons are raised from the top of the filled band, in view of the large absorption coefficient ($\sim 10^5$/cm) found by Tyler. Since the photoconductivity measurements also show a large increase starting at this point, the transition must be either to the conduction band directly, or else to states lying sufficiently close to the base of the conduction band that thermal transfer into the band has a high probability at room temperature. The direct transfer seems unlikely, among other reasons, because this would call for an improbably large value for the electron affinity (1.3–1.5 ev), for which values in the range 0.7–0.9 ev seem to be currently favored.

The band separation may be taken to be a little more than 3.7 ev, and the temperature variation data indicate that this band separation decreases at the rate of 7×10^{-4} ev per degree C. This rate of change of band separation is in reasonably good agreement with the well-known displacement of absorption bands, usually taken to be 1A per degree C.

In the case of photoelectric emission from activated BaO, there is a conspicuous increase for photon energies just above the 3.7-ev absorption edge. Both our photoconductivity studies and observations made by Apker[5] on energy distribution of photoelectrons indicate that there does not exist any concentration of electrons in states at this depth below vacuum potential. A possible explanation has been advanced by Apker which assumes that photoemission in this region is largely caused by interaction between excitons and electrons in the donor sites. According to this suggestion, the high energy incident photons create excitons near the surface of the crystal. An exciton may dissociate thermally to form a conduction electron, or it may recombine, or it may encounter an electron in a donor site near the surface and, by transfer of its excitation energy, cause this electron to be emitted from the surface. Since the high absorption coefficient in this region indicates a high density of excitions near the surface, the probability of electron release by this process might be expected to be higher than for the direct photoelectric process.

[5] L. Apker (private communication).

A rise in temperature should increase the probability that an exciton would dissociate thermally, with corresponding increase in photoconductivity, as has been observed, before it encounters an electron at a donor site. Hence, the photoemission in the absorption region should decrease with increasing temperature, as is observed. The subsequent rise in photoemission for temperatures above 600°K may perhaps be accounted for by assuming that this represents thermionic emission of electrons which reach the conduction band by exciton dissociation.

The 2.5-ev peak in the photoemission from activated BaO, caused by irradiation in the absorption region, indicates the presence of a number of donor sites at this depth below vacuum potential, most of which are normally unoccupied but which may be filled by electrons from the conduction band. The large rise beyond 3.7 ev, and its smaller dependence on irradiation, argues the presence of larger number of occupied sites, which may be distributed down to at least 3.7 ev below vacuum potential. On the other hand, in the case of photoemission from the unactivated BaO, there is no sharp rise for photon energies above 3.7 ev, nor is there any evidence of a peak in the neighborhood of 2.5 ev. This would seem to indicate a very low density of donor sites, whether occupied or not, in the unactivated state. This conclusion, however, is hardly compatible with the observed uniformity of slope of the Richardson plots.

A detailed interpretation of the photoemission data is rather hazardous until a determination can be made as to which of the features are characteristic of the volume properties of the BaO crystals as distinguished from those which are representative of the surface conditions existing.

Photoconductivity induced by photons with energy less than 3.7 ev is presumably due to electrons raised to the conduction band from donor or acceptor sites. The increase observed on activation may be largely accounted for by the increased density of occupied donor sites, which also produce the rise in thermionic emission. In addition, there may be an increase in mobility of electrons in the conduction band, resulting from a reduction of trap density. However, since this latter would affect equally the photoconductivity in all spectral regions, while the increase in the absorption region is always proportionately larger than that in the low energy tail, some further mechanism is required. This could be provided, on the exciton hypothesis, by the assumption that the probability of exciton recombination before thermal dissociation is relatively large in the unactivated state and that it is reduced by activation.

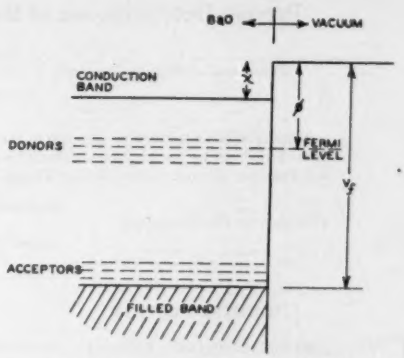

FIG. 14. Energy level diagram for BaO.

The authors wish to express their indebtedness for numerous suggestions and discussions to Professor L. P. Smith and to their other colleagues at RCA Laboratories. In addition, they have profited from discussions with Dr. C. Herring and others of Bell Telephone Laboratories, and with Dr. L. Apker, Dr. W. W. Tyler, and others at General Electric Research Laboratories

Precise Determination of the Magnetic Moment of the Deuteron

BERNARD SMALLER
Department of Physics, University of Chicago and Argonne National Laboratory, Chicago, Illinois
(Received April 16, 1951)

A precision measurement of the ratio of the magnetic moment of the proton to that of the deuteron has been carried out by the magnetic resonance method. The measurements were made using mixtures of H_2O and D_2O and also mixtures of H_2 and D_2 gas. The result for the H_2O:D_2O mixture is

$$\mu_H/\mu_D=3.2571999\pm0.0000012,$$

while for the H_2:D_2 mixture

$$\mu_H/\mu_D=3.2571990\pm0.0000010.$$

I. INTRODUCTION

THE hyperfine structure splittings observed in atoms are closely related to the magnetic moments of the nuclei of these atoms. In the case of hydrogen and deuterium, in particular, it should be possible to calculate the ratio of the hyperfine structure splittings from the ratio of the nuclear magnetic moments to a very high degree of accuracy. When accurate measurements of these quantities[1] were made, however, their values were not in complete accord with the Breit-Meyerott formula,[2]

$$\kappa_{\text{theor}}=\nu_D/\nu_H=\tfrac{3}{4}(m_D/m_H)^3\mu_D/\mu_H. \quad (1)$$

Here, ν_D/ν_H is the ratio of the hyperfine splitting in deuterium and hydrogen, m_D/m_H is the ratio of the reduced masses of an electron in these atoms, and μ_D/μ_H is the ratio of their nuclear moments. The measurements of the hyperfine splitting gave a value of ν_D/ν_H which was larger than that given by Eq. (1) by 17 parts in 10^5, whereas the estimated experimental uncertainty was only 1 part in 10^5.

It was shown by Bohr[3] that most of this discrepancy could be accounted for by taking into consideration the structure of the deuteron. He pointed out that when the electron is close to the deuterium nucleus, it moves rapidly compared with the nuclear motion and centers its motion around the proton rather than around the deuteron center of mass. The interaction between the electron and nuclear spins is increased thereby. For the order of magnitude of this effect, Bohr obtained the formula

$$\epsilon=\Delta\kappa/\kappa=-(\mu_N/\mu_D)d/a=1.84\times10^{-4}, \quad (2)$$

where d and a represent the radii of the deuterium nucleus and atom, respectively.

The present measurement was undertaken at the instigation of Professor Rabi as part of a campaign to press to the limit both the experimental and theoretical possibilities of this subject. Accordingly, a careful evaluation of all the known effects of nuclear motion on the hyperfine structure was made by Low[4] with the result:

$$\epsilon_{\text{theor}}=(1.83\pm0.22)\times10^{-4}. \quad (3)$$

The uncertainty given is due mostly to the uncertainties in the knowledge of the electronic wave function of the deuteron. An improved measurement of ν_D/ν_H was made by Prodell and Kusch[5] with the result,

$$\nu_D/\nu_H=0.230486536\pm0.00000010.$$

This paper reports a measurement of μ_D/μ_H with accuracy comparable to that obtained for ν_D/ν_H.

II. MAGNETIC RESONANCE METHOD

The measurement was based on the magnetic resonance method.[6,7] The technique was a further refinement of the one which was used by Anderson,[8] hereafter referred to as **I**, in a measurement of the magnetic moment of He^3. The sample consisted of a mixture of deuterium and hydrogen gases under pressure. Measurements were also made with a mixture of H_2O and D_2O. Two rectangular small coils were placed at right angles to one another but arranged to include the same volume of the gas mixture. Each coil was connected as one arm of its own "Twin T" radiofrequency bridge. The coils were placed between the poles of an electromagnet with their axes at right angles to that of the poles of the magnet.

Under these circumstances, a substance with spin I may orient itself in $2I+1$ ways with respect to the direction of the magnetic field, each having a different energy value. Transitions between neighboring states will be induced where the frequency of the signal applied to the coil satisfies the resonance condition,

$$2\pi f=|\gamma|H, \quad (4)$$

where $\gamma=\mu/\hbar I$ is the ratio of the magnetic moment to the angular momentum of the substance, f is the frequency in cycles per second, and H is the magnetic field in gauss.

The magnetic field is modulated about the resonance value by a small amount of 25 cycles per second. Under

[1] J. E. Nafe and E. B. Nelson, Phys. Rev. **73**, 718 (1948).
[2] G. Breit and E. R. Meyerott, Phys. Rev. **72**, 1023 (1947).
[3] A. Bohr, Phys. Rev. **73**, 1109 (1948).
[4] F. Low, Phys. Rev. **77**, 361 (1950).
[5] A. G. Prodell and P. Kusch, Phys. Rev. **79**, 1009 (1950).
[6] Purcell, Torrey, and Pound, Phys. Rev. **69**, 37 (1946).
[7] Bloch, Hansen, and Packard, Phys. Rev. **69**, 127 (1946); **70**, 474 (1946); F. Bloch, Phys. Rev. **70**, 460 (1946).
[8] H. L. Anderson, Phys. Rev. **76**, 1460 (1949).

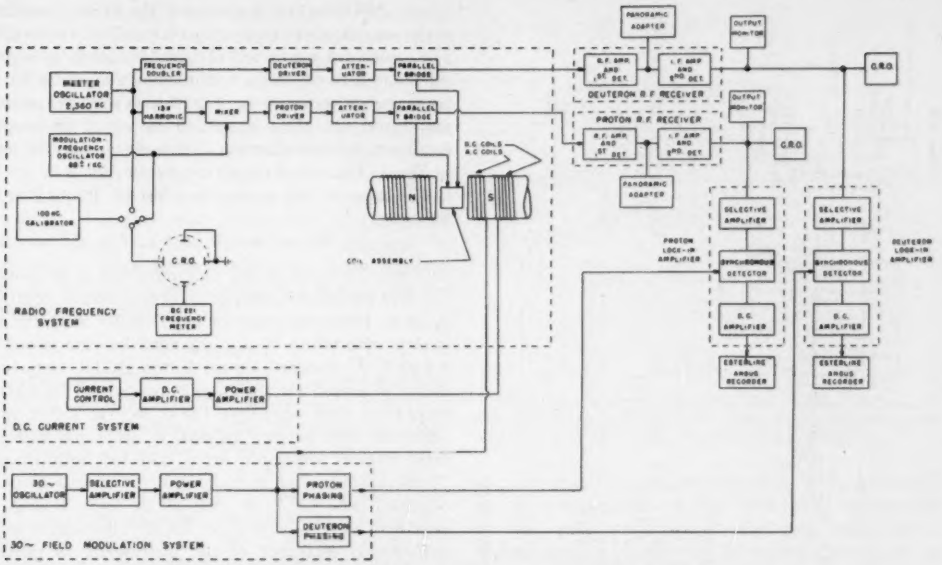

FIG. 1. Block diagram of nuclear magnetic resonance apparatus.

suitable conditions, the transitions which occur each time the resonance value of the field is traversed produced a change in the impedance of the coil and an unbalance of the bridge. Thus, the magnetic resonance effect produces a 25-cycle modulation in the radio-frequency signal which feeds the bridge, and this may be detected by means of an ordinary radio receiver. The extreme sharpness of the resonance which may be obtained makes possible the great accuracy of the method.

It is seen that a measurement of γ requires a measurement of both the frequency f and the magnetic field H. However, the ratio of the quantities γ for two substances can be obtained from a measurement of the ratio of two frequencies provided the resonances are observed in the same magnetic field at the same time. This was the technique of the present experiments.

The object of the measurement was to determine the ratio of the γ's for hydrogen and deuterium to a precision of a few parts in 10^7. The limit to the precision was set by the breadth of the resonance, which in turn was determined by the inhomogeneity of the magnetic field over the sample, and by the constancy of the magnetic field in time. By carefully lapping the pole faces of the magnet and by using a fairly small sample which could be moved about between the poles, it was possible to find a place where the half-width of the resonance at 7000 gauss amounted to 0.018 gauss. The center of the resonance curve was estimated to ± 0.0005 gauss. The magnet was the same as was used in **I**, but the constancy of its field with time was considerably improved.

It is important to recognize that the quantity measured in this experiment may be close to, but is not necessarily equal to, the ratio of the *nuclear* gyromagnetic ratios. Equation (4) holds for the *nuclear* gyromagnetic ratio only if H is the magnetic field at the nucleus. Thus, even though the external magnetic field is the same for the two substances, local differences in magnetic field might occur because of electronic and nuclear motions in the neighborhood of the nucleus under observation. In the previous measurements, this comparison was made using samples of water. A precision comparison using a mixture of heavy and light water was also made in the present work. These molecules are, indeed, similar to a high degree; but differences in their rotational and vibrational properties could be expected to introduce differences in the magnetic field at the nucleus amounting to several parts in 10^7. For this reason, the comparison was also made using hydrogen and deuterium gas mixtures. For these molecules, fairly accurate experimental data on the rotational and vibrational behavior are available, together with reasonably manageable electronic wave functions, so that at least the order of magnitude of the corrections can be estimated with some confidence.

A. Radiofrequency System

The measurements were carried out at a magnetic field of 7223 gauss. The corresponding resonance frequencies are near 30,750 kilocycles per second for the proton and near 4720 kilocycles per second for the deuteron. To obtain the resonances simultaneously at

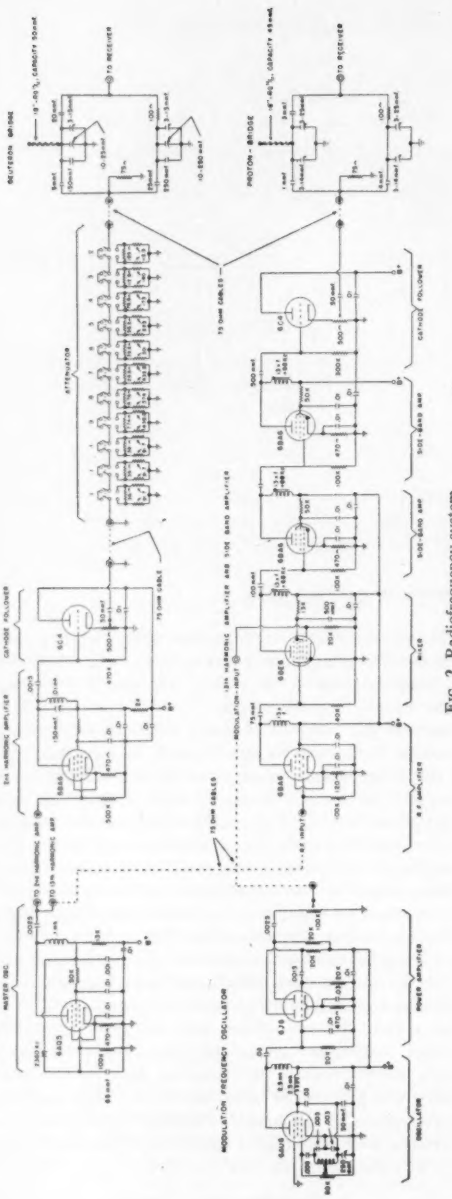

FIG. 2. Radiofrequency system.

the same magnetic field, at least one of these frequencies must be variable. Instead of the two oscillator arrangements used in I, advantage was taken of the fact that the required frequency ratio is close to 13/2. A master crystal was used to generate a fundamental frequency, f_0, near 2360 kilocycles per second. The second harmonic of this was amplified and used to drive the deuteron coil. The proton frequency was obtained by using the upper side band derived from a variable modulation oscillator operating at frequency f_m near 68 kilocycles per second and mixed with the thirteenth harmonic of the master oscillator. A block diagram of the scheme may be seen in Fig. 1. The actual circuit is given in Fig. 2.

The ratio of the proton to deuteron frequencies is given by

$$R=f_H/f_D=(13/2)+f_m/2f_0. \tag{5}$$

The relative error in the determination of R is only 1/450 of the relative error in the determination of either f_m or f_0. For an accuracy of 1 part in 10^7 in R, the accuracy with which f_0 and f_m need be determined is 3×10^{-5}. A standard Signal Corps BC221 frequency meter was used for these measurements. This instrument has a dual range from 125 kc sec^{-1} to 250 kc sec^{-1} and from 2000 kc sec^{-1} to 4000 kc sec^{-1} and uses the same vernier capacitor drum dial for both ranges. Through the use of harmonics, a continuous range is obtained from 125 kc sec^{-1} to 20 mc sec^{-1}. It may be read with a precision of about 2×10^{-5}. Instead of using the crystal oscillator of the instrument to provide check calibration points, a more accurate method was used. A General Radio 1101A–100 kc sec^{-1} frequency standard was used to provide check points by utilizing the optimum combination of harmonics to provide a Lissajou figure. For the modulating frequency, f_m, a 15:11 frequency ratio was used to establish a check point at $15/11\times100=136.364$ kc sec^{-1}. For the master frequency, f_0, a 47:2 frequency ratio was used to provide a check point at 2350.000 kc sec^{-1}. The 100-kc sec^{-1} standard was checked against WWV. The drifts to which it is subject can produce only quite negligible errors.

B. Sample and Coil Arrangement

For the measurements with the gases, a brass cell was used which could be filled with a suitable mixture of hydrogen and deuterium under pressure. Two coils were used having a rectangular cross section and placed at right angles to one another and to the magnetic field. The proton coil nested snugly inside the deuteron coil. The space in the cell exterior to the coils was filled with non-hydrogen-containing Teflon plastic, thereby confinding the gas to the region inside the coils. The construction is illustrated in Fig. 3. The volume enclosed by the coils was 0.613 cm^3, small enough to bring the inhomogeneity of the field over the sample down to less than 3×10^{-6}. A typical coil assembly used for the water samples is shown in Fig. 4. Here the deuteron coil was wound on the outside of a small glass tube. The proton coil was placed inside the tube. Care was taken to fill the tube with the water sample so that very little of the sample was outside the coils. The volume of the sample was about 0.23 cm^3.

This arrangement is not ideal, since the proton coil measures a different average over the sample volume than does the deuteron coil. The error was estimated to be less than 2×10^{-7}. The obvious procedure for eliminating this source of error by interchanging the roles of the two coils was not practical in the present experiment because of the large difference in inductance of the two coils. Evidence that it did not amount to more than this is had from the general consistency of the data, which were taken with a variety of coils and coil positions over a period of more than one year. In particular, a measurement made with the coils rotated through 90° gave a result which was not outside the experimental uncertainty.

C. Detection

The output of the bridge was connected to a National HRO-5A radio receiver. The balance of the bridge was judged with a panoramic adapter at the output of the first detector, and it could also be read directly on a microammeter at the output of the second detector.

In a typical experiment using 880 lb/in² of D_2 and 320 lb/in² of H_2, the input into the deuteron bridge was set to 100 millivolts and the rf voltage across the deuteron coil, as calculated from the constants of the bridge circuit, was 175 millivolts. The bridge was adjusted to resistive balance and reactive unbalance in the amount of about 10 microvolts at the input of the receiver. The gain of the receiver was set to give a carrier output of 2.5 volts at the second detector. The amplitude of the signal obtained was about one-fourth of the maximum obtainable by increasing the radio-frequency input power to the bridge while maintaining the carrier level constant at the second detector. The effects of saturation were kept small thereby. The proton bridge and receiver were operated under identical conditions, except for the input voltage being reduced to about 20 millivolts.

The property of the "Twin T" bridge of balancing separately the reactive and resistive components of the signal is an important feature of the present measurement. The presence of an appreciable amount of resistive unbalance in the signal results in a systematic shift in the center of symmetry of the pattern. This could easily be mistaken for an apparent difference in the value of the resonant field. In the present measurements, the resistive unbalance was always less than 1/100 the reactive unbalance. A special experiment showed that, with a resistive unbalance ten times greater than that usually used, the shift in the center of the pattern was not detectable.

D. Magnetic Field Control

The magnet used in this experiment was the same as that used in **I**. It had a 5-inch-diameter pole with a 1-inch gap and was provided with a high voltage, low current, field winding so that precise electronic control of the magnet current could be arranged. The dc voltage

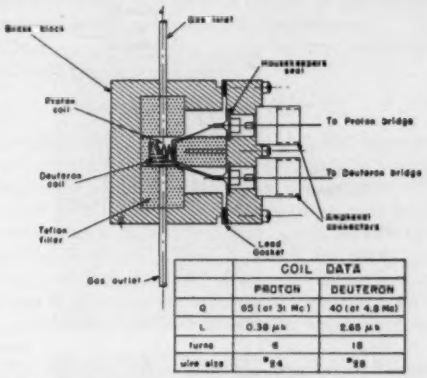

	COIL DATA	
	PROTON	DEUTERON
Q	65 (at 31 Mc)	40 (at 4.8 Mc)
L	0.38 μh	2.65 μh
turns	6	18
wire size	#24	#28

FIG. 3. Gas chamber assembly for nuclear resonance measurement. Axes of proton and deuteron coil are perpendicular to each other and to magnetic field, H_0 (directed into the figure).

amplifier used in the current regulator was improved to provide a loop gain of the feed-back circuit of 6000. The dc field sweep rate was controlled by a motor-driven Helipot and was usually set to change the field at the rate of 3.0 milligauss per second. Ample time was afforded thereby for the response of the lock-in amplifiers. The deuteron and proton patterns were usually observed with a time difference less than three seconds. Thus, the requirement on the regulator was to keep the field constant over times of only about this duration. Occasionally, a shift in magnetic field of as much as 3×10^{-6} was detected during the traversal of a resonance pattern. Such patterns were not excluded from the data, and they contributed their share to the lack of precision in the final result. Inconsistency of the field, together

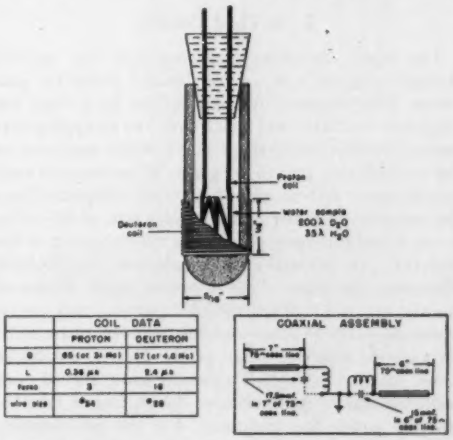

	COIL DATA	
	PROTON	DEUTERON
Q	65 (at 31 Mc)	37 (at 4.8 Mc)
L	0.38 μh	2.4 μh
turns	3	16
wire size	#24	#28

FIG. 4. Water chamber assembly for nuclear resonance measurement. Axes of proton and deuteron coil are perpendicular to each other and to magnetic field, H_0 (directed into the figure).

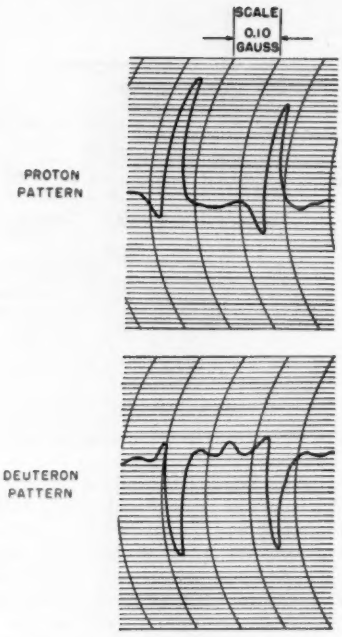

FIG. 5. Proton and deuteron resonance patterns in H_2-D_2. Dispersion signal patterns as they appear at output of lock-in amplifiers; ac sweep set to 0.024 gauss.

with inhomogeneity of the field, constituted the major source of inaccuracy in these measurements. Typical patterns are shown in Fig. 5 for the H_2-D_2 mixture and in Fig. 6 for the H_2O-D_2O mixture.

E. ac Field Control

The small sinusoidally varying field was applied through a separate set of coils wound about the pole pieces. The frequency was determined by a fixed low frequency oscillator and was coupled to an appropriate power amplifier permitting control of the amplitude of the ac field from zero to 2.5 gauss. Measurements were usually made with an amplitude of 24 milligauss. Since the selective amplifier had a band width of 0.5 cycle, it was found necessary to stabilize the frequency to less than 0.1 cycle to insure a stable gain from the amplifier. Moreover, the phase of the resonance signal influenced the size and shape of the recorded pattern; and, hence, it was necessary to avoid variable unknown phase shifts through the selective stage of the lock-in amplifiers. Thus, for the D_2O-H_2O measurements, the 30-cycle oscillator was of multivibrator design locked into the 60-cycle power line frequency. For the gas measurements, it had become necessary to avoid interference effects from adjacent motor generators, and so a 25-cycle oscillator was used, locking into the 100-cycle subharmonic of the 100-kc frequency standard. For studies of frequency modulation effects, the 100-cycle signal was used directly. The phasing arrangement was of the variable RC type driven from the output of a center-tapped transformer which permitted phase shifts from zero to almost 180 degrees.

F. Line Shape

In the initial experiments, we were puzzled by an apparent splitting of the deuteron line. Following a suggestion by Pound, the cause was sought and found to be a frequency modulation effect. The frequency modulation comes because of the use of the 25-cycle magnetic field modulation. In the absence of this modulation, the nuclei precess with frequencies in a narrow band about the central frequency given by Eq. (3). When the modulation is applied, however, side bands appear in the spectrum of the precessional frequency spaced by almost integral multiples of the modulation frequency on either side of the central frequency. The amplitude of the modulation determines the amplitude of the side bands. Where the modulation amplitude is large, the distant side bands contribute and the pattern obtained is broadened. A series of maxima will appear if the width of the resonance is small compared with the modulation frequency. In the present case, the width of the resonance was determined by the inhomogeneity in the magnetic field. The effect was particularly marked when the water samples were used, since then this inhomogeneity amounted to about 18 milligauss for the proton and 36 milligauss for the deuteron. The corresponding line widths are 23 cycles/sec for the deuteron and 77 cycles/sec for the proton. Thus, with a modulation frequency of 30 cycles/sec, a splitting in the line could be expected for the deuteron but not for the proton, and this was as observed. Splitting in the proton pattern was observed when the modulation frequency was increased to 100 cycles/sec.

A closer understanding of the effects of frequency modulation was obtained by applying the analysis of Karplus[9] to the present case. When saturation effects are unimportant, the equations of motion of the magnetic moment of a collection of nuclei in a homogeneous magnetic field $H(t)$ in the z direction, acted upon by a rotating magnetic field of amplitude H_1 and angular frequency ω may be written,[10] in terms of the complex function $F=v+iu$,

$$dF/dt=[\omega_r+i\Delta\omega(t)]F=-|\gamma|H_1M. \qquad (6)$$

Here u and v are the components of the magnetic moment in- and out-of-phase, respectively, with the rotating field H_1; $|\gamma|$ is the absolute value of the gyromagnetic ratio; $\Delta\omega=|\gamma|H_0(t)-\omega$; ω_r is the inverse of the relaxation time; and $M=\chi H_0(t)$ is the equilibrium magnetic moment.

[9] R. Karplus, Phys. Rev. **73**, 1029 (1948).
[10] B. A. Jacobsohn and R. K. Wangsness, Phys. Rev. **73**, 942 (1948).

For sinusoidal modulation of the magnetic field

$$\Delta\omega(t)=\tilde{\omega}+\omega_m\cos\omega_s t. \tag{7}$$

The time-independent solution of Eq. (6) is

$$F=|\gamma|H_1M_0\int_0^\infty dT \times\exp\left[-iT\tilde{\omega}-T\omega_r-i\omega_m\int_{t-T}^{t}\cos\omega_s t'dt'\right]. \tag{8}$$

The exponential in the integrand is expanded in a fourier series in terms of the ordinary bessel function $J_k(x)$,

$$\exp[-i\beta\sin x]=\sum_{k=-\infty}^{\infty}J_k(\beta)\exp[-ikx]. \tag{9}$$

On integrating, Eq. (8) becomes

$$F=-i|\gamma|H_1M_0\sum_{k=-\infty}^{\infty}\sum_{l=-\infty}^{\infty}J_k\left(\frac{\omega_m}{\omega_s}\right)J_l\left(\frac{\omega_m}{\omega_s}\right) \times\exp[i(k-l)\omega_s t]\frac{k\omega_m+\tilde{\omega}+i\omega_r}{(k\omega_m+\tilde{\omega})^2+\omega_r^2}. \tag{10}$$

In the experiments, the bridge was usually unbalanced to give the dispersion signal, which is the imaginary part of F. Moreover, the detector system responded only to the fundamental of the sweep frequency ω_s, so that only terms with $k-l=\pm1$ contribute. The signal is proportional to

$$u=A\cos\omega_s t+B\sin\omega_s t,$$

where

$$A=\sum_{k=0}^{\infty}\frac{2k\omega_s}{\omega_m}J_k^2\frac{2k\omega_s(k^2\omega_s^2+\omega_r^2-\tilde{\omega}^2)}{([k\omega_s+\tilde{\omega}]^2+\omega_r^2)([k\omega_s-\tilde{\omega}]^2+\omega_r^2)}, \tag{11}$$

$$B=\sum_{k=0}^{\infty}\left(\frac{2k\omega_s}{\omega_m}J_k^2-2J_kJ_{k+1}\right) \times\frac{2\omega_r(k^2\omega_s^2+\omega_r^2+\tilde{\omega}^2)}{([k\omega_s+\tilde{\omega}]+\omega_r^2)([k\omega_s-\tilde{\omega}]^2+\omega_r^2)},$$

$$J_k=J_k(\omega_m/\omega_s).$$

In the synchronous detector, this signal is mixed with a reference signal $V=\cos(\omega_s t-\theta)$, and the product of the two is integrated to give the dc output which drives the Esterline Angus recorder:

$$V_0\propto\oint uV dT=A\cos\theta+B\sin\theta. \tag{12}$$

The size and shape of the pattern may be altered markedly by the setting of the phase angle θ. For purposes of frequency comparison, the important feature of (10) and (11) is that the pattern is symmetric with respect to $\tilde{\omega}$ and this dictates the use of the center of symmetry of the pattern in the comparisons.

There is an optimum phase setting which gives maximum response at $\tilde{\omega}=0$.

$$\theta_{\text{opt}}=\tan^{-1}[B(\tilde{\omega}=0)/A(\tilde{\omega}=0)]. \tag{13}$$

At phase angles 90° removed from this, the response at $\tilde{\omega}=0$ becomes zero. When $\omega_s>\omega_r$, frequency modulation effects occur which cause a splitting in the pattern where θ is not close to θ_{opt}. A comparison of patterns as calculated with $\omega_s/\omega_r=1.22$ and $\omega_m/\omega_s=0.64$ with those observed is given in Figs. 7 and 8 for $\theta=\theta_{\text{opt}}$ and $\theta=\theta_{\text{opt}}+\pi/2$, respectively. Such curves confirm the general behavior outlined here and form the basis for the estimates of field inhomogeneity which have been given.

The width of the pattern is minimized by lowering the modulation amplitude until only the terms involving $k=0, 1$ contribute appreciably. Beyond this, the amplitude of the signal is reduced without further reduction in width.

III. RATIO DETERMINATION

A. Procedure

It was found convenient to follow a set procedure for each separate determination. For the D_2O:H_2O system,

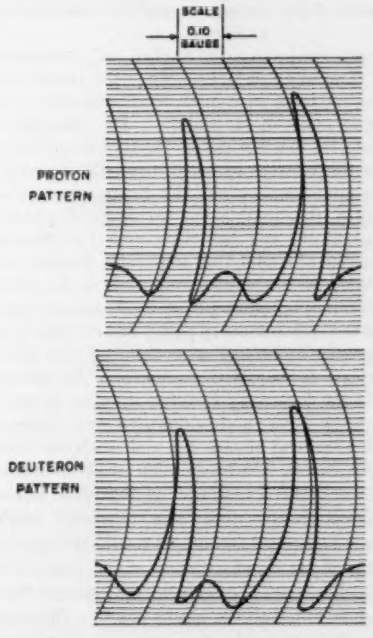

FIG. 6. Proton and deuteron resonance patterns in H_2O-D_2O. Dispersion signal patterns as they appear at output of lock-in amplifiers; ac sweep set to 0.024 gauss.

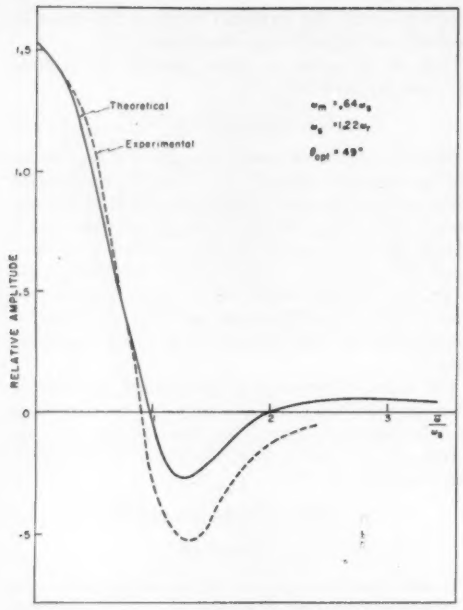

FIG. 7. Resonance line shape for $\theta=\theta_{opt}$. Line has symmetry about the $\tilde{\omega}=0$ axis. Curves are normalized at their maximum.

the sample was prepared in a small vial containing the desired ratio of D to H and Mn^{++} ion concentration. (The gas mixtures were made from a manifold system containing tanks of H_2 and D_2.) The radiofrequency power was set to a low value. The proton and deuteron detector phases were varied through 180 degrees; and the maximum amplitude of the dispersion pattern was determined, thus establishing the optimum phase. The signal amplitude and line width were then determined as a function of modulation amplitude, yielding a value for ω_r. With the modulation amplitude set for minimum line width and optimum phase, a saturation curve was run and the radiofrequency power was reduced to about 0.10 the value at which $\frac{1}{2}$ saturation had been obtained. (In the case of the gas measurements, the values of rf power to the deuteron coil were somewhat higher.)

Frequency checks and calibrations were made at the beginning and end of each run and at several intervals during its course. The modulation oscillator was set to a sequence of values, straddling the value where the patterns coincided in time. The steps were usually 13 cycles/sec apart and constantly monitored against the frequency meter by observation of the Lissajou figure on the oscilloscope. The bridges were balanced to a null and then adjusted to the proper reactive unbalance so that input level at the receivers was 10 microvolts. This adjustment was usually checked at each setting of the modulation oscillator. With the correct pure dispersion pattern attained of approximately equal height in both channels, a series of runs was taken of the line pattern in increasing and decreasing fields and the average displacement of the center of the patterns noted.

B. Results

The detailed measurements are given in Tables I and II for water and gas samples, respectively, where the displacement is given in milligauss. The value of modulation frequency for zero displacement between the center of the deuteron and proton pattern (i.e., identical magnetic field) was determined by the method of least squares. The results for the aqueous system are given in Table III, while those for the gas are shown in Table IV.

In any given run the relative probable error amounted to about 2×10^{-7}, owing primarily to the uncertainty in selection of the line center. The relative error in establishing the frequency ratio amounted to about 1×10^{-7}. In order to reveal the presence of other systematic errors, the experimental conditions were varied in the various runs. Thus, there was some question whether the central field for the two substances was at precisely the same position. Accordingly, in all measurements with water samples new coils were constructed for each determination. For the gas, measurements were taken with coils rotated 90° from their conventional position.

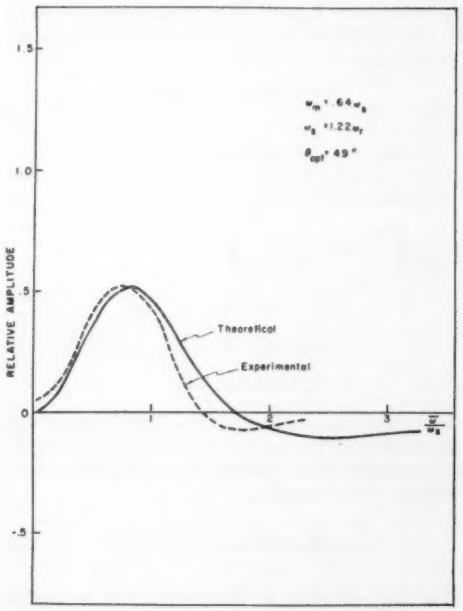

FIG. 8. Resonance line shape for $\theta=\theta_{opt}+\frac{1}{2}\pi$. Line has symmetry about $\tilde{\omega}=0$ axis, thus presenting a doublet appearance. Both curves are normalized at their maximum.

TABLE I. Difference in resonance values of the magnetic field for D+H for various modulation frequencies (using H_2O-D_2O mixture).

Run No.	$\frac{Mn^{++}}{D^+}$	f_0 Master oscillator frequency (cycles sec^{-1})	f_m Modulation oscillator frequency (cycles sec^{-1})	$\langle H(D)-H(H)\rangle_{Av}$ (milligauss)
31	0	2360290	68030.8	−12.7
			68017.6	−9.1
			68004.4	−5.2
			67991.2	−1.4
			67978.0	+1.1
			67964.8	+4.2
			67951.6	+5.6
			67938.4	+9.5
33	1×10^{-6}	2360250	68030.8	−10.5
			68017.6	−8.0
			68004.4	−6.3
			67991.2	−2.5
			67978.0	+0.5
			67964.8	+3.0
			67951.6	+6.9
			67938.4	+11.3
35	1.4×10^{-5}	2360270	68004.4	−8.8
			67991.2	−6.4
			67984.6	−3.6
			67978.0	−1.3
			67964.8	0
			67951.6	+2.7
			67938.4	+7.4
37	1×10^{-5}	2360290	68017.6	−13.1
			68004.4	−12.6
			67991.2	−1.9
			67984.6	−5.8
			67978.0	−1.2
			67971.4	−2.6
			67964.8	0
			67951.6	+2.6
36	1×10^{-4}	2360310	68017.6	−13.6
			68004.4	−6.2
			67991.2	−4.2
			67984.6	−2.5
			67978.0	+2.4
			67964.8	+4.0
			67951.6	+9.9
			67938.4	+9.4

TABLE II. Difference in resonance values of the magnetic field for D+H for various modulation frequencies (using H_2-D_2 mixture).

Run No.	f_0 Master oscillator frequency (cycles sec^{-1})	f_m Modulation oscillator frequency (cycles sec^{-1})	$\langle H(D)-H(H)\rangle_{Av}$ (milligauss)
47	2360250	68004.4	−8.4
		67978.0	−7.0
		67964.8	+3.1
		67951.6	+3.5
		67938.4	+3.7
		67912.0	+12.3
49	2360270	68004.4	−11.3
		67991.2	−8.0
		67978.0	−4.0
		67964.8	−1.7
		67951.6	0
		67938.4	+5.4
		67925.2	+7.3
56	2360330	68004.4	−13.2
		67991.2	−6.5
		67978.0	−2.1
		67964.8	+1.6
		67951.6	+3.4
		67938.4	+5.0
		67925.2	+6.0
57	2360330	67993.4	−2.0
		67959.2	+7.0
		67940.8	+9.8
58	2360200	68004.4	−4.6
		67991.2	−2.6
		67978.0	0
		67964.8	+4.1
		67951.6	+5.7
		67938.4	+9.3
59	2360170	68004.4	−3.4
		67991.2	−5.1
		67978.0	−1.1
		67964.8	−4.9
		67951.6	0
		67938.4	0
		67925.2	+5.9
60	2360250	68004.4	−4.3
		67991.2	−3.9
		67978.0	−2.7
		67964.8	−0.3
		67951.6	+0.5
		67938.4	+1.8
		67925.2	+5.3

Measurements were also made with the coil in different positions in the magnetic field. For some measurements the dc field sweeping rate was varied, the recording systems were interchanged, and the radiofrequency power level altered. In the water measurements different amounts of manganese ion were added, while for the gas the pressure was varied to some extent. The effect of all of these changes can be judged from the self-consistency of the several runs and appears to be of the order of 2×10^{-7}.

An additional uncertainty of about 1×10^{-7} should be included due to the magnetic shielding correction. This correction, when calculated using Ramsey's formula[11] and new values for the rotational field,[12,13] is

[11] N. F. Ramsey, Phys. Rev. **78**, 699 (1950).
[12] Kolsky, Phipps, Ramsey, and Silsbee, Phys. Rev. **79**, 883 (1950).
[13] Kolsky, Phipps, Ramsey, and Silsbee, Phys. Rev. **80**, 483 (1950).

TABLE III. Ratio of the magnetic moment of the proton to that of the deuteron in H_2O-D_2O.

Run No.	Mn^{++}/D^+	μ_H/μ_D	Probable error
31	0	3.25720041	±0.00000022
33	1.0×10^{-6}	3.25720065	0.00000022
35	1.4×10^{-5}	3.25719906	0.00000023
37	1.0×10^{-5}	3.25719906	0.00000079
36	1.0×10^{-4}	3.25720014	0.00000068
	Mean	3.25719986	±0.00000023

very closely the same for both H_2 and D_2. However, a difference in the magnetic shielding constant, σ, arises because of changes in the amplitude of the molecular vibration.[14] For the first term in Ramsey's formula, Newell[15] has calculated that the contribution to σ is greater for D_2 by $(1.1\pm0.2)\times10^{-7}$. He points out, however, that this change could be canceled by the effect of the molecular vibration in the second term.

The result for the ratio of the magnetic moments of the proton and the deuteron from the measurements with the gas is thus

$$\mu_H/\mu_D=3.2571990\pm0.0000010.$$

The correction in the case of the water measurements is less certain and may possibly be twice as large as for the gas. The result of the water measurements is, thus,

$$\mu_H/\mu_D=3.2571999\pm0.0000012.$$

TABLE IV. Ratio of the magnetic moment of the proton to that of the deuteron in H_2-D_2.

Run No.	Pressure (lb/in²) H_2	Pressure (lb/in²) D_2	μ_H/μ_D	Probable error
47	300	700	3.25719876	±0.00000069
49	300	500	3.25719803	0.00000022
56	520	880	3.25719818	0.00000060
57	300	500	3.25720074	0.00000016
58	320	880	3.25720064	0.00000024
59	660	740	3.25719854	0.00000096
60	660	740	3.25719825	0.00000049
		Mean	3.25719902	±0.00000030

[14] G. F. Newell, Phys. Rev. **80**, 476 (1950).
[15] G. F. Newell (private communication).

A comparison of these results with previous determinations of the ratio μ_D/μ_H is given in Table V. The present result is in agreement with that of Levinthal, but with an accuracy of about fifteen times that of the latter. However, it lies outside the stated error of the values given by Lindstrom, as well as that of Bitter *et al.* and of Siegbahn.

Using the value of μ_H/μ_D as determined with the gas and the recent value of m_p/m_e given by Sommer,[16] the expected value of the hyperfine structure ratio ν_H/ν_D is obtained from Eq. (1). The deviation from that measured by Prodell and Kusch[5] is thus

$$\epsilon=\Delta\kappa/\kappa=1.702\pm0.007\times10^{-4}.$$

TABLE V. Comparison with previous values of μ_D/μ_H.

Author	Sample	μ_D/μ_H	Stated error
Bloch[a]	Water	0.3070126	±0.000002
Bitter[b]	Liquid H_2	0.307021	0.000005
Siegbahn[c]	Water	0.3070183	0.0000015
Wimett[d]	Water	0.3070117	0.0000017
Lindstrom[e]	Water	0.30701337	0.00000050
Levinthal[f]	Water	0.3070117	0.0000015
Present work	Water	0.30701217	0.00000012
Present work	Gas	0.30701225	0.00000010

[a] Bloch, Graves, Packard, and Spence, Phys. Rev. **71**, 551 (1947).
[b] Bitter, Alpert, Nagle, and Poss, Phys. Rev. **72**, 1271 (1947).
[c] K. Siegbahn and G. Lindstrom, Nature **163**, 211 (1949).
[d] T. F. Wimett, M.I.T. Research Laboratory of Electronics Report (July, 1949).
[e] G. Lindstrom, Phys. Rev. **78**, 817 (1950).
[f] E. C. Levinthal, Phys. Rev. **78**, 204 (1950).

This value is consistent with the theoretical estimate of this required correction, but possesses a considerably higher precision and thereby provides a critical test of the theory of the structure of the deuteron.

The author is greatly indebted to Professor H. L. Anderson for the suggestion of the problem and for the invaluable advice during its course. He also wishes to express his appreciation to Mr. E. Yasaitis, without whose able assistance the project would have been seriously handicapped, and to Dr. O. C. Simpson, under whose direction this work was undertaken, for his interest and encouragement.

[16] Sommer, Thomas, and Hipple, Phys. Rev. **80**, 487 (1950).

On the Inertia of Oscillating Ferromagnetic Domain Walls*

GEORGE T. RADO
Naval Research Laboratory, Washington, D. C.
(Received March 30, 1951)

It is shown that the inertia of an oscillating ferromagnetic domain wall can be calculated without making any assumptions with regard to the damping mechanism. Physical considerations other than damping are used to formulate appropriate approximations. The particular distribution of spin orientations in an oscillating wall is discussed, and the possibility of dynamic interactions between domain rotations and the wall displacement is pointed out. The inertia of a wall in periodic motion is found to agree with that obtained by Döring for the special case of uniform motion. It is concluded that the inertia depends solely on characteristics of the wall at rest, provided the distortion of the moving wall is sufficiently small to insure the linearity of the equation of motion.

I. INTRODUCTION

ABOUT three years ago Döring[1] showed theoretically that a moving ferromagnetic domain wall possesses an apparent inertial mass which appears as a consequence of the angular momentum that is associated with the magnetic moment of the electrons responsible for the spontaneous magnetization. Döring's work is described briefly in Sec. II. Since domain walls are subject to certain elastic restoring forces which may be estimated from the finite value of the observed initial susceptibility, the discovery of wall inertia enabled Döring to predict the existence of natural frequencies of oscillation for domain walls. It is to be expected, therefore, that the magnetic spectrum of a ferromagnetic substance will contain a (broad) resonance which is distinct from the now well-known rotational resonance connected with the Larmor precession of domains in the internal anisotropy field. Recent studies[2] of ferrite-type materials at this laboratory included the first observation of such a wall resonance, and led to an experimental method for identifying this inertia effect in the presence of a rotational resonance.

Döring's calculation of the apparent mass of a wall, as well as Becker's[3] simplification of the theory, is concerned with a domain wall in *uniform motion* and assumes that the value of the wall velocity is limited by microscopic eddy currents or some other damping processes. Kittel's[4] recent extension of Becker's method also refers to a uniformly moving wall, and is based on the phenomenological damping mechanism originated by Landau and Lifshitz.[5]

Since experimental interest has lately been focused on walls in *oscillatory motion*, and since neither the nature nor the origin of the damping processes in nonconducting ferromagnetic substances is presently understood, it is of interest to inquire whether the concept of wall inertia is valid for any state of wall motion and independent of the damping mechanism. It is the purpose of the present paper to investigate this question by an explicit calculation of oscillatory wall motion. As shown toward the end of Sec. II, the velocity of such walls is inherently limited by their inertia, so that this phenomenon can be studied theoretically without assuming any damping mechanism whatsoever. It is also shown that an oscillating wall, in contrast to a uniformly moving wall, is influenced by dynamic interactions between the wall displacement and domain rotations. The physical consideration of the inertia and interaction effects then leads quite naturally to the approximations appropriate for the mathematical treatment (Sec. III) of a particular type of wall. A form of the distribution of spin orientations suggested by physical considerations is shown to be a satisfactory approximation. This form differs significantly from that in a uniformly moving wall. In Sec. IV the wall inertia derived from the spin orientations is generalized to any type of wall and the effects of damping are noted. It is concluded, in effect, that under the conditions likely to be encountered experimentally, the inertia is an intrinsic property of a domain wall, and its value depends solely on characteristics of the wall at rest.

II. PHYSICAL CONSIDERATIONS

Consider a free domain wall which separates two domains magnetized parallel to the unit vectors $\mathbf{i}_1$ and $\mathbf{i}_2$. If this wall is to move under the influence of a homogeneous magnetic field, $\mathbf{H}_a$, it is for energetic reasons necessary that

$$\mathbf{H}_a \cdot (\mathbf{i}_1 - \mathbf{i}_2) \neq 0. \tag{1}$$

Since the electronic magnetic moments are gyroscopic, however, an $\mathbf{H}_a$ satisfying Eq. (1) cannot "directly" give rise to the "flipping over" of the spins which takes place in the moving wall. It may seem, therefore, as if Eq. (1) were not a sufficient condition for wall motion. But the torque exerted by $\mathbf{H}_a$ on the spins distorts the shape of the wall by producing an increase in the component of magnetization antiparallel

* Presented at the New York meeting of the American Physical Society, February 3, 1951 [Phys. Rev. 82, 340(A) (1951)].
[1] W. Döring, Z. Naturforsch. 3a, 374 (1948).
[2] Rado, Wright, and Emerson, Phys. Rev. 80, 273 (1950).
[3] R. Becker, Proceedings of the Grenoble Conference, July, 1950. An even simpler derivation was presented by Professor Becker in a lecture delivered in December, 1950, at Catholic University, Washington, D. C.
[4] C. Kittel, Phys. Rev. 80, 918 (1950).
[5] L. Landau and E. Lifshitz, Physik. Z. Sowjetunion 8, 153 (1935).

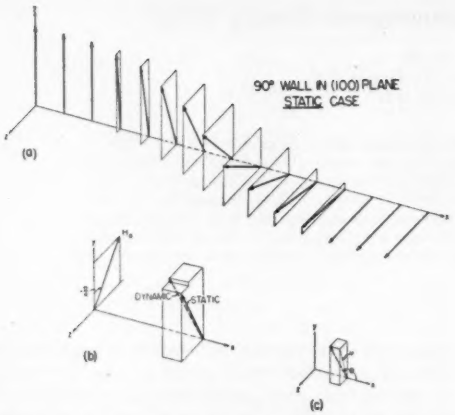

FIG. 1. (a) Schematic representation of static spin orientations in a 90° domain wall parallel to the (100) plane of a material with positive crystalline anisotropy. Note that in this particular static case all the spins are parallel to the plane of the wall. (b) Illustration of the effect of an applied field on the orientation of a spin at a given distance from the instantaneous center of the wall. The distortion of the moving wall, indicated by the deviation of the vector labeled "dynamic" from the (100) plane, is responsible for the dynamic demagnetizing field which exists in the wall during motion. In the case shown, the wall moves toward the positive x direction. (c) Polar coordinates used in the mathematical treatment.

to the "wall-normal,"[6] $\mathbf{w}$, and this additional magnetization, in turn, generates a non-uniform demagnetizing field oriented parallel to $\mathbf{w}$. In the gyroscopic sense it is the additional demagnetizing field inside the moving wall that makes the "flipping-over" of the spins possible, and thus Eq. (1) is indeed a sufficient condition for wall motion. The simple example of Fig. 1 is especially suited to illustrate the above remarks because in that particular 90° wall there is no magnetization normal to the plane of the wall (yz plane) as long as the wall is at rest (Fig. 1(a)). If, however, an $\mathbf{H}_a$ is applied (Fig. 1(b)) in the direction shown (which satisfies, of course, Eq. (1)), then the distribution of spin orientations moves toward the positive x-direction and the immediate (rather than ultimate) cause of this motion is the torque exerted on the spins by the demagnetizing field oriented along $+x$ inside the moving wall.

Although these gyroscopic effects are included in the calculations of Landau and Lifshitz, it was Döring who first pointed out that the wall distortion attendant on wall motion causes the surface energy, σ, of a moving wall to exceed the surface energy, σ_0, of the same wall at rest. He found, in particular, that for the case of uniform motion

$$\Delta\sigma=\sigma-\sigma_0=(m_w/2)v^2, \tag{2}$$

where v is the wall velocity and m_w denotes the apparent (inertial) mass per unit wall area. For a cubic lattice described by the lattice constant, a, the value of m_w is given by

$$m_w=\sigma_0/(2\pi\gamma_g^2Ja^2n\sin^2\theta_w), \tag{3}$$

where J represents an average exchange integral between neighboring spins, n is the effective number of spins per unit volume, θ_w is defined by

$$\cos\theta_w=\mathbf{w}\cdot\mathbf{i}_1=\mathbf{w}\cdot\mathbf{i}_2, \tag{4}$$

and γ_g, the magneto-mechanical ratio, is taken as[7]

$$\gamma_g=2\mu_B/\hbar=e/mc \tag{5}$$

because spin-orbit effects are neglected. It is interesting to note, as Becker[8] has emphasized, that the apparent kinetic energy, $\Delta\sigma$, is simply the magnetic energy per unit wall area stored in the additional demagnetizing field which exists within the moving wall.

In deriving Eqs. (2) and (3), Döring made two assumptions whose combined effect is to insure that the shape of the moving wall is distorted by only a small amount with respect to that of the wall at rest. The first assumption is somewhat arbitrary in that it postulates that v is sufficiently small that

$$(\hbar vn/2K\delta)\cong 1. \tag{6}$$

Here K is the first-order anisotropy constant and

$$\delta=(Ja^2n/4K)^{\frac{1}{2}} \tag{7}$$

is the wall thickness parameter. The second assumption is a recognition of the fact that in many materials

$$\lambda=K/(2\pi M_s^2)\ll 1, \tag{8}$$

where $M_s(=n\mu_B)$ is the saturation magnetization. Accordingly, terms of the order λ^2 are neglected in the final expression for σ.

The inertia effect anticipated for the case of a domain wall in undamped oscillatory motion leads one to suppose that the wall velocity is proportional to the applied field,[9] $H_a=H_0\exp(i\omega t)$, provided H_0 is sufficiently small, and $\omega\neq 0$. As shown below, these conditions can be met by restricting H_0 to the range

$$p=\gamma_gH_0/\omega\ll 1 \tag{9}$$

for any finite value of ω. The relation (9) implies that the period of oscillation of the applied field is much smaller than its Larmor period. Consequently, the direction of $\mathbf{H}_a$ is reversed before it is possible for the internal demagnetizing field (which is established by the effect

[6] In the case of a moving wall it is convenient to define the wall-normal as being a unit vector, $\mathbf{w}$, which is perpendicular to the plane of the wall and parallel to the wall velocity vector, $\mathbf{v}$.

[7] μ_B is the Bohr magneton, e/mc the specific electronic charge, and $2\pi\hbar$ the Planck constant.

[8] Both treatments of Becker avoid Döring's more rigorous perturbation calculation by neglecting at the outset the changes, due to wall motion, of the exchange and anisotropy torques acting on the spins. The resulting simplification of the problem leads to a clarifying emphasis on the essential role of the demagnetizing field in the interior of a moving wall.

[9] In any actual ferromagnetic material the wall oscillations are always damped, and $v\propto H_a$ for sufficiently small values of H_a.

of $\mathbf{H}_a$ on the spins) to be altered appreciably. Since it is the demagnetizing field that drives the wall, there is seen to be a tendency for the wall to oppose a change in its state of motion. This tendency is basically a consequence of the gyroscopic nature of the spins and may be regarded as the physical basis of the wall inertia effect.[10]

The domain rotations which accompany any wall displacement in an alternating field give rise to an instantaneous component of magnetization parallel or antiparallel to $\mathbf{w}$, and thus they affect the demagnetizing field inside the wall. This means that in oscillating walls, unlike in uniformly moving walls, there must be a dynamic coupling between wall displacements and domain rotations. Since damping mechanisms are not considered at present, the desired proportionality between v and H_a requires that ω be restricted to the range

$$q=\frac{\omega}{\gamma_0(2K/M_s)}\ll 1, \tag{10}$$

which corresponds to values of ω well below the Larmor resonance frequency of rotations in the internal anisotropy field.

The approximations (9) and (10) state that terms of the order p^2 and q^2 are to be neglected in comparison to unity. They are necessitated by the requirement of small wall distortion, or the essentially equivalent requirement of $v\propto H_a$. It may be noted that with the help of Eqs. (31), (38), and (33), which will be derived in Sec. III, the approximation (9) can be shown to be equivalent to the statement that the dynamic demagnetizing field at any point in the wall is much smaller than the maximum conceivable value, $4\pi M_s$. Furthermore, Eqs. (16a) and (28a) indicate, as expected, that the approximation (10) causes the contribution of the domain rotations to the demagnetizing field to be much smaller than the contribution (due to the effect of H_a) of the spins in the wall. Finally, it should be mentioned that in calculating σ it proves convenient (although not necessary) to assume that the magnetic constants of the material in question satisfy the approximation (8) sufficiently well to justify neglecting terms of order λ (rather than λ^2) in comparison to unity.

III. MATHEMATICAL TREATMENT

Let $\mathbf{i}_x$, $\mathbf{i}_y$, and $\mathbf{i}_z$ be unit vectors along the cubic axes of a crystal with cubic symmetry, and let

$$\mathbf{s}=\alpha\mathbf{i}_x+\beta\mathbf{i}_y+\gamma\mathbf{i}_z \tag{11}$$

be a unit vector parallel to an arbitrary spin. The equation of motion[1,5] may be written in the form

$$(\hbar/2)(\partial\mathbf{s}/\partial t)=\mathbf{T}_J+\mathbf{T}_K+\mathbf{T}_H, \tag{12}$$

where

$$\mathbf{T}_J=(Ja^2/2)\mathbf{s}\times\nabla^2\mathbf{s}, \tag{13}$$

$$\mathbf{T}_K=(2K/n)\mathbf{s}\times(\alpha^3\mathbf{i}_x+\beta^3\mathbf{i}_y+\gamma^3\mathbf{i}_z), \tag{14}$$

$$\mathbf{T}_H=\mu_B\mathbf{s}\times\mathbf{H}, \tag{15}$$

are the torques[11] due to exchange, anisotropy, and magnetic field, respectively, and $\mathbf{H}$ includes $\mathbf{H}_a$ as well as any demagnetizing field. Equation (12) is general except for the fact that magnetoelastic torques, damping torques, and torques due to lattice imperfections are neglected. However, the following calculations refer to a particular kind of 90° wall (Fig. 1(a)) in a substance with positive anisotropy, and they assume that the domains adjacent to the wall are of semi-infinite extent. It is also assumed that the direction of $\mathbf{H}_a$ bisects the angle between $\mathbf{i}_y$ and $(-\mathbf{i}_z)$ (Fig. 1b). The problem is thus simplified because in this particular case the domains precess in such a way that their components of magnetization parallel to $\mathbf{w}$ (i.e., parallel to $\mathbf{i}_x$) are equal at all times. Generalizations of the present model will be discussed in the next section.

The components of $\mathbf{H}$ are given by

$$H_x=4\pi M_s({}^{\infty}\alpha-\alpha), \tag{16a}$$

$$H_y=2^{-\frac{1}{2}}H_0e^{i\omega t}, \tag{16b}$$

$$H_z=-2^{-\frac{1}{2}}H_0e^{i\omega t}, \tag{16c}$$

where ${}^{\infty}\alpha$ is the value of α in either domain, i.e., at $x=\pm\infty$. The demagnetizing field, H_x, is seen to be obtained from the condition that the component of the induction parallel to $\mathbf{w}$ must be continuous across the wall. Equation (16a) shows that the domain rotations affect H_x, and thus implies that they are coupled to the wall motion.

It is convenient to introduce the polar coordinates θ and ϕ with respect to the wall normal as polar axis (Fig. 1(c)), and to consider $\alpha(=\cos\theta)$ and ϕ, rather than α, β, and γ, as the independent variables. Figure 1(a) indicates that both α and ϕ can depend on x and t only. Before solving Eq. (12), however, it is useful to introduce the dimensionless quantity

$$\xi=(1/\delta)(x-X) \tag{17}$$

as a measure of the distance of an arbitrary spin from the instantaneous center of the wall. Here X is the time-dependent wall displacement which is related to the wall velocity, v, by $v=dX/dt$. On the basis of the physical situation discussed in Sec. II it seems reasonable to suppose that α and ϕ are each given by a function of ξ

[10] It may be noted that, irrespective of damping, the susceptibility due to wall motion is determined essentially by the inertia effect provided the driving frequency is large compared with the wall resonance frequency. This fact might be used for determining m_w by an experiment which does not involve domain rotations; the result may then be compared with the m_w obtained from the measured wall resonance frequency.

[11] The corresponding energy densities are given by

$$E_J=(Ja^2n/4)[(\nabla\alpha)^2+(\nabla\beta)^2+(\nabla\gamma)^2],$$
$$E_K=K(\alpha^2\beta^2+\beta^2\gamma^2+\gamma^2\alpha^2)=(K/2)[1-(\alpha^4+\beta^4+\gamma^4)],$$
$$E_H=-M_s\mathbf{s}\cdot\mathbf{H}.$$

These expressions are discussed in connection with static domain theory by C. Kittel, Revs. Modern Phys. **21**, 541 (1949). It may be noted that the above value of E_J assumes a spin of $(\frac{1}{2})\hbar$; the corresponding value of E_J in Kittel's review (Eq. 2.1.11), on the other hand, is specialized to a body centered cubic lattice.

plus a small time-dependent perturbation describing the wall distortion. It proves advantageous to postulate solutions of the particular form

$$\alpha(\xi, t)=\alpha_0(\xi)+\alpha_1(\xi)pe^{i\omega t}, \tag{18}$$

$$\phi(\xi, t)=\phi_0(\xi)+\phi_1(\xi)qpe^{i\omega t}, \tag{19}$$

$$v(t)=(4\pi M_s\gamma_g\delta)V_0pe^{i\omega t}, \tag{20}$$

where the absolute values of the dimensionless quantities α_0, α_1, ϕ_0, ϕ_1, and V_0 will be shown to be of order unity or smaller. These solutions mean that the spins in the oscillating wall perform small precession-like motions with respect to the orientations which they would have if the shape of the oscillating wall were the same as that of the wall at rest. The corresponding solutions for the case of uniform motion, on the other hand, are functions of the single variable $(x-vt)$, so that the distortion of the uniformly moving wall (relative to the wall at rest) is independent of time. This difference between the two sets of solutions might seem to be of formal significance only. But Landau and Lifshitz[5] assumed, in fact, that even in an oscillating wall the quantity $(x-vt)$ is the single independent variable, and consequently they were led to the incorrect result that in the case of vanishing damping a free oscillating wall gives rise to an infinite susceptibility at any frequency.

Equations (18), (19), and (20) may now be substituted into Eq. (12) by using the relations

$$\partial/\partial t=-(v/\delta)(\partial/\partial\xi), \tag{21}$$

$$\nabla^2=\partial^2/\partial x^2=(1/\delta^2)(\partial^2/\partial\xi^2), \tag{22}$$

which follow from Eq. (17). The resulting scalar equations are evaluated by equating the coefficients of separate powers of p to zero. Using the boundary conditions

$$\alpha_0=0, \quad \phi_0=0, \quad \text{at} \quad \xi=-\infty, \tag{23a}$$

$$\alpha_0=0, \quad \phi_0=\pi/2, \quad \text{at} \quad \xi=+\infty, \tag{23b}$$

one obtains for the zeroth approximation in p

$$4(d^2\phi_0/d\xi^2)-\sin4\phi_0=0, \tag{24}$$

$$\alpha_0=0. \tag{25}$$

Since ϕ_0 must satisfy the additional boundary condition that $d\phi_0/d\xi=0$ at $\xi=\pm\infty$, Eq. (24) gives

$$d\phi_0/d\xi=(\tfrac{1}{2})\sin2\phi_0, \tag{26}$$

which leads to

$$\phi_0=\text{arc tan}e^{\xi} \tag{27}$$

if ξ is measured from the instantaneous center of the wall ($\xi=0$ when $\phi_0=\pi/4$). It is interesting that in the limiting case of $H_0=0$ (where $v=0$, and hence $\xi\equiv x$), the Eqs. (25), (26), and (27) agree with Néel's[12] results for the static spin orientations in the type of domain wall under consideration. Equation (25) shows, in particular, that in the static case all the spins are parallel to the plane of the wall (yz plane).

If the scalar equations resulting from Eqs. (12), (21), and (22), are evaluated to the first approximation in p, it is found that the time dependence is eliminated and that [owing to Eq. (16a)] one of the two equations for $\alpha_1(\xi)$ and $\phi_1(\xi)$ obtained in this way contains the unknown quantity $\alpha_1(\infty)$. It is therefore convenient to begin by solving these two equations for those regions ($\xi=\pm\infty$) which are occupied by the domains. In these regions $d^2\alpha_1/d\xi^2=d^2\phi_1/d\xi^2=0$ (because all the spins are parallel), α_0 and ϕ_0 are given by Eqs. (23) and the use of Eq. (10) leads to the solutions

$$\alpha_1(\infty)=-2^{-\frac{1}{2}}iq^2/(1-q^2)\approx 0, \tag{28a}$$

$$\phi_1(\infty)=-2^{-\frac{1}{2}}/(1-q^2)\approx -2^{-\frac{1}{2}}. \tag{28b}$$

Equations (28a) and (10) make it now possible to obtain the relatively simple equations

$$d^2\phi_1/d\xi^2-(\cos4\phi_0)\phi_1=2^{-\frac{1}{2}}(\cos\phi_0+\sin\phi_0)+i\alpha_1, \tag{29}$$

$$\alpha_1-\lambda[(d^2\alpha_1/d\xi^2)-\alpha_1(1-3\sin^2\phi_0+3\sin^4\phi_0)]=-(V_0/2)\sin2\phi_0 \tag{30}$$

which determine $\alpha_1(\xi)$ and $\phi_1(\xi)$ for any arbitrary spin. At first sight it might seem as if such a determination could not be carried out because the parameter V_0 is unknown. However, it will be shown below that V_0 must have one definite (and calculable) value if ϕ_1 is to represent the distortion of a wall that moves in accordance with the solutions postulated in Eqs. (18), (19), and (20).

The calculation of the wall inertia is based on Eq. (30) and does not require a knowledge of V_0. This equation may be simplified considerably by neglecting[13] the term proportional to λ, as mentioned in Sec. II. Using Eqs. (30), (18), (25), (20), and (28a), Eq. (16a) then leads to the value

$$H_x=-4\pi M_s\alpha=(v/2\gamma_g\delta)\sin2\phi_0 \tag{31}$$

for the demagnetizing field. The excess surface energy of the moving wall ($\Delta\sigma=\sigma-\sigma_0$) is due not only to the energy stored in H_x but contains contributions due to anisotropy and exchange also. However, the latter contributions may be neglected because they are smaller than the demagnetizing energy by a factor[14] of the order λ. Thus one obtains

$$\Delta\sigma=(\delta/8\pi)\int_{-\infty}^{\infty}H_x^2d\xi=(\tfrac{1}{2})(1/8\pi\gamma_g^2\delta)v^2, \tag{32}$$

so that the apparent mass per unit wall area is given by

$$m_w=(1/8\pi\gamma_g^2\delta). \tag{33}$$

[12] L. Néel, Cahiers phys. **25**, 1 (1944).

[13] If the λ term is not neglected, Eq. (30) may be solved formally by a power series expansion in λ. The resulting expression for α_1 is still proportional to V_0.

[14] A simple calculation, based on the expressions given in footnote 10, shows that the contributions to $\Delta\sigma$ due to anisotropy and exchange are each of the order K. The contribution due to demagnetization, on the other hand, is of the order M_s^2.

This value is interesting because it agrees precisely with that obtained from Döring's formula, Eq. (3), which was derived for a uniformly moving wall. To show this correspondence it is merely necessary to observe that $\theta_\infty=\pi/2$, and $\sigma_0=K\delta$, for the type of wall under consideration.

Before calculating the wall velocity it should be recalled that the consequences of the equation of motion [Eq. (12)] must be sufficient to determine α and ϕ as functions of x and t; thus the unknown parameter v (or the dimensionless constant V_0) is necessarily an "artificial unknown" which was introduced, through the use of the coordinate ξ, merely to obtain those spin orientations which correspond to a moving wall. Consequently V_0 must be calculable from Eqs. (29) and (30) even though these do contain two "essential unknowns" (α_1 and ϕ_1). Combining Eqs. (29) and (30), and introducing $U(\xi)=\phi_1(\xi)-\phi_1(\infty)$, one obtains an equation which can be written in the form

$$\frac{1}{\sin 2\phi_0}\frac{d}{d(2\phi_0)}\left[\sin 2\phi_0\frac{dU}{d(2\phi_0)}\right]+\left(2-\frac{1}{\sin^2 2\phi_0}\right)U=F(V_0,\phi_0) \quad (34)$$

if the independent variable is changed from ξ to ϕ_0 by means of Eq. (26). Here

$$F(V_0,\phi_0)=[-(iV_0/2)\sin 2\phi_0+2^{-\frac{1}{2}}(\cos\phi_0+\sin\phi_0+2\sin^2 2\phi_0-1)]\sin^{-2}2\phi_0, \quad (35)$$

and $U(\phi_0)$ is subject to the boundary conditions

$$U(0)=U(\pi/2)=0. \quad (36)$$

Since the homogeneous part of Eq. (34) possesses the eigenfunction $P_1^1(\cos 2\phi_0)$ (which is the associated Legendre function $\sin 2\phi_0$), it follows from the theory of orthogonal functions[15] that the inhomogeneous Eq. (34) does not, in general, have a solution satisfying the same boundary conditions (Eq. (36)) as the homogeneous part of Eq. (34). Such a solution exists, in fact, only if the P_1^1 component of the inhomogeneous part vanishes. It is therefore possible to calculate[16] V_0 from the requirement that

$$\int_{-1}^{1}F(V_0,\phi_0)P_1^1(\cos 2\phi_0)d(\cos 2\phi_0)=0. \quad (37)$$

On this basis one obtains $V_0=2^{\frac{1}{2}}/i$, showing that $|V_0|$, (and hence $|\alpha_1|$ and $|\phi_1|$) is of order unity in accordance with the original assumption. Equation (20) than leads to the final result

$$v=(2^{\frac{1}{2}}M_s/i\omega m_\infty)H_0e^{i\omega t}, \quad (38)$$

where m_∞ is given by Eq. (33).

The value of ϕ_1 may now be calculated by expanding Eq. (34) in a series of associated Legendre functions of the type $P_n^1(\cos 2\phi_0)$. It is more interesting, however, to consider some of the consequences of Eq. (38), even though this equation cannot be used to predict v for any actual ferromagnetic substance because the damping and restoring forces acting on the wall have not been taken into account. Assuming that the value of m_∞ for the oscillating wall is known to be given by Eq. (33), one can equate the inertial force per unit wall area and the pressure exerted by the applied field on the wall. The solution of the simple equation

$$m_\infty(dv/dt)=M_s[2^{-\frac{1}{2}}-(-2^{-\frac{1}{2}})]H_0e^{i\omega t} \quad (39)$$

obtained in this manner is easily seen to be identical with Eq. (38). This fact permits two conclusions. (1) As expected on the basis of Eqs. (16a) and (28a), the dynamic coupling between the wall displacement and the domain rotations is negligible because of the approximations used. (2) The work per unit wall area required to displace the oscillating wall by an amount dX is identical with that required to turn the spins contained in a volume dX from the $+z$ direction to the $+y$ direction. Consequently, the amount of work required to produce the distortion existing in the oscillating wall is negligible because of the approximations used.

IV. GENERALIZATIONS

The results obtained in Sec. III may be generalized by allowing the direction of $\mathbf{H}_a$ to be arbitrary instead of requiring it to be parallel to the $[01\bar{1}]$ direction. It can easily be shown that the value of m_∞ is not changed from that given by Eq. (33), and that Eq. (38) for v still applies provided H_0 is replaced by its component along the $[01\bar{1}]$ direction. The proof of the latter statement involves primarily a redefinition of the function U; but the details of the calculation may be omitted because the inequality (1) clearly indicates that only the component of $\mathbf{H}_a$ parallel to the $[01\bar{1}]$ direction is energetically capable of displacing the particular wall considered here. If $\mathbf{H}_a$ is periodic without being sinusoidal, then the problem can be generalized by means of a fourier development provided the maximum amplitude of $\mathbf{H}_a$ is sufficiently small. The method given in Sec. III could also be extended to any arbitrary domain wall without requiring the introduction of new concepts. Such calculations would show, in agreement with Döring's analysis, that the static spin orientations do not generally lie in the plane of the wall, and that Döring's result for the inertia, Eq. (3), is still valid for the oscillatory case.

As pointed out previously,[2] the damping existing in actual ferromagnetic substances may influence the apparent mass of a wall. This effect was evaluated by

[15] See, for example, E. Madelung, *Die mathematischen Hilfsmittel des Physikers* (Verlag. Julius Springer, Berlin, 1936), pp. 196 and 201.

[16] A somewhat similar method was used by Landau and Lifshitz (reference 5) in connection with a related problem. However, their result for v diverges in the case of vanishing damping, as mentioned previously.

Kittel[4] for the case of a uniform motion by using the particular phenomenological damping torque introduced by Landau and Lifshitz. By taking this torque into account in the oscillatory case also, the wall velocity would be limited without having to use the approximations[17] (9) and (10). However, the effect of damping on m_w is quite small, and in the case studied experimentally[2] this correction is well within the accuracy of the approximations used in the theories of inertia. Since not even the mathematical form of the Landau-Lifshitz damping torque has been verified by existing experimental results, it seems preferable not to consider the damping effects at present. If unexpected developments in the study of the damping mechanism are excluded, one may therefore conclude that the inertia of a wall is independent of the state of motion, and dependent solely on characteristics of the wall at rest, provided the distortion of the moving wall is sufficiently small to ensure the linearity of the dynamic wall problem.

[17] It is interesting to consider some numerical values in connection with these approximations. For $\gamma_0 H_0$ one may use 2.8×10^8 cycles/sec, corresponding to the representative value of $H_0=0.1$ oersted; $\gamma_0(2K/M_s)$, on the other hand, is about 1.5×10^9 cycles/sec for iron, and about 2.5×10^9 cycles/sec for the particular ferrite which showed an experimental wall resonance (reference 2) at about 5×10^7 cycles/sec.

The author wishes to thank Mr. W. S. Ament for helpful discussions on orthogonal functions, and Dr. M. H. Johnson for valuable comments on the manuscript.

PHYSICAL REVIEW VOLUME 83, NUMBER 4 AUGUST 15, 1951

On the Sensitivity of Photographic Grains to Electrons*†

DAVID OKRENT‡ AND A. K. SOLOMON
Biophysical Laboratory, Harvard Medical School, Boston, Massachusetts, and Physics Department, Harvard University, Cambridge, Massachusetts

(Received December 26, 1950)

Three single-grain-layer photographic emulsions have been exposed to a measured quantity of monoenergetic electrons, varying in energy from 7 to 112 kev. Two of the coatings (both chlorobromides) had high background fog, which introduced considerable error in the counting procedure. Also, neither of these films was especially sensitive to electrons. Nevertheless, it could be ascertained that the sensitivity of these coatings was fairly constant up to 50 to 70 kev, after which it dropped off slowly. These two coatings were prepared in almost identical fashion and showed a similar response to white light, yet their sensitivity to electrons differed by a factor of 8 or 9.

The third coating was a fine-grained bromoiodide, similar to the emulsions used in nuclear track plates. This coating was essentially fog-free, and reproducible results were obtained. The sensitivity was highest at low electron energies (approaching unity), dropping rapidly at first, then leveling off for higher energies. The curve of developability probability as a function of electron energy bears a close resemblance to the curve of space rate of energy loss for the electron. It also is in fairly good agreement with curves based on grain count data for electron tracks reported by Ross and Zajac.

It was estimated that at 112 kev the electron forms about 62 ion pairs in passing through the center of a grain in this third coating. Since the sensitivity is still appreciable at this energy, this number of ion pairs should roughly represent a quantity which is approaching the lower limit of the number required to render the average grain in this coating developable. This is to be compared with the data that Webb has published, namely, that about 40 quanta of light are needed on the average to render a photographic grain developable.

I. INTRODUCTION

WHEN light of the proper wavelength is incident on a photographic emulsion, some of the silver halide grains (the number depending on the amount of exposure) are altered in such a way that they react differently toward certain reducing agents known as developers. That is to say, those grains which have been affected sufficiently by the light are reduced to metallic silver by the developer, while the other grains are not reduced at all. This developable state is called the latent image and is not susceptible to direct observation.

The latent image consists of a submicroscopic speck of silver, sufficiently large and properly located to produce developability. According to the Gurney-Mott[1] theory of latent image formation, the absorption of a light quantum by the photographic grain raises a bound electron into the conduction band or into an exciton level, the exciton being subsequently dissociated by thermal motion. Freed electrons will migrate and be trapped at imperfections in the crystal, whereupon positive silver ions will diffuse to the trapped electrons and be neutralized. Sufficient repetition of this process at a suitably located point will result in the formation of a latent image.

A high velocity charged particle striking a photographic grain should have a similar action. Coulomb

* This paper is a summary of the thesis submitted by David Okrent in partial fulfillment of the requirements for the Ph.D. in physics.

† This work was supported in part by the AEC, the ONR, and the American Cancer Society.

‡ AEC Predoctoral Fellow. Present address: Argonne National Laboratory, Chicago, Illinois.

[1] R. W. Gurney and N. F. Mott, Proc. Roy. Soc. (London) **A164**, 151 (1938).

forces will free bound electrons along the path of the particle in the grain, and if the number released is sufficient, a latent image will be formed. If a single particle does not give up sufficient energy to the grain, several hits on an individual grain may be required.

For particle energies below that producing minimal ionization in the surrounding medium, the space rate of energy loss for the various charged particles will vary almost inversely with the energy of the particle. The greater the energy of the incident particle, the smaller is the space rate of energy loss. Webb[2] has given theoretical curves of the space rate of energy loss in air for alpha-particles, deuterons, mesons, and electrons, based on calculations for the proton by Smith.[3]

For alpha-particles of polonium the space rate of energy loss is so high that the number of electrons freed in a transpierced photographic grain is well above the minimum required for latent image formation. Thus, Webb[4] has measured the developability probability[4a] to be unity in this case. Indeed, for alpha-particles of 380 Mev, the probability is still so high that a recognizable track is left in nuclear track plates. Of course, the grain spacing is much greater at the high energy end of the track, since here not every transpierced grain will have sufficient electrons released to form a latent image.

For lighter particles, the space rate of energy loss, and hence the probability of developability, becomes proportionately less for the same particle energy.

Many measurements have been made on the sensitivity of photographic emulsions to electrons, including those reported by Baker, Ramberg, and Hillier,[5] Borries,[6] Charlesby,[7] Cranberg and Halpern,[8] and Ellis and Aston.[9] These papers all present Hurter-Driffield curves of density as a function of exposure for various emulsions and conditions, where the density is defined as the logarithm to the base 10 of the ratio of the intensity of the original beam of light to the intensity of the beam which is transmitted through the silver deposit in the emulsion. All measurements were made with relatively thick, multi-grain-layer emulsions in which the incident particles lost a considerable part, if not all, of their energy in their passage through the emulsion. These measurements were not intended to supply information on the response of individual photographic grains, but rather to obtain data on the gross sensitivity of the emulsion. This paper, on the other hand, reports on some direct measurements of the developability probability for individual photographic grains exposed to monoenergetic electrons in the energy range 7 to 115 kev. Special single-grain-layer emulsions were used to avoid an averaging process on the effect of the electron over its energy range while in the emulsion. The single-grain-layer emulsion also made it feasible to count individual grains visually with the aid of a microscope.

The films were exposed to measured quantities of uniformly distributed, monoenergetic electrons for

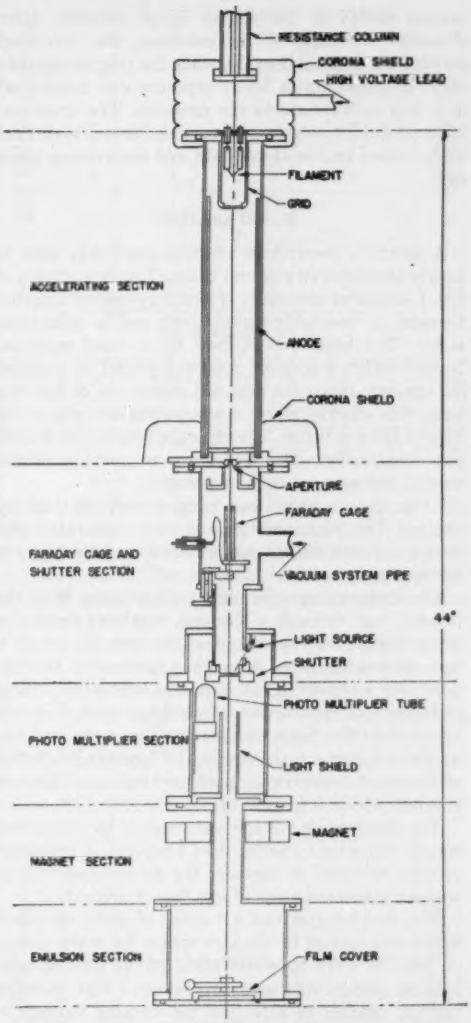

FIG. 1. Schematic, scale diagram of electron gun used to expose single-grain-layer film to monoenergetic electron beam.

[2] J. H. Webb, Phys. Rev. **74**, 511 (1948).
[3] J. H. Smith, Phys. Rev. **71**, 32 (1947).
[4] J. H. Webb, J. Opt. Soc. Am. **38**, 312 (1948).
[4a] The developability probability is defined as the probability that a photographic grain will form a latent image and be rendered developable if it is transpierced by an incident particle.
[5] Baker, Ramberg, and Hillier, J. Appl. Phys. **13**, 450 (1942).
[6] B. v. Borries, Physik. Z. **43**, 190 (1942).
[7] A. Charlesby, Proc. Phys. Soc. (London) **52**, 657 (1940).
[8] L. Cranberg and J. Halpern, Rev. Sci. Instr. **20**, 641 (1949).
[9] C. D. Ellis and G. H. Aston, Proc. Roy. Soc. (London) **A119**, 645 (1928).

various points in the energy range covered. After chemical processing of the emulsion, the developed grains were counted directly, while the original number of undeveloped grains before exposure was determined in a way appropriate to the emulsion. The developability probability was then determined from a statistical study, based on the above data and the average grain size.

II. APPARATUS

A specially constructed electron gun[10] was used to supply the required electron beam. The gun, shown in Fig. 1, consisted essentially of a battery-heated tungsten filament, a resistance-biased grid, and a cylindrical anode. The beam was defined by a small aperture, beyond which a faraday cage was placed to measure the current. When the cage was swung out of line, the beam was intercepted by a camera shutter lying in its path to the film below. The exposure time was measured photoelectrically. The deflecting magnet permitted several exposures on each film sample.

Large variations in beam current were obtained by varying the bias resistor and the filament-to-grid distance. Finer control was attained by adjusting the filament temperature.

The current from the electron beam ran from the faraday cage through a shielded, insulated conductor to the input of a vibrating reed electrometer, where it was allowed to bleed through a calibrated resistor, providing a steady signal. Readings were taken before and after each exposure and the average used. It is estimated that the beam current readings were accurate within 2.5 percent absolutely, 1.5 percent relatively, while the photoelectrically measured exposure time was accurate within 0.75 percent.

The accelerating voltage was supplied by a dc power supply regulated to better than 1 percent. A resistance column was used to measure the accelerating voltage with an estimated error of less than 2 percent.

The electron gun had a volume of about six liters, which was opened to the atmosphere for every change of film. A VMF-50 oil-diffusion pump with suitable backing pumps was used to provide a fast pumping system, capable of attaining the working vacuum of 10^{-4} mm of Hg within a reasonable time.

III. DEVELOPING PROCEDURE

The film was loaded, unloaded, and developed in complete darkness. Usually, three or four exposures were made on each film strip, the latter coming from one long roll for each emulsion examined. Considerable care had to be exercised in handling the film, since it did not have the thin protective layer of gelatin sometimes coated on ordinary emulsions. Thus, the film was especially sensitive to any mechanical pressure or abrasion.

[10] D. Okrent, thesis, Harvard University (1950).

All films were developed within thirty minutes after exposure to avoid effects due to latent image fading. The temperature of the developer was controlled by a large water bath to $\pm 0.5°F$; a thermometer was placed directly in the developer immediately before use to check the temperature.

Three distinct single-layer-films or coatings were used, two of which were subjected to the same developing procedure. These two coatings (designated J-4916 and J-8957) were developed in fresh D-19 developer at 68°F for 80 seconds, placed in a short stop bath, washed thoroughly, and hung up to dry. Since both developed and undeveloped grains were to be counted, these coatings were not "fixed." The background fog was considerable and increased with increased development time; hence, the development time was limited to 80 seconds.

In the third coating (designated J-10217) the grains were considerably smaller and crowded together very closely. At 2500× magnification it was extremely difficult to count the total number of grains in a reasonably large field of view. It was impossible to distinguish accurately between developed and undeveloped grains. Hence, this coating had to be fixed after development. The development time was increased to three minutes so that the developed grains would be larger and more dense. This improved the ease of counting.

All three coatings were specially prepared on an experimental basis by the Research Laboratory of the Eastman Kodak Company.[10a] The first two coatings (J-4916 and J-8957) were prepared at different times but from a similar type of base emulsion (a chlorobromide). Relatively small changes in emulsion technique were made in preparing the two. Routine tests by Eastman indicated that these two coatings had comparable sensitivities to white light, certainly within a factor of two. The third coating (J-10217) was a bromoiodide emulsion of finer grain and had quite different over-all characteristics. It was similar to the emulsions used in nuclear track plates.

IV. COUNTING PROCEDURE

Before a grain count was made, the cross-sectional area of the beam, as measured by the size of the spot on the film, had to be determined in order to calculate the electron density per unit area. Since the spots were small (0.2 cm^2), oval-shaped, weak, and not perfectly defined, this was a difficult problem. It was decided to enlarge the spot by projection, copy the image, and compare its area with that of a projected standard. The area comparison was actually made by weighing on an analytical balance the paper sections on which the areas had been outlined.

[10a] A clear gelatin layer is superposed on film support, and on the clear gelatin layer rests a very thin layer of silver halide emulsion. These were experimental films supplied for this particular experiment and are not offered for general sale by the Eastman Kodak Company.

The counting was done on a Bausch and Lomb research microscope, using an oil-immersion, apochromatic objective, and 25× binocular eyepieces. To reduce the counting field, an eyepiece disk with ruled squares was installed and only those grains falling within one square were counted.

For the first two coatings, the background fog was very high, being of the order of one grain in nine. Since low exposures were used to keep down the probability of multiple hits, and since the films turned out to be rather insensitive to electrons, the end result was a greater background count than induced count. Hence, the counting process became rather irreproducible, with variations of more than 20 percent in counts which were repeated.

Various methods for removing background fog in advance of exposure have been published. The possibility of non-uniform treatment, and other similar considerations, ruled out such a procedure in this experiment.

Fortunately, the third coating (J-10217) had essentially no fog, and the results were reproducible. This coating was given a wide range of exposures for each energy. When all spots were not sufficiently dark for area measurements, only the darkest were measured and the results used for all exposures. This procedure did not permit exact area measurements; a few percent variation existed between the data and a smooth curve drawn through the points when area was plotted as a function of energy.

Sampling was done at random. Since the undeveloped grains had been dissolved away, only the number of developed grains in each counting sample was noted and the average over all of the samples calculated. The total number of grains originally present in the coating for an area the size of the sample area was then determined by examining both unprocessed film and fully exposed and developed film.

It was assumed that the original number of unexposed grains per sample area did not vary significantly along the length of the film. Since data runs at the various accelerating voltages were mixed in order, a deviation from this assumption would have introduced no consistent error.

The number of grains counted per exposure varied from a few hundred to over a thousand. All grains which appeared were counted, regardless of any grain clumping. Clumping did not appear to be a significant factor, however; at low exposures practically none appeared. At very high exposures, especially at the low accelerating energies, the grains became so numerous that accurate counting was quite difficult and errors were introduced.

V. RESULTS

The results for the first coating (J-4916, a chlorobromide) are presented in Fig. 2. Two different measures of the sensitivity of this emulsion are plotted as a function of the energy of the incident electrons. The left-hand ordinate represents the ratio of the fraction of grains rendered developable to the fraction hit by one or more electron. This is really the developability probability[10b] for a single hit, so long as the likelihood of multiple hits is kept low.

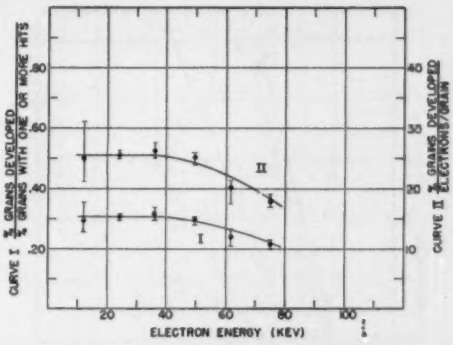
CURVE I % GRAINS DEVELOPED / % GRAINS WITH ONE OR MORE HITS
CURVE II % GRAINS DEVELOPED / ELECTRONS/GRAIN
ELECTRON ENERGY (KEV)
I
II

FIG. 2. Developability probability (the ratio of percent grains developed to percent grains with one or more hits) for first coating, J-4916, a chlorobromide, as a function of electron energy. Curve II gives a grosser measure of sensitivity, the ratio of percent grains developed to electrons per grain. All data is for exposures such that the probability of one or more hits per grain lies between 0.24 and 0.35.

The ordinate of the second curve plotted in Fig. 2 is the ratio of percentage of grains developed to electrons/grain. This quantity is a measure of the gross sensitivity of the coating and is particularly useful for comparing the first two coatings, which were exposed to very different intensities. The spread in data is indicated by the vertical bars through the points representing average values. This spread was considerably larger at first, but

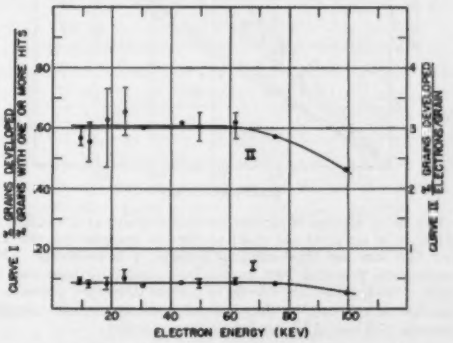
CURVE I % GRAINS DEVELOPED / % GRAINS WITH ONE OR MORE HITS
CURVE II % GRAINS DEVELOPED / ELECTRONS/GRAIN
ELECTRON ENERGY (KEV)
I
II

FIG. 3. Developability probability and ratio of percent grains developed to electrons per grain for second coating, J-8957, a chlorobromide, as a function of electron energy. The probability of one or more hits per grain lies between 0.87 and 0.95 for all data points. At this high level of exposure, curve II becomes a better criterion of comparison with the first coating.

[10b] The method of computing developability probability, as well as data for a sample run, are given in the Appendix.

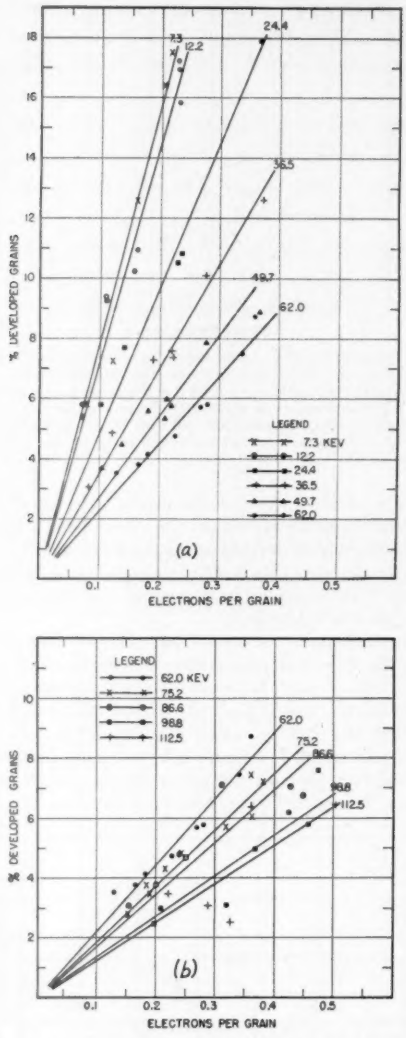

FIG. 4. (a) Curves of percent developed grains as a function of exposure in electrons per grain at electron energies between 7.3 and 62.0 kev for third coating, J-10217, a bromoiodide. This coating was prepared from an emulsion similar to those used in nuclear track plates. (b) Curves of percent developed grains as a function of exposure in electrons per grain at electron energies between 62.0 and 112.5 kev for the same coating.

by counting two or three times as many grains, the spread was reduced. The only experimental points used were those for which the probability of one or more hits lay between 0.24 and 0.35. Data points for slightly higher electron intensities did bracket the curve, however.

The data are not good enough to define the exact shape of the curve. One can state only that it is comparatively flat up to 50 kev, after which the sensitivity falls off slightly.

The results for the second coating (J-8957, also a chlorobromide) are presented in Fig. 3. The ordinates and abscissa are the same as in Fig. 2. For energies where only one experimental point was available, no spread in data was shown, but the usual wide variation in repeated measurements still existed.

The general shape of the curves, as well as the data spread, are similar to that obtained with the first coating. The sensitivity remained relatively constant up to about 60 kev, after which it dropped slowly. Curve I in Fig. 3 appears somewhat flatter because of the smaller values of the ordinate. However, the absolute sensitivity was much lower for the second coating, despite the fact that the two were intended to be very similar, when manufactured. Indeed, rough tests by Eastman showed that upon gross exposure to 100-kev x-rays, approximately the same density was produced for a given exposure; also, upon exposure to white light, a factor of 2 bracketed the variation in the density.

The results obtained in this experiment indicate a much greater difference in sensitivity to electrons for the two coatings. When the developability probabilities are compared, it appears that the first coating is about four times as sensitive. However, in order to get a visible spot with the second coating, much greater electron intensities had to be used. For the data plotted, the probability of one or more hits lies between 0.87 and 0.95. At this high probability, the Poisson law of fluctuations of small numbers dictates that additional electrons have relatively little chance of piercing an untouched grain. Hence, a comparison of the gross sensitivity, as measured by the ratio of the percentage of grains developed to electrons/grain, indicates that the first coating was 8 or 9 times as sensitive.

The results on electron sensitivity, when compared with the tests with white light by Eastman, indicate that there may be discrepancies between relative speeds to electrons as compared with white light exposures. There are other data to this effect.[11]

The apparent discrepancy in sensitivity to x-rays and electrons is unexplained. The x-rays should have produced their photographic effects by the agency of high energy photoelectrons, so that one would expect the results to be comparable. It should be noted that the accuracy of the x-ray tests was rather low because of the low total densities resulting.

The results for the third coating (J-10217, the bromoiodide) are presented in Fig. 4, (a) and (b). At each accelerating voltage this coating was exposed to a wide range of electron intensities. The percentage of developed grains is plotted as a function of electrons/grain for each accelerating voltage. (The average measured cross-

[11] H. C. Yutzy, private communication.

sectional area for the individual grains in this coating was 0.9×10^{-8} sq cm±8 percent. The grains were essentially spherical.) Straight line curves were drawn through the data, their slopes having been computed to minimize the mean square deviation from the curve.

In Fig. 5 the developability cross section is plotted as a function of electron energy for the third coating. The data for this curve are derived from Fig. 4, (a) and (b), by reading off the percentage of developed grains corresponding to 0.2 electron per grain for all voltages, and then computing the fraction having one or more hits (a constant over all voltages, of course). If a different choice for electrons per grain were made, the absolute values for developability cross section would differ slightly, but the shape of the curve would be the same.

The results for this coating differ markedly from those of the first two coatings. Instead of having a long plateau, the sensitivity drops off sharply from a high point at the lower energies. The exact shape of the curve below 15 kev is somewhat in doubt, since the data were rather irreproducible at 7 kev.

In Fig. 4 it can be seen that for low and moderate exposures, the percentage of grains developed is a linear function of the number of electrons/grain. To investigate the shape of the curve for higher exposures, data were taken at a later date for two voltages (18.3 and 75.2 kev) over an extended exposure range. The results are presented in Fig. 6. As was anticipated, the percentage of grains developed rises linearly at first, then slows off as the electrons per grain is increased. At least part of this decrease in slope is due to electrons being wasted on grains already developable. This would account for the low energy curve deviating from a straight line earlier than the high energy curve.

It is interesting to note that when the percentage of grains developed is plotted as a function of grains hit by one or more electrons, the curve straightens out for

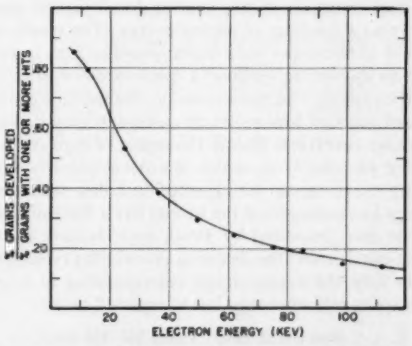

FIG. 5. Developability probability for coating J-10217 as a function of electron energy. This curve is derived from Figs. 4(a) and 4(b) by reading off the percent developed grains corresponding to 0.2 electron per grain (an arbitrary choice) for all voltages and performing the required computations.

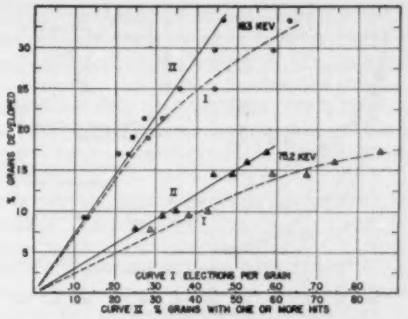

FIG. 6. Curves of percent grains developed as a function both of electrons per grain and percent grains with one or more hits at 18.3 and 75.2 kev for coating J-10217.

the exposure range used. The data for 75.2 kev fall right on a straight line; the curve for 18.3 kev is less definite.

If the developability probability remained constant for every electron-grain collision, independent of previous collisions which had not produced developability, then the curve of percent grains developed as a function of percent grains with one or more hits would be a 45° straight line for a developability probability of unity. For lower probabilities the curve should be below the 45° line initially, but rise steeply to meet it at 100 percent developed grains. This condition probably does not represent fact, since an electron which has not produced developability nevertheless would have freed some bound electrons in the silver halide grain. Thus, it might be anticipated that the task of a second electron would be simpler.

The data presented in Fig. 6 were taken at a later date than that in Fig. 4, so that there may have been some change in film characteristics. Also, the counting was done at different times, so that the sampling procedure, a rather arbitrary thing, probably differed somewhat. In any event, the sensitivity at both voltages is up to 20 percent higher in Fig. 6 than in Fig. 4. This was also true of some scattered data taken at other voltages. This variation, primarily in absolute sensitivity, is another indication of the difficulties inherent in sensitivity measurements with photographic emulsions.

VI. SOURCES OF ERROR

As indicated in Sec. II, the error in any meter measurements is believed to have been small, i.e., of the order of 2 percent. Considerably larger errors were introduced, however, in the measurement of spot area and the correction for background fog in the first two coatings. These inaccuracies, coupled with those introduced in the counting procedure, completely overshadow any of the former errors.

It is believed that an estimate of accuracy within 20 percent, relatively and absolutely, for the data pre-

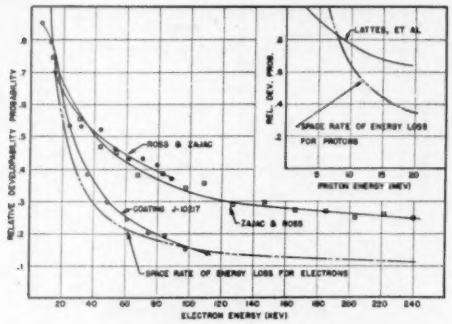

FIG. 7. Relative developability probability as a function of electron energy computed from grain counts for electron tracks in an experimental emulsion as given by Ross and Zajac (see reference 14) and in Kodak NT4 plates, as reported by Zajac and Ross (see reference 15). The results for coating J-10217, as well as an approximate curve of space rate of energy loss for the electron are presented for comparison. In the upper right-hand corner, a curve of relative developability probability computed from grain counts along proton tracks in Ilford plates as reported by Lattes *et al.* (see reference 17) is compared with an approximate curve of space rate of energy loss for the proton over the limited range available.

sented in Figs. 2 and 3 would be somewhat optimisitic. The data for the third coating were much more reproducible, thanks to the lack of background fog; and it is estimated that the data in Fig 4, (a) and (b), are correct within 10 percent relatively, and 20 percent absolutely.

No mention has been made, thus far, of a correction for backscattered electrons. Certainly, some of the incident electrons suffered collisions with nuclei or bound electrons in the gelatin layer and cellulose ester backing after penetrating the layer of silver halide grains. It turns out that this effect is small here, however. If we consider the contribution from single nuclear scattering for a scatterer of atomic number equal to 4, we find that roughly 1 percent of the incident electrons will be backscattered, using either the Mott or Rutherford formula.

Neher[12] has found experimentally that the total backscattering of monoenergetic, high speed electrons from thin and thick foils is of the same order as that predicted by the Mott theory, if we neglect backscattered electrons of very low energy. The results of Zumwalt[13] on backscattering of beta-rays indicate that less than 4 percent of the particles incident on the single-layer film should emerge in a backward direction.

Thus, in view of the considerably larger errors elsewhere, it was decided that any correction for backscattering was an unnecessary refinement at this time.

VII. DISCUSSION OF RESULTS

It is possible to obtain information on the sensitivity of photographic grains to particles as a function of particle energy by studying the variation in grain density along tracks in nuclear track plates. Measurements on grain density along tracks of β-particles have been reported by Ross and Zajac.[14,15] In the first paper the grain density in an experimental emulsion for tracks left by 100-kev electrons is given as a function of distance from the end of the track. Only unbranched tracks starting at the surface of the emulsion and having an initial direction within 40° of the central ray direction were used here. The branches, were caused by delta-rays and could not be identified with certainty if their energy was below 20 kev.

The second paper gives the mean density of grains for electron tracks in Kodak NT4 plates corresponding to an electron energy of about 250 kev. The reported counts, however, for grain number in any portion of the track, included the grains belonging to any branch produced in that portion.

With the aid of the experimental range-energy data given in the two papers, these data on grain density can be transformed into curves of relative developability probability as a function of electron energy. A rough computation has been made and the results are presented in Fig. 7. The results for the third coating (J-10217) are plotted on the same axes, as is an approximate curve of space rate of energy loss for the electron as a function of electron energy. The resemblance of the latter two is obvious; the results derived from Ross and Zajac are in good agreement with them qualitatively, fair agreement quantitatively.

Measurements on grain density for heavy particles, including alpha-particles, tritons, deuterons, protons, and mesons, have been reported by Wilkins and St. Helens,[16] Lattes, Occhialini, and Powell,[17] Brock and Gardner,[18] and Berlman,[19] among others. Lattes, Occhialini, and Powell report the variation in grain density for the longest tracks, namely, 2150 microns, corresponding to 21-Mev protons. Using the range-energy curve for protons, as given by Webb,[2] this data has been transformed into relative developability probability as a function of proton energy. The results are plotted in the upper right-hand corner of Fig. 7, along with an approximate curve of space rate of energy loss for the proton. The two curves do not match over this limited range of proton energy, although they do show a similar curvature. This is the region of high developability probability in which the developability probability curve cannot be expected to follow the rate of energy loss curve, since the former has a limit of unity.

The data presented by Brock and Gardner for the alpha-particle and the deuteron give similar results, but again only the energy range corresponding to a very high space rate of energy loss is reported herein.

[12] H. V. Neher, Phys. Rev. **38**, 1321 (1931).
[13] L. R. Zumwalt, MDDC-1346 (unpublished).
[14] M. A. S. Ross and B. Zajac, Nature **162**, 923 (1948).
[15] B. Zajac and M. A. S. Ross, Nature **164**, 311 (1949).
[16] T. R. Wilkins and H. J. St. Helens, Phys. Rev. **54**, 783 (1938).
[17] Lattes, Occhialini, and Powell, Nature **160**, 453 (1947).
[18] R. L. Brock and E. Gardner, Rev. Sci. Instr. **19**, 299 (1948).
[19] I. B. Berlman, Phys. Rev. **80**, 96 (1950).

One other bit of information can be gleaned from the results. Webb[4] has found that on the average about 40 quanta of light had to be absorbed by a photographic grain to produce developability. This information was gained by exposing single-grain-layer photographic plates, prepared from a non-color-sensitized, slow-speed, uniform-grain-size emulsion to monochromatic light of three different wavelengths. On the other hand, by considering the limiting sensitivity of nuclear track plates available in April, 1948, Webb[3] estimated that about 150 ion pairs per grain were formed by the particle as it entered this threshold.

The results for the third coating indicate that at 110 kev there is still an appreciable sensitivity present. By following Webb,[3] we can estimate the number of ion pairs formed for this electron energy and thus gain information on the number of ion pairs which will render a grain developable. Van Heerden[20] (as quoted by Webb) found that 7.6[21] ev is required to produce each ion pair for the case of high speed beta-particles passing through silver chloride. From the space rate of energy loss curve for the electron, we find that at 110 kev it loses about 0.0045 Mev/cm in air. The maximum number of ion pairs produced in a photographic grain for a particle of this energy-loss value can be found by multiplying the rate of energy loss in air by the stopping power of silver bromide relative to air (3000), multiplying by the diameter of the grain (0.35 micron), and dividing by the electron volts used per ion pair. Then we find that

$$\text{ion pairs/grain} = 0.0045 \times 10^{6} \times 3000 \times 3.5 \times 10^{-5} / 7.6 = 62 \text{ ion pairs/grain.}$$

This approximate number does not represent the average number of ion pairs produced along a straight line which are needed to render the grain developable, but rather something which approaches the lower limit. It is not surprising that this process seems less efficient than the random absorption of light quanta throughout the grain. Since all the ion pairs are produced in a very short time and along an essentially straight line, losses due to recombination should be favored. Also, there is direct evidence[2] of inefficiency in the photographic process for light exposures of duration less than 10^{-3} sec as compared with equal exposure over a longer time. Thus, the very short duration of exposure when incident particles are considered should provide further loss in efficiency.

Considerable thanks are due to the Eastman Kodak Company in general, and Drs. H. C. Yutzy and J. Spence in particular, for supplying the single-grain-layer emulsions used in these tests, as well as suggestions in development procedure. Acknowledgment is made to Dr. C. E. Hall of M.I.T. and Drs. V. K. Zworykin, J. Hillier, and S. G. Ellis of the RCA Laboratories for their assistance in the design of the electron gun. Much gratitude is also due to Messrs. Robert Dooley and D. C. Caton for their friendly assistance in the construction and assembly of the electron gun and its associated instruments.

APPENDIX

The developability probability is computed in the following manner. The area of the exposed spot is read from the curve of spot area as a function of electron energy. The average electrometer reading in millivolts is converted to number of electrons and then combined with the shutter open time and spot area to give electrons/sq cm. Using this value and the average measured grain area, the poisson law of fluctuations of small numbers is then applied to compute the fraction of grains hit by one or more electrons.[4]

The fraction of the total number of grains present which has been rendered developable is determined from the microscopic counting data after correction for fog. This fraction, divided by the fraction of grains hit, is equal to the developability probability.

Typical data for one exposure of coating J-4916 was as follows:

1. Accelerating voltage	49.7 kv
2. Average electrometer reading	7.05 mv
3. Shutter-open time	0.150 sec
4. Fraction grains rendered developable	0.101
5. Spot area (read from curve)	0.183 sq cm
6. Average grain area	2.24×10^{-9} sq cm.

The bleed resistor on the electrometer was 1.98×10^{8} ohms; hence, the total beam current was 3.56×10^{-11} ampere, corresponding to a charge density of 1.82×10^{8} electrons/sq cm delivered to the coating. The number of electrons per grain, therefore, amounted to 0.407. From the poisson distribution we then find the number of grains suffering one or more hits to be 0.335, so that the developability probability is equal to 0.301.

[20] P. J. Van Heerden, *N. V. Noord-Hollandsche Uetgevers Maatschappy* (Amsterdam, 1945).

[21] W. L. Whittemore and J. C. Street [Phys. Rev. **76**, 1786 (1949)] report a value of 6.6±0.7 ev, while Hofstadter, Milton, and Ridgeway [Phys. Rev. **72**, 977 (1947)] obtained a variety of much higher values. Van Heerden's value was used to make the result directly comparable with that of Webb.

The Absolute Energy Loss of 18-Mev Protons in Various Materials*†

DONALD C. SACHS‡ AND J. REGINALD RICHARDSON
Department of Physics, University of California, Los Angeles, California
(Received March 13, 1951)

The absolute energy loss of 17.77±0.03-Mev protons upon passing through various materials was measured using the U.C.L.A. 41-inch FM cyclotron. A ribbon foil of thorium, mounted inside the dee, was used to deflect the circulating proton beam above the median plane of the cyclotron magnetic field. This scattered beam of protons, confined to a plane above the median plane, described a circular path in the magnetic field through a slit system. At the 180° point, the beam was made to pass through a thin metallic foil. The protons traveled an additional 210° to an ionization chamber detector. It was possible to move the detector to different cyclotron radii. The displacement of the proton intensity distribution caused by the presence of the metallic foil was a measure of the absolute energy loss in the foil. It was possible to calculate the stopping power and the mean excitation potential for each material investigated. The results for aluminum yield a value of 156±3 electron volts for the mean excitation potential. Other materials examined included Ni, Cu, Rh, Ag, Cd, Sn, Ta, Au, and Nylon.

Some information was obtained concerning the corrections to be applied to the stopping power formula; hence, the variation of these corrections with the atomic number of the stopping material was determined.

INTRODUCTION

IT is well known that the energy of a high speed charged particle is reduced upon passing through matter as a consequence of its many inelastic collisions with the atoms of the stopping material.

Bohr[1] was the first to develop a theory of stopping power $(-dE/dx)$ on the basis of classical mechanics. Subsequently, Bethe[2] and Bloch[3] applied the methods of quantum mechanics to the problem, the latter using the Fermi-Thomas statistical model of the atom. From the quantum statistical treatment, one derives the following relation for the stopping power:

$$-dE/dx=(4\pi e^4z^2/mv^2)NZ\ln(2mv^2/I), \quad (1)$$

where E is the energy, ez is the charge, and v is the velocity of the incident particle. The quantity x is the distance traveled by the particle through the stopping material. N is the number of atoms per cubic centimeter of the stopping material, Z is its atomic number, I is the mean excitation potential of the atom, and m is the electron mass. One condition for the validity of Eq. (1) is that the velocity of the incident particle be large compared with that of the electrons in the atoms of the stopping material. That is, in terms of energy,

$$E(\text{incident})\gg(M/m)E(\text{electron}), \quad (2)$$

where M is the mass of the incident particle and E (electron) is the ionization potential of the electron in the atom. When the inequality (2) is not satisfied for all electrons in the atom, then Eq. (1) is not valid as written and corrections must be applied.

These corrections have been calculated by Livingston and Bethe[4] for light elements where only the K electrons fail to satisfy condition (2). The corrected stopping power formula takes the form

$$-dE/dx=(4\pi e^4z^2/mv^2)N[Z\ln(2mv^2/I)-C], \quad (3)$$

where C is the total correction, including electrons in all the shells. Livingston and Bethe present a curve of the variation of C_k with $1/\eta$, which is a function of the energy of the incident particle. However, corrections for cases in which electrons of other shells do not satisfy the condition (2) have not yet been determined analytically or empirically.

It is difficult to determine the average excitation potential, I, purely theoretically with much accuracy; attempts in this direction[2] have met with little success. Therefore, I must be determined from the experimental data on stopping. Relative values of the mean excitation potentials have been obtained by Wilson,[5] Kelly,[6] Teasdale,[7] and by Bakker and Segrè.[8] Wilson determined the stopping power of aluminum relative to air for protons of energies to 4.0 Mev; the latter paper gives the stopping powers of various elements relative to Wilson's aluminum value for 340-Mev incident protons. The experiment described here is the first to measure absolute proton stopping powers.

THE DEFLECTION METHOD

Heretofore, in most cyclotron experiments which examined the stopping power of various materials, it has been necessary to use a beam of particles which was deflected so as to go outside the cyclotron tank. However, in the work described here, a unique method of deflection[9] was used and the experiment was carried on inside the tank of the U.C.L.A. 41-inch FM cyclo-

* This paper includes parts of a thesis submitted by one of the writers (D.C.S.) in partial fulfillment of the requirements for the Doctor of Philosophy degree at the University of California at Los Angeles.

† The experiment was assisted by the joint program of the ONR and AEC.

‡ AEC Predoctoral Fellow, 1948–50. Now at the Stanford Research Institute, Stanford, California.

[1] N. Bohr, Phil. Mag. **25**, 10 (1913).

[2] H. A. Bethe, Ann. Physik **5**, 325 (1930).

[3] F. Bloch, Z. Physik **81**, 363 (1933).

[4] M. S. Livingston and H. A. Bethe, Revs. Modern Phys. **9**, 285 (1937).

[5] R. R. Wilson, Phys. Rev. **60**, 749 (1941).

[6] E. L. Kelly, Phys. Rev. **75**, 1006 (1949).

[7] J. G. Teasdale, UCLA Technical Report No. 3 (1949), unpublished.

[8] C. J. Bakker and E. Segrè, UCRL 850 (1950), unpublished (referred to here as BS).

[9] C. E. Leith, Phys. Rev. **7**, 89A (1950).

tron. The deflector took the form of a thorium foil (see Th in Fig. 1) mounted just inside the dee with its plane including a radial line and the vertical component of the magnetic field. When the circulating proton beam impinged upon the thorium foil, there was a slight decrease in the average energy coupled with a great deal of multiple scattering in the foil. The protons that were deflected upward were used in this experiment.

One can define the usual positive dimensionless quantity, n, as

$$n=-(r/H)\partial H/\partial r, \tag{4}$$

where r and H denote the cyclotron radius and magnetic field respectively. If one takes Z as the coordinate perpendicular to the cyclotron pole faces, it can be shown that the Z-component velocity of the particle away from the median plane due to scattering is opposed by the Z-component of force toward the median plane due to magnetic focussing forces. Considering the case of $Z=Z_0=0$ at zero time, i.e., a particle scattered at the median plane, one obtains

$$Z=(\phi r/n^{\frac{1}{2}})\sin(n^{\frac{1}{2}}\theta)=\phi s[\sin(n^{\frac{1}{2}}\theta)/n^{\frac{1}{2}}\theta], \tag{5}$$

where ϕ is the angle relative to the median plane through which the thorium foil deflects the particle and $s=r\theta$ is the particle path length. For a given scattering angle, ϕ, and for the value of n corresponding to the cyclotron radius used, the product $s[\sin(n^{\frac{1}{2}}\theta)/n^{\frac{1}{2}}\theta]$ remains relatively constant for values of θ between 180° and 390°. The explanation lies in the fact that the wavelength of the harmonic motion is long compared with the particle path length in this interval. If one considers the more general case where a particle off the median plane is deflected but where $Z_0 \ll \phi r/n^{\frac{1}{2}}$, one obtains an equation similar to Eq. (5) above. From this analysis it was computed that protons scattered from the thorium as much as one-fourth inch from the median plane will travel around the vacuum tank without hitting the dee or upper pole face. This conclusion was verified by experiment.

APPARATUS

A schematic drawing of the geometry of the experiment is shown in Fig. 1. The slit, S_1, was the "defining" or central slit and it took the form of an aluminum plate with a slot cut out of it. The slit, S_2, was the "foil" slit and it was equipped with copper out-rigger fins to stop those deflected protons which missed the slit. The ionization chamber, C, which moved on a radial track, T, was located in a plane above the dee structure and thorium foil as indicated in the end view of the cyclotron tank shown in Fig. 1. The slit, S_3, was the chamber slit and was mounted in front of the aluminum window of the ionization chamber.

The positions of the thorium, the slits, and the motion of the ionization chamber along its track were measured with a special precision-built measuring device. With the aid of a magnifying glass, one could read the scales to an accuracy of ±0.1 mm. The procedure was to measure the positions of the thorium, slits, and chamber motion both before and after a series of runs. There were two different sets of slit widths used in this experiment; the first (Geometry I) produced a well-defined proton beam that was adapted to the investigation of the thin aluminum foils, while the second (Geometry II) provided the larger beam intensity necessary for testing the thicker foils and heavier elements.

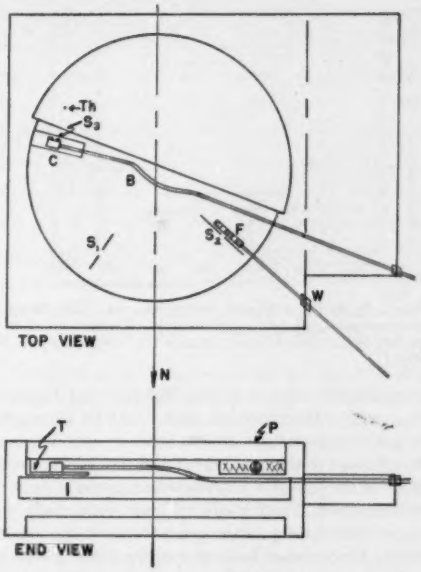

FIG. 1. A schematic drawing of the geometry of the absolute energy loss experiment.

So that it would be possible to investigate more than one material or thickness during a cyclotron run, a foil frame (see F in Fig. 1) was built to hold the foils and was fastened to a rod which passed into the cyclotron tank through a Wilson seal.

The ionization chamber was of the parallel-plate type, it was filled with air at atmospheric pressure, and was operated at saturation. The ionization current was measured by means of a conventional electrometer tube circuit.

To be certain that the intensity distribution of the deflected proton beam was obtained with constant cyclotron operating conditions, a means for moving the chamber during cyclotron operation was devised. It was arranged so that an observer outside the cyclotron building could both change and read the position of the chamber.

The circulating proton beam was monitored using a Beckman radiation meter located near the vacuum tank and connected to a 0–100 microampere meter in the control room. The magnetic field of the cyclotron

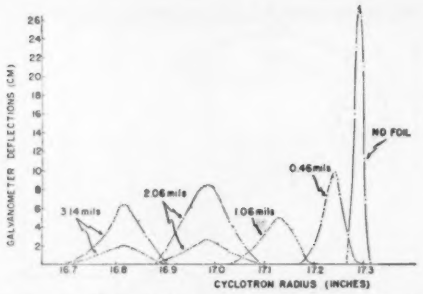

FIG. 2. A plot of a typical energy loss run. This shows the displacements of the proton momentum distributions after the beam has been made to pass through thin aluminum foils (Geometry I).

was monitored with a special flip coil and fluxmeter arrangement. The magnetic field could be maintained constant to ±4 parts in 15,000.

In addition to the usual determination of the surface density of the foils, the thickness variations of each foil were measured. These measurements were made with a copper target x-ray beam and a thin window electron counter. Only those foils whose thickness variations (rms deviation) was less than one percent were selected for the energy loss experiment. The foils were considered chemically pure, since the largest total impurity was 0.2 percent, while the aluminum foils were 99.9 percent aluminum.

The energy of the incident protons and the energies lost in the foils were determined by measuring the magnetic field values along the proton paths. With this information, it was possible to plot the proton trajectories graphically. The magnetic field was measured with a nuclear resonance absorption device similar to the one described by Hopkins.[10] It was possible to reproduce resonance absorption readings to ±7 gauss or ±0.05 percent. The proton energy determination method that was employed is described by Parkins and Crittenden.[11]

TABLE I. Mean excitation potential of aluminum.

Surface density (mg/cm²)	Most probable energy loss (Mev)	Most probable energy loss (10^4) g/cm² (with probable error)	Mean excitation potential (ev) (with probable error)
7.153[a]	0.153	0.3422±0.0085	168.3±20.2
14.054[a]	0.301	0.3432±0.0050	168.4±12.6
21.432	0.465	0.3476±0.0037	160.6±8.0
21.532[a]	0.470	0.3497±0.0040	155.6±8.9
33.875	0.737	0.3485±0.0028	162.8±6.5
38.395	0.839	0.3500±0.0020	162.0±4.7
47.457	1.048	0.3538±0.0017	156.7±7.7
57.493	1.276	0.3555±0.0025	157.1±5.5
67.294	1.515	0.3607±0.0024	150.0±5.0
76.849	1.737	0.3621±0.0018	150.8±3.8

[a] These measurements were made with Geometry I; the remaining measurements were made using Geometry II.

[10] N. J. Hopkins, Rev. Sci. Instr. **20**, 401 (1949).
[11] W. E. Parkins and R. Crittenden, J. Appl. Phys. **17**, 447 (1946).

RESULTS

Energy

The incident or "no foil" energy was determined to be 17.77 Mev with an energy spread of ±0.15 percent. From the accuracy of the energy loss measurements and the energy calibration (i.e., the change in energy corresponding to a certain change in cyclotron radius), the probable error in the energy loss determination was fixed at ±0.004 Mev. It must be noted that, since the mean excitation potential, I, appears in the argument of the logarithm in Eq. (3), its value will be sensitive to small changes in (dE/dx). A one percent probable error in (dE/dx) will be magnified to almost 6 percent in I.

Aluminum

Figure 2 shows a plot of a typical aluminum foil run. The displacement of the foil intensity distribution maxima from the "no foil" maximum represents the magnitude of the most probable energy loss in the foil. The two curves for the 2.06- and 3.14-mil foils correspond to different electrometer sensitivity settings. In both cases, the data for the lower curves were taken with the same setting as used for the "no foil" data. However, the sensitivity was later increased and the higher distribution curves resulted. The results of the aluminum runs are shown in Table I. The values of C_k from Livingston and Bethe[6] corresponding to the average energy were used in the calculation of the mean excitation potential. Consideration of all ten values in Table I gives a weighted average for the mean excitation potential of 156.2±2.0 electron volts. The first two values correspond to fairly thin foils and have a relatively large associated error. If these are thrown out, the weighted average is changed to 155.8±1.8 electron volts. Using the standard error, we then state our result as 156±3 electron volts. This result must be compared with the value of 150 electron volts determined by Wilson.[5] Since Wilson's standard error in the stopping power seems to have been about 3 percent, his standard error in the mean excitation potential was approximately 15 percent.

TABLE II. Weighted averages of the uncorrected mean excitation potentials.

Element	Weighted average uncorrected mean excitation potential (ev)	Root mean square deviation (ev)	Percent rms deviation
Al	161.4	2.0	1.2
Ni	375	19	5.1
Cu	412	6.3	1.5
Rh	760	17	2.2
Ag	766	21	2.7
Cd	766	32	4.2
Sn	831	47	5.6
Ta	1092	25	2.3
Au	1290	40	3.1

Corrections in Stopping Formula

The uncorrected mean excitation potentials of the elements other than aluminum which were investigated can be found in Table II. These results were computed using Eq. (1), and are not corrected for nonparticipating electrons.

It was thought that further use could be made of these data in the following way: BS,[8] using 340-Mev protons, were working with a $(m/M)E(\text{incident})=185$ kev, and thus one could assume that the condition of Eq. (2) would be met for all the electronic shells of the elements which they investigated. Hence, one could compare the BS results for the relative mean excitation potentials with the uncorrected results of the present investigation, and thereby obtain the corrections to the stopping formula corresponding to each element. The second column of Table III shows the BS results referred to the I_{AL} of the present investigation. One of

TABLE III. Corrections to be applied to the stopping power formula.

Element	Mean excitation Potential (ev) (from BS)	C/Z
Al	155.8[a]	0.037
Ni	270	0.328
Cu	290	0.351
Rh	425	0.579
Ag	438	0.560
Cd	454	0.526
Sn	470	0.574
Ta	690	0.460
	567[b]	(0.668)
Au	747	0.546
	594[b]	(0.771)

[a] Normalized to present results.
[b] C_k correction equal to 0.30 applied; value taken from Livingston and Bethe curve.

the features of the BS results was that for elements between $Z=47$ and $Z=92$ the quantity I/Z was essentially constant. This fact was used in determining the approximate corrected potentials of nickel, rhodium, cadmium, tantalum, and gold. The results of the correction determinations are listed for each element as C/Z, the total correction divided by the atomic number, in the third column of Table III. A plot of this quantity *vs* the atomic number is shown in Fig. 3. It is evident from this plot that the curve begins to bend over after rising steadily to about $Z=40$. Before proceeding, however, one had to be sure this bending over of the curve was not a function of the method of analysis.

When the energies of the K electrons of tantalum and gold were calculated from x-ray absorption edge data, it became evident that even at the very high incident energy of 340 Mev one had to considered C_k corrections in these high Z elements. Nevertheless, this

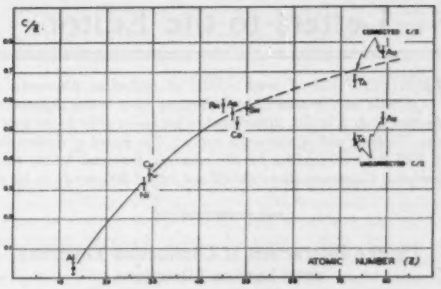

FIG. 3. A plot of the correction quantity C/Z for 18-Mev protons *vs* the atomic number of the stopping substance.

C_k correction could not change the nonlinearity of the curve in Fig. 3, since this would require that C_k/Z be comparable to C/Z, which in turn would change I by about a factor of three. As an approximation for tantalum and gold, it is possible to use the C_k as read off the Livingston and Bethe curve. These corrected C/Z points are shown in Fig. 3 and the dotted portion of the curve indicates the approximate plot.

For a given particle velocity, the value of C/Z increases with increasing atomic number since more electrons become ineffective in stopping at higher Z. However, Fig. 3 indicates that after $Z=40$, the fractional increase in the number of ineffective electrons is comparable to the fractional increase in the total number of electrons. The reason for this is found in the fact that the electrons in outer shells are more effective in the stopping process than those in the inner shells. Thus, an added electron in tantalum or gold will not increase the fractional number of ineffective electrons as much as the addition of an electron to nickel or copper.

Nylon

Since Nylon[12] is a material used widely for counter windows and as a target in scattering experiments, it was included in this investigation of absolute energy loss. Because the stopping number was very large, the calculation of the mean excitation potential was insensitive to the addition of the C_k correction. The calculated weighted average of I_{Nylon} was 38.5 ± 0.5 electron volts. No effort was made to determine the individual excitation potentials of the component atoms. For equal energy losses in the Nylon and aluminum, the mass stopping power relative to aluminum was computed to be 1.21 ± 0.02.

The writers wish to thank Mr. Plunkett and Mr. Jones of the cyclotron crew and Mr. Griffiths of the Physics Shop for their cooperation.

[12] The sample used was supplied by the Goodyear Tire and Rubber Company.

Letters to the Editor

PUBLICATION of brief reports of important discoveries in physics may be secured by addressing them to this department. The closing date for this department is five weeks prior to the date of issue. No proof will be sent to the authors. The Board of Editors does not hold itself responsible for the opinions expressed by the correspondents. Communications should not exceed 600 words in length.

On the Interaction of Conduction Electrons with Lattice Vibrations

S. D. DRELL
Stanford University, Stanford, California
(Received June 28, 1951)

BARDEEN[1-4] and Fröhlich[5,6] have recently proposed theories of superconductivity based on interactions between conduction electrons and the zero-point vibrations of the lattice. In his development, Bardeen views this interaction as giving rise to Brillouin zone boundaries with small energy gaps ($\sim kT_c$) at the Fermi surface of the electron distribution. Electrons with energies near the Fermi surface have small effective mass in consequence of the high curvature in their energy *versus* wave number relation at a zone boundary. Bardeen suggests that these are the superconducting electrons and indicates that it is possible to give a consistent interpretation for properties of superconductors in terms of the large diamagnetism exhibited by a gas of noninteracting electrons with small effective mass.

In this note we study the effective mass of conduction electrons which interact with the zero-point lattice vibrations. Fröhlich has calculated, with second-order perturbation theory, the self-energy of an electron interacting with the lattice normal modes of vibration (the phonon field). The energy denominators vanish and this perturbation procedure becomes invalid for virtual intermediate states which conserve energy.[7] Bardeen has avoided this difficulty with a variational treatment that leads to band structure in the energy *versus* wave number curve for the electrons. However, this result is obtained only after a questionable approximation for the mean energy of the virtual intermediate electron plus phonon states. We have calculated the energy of electrons interacting with the lattice vibrations by means of a Bloch-Nordsieck–type canonical transformation.[8] The B-N treatment is particularly suited to this type of problem, in which the energies associated with the crystal normal modes that are excited at low temperatures are very small compared with the electron energies. In this case neglect of electron recoil upon scattering with phonons introduces but a small error. Perturbation theory is avoided and, along with it, the vanishing energy denominators. We interpret our result as arguing against the conclusion that electrons have small effective mass in consequence of their interactions with the lattice normal modes.

The hamiltonian for electrons moving in a periodic lattice potential and interacting with normal modes of the crystal may be written as in reference 1. Neglect of the electrons' recoil upon scattering with the phonon field gives a hamiltonian that is linear in the electron momentum operators $-i\hbar\,\mathbf{grad}_j$. The Schrödinger equation with this hamiltonian is exactly soluble by means of a canonical transformation of the type introduced originally by Bloch and Nordsieck[9] in their study of the "infrared catastrophe," and used more recently in attempts at nonperturbation solutions for meson problems.[9] The eigensolutions correspond to a product of Bloch functions for individual electrons moving in a periodic lattice potential, multiplied by hermite functions for displaced zero-point oscillations of the phonon field, and multiplied by a factor expressing the interactions between the different electrons in consequence of their coupling with the lattice vibrations. The energy eigenvalues differ from those of the band theory for electrons moving in the periodic potential of the static lattice in the following way. In the periodic potential of a static lattice with period $\mathbf{a}$, there occur forbidden energy bands for electrons with momenta in the neighborhood of $m\dot{v}_i=\pi\hbar(n_i/a_i)$, where the n_i are integers. Electrons with these momenta suffer Bragg reflection. The lattice vibrations have the period $\mathbf{L}$, the crystal dimensions, and they superimpose, on the above bands, forbidden energy bands for electrons which satisfy an analogous Bragg condition with the lattice vibrations,

$$\omega_f^2=[\mathbf{v}\cdot(\mathbf{\Lambda}_f-\mathbf{k}_n)]^2. \tag{1}$$

Here ω_f, the angular frequency of the lattice vibrations with wave vector $\mathbf{\Lambda}_f=2\pi(f_1/L_1, f_2/L_2, f_3/L_3)$, is given by $\omega_f=s\Lambda_f$; s is the velocity of sound in the crystal, the f_i are integers, and $\mathbf{k}_n=2\pi(n_1/a_1, n_2/a_2, n_3/a_3)$ is a reciprocal lattice vector.[10] The width of these forbidden bands is

$$\sim(\text{amplitude of the lattice potential})/(\text{number of unit cells in the crystal})^{\frac{1}{2}}.$$

It is thus very small. These narrow forbidden bands occur throughout the electron distribution at momentum values that satisfy the condition in Eq. (1). They do not critically change the energy levels of the conduction electrons and hence do not critically alter their effective mass. A first-order perturbation treatment of the neglected electron recoil yields a small correction ($\sim s/v$) to these results.

In summary, our calculations do not indicate a small effective mass for electrons in consequence of their interactions with lattice vibrations. The energy shell distribution as proposed by Fröhlich does not appear to be energetically preferred. When other important factors such as the interelectron coulomb repulsion are considered, one may hope to find an adequate theory of superconductivity developed along lines of these very attractive physical proposals of Bardeen and Fröhlich. A manuscript discussing the details of this calculation is in preparation. Valuable discussions with Professor L. I. Schiff are gratefully acknowledged.

[1] J. Bardeen, Phys. Rev. **80**, 567 (1950).
[2] J. Bardeen, Phys. Rev. **81**, 469 (1951).
[3] J. Bardeen, Phys. Rev. **81**, 829 (1951).
[4] J. Bardeen, Phys. Rev. **81**, 1070 (1951).
[5] H. Fröhlich, Phys. Rev. **79**, 845 (1950).
[6] H. Fröhlich, Proc. Phys. Soc. (London) **A64**, 129 (1951).
[7] Fröhlich takes principal values in the integration over intermediate states.
[8] F. Bloch and A. Nordsieck, Phys. Rev. **52**, 54 (1937).
[9] Lewis, Oppenheimer, and Wouthuysen, Phys. Rev. **73**, 127 (1948); S. D. Drell, Phys. Rev. **83**, 555 (1951).
[10] These bands do not appear in Fröhlich's work because he takes principal values for his integrals over the intermediate states.

Anomalous Intensity Distribution of Rotation Lines in Fundamental Vibration Bands in Triatomic Molecules*

HARALD H. NIELSEN
Department of Physics and Astronomy, Ohio State University, Columbus, Ohio
(Received June 21, 1951)

A MECHANISM will be discussed here to account for the anomalous intensity distribution of the rotation lines in certain fundamental bands in the infrared spectra of triatomic molecules, notably in the 3.8-μ band in the H_2S spectrum. The theory assumes that it is necessary to take into account the mixing of the wave functions for a given rotation state in a vibration level with the wave functions of rotation states in other vibration levels in order to calculate the intensities with accuracy. The mixing must be between wave functions of the first excited states of the three vibration frequencies to give a first-order effect. Such a mixing may come about through the coupling of the vibrations through the Coriolis operator $p_z P_z/I_{zz}$, the z axis having been chosen as the axis of spin of the molecule. The mixed wave function

for the first excited state of the unsymmetrical vibration ν_3 takes the form

$$\psi(0,0,1,J,K,M)=\{\psi^0(0,0,1)-iKC\sum_{s=1}^{3}[\zeta_{3s}/(\omega_3-\omega_s)]$$
$$\times[(\omega_3+\omega_s)/(\omega_3\omega_s)]^{\frac{1}{2}}\}\psi^0(V_s=1,V_{s'}=0)\}\Theta(\theta,\psi)e^{iK\xi},$$

C being $h/8\pi^2I_{aa}c$ and ζ_{3s} the Coriolis coupling factors which depend upon the nature of the normal coordinates. Similar wave functions are obtained for the first excited states of ν_1 and ν_2.

Assuming the dipole moment induced by vibration to be

$$E=\sum_{s=1}^{3}a_sq_s,$$

where a_s is a constant and q_s are the normal coordinates the intensities of the lines in ν_s ($s=1$, 2 or 3) are proportional to the squares of the matrix elements $(0,0,0,K|I|V_s=1,V_{s'}=0,K\mp1)$, which are the following

$$(0,0,0,K|I|V_s=1,V_{s'}=0,K\mp1)$$
$$=\{a_s\pm\Sigma'_{s'}a_{s'}(K\zeta_{3s'}C/\Delta_{s'})[(\omega_s+\omega_{s'})/(\omega_s\omega_{s'})]^{\frac{1}{2}}\},$$

$\Delta_{s'}$ being $\omega_3-\omega_{s'}$.

It is, of course, well known that in molecules like H_2O and H_2S the band ν_3 is intense compared with the band ν_2, which is intense compared with ν_1, i.e., $a_2\gg a_3\gg a_1$. Taking ω_1, ω_2, and ω_3 to be 2610 cm^{-1}, 1290 cm^{-1}, and 2684 cm^{-1} for H_2S and letting $C=h/8\pi^2I_{aa}c$ be approximately 5 cm^{-1} and finally assuming the values of $\zeta_{31}=4.5\times10^{-3}$ and $\zeta_{32}=-1.0$ calculated by Darling and Dennison[1] for water vapor to be valid for H_2S as well, it may be shown that the term in I containing a_1K may be neglected. Moreover, the factor I will decrease to zero as the term containing a_3K approaches 1.4×10^3a_2 for transitions of the type $K\rightarrow K-1$. I will, for the same value of K, have assumed double its original value for transitions of the type $K\rightarrow K+1$. Since $a_2\gg a_3$, the above may happen for small values of K (i.e., $K\approx10$). The general effect upon the intensities is to enhance the transitions $K\rightarrow K+1$ at the expense of the transitions $K\rightarrow K-1$. By choosing the ratio of a_2 to a_3 in the proper manner the transitions $K\rightarrow K-1$ can almost entirely be suppressed so that, as in the case of H_2S, only about one-half of the band may be observed.

The effect of the perturbation on the band ν_2 is small and would probably not be observable. The effect of the perturbation on ν_1 is less readily estimated, but would probably not be observable as long as $a_2\gg a_1$.

* This work was assisted by the ONR.

[1] B. T. Darling and D. M. Dennison, Phys. Rev. **57**, 128 (1940).

Magnetic Moments of Even-Odd Nuclei

F. Bloch
Department of Physics, Stanford University, Stanford, California
(Received June 27, 1951)

THE success of the shell model[1] indicates that it is a good approximation to consider even-odd nuclei as single-particle systems with the odd nucleon moving in a spherically symmetrical potential provided by the even-even core. The model leads thus to the basic classification of nuclear states by the orbital angular momentum lh of the odd nucleon as well as by the spin I and to the expectation that the magnetic moment μ should have one of the two Schmidt values,[2] determined by $l=I\pm\frac{1}{2}$.

Two modifications have been proposed to explain the observed deviations from these values:

A.—l is not a good quantum number, and nuclear states represent actually a mixture of states[3] with $l=I+\frac{1}{2}$ and $l=I-\frac{1}{2}$.

B.—A tidal wave which contributes to μ can be formed in the core by the interaction with the odd nucleon.[4]

It has been pointed out before[4] that either modification has its peculiar serious difficulties: modification A requires a considerable mixing of states which, according to the shell model, are widely separated in energy and which have different parity in the odd nucleon; modification B fails to give deviations from the Schmidt values for nuclei with $I=\frac{1}{2}$, while they occur here actually with comparable magnitude as for other nuclei. Unless they are considered as small corrections, insufficient to explain the observed deviations, both proposals require besides a major departure from essential features of the shell model.

TABLE I. The effective intrinsic moment μ' of the odd nucleon, calculated from the Landé formula for an even-odd nucleus with magnetic moment μ, spin I and for both values of the orbital quantum number $l=I\pm1/2$.

	Odd proton	Odd neutron
l	μ'_P	μ'_N
$I-1/2$	$\mu-I+1/2$	μ
$I+1/2$	$I+(3/2)-(I+1/I)\mu$	$-(I+1/I)\mu$

We propose an alternative interpretation of the empirical results which is compatible with a strict adherence to the shell model.

C.—The intrinsic magnetic moment of the odd nucleon is affected by the binding to the core; depending upon the nucleus, it can differ by an appreciable amount from the magnetic moment of the free nucleon.

Accepting this interpretation, one can use the Landé formula to determine the effective intrinsic moments μ_P' or μ_N' of the odd proton or neutron, respectively, from the observed magnetic moment μ and spin I of an even-odd nucleus. They are given in Table I for either alternative $l=I\pm\frac{1}{2}$ in units of the nuclear magneton.

Using available data for both odd-proton and odd-neutron nuclei, we have plotted in Fig. 1 the corresponding deviations $\Delta\mu_P=\mu_P-\mu_P'$ and $\Delta\mu_N=-(\mu_N-\mu_N')$ of the intrinsic moment from its magnitude $\mu_P=2.79$ and $-\mu_N=1.91$ in the free nucleon against the number n of odd nucleons up to $n=83$. For each nucleus the assignment of l in Table I was made according to the shell model, i.e., according to the Schmidt value which is closer to μ; it leads in our presentation equivalently to the smaller deviation $\Delta\mu$.

Within minor fluctuations and particularly up to $n=40$, the odd neutron points not only follow remarkably well those for the odd protons[5] but the plot reveals also a certain regularity for both: a very coarse general trend, indicated by C_1, exhibits an initial rise to the approximately constant value $\Delta\mu\cong1$ for $n>20$. A pronounced alternating variation is superimposed on this general trend and is indicated by C_2; its periods are evidently related to the shells, closed at $n=2$, 8, 20, 50, 82, insofar as the maxima occur approximately in the middle and the minima towards the end of each shell. Possible secondary variations in the second half of the fourth and fifth shell are indicated by

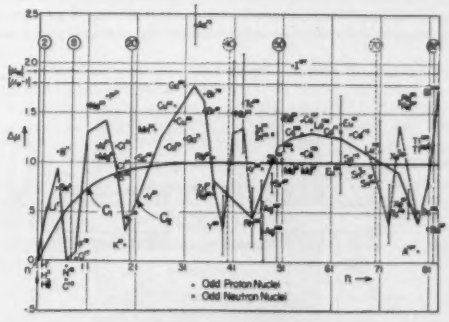

FIG. 1. The defect $\Delta\mu$ of the effective intrinsic moment of the odd nucleon *versus* the number n of odd nucleons in even-odd nuclei. Odd-proton nuclei are indicated by dots, odd-neutron nuclei by crosses. The encircled numbers on top represent the closing of shells; the subshells closed before the filling of the $g_{9/2}$ and $h_{11/2}$ states, are indicated by broken numbers and circles.

broken lines; they are similar to each other and may relate to the filling of the $g_{9/2}$ states (for $40<n\leq 50$) and $h_{11/2}$ states (for $70<n\leq 82$) in the scheme of Mayer, but more accurate data in these regions are required to establish their reality. The remaining minor fluctuations of the order of 0.2 magneton seem rather irregular.

Current theories suggest that our presentation should be plausibly interpreted as a variation of the "anomalous moment," due to modifications of the meson field by the binding of the odd nucleon.[6] Accordingly, the values $|\mu_P-1|$ and $|\mu_N|$ of $\Delta\mu$ in Fig. 1 represent the limits where the anomalous moment would be completely quenched; with very few exceptions, the points are seen to fall between zero and these limits, indicating partial quenching as the general case. We hope that further developments of the meson theory of nuclear forces will tend to corroborate this interpretation and to explain the characteristic features of our plot.[7]

[1] Haxel, Jensen, and Suess, Phys. Rev. **75**, 1766 (1949); E. Feenberg and K. C. Hammack, Phys. Rev. **75**, 1877 (1949); L. W. Nordheim, Phys. Rev. **75**, 1894 (1949); M. G. Mayer, Phys. Rev. **75**, 1969 (1949), **78**, 16 (1950); E. Feenberg, Phys. Rev. **77**, 771 (1950).

[2] T. Schmidt, Z. Physik **106**, 358 (1937).

[3] L. W. Nordheim (reference 1), and A. L. Schawlow and C. H. Townes [Phys. Rev. **82**, 268 (1951)] have recently pointed out that approximately equal mixtures are found for nuclei with the same spin and the same number of odd protons or odd neutrons.

[4] L. L. Foldy and F. T. Milford, Phys. Rev. **80**, 751 (1950).

[5] In spite of its different interpretation, this agreement is closely related to that observed by Schawlow and Townes (reference 3) for nuclei of equal spin; it is noteworthy, however, that it holds also for O^{17} and F^{19} with spins 5/2 and 1/2, respectively.

[6] F. Villars [Phys. Rev. **72**, 256 (1947); Helv. Phys. Acta **20**, 476 (1947); **21**, 354 (1948)] has previously considered such variations, due to exchange currents of the meson field, and has applied them successfully to the nuclei H^3 and He^3.

[7] The mechanism introduced by F. Villars (reference 6), will certainly have to be considered in this connection. In another approach, which seems to us more promising, nonlinear terms are introduced in the meson field to explain the validity of the single-particle model and the saturation of nuclear forces; they appear at the same time to lead quite naturally to the quenching of the anomalous moments, postulated here. (Private communication by L. I. Schiff and S. D. Drell.)

Resonant Scattering of Slow Neutrons by Cadmium

B. N. Brockhouse, D. G. Hurst, and M. Bloom
Atomic Energy Project, National Research Council of Canada, Chalk River, Ontario, Canada
(Received June 21, 1951)

SCATTERING of slow neutrons by cadmium has been measured over a range of neutron energy (0.02 to 0.4 ev) which includes the resonance at 0.176 ev. The apparatus shown in Fig. 1 was mounted on the arm of the crystal spectrometer previously described,[1] replacing the usual counter and shielding. Two circular apertures in slabs of boron carbide limited the monoenergetic beam to ½-inch diameter. Scattered neutrons were detected in six boron trifluoride counters symmetrically arranged in an annular bank about the neutron beam. To reduce background, the scattering chamber was evacuated and the equipment was shielded with paraffin wax and boron carbide. A thin sample of vanadium was used as a standard scatterer because of the almost complete lack of coherent scattering in vanadium.[2]

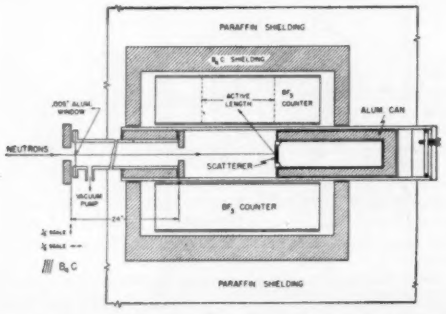

FIG. 1. Resonant scattering apparatus. The vertical and horizontal scales are such that the figure is compressed horizontally in a ratio 2:1.

The counting rates from the standard scatterer and from specimens of cadmium thick enough to absorb nearly all the incident neutrons were measured under the same conditions. The ratio of scattering to absorption cross sections for cadmium is then given by $\sigma_s/\sigma_a = KN_v\sigma_{sv}N/N_v$, provided $\sigma_s \ll \sigma_a$, where K is an instrumental constant, n_v is the number of vanadium atoms per cm², σ_{sv} is the scattering cross section of vanadium, and N and N_v are the counting rates due to cadmium and vanadium, respectively.

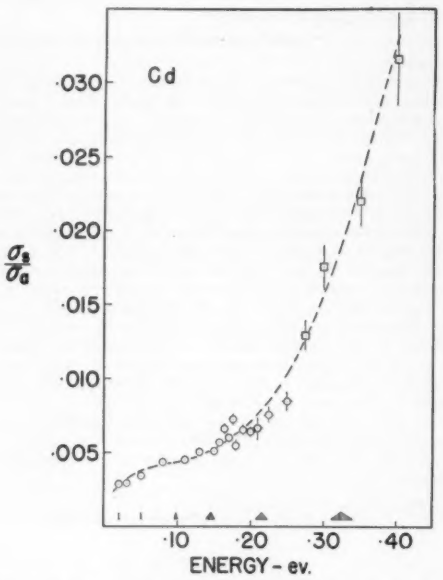

FIG. 2. Ratio of scattering to absorption cross sections in Cd. The circles and squares are experimental points with their standard deviations. The dashed curve is the Breit-Wigner curve calculated with $E_0=0.176$ ev, $\Gamma_a=0.115$ ev, $\sigma_{s0}=7200$ barns, $\sigma p=5.3$ barns, $a=6.5\times10^{-13}$ cm, $f=0.1230$, $g=0.75$. The triangles indicate the resolution of the apparatus.

The essentially cylindrical symmetry of the apparatus permits the calculation of the angular distribution of the scattered neutrons for both specimen and standard. From these distributions and the measured counter sensitivity the constant K was computed. A small energy dependence of K, due to absorption in the vanadium, was taken into account.

The quantity $n_v\sigma_{sv}$ was determined by measuring the transmission of the standard vanadium sample as a function of energy. The total cross section of the sample was linear in $1/v$. The $1/v$ term was identified with absorption and the constant term with scattering. This constant term, which is considered accurate to ±3 percent, was used as $n_v\sigma_{sv}$.

The ratio σ_s/σ_a for cadmium is shown in Fig. 2 with standard deviations. A correction for contamination of the beam by higher diffraction orders has been applied.

In the same figure a curve is drawn showing the ratio predicted

by the Breit-Wigner formula for a single level,[3] namely,

$$\frac{\sigma_s}{\sigma_a}=\left(\frac{E}{E_0}\right)^{\frac{1}{2}}\frac{\Gamma_{n0}}{\Gamma_a}+8.76\times10^{9}\frac{(E-E_0)E^{\frac{1}{2}}}{\Gamma_a}a+\frac{\sigma_p}{\sigma_a},$$

where

$$\Gamma_{n0}/\Gamma_a=4.82\times10^{18}E_0\sigma_{a0}/4\pi gf, \quad \Gamma_{n0}\ll\Gamma_a,$$

$$g_{i\pm\frac{1}{2}}=\tfrac{1}{2}[1\pm1/(2i+1)],$$

E is the neutron energy in ev, Γ_n and Γ_a are, respectively, the neutron and absorption widths in ev, σ_p is the potential scattering cross section of the mixture of isotopes, a is the potential scattering length of the resonant isotope, i is its spin, and f is its abundance. The subscript 0 refers to the energy of the resonance. Values of Γ_a, σ_{a0}, E_0, σ_p were obtained from transmission measurements of Rainwater *et al.*[4] g was taken to be 0.75 in agreement with Beeman,[5] corresponding to spin 1 for the compound nucleus Cd^{114}. The scattering length a was assumed to be $(\sigma_p/4\pi)^{\frac{1}{2}}$; i.e., the potential scattering of the resonant state was assumed to be the same as that of the average for the element.

The general agreement is excellent, except that in the region 0.180 to 0.250 ev the measured values are low in comparison with those at lower energies. A possible cause is discussed in the following letter in connection with scattering by Sm_2O_3. This agreement is further support for the Breit-Wigner formulation, in particular for the proportionality of neutron width to wave number.

[1] Hurst, Pressesky, and Tunnicliffe, Rev. Sci. Instr. **21**, 705 (1950).
[2] C. G. Shull and E. O. Wollan, Phys. Rev. **81**, 527 (1951). Use of vanadium as a standard was suggested by Dr. G. H. Goldschmidt.
[3] See, for example, Feshbach, Peaslee, and Weisskopf, Phys. Rev. **71**, 145 (1947).
[4] Rainwater, Havens, Wu, and Dunning, Phys. Rev. **71**, 65 (1947).
[5] W. W. Beeman, Phys. Rev. **72**, 986 (1947).

Resonant Scattering in Samarium and Gadolinium

B. N. Brockhouse and D. G. Hurst
Atomic Energy Project, National Research Council of Canada, Chalk River, Ontario, Canada
(Received June 21, 1951)

SAMARIUM.—Scattering of low energy neutrons by samarium has been investigated by the method outlined in the preceding letter.[1] The ratio σ_s/σ_a for neutrons of energy 0.02 ev to 0.150 ev is shown in Fig. 1 for two samples of Sm_2O_3. The dotted curves are Breit-Wigner curves which involve only parameters from the literature. The resonance at 0.096 ev has been assigned[2] to Sm^{149}. Since the spin of this isotope is not known, curves for several values of spin have been plotted. In the formula (see preceding letter) σ_{a0}, Γ_a, E_0 were taken from the transmission data of Sturm,[3] and a was calculated from the Amaldi[4] $A^{\frac{1}{3}}$ relation for nuclear radii. The potential cross section for this value of a is 9 barns, and if 4 barns is taken as the scattering cross section of oxygen, the potential cross section of $\frac{1}{2}(Sm_2O_3)$ is $\sigma_p=9+6=15$ barns. The two most recent determinations[5,6] of isotope abundance give $f=0.1368$ for Sm^{149} when weighted according to their stated accuracies.

The shapes of the experimental and theoretical curves are closely alike. Comparison of the curves suggests that the spin of Sm^{149} is high ($i>\frac{3}{2}$), in agreement with Brix and Kopfermann,[7] who found $i>\frac{1}{2}$, and that the spin of the compound nucleus Sm^{150} is $i+\frac{1}{2}$. On the Mayer shell model[8] the spin of Sm^{149} is expected to be 9/2. Larger ground-state spins are not observed. The agreement between theory and experiment for spin 9/2 is within the combined experimental errors of the transmission measurements and these results.

In this discussion three related effects have been neglected. These are Bragg scattering, the Debye correction to the scattering cross sections, and the change of neutron energy due to recoil of the nucleus. The first and third do not occur together. Insufficient data exist for accurate calculation of these effects but qualitative examination suggests that they are small. The general result is to raise the measured value of the ratio σ_s/σ_a at low energies compared with its value at high energies. It may be significant that the deviations between theory and experiment shown in Fig. 1, and also in Fig. 2 of the preceding letter, are in this direction.

The samarium oxide, as received, contained an amount of volatile material, presumably water and CO_2, sufficient to affect the measurements seriously. This was removed by heating one sample for 24 hours in a vacuum at 500°C, and the other in air at 700°C. The fact that the two samples of different origin and heat treatment gave essentially the same result indicates that there was no serious contamination.

Gadolinium.—Measurements of σ_s/σ_a were made on a sample of Gd_2O_3 in the condition received. The experience with Sm_2O_3 suggests that the measured values are about 20 percent too high, because of contamination. Nevertheless, the results are of some interest.

Sturm[3] and Brill and Lichtenberger[9] fitted their transmission measurements in the region 0.01 to 0.20 ev by a one-level Breit-Wigner formula for absorption. Our measurements of σ_s/σ_a lie significantly below all the Breit-Wigner curves calculated from their data, being about 15 percent below the lowest curve, that with $g=0.75$. Any correction for contamination increases the discrepancy.

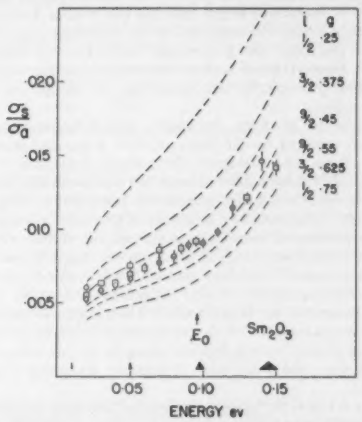

FIG. 1. Ratio of scattering to absorption cross sections in Sm_2O_3. The circles and squares are experimental values, with their standard deviations, for two samples of different origin. The dashed curves are the Breit-Wigner curves calculated with $E_0=0.096$ ev, $\sigma_0=15{,}500$ barns, $\Gamma_a=0.074$ ev, $\sigma_p=15$ barns, $a=8\times10^{-12}$ cm, and $f=0.1368$, for different values of i and g.

We believe this disagreement shows that the low energy absorption in gadolinium cannot be described by a one-level formula. This is supported by measurements of Lapp *et al.*,[2] which show cross sections for pile neutrons of 2.5×10^{3} barns for Gd^{157} and 0.7×10^{3} barns for Gd^{155}. The cross section for Gd^{157} is the larger by a factor of 3.5; hence, description in terms of one level of Gd^{158} may have a limited meaning. If so, the conclusion may be drawn that the g-value for Gd^{157} is high and hence that its spin is low, and that the compound nucleus Gd^{158} has spin $i+\frac{1}{2}$.

[1] Brockhouse, Hurst, and Bloom, Phys. Rev. **83**, 839 (1951), (preceding letter).
[2] Lapp, Van Horn, and Dempster, Phys. Rev. **71**, 745 (1947).
[3] W. J. Sturm, Phys. Rev. **71**, 757 (1947).
[4] Amaldi, Bocciarelli, Cacceapuoti, and Trabacchi, Nuovo cimento **3**, 203 (1946).
[5] J. Mattauch and H. Scheld, Z. Naturforsch. **3a**, 105 (1948).
[6] Ingham, Hayden, and Hess, Phys. Rev. **73**, 180 (1948).
[7] P. Brix and H. Kopfermann, Z. Physik **126**, 344 (1949). K. Murakawa and J. S. Ross have reported the spin of Sm^{149} to be 5/2 [Phys. Rev. **82**, 967 (1951)].
[8] M. G. Mayer, Phys. Rev. **75**, 1969 (1949); **78**, 16 (1950).
[9] T. Brill and H. V. Lichtenberger, Phys. Rev. **72**, 585 (1947).

Lower Limit for the Lifetime of the 0.8-Mev Excited Level of Mo^{96}

FRANZ R. METZGER
Department of Physics, University of Illinois, Urbana, Illinois*
(Received July 5, 1951)

THE method of delayed coincidences yields upper limits for the lifetimes of nuclear levels which are shorter than $\sim 10^{-10}$ sec. Resonant nuclear scattering of gamma-rays,[1,2] on the other hand, is more easily observed the shorter the lifetime and will therefore enable one to determine very short lifetimes or set lower limits to them. The two methods thus complement each other.

The cross section for nuclear resonant scattering is large at resonance ($\sim 2\times 10^{-21}$ cm^2 at one Mev); but in general the gamma-rays are off resonance owing to the energy transferred to the recoiling nuclei in the emission process as well as in the absorption process. In optics, where resonance fluorescence is a well-known phenomenon, this energy transfer is small compared with the energies of thermal motion; for gamma-rays the recoil energies are orders of magnitude larger than the line widths. For a given off-resonance energy the reduction in the scattering cross section is smaller the larger the gamma-ray width, i.e., the faster the transition. Observation of nuclear resonance scattering will therefore be most probable for fast transitions, i.e., transitions of low multipole order.

According to Medicus, Preiswerk, and Scherrer,[3] the last gamma-ray emitted in the decay of Tc^{96} is an electric dipole. For this reason we investigated the resonant scattering in Mo^{96} into which Tc^{96} decays. Mo^{96} seemed to be a favorable choice for another reason: the 0.8-Mev gamma-ray transition to the ground state of Mo^{96} is preceded by a cascade of two other gamma-rays. After the emission of these two gamma-rays the nucleus will have a certain momentum which depends on the angle between the two gamma-rays. If the third gamma-ray is emitted before the recoiling nucleus comes to rest, its energy (0.8 Mev) will be changed because of the Doppler effect. Thus, in a small percentage of the disintegrations of Tc^{96}, the resonance condition for the transition to the ground state is fulfilled owing to the preceding radiation; therefore, the observation of resonant scattering is greatly facilitated.

Using a 0.1 m-C Tc^{96} source we observed the radiation scattered by about 100 degrees from a sheet of molybdenum. Sodium iodide scintillation counters were used as detectors. At low discriminator settings the counting rate was primarily due to the soft Compton scattered quanta. At high discriminator settings the main contribution was due to the unmodified radiation arising from coherent scattering and resonant scattering. The amount of coherent scattering was estimated in a separate experiment using a cadmium scatterer in place of the molybdenum.

With a molybdenum sheet of 0.57 g/cm^2 the contribution of the resonant scattering was found to be less than 20 counts per minute, whereas the counting rate due to Compton scattering was 20,000 counts per minute. This result indicates that the width of the 0.8-Mev gamma-ray is several orders of magnitude smaller than the width of the recoil distribution.

In order to insure that our equipment had the expected sensitivity, we investigated the coherent scattering of Co^{60} gamma-rays from lead and zinc radiators. The amount of coherent scattering observed agreed reasonably well with the values calculated from Franz's[4] formula (7×10^{-4} and 9×10^{-5} times the Compton cross section, respectively). This formula had been checked at lower energies by Moon[5] and Storruste.[6] We therefore feel confident that our failure to detect resonant nuclear scattering from Mo^{96} is due to the small width of the gamma-line.

After applying all the necessary corrections to our experimental data, we find that the gamma-ray width Γ of the 0.8-Mev transition to the ground state of Mo^{96} is $\leqslant 10^{-2}$ ev. From Weisskopf's[7] formula for the transition probability one calculates a maximum width of one ev for an electric dipole transition, and a width of 1.1×10^{-2} ev for a magnetic dipole transition.

From our experiment we conclude that either the matrix element for the electric dipole transition is strongly reduced or that the transition to the ground state of Mo^{96} is of a higher multipole order.

From $\Gamma \leqslant 10^{-2}$ ev one finds for the half-life of the 0.8-Mev excited state in Mo^{96} $T_{\frac{1}{2}} \geqslant 0.5\times 10^{-13}$ sec.

* This work was supported in part by the joint program of the ONR and AEC.
[1] W. Kuhn, Z. Physik **43**, 56 (1927).
[2] E. Pollard and D. E. Alburger, Phys. Rev. **74**, 936 (1948).
[3] Medicus, Preiswerk, and Scherrer, Helv. Phys. Acta **23**, 299 (1950).
[4] W. Franz, Z. Physik **98**, 314 (1935).
[5] P. B. Moon, Proc. Phys. Soc. (London) **A63**, 1189 (1950).
[6] A. Storruste, Proc. Phys. Soc. (London) **A63**, 1197 (1950).
[7] Privately circulated notes, to appear as part of a book on nuclear physics.

The Differential Cross Section for High Energy Nucleon-Nucleon Collisions

H. S. GREEN AND H. MESSEL
School of Theoretical Physics, Dublin Institute for Advanced Studies, Dublin, Ireland
(Received July 2, 1951)

IN an attempt to account theoretically for the lateral and angular spread of the penetrating particles in high energy cosmic-ray showers, we have developed a method for deriving the differential from a given total cross section for inelastic nucleon-nucleon collisions in the laboratory frame of reference. An integral equation was set up for the differential cross section and solved assuming that in the c.m. frame of reference it was of the form $R+S\cos^2\bar{\Theta}$, where R and S are functions of the incident and scattered energies only, and $\bar{\Theta}$ is the scattering angle.

We define $W(U, c)dUdc$ as the probability in the laboratory frame of reference of finding a nucleon with total energy in the interval U, $U+dU$ and scattered at an angle whose cosine lies in the interval c, $c+dc$. Similarly $F(U)dU$ gives the total probability of finding a nucleon with energy in the interval U, $U+dU$. These two functions are related by the integral equation

$$\int W(U, c)dc = F(U). \tag{1}$$

The differential probability $W(U, c)dUdc$ is invariant under Lorentz transformation and we may therefore write

$$W(U, c)dUdc = (R+S\bar{c}^2)d\bar{U}d\bar{c}, \tag{2}$$

where the barred symbols refer to c.m. coordinates. Writing $\bar{U}=\cosh\bar{u}$, and $U_0=\cosh 2v$ for the energy of the incident nucleon we have found from (1)

$$R(\cosh\bar{u}) = (d/d\bar{u})\{\sinh^{-1}\bar{u}g'(v-\bar{u})\}, \tag{3}$$

$$\begin{aligned} S(\cosh\bar{u}) = &-\sinh^{-2}\bar{u}(d/d\bar{u})\{\sinh\bar{u}g'(v-\bar{u})\} \\ &-\tfrac{1}{2}(\sinh\bar{u}\sinh v)^{-2}[\sinh v\{f'(v+\bar{u})-f'(v-\bar{u})\} \\ &-\cosh v\{f(v+\bar{u})-f(v-\bar{u})\}], \end{aligned} \tag{4}$$

where the primes indicate derivatives, and

$$f(u) = F(\cosh u), \tag{5}$$

$$g(u) = \{4\cosh v\sinh(u-v)\}^{-1}\{f(u)-f(2v-u)\}. \tag{6}$$

Thus starting from the general total probability function $F(U)dU$ we have without specializing it found the differential probability function $W(U, c)dUdc$.

To obtain explicit results we adopted the form of $f(u)$ found by Messel[1] to account best for the vertical development of the high energy nucleon component of the cosmic radiation:

$$f(u) = 20(U_0-1)^{-5}(\cosh u-1)(U_0-\cosh u)^3. \tag{7}$$

In the ultra-relativistic approximation (7) leads to

$$R = -S = 30\bar{c}^{-6v}(\exp v-\exp\bar{u})\exp(3\bar{u}). \tag{8}$$

We have calculated the mean square angle of scatter for a single

nucleon-nucleon collision using (8) and found

$$\langle\Theta^2\rangle_{Av}=4U_0^{-1}\text{ (radians)}^2. \quad (9)$$

The primary energy U_0 is measured in proton mass units.

Consideration of this result leads us to the conclusion that the lateral spread of the high energy nucleon component of the cosmic radiation in extensive air showers must be considerably greater than that for the majority of electrons whose mean square angular deflection is proportional only to U_0^{-2}.

The details and full discussion of the above work will be given in a subsequent publication. We are indebted to Professor E. Schrödinger for valuable suggestions in the course of the above work.

[1] H. Messel, Proc. Phys. Soc. (London), to be published.

Two-Step Isomeric Transition in Hf^{179m}*

E. der Mateosian and M. Goldhaber
Brookhaven National Laboratory, Upton, New York
(Received July 5, 1951)

A 19-sec activity was reported in Hf by Flammersfeld,[1] and was assigned to Hf^{179m} by Muehlhause.[2] Hole[3] measured the energy of the conversion electrons in a β-ray spectrometer and obtained a value of 150 kev for the transition energy. The authors,[4] who investigated the unconverted gamma-rays in a scintillation spectrometer, found an intense gamma-ray line of 215-kev energy and suggested the possibility of a two-step isomeric transition. The measurements of Hole were repeated and confirmed by Burson *et al.*,[5] who found 160 kev for the internally converted transition. Thus it was apparent that two gamma-rays were involved in these measurements, a highly internally converted transition of 160 kev and a weakly converted transition of 215 kev.

To test the possibility of a two-step isomeric transition a number of experiments were carried out. Since previous investigations of the lifetime and the assignment of the 19-sec activity to Hf^{179m} had been based on observations of conversion electrons, it was necessary to determine whether the 215-kev gamma-rays were also associated with Hf^{179m}. Enriched isotopes of Hf (Hf^{176}, Hf^{177}, Hf^{178}, and Hf^{179}) were irradiated in the Brookhaven reactor and the 215-kev line was observed with a scintillation spectrometer. It appeared most intense in $Hf^{178}+n$. The γ-rays were found to decay with a half-life of 19 sec.

To record the expected coincidences in such a short-lived activity we made use of the following scheme. The Hf^{179m} sample was placed between two scintillation crystals mounted on RCA 5819 tubes. The pulse from one photomultiplier was used to start the sweep of an oscilloscope, while the pulse from the other photomultiplier was impressed upon the screen (y axis) of a cathode-ray tube. Under these conditions, the distribution seen is due to pulses in coincidence with the triggering pulses. By using either NaI-Tl or anthracene crystals, the detectors were made sensitive to gamma-rays or electrons, respectively. By triggering the sweep with electron pulses from an anthracene crystal and impressing the gamma-ray pulses from a NaI-Tl crystal upon the screen, the pulse distribution due to the 215-kev gamma-ray was seen (Fig. 1), indicating the existence of coincidences with a time delay <0.5 μsec. In coincidence with gamma-rays >160 kev an electron distribution with an upper limit of $\sim$95 kev was obtained. Adding the K-work function of Hf we find $\sim$150 kev for the energy of the highly converted transition, in good agreement with the beta-spectrographic investigations. The photon pulses obtained in coincidence with gamma-rays >160 kev showed only the Hf K-x-rays. The 160-kev transition is evidently highly converted, as already noticed by Hole,[3] who found a conversion coefficient $\epsilon>19$. A search was made for L conversion electrons from the 215-kev transition with the help of an anthracene crystal. An upper limit of 10 percent of the intensity of the K electrons of the 160-kev transition was established. (The K conversion electrons would approximately coincide with L conversion electrons from the 160-kev transition.) No cross-over transition of (160+215) kev=375 kev was detected. If present, it takes place in <1 percent of the transitions. With the help of the K conversion coefficients calculated by Rose *et al.*[6] (see Table I) and the empirical lifetime energy relations and K/L ratios given by Goldhaber and Sunyar[7] the results given above allow us to conclude that the 160-kev transition is an $M3$ transition and that the 215-kev transition corresponds to a spin change $\Delta I\leq 2$, with an $M2$ transition excluded.

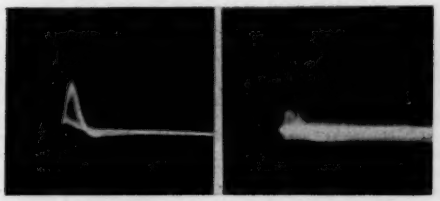

(a) (b)

FIG. 1. (a) Te^{129m} γ-rays (159 kev) for calibration; (b) Hf^{179m} γ-rays (215 kev) and Hf K x-rays which coincide with conversion electrons preceding them.

TABLE I. K conversion coefficients.[a]

E(kev)	α_1	α_2	α_3	β_1	β_2	β_3
160	0.088	0.31	0.93	1.05	5.4	20.0
215	0.043	0.14	0.43	0.47	2.1	7.0

[a] See reference 6.

A final level assignment must await a measurement of the ground-state spin of Hf^{179} (known to be $\leq\frac{1}{2}$)[8] and the determination of the character of the 215-kev transition. The following tentative decay scheme is compatible with existing knowledge and shell theory, but is not unique:

$$h_{9/2} \xrightarrow{160\text{ kev}} p_{3/2} \xrightarrow{215\text{ kev}} p_{1/2}.$$

* Research carried out under contract with the AEC.
[1] A. Flammersfeld, Z. Naturforsch. 1, 190 (1946).
[2] C. O. Muehlhause, private communication.
[3] N. Hole, Arkiv Mat. Astron. Fysik 35A, No. 9 (1948).
[4] E. der Mateosian and M. Goldhaber, Phys. Rev. 82, 115 (1951).
[5] Burson, Blair, Keller, and Wexler, Phys. Rev. 83, 62 (1951).
[6] Rose, Goertzel, Spinrad, Harr, and Strong, Phys. Rev. 83, 79 (1951).
[7] M. Goldhaber and A. W. Sunyar, Phys. Rev., to be published.
[8] K. Way *et al.*, "Nuclear data," Natl. Bur. Standards (U. S.) Circ. No. 499 (1950).

On the Decay of Neutral V-Particles*

R. B. Leighton, S. Dean Wanlass, and William L. Alford
California Institute of Technology, Pasadena, California
(Received July 5, 1951)

SEVERAL new examples of the decay of neutral V-particles[1-4] have been obtained recently at Pasadena, using two new magnet cloud chambers arranged to respond to cosmic-ray penetrating showers. Nine of these are of special interest in that it is possible to draw some conclusions as to the identity of the charged secondaries in each case. The momentum and estimated specific ionization (relative to the minimum for fast, singly charged particles) and the mass-value computed from these quantities are tabulated for each charged decay-particle in Table I.

It is apparent from this table that all of the negative particles are mesons; one of these underwent a sudden deflection in flight, the angular deviation of 6° being within the allowable range for a $\pi-\mu$-decay, so that the negative particles are indeed probably π-mesons.

On the other hand, it is also apparent that most of the positive particles are surely much heavier than mesons, and while the

TABLE I. Numerical data relating to V-particle decay.

Frame	P_+ Mev/c	$I_+/I_{\min}$	M_+ m_e	P_- Mev/c	$I_-/I_{\min}$	M_- m_e	θ deg	Q' Mev
6724	700±200	1.7±0.3	1500±700	47±2	6±2	280±60	157	65±20
7029	172±10	8±3	1200±300	136±5	1.5±0.3	260±60	96	55±10
7800	178±25	>15	>1500	172±25	1.7±0.3	340±150	37	50±20
8796	620±100	1.3±0.2	870±600	117±5	1.5±0.3	225±70	44	21±5[a] 130±30[b]
9489	370±50	2.5±1	1100±500	180±20	1.3±0.2	250±100	52	53±10
10876	475±75	1.8±0.7	1100±600	101±5	2.0±0.5	260±50	70	32±5
11373	350±100	5±2	1800±900	65±10	3.5±1.5	260±70	134	35±5
12418	500±100	<1.3	<850	216±20	<1.3	<320	39	93±20[b]
12717	850±200	<1.3	<1500	125±25	1.7±0.5	270±120	71	63±20

[a] Calculated for $\pi+p$ decay. [b] Calculated for $\pi+\pi$ decay.

calculated mass-values fall somewhat short of a proton mass, they are assumed for the present to be protons.

Also given in Table I are the Q'-values which would correspond to a two-body decay of the V^0 into a proton and a π-meson. A rigorous formula for Q' is

$$Q'=(M_1+M_2)\{[1+2Q_1/(M_1+M_2)]^{\frac{1}{2}}-1\}.$$

Here, M_1 and M_2 are the rest-masses of the two particles into which the V^0 decays and

$$Q_1=(E_1E_2-M_1M_2-P_1P_2\cos\theta)/(M_1+M_2),$$

where P_1 and P_2 are the momenta of the two decay particles and E_1 and E_2 are their total energies, all measured in energy units, while θ is the total angle included between the decay-particle tracks. If $Q'\ll(M_1+M_2)$, a very good approximation is $Q'\approx Q_1$.

The energies released in these decays do not appear to be consistent with the assumption of a unique two-body decay process for a V^0. The Q'-values found by the Manchester group[3] and by the Indiana group[4] show a similar variation, and fit quite well into the range found here. One, or possibly two, of the decays seem to be of the type suggested by the Manchester workers,[3] in which both particles are mesons. The Q'-values for an assumed two-body decay into two π-mesons is given for these two cases. These Q'-values are about twice as large as those obtained for $\pi+p$ decay.

The present results, and those of other observers, are so far consistent with the assumption that several different V^0 particles exist, all of comparable lifetime, one or more of which decays into two mesons, and two or more into a proton and meson, the latter with energy releases of about 32 Mev and about 55 Mev.

However, all of the results obtained so far can also be explained in terms of a single three-body decay process having a fixed Q-value, in which a neutral V-particle always decays into two mesons and a nucleon, thus:

$$V^0\rightarrow\text{meson}+\text{meson}+\text{nucleon}+Q,$$

where the distribution of charge between the nucleon and the mesons is such that any of the three particles is about equally likely to be neutral. This would agree with the observation that about one-third of the decays seem to involve two charged mesons, and about two-thirds a proton and a meson.

In a decay process such as the above one, in which one of the products is much heavier than the others, most of the kinetic energy released in the decay in the center-of-mass system is carried off by the lighter particles. If there are two similar lighter particles, they will, on the average, have energies equal to about half the total energy available in the decay, and the distribution of energies carried by each of them will be approximately symmetrical about this average.

It has been pointed out by Feynman that the "fictitious mass," calculated for the V^0 as if the decay produced only the two observed particles, is relativistically invariant, since it is of the form

$$M'^2=(E_1+E_2)^2-(\mathbf{P}_1+\mathbf{P}_2)^2$$

or, equivalently,

$$M'^2=(E_v-E_0)^2-(\mathbf{P}_v-\mathbf{P}_0)^2,$$

where M' is the fictitious mass, E_1, E_2, E_0, and E_v are the total energies (mass plus kinetic) of the two charged particles, the neutral decay particle, and the V^0, respectively, and $\mathbf{P}_1$, $\mathbf{P}_2$, $\mathbf{P}_0$, and $\mathbf{P}_v$ are similarly their vector momenta. Since M' is invariant, it may be calculated in the c.m. system of the V^0, where $\mathbf{P}_v=0$ and $E_v=M_v$, with the result

$$M'^2=(M_v-M_0)^2-2M_vT_0.$$

Thus, the distribution of M'^2 is proportional to the distribution of kinetic energy T_0 carried by the neutral decay particle in the c.m. system of the V-particle. M' will fall from case to case between the limits (M_1+M_2) and (M_1+M_2+Q); in those decays where the charged products are a proton and a meson, M' should usually be somewhat less than $(M_1+M_2+\frac{1}{2}Q)$.

A histogram of the values of Q' for the cases of $\pi+p$ decay is shown in Fig. 1. Included in it are the cases here described and

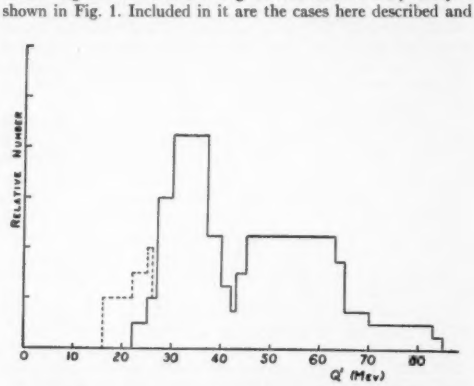

FIG. 1. Histogram of energies released in neutral V-particle decay. Each decay is represented by a rectangle whose half-width is equal to the stated uncertainty for that case, and whose height is such that each contributes an equal area to the diagram. The total number of cases represented is eleven, plus one (shown dotted) which might not be a valid $\pi+p$ decay.

four cases published by other workers.[3,4] From this histogram it is apparent that, if the foregoing three-body decay scheme were correct, the Q of the decay should be in the range 100–150 Mev.

Finally, a remark should perhaps be made regarding the problem of distinguishing between two-body and three-body decay of a V^0 by means of the "coplanarity" of the decay tracks with a star or other origin from which the V^0 can be assumed to have traveled. If the decay were a three-body process involving two light particles and a heavy one, as is suggested above, the heavy particle would usually possess a much larger momentum in the laboratory system than either of the two lighter particles, and its path would therefore lie more nearly along the V^0 path. Therefore, in those cases where the charged products were a meson and proton, the "coplanarity" would appear to be rather good, so that the decay would appear to be consistent with a two-body one, while in those cases where the charged products were both mesons, the "coplanarity" would be rather poor. This might explain the observed

results[2] that in a majority of cases where an origin is present, the tracks appear to be coplanar with it, within the rather limited accuracy of measurement.

* Assisted in part by the joint program of the ONR and AEC.
[1] G. D. Rochester and C. C. Butler, Nature **160**, 855 (1947).
[2] Seriff, Leighton, Hsiao, Cowan, and Anderson, Phys. Rev. **78**, 290 (1950).
[3] Armenteros, Barker, Butler, Cachon, and Chapman, Nature **167**, 501 (1951).
[4] Thompson, Cohn, and Flum, Phys. Rev. **83**, 175 (1951).

Erratum: The Angular Correlation Theorem and the Elimination of Interference Terms

[Phys. Rev. **83**, 189 (1951)]

H. A. Tolhoek and S. R. de Groot
Institute for Theoretical Physics, University of Utrecht, Netherlands

EQUATIONS (3) and (5) should read as follows:

$$(e_1|\rho|e_2)=NS_1(i|H_1|e_1)^*(i|H_1|e_2), \tag{3}$$

$$S_1(i|H_1|e_1)^*(i|H_1|e_2)=0 \quad (e_1\neq e_2). \tag{5}$$

Neutron-Proton Scattering with Repulsive Forces

P. O. Olsson
Stockholm Hogskola and Royal Institute of Technology, Stockholm, Sweden
(Received June 22, 1951)

THE neutron-proton scattering at 90 and 260 Mev has been calculated using central forces and a square well with an impenetrable inner sphere. The radius of the sphere was varied between the limits 0 and 1.2×10^{-13} cm and the depth of the well between 38 and 140 Mev. The low energy scattering could be made to agree with experiment within wide ranges of the hard sphere radius and well depth. At 90 Mev the neutral total cross section varied between 0.20 and 0.28 barn, whereas the cross sections for the charged and symmetric theories could be brought in agreement with the experimental value of 0.079 barn. (These theories were considered in order to be able to compare results with earlier calculations.) The angular distribution was in poor agreement with experimental values, being much the same as those obtained for an ordinary well.

At 260 Mev the cross sections obtained were much too large, being about three times the experimental value of 0.038 barn. For the charged and symmetric theories the cross sections were generally larger than the corresponding values at 90 Mev. This increase of the cross sections with increasing energy was caused by too rapid an increase of the P- and particularly the D-phases. The effect is explained by the fact that the attractive outer region must be made much stronger for a model with a repulsive core than for an ordinary well, and the phase-decreasing effect of the repulsive core will be comparatively unimportant for the P- and D-phases. If the radius of the inner core is further increased, the depth of the outer region must be increased too in order to maintain low energy agreement, but the effect of the inner core will be more pronounced so that the S-phase will become negative. Negative S-phases will give angular distributions having maxima at 90° in contradiction with the U-shaped distribution expected from experiment.[1]

The conclusion from these considerations is that a strong repulsion can hardly be present in the neutron-proton interaction in triplet states of even parity.

The possibility of introducing repulsive forces into the proton-proton interaction has recently been investigated by Jastrow,[2] and later investigations have been extended also to the neutron-proton case.[3] Jastrow reports reasonable agreement with available experimental data, but the repulsion used is assumed to have negligible range in the triplet states. It seems strange to us that, if a repulsion is really present, it should be so strongly spin-dependent.

The investigations related above were carried out on a suggestion by Professor O. Klein, to whom I wish to express my gratitude.

[1] Kelley, Leith, Segrè, and Wiegand, Phys. Rev. **79**, 96 (1950).
[2] R. Jastrow, Phys. Rev. **79**, 389 (1950).
[3] R. Jastrow, Phys. Rev. **81**, 165 (1951).

The Magnetic Moment of S^{33}

S. S. Dharmatti and H. E. Weaver, Jr.
Stanford University, Stanford, California*
(Received July 5, 1951)

EMPLOYING the nuclear induction spectrometer described earlier by Proctor,[1] signals of S^{33} with a natural line width of about one gauss were detected in chemically pure CS_2. The resonant frequency was compared with that of N^{14} in a 3.2 normal solution of HNO_3 with the result

$$\nu(S^{33})/\nu(N^{14})=1.06174\pm0.00013. \tag{1}$$

Using the known magnetic moment[2] of N^{14} and the fact that the spin of S^{33} is $\frac{3}{2}$,[3] the value of the magnetic moment was found to be

$$\mu(S^{33})=+0.64292\pm0.00014. \tag{2}$$

The positive sign in Eq. (2) was verified by comparing the sign of the S^{33} signal with that of N^{14} and H^1. In the case of H^2 a careful comparison of signal magnitudes was also carried out and within the experimental error gave a result consistent[4] with the spin and natural abundance (0.74 percent) of S^{33}. The earlier determination of $\mu(S^{33})=0.632\pm0.010$ nm by Eshbach, Hillger, and Jen[5] is in agreement with the more precise value of Eq. (2).

Signals of S^{32} were not observed in other liquid sulfur compounds. This was probably due to the fact that the line widths, resulting from quadrupole[6] effects, were too broad.

We would like to express here our gratitude to Professor Felix Bloch for many helpful consultations during the course of this work.

* Assisted by the joint program of the AEC and ONR.
[1] W. G. Proctor, Phys. Rev. **79**, 35 (1950).
[2] W. G. Proctor and F. C. Yu, Phys. Rev. **81**, 20 (1951).
[3] C. H. Townes and S. Geschwind, Phys. Rev. **74**, 626 (1948).
[4] F. Bloch, Phys. Rev. **70**, 460 (1946).
[5] Eshbach, Hillger, and Jen, Phys. Rev. **80**, 1106 (1950).
[6] C. H. Townes and B. P. Dailey, J. Chem. Phys. **17**, 782 (1949), report a quadrupole moment for S^{33} of about -0.08×10^{-24} cm².

The Reactions of He^3+He^3

W. M. Good, W. E. Kunz, and C. D. Moak
Oak Ridge National Laboratory, Oak Ridge, Tennessee
(Received June 11, 1951)

THE following reactions can be expected to compete when He^3 is captured by He^3:

$$He^3+He^3\rightarrow He^4+H^1+H^1+12.82, \tag{1}$$

$$He^3+He^3\rightarrow Li^6+H^1+11.02 \text{ Mev} \tag{2}$$

$$\downarrow$$

$$He^4+H^1+1.8 \text{ Mev}.$$

Three μa of He^{3+} at 300 kev were obtained by accelerating a mixture of He^3 and He^4 in a Cockroft-Walton generator. The three μa of He^{3+}, which constituted about two percent of the beam, were magnetically separated and directed against a clean 5-mil aluminum foil as shown in Fig. 1. Behind this foil was located a proton counter. After two hours of bombardment, the counting rate of the counter rose some fifteen times background.

Figure 2 shows the spectrum of protons observed by two different methods when two separate clean 5-mil aluminum foils were bombarded by the He^3. In the first method the detector was

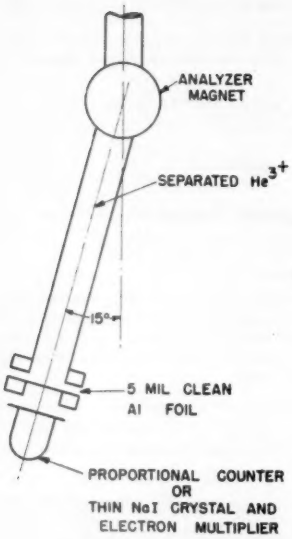

FIG. 1. Experimental set-up for observing the reactions of He^3+He^3.

a proportional counter biased to detect only protons at the end of their range, and the counting rate was observed *vs* thickness of aluminum absorber. In Fig. 2, the result of a single experiment is given with the thickness of aluminum, including that of the 5-mil target, converted to its energy equivalent. There appears a large yield of 14.7-Mev protons from the reaction $He^3+H^2 \rightarrow He^4+H^1+18.32$ Mev. This reaction always appears as a result of an accumulation on the target of deuterium which inevitably gets into the machine. The 14.7-Mev protons were used as an energy reference. In the second method a differential pulse-height selector was used to study the pulse-height spectrum produced by the protons in a thin NaI crystal. In this case, the 14.7-Mev protons from the impurity reaction He^3+H^2 served to calibrate the energy of the pulses. Figure 2 shows the spectrum obtained after converting the pulse height to energy, taking account of energy losses in the 5-mil window.

To aid in interpreting these very preliminary results, the statistical proton energy distribution for the three-body breakup

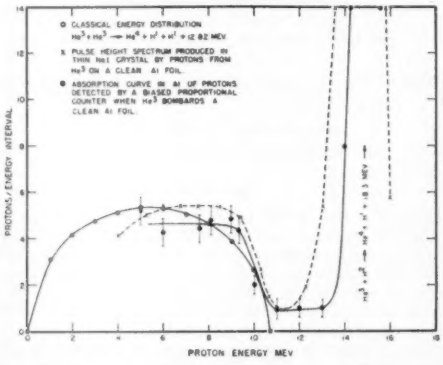

FIG. 2. Energy distribution of protons from bombarding He^3 on clean aluminum.

(1) is given for comparison. The maximum observed proton energy agrees closely with that expected from the three-body breakup. The departure in shape of the calculated distribution from that observed cannot be accounted for by center-of-gravity motion, and suggests at least some of the competing reaction (2), namely, a breakup of Be^6 into Li^5 and a proton followed by the decay of Li^5 to He^4 and another proton. That the protons cannot originate from capture of He^3 on aluminum itself seems virtually certain because of the build-up in the counting rate, and such protons would have a maximum energy of 11.7 Mev, which is clearly not the case observed here. Actually, a reaction on aluminum would be expected to show resolvable group structure rather than a continuum. In addition, the very high coulomb barrier would make such a reaction most unlikely.

It is concluded at present that the reaction being observed is that of He^3 on He^3 which has accumulated on the target. These data are preliminary and a further study of the reaction is under way.

The authors are indebted to Dr. M. E. Rose for discussion of the problem.

A Numerical Variational Method*

R. E. MEYEROTT,† P. J. LUKE,‡ W. W. CLENDENIN, AND S. GELTMAN
Yale University, New Haven, Connecticut
(Received July 2, 1951)

RELAXATION methods in eigenvalue problems have been discussed by Southwell,[1] by Allen and others,[2] and by Fox.[3] The solution consists of two steps. First, the differential equation of the problem is replaced by a set of finite difference equations. Secondly, the solution so obtained is used in the Rayleigh-Ritz expression for the energy parameter. The energy parameter used in the difference equations must be equal to that found from the Ritz integral. For this reason a procedure which requires the consistency of these two values of the energy parameter is of interest and is described below.

At the suggestion of Professor G. Breit, the problem was set up on the basis of the variational principle for one and two independent variables. For one variable, the interval of the independent variable is subdivided by a set of equally spaced net points. The values at these points are used as variational parameters. Elsewhere the trial function is defined by a linear interpolation formula. The Rayleigh-Ritz energy integral then leads to a set of simultaneous linear equations in the variational parameters similar to those of Fox. The coefficients involve the energy and integrals of the potential energy. The equations may then be used in the same manner as the relaxation equations.

A similar procedure is used for two independent variables. The plane of the independent variables is divided by equidistant lines parallel to the axes of independent variables into square panels. The values of the function at the corner points of the panels are used as variational parameters and the function is defined elsewhere by an interpolation formula. The variational method again leads to a set of linear equations similar to the relaxation equations.

In both cases the equations contain fourth- and higher order differences similar to the difference correction obtained by Fox. The fourth-order differences in the variational equations are the negative of those obtained by Fox.

The method is well suited to the improvement of an approximate solution which is known precisely, but which only approximately satisfies the differential equation and boundary conditions. The procedure is analogous to that described previously and leads to similar difference equations which, however, include inhomogeneous terms depending on the approximate solution and on the differential equation. On the boundary the correction function is defined so that the sum of correction function and approximate solution satisfy the boundary conditions. Elsewhere it is defined in terms of net point values and an interpolation formula. The large number of variational parameters, one for each net point, make it

practical to obtain an accurate correction function. This method has been used in the calculation of a wave function and energy value for the $1s2s\ ^3S$ state of ionized lithium.[4] The approximate solution is a finite series of product-type functions. Comparison of the energy value obtained with the experimental energy is of help in determining the goodness of the wave function.

* Assisted by the joint program of the ONR and AEC.
† Now at Argonne National Laboratory, Chicago, Illinois.
‡ Now at the Applied Physics Laboratories of Johns Hopkins University, Silver Spring, Maryland.
[1] R. V. Southwell, *Relaxation Methods in Engineering Science* (Oxford University Press, London, 1940).
[2] Allen, Fox, Motz, and Southwell, Trans. Roy. Soc. (London) **A239**, 488 (1942).
[3] L. Fox, Proc. Roy. Soc. (London) **A190**, 31 (1947).
[4] Luke, Meyerott, and Clendenin, Phys. Rev. **83**, 847 (1951).

Wave Function of Ionized Lithium*

P. J. Luke,† R. E. Meyerott,‡ and W. W. Clendenin
Yale University, New Haven, Connecticut
(Received July 2, 1951)

A WAVE function of singly ionized lithium in the $1s2s\ ^3S$ state has been calculated and used to find the hyperfine splitting coupling factor. The wave function depends only on the size and shape of the electronic triangle, not on its orientation. It is convenient to take as coördinates the distances r_1 and r_2 of electrons 1 and 2 from the nucleus and the angle θ between r_1 and r_2. The differential equation satisfied by $\varphi=r_1r_2\psi$, where ψ is the wave function, is given in Breit and Doermann's paper,[1] Eq. (39). The boundary conditions require that φ vanish when either r_1 or r_2 is zero or infinity. The antisymmetry of the wave function requires that φ vanish whenever r_1 equals r_2. It suffices to compute φ in the region $r_1>r_2$, as the function may be obtained elsewhere from the antisymmetry condition.

The function φ is expanded in a series of Legendre polynomials,

$$\varphi(r_1,r_2,\theta)=\sum_{l=0}^{\infty}(2l+1)^{\frac{1}{2}}\Phi_l(r_1,r_2)P_l(\cos\theta). \quad (1)$$

Substitution in the differential equation results in a set of simultaneous differential equations for the functions Φ_l. The differential equation for Φ_0, which may be shown to be the dominant term in the expansion of φ, is

$$\left[\frac{\partial^2}{\partial r_1^2}+\frac{\partial^2}{\partial r_2^2}+\frac{\lambda}{4}+\frac{Z-1}{Zr_1}+\frac{1}{r_2}\right]\Phi_0=\frac{1}{Zr_1}\sum_{m=1}^{\infty}(2m+1)^{\frac{1}{2}}\left(\frac{r_2}{r_1}\right)^m\Phi_m. \quad (2)$$

To solve this equation, Φ_0 is expressed as $\Phi_0^{(0)}+\Phi_0^{(1)}$, where $\Phi_0^{(0)}$ is the solution of the homogeneous equation for a particular value λ_0 of the energy parameter. The function $\Phi_0^{(0)}$ is expressed as $\varphi^{(0)}+\varphi^{(1)}$; $\varphi^{(0)}$ is a sum of product-type solutions each of which satisfies the separable homogeneous equation. The coefficients of these terms are adjusted so that the integral of the square of $\varphi^{(0)}$ along $r_1=r_2$ is a minimum. The function $\varphi^{(1)}$ satisfies the homogeneous equation and cancels $\varphi^{(0)}$ along $r_1=r_2$. The relatively small function $\varphi^{(1)}$ was computed by a numerical variational method described elsewhere.[2] Three terms were used for $\varphi^{(0)}$ and a value of λ_0 equal to $-1.1354467RhcZ^2$, where R is Rydberg's constant, was chosen. This value is slightly lower than the value $-1.1354RhcZ^2$ obtained by Breit and Doermann.

The functions Φ_1 and Φ_2 were computed by numerical methods similar to that used for $\varphi^{(1)}$. An estimate of Φ_2 showed it to have a negligible effect. Using Φ_1 and Φ_2, the function $\Phi_0^{(1)}$ was computed numerically.

Substitution of the series expansion of φ in the Rayleigh-Ritz integral gave the energy. The principal additions to λ_0 came from the two terms of the form $\int\int(1/r_1)\Phi_0(r_2/r_1)^{\frac{1}{2}}\Phi_1dr_1dr_2$ which are due to the electronic potential energy. These amounted to $-290\times10^{-6}RhcZ^2$. The remaining terms in the integral were small and tended to cancel one another. Their sum was $+13\times10^{-6}RhcZ^2$. These results give $-1.135724RhcZ^2$ for the energy. This is to be compared with the experimental value, corrected for the relativistic effect and nuclear motion, of $-1.135721\pm0.000026RhcZ^2$.

The correction factor $1+\epsilon$ appearing in the expression of Breit and Doermann for the hyperfine splitting was computed to be 1.06190 ± 0.00003. The uncertainty here is due to uncertainty in the function $\Phi_0^{(1)}$.

The possibility of using separability and the successive corrections has been pointed out to us by Professor G. Breit. Acknowledgment is made of preliminary trials of the method by Dr. S. Share, then at the University of Wisconsin, and of help from Mr. S. Geltman in some of the work.

* Assisted by the joint program of the ONR and AEC.
† Now at the Applied Physics Laboratories of Johns Hopkins University, Silver Spring, Maryland.
‡ Now at Argonne National Laboratory, Chicago, Illinois.
[1] Breit and Doermann, Phys. Rev. **36**, 1732 (1930).
[2] Meyerott, Luke, Clendenin, and Geltman, Phys. Rev. **83**, 846 (1951).

Ferromagnetic Resonance Absorption in $MnOFe_2O_3$ at Low Temperature

Toshiiko Okamura and Yosiharu Torizuka
Research Institute for Scientific Measurement, Sendai, Japan
(Received June 25, 1951)

RECENTLY, it has been discovered experimentally that the intensity of magnetization of nickel[1] and mangan ferrite[2] decreases at low fields in a certain temperature range, and that a transition like that of magnetite also exists in these complete inverted spinels.

In order to study the mechanism of these transitions, microwave resonance experiments have been undertaken by many physicists,[3-5] and various interesting results have been obtained. For the same purpose, the present resonance experiment with mangan ferrite was made at 3.22-cm wavelength from +150°C to liquid nitrogen temperature, and the relative absorption with varying static magnetic field was observed at various temperatures on a sintered disk-formed specimen, whose diameter was 4 mm and whose thickness was 0.3 mm.

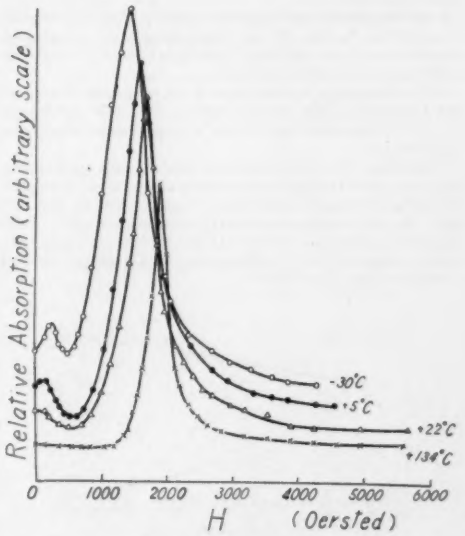

FIG. 1. Curves of absorption *versus* dc magnetic field for $MnOFe_2O_3$; temperature range +134° to −30°.

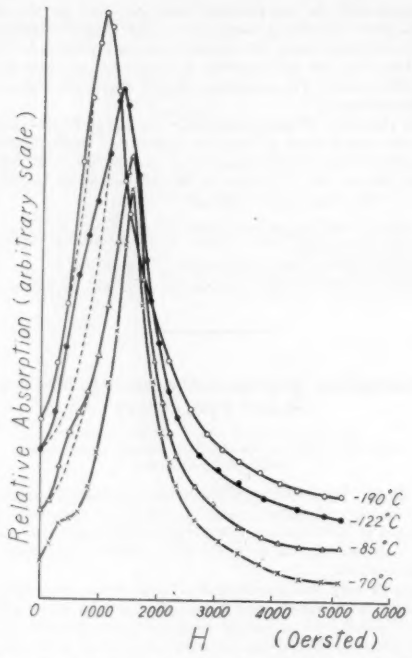

FIG. 2. Curves of absorption *versus* dc magnetic field for $MnOFe_2O_3$; temperature range $-70°$ to $-190°$.

Figures 1 and 2 show the curve of relative absorption with varying applied dc magnetic field at temperatures ranging from $+135°C$ to $-190°$.

In the temperature range of about $+20°$ to $-70°$, double peaks were observed; further, with decreasing temperature, a small peak overlaps the ordinary large peak, tending to form an asymmetrical resonance curve as shown in Fig. 2.

From the magnetic measurement, it was previously determined that the transition of the mangan ferrite began at $+20°$ and finished at $-150°$, below which the intensity of magnetization appears almost constant.

To ascertain the behavior of these double peaks more clearly, the resonance field strengths were plotted as a function of temperature in Fig. 3; the open circles denote resonance fields for high field peaks, the solid circles resonance fields for low field peaks. From this figure, it is seen that the way in which the resonance fields vary with temperature in the transition region is qualitatively the same as in the case of nickel ferrite.[4]

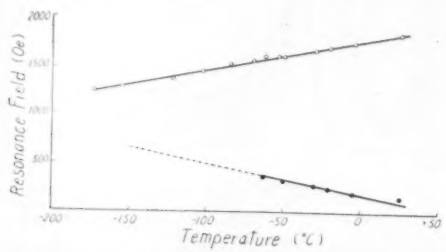

FIG. 3. Resonance fields for high and low field peaks *versus* temperature.

In this experiment, when another specimen of different size was used, the double peaks were always found in the same temperature range.

Thus, it is concluded that the double peaks are not caused by an internal cavity effect,[6] but rather by formation of an ordering pattern of some ferrous ions.

Details of this work will be published in *The Science Reports of the Tôhoku Imperial University.*

[1] T. Okamura, Nature, to be published.
[2] T. Okamura and J. Simoizaka, to be published.
[3] L. R. Bickford, Phys. Rev. **78**, 449 (1950).
[4] T. Okamura and Y. Torizuka, "Ferromagnetic resonance absorption in $NiOFe_2O_3$ at low temperature," Science Repts. Tôhoku Imp. Univ., to be published.
[5] T. Okamura and Y. Torizuka, "Microwave resonance adsorption in magnetite at low temperature," Science Repts. Tôhoku Imp. Univ., to be published.
[6] Yager, Galt, Merritt, and Wood, Phys. Rev. **80**, 744 (1950).

The Beta-Spectrum of S^{35} Using Window Corrections*

R. B. HELLER, E. F. STURCKEN, AND A. H. WEBER
St. Louis University, St. Louis, Missouri
(Received July 5, 1951)

ALBERT and Wu[1] have determined the negatron spectrum of S^{35} as a straight line Fermi plot from 166 kev down to 16 kev for a 1-$\mu g/cm^2$ source employing a solenoidal spectrometer. Langer *et al.*,[2] using a small 180° spectrometer, found the spectrum linear down to about 50 kev with a source of about 10 $\mu g/cm^2$. Salmi,[3] also using a 180° spectrometer, obtained linearity in the Fermi plot down to about 42 kev. The emphasis in these investigations has been upon minimizing the distortion in the low energy region by the use of extremely thin sources and source backings. Gross and Hamilton,[4] employing an electrostatic type of spectrometer, report linearity in the Fermi plot down to about 6 kev.

We have measured the transmission of slow beta-rays by Nylon films and so decided to investigate the effect these correction curves would have on the low energy spectrum of reasonably thin S^{35} sources and source backings. The St. Louis University thin lens spectrometer was employed, with the outermost layers only of the magnet coil energized so as to minimize spherical aberration in the moderately low energy region. The resolution of the instrument was about 2.5 percent.

The source was CdS^{35} prepared from highly active elemental S^{35} obtained from Oak Ridge in a benzene solution. A circular area source 0.5 cm in diameter was prepared in the following manner. A 30A layer of Al was evaporated on a Nylon backing weighing less than 10 $\mu g/cm^2$. This Nylon film was chosen from the same batch used to obtain the corrections of reference 5. The CdS was deposited from a warm water mixture onto an area of 0.5 cm in diameter upon which had previously been placed a 5 percent solution of Lilly insulin (40 units per cc). The source was rapidly dried under an infrared heat lamp. The deposit did not form a perfectly uniform layer. Assuming uniform spreading the source weighed less than 10 $\mu g/cm^2$. A thin line of conducting Aquadag

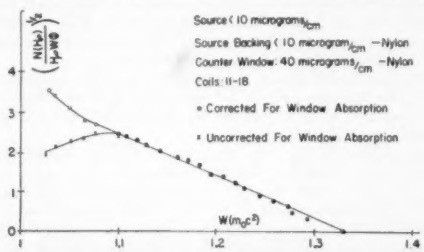

FIG. 1. Fermi plot of S^{35}. The end-point energy is 167 kev.

was ruled from the edges of the Al-covered Nylon backing to ground.

The counter window was about 45 $\mu g/cm^2$ of Nylon whose transmission properties were known.[5] Figure 1 shows that the Fermi plot of the uncorrected data is linear down to about 48 kev, and the data corrected for window absorption is linear to about 32 kev. It must be realized that back scattering of source mounts which are thicker than about 10 $\mu g/cm^2$ may give an excess of low energy betas which in turn may be absorbed or scattered by the counter window to produce a partial canceling of the two effects (source backscattering and counter window absorption).

The present results constitute additional evidence that the beta-spectrum of S^{35} observed with favorable experimental techniques is an allowed Fermi spectrum.

* This document is based on work performed under contract with the AEC.

[1] R. D. Albert and C. S. Wu, Phys. Rev. **74**, 847 (1948).
[2] Langer, Motz, and Price, Phys. Rev. **77**, 798 (1950).
[3] E. W. Salmi, Ph.D. dissertation, Department of Physics, University of Michigan (1950), unpublished.
[4] L. Gross and D. K. Hamilton, Phys. Rev. **80**, 484 (1950).
[5] Heller, Sturcken, and Weber, Rev. Sci. Instr. **21**, 898 (1950).

The Effect of Bohr Orbit Binding on Negative μ-Meson β-Decay*

C. E. Porter and H. Primakoff†
Department of Physics and Laboratory for Nuclear Science and Engineering, Massachusetts Institute of Technology, Cambridge, Massachusetts
(Received June 26, 1951)

THE phenomenon of the β-decay of μ-mesons is currently attracting both experimental and theoretical interest.[1,2] In the present note we have calculated the effect of binding the negative μ-meson into its lowest Bohr orbit[3] on the negative electron momentum spectrum characterizing the process: $\mu^- \to e^- + 2\nu$;[2] the orbital motion of the μ^- meson induced by the binding results in a "Doppler smearing" of the e^- spectrum. Similar Doppler smearing calculations have been previously made assuming a two-particle mode of decay of the μ^- meson.[4]

The principal result of our investigation is the prediction of a tailing of the e^- spectrum beyond the cut-off momentum appropriate to a meson which is free and stationary before decay, i.e., effectively, a tailing beyond the cut-off momentum of the e^+ spectrum from μ^+ mesons. This is shown in Fig. 1. A simple estimate based on the conservation laws gives the order of magnitude of the calculated Doppler smearing of the e^- spectrum:

$$\mathbf{p}_\mu = \mathbf{p}_e + \mathbf{n}_1 + \mathbf{n}_2; \quad \mu c^2 = c([p_e^2 + (mc)^2]^{\frac{1}{2}} + n_1 + n_2) \tag{1}$$

with $\mathbf{n}_1$ practically parallel to $\mathbf{n}_2$ when $|\mathbf{p}_e| \cong \frac{1}{2}\mu c$. We then have, from Eq. (1),

$$(p_e{}^-)_{max} \cong \tfrac{1}{2}\mu c[1 + (p_\mu)_{kr}/\mu c] \cong (p_e{}^+)_{max}(1 + Z\alpha) \tag{2}$$

for lowest Bohr orbit binding about a nucleus of charge Ze (here, $\alpha = 1/137$), in qualitative agreement with the more detailed results below.

In our complete calculations we have considered explicitly the "antisymmetric charge exchange" tensor coupling and the "charge retention" axial vector coupling;[2] these constitute the two extreme cases of $e^\pm$ momentum spectra with regard to shape near cutoff,[2] and have the further desirable property that, upon neglect of terms in $m/\mu \cong 1/210$, all other coupling types yield e^+ and e^- momentum spectra which are linear combinations of the two in question.

To a sufficient approximation in the relatively small parameter $Z\alpha$, we then find the following e^+ and e^- momentum spectra:

$$\{P(p_e)dp_e/\mu c\}_{e^+} = (96/\tau)(p_e/\mu c)^2(1 - 2p_e/\mu c)S(2p_e/\mu c)(dp_e/\mu c),$$
antisym. ch. ex.—tensor, (3a)

$$\{P(p_e)dp_e/\mu c\}_{e^+} = (96/\tau)\tfrac{1}{2}(p_e/\mu c)^2[1 - \tfrac{2}{3}(2p_e/\mu c)]S(2p_e/\mu c)(dp_e/\mu c),$$
ch. ret.—axial vector, (3b)

where $S(x) = 1$ for $0 \leqq x \leqq 1$, $S(x) = 0$ for $x > 1$, τ = meson decay mean life,[4,6] and

$$\left\{\frac{P(p_e)dp_e}{\mu c}\right\}_{e^-} = \left\{\frac{P(p_e)dp_e}{\mu c}\right\}_{e^+}\left[S\left(\frac{2p_e}{\mu c}\right)\right]^{-1} S\left(\frac{p_e}{\mu c}\right) \times \left\{\frac{1}{\pi}\left[\tan^{-1}\left(\frac{1-2y}{Z\alpha}\right) + \tan^{-1}\left(\frac{1}{Z\alpha}\right)\right] + Z\alpha\left(\frac{2}{\pi}\right)\frac{1-y}{1-2y}\left[1 - \frac{1}{3}\left(\frac{1-y}{y}\right)\frac{(Z\alpha)^2}{(Z\alpha)^2 + (1-2y)^2}\right]\right\},$$
antisym. ch. ex.—tensor, (4a)

$$\left\{\frac{P(p_e)dp_e}{\mu c}\right\}_{e^-} = \left\{\frac{P(p_e)dp_e}{\mu c}\right\}_{e^+}\left[S\left(\frac{2p_e}{\mu c}\right)\right]^{-1} S\left(\frac{p_e}{\mu c}\right) \times \left\{\frac{1}{\pi}\left[\tan^{-1}\left(\frac{1-2y}{Z\alpha}\right) + \tan^{-1}\left(\frac{1}{Z\alpha}\right)\right] + Z\alpha\left(\frac{2}{\pi}\right) \times \frac{1-y}{(Z\alpha)^2 + (1-2y)^2}\left[(1-2y) - \frac{2(Z\alpha)^2(1-3y/2)}{3\ \ y(1-4y/3)}\right]\right\},$$
ch. ret.—axial vector, (4b)

with $y \equiv p_e/\mu c$.

The expressions in Eqs. (3) and (4) are obtained by standard perturbation calculations of the corresponding transition |M.E.|[2]; in these |M.E.|[2] we use Schrödinger plane-wave and bound state wave functions for the μ^+ and μ^-, respectively, Dirac plane-wave wave functions for the e^+ and e^-, and Majorana plane-wave wave functions for the neutrinos. As a result, the momentum conservation quantity $\delta(\mathbf{p}_\mu - \mathbf{p}_e - \mathbf{n}_1 - \mathbf{n}_2)\delta(\mathbf{p}_\mu)$ appropriate to μ^+ decay, is replaced to a good approximation by the corresponding quantity

$$\delta(\mathbf{p}_\mu - \mathbf{p}_e - \mathbf{n}_1 - \mathbf{n}_2)\{(8/\pi^2)(Z\alpha\mu c)^{-4}[1 + p_\mu{}^2/(Z\alpha\mu c)^2]^{-4}\}$$

in the case of μ^- decay, where in the last expression, the second factor represents the normalized momentum probability distribution of the bound μ^- moving about the point charge nucleus Ze. The integration over $\mathbf{p}_\mu$ in the calculation of the μ^- decay transition probability is then immediate; the integration over $\mathbf{n}_1$ and $\mathbf{n}_2$, however, appears possible only upon use of the integral representation,

$$[1 + (\mathbf{x} + \mathbf{x}_1 + \mathbf{x}_2)^2]^{-4} = (192\pi)^{-1} \times \int d\mathbf{q} q^3 (\pi/2iq)^{\frac{1}{2}} H_{3/2}{}^{(1)}(iq)\ \exp(i\mathbf{q}\cdot[\mathbf{x} + \mathbf{x}_1 + \mathbf{x}_2]),$$

and even then is both difficult and tedious.

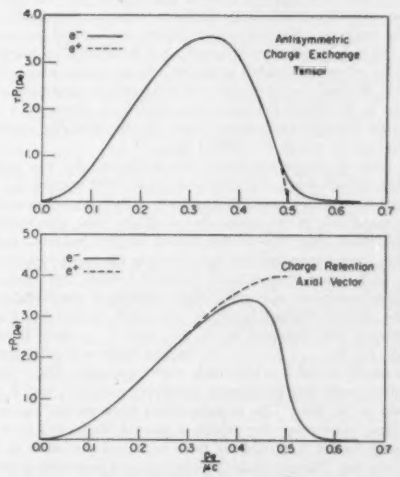

FIG. 1. Negative and positive electron momentum spectra from Eqs. (4) and (3), for $Z/137 = 0.1$.

Plots of the e^- momentum spectra given in Eq. (4) are shown in Fig. 1 for $Z/137=0.1$ (μ^- decay in Si) along with plots of the e^+ spectra given in Eq. (3) where effectively $Z/137=0$ (μ^+ decay).[6] It will be seen that e^+ momentum spectra with a relatively large number of electrons near cutoff give an enhanced e^- tailing effect. It is interesting to note that the recent work of Sagane *et al.*[1] seems to indicate the tensor coupling spectrum of Eq. (3a); in the perhaps analogous phenomenon of nucleon β-decay, recent work also seems to favor tensor coupling.[7]

* Assisted by the joint program of the ONR and AEC.
† On leave from Washington University, St. Louis, Missouri.
[1] Leighton, Anderson, and Seriff, Phys. Rev. **75**, 1432 (1949); Sagane, Gardener, and Hubbard, Phys. Rev. **82**, 557 (1951); H. W. Hubbard, Phys. Rev. **83**, 893(A) (1951).
[2] J. Tiomno and J. A. Wheeler, Revs. Modern Phys. **21**, 144 (1948); L. Michel, Proc. Phys. Soc. (London) **A63**, 514, 1371 (1950); Compt. rend. **232**, 391 (1951). Recently, S. Ogawa and S. Kamefuchi, Prog. Theor. Phys. **5**, 311 (1950), have discussed the possibility of neutrinoless decay of bound μ^- mesons with the emission of monoenergetic 100-Mev electrons.
[3] It will be recalled that practically all μ^- mesons stopped in matter are captured, previous to decay, into lowest Bohr orbits about the nuclei of the slowing-down material. See E. Fermi and E. Teller, Phys. Rev. **72**, 399 (1947).
[4] E. Corinaldesi, Nuovo cimento **4**, 132 (1947); H. Primakoff, Phys. Rev. **74**, 878 (1948).
[5] With neglect of terms in m/μ, (3a) and (3b) agree with the results of reference 2. (The corresponding formulas of Tiomno and Wheeler (their Eqs. (27) and (32)) seem, however, to contain misprints.) The relation between τ and the dimensionless field interaction coupling constant, $G^2/\hbar c$, is: $\tau^{-1}=[(9/16\pi^4)(1/96)(\mu/m)^5(mc^2/\hbar)](G^2/\hbar c)_{\text{tensor}}$; $\tau^{-1}=[(1/2\pi^3)(1/96)\times(\mu/m)^5(mc^2/\hbar)](G^2/\hbar c)_{\text{axv. vector}}$.
[6] It may be noted that the Bohr orbit binding of the μ^- causes a slight difference, $\approx(Z\alpha)^2\times100$ percent, between the mean lives of the μ^- and μ^+.
[7] L. M. Langer and R. J. D. Moffat, Phys. Rev. **82**, 635 (1951).

Multiple Coulomb Scattering of High Energy Protons in Photographic Emulsions*

MARTIN J. BERGER, J. J. LORD, AND MARCEL SCHEIN
Department of Physics, University of Chicago, Chicago, Illinois
(Received June 25, 1951)

MEASUREMENTS of the multiple coulomb scattering of fast charged particles in photographic emulsions reported in the recent literature have been confined to groups of cosmic-ray particles,[1] and to electrons produced by gamma-rays[2] or accelerated by a synchrotron.[3] Their results, when expressed in terms of a universal "scattering constant" for the photographic emulsion, show some disagreement. Because of the value of a precise knowledge of this quantity for practical applications such as mass and energy determinations, an investigation was therefore undertaken of the multiple scattering of artificially accelerated protons. In order to obtain sufficient accuracy, it was essential to investigate a group of monoenergetic particles whose energy was precisely known. We had an opportunity of doing this by analyzing proton tracks in an Ilford G5 plate that had been exposed by being dropped through the proton beam of the Berkeley cyclotron, which had an energy $E=340\pm1$ Mev.

A total of 150 tracks have been analyzed, and the analyzed section of each track was on the average 5000 microns (μ) long. In order to avoid possible emulsion distortion, measurements were made only in the central section of the plate, and sections of tracks closer than 50μ to the surface of the emulsion were excluded. Owing to energy loss by ionization, the mean proton energy over each track was reduced to 337 ± 1 Mev. The coordinate method of analysis was used, which consists of the measurement of the lateral displacements of the track caused by multiple scattering. The distances $y_1, y_2, \cdots, y_j, \cdots, y_n$ from successive points $P_1, P_2, \cdots, P_j, \cdots, P_n$ on the track to a reference line, very nearly parallel to the track, were measured. The distance s (minimum cell length) between successive points P_j and P_{j+1} was chosen to be 250μ. The measurements were carried out with a precision microscope for which a special stage has been constructed having a rectilinear motion with a deviation of 0.04μ over one cm. The apparatus was located in a basement room kept at very constant temperature, and mounted on a solid base to eliminate vibrations.

The set of second differences of the lateral displacements $\Delta^2y_j=y_{j+2}-2y_{j+1}+y_j$ obtained from a given track provides a measure of the multiple scattering. The mean value $\langle|\Delta^2y|\rangle_{Av}$ was computed from the Δ^2y_j obtained from all the 150 measured tracks, which are equivalent to a single track 75.3 cm long (with a constant energy of 337 Mev). The amount of multiple scattering is then expressed in the usual manner in terms of a "scattering constant" K_s defined by the relation:

$$\langle|\alpha|\rangle_{Av}=\langle|\Delta^2y|\rangle_{Av}(1/s)=K_s(Z/pv),$$

where $\langle|\alpha|\rangle_{Av}$ is the mean chord angle between successive chords through the points dividing the track into cells; Z, p, and v are the charge, momentum, and velocity of the scattered particle, and s is the cell length. ($\langle|\alpha|\rangle_{Av}$ is expressed in degrees, (pv) in Mev, and s in microns.)

The experimental results are shown in Table I. It must be mentioned that in order to minimize statistical fluctuations the standard procedure was followed of computing all mean values $\langle|\Delta^2y|\rangle_{Av}$ so as to include only individual Δ^2y_j with absolute values smaller than four times the experimental mean. This resulted in a loss of approximately 1.4 percent of the data, which appears to verify the presence of an expected non-gaussian tail in the distribution of multiple scattering deflections. It can be seen from Table I that within the limits of error K_s is proportional to $(s)^{\frac{1}{2}}$ for cell lengths in the range from 750 to 250μ. Assuming that this relation is valid down to $s=100\mu$, one obtains by extrapolation K_{100}, which may be compared with the results of other authors:

	K_{100}
Fowler[1] (cosmic-ray particles)	32.7
Recent work at Bristol[4]	26
Voyvodic and Pickup[2] (Li(p, γ) gamma-ray electrons)	21.3±1.0
Corson[3] (40-, 115-, 195-, and 280-Mev electrons)	26 ±1
BLS (average of values in Table I for 337-Mev protons)	24.1±0.8.

TABLE I. Multiple scattering of (337±1)-Mev protons in Ilford G5 emulsions.

Cell length (microns)	Number of cells	$\langle|\Delta^2y|\rangle_{Av}$ (microns)	K_s	$K_{100}=K_s(100/s)^{\frac{1}{2}}$
250	3005	0.2880	38.6±1.3	24.4±0.8
500	1480	0.8064	54.1±1.7	24.2±0.8
750	970	1.448	64.7±2.5	23.6±0.9

A more complete description and a theoretical analysis, as well as the results of further measurements at 340 Mev and other proton energies now in progress, will be presented in a forthcoming publication.

The authors would like to express their gratitude to Professors E. O. Lawrence and W. Barkas for their excellent cooperation in exposing plates for us in the Berkeley cyclotron.

* Assisted by the joint program of the ONR and AEC.
[1] P. H. Fowler, Phil. Mag. **41**, 169, 413 (1950).
[2] L. Voyvodic and E. Pickup, Phys. Rev. **81**, 471, 890 (1951).
[3] D. R. Corson, Phys. Rev. **83**, 217(A) (1951).
[4] Mentioned by Dainton, Fowler, and Kent, Phil. Mag. **42**, 317 (1951).

On a Formulation of Quantum Electrodynamics

J. G. VALATIN
Institute for Theoretical Physics, University of Copenhagen, Copenhagen, Denmark
(Received July 2, 1951)

DIFFICULTIES arising from the supplementary condition in the formulation of quantum electrodynamics as given by Fermi have been pointed out several times.[1-3] Taking over an idea of Novobátzky,[4] but following a different course, we want to avoid the supplementary condition and the corresponding com-

plications by introducing only two kinds of transverse and one kind of scalar photon, instead of the four kinds of photon variables of the Fermi electrodynamics.

Starting from the interaction representation, the states of free transverse photons can be described in a relativistic way by means of the 6-vector solutions $F_{\mu\nu}^{(1)}$ of the vacuum maxwell equations:

$$\begin{aligned}\partial_\mu F_{\mu\nu}^{(1)}&=0,\\ \partial_\kappa F_{\mu\nu}^{(1)}+\partial_\nu F_{\kappa\mu}^{(1)}+\partial_\mu F_{\nu\kappa}^{(1)}&=0.\end{aligned}\tag{1}$$

These equations insure that $F_{\mu\nu}^{(1)}$ represents transverse waves in any reference system. Quantization gives for the operators $F_{\mu\nu}^{(1)}$ the well-known covariant commutation relations of the field strengths. Using hyperplanes σ perpendicular to a timelike direction n_μ, the interaction between the transverse photon field and the current j_μ of the electrons can be introduced by means of an interaction hamiltonian

$$H_1^{(1)}=-\int_\sigma d\sigma' j_\mu(x') A_\mu^{(1)}(x'),\tag{2}$$

where the potential $A_\mu^{(1)}$ is defined with respect to the direction n_μ by means of the field $F_{\mu\nu}^{(1)}$, as

$$A_\mu^{(1)}=-\partial^{-1}F_{\mu\nu}^{(1)}n_\nu.\tag{3}$$

$\partial=n_\kappa\partial_\kappa$, and ∂^{-1} is a suitably defined inverse operator.[3] From Eqs. (1) and (3) and from the commutation relations for the $F_{\mu\nu}^{(1)}$, $A_\mu^{(1)}$ satisfies the equations $A_\mu^{(1)}n_\mu=0$, $\partial_\mu A_\mu^{(1)}=0$, $\Box A_\mu^{(1)}=0$, and the commutation relations of the transverse potential of the Fermi electrodynamics. A different choice of n_μ means only a different choice of the gauge of the potential $A_\mu^{(1)}$. Adding to Eq. (2) the covariant expression of the coulomb interaction energy, we have the usual form of quantum electrodynamics with the coulomb interaction treated separately. The present formulation has, however, the advantage of a relativistic description of the states of light quanta.

In order to describe the coulomb interaction as transmitted by a field, we introduce besides $F_{\mu\nu}^{(1)}$ another field, characterized by the four-vector B_μ, which satisfies in vacuum equations analogous to (1),

$$\begin{aligned}\partial_\mu B_\mu&=0,\\ \partial_\nu B_\kappa-\partial_\kappa B_\nu&=0.\end{aligned}\tag{4}$$

According to Eq. (4), $B_\mu=\partial_\mu Q$ can be deduced from a single scalar function $Q(x)$. The canonical formalism and the quantization of Eq. (4) can be worked out easily and correspond to the theory of a scalar meson with zero rest mass. In characterizing the states of scalar photons with the solutions of Eq. (4), we can introduce an interaction with the electrons by means of an interaction hamiltonian $H_1^{(2)}$ of the form (2), with a potential

$$A_\mu^{(2)}=-\partial^{-1}B_\mu=-\partial_\mu\partial^{-1}Q\tag{5}$$

instead of $A_\mu^{(1)}$.

The potentials $A_\mu=A_\mu^{(1)}+A_\mu^{(2)}$ satisfy the commutation relations

$$\begin{aligned}[A_\mu(x),A_\nu(x')]&=id_{\mu\nu}D(x-x'),\\ d_{\mu\nu}&=\delta_{\mu\nu}-2\partial_\mu\partial_\nu\partial^{-2}-n_\mu\partial_\nu\partial^{-1}-n_\nu\partial_\mu\partial^{-1}.\end{aligned}\tag{6}$$

The interaction hamiltonian $H_1=H_1^{(1)}+H_1^{(2)}$ together with the commutation relations (6) describes correctly the interactions between electrons and the electromagnetic field.

By means of a canonical transformation, very similar to that used in the Fermi electrodynamics, the scalar photon variables can be eliminated. A wave equation is obtained in which the interaction energy $H_1^{(2)}$ is replaced by the direct coulomb interaction energy. In order to obtain the correct sign of the coulomb interaction one has to choose in the commutation relation for the scalar field $Q(x)$ the sign corresponding to the time-component photons of the Fermi electrodynamics. The scalar field and quanta do not represent measurable quantities, but are related to the gauge of the potentials. This corresponds to the fact that also in classical theory the retarded transmission of the coulomb interaction corresponds to potential waves only.

In calculating the S-matrix in the unseparated treatment, the commutation relations, Eq. (6), may be replaced, as can be shown, by the simpler relations of the Fermi electrodynamics. The additional terms of Eq. (6) do not give any contribution.

In transforming the equations to the Heisenberg representation, the potentials $\mathbf{A}_\mu$ do not satisfy the Lorentz condition, but $\partial_\mu\mathbf{A}_\mu$ depends on the currents and on n_μ which plays the role of a gauge vector. The fields $\mathbf{F}_{\mu\nu}=\partial_\mu\mathbf{A}_\nu-\partial_\nu\mathbf{A}_\mu$ satisfy, however, the maxwell equations,

$$\partial_\mu\mathbf{F}_{\mu\nu}=-\mathbf{j}_\nu.\tag{7}$$

$\mathbf{F}_{\mu\nu}$ is independent on the scalar field variables.

As shown by Professor C. Møller, one can build up the theory also by starting directly from the Heisenberg representation and introducing suitable energy-momentum expressions and the corresponding commutation rules.

Details will be published in the *Proceedings of the Copenhagen Academy*.

[1] F. J. Belinfante, Physica **12**, 17 (1946); Phys. Rev. **76**, 226 (1949).
[2] S. T. Ma, Phys. Rev. **75**, 535 (1949); **80**, 729 (1950).
[3] F. Coester and J. M. Jauch, Phys. Rev. **78**, 149, 827 (1950).
[4] K. F. Novobátzky, Z. Physik **111**, 292 (1938); Mat. Fiz. Lapok Budapest **48**, 312 (1941).

Molecular Constants of $Cs^{133}Cl^{35}$

R. G. Luce and J. W. Trischka
*Syracuse University, Syracuse, New York**
(Received June 18, 1951)

THE radiofrequency spectra of cesium chloride were studied by means of the electric resonance method of molecular beam spectroscopy.[1,2] Lines were observed arising from the $J,m_J\rightarrow J,m_J'$ transitions 2,0→2,1; 3,0→3,1; 4,0→4,1; 4,1→4,2; and 5,1→5,2. Lines arising from molecules in six different vibrational states were resolved. Evidence for the quadrupole interaction of Cs and Cl was seen in the broad lines observed at low frequencies, but no fine structure due to these interactions could be resolved. Cs has but one isotope; however, Cl has two with an abundance ratio of 3:1. The spectrum of the less abundant specie could be discerned superimposed on the spectrum of the more abundant one in the predicted position.

It was possible to observe the 2,0→2,1; 3,0→3,1; and 4,1→4,2 transitions in electric fields of sufficient magnitude to obtain values of the permanent dipole moment, μ, and the moment of inertia, A. Consistent results were obtained for the three transitions and the weighted average $A=384\pm7\times10^{-40}$ cgs unit and $\mu=10.5\pm0.25$ Debyes for the zeroth vibrational state. The rotational constant B_v is, then, 0.0736 ± 0.0015 cm^{-1}. The constant α_e was calculated using the separation of the observed lines corresponding to different vibrational states and a theoretical value[3] of $\omega_e=299$ cm^{-1}. We found $\alpha_e=0.52\pm0.05\times10^{-3}$ cm^{-1}.

The internuclear distance, r_v, of vibrational state v may be calculated from the moment of inertia, and a value $r_0=2.88\pm0.03$A was obtained. The internuclear distance has been measured by Maxwell, Hendricks, and Mosley[4] using the electron diffraction method, with a resulting value of $r=3.06\pm0.03$A. This result, however, is an average over the vibrational states present, and for their observation temperature $v=3$ is the median vibrational state. Using our value of α_e, we get $r_0=3.02\pm0.03$A as the number to be compared with the electric resonance value above. It is seen that the discrepancy of 5 percent between the two values is well outside the limits of estimated experimental errors for both methods.

It is to be expected that both nuclei contribute to the quadrupole interaction present. If the interaction for one of the nuclei is predominant, the resolving power of the spectrometer was such that some fine structure lines should have been resolved. If, however, the interaction of the two nuclei are of the same order, the large number of lines present would make any resolution impossible. As no structure was observed, this latter condition is concluded

to prevail. If calculations are made assuming the entire interaction to be due to one nucleus alone, it is possible to place maximum values on the interactions present from the separate nuclei. This leads to values of 3 Mc and 4 Mc as the maximum possible values of the interaction constant, $|eqQ/h|$, for Cl and Cs, respectively.

* Supported in part by the ONR.
[1] H. K. Hughes, Phys. Rev. **72**, 614 (1947).
[2] J. W. Trischka, Phys. Rev. **74**, 718 (1948).
[3] E. S. Rittner, to be published.
[4] Maxwell, Hendricks, and Mosley, Phys. Rev. **52**, 968 (1937).

The Positron to γ-Ray Ratio in Zn^{65}

GEORGE M. GRIFFITHS
Department of Physics, University of British Columbia, Vancouver, Canada
(Received June 27, 1951)

IN connection with the calibration of Zn^{65} and Co^{60} sources, the following measurements were made which indicate a ratio of 1 positron to 65 ± 5 γ-rays for 250-day Zn^{65}.

Two scintillation counters were placed at equal distances from, and on opposite sides of, a small zinc source, and coincidence and single channel counting rates were obtained. The source was surrounded by aluminum foil, so that for each positron there were two annihilation quanta emitted in very nearly opposite directions. If the source produced N_+ positrons and N_γ γ-rays per unit time and the plane angles subtended by the counters at the source were large compared with the small departure from collinearity of the annihilation quanta,[1] then the positron to γ-ray ratio is approximately given by

$$N_+/N_\gamma = N_c{}^+\epsilon_1{}^\gamma/2\epsilon_1{}^+\epsilon_2{}^+(N_1{}^\gamma+N_1{}^+) = N_c{}^+\epsilon_2{}^\gamma/2\epsilon_1{}^+\epsilon_2{}^+(N_2{}^\gamma+N_2{}^+),$$

where N is a counting rate, ϵ a counter efficiency, superscripts $+$ and γ refer to annihilation radiation and nuclear γ-rays, respectively, and subscripts 1, 2, and c refer to counters 1, 2 and the coincidence counter, respectively. This approximate formula holds for the case when the ratio N_+/N_γ is small, as it is for Zn^{65}. Note that the solid angle factor does not appear. Thus, with the above-mentioned measurements, corrected for background, dead time, and accidental coincidences, we require only the counter efficiencies[2] at 0.51 and 1.11 Mev in order to calculate N_+/N_γ.

The efficiency for the Zn^{65} γ-ray (1.11 Mev) was assumed to be the same as that for the Co^{60} γ-rays (1.17 and 1.33 Mev). By means of a standard coincidence method (applicable for a source giving cascaded radiations of about the same energy) the efficiency for Co^{60} γ-rays was found to be 17 percent when the quanta traversed one inch of a clear anthracene block ($1''\times1''\times\frac{1}{2}''$) mounted on the end of an RCA 5819 photomultiplier. Within experimental errors this is equal to the efficiency as calculated using the Klein-Nishina formula. When the geometry was such that 180° backscattered quanta (0.2 Mev) from one counter could enter the second counter, the coincidence rate increased because of single quanta producing pulses in both counters. From the amount of the increase we calculated that the counter efficiencies for the 0.2-Mev backscattered quanta were about 30 percent, close to the theoretically expected value of 38 percent. The experimental value is low, owing to absorption of some of the backscattered quanta in the scattering crystal and to the smaller number of photons excited in the crystal by the low energy quanta. Since these measurements agree reasonably well with the theory, we assumed that the efficiency for the annihilation radiation was 25 percent as given by the Klein-Nishina formula.

Owing to the small departure from collinearity of annihilation quanta, the ratio N_+/N_γ increased as the counters were moved closer to the source, and angular correlation curves at the larger distances showed the characteristic tails.[1] These effects were not detectable with the counters closer than 40 cm to the source. The result of 1 positron in 65 ± 5 γ-rays is the average of 4 measurements with the counters 35 cm from the source (the ±5 includes an estimate of the error involved in the efficiency figures). This result is not in agreement with the decay scheme presented in *Nuclear Data*[3] but is in rough agreement with the results in the *Trilinear Chart of Nuclear Species*.[4] The data for Zn^{65} in the latter publication was based primarily on unpublished work of Dr. W. C. Peacock.[5] Taking his value of 50 percent K-capture to the 1.11-Mev level of Cu^{65}, one finds that 0.8 percent of the Zn^{65} disintegrations are by positron emission.

I wish to express my thanks to Dr. K. C. Mann for providing the Zn^{65} and to the Ontario Research Council for a scholarship.

[1] P. E. Argyle and J. B. Warren, Can. J. Phys. **29**, 32 (1951).
[2] Mann, Rankin, and Daykin, Phys. Rev. **76**, 1719 (1949).
[3] National Bureau of Standards, *Nuclear Data* (U. S. Government Printing Office, Washington, 1950), Circ. 499.
[4] *Trilinear Chart of Nuclear Species*, edited by W. H. Sullivan (John Wiley and Sons, Inc., New York, 1949).
[5] Private communication from W. H. Sullivan.

Paramagnetic Resonance Absorption in Three Chlorides of Copper

J. ITOH, M. FUJIMOTO, AND H. IBAMOTO
Faculty of Science and Institute of Scientific and Industrial Research, Osaka University, Osaka, Japan
(Received June 4, 1951)

WE have measured the microwave paramagnetic resonance absorption in single crystals[1] of $CuCl_2\cdot2H_2O$, $K_2CuCl_4\cdot2H_2O$, and $(NH_4)_2CuCl_4\cdot2H_2O$ at 3100 Mc/sec and at

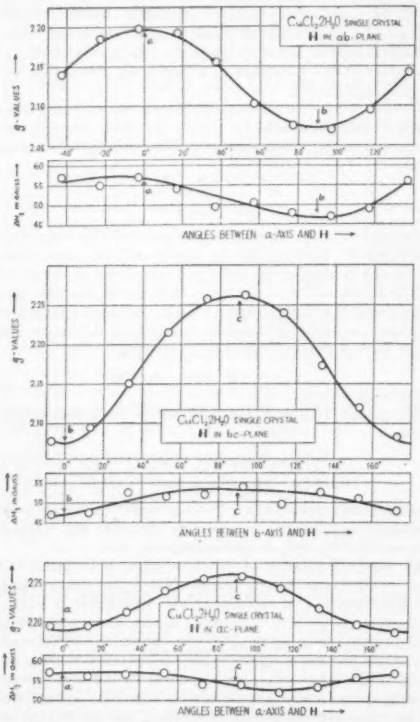

FIG. 1. Variation of g-values and half-widths (ΔH_1) with angle between the static field **H** and the crystal axis in $CuCl_2\cdot2H_2O$, at 3100 Mc/sec. The figures indicate these angular dependences for the cases in which **H** rotates about the c axis, the a axis, and the l axis, respectively.

room temperature. Also, we calculated g-values for these crystals and compared them with the experimental results.

The measurements were made by the usual standing wave method. The crystal structure of $CuCl_2 \cdot 2H_2O$ is orthorhombic, while the other two are tetragonal. The unit cell of these crystals contains two molecules. In the case of copper chloride, one of the molecules is derived from the other by a translation from the point $(0, 0, 0)$ to $(\frac{1}{2}, \frac{1}{2}, 0)$ followed by a reflection in the $b-c$ plane. In the case of potassium and ammonium salts, one is derived from the other by a translation from the point $(0, 0, 0)$ to $(\frac{1}{2}, \frac{1}{2}, \frac{1}{2})$ followed by a reflection in the $(1, 0, 0)$ plane. Therefore, one may generally expect two resonance peaks. Actually, however, we obtained only one resonance maximum for all directions of the static magnetic field, which means that exchange coupling between copper ions is sufficiently strong that one resonance maximum occurs at the arithmetical mean of the two expected resonance fields.

Angular dependences of g-values and half-width values obtained experimentally for copper chloride and for the potassium salt are

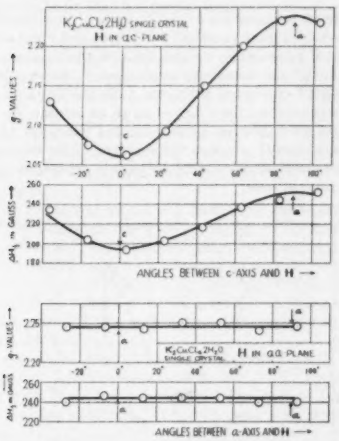

FIG. 2. Variation of g-values and half-widths ($\Delta H_{\frac{1}{2}}$) with angle between the static field **H** and the crystal axis in $K_2CuCl_4 \cdot 2H_2O$, at 3100 Mc/sec. Figures indicate these angular dependences for the cases in which **H** rotates about the a axis and the c axis, respectively.

shown in Fig. 1 and Fig. 2. Those for the ammonium salt are almost the same as those for the potassium salt.

Since in these crystals the crystalline electric field at the position of the copper ion is of rhombic symmetry, we extended the calculation of Polder,[2] who treated the case of a tetragonal field, to the case of a rhombic field. Also, we have calculated self-consistent values for the induced moments of water molecules and chlorine ions; and then the expansion coefficients of the crystalline field at the position of copper ions were computed up to the fourth-order terms. Here, we assumed each ion or each water molecule to be a point charge and/or a point dipole at the position predicted by the x-ray analysis of Harker[3] and Chrobak.[4] The g-values thus calculated, and also the experimental g-values, are shown in Table I. As mentioned above, by the effect of exchange coupling, only the value $\frac{1}{2}(g_a+g_b)$ can be obtained experimentally for the potassium and ammonium salts; these values are shown also in the table. The agreement is satisfactory for all of these salts.

TABLE I. Calculated and experimental g-values.

	$CuCl_2 \cdot 2H_2O$		$K_2CuCl_4 \cdot 2H_2O$		$(NH_4)_2CuCl_4 \cdot 2H_2O$	
	Exp.	Calc.	Exp.	Calc.	Exp.	Calc.
g_a*	2.195	2.248		2.290		2.122
$(g_a+g_b)/2$			2.24	2.28	2.25	2.23
g_b*	2.075	2.052		2.278		2.336
g_c	2.26	2.278	2.06	2.04	2.05	2.01

* g_a and g_b for the potassium and ammonium salts mean the g-values for the molecule at $(0, 0, 0)$ in the direction $(1, 1, 0)$ and $(\bar{1}, 1, 0)$, respectively.

The shapes of the absorption curves are not gaussian, but lie between gaussian and Lorentz-type absorption curves. Those for the potassium and ammonium salts almost coincide with the latter. Therefore, the experimental half-width $\Delta H_{\frac{1}{2}}$ may not be compared directly with the theoretical value of $(\langle\Delta H^2\rangle_{Av})^{\frac{1}{2}}$ calculated by Van Vleck's formula.[5] $\Delta H_{\frac{1}{2}}$ is much smaller than 2.36 $(\langle\Delta H^2\rangle_{Av})^{\frac{1}{2}}$, which corresponds to the theoretical half-width in the case of a gaussian-type absorption curve. Moreover, the angular dependance of $(\langle\Delta H^2\rangle_{Av})^{\frac{1}{2}}$ is not similar to the experimental results. The width for copper chloride is still narrower than that for copper sulfate pentahydrate, suggesting still stronger exchange coupling.

The details of the experiment and the calculations will be published elsewhere.

[1] These single crystals were made available by the courtesy of Dr. R. Kiriyama of the Department of Chemistry, to whom we express our gratitude.
[2] D. Polder, Physica **9**, 709 (1942).
[3] D. Harker, Z. Krist. **93**, 136 (1936).
[4] L. Chrobak, Z. Krist. **88**, 35 (1934).
[5] J. H. Van Vleck, Phys. Rev. **74**, 1168 (1948).

Production of Neutral Mesons by γ-Rays Incident on Hydrogen*

A. SILVERMAN AND M. STEARNS
Cornell University, Ithaca, New York
(Received July 5, 1951)

THE reaction $\gamma+H^1 \rightarrow \pi^0+H^1$ has been investigated by bombarding thin polyethylene and carbon targets with bremsstrahlung radiation from the 310-Mev Cornell synchrotron. The experimental arrangement is shown schematically in Fig. 1.

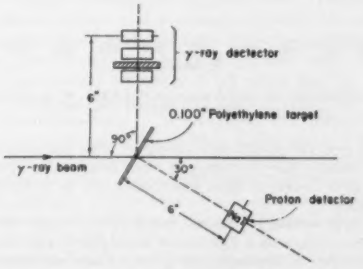

FIG. 1. Experimental arrangement (schematic).

The reaction is observed by detecting coincidences between the recoil proton and one of the decay γ-rays from the neutral meson. The energy and angle of the recoil proton are measured, and these two quantities, combined with the conservation equations, uniquely determine the energy of the incident γ-ray and the energy and angle of the neutral meson. In this manner it is possible to get the cross section for the production of neutral mesons as a function of γ-ray energy despite the continuous spectrum of the incident radiation. The technique of detecting the two decay γ-rays used by Steinberger, Panofsky, and Steller[1] does not give the meson energy directly, since a measurement of the angle between the two γ-rays does not uniquely determine the meson energy.

The γ-ray counter is similar to one described by Steinberger, Panofsky, and Steller[1] and is placed in the direction of the neutral meson for maximum efficiency. The proton counter is a thick NaI crystal in which the recoil proton comes to rest. The pulse height is thus a measure of the proton energy.

Most of the runs were taken with the proton counter at $30°\pm3°$ to the beam as shown in Fig. 1. For incident γ-rays between 200 and 310 Mev the corresponding neutral meson angle is $90°\pm10°$. The γ-ray counter was correspondingly set at 90° (Fig. 1) with an angular aperture of $\pm5°$.[2] The hydrogen target was 0.23 g/cm² slab of polyethylene and the carbon background was determined by making additional runs with a carbon target of equal stopping power for protons. The carbon background constituted about 22 percent of the total counts, varying from 10 percent in the highest energy interval to about 40 percent in the lowest. Accidentals were less than 5 percent and were measured directly by recording coincidences between the two counters with one channel delayed by more than twice the resolving time of the system.

Several auxiliary experiments were performed to check that the coincidences observed were due to the above reaction. These included studying the effect of removing the lead converter in the γ-ray counter, the change in counting rate as a function of the angle of the γ-ray detector, and the change in maximum energy of the recoil protons as a function of the angle of the proton counter.

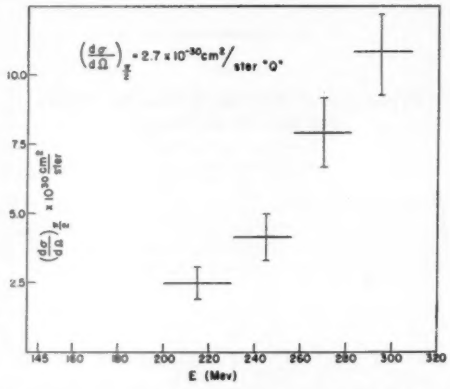

FIG. 2. Cross section for neutral meson production at 90° in the laboratory system as a function of incident γ-ray energy.

In each case the results were consistent with the production of neutral mesons from hydrogen. A more detailed description and quantitative results of these experiments will be published in a later paper.

The cross section for neutral meson production at 90° in the laboratory system as a function of the incident γ-ray energy is shown in Fig. 2. The indicated errors include estimated instrumental as well as statistical errors. The curve can be fitted with the power law $d\sigma/d\Omega = k(E_\gamma - \mu c^2)^{1.5\pm0.5}$, where E_γ is the incident γ-ray energy and μc^2 the rest mass of the neutral meson. The curvature is in sharp contrast with that of the equivalent cross section for π^+ mesons which approximates a one-half power law.[3] The absolute magnitudes of the two cross sections are roughly the same at 300 Mev.

A run was taken with the proton counter at 45°. The range of proton energies measured at this angle corresponds to γ-rays between 250 and 310 Mev. For these energies the corresponding neutral meson laboratory angle is $60°\pm10°$. The ratio of the differential cross sections at 60° and 90° (laboratory angles) for 250–310-Mev incident γ-rays is $(d\sigma/d\Omega)_{60°}/(d\sigma/d\Omega)_{90°} = 1.50 \pm 0.25$. In the center-of-mass system the corresponding ratio becomes $(d\sigma/d\Omega)_{76°}/(d\sigma/d\Omega)_{112°} = 1.10\pm0.20$.

Attempts have been made to calculate these cross sections using both weak and strong coupling theories. The weak coupling approximation seems to give results in disagreement with the experimental results.[4] Brueckner and Case,[5] using a strong coupling theory involving an excited state of the nucleon, calculate results which seem to be in good agreement with the experimental ones.

* This work was done under an ONR contract.

[1] Steinberger, Panofsky, and Steller, Phys. Rev. **78**, 802 (1950).

[2] The proton Compton scattering cannot contribute, since for protons scattered at 30° the γ-ray is scattered at approximately 110°.

[3] Bishop, Steinberger, and Cook, Phys. Rev. **80**, 291 (1950).

[4] M. F. Kaplon, Phys. Rev. **83**, 712 (1951).

[5] K. A. Brueckner and K. M. Case, Phys. Rev. (to be published).

The Room Temperature Solubility of Iron in Copper

T. S. HUTCHISON AND JAMES REEKIE
Department of Physics, Royal Military College of Canada, Kingston, Ontario, Canada
(Received June 18, 1951)

THE room temperature solubility limit of iron in copper was determined some years ago by Hanson and Ford[1] and stated to be about 0.2 percent by weight. Other workers have suggested that the solubility is exceedingly small at room temperature,[2] while recent results,[3] concerned primarily with the effect of internal strain in copper-iron alloys, have tended to confirm the work of Hanson and Ford. We have reinvestigated this point by making direct measurements, at room temperature, of the density and of the lattice parameter of a number of copper-iron alloys containing up to 1.4 percent iron.

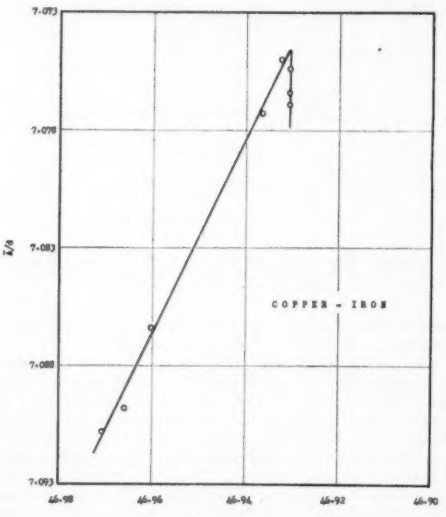

FIG. 1. Graph of $\bar{A}/d$ *vs* a^2 which shows a continuous linear variation of $(\bar{A}/d)$ with a^2 up to a solubility limit of 0.26 percent by weight of iron.

The specimens, in the form of rods about 3 mm in diameter and 15 cm long, were originally vacuum annealed for 10 hours at 900°C and then furnace cooled to 25°C over a period of about 10 hours. Density measurements were then made by weighing the rods in air and in water under closely controlled temperature conditions, making all necessary corrections, to obtain values which are considered accurate to about 1 part in 5000.

For the lattice parameter determination, filings were prepared from the original specimens and annealed under the same conditions as the rods. The more general method of annealing the bulk metal, filing, and then stress-relieving the filings with a lower temperature anneal, proved unsatisfactory. It is difficult in this latter procedure to insure that no precipitation of the iron occurs during filing.

Lattice parameters were obtained from measurements of Debye-Scherrer x-ray photographs taken in an 11.46-cm diameter circular camera, using both cobalt and copper unfiltered radiations. Extrapolated values of lattice parameter were deduced in the usual way by computing the spacings and plotting against the Nelson-Riley extrapolation function;[4] the value of a thus obtained is estimated to be correct to within $\pm 1\times 10^{-4}$A. It is found that a decreases from a value of 3.6081A for pure copper to 3.6071A when the copper contains about 0.25 percent iron. For higher iron content the parameter remains constant. This, taken in conjunction with the fact that the atomic radius of iron is close to that of copper, excludes the possibility of an interstitial solution.

In the case of an alloy in the form of a substitutional solid solution it can be shown that the density is given by

$$d = n\bar{A}m_H/a^3.$$

In this expression n is the number of atoms in the unit cell of volume a^3, $\bar{A}$ is the average atomic weight of the alloy (relative to hydrogen and calculated from the weight percentages of the constituents), and m_H is the mass in grams of the hydrogen atom. For simple substitution, in the case of a face-centered cubic structure, $n=4$. Thus in the case of a solution of iron in copper we should find that a^3 is a continuous linear function of $\bar{A}/d$ up to the limit of solubility.

Taking our observed values of d and a, we have plotted $\bar{A}/d$ against a^3, obtaining the result shown in Fig. 1. The approximate linearity of the graph shows that substitution takes place up to an $\bar{A}/d$ value of 7.075, which corresponds to a room temperature solubility limit of about 0.26 percent by weight of iron. For higher percentages the fact that the lattice parameter is found to remain practically constant indicates that precipitation of the iron occurs beyond this limit.

We are greatly indebted to Mr. F. E. Hetherington for carrying out the density measurements, and to Mr. F. T. Hedgcock for assistance with the x-ray calculations. The Metals Division of Imperial Chemical Industries, Ltd., very generously supplied the alloys used.

[1] D. Hanson and G. W. Ford, J. Inst. Metals **32**, 333 (1924).
[2] F. Bitter and A. R. Kaufmann, Phys. Rev. **56**, 1044 (1939); see also M. Hansen, *Der Aufbau der Zweistofflegierungen* (Verlag. Julius Springer, Berlin, 1936). G. Tammann and W. Oelsen, Z. anorg. u. allgem. Chem. **186**, 267 (1930). A. J. Bradley and H. J. Goldschmidt, J. Inst. Metals **65**, 403 (1939).
[3] F. E. Hetherington and J. Reekie (to be published).
[4] J. B. Nelson and D. P. Riley, Proc. Phys. Soc. (London) **57**, 160 (1945).

On the Angular Distribution of the π^+ Mesons from 341-Mev Protons on Protons*

MARIAN N. WHITEHEAD AND CHAIM RICHMAN
Radiation Laboratory, Department of Physics, University of California, Berkeley, California
(Received July 5, 1951)

STUDIES of the production of π^+ mesons by 341-Mev protons on protons[1,2] have shown a continuous spectrum of mesons with a pronounced peak at the high energy end. It was suggested[2] that besides the reaction $p+p\rightarrow n+p+\pi^+$, a second reaction takes place, namely, $p+p\rightarrow d+\pi^+$, which could be expected to give a considerable yield of mesons in a line spectrum separated from the continuous spectrum produced by the first reaction by 2.2 Mev as measured in the center-of-mass system. Recently it was shown by Crawford *et al.*[4] that deuterons do come off in coincidence with the π^+ mesons around the peak energy. They did not measure the absolute yield. The reaction $p+p\rightarrow d+\pi^+$ is of great interest, since, as has been pointed out by Marshak and Cheston[5] and independently by M. H. Johnson, a measurement of the inverse process will by means of detailed balancing determine the spin of the π^+ meson.

It is very important for the sake of the complete detailed balancing arguments as well as for the theory of this process[6] to find the angular distribution of the mesons. The measurements of the meson yield at 0°,[1] and at 18° and 30°[2] show a non-isotropic distribution when transformed to the center-of-mass system and suggest that the total meson yield goes something like $\cos^2\theta$, where θ is the angle in the center of mass of the mesons with respect to the line of the protons. To determine the angular distribution more precisely we have measured the yield in the laboratory at 60°. The method we used is the same as was used to measure the yield at 0°, that is, to take a polyethylene-carbon difference. As before, the mesons are detected by means of nuclear emulsions. The spectrum obtained is shown in Fig. 1. The errors shown are the statistical

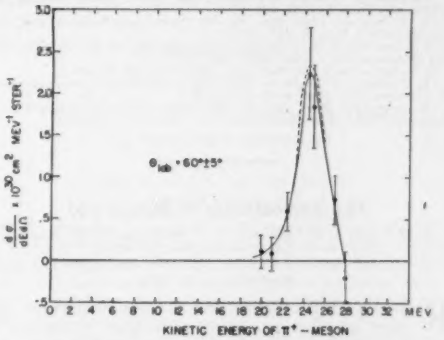

FIG. 1. Spectrum of π^+-mesons at $\theta_{lab}=60°\pm5°$ to the proton beam.

probable errors. Because of the low yield from hydrogen the subtraction method becomes more difficult here, and no data were obtained at the low energy end of the spectrum. The spectrum shows the characteristic peak to be around 25 Mev. The energy of the beam was 341±3 Mev. The angle at which the mesons were observed was determined to be 58°±5°. From energy and momentum conservation, the energy of the meson peak if it is produced by the formation of a deuteron would be 25±2 Mev at 60°, using a meson mass equal to $(276.2\pm2.3)m_e$. We believe that the energy of the peak is the best measure of the angle at which the mesons emerge with respect to the beam. The dotted curve is the spectrum corrected for nuclear interaction of the mesons in the absorber, assuming nuclear area for this interaction. The total cross section for the production of mesons in the peak at this angle is $(8.0\pm2)\times10^{-30}$ cm^2 sterad^{-1}.

The measurements of the yield of mesons at the various angles which have so far been made do not tell us whether a deuteron comes off in coincidence with every meson observed at the peak. However, the phenomenological calculations of Watson and Brueckner,[6] when compared to the meson spectrum at 0°, lead one to believe that most of the mesons in the peak come from the reaction in which a deuteron is formed. Because of the experimental uncertainties in our spectrum at 60°, it is more difficult to make comparisons with the theory at this angle. We will assume that here too the peak is primarily due to the reaction $p+p\rightarrow d+\pi^+$ and calculate the angular distribution in the center of mass on this basis. The integrated cross section due to the peak at 0° is $(1.3\pm0.26)\times10^{-33}$ cm^2 sterad^{-1} in the laboratory frame. Comparing this cross section with the cross section at 60°, we obtain the following formula for the differential cross section in the center of

mass as a function of θ, the angle in the center of mass:

$$(d\sigma/d\Omega)_{cm} = (3.20\pm0.78)(0.071\pm0.068+\cos^2\theta)$$

$$\times 10^{-29} \text{ cm}^2 \text{ sterad}^{-1}.$$

The total cross section for the mesons in the peak is therefore $(1.62\pm0.49)\times10^{-28}$ cm^2. This suggests that the meson comes off almost entirely in a P-wave, and since the majority of the mesons of the entire spectrum are in the peak, it would follow that the total spectrum is approximately in a P-wave.

It is a pleasure to acknowledge the continued encouragement we have received from Professors E. O. Lawrence and R. L. Thornton. Mr. Dan Hamlin was of great help with the scanning of the plates. We are indebted to Dr. K. M. Watson and Mr. E. M. Henley for discussions of the theoretical aspects of the problem. We would like to thank Mr. J. Vale and the cyclotron crew for making the bombardments.

* This work was supported by the AEC.

[1] Cartwright, Richman, Whitehead, and Wilcox, Phys. Rev. **78**, 823 (1950), and Phys. Rev. **81**, 652 (1951).
[2] V. Z. Peterson, Phys. Rev. **79**, 407 (1950), and Peterson, Iloff, and Sherman, Phys. Rev. **81**, 647 (1951).
[3] G. Chew and E. Hart, private communication. See also Morand, Cüer, and Moucharafyeh, Compt. rend. **226**, 1974 (1948).
[4] Crawford, Crowe, and Stevenson, Phys. Rev. **82**, 97 (1951).
[5] R. E. Marshak, Rochester High Energy Conference, December, 1950. W. Cheston, Phys. Rev., to be published.
[6] K. Brueckner, Phys. Rev. **82**, 598 (1951). K. M. Watson and K. A. Brueckner, Phys. Rev. **83**, 1 (1951).

The Radioactivity of Barium 140

J. M. Cork, J. M. LeBlanc, A. E. Stoddard, D. W. Martin, C. E. Branyan, and W. J. Childs
*University of Michigan, Ann Arbor, Michigan**
(Received June 28, 1951)

RADIOACTIVE barium of half-life about 13 days was first noted[1] as a product of the bombardment of uranium by neutrons, even before the phenomenon of nuclear fission was recognized. Subsequent studies[2] have shown the activity to be in Ba^{140}, in which the beta-decay to La^{140} is complex and accompanied by gamma-emission. Three gamma-rays had been reported[3] with energies of 0.16, 0.30, and 0.54 Mev.

TABLE I. Summary of electron lines.

Electron energy (kev)	Relative intensity	Interpretation	Gamma-energy (kev)
23.3	20	L_1(Z=57)	29.6
23.7	2	L_2	29.6
24.1	1	L_3	29.6
28.2	10	M	29.6
29.3	5	N	29.6
79.8	1	K	118.5
93.1	4	K	131.8
123.3	10	K	162.0
156.0	5	L	162.3
160.8	2	M	162.2
265.5	4	K	304.2
382.8	1	K	421.5
397.1	1	K	435.8
498.0	4	K	536.7
530.0	1	L	536.3

A continued study of the fission product as supplied by the Oak Ridge National Laboratory, using photographic magnetic spectrometers, leads to a more accurate evaluation of energies and shows the existence of certain previously unreported gamma-rays. The barium radioactivity will usually be in equilibrium with the daughter, radioactive lanthanum. It appears, however, that in the original chemical separation of Ba^{140}, the La^{140} is carried down in excess of the equilibrium amount. This leads to a change in the relative intensity with time of the electron lines due to La^{140} as compared with the electron lines due to Ba^{140} and thus aids in their identification. The half-life curve of the specimen is complex, showing an initial 41-hour decay before settling into the longer barium half-life, now found to be 13.4 days. The K-L-M differences of the electron energies also make it possible, in most cases, to distinguish those electron lines associated with each activity.

A summary of the electron energies (believed to be accurate to ±0.2 percent) together with an arbitrary estimate of their relative intensities, and proposed gamma-origin is presented in Table I. A

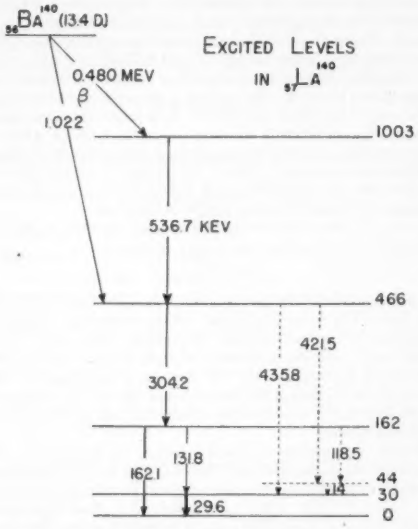

FIG. 1. Energy levels in La^{140} following beta-emission from Ba^{140}.

decay scheme had been proposed by Beach *et al.*, using their three observed gamma-energies, in which an unobserved gamma of 76 kev would have been required. It is now quite certain this gamma-ray does not exist. The observed gamma-energies do, however, fit very satisfactorily a modification and enlargement of the level scheme as shown in Fig. 1. The gamma-rays of greater intensity are represented as transitions with darker lines. The transitions shown as dotted lines are less certain, since only the "K" electron line was observed for each of these gamma-rays and there is some possibility that any or all of this activity is in the daughter product. In order to complete the scheme a gamma-ray of energy 14 kev would be required. This energy is slightly below the limit of the spectrometers.

* This project received the joint support of the ONR and AEC.
[1] O. Hahn and F. Strassmann, Naturwiss. **27**, 11 (1939).
[2] C. Mandeville and M. Shapiro, Phys. Rev. **76**, 718 (1949); W. Lyon, ONRL-286 (1949), unpublished.
[3] Beach, Peacock, and Wilkinson, Phys. Rev. **76**, 1624 (1949).

Gamma-Radiation from Lanthanum 140

J. M. Cork, A. E. Stoddard, J. M. LeBlanc, C. E. Branyan, D. W. Martin, and W. J. Childs
*University of Michigan, Ann Arbor, Michigan**
(Received June 28, 1951)

A PREVIOUS study of the radioactivity from La^{140} (41.4 hr) showed[1] the presence of twelve low energy gamma-rays, with an indication of others at higher energy. A contemporary report noted[2] the beta-decay of La^{140} to be complex with energies of 1.32, 1.67, and 2.26 Mev; but only five gamma-rays, mainly at higher energy, were found. The present spectrometric investigation,

TABLE I. Electron energies from La^{140}.

Electron energy (kev)	Relative intensity	Interpretation	Gamma-energy (kev)
62.1	2	$L^1(Z=58)$	68.7
68.9	4	K^2	109.2
70.1	1	K^3	110.4
90.3	7	K^4	130.6
102.7	4	L_2^3	109.3
108.0	1	M^3	109.3
124.3	1	L_1^4	130.9
132.7	2	K^5	173.0
201.1	3	K^9	241.4
225.1	3	K^7	265.4
288.3	10	K^8	328.6
322.0	4	L_2^8	328.6
326.0	1	M^8	327.4
391.0	2	K^9	431.3
446.0	7	K^{10}	486.3
480.0	2	L_1^{10}	486.6
484.9	1	M^{10}	486.3
711.5	1	K^{11}	751.8
775.5	5	K^{12}	815.8
808.2	1	L_1^{12}	814.8
886	1	K^{13}	926
1557	3	K^{14}	1597
1591	1	L_1^{14}	1598
1864	1	K^{15}	1904

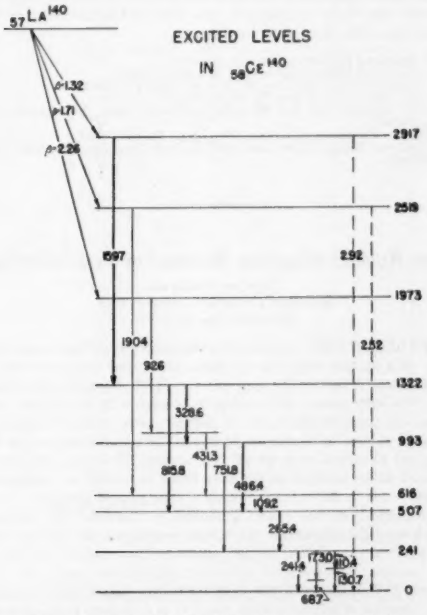

FIG. 1. Nuclear levels in Ce^{140} following beta-decay in La^{140}.

TABLE II. Gamma-energies.

Arbitrary designation	Energy (kev)	Arbitrary designation	Energy (kev)
1	68.7	10	486.4
2	109.2	11	751.8
3	110.4	12	815.8
4	130.7	13	926
5	173.0	14	1597
6	241.4	15	1904
7	265.4	16	(2.52 Mev)
8	328.6	17	(2.92 Mev)
9	431.3		

employing a stronger source obtained as a fission product from the Oak Ridge National Laboratory, closely confirms most of our earlier interpretation and adds several previously unobserved gamma-rays.

A summary of the energies of the conversion electron lines, together with their approximate intensities and interpretation, is presented in Table I. The averaged values of the derived gamma-rays, shown in column 4, are collected in Table II, each designated by an arbitrary index number. The gamma-rays fit remarkably well a nuclear level scheme as shown in Fig. 1. The high energy gamma-rays previously reported at 2.5 Mev by Wattenberg and at 2.9 Mev by Bishop are included as 2.52 and 2.92 Mev, since as such they appear as cross-overs in the proposed level scheme, although they were not observed by conversion electrons.

* This project received the joint support of the AEC and ONR.
[1] Cork, Keller, Rutledge, and Stoddard, Phys. Rev. **76**, 1886 (1949).
[2] Beach, Peacock, and Wilkinson, Phys. Rev. **76**, 1624 (1949).
[3] A. Wattenberg, Argonne National Laboratory Report ANL 4076 (1947), unpublished; Bishop, Wilson, and Halban, Phys. Rev. **77**, 416 (1950).

The Application of Wooldridge's Theory of Secondary Emission*

E. M. BARODY
Battelle Memorial Institute, Columbus, Ohio
(Received June 28, 1951)

AN interesting letter by Brophy[1] has pointed out how Wooldridge's result[2] for the variation of the secondary emission coefficient with primary energy can be put into a very convenient form, and has compared this result with a particular form of free electron theory, and with experiment. We have been working along similar lines and have reached conclusions in general agreement with those of Brophy. However, there are certain differences and extensions which are presented below.

There seems to be an error in the form of Wooldridge's Eq. (53) as first given in the letter. It becomes correct if δ_{max} is replaced by δ_m, the value which Wooldridge's δ would approach for large primary energy. The corresponding definition of K is $(1/2\delta_m)\times[1-(W_s/E_0+E_p)^{\frac{1}{2}}]$. The other substitutions listed by Brophy then lead to

$$\delta/\delta_m = 1 - A\exp(-x^2) + B\exp(-x^2)\int_0^x \exp(t^2)dt, \qquad (1)$$

where A, B, and M are defined in Brophy's letter,[3] and $\delta_m = (1-M)/K$.

Various implications of the above relations have been investigated. It was found that δ reaches a maximum given by

$$\delta_{max}/\delta_m = 1 + (MK^{\frac{1}{2}}/x_{max}) \qquad (2)$$

at $x = x_{max}$, where

$$\int_0^{x_{max}} \exp(t^2)dt - \frac{\exp(x_{max}^2)}{2x_{max}} = \frac{A}{B}. \qquad (3)$$

Dividing Eq. (1) by Eq. (2) gives an equation for δ/δ_{max} which should replace Brophy's Eq. (2).

The extent to which this new statement of Wooldridge's result predicts a universal relationship between δ/δ_{max} and $E_p/E_{p\,max}$ has been explored. For most metals the parameter M may be estimated to fall in the range 0.75 to 0.90. The corresponding range of K is determined by the experimental values of δ_{max} almost all of which fall between 0.5 and 1.6. Calculation shows that for any reasonable values of M and K, a graph very much like the quantum-mechanical curve in Fig. 1 of Brophy's letter is obtained, although a significant variation in the rate of decrease at high energies is found. The amount of this variation is easily determined from the following approximation, which applies extremely well for all $E_p \geq E_{p\,max}$:

$$\delta/\delta_{max} = [1+\gamma(E_{p\,max}/E_p)^{\frac{1}{2}}]/(1+\gamma). \qquad (4)$$

Here, $\gamma = MK^{\frac{1}{2}}/x_{\max}$, and is expected to lie in the approximate range 0.15 to 0.30. At $E_p = 2E_{p\,\max}$, for example, the predicted range of $\delta/\delta_{\max}$ corresponding to these figures is 0.96 to 0.93. These numbers agree rather well with experiment, the available data suggesting that the correct range is something like 0.95 to 0.90.

It is hoped that the above and related material can be treated more fully in a later publication.

* Sponsored by the Army Signal Corps and the Air Force.
[1] James J. Brophy, Phys. Rev. **82**, 757 (1951).
[2] D. E. Wooldridge, Phys. Rev. **56**, 562 (1939).
[3] However, there is a misprint in the definition of A. The upper limit of the integral should be $K^{\frac{1}{2}}$, rather than K.

Angular Distributions for (d,p) and (d,n) Reactions in Light Nuclei

S. T. Butler*
Department of Mathematical Physics
AND
J. L. Symonds†
Physics Department, University of Birmingham, Birmingham, England
(Received June 25, 1951)

In this note, we wish to point out that the experimental angular distributions recently reported[1,2] for the reactions $T(d,n)He^4$ and $He^3(d,p)He^4$ can be explained by means of the stripping process.[3] Figure 1, for example, is a comparison between the

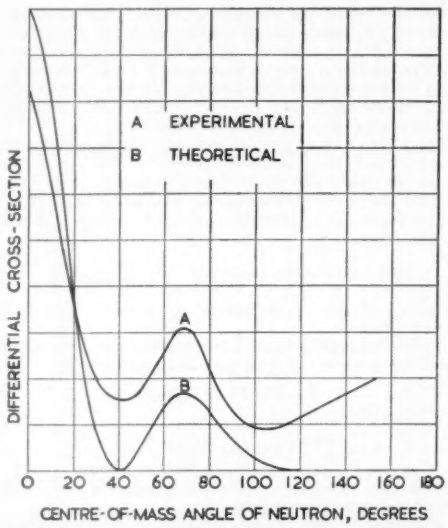

FIG. 1. Comparison between experimental and theoretical angular distributions for the reaction $T(d,n)He^4$ for 10.5-Mev deuterons. (Theoretical curve calculated assuming "radius" of tritium plus range of nuclear forces $=4.3\times10^{-13}$ cm.)

theoretical and experimental distributions for the $T(d,n)He^4$ reaction for an incident deuteron energy of about 10.5 Mev (lab.), and the distributions for the mirror reaction are almost identical. The theoretical curve has been calculated assuming the captured proton carries with it zero orbital angular momentum (consistent with the known spins and parities of the initial and final nuclei involved), and the experimental curve is a replica of that drawn by Brolley *et al.*[1] through their experimental points.

It is seen that good agreement is obtained for the positions of the two peaks at 0° and 68° in the center-of-mass system, although beyond 100° the two curves diverge. The relative heights of the two maxima do not quite correspond, but the agreement is nevertheless remarkably good. The absolute magnitude of the differential cross section in the forward direction (about 16 millibarns) is also quite compatible with an approximate estimate made assuming a stripping process.

This indicates that stripping plays a major part in determining the angular distributions. Compound nucleus formation, then, can at most be the cause of the slowly varying difference between the two curves, although even this is not certain, since the theoretical treatment of the stripping process does not claim to be rigorous for the smaller incident deuteron angular momenta. The similarity between the distributions for the above mirror reactions follows immediately, therefore, from the fact that T^3 and He^3 have the same symmetry properties and similar binding energies, and does not necessarily imply similarity in the properties of the compound nuclei, as suggested by Brolley *et al.*[1]

From a comparison of the experimental[4,5] and theoretical angular distributions of protons from the $d-d$ reaction at incident energies of 8–10 Mev, it seems likely that in this reaction, also, the main features of the curve can be explained by stripping. Only a qualitative comparison has been made as yet, however, since the theory has to be modified in this case to take account of the identity of the two initial particles.

* Australian National University Scholar.
† Australian National University Research Fellow.
[1] Brolley, Fowler, and Stovall, Phys. Rev. **82**, 502 (1951).
[2] J. C. Allred, Phys. Rev. **77**, 753 (1950).
[3] S. T. Butler, Phys. Rev. **80**, 1095 (1950); Proc. Roy. Soc. (London), to be published.
[4] Leiter, Rodgers, and Kruger, Phys. Rev. **78**, 663 (1950).
[5] Burrows, Burge, Gibson, and Rotblat, Proc. Roy. Soc. (London), to be published.

The Nuclear Magnetic Moment of Praseodymium

Dudley Williams
Ohio State University, Columbus, Ohio
(Received June 21, 1951)

Preliminary reports from this laboratory[1,2] gave accounts of a nuclear magnetic resonance absorption peak observed in a solution of praseodymium nitrate. The observed absorption line was very strong and unexpectedly narrow in view of the fact that the praseodymium ion is paramagnetic, but the observed peak could not be attributed to any of the impurities listed in the original chemical analysis of the sample. However, studies of several other praseodymium salts failed to reveal an absorption peak—even in the case of another nitrate sample prepared in our laboratory from the oxide. Therefore, a check of the chemical analysis of the original nitrate sample was requested. Although the supplier of the original sample reaffirmed his original analysis of the sample, a subsequent spectroscopic analysis made by Professor J. I. Watters of the local chemistry department revealed the presence of a considerable quantity of rubidium in the sample.

The ratio of the resonance frequency of Rb^{87} to the proton frequency is 0.327100 ± 0.000023 in a sample of Rb_2CO_3 solution, whereas the "best" value for the corresponding ratio for the "praseodymium nitrate" sample was 0.32698 ± 0.00016. Hence, there can be little doubt that the observed peak was due to the rubidium, which was not detected in the chemical analysis of the sample.

Therefore, it becomes necessary to retract the previously reported value for the praseodymium moment. The writer must accept full responsibility for the error in not insisting that the original chemical analyses be checked by spectroscopic methods. The close agreement of the ratios listed above is actually a tribute to the experimental skill of W. H. Chambers and R. E. Sheriff, former graduate students, who made the original frequency

measurements. The writer wishes to express his appreciation to Dr. Yu Ting for his assistance in further work on praseodymium and to Professor J. I. Watters of the chemistry department for making the spectroscopic analysis, which revealed the presence of the rubidium.

[1] J. E. Mack, Revs. Modern Phys. **22**, 64 (1950).
[2] Chambers, Sheriff, and Williams, Phys. Rev. **78**, 482 (1950).

Elastic Scattering of 340-Mev Protons*

R. E. Richardson, W. P. Ball, C. E. Leith, and B. J. Moyer
Radiation Laboratory, Department of Physics, University of California, Berkeley, California
(Received June 18, 1951)

PREVIOUS workers have observed portions of the diffraction patterns in elastic scattering of 14[1]- and 90[2]-Mev neutrons by nuclei. An experiment is now under way at this laboratory to investigate the elastic scattering of 340-Mev protons.

The DeBroglie wavelength of 340-Mev protons is appreciably less than nuclear radii, and because of this it is possible to observe a greater portion of the Fraunhofer diffraction pattern than has hitherto been observed.

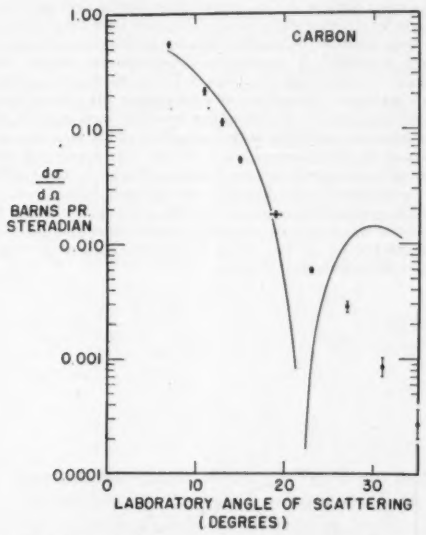

FIG. 1. Differential elastic scattering cross section of carbon for 340-Mev protons as a function of angle. The curve is the prediction of the transparent nucleus theory.

The bombarding energy in this experiment is much larger than the coulomb barrier energies of the target nuclei. Rutherford scattering is therefore important only at very small angles. The use of protons makes possible selection of a very small energy interval, which could not be done in the neutron-nucleus experiments.[1,2]

Incident protons are provided by the external beam of the 184-inch synchrocyclotron, removed from the orbit by scattering into a magnetic deflecting channel.[3] Scattered protons are detected by a triple-coincidence, scintillation counter telescope placed 48 inches from a thin scatterer. The photomultiplier signals are clipped, amplified, and limited; then coincidences are made in a coincidence circuit of approximately 2×10^{-8} second resolving time. Elastically scattered protons are selected by inserting a copper absorber between the second and third phosphors of such thickness that only protons of energy greater than 330 Mev may be detected. The detection threshold for the carbon points was 315 Mev.

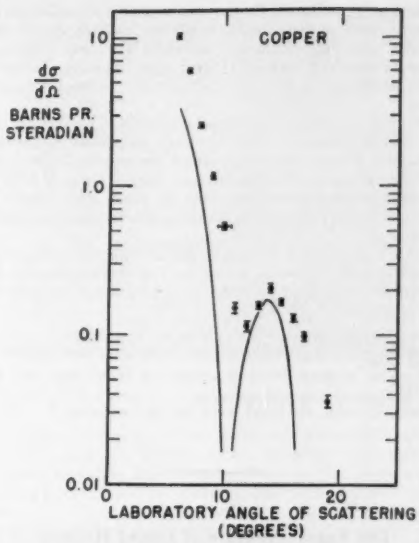

FIG. 2. Differential elastic scattering cross section of copper for 340-Mev protons as a function of angle. The curve is the prediction of the transparent nucleus theory.

Diffraction patterns are shown in Figs. 1 to 3 for some of the

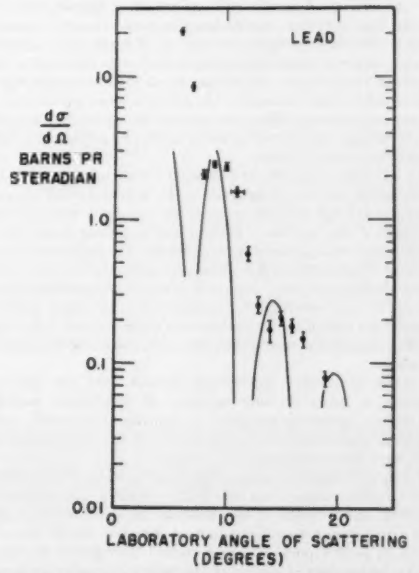

FIG. 3. Differential elastic scattering cross section of lead for 340-Mev protons as a function of angle. The curve is the prediction of the transparent nucleus theory.

elements so far measured. The curves drawn are the predictions of the transparent nucleus theory[4] neglecting coulomb effects and using constants which fit the neutron results. The errors shown are the usual standard deviations based upon counting statistics. Further calibration is under way to detect any possible systematic errors.

The lack of sharp minima may be partially explained by the finite angular resolution. It is noteworthy that, while the angular resolution is the same for all data shown, the smearing is greater in the lighter elements. The transparency effect is expected to be a smooth function of mass number, but the model upon which it is based may not be correct for light nuclei, with their small numbers of nucleons.

Further experiments are contemplated with much improved angular resolution in order to look for any dissimilarities in the patterns from adjacent nuclei whose structures are expected to differ appreciably.

* This work was performed under the auspices of the AEC.
[1] Amaldi, Bacciarelli, Cacciapuoti, and Trabacchi, Nuovo cimento 3, 15, 203 (1946).
[2] Bratenahl, Fernbach, Hildebrand, Leith, and Moyer, Phys. Rev. 77, 597 (1950).
[3] C. E. Leith, Phys. Rev. 78, 89 (1950).
[4] Fernbach, Serber, and Taylor, Phys. Rev. 75, 1352 (1949).

The Vapor Pressure of Liquid Helium at the Lambda-Point

EARL LONG AND LOTHAR MEYER
Institute for the Study of Metals, University of Chicago, Chicago, Illinois
(Received June 21, 1951)

THE vapor pressure of liquid helium at the lambda-point was established by Schmidt and Keesom[1] as 38.3±0.2 mm Hg, corresponding to a temperature of 2.186°K in the so-called 1937 to 1949 temperature scale.

In the course of experiments on adsorbed helium films we recently had occasion to redetermine this pressure, using in principle the same method as that of Schmidt and Keesom. A copper-vapor pressure thermometer bulb was mounted at the bottom of the cryostat, connecting to an oil manometer which could be used either to measure the absolute vapor pressure or to measure any pressure differences between the vapor pressure bulb and the pressure at the top of the cryostat. In addition the bath was provided with a stirrer.

The criterion Schmidt and Keesom used to determine the lambda-point pressure is as follows: In helium I with its poor heat conductivity vertical temperature gradients arise because the liquid at the bottom of the cryostat is boiling under higher pressure than the liquid at the top, owing to the hydrostatic pressure head. These temperature differences instantly disappear when passing the lambda-point, as a consequence of the sudden extreme increase in heat conductivity of the liquid. A vapor pressure thermometer placed at the bottom of a cryostat bath will therefore show a higher pressure than the bath, above the λ-point but not below.

A series of careful experiments showed that the expected difference in vapor pressure appeared at 38.10±0.02 mm Hg (and higher pressures) measured at the top of the bath, using Octoil-S oil manometers and an accurate wide-bore Hg manometer, which were intercompared.

At this and higher pressures the vapor pressure thermometer showed higher values than the bath pressures, the differences depending on the height of the bath and the speed of the stirrer. Below this pressure no differences were observed (±0.05 mm oil). Moreover, at this point bubbling started throughout the liquid and the fluctuations in control of the bath temperature increased to the relatively high values known for the He I region.

We therefore believe that the vapor pressure of liquid helium at the λ-point (p_λ) should be revised to

$$p_\lambda = 38.10 \text{ mm Hg}.$$

In the conventional temperature scale this would reduce the λ-temperature to 2.184°K. However, Kistemaker[2] reports that a vapor pressure of 38.25 mm Hg corresponds to a temperature of only 2.17°K, which would reduce T_λ to 2.169°K. The uncertainty of the λ-temperature seems at present to be at least 0.01°.

[1] G. Schmidt and W. H. Keesom, Leiden Comm. 22, No. 250b (1937); Physica 4, 963 (1937).
[2] J. Kistemaker, thesis, Leiden (1945), Table XXI; Physica 12, 281 (1946); Leiden Comm. Suppl. No. 95a (1948).

On the Decay of I^{131}

SIGVARD THULIN
Nobel Institute of Physics, Stockholm, Sweden
(Received July 3, 1951)

ALTHOUGH the decay scheme of I^{131} has been extensively studied, there still remain several inconsistencies. The greatest difficulty seems to be associated with the position of those levels from which the high energy γ-rays are emitted. The present investigation concerns this question.

The upper limit of the low energy β-component is of great importance for the whole decay scheme. Energies from 250 to 336 kev have been reported.[1-5] A redetermination of this energy therefore seemed desirable. A carrier-free β-spectrometer sample was obtained by separating *n*-irradiated Te in the electromagnetic isotope separator. The activity of mass number 131 was collected on a 0.15 mg/cm² Al foil. According to earlier measurements on other separated activities, such a sample does not give any distortion of the β-continuum above 50 kev. The β-spectrum was measured in a magnetic lens spectrometer. The upper limits of the two β-components were found to be 607 and 255±30 kev. A β-sample, prepared by evaporation of the *n*-irradiated Te on 0.15 mg Al/cm² was measured in another spectrometer and gave the value 260 kev for the low energy component. This result would support the term scheme of Kern.

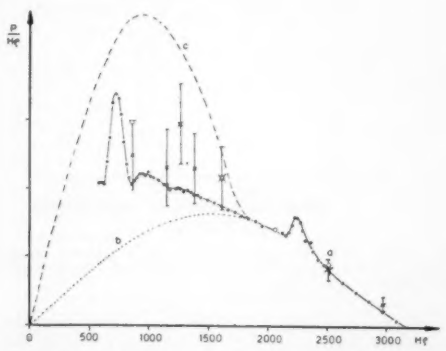

FIG. 1. Coincidence spectrum of I^{131}: *a* = β-spectrum measured in one of the lenses; *b* = 607-kev β-component. The crosses and circles are the measured coincidence points corrected for coincidence background and normalized to the upper part of curve *a*. *c* = theoretical coincidence spectrum, assuming that the 284- and 638-kev γ-transitions feed the 80-kev level with approximately the same intensity.

Some of the inconsistencies mentioned above might be clarified by coincidence measurements. For this reason, coincidences were measured in a double-lens β-spectrometer (β-spectrogoniometer)[6] between the *K* conversion line of the 80-kev γ-ray and different energies of the β-continuum. The results are shown in Fig. 1. The

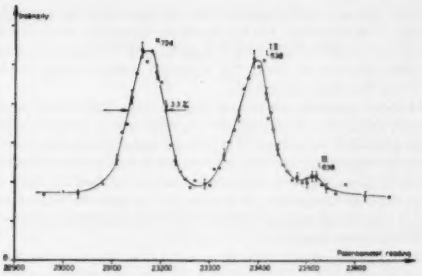

FIG. 2. The K_{724} and L_{638} photolines from a uranium converter.

presence of coincidences between the 80-kev γ-ray the 607-kev β-component definitely rules out the third decay scheme of Cork *et al.*[7] It seems probable that there is a small coincidence effect also between the 80-kev γ- and the 255-kev β-component.

Earlier measurements indicate that the energy difference between the two high energy γ-rays (724 and 638 kev) is approximately 80 kev, i.e., the energy of a third γ-ray. A high precision determination of this energy difference can be obtained by measuring the photoelectron lines from a uranium converter, since the K_{724} line and L_{638} line appear as a narrow doublet. Such a measurement was carried out in the double focusing spectrometer using a 250-mC I^{131} sample and a uranium radiator (1.3 mg/cm^2). The doublet is shown in Fig. 2. The energies of the two γ-rays were found to be 638.9$\pm$0.6 kev and 723.9$\pm$0.7 kev. The relative intensity, estimated from the K photo lines, is 7.8:1. The energy difference as determined from the doublet lines is 85.7$\pm$0.4 kev. A difference of 80.1 kev would give a doublet with approximately twice as large a distance between the lines. The value 85.7 kev definitely excludes the possibility of a cross-over transition for the 724-kev γ-ray as assumed by Zeldes *et al.*[8] and Bell *et al.*,[2] which, in fact, had seemed to be a satisfactory suggestion.

[1] Kern, Mitchell, and Zaffarano, Phys. Rev. **75**, 1632 (1949); **76**, 94 (1949).
[2] Bell, Cassidy, and Kelley, Phys. Rev. **82**, 103 (1951).
[3] I. Feister and L. F. Curtiss, Phys. Rev. **78**, 179 (1950).
[4] F. Metzger and M. Deutsch, Phys. Rev. **74**, 1879 (1948).
[5] Verster, Nijgh, van Lieshout, and Bakker, Physica, to be published.
[6] K. Siegbahn, Arkiv Mat. Astron. Fysik, to be published.
[7] Cork, Rutledge, Stoddard, Branyan, and Childs, Phys. Rev. **81**, 482 (1951).
[8] Zeldes, Brosi, and Ketelle, Phys. Rev. **81**, 642 (1951).

A Photographic Study of the $\pi^+ \rightarrow \mu^+ \rightarrow \beta^+$ Decay Process and the Energy Spectrum of the β^+

H. BRAMSON AND W. W. HAVENS, JR.
Columbia University, New York, New York
(Received June 29, 1951)

AN investigation of meson decay has been undertaken using thick electron sensitive emulsions and the beam of mesons produced by the 385-Mev Nevis cyclotron.

The emulsions were exposed in a collimating chamber[1] which yields plates of low background while restricting entrance of π-mesons to a nearly monoenergetic monodirectional beam of π^+ mesons. The μ^+ mesons entering these plates can, except in exceedingly rare instances[1] be readily distinguished from the main π^+ beam. In addition, the appearance of the decay particle at the terminus of the μ^+ meson can be regarded as a final check of its identification.

Ilford G5 emulsions, approximately 0.6 mm and 1 mm thick, were used in order to investigate the energy spectrum of the charged particle from the decay of the μ^+ meson. To date, 1158 cases of π^+ decay have been observed where the μ's have ended in

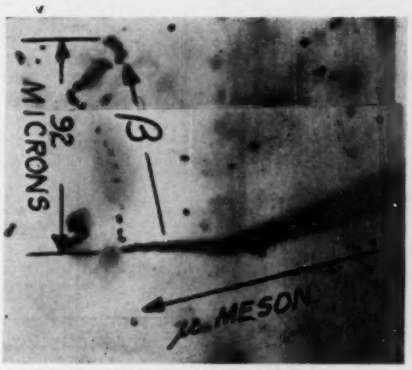

FIG. 1. Slow positron of a $\pi \rightarrow \mu \rightarrow \beta$-sequence in 1-mm emulsion.

the emulsion. In each of these cases, an attendant minimum ionization track was always visible, attesting to the uniform minimum ionization achieved throughout the film. Steep angles of the decay track did not introduce difficulties in their identification.

Throughout these studies anomalous ranges of μ-mesons were searched for without success. Since W. F. Fry[2] has reported four μ meson ranges which were clearly anomalous, our results were rescanned, specifically in a search for μ-meson ranges less than 420 microns. However, no such anomalous events have been found. Therefore, we believe either that such events are not as common as indicated by Fry's results, or that the statistical fluctuations of scattering measurements and grain counting over such short track lengths can permit such variations in usual μ-meson tracks to account for Fry's results.

Three interesting examples of μ^+ decays are shown here. Figure 1 shows the slowest positron yet observed in this study. From its range, which lies entirely within the emulsion, the energy was estimated to be about 0.1 Mev. Figure 2(a) shows an instance of an unusually sharp scattering of the decay particle shortly

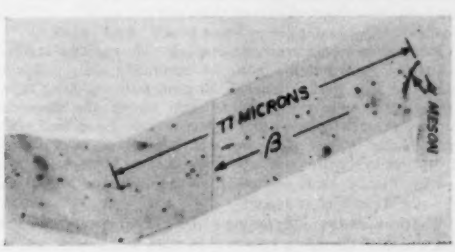

(a)

(b)

FIG. 2. (a) Instance of large scattering of positron (0.6-mm emulsion). (b) Example of positron annihilation in 1-mm emulsion. (Annihilation takes place 4900 microns from μ-meson, 190 microns beneath air surface, 600 microns above glass surface.)

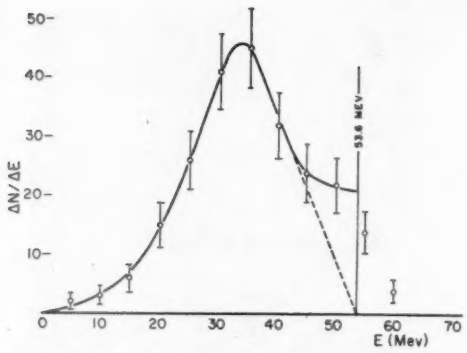

FIG. 3. Spectrum of 117 positrons from μ^+ meson decay. Each point represents the number of positrons per 10-Mev energy interval. The vertical lines indicate the statistical spread. The smooth curve represents the best match to the observed points. The dotted portion represents the best match to the data by a curve approaching zero at the upper energy end.

after leaving the μ-meson. Similar large scatterings (at least eight times the average scattering, including the large scatterings) are found to occur with a frequency of about 10 percent within the first g/cm^2 of emulsion. With a fair bremsstrahlung loss possible in these events, this comprises a possible source of error in techniques employing appreciable "dead" mass to stop the μ-meson. Figure 2(b) shows one of six events in which the decay particle disappears. In view of the uniform minimum ionization achieved, this disappearance is interpreted to be an annihilation process. Hence, in addition to having the same charge as the positron, and a mass not much heavier (if at all),[3] this decay particle is now observed to have a third property in common with the positron, that of annihilation.

The use of nuclear emulsions for investigating the energy spectrum of the positron from μ^+ decay has several advantages. In a few hours of cyclotron running time, $1500\pi \rightarrow \mu \rightarrow \beta$ sequences were obtained. A qualitative examination of the β-tracks can be made at a rate of 40/day/scanner. Positrons of all energies give substantially the same grain density;[4] hence, all energies are recorded with almost equal sensitivity. The complete history of the positron is observed; therefore, there is no possibility of failing to observe appreciable energy losses in any "dead" mass.

However, some disadvantages also exist. The results of multiple scattering measurements must be accurately correlated with energy. A long track is required for good accuracy. Long tracks imply appreciable energy degradation during the measuring process through collision and radiation loss. Long tracks also discriminate against slow positrons because of outscattering. Distortion in the processed emulsion will cause lower estimates of energy. Finally, these scattering measurements are tedious and exacting if precision is desired.

The modification of the stage and drive of a conventional microscope enabled the measurements to be made with greater ease and speed. The effective track length depends upon the shortest "foil" thickness feasible, below which the noise level becomes critical. After some investigation, it was found possible to make Fowler-type measurements of track ordinates with a mean deviation of 0.03 micron. This permitted the use of intervals as short as 50 microns for the fastest particles observed, with a noise error of less than 2 percent in the most unfavorable cases. Therefore, a 1500-micron track length was selected at the minimum acceptable for the desired statistical accuracy: 10 percent standard deviation. Outscattering is then less than 2 percent above 20 Mev, reaching 10 percent at 11 Mev and 38 percent at 5 Mev. The average bremsstrahlung loss is 7 percent for the 2.91-cm radiation length in G5 emulsion. Hence, individual variations from this average loss are much smaller than the statistical uncertainty in energy determination. On all plates no distortion was noted in the central portions for the track lengths used. Taking into account all these sources of error, the standard deviation per track is probably less than 11 percent.

Average multiple scattering angles were calibrated against energy using the Scott-Snyder[5] theory, which from Corson's[6] work appeared to be best. The energy spectrum uncorrected for outscattering resulting from the first 117 decays is shown measured in Fig. 3. The spectrum appears to have a marked non-zero cutoff at the high energy end, as is indicated by both the experimental points and the straggling beyond cutoff (taking the μ-meson mass as 209 electron masses).

It is interesting to note that if (a) the Scott-Snyder-theory provides a perfect calibration and (b) the relativistic momentum of the positron is, on the average, equal to that of each neutrino, then the average energy: 35.76 ± 0.37 Mev, gives the mass of the μ-meson as 209.3 ± 2.2 electron masses. In the absence of an accurate independent verification of the Scott-Snyder theory in this energy region, this excellent agreement with recent values[7] might best be taken as an indication of the high accuracy of this theory as applied here.

We wish to thank Drs. Friedman and Rainwater for kindly lending us their exposure chamber and some plates for our earlier work. We are also grateful to Miss Marjorie Fogarty and Mrs. Carol Major for their invaluable assistance in locating the events, and to Mr. Aurel Seifert for aiding with some of the measurements.

[1] H. L. Friedman and J. Rainwater, Phys. Rev. **81**, 644 (1951).
[2] Using C2 emulsions; Nuovo cimento, letter in publication.
[3] E. P. Hincks and B. Pontecorvo, Phys. Rev. **75**, 698 (1949); J. C. Fletcher and H. K. Forster, Phys. Rev. **75**, 204 (1949).
[4] E. Pickup and L. Voyvodic, Phys. Rev. **80**, 89 (1950).
[5] W. T. Scott and H. S. Snyder, Phys. Rev. **76**, 220 (1949).
[6] D. R. Corson, Phys. Rev. **80**, 303 (1950); and private communication.
[7] W. H. Barkas, UCRL Report 1285, unpublished.

On a One-to-One Correspondence between Infinitesimal Canonical Transformations and Infinitesimal Unitary Transformations

D. C. RIVIER*
Palmer Physical Laboratory, Princeton University, Princeton, New Jersey
(Received July 2, 1951)

IT is well known that there is an analogy between the group of the canonical transformations of classical mechanics and the group of the unitary transformations of quantum mechanics, insofar as in the latter we exclude degrees of freedom without classical analog.[1] Until now, however, this analogy has been found to be not very simple; more precisely, no general homomorphism has been given between the two groups.[2,3] Among the reasons for that are the ambiguities in the definition of the quantum-mechanical function $F(\mathbf{p}, \mathbf{q})$ of the noncommutable operators $\mathbf{p}$, $\mathbf{q}$ with

$$[\mathbf{p}, \mathbf{q}] = -i\hbar\mathbf{1}, \tag{1}$$

corresponding to the classical function $F^c(p, q)$ of the commutable variables[4] p, q. In order to have an actual significance, such a correspondence must be independent of the choice of the variables p, q, at least within a certain subset of the group of canonical transformations.

The first step in finding a correspondence between canonical transformations and unitary transformations is to give this correspondence between $F^c(p, q)$ and $F(\mathbf{p}, \mathbf{q})$. We propose the following one: to every classical real function $F^c(p, q)$ which may be written as a fourier integral

$$F^c(p, q) = \int dx \int dy f^c(x, y) e^{i(px+qy)}, \quad \bar{f}^c(-x, -y) = f^c(x, y) \tag{2}$$

($^-$ means imaginary conjugate) corresponds the quantum-me-

chanical function

$$F(\mathbf{p},\mathbf{q})=\int dx\int dy f(x,y)e^{i\mathbf{p}x}\cdot e^{i\mathbf{q}y},$$
$$f(x,y)=\tfrac{1}{2}(1+e^{-i\hbar xy})f^c(x,y). \tag{3}$$

The operator $F(\mathbf{p},\mathbf{q})$ has the following properties: (1) it is hermitian; (2) it is "well ordered," i.e., it may be written as a sum of terms where the $\mathbf{p}$ are on the left of the $\mathbf{q}$; (3) for $\hbar$ going to 0, F is reduced to F^c, which expresses the condition of correspondence. All these properties are invariant under the operations of derivation or integration.[5]

The infinitesimal canonical transformation generated by the real function $F^c(p,q)$ is described by the following equations:

$$\begin{cases} p'=p+\alpha\{F^c(p,q),p\}=p-\alpha\partial F^c/\partial q & (\alpha \text{ real}),\\ q'=q+\alpha\{F^c(p,q),q\}=q+\alpha\partial F^c/\partial p. \end{cases} \tag{4}$$

By application of Taylor's formula, we get the transform $G^c(p',q')$ of any real function $G^c(p,q)$, neglecting terms in $\alpha^2,\alpha^3,\cdots$,

$$G^c(p',q')=G^c(p,q)+\alpha\{F^c(p,q),G^c(p,q)\} \tag{4a}$$

with the definition for the poisson bracket

$$\{F^c(p,q),G^c(p,q)\}=\frac{\partial F^c}{\partial p}\frac{\partial G^c}{\partial q}-\frac{\partial G^c}{\partial p}\frac{\partial F^c}{\partial q}.$$

Now we want to extend the notion of a canonical infinitesimal transformation to the case where the commutable variables p,q are replaced by the noncommutables $\mathbf{p},\mathbf{q}$, and, at the same time, the functions $G^c(p,q)$, $F^c(p,q)$, etc., replaced by $G(\mathbf{p},\mathbf{q})$, $F(\mathbf{p},\mathbf{q})$, $\cdots$, etc. This extension must satisfy the following conditions: (1) the new variables $\mathbf{p}',\mathbf{q}'$ must be hermitian; (2) the correspondence $F^c(p,q)\to F(\mathbf{p},\mathbf{q})$ must be the same as the correspondence $F^c(p',q')\to F(\mathbf{p}',\mathbf{q}')$ (invariance of the law of correspondence (2), (3) with respect to a canonical infinitesimal transformation). The only possible extension of (4) satisfying these conditions is

$$\begin{cases} \mathbf{p}'=\mathbf{p}-\alpha\partial F/\partial\mathbf{q},\\ \mathbf{q}'=\mathbf{q}+\alpha\partial F/\partial\mathbf{p}. \end{cases} \tag{5}$$

The condition (2) gives the transform $G(\mathbf{p}',\mathbf{q}')$ of $G^c(p',q')$:

$$G(\mathbf{p}',\mathbf{q}')=\int dx\int dy g(x,y)\exp\{i\mathbf{p}'x\}\exp\{i\mathbf{q}'y\}$$
$$=\int dx\int dy g(x,y)\exp\{ix(\mathbf{p}-\alpha\partial F/\partial\mathbf{q})\}$$
$$\times\exp\{iy(\mathbf{q}-\alpha\partial F/\partial\mathbf{p})\}. \tag{6}$$

Easy calculation gives, neglecting terms in $\alpha^2,\alpha^3,\cdots$,

$$\exp\{ix(\mathbf{p}-\alpha\partial F/\partial\mathbf{q})\}=\exp\{ix\mathbf{p}\}+\alpha(i/\hbar)\exp\{i\mathbf{p}x\}$$
$$\times(\exp\{-x\hbar\partial/\partial\mathbf{q}\}-1)F(\mathbf{p},\mathbf{q})\cdots.$$

Substituting in (6) and using Fourier's development of $F(\mathbf{p},\mathbf{q})$, we have

$$G(\mathbf{p}',\mathbf{q}')=G(\mathbf{p},\mathbf{q})+\alpha(i/\hbar)\int dx\int dy\int dx_1\int dy_1 g(x,y)f(x_1y_1)$$
$$\times\begin{bmatrix}\exp\{-i\hbar xy_1+i(x+x_1)\mathbf{p}\}\exp\{i(y+y_1)\mathbf{q}\}\\ -\exp\{-i\hbar x_1y+i(x+x_1)\mathbf{p}\}\exp\{i(y+y_1)\mathbf{q}\}\end{bmatrix}$$

or, finally, still neglecting terms on $\alpha^2,\alpha^3,\cdots$, we have

$$G(\mathbf{p}',\mathbf{q}')=G(\mathbf{p},\mathbf{q})+\alpha(i/\hbar)[F(\mathbf{p},\mathbf{q}),G(\mathbf{p},\mathbf{q})],$$
$$[A,B]=AB-BA. \tag{7}$$

In other words, the extension of the infinitesimal canonical transformation (4, 4a) generated by the classical function $F^c(p,q)$ is the infinitesimal unitary transformation

$$\begin{cases} \mathbf{p}'=\mathbf{p}+\alpha(i/\hbar)[F(\mathbf{p},\mathbf{q}),\mathbf{p}]=U\mathbf{p}U^{-1},\\ \mathbf{q}'=\mathbf{q}+\alpha(i/\hbar)[F(\mathbf{p},\mathbf{q}),\mathbf{q}]=U\mathbf{q}U^{-1}, \end{cases} \tag{5'}$$

$$G(\mathbf{p}',\mathbf{q}')=G(\mathbf{p},\mathbf{q})+\alpha(i/\hbar)[F(\mathbf{p},\mathbf{q}),G(\mathbf{p},\mathbf{q})]=UG(\mathbf{p},\mathbf{q})U^{-1} \tag{5a'}$$

"generated" by the hermitian operator $F(\mathbf{p},\mathbf{q})$ or also performed by the unitary operator $U=1+\alpha(i/\hbar)F(\mathbf{p},\mathbf{q})$.

On the whole, the infinitesimal unitary transformations appear here as a suitable generalization of the infinitesimal canonical transformations for noncommutable variables, preserving chiefly the hermitian character of the suitably defined function of these noncommutable variables. Obviously, there is a one-to-one correspondence between an infinitesimal canonical transformation and its unitary extension.

* Fellow of the Swiss Commission for Scholarships in Mathematics and Physics.

[1] P. A. M. Dirac, *The Principles of Quantum Mechanics* (Clarendon Press, Oxford, England, 1947), third edition, pp. 105, 106.

[2] P. A. M. Dirac, Revs. Modern Phys. **17**, 195 (1945); see also P. Jordan, Z. Physik **37**, 383 (1926); **38**, 513 (1928).

[3] Léon van Hove, *Sur certaines représentations unitaires d'un groupe infini de transformations*, thèse d'agrégation, Bruxelles (1951); *Sur le problème des relations entre les transformations unitaires de la mécanique quantique et les transformations canoniques de la mécanique classique* (to be published). The author is greatly indebted to Dr. van Hove for sending him these papers before publication.

[4] To simplify the notation, we consider only the case of two canonical variables; generalization to $2n$ variables causes no trouble.

[5] The correspondence given here between F^c and F is a slight modification of that proposed by H. Weyl (reference 6), using the notion of well-ordered function introduced by P. Jordan (see reference 2).

[6] H. Weyl, Z. Physik **46**, 1 (1927); *The Theory of Groups and Quantum Mechanics* (Dover Publications, New York, 1949), pp. 274, 275.

Neutron Crystal Monochromators*

R. J. Weiss†
Watertown Arsenal, Watertown, Massachusetts
AND
J. Hastings and L. Corliss
Brookhaven National Laboratory, Upton, New York
(Received July 5, 1951)

A POLYCHROMATIC beam of thermal neutrons from the Brookhaven reactor, collimated to about one-minute divergence (slit geometry), was diffracted from a single crystal and the contour of the diffracted beam was determined with a slit mounted on a comparator in front of a BF_3 counter. Coherent regions of the crystal tilted with respect to one another will diffract through slightly different angles according to the Bragg law. It was found that the diffracted beams invariably exhibited several maxima for crystals grown from the melt, and these have been attributed to the lineage structure of such crystals. Lineages are large regions of the crystal tilted with respect to one another but not to such an extent as to call them grains.[1] Within each lineage region there are coherent domains (commonly called mosaic blocks) tilted with respect to one another to a lesser degree than lineages and about 5000A in size[2] in annealed specimens. The existence of lineage is

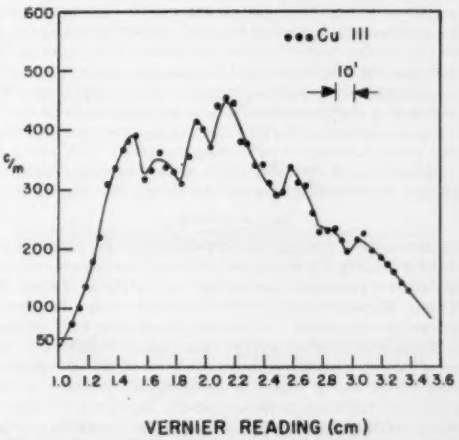

FIG. 1. Contour of Bragg peak from a diffracting plane perpendicular to growth direction, showing lineage.

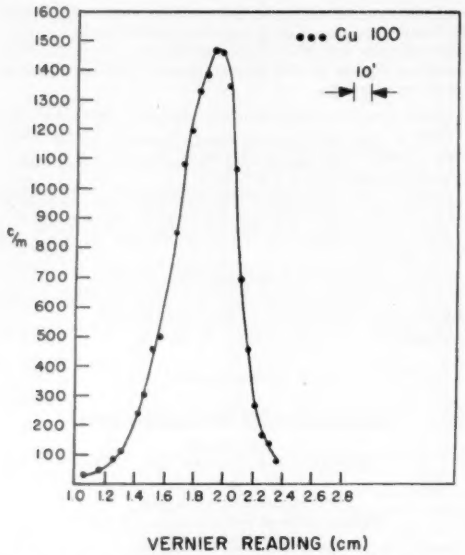

FIG. 2. Contour of Bragg peak from a diffracting plane parallel to growth direction, showing decrease in lineage.

well known to metallurgists, but has not as yet been specifically correlated with the diffraction of neutrons. The lineage structure is a result of the growth process and appears as a fibrous structure in the direction of growth. Figure 1 is a diffraction pattern of a crystal from a diffracting plane approximately perpendicular to the growth direction, with the beam intercepting many lineage regions. Figure 2 is a diffraction pattern from a diffracting plane parallel to the growth direction. In the latter case the beam was parallel to the fibers and intercepted only 2 lineage regions.

These results are important in connection with neutron crystal monochromators, since neutron beams are large enough and penetrate deeply enough to be affected by lineage. In a previous search for good monochromating crystals, double-crystal rocking curves were taken[2] at Oak Ridge, and an attempt was made to interpret the results with the dynamical theory of x-ray diffraction assuming the angular distribution of coherent domains to be gaussian. In most cases the reflectivities were too small by a factor of 2, and it now appears that the discrepancy may be due to lineage (two of the crystals were checked with the present apparatus and were found to contain pronounced lineage). The lineage structure is lost to a great extent in double-crystal rocking curves.

The wavelength resolution, $\Delta\lambda/\lambda$, of a crystal monochromator is related to the angular spread of the coherent domains, $\Delta\theta$, by

$$\Delta\lambda/\lambda = \Delta\theta/\tan\theta_B,$$

where θ_B is the Bragg angle. Twenty assorted crystals grown from the melt (Be, Mg, Cu, Ni, Pb, Bi, NaCl, LiF) were examined, and all contained pronounced lineage with an average $\Delta\theta$ of about 30 minutes. Thermal annealing of lead in general reduced this, and in one case $\Delta\theta$ was reduced to 2.5 minutes. On the other hand, $\Delta\theta$ may be increased by about an order of magnitude by straining crystals below their temperature of recrystallization. In crystals used for monochromators, $\Delta\theta$ should be approximately the same as the geometrical resolution of the instrument. Because of its ease of growth, its high coherent cross section and low absorption, and the ability to vary the lineage to some extent, it appears that lead makes a suitable monochromator for neutrons.

We are grateful for many helpful discussions with Dr. A. W. McReynolds of Brookhaven National Laboratory and Dr. L. D. Jaffe of Watertown Arsenal.

* Research carried out under contract with the AEC.
† Permanent duty station, Brookhaven National Laboratory.
[1] M. J. Buerger, Z. Krist. **89**, 195 (1934).
[2] B. L. Averbach and B. E. Warren, J. Appl. Phys. **20**, 1066 (1949).
[3] Pasternack, McReynolds, Weiss, and Corliss, Phys. Rev. **81**, 326 (1951).

Radioactivity of F^{17}

V. PEREZ-MENDEZ AND P. LINDENFELD
Pupin Physics Laboratories, Columbia University, New York, New York
(Received June 21, 1951)

THE gamma-radiation from F^{17} has been re-examined with a scintillation counter and a pulse-height analyzer.

Distilled water was bombarded with deuterons in the internal beam of the 36-in. cyclotron and half-lives were measured at different pulse-height settings. With the increased activity which was produced in this way, and the better energy discrimination, it was found that the previously reported gamma-rays[1] of energy higher than that of annihilation radiation had a half-life distinctly shorter than that of F^{17}.

The large chemical activity of fluorine and of the ozone which is produced when gaseous oxygen is bombarded makes it likely that some impurity was carried along in the previous experiments.

We conclude that F^{17}, in common with other mirror image nuclei which have been investigated with spectrometers, does not emit any nuclear gamma-radiation.

[1] V. Perez-Mendez and P. Lindenfeld, Phys. Rev. **80**, 1097 (1950).

Measurement of Some Internal Conversion Coefficients*

A. W. SUNYAR
Brookhaven National Laboratory, Upton, New York
(Received July 5, 1951)

THE lifetime-energy relations of Axel and Dancoff[1] lead to the interpretation that the isomeric transitions in Cd^{111m} (48.6 min, 149 kev), Cs^{134} (3.15 hr, 128 kev), and Ta^{182m} (16.4 min, 180 kev) are of multipole order $\Lambda=4$; i.e., electric 2^4-pole ($E4$) and/or magnetic 2^3-pole ($M3$). Measured K/L ratios for these transitions,[2] when compared with the approximately calculated ones of Hebb and Nelson,[3] support the interpretation that these transitions are of the $E4$ type ($\Delta I=4$, no parity change). In addition, the conversion coefficient for Cd^{111m} has been recently reported[4] to agree with that theoretically expected[5] for an $E4$ transition. This is in direct contradiction to the predictions of the strong spin-orbit coupling shell model for Cd^{111m}. The second step (247 kev) of this two-step isomeric transition is an $E2$ transition on the basis of its conversion coefficient.[4] The ground-state spin and magnetic moment of Cd^{111} indicate that it may be designated as an $s_{1/2}$ state. In terms of the shell model the decay of Cd^{111m} would thus be most naturally designated by the transitions

$$h_{11/2} \xrightarrow{149\text{ kev}} d_{3/2} \xrightarrow{247\text{ kev}} s_{1/2}$$

as pointed out by Johansson.[6] The 149-kev transition would be of the $E3$ type ($\Delta I=3$, change in parity). In terms of the classification of Axel and Dancoff,[1] the observed lifetime of the 149-kev transition would then be $\approx 10^7$ times slower than the calculated lifetime.

Weisskopf has recently derived new lifetime-energy relations[7] which give considerably smaller radiation probabilities for all electric transitions with $\Delta I \geq 2$. (The factor is, however, too small to account for the observed discrepancy.) The reclassification of

isomers by Goldhaber and Sunyar[6] has shown that the group of isomers previously identified with $\Delta=4$ ($E4$ and $M3$ transitions) consist really of transitions with $\Delta I=3$ ($E3$ and $M3$ transitions), and that the calculated K/L ratios of Hebb and Nelson[3] for electric transitions with $\Delta I \geq 3$ yield spin changes one unit too high. In the new classification, Cd^{111m}, Cs^{134m}, and Ta^{182m} are $E3$ transitions. These transitions are the slowest of the $E3$ group and in fact are nearly slow enough to be compatible with Weisskopf's $E4$ lifetime formula. The K/L ratios for these transitions clearly

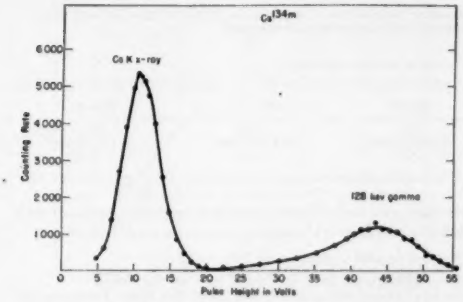

FIG. 1. Pulse-height distribution from Cs^{134m}.

indicate their electric character. An accurate measurement of the internal conversion coefficients will thus decide in favor of $E3$ or $E4$.

Measurements of the conversion coefficients have been made with a scintillation counter using a 1-cm cube crystal of NaI (Tl). A single-channel differential discriminator was used for determining the pulse height distribution. The K conversion coefficient was determined by comparing the intensity of the K x-rays relative to that of the unconverted gamma-ray. The heights of the

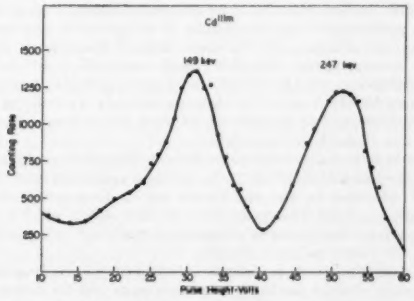

FIG. 2. Pulse-height distribution from Cd^{111m}, showing the unconverted 149-kev and 247-kev gamma-rays.

photopeaks above background give directly the K conversion coefficient when corrections are applied for the following factors: (1) the percent absorption of the radiations in NaI 1-cm thick;[9] (2) the ratio of photoelectric cross section to total absorption cross section,[10] including the effect of Compton scattering by Na in the crystal; (3) the fluorescent yield for the x-rays;[11] (4) the variation of half-width for a photopeak with γ-energy; (5) the change in the fractional acceptance interval, $\Delta E/E$, of the channel with discriminator setting; (6) variation, if any, of the absolute channel width ΔE with discriminator setting. The method has been checked by a measurement of the x/γ-ratio for Te^{123m}. The computed value expected from previous measurements of electron intensities[12] is 0.61, while the measured value is 0.59 ± 0.08.

The sources were prepared by slow neutron bombardment in the Brookhaven reactor. In the case of cadmium, the separated isotope Cd^{110} obtained from Oak Ridge was used.

A typical pulse height distribution from which x/γ-ratios are obtained is shown in Fig. 1 for Cs^{134m}. In Fig. 2 are shown the photopeaks of the 149- and 247-kev gamma-rays of Cd^{111m}, from which the $\gamma 149/\gamma 247$ ratio may be computed. The conversion coefficient for the 247-kev gamma-ray is known,[4] and hence the total conversion coefficient for the 149-kev gamma-ray is determined. The known K/L ratio for this transition[4] allows α_K to be determined. The experimental results are summarized in Table I.

TABLE I. Experimental and theoretical conversion coefficients.

Isomer	E(kev)	Measured α_K	Theoretical α_K[a] $E3$	$E4$
Cd^{111m}	149	x/γ: 1.45 ± 0.4	$>1.5\pm0.3$	1.4	7.1
		$\gamma 149/\gamma 247$: 1.60 ± 0.5		
Cs^{134m}	128	2.2 ± 0.4		~2.45	~12
Ta^{182m}	180	0.8 ± 0.3		0.69	2.05

[a] See reference 5.

The measurements are compatible only with the conclusion that all of the transitions are of the $E3$ type in spite of their comparatively long lifetime.

* Research carried out under contract with the AEC.

[1] P. Axel and S. M. Dancoff, Phys. Rev. **76**, 892 (1949).
[2] National Bureau of Standards Circular **499** (1950), unpublished.
[3] M. H. Hebb and E. Nelson, Phys. Rev. **58**, 486 (1940).
[4] C. L. McGinnis, Phys. Rev. **81**, 734 (1951). A private communication from Dr. A. C. Helmholz to Dr. M. Goldhaber states that a later measurement by Mr. McGinnis agrees with that expected for an $E3$ transition.
[5] Rose, Goertzel, Spinrad, Harr, and Strong, privately circulated tables.
[6] S. Johansson, Phys. Rev. **79**, 896 (1950).
[7] V. F. Weisskopf and J. Blatt, privately circulated chapter from forthcoming book on nuclear theory.
[8] M. Goldhaber and A. W. Sunyar, Phys. Rev. (to be published).
[9] A. H. Compton and S. K. Allison, *X-Rays in Theory and Experiment* (D. Van Nostrand Company, Inc., New York, 1935).
[10] M. T. Jones, Phys. Rev. **50**, 110 (1936).
[11] Steffen, Huber, and Humbel, Helv. Phys. Acta **22**, 167 (1949).
[12] Katz, Hill, and Goldhaber, Phys. Rev. **78**, 9 (1950).

Disintegration of Sn^{119m}

R. D. HILL
*University of Illinois, Urbana, Illinois**
(Received June 29, 1951)

EARLIER experiments[1] on the disintegration of Sn^{119m} showed the existence of a strongly converted 69-kev transition, of 250-day half-life, and probably $M4$ character. It was suggested that this transition should be followed by a second transition, probably of $M1$ character.

The first sources proved to be too weak to measure an accurate energy of the first transition or to observe the existence of the

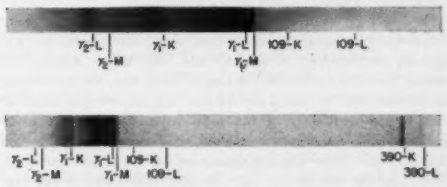

FIG. 1. Conversion spectra of Sn^{119m}. Upper spectrum, 100-gauss magnet. Lower spectrum, 200-gauss magnet. $\gamma_1=65.3$ kev, $\gamma_2=24.2$ kev; 109-kev transition from Te^{119m}, 390-kev transition from In^{119m} (produced from Sn^{119} and Sn^{122} by neutron capture and subsequent decay).

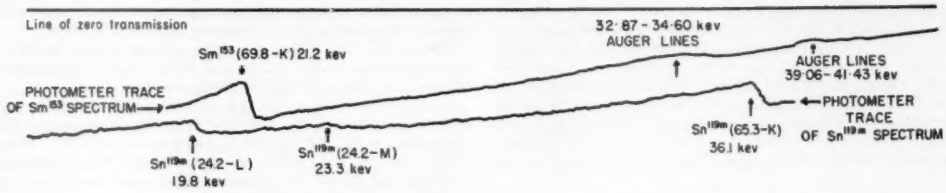

FIG. 2. Microphotometer traces (redrawn) of Sn^{119m} and Sm^{152} spectra in the region from 19 to 42 kev. The similarity of the 19.8-kev line with other conversion lines (e.g., 21.2 and 36.1 kev) and the contrast with Auger lines are exhibited.

TABLE I. Intensities of conversion lines in Sn^{119m} electron spectrum.

Line	24.2-L_I	24.2-M_I	65.3-K	65.3-L_{III}	65.3-M_V
Energy (kev)	19.8	23.3	36.1	61.4	64.8
Density	0.050±0.005	0.020±0.005	0.110±0.005	0.715±0.005	0.205±0.005
Intensity (arb)	5.2	1.2	1.6	3.1	0.8

second. A crude estimate[3] of the slow neutron capture cross section of Sn^{118} for the production of Sn^{119m} was 0.004 barn. Much more intense sources have now been produced by irradiating a Sn^{118} sample (enriched to 91 percent) in a high neutron flux for a period of five months.[3]

Electron spectra of Sn^{119m} taken with 180° magnetic spectrographs are shown in Fig. 1. Two γ-transitions of 24.2±0.5 and 65.3±0.5 kev are observed. The energy of the former is computed on the basis of conversions mainly in the L_I and M_I shells. Also present in the spectrum is the well-known 390-kev γ-transition of In^{113m}, produced from Sn^{113}, which is itself produced from 0.2 percent of Sn^{112}. Although a lifetime check for a period of ~250 days has not yet been made, the 24.2-kev transition is clearly identified as the second transition of Sn^{119m}, since it agrees well with the value of 20±5 kev determined recently for this transition by Scharff-Goldhaber *et al.*,[4] who used scintillation and proportional counters.

Since the conversion lines of the 24.2-kev transition lie within the region of the Auger lines from the Sn and In x-rays, it is important to verify that the 24.2-L and 24.2-M are not Auger lines. (From the intensity of the 390-kev conversion lines it can be shown that the In x-ray intensity, arising mainly from the 110-day K-capture activity of Sn^{113}, is approximately equal to the intensity of the Sn x-rays arising from conversion of the 65-kev Sn^{119m} transition. On this basis also, the capture cross section of Sn^{118} comes out to be 0.003 barn.) It should first be noted that the appearance of the 24.2-L conversion line is different from that of an Auger group. This is clearly shown in Fig. 2, where the photometer traces of Sn^{119m} and Sm^{152} spectra, in similar energy regions, are compared. It is also clear from the intensity analysis that the 24.2-L line is approximately 15 times more intense than that of all the indium Auger lines put together.

Measurement of the intensity of the 24.2-kev transition presents some difficulty on account of the low energies of the conversion lines. Previously, analysis of the intensity of such low energy lines has not been attempted because of the difficulty of correcting for photographic sensitivity and source absorption.

The values given in Table I have been derived using large corrections for photographic sensitivity, which are consistent with Cranberg and Halpern's values,[5] and also using Richardson's analysis[6] in order to correct for source thickness. These intensity values show that the 24.2-L and 24.2-M lines represent a transition which is approximately of the same intensity as the 65.3-kev transition. Theoretically, this should be the case, since the value of the L_I shell conversion coefficient for an $M1$ transition of 24.2 kev is 7.5.[7] An indication that the corrections are of the right magnitude is shown by the L/M ratios for both transitions, which are ~4, a value which we have usually observed in previous work. The K/L ratio of the 65.3-kev transition is 0.51. This value is lower than previously obtained and is in excellent agreement with Goldhaber and Sunyar's[8] empirical curves for an $M4$ transition.

* Assisted by joint program of the ONR and AEC.
[1] J. W. Mihelich and R. D. Hill, Phys. Rev. **79**, 781 (1950).
[2] J. W. Mihelich and R. D. Hill, Phys. Rev. **77**, 743 (1950).
[3] Enriched isotope obtained from Y12 plant, Oak Ridge, Tennessee, and irradiated by special arrangement with AEC, Isotopes Division, Oak Ridge, Tennessee.
[4] Scharff-Goldhaber, der Mateosian, Goldhaber, Johnson, and McKeown, Phys. Rev. **83**, 480 (1951).
[5] L. Cranberg and J. Halpern, Rev. Sci. Instr. **20**, 641 (1949).
[6] H. O. W. Richardson, Proc. Phys. Soc. (London) **63**, 234 (1950).
[7] Gellman, Griffith, and Stanley, Phys. Rev. **80**, 1028 (1950).
[8] M. Goldhaber and A. W. Sunyar, Phys. Rev., to be published.

Three-Quantum Decay of Positronium*

MARTIN DEUTSCH
Department of Physics and Laboratory for Nuclear Science and Engineering, Massachusetts Institute of Technology, Cambridge, Massachusetts
(Received June 25, 1951)

THE rate of decay by three-photon annihilation of ortho-positronium—the ground state of the bound electron-positron system with spin one—has been calculated theoretically with three different results: Ore and Powell[1] find $\lambda_0=7.2\times10^6$ sec^{-1}, Lifshitz[2] gives $\lambda_0=1.13\times10^7$ sec^{-1}, Ivanenko and Sokolov[3] obtain $\lambda_0=1.6\times10^6$ sec^{-1}. Since the three papers start with the same physical assumptions, the discrepancy must be due to errors in at least two of the three calculations.

We have now determined this decay rate experimentally and find $\lambda_0=(6.8\pm0.7)\times10^6$ sec^{-1}, in excellent agreement with the value calculated by Ore and Powell and in disagreement with the other authors. This seems to be the first case in which close experimental verification of a theoretical result has been possible for a third-order radiation process.

In a previous communication[4] we have reported the abundant formation of ortho-positronium in some gases and the action of nitric oxide in low concentration to destroy it by rapid conversion to the para state. This property of NO permits us to separate effects due to ortho-positronium from other phenomena. By this means we have found that in dichlorodifluoromethane ("Freon 12") at pressures above about 0.4 atmosphere substantially all annihilation processes occurring with delays exceeding 8×10^{-8} sec are due to ortho-positronium. At lower pressures a second group appears which is not suppressed by NO and shows a rapid decay depending strongly on pressure. We make the hypothesis that this behavior is due to a large "positron attachment coefficient" of CCl_2F_2 which results in an anomalously large molecular annihilation cross section for free positrons. It may not be accidental that Freon is known to show extremely strong electron attachment.

Whatever the exact mechanism for suppressing the free posi-

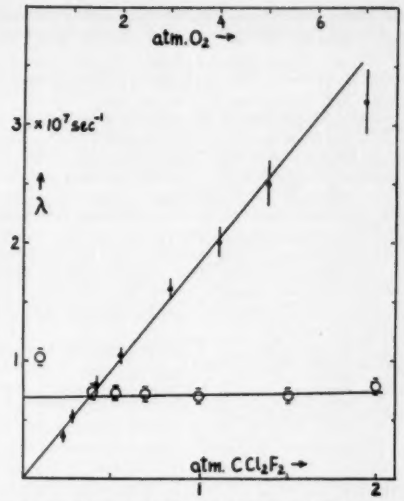

FIG. 1. Rate of decay of annihilation radiation in CCl_2F_2 (open circles) and in O_2 (full circles). The pressure scales are adjusted so that the abscissa corresponds to the same electron density in both gases.

trons, the delayed annihilation radiation in Freon at moderately high pressure seems to be due entirely to ortho-positronium. Its decay rate should depend somewhat on gas pressure p so that $\lambda=\lambda_0+ap$. The pressure proportional term represents annihilation in collisions with Freon or impurity molecules.

The method used to measure the decay rate was the same as in the previous communication.[4] Figure 1 shows the results as a function of gas pressure. The straight line represents the equation $\lambda=6.8\times10^6+0.3\times10^6p$. The value $\lambda_0=6.8\times10^6$ sec^{-1} for the rate of three-quantum decay, obtained by extrapolating the line to zero pressure, should be good to ten percent. The coefficient $a=0.3\times10^6$ sec^{-1} atmos^{-1} is rather uncertain. In any case, a is small, in agreement with calculations of Ore concerning the great stability of positronium against collisions in most gases. The point in Fig. 1 at 0.1 atmosphere which does not fall on the straight line is included to show the effect of free positrons at low pressures.

For comparison, Fig. 1 also shows the decay rate of annihilation radiation in oxygen as a function of pressure. In this gas, at pressures above about 0.5 atmosphere all positronium is converted to the para state so rapidly that substantially all delayed annihilation radiation is due to free positrons decaying in collisions. The rate of decay is, therefore, directly proportional to gas density as shown in Fig. 1. A more detailed discussion of both curves will be given in a later communication.

We wish to thank Professor H. Primakoff for valuable discussions.

* Supported in part by the joint program of the AEC and ONR.
[1] A. Ore and J. L. Powell, Phys. Rev. **75**, 1696 (1949).
[2] E. M. Lifshitz, Doklady Akad. Nauk S.S.S.R. **60**, 211 (1948).
[3] D. Ivanenko and A. Sokolov, Doklady Akad. Nauk S.S.S.R. **61**, 51 (1948).
[4] M. Deutsch, Phys. Rev. **82**, 455 (1951).

A Tentative Interpretation of the Second Maximum in the Transition Curve for Cosmic-Ray Showers

TSAI-CHÜ
Observatoire du Pic du Midi, Bagnères-de-Bigorre, France
(Received June 13, 1951)

THE experimental results on the second maximum still remain in controversy. Bothe *et al.*[1,2] have repeatedly reported the second maximum in the transition curve at 15-cm Pb. While others found a small hump not necessarily at the same place or even nothing at all, formerly Clay,[3] and recently Kameda and Miura,[4] Fenyves and Haiman,[5] and Chaudhary[6] confirmed its existence. The explanation probably lies in the interpretation of this phenomenon, and the discrepancy in experimental results arises possibly from the differences in the arrangement of counters[6] or in the sensitivity of counters to low energy photons.

The nature of primary and secondary particles of the narrow showers responsible for the second maximum remains unknown. Schmeiser and Bothe[7] found that the second maximum is more prominent in the basement than under the roof. Absorption measurements[7] on the secondary particles produced in 1.5 cm Pb as well as in 15 cm Pb show that their coefficients of absorption are much smaller than those of electrons; the particles from 1.5 cm Pb are even more penetrating. In adjacent absorbers these penetrating particles produce further soft showers, the so-called *Zusatzstrahlung*.[8] Bothe[1] considered the narrow showers as the production of mesons by mesons, a new process not yet definitely confirmed by other experiments. In a sub-basement under about 60 cm concrete and with 15 cm Pb above a cloud chamber, Shutt[9] observed many showers containing two penetrating particles making an angle around 6 degrees, the frequency being 1 shower for every 4000 single penetrating particles; Jánossy[10] gave 1 in 12,000. The frequency of a meson accompanying a knock-on electron, which constitutes essentially the background of the transition curve, is 6.9 per 100 mesons[11] near sea level. Therefore, in a cloud chamber the knock-on phenomenon is at least 280 times more frequent than a penetrating pair originating from the lead above it. The selection by counters due to absorption and arrangements reduces the knock-on electrons, but a maximum as large as 35 percent (curve C^3)—that means the frequency of penetrating showers is increased about one hundred times by counters—can never be expected due to penetrating showers. Furthermore, a small maximum probably exists in the transition curve (curve d^3) for non-ionizing primaries; about 65 percent of narrow showers from 1.5-cm Pb are produced by non-ionizing primaries[6] and 25 percent from 15-cm Pb;[6] these facts quickly rule out the meson as the primary.

Kameda and Miura[4] proposed nucleons as primaries. Small angle showers are less penetrating, according to theory and experiment, but frequency considerations still render this proposal impossible. The nucleon intensity decreases much faster than the knock-on electrons in the underground, while the secondary mesons are not shower-producing. Transition curves for penetrating showers are either saturated at great thicknesses[10] or even increase appreciably;[9] no experiment[12] gives a sharp maximum. Only the soft components associated with the penetrating particles, such as knock-on electrons and gamma-radiations in nuclear phenomena, could probably produce a maximum. The striking difference[6] in the contribution of ionizing and non-ionizing primaries at 1.5 and 15 cm Pb cannot be understood with the known properties of protons and neutrons. Because nucleons have a comparatively long mean free path for showers of small multiplicity,[13] it is surely impossible that there are more penetrating showers at 1.5 cm Pb than at 15 cm.

It seems that narrow showers are intimately connected with the soft component. The only thing necessary is to explain the abnormal coefficient of absorption and the possibility of a second maximum appearing. Without introducing new unstable particles,[6] I have tentatively applied the idea of Cocconi and Greisen[14] to explain a small maximum[15] (it may be called rather an irregularity at present) between 5 and 10 cm in the transition curve. A similar irregularity in the same region was present in the curve of Altmann, Walker, and Hess,[16] and also in the Hg curves of Clay.[3] Cascade showers die out by leaving a large number of photons of the order of critical energy, their minimum coefficient of absorption, 0.19 per radiation length (or 1/2.7 per cm lead), being much smaller than that of electrons. The surviving photons degrade their energy mainly by the Compton process, and less frequently by pair production. Some electrons produce further brems-

strahlung, while the positrons annihilate and produce photons. If the multiplication or the cascade of very low energy photons compensates more than the decrease in photon-efficiency of counters, the transition curve rises again and reaches a maximum after about 5 cm Pb (twice the mean free path of the photons of minimum absorption). The counters are triggered essentially by the production of photoelectrons or Compton electrons on their metallic walls. Counters of thin glass walls covered with metal increase the maximum appreciably. The small angle arrangements of Bothe constitute another factor favorable to the maximum. Owing to Compton and coulomb scattering, low energy photons and electrons deviate widely from their origin. The concurrent particles of the shower proper may easily miss the detector, but scattering increases the chance to detect its residual rays. All the difficulties, such as the large magnitude of the maximum, the differences in the behavior of ionizing and non-ionizing primaries, the independence of angle and multiplicity,[8] the associated *Zusatzstrahlung*, etc., can be understood very well. The irregularity between 5 and 10 cm probably arises from the discontinuity in the energy spectrum of soft components; near sea level low energy electrons, and particularly photons, are more abundant below 200 Mev.[17] To avoid the nuclear phenomena and to eliminate the softer primaries, underground measurements should give better results. Whether this hypothesis is good or not can be decided by experiments.

[1] W. Bothe, Revs. Modern Phys. **11**, 82 (1939), and the references contained in this article.
[2] W. Bothe and H. Thurin, Phys. Rev. **79**, 544 (1950).
[3] J. Clay, Revs. Modern Phys. **11**, 287 (1939); **21**, 82 (1949).
[4] T. Kameda and I. Miura, Prog. Theor. Phys. **5**, 323 (1950).
[5] E. Fenyves and O. Haiman, Nature **165**, 244 (1950).
[6] P. K. Sen Chaudhary, Phys. Rev. **81**, 274 (1951).
[7] K. Schmeiser and W. Bothe, Ann. Physik **32**, 161 (1938).
[8] K. Schmeiser, Z. Physik **110**, 443 (1938); **112**, 501 (1939).
[9] R. P. Shutt, Phys. Rev. **69**, 261 (1946).
[10] L. Jánossy, Proc. Roy. Soc. (London) **A179**, 361 (1941); Phys. Rev. **64**, 345 (1943); L. Jánossy and G. D. Rochester, Proc. Roc. Soc. (London) **A183**, 181 (1944).
[11] Brown, McKay, and Palmatier, Phys. Rev. **76**, 506 (1949).
[12] Up to the present time the only exception seems to be the experiment of Kameda and Miura. Their transition curves for narrow and wide angle penetrating showers are at complete variance with other workers. It is not clear that they are really contributed entirely by penetrating particles. One does not know whether their first and second maxima at 5 and 17 cm are really the second and third maxima (total thicknesses of lead equal to 15 and 27 cm) or not.
[13] W. D. Walker, Phys. Rev. **77**, 687 (1950).
[14] Cocconi, Cocconi Tongiorgi, and Greisen, Phys. Rev. **75**, 1063 (1949); K. Greisen, Phys. Rev. **75**, 1071 (1949).
[15] R. Maze and Tsai-Chü, Compt. rend. **232**, 224 (1951).
[16] Altmann, Walker, and Hess, Phys. Rev. **58**, 1011 (1940).
[17] D. J. X. Montgomery, *Cosmic Ray Phys.cs* (Princeton University Press, Princeton, New Jersey, 1949), p. 263.

PHYSICAL REVIEW VOLUME 83, NUMBER 4 AUGUST 15, 1951

Proceedings of the American Physical Society

Minutes of the Meeting at Schenectady, New York, June 14–16, 1951

THE 307th meeting of the American Physical Society, being the 1951 Summer Meeting in the East, was one of the delightful small meetings which more or less alternate with those that are huge and congested; and it was particularly delightful because of the excellent planning of our hosts, who were the General Electric Company and Union College. It was held at Schenectady, New York, on Thursday, Friday, and Saturday, June 14, 15, and 16, 1951. The attendance was over 400; this is believed to have made it the largest summer meeting which we have ever held, apart from the Semi-Centennial Meeting of 1949. The programme comprised sixty-four contributed papers and seventeen invited papers, their topics distributed widely over the field of physics: it is reproduced *in toto* on the following pages. Cool rain fell throughout the Thursday and the Friday, distressing to those who did not remember that sunny June days in the Northeast are likely to be hot, distressing also to our hosts of General Electric who had hoped to offer us the hospitality of their gardens as well as that of their laboratory "The Knolls." Mention should be made that General Electric provided a fleet of buses to take our members to and fro between their living-quarters and the Knolls, and gave us a reception on the Thursday afternoon; and that Union College extended to our members the privilege of living in its new dormitory, and put three of its buildings at our disposal for the scientific sessions. The heads of the very efficient Local Committee were L. R. Apker and M. H. Hebb of General Electric, and H. E. Way of Union College.

The banquet of the Society was held in the Van Curler Hotel on the Friday evening with an attendance of 170. Messrs. Hebb and V. Rojansky made brief and witty remarks, and V. J. Schaefer gave the principal after-dinner speech under the title "Cloud Physics."

The Council met on the Friday afternoon, and elected three candidates to Fellowship and one hundred and forty-seven to Membership: their names are appended. It was decided that beginning in 1952, *Journal of Chemical Physics* shall be offered to our members on membership subscription as an "option" alternative to *Physical Review*—without payment beyond regular dues. Also beginning in 1952, as stated in the Minutes of the Washington meeting, an extra payment of $2.00 (in addition to dues) will be required from each member who subscribes to either section of Science Abstracts and an extra payment of $7.50 from any member who subscribes to both. The Society will also make an annual grant or subsidy to the management of "Science Abstracts" as a contribution to the fixed charges of that journal, and the Council approved a specific proposition, in line with the report of the Committee on Science Abstracts at the Washington meeting.

Reports reaching the office of the Society indicate that we have lost through death Arnold Sommerfeld

(Honorary Member) and Edward Bennett, A. Wilmer Duff, C. F. Eyring, H. E. Marsh, Hantaro Nagaoka, Yoshio Nishina, Tokiharu Okaya, R. T. Ratliff, and A. H. Rollefson.

Elected to Fellowship at the Schenectady meeting: W. W. Beeman, Claude Cherrier, and Erich Regener.

Elected to Membership at the Schenectady meeting: Robert P. Abrahams, Ralph M. Adams, Denis Aliaga-Kelly, Harold W. Anderson, James K. Anderson, LeRoy E. Anger, Edwin L. Armstrong, Frank G. AtLee, Jr., Alfred E. Attard, Paul Avignon, Herman W. Bandel, Emanuel Baskir, Zoltan Bay, Ralph E. Beatty, Jr., John F. Bedinger, Emanuel Belmont, George Bemski, Roger J. Blin-Stoyle, Clyde M. Bliven, Theodore Bowen, Malcolm K. Brachman, Lee C. Bradley III, Chancellor Bramblett, John C. Cacheris, Joseph E. Cahill, Piero C. Caldirola, Nazzareno P. Cedrone, Te-Ning Chin, William Chinowsky, Edward L. Chupp, Armand Cioccio, Stanley J. Ciosek, David Cohen, Kenneth M. Crowe, Paul H. Cutler, Richard W. Damon, Lucien A. D'Asaro, William J. Davis, Jr., Peter T. Demos, George Derderian, Leon M. Dorfman, James B. Dozier, Jr., Richard M. Drisko, Ralph D. Drosd, Thomas A. Green, Daniel H. Greenberg, Alford J. Greenwald, Ernest M. Grunwald, George L. Guthrie, Sister M. Bernarda Handrup, Charles W. Durieux, Seymour Edelberg, Walter G. Elwell, Harald A. Enge, Ismael V. Escobar, Bill W. Fain, Craig S. Fenn, Robert J. Friauf, George C. Fullmer, Harvey L. Garner, John H. Gibbons, Howard B. Glenn, Samuel Globe, Joseph M. Green, Lloyd H. Groth, Daniel W. Healy, Jr., Hans Heil, Robert B. Heller, Rudolf Hermann, Bernard Herzog, Abraham Hirschman, Erik V. Hulthen, Andrew R. Hutson, Thomas O. Jeffries, David W. Juenker, C. C. Jonker, Adolph S. Jursa, Quentin C. Kaiser, Bernard Kaplan, Thomas A. Kaplan, Robert J. Kerr, Alvin E. Kiel, Raymond A. Kinmonth, Jr., Joseph M. Krafft, Albert L. Latter, Michael Leichter, William H. Lupton, Leo Mandelkern, Raymond F. McCartney, Clyde L. McCrary, Clayton J. McDole, Bruce J. McDonald, Edgar A. McLean, William H. McMaster, John W. Michener, Robert H. Mills, Jean A. Minken, James O. Montague, June O. Montgomery, Marion M. M. Morgan, Thomas A. Morgan, Edward L. Murphey, Irving Nadelhaft, James R. Novotny, M. Thomas O'Shaughnessy, Edward D. Padgett, DeWitt R. Petterson, Sanborn F. Philp, Vernon C. Plane, David G. Proctor, David Reiner, Michel C. Renardier, Stanley E. Rittenburg, James P. Rodman, Herbert Rabin, David C. Rahm, Eugene C. Raka, Marc H. Ross, Bernard Roth, Jean L. Ryan, George Saphir, Norman M. Schaeffer, Morris F. Scharff, Curtis L. Scoville, Aaron J. Seriff, John D. Servis, Frank H. Shelton, Edwin Shotland, Robert H. Silsbee, A. Lee Smith, Anne Smith, Harold D. Smith, Helmut Sommer, David E. Soule, B. Frank Sterling, Jr., Yoshio Tanaka, Fred W. Thalgott, John M. Tinker, Robert A. Uphaus, Jack Uretsky, Warren P. Waters, Christopher B. Walker, Dean A. Watkins, Arthur E. Williamson, Jr., Edward J. Winhold, Albert M. Wittenberg, and Max Wolfsberg.

KARL K. DARROW, *Secretary*,
American Physical Society
Columbia University
New York 27, New York

Errata Pertaining to Papers C4, F3, F7, H9, and J2

C4, by J. E. Goldman. In lines 13 and 14, "too close for a strong exchange interaction" should read "too close for a strong positive exchange interaction." In line 17, "face-centered cubic" should read "simple cubic."

F3, by H. W. Boehmer and J. E. Coolidge. The by-line should read, "H. W. Boehmer, University of Colorado, and J. E. Coolidge, Pennsylvania State College." In line 15, "$I(\theta)=I(0)\cos\lambda\theta$" should read "$I(\theta)=I(0)\cos^{\lambda}\theta$."

F7, by J. E. MacDonald and D. L. Falkoff. In line 14, "it is" should read "it is not." In line 15, "all" should read "these." In line 16, "provided" should read "even when."

H9, by F. A. Grant. The by-line should read, "F. A. Grant, University of Maryland (Introduced by Raymond Morgan). Footnote* should read "Supported by Bureau of Ships Contract."

J2, by K. W. DeSorbo and W. C. Dunlap, Jr. In line 12, "0.12 ev" should read "0.03 ev."

PROGRAMME

THURSDAY MORNING AT 10:00

Knolls Auditorium

(J. H. VAN VLECK presiding)

A1. Opening Address. C. G. SUITS, *General Electric Company.*

A2. Nuclear Research with X-rays up to 100 Mev. GEORGE BALDWIN, *General Electric Company.* (35 min.)

A3. Report on the McGill University Radiation Laboratory J. S. FOSTER, *McGill University.* (35 min.)

A4. The Research Programme of the Berkeley Linear Accelerator. W. K. PANOFSKY, *University of California, Berkeley.* (35 min.)

THURSDAY AFTERNOON AT 2:00

Knolls Auditorium

(C. G. SUITS presiding)

B1. Lightning. K. B. MCEACHRON, *General Electric Company. Pittsfield.* (40 min.)

B2. Periodic Deviations of Thermionic Emission from the Schottky Law: Experiments. W. B. NOTTINGHAM, *M.I.T.* (30 min.)

B3. Periodic Deviations of Thermionic Emission from the Schottky Law: Theory. N. H. FRANK, *M.I.T.* (30 min.)

THURSDAY AFTERNOON AT 2:45

Knolls 441

(J. H. HOLLOMON presiding)

Magnetism; Physics of Metals

C1. The Magnetic Susceptibility of Metallic Uranium in the Range −195°C to 1060°C.* C. J. KRIESSMAN, JR.,† AND T. R. MCGUIRE, *U. S. Naval Ordnance Laboratory.*—The magnetic susceptibility of uranium was found to increase uniformly from $1.65\pm0.02\times10^{-6}$ at −195°C up to $1.98\pm0.02\times10^{-6}$ at 800°C. These results are in agreement with those of Bates,[1] who made measurements in the range 20 to 350°C. An abrupt increase of about 6 percent in the susceptibility was found at 800°C with a second but smaller sudden increase at 940°C. The susceptibility discontinuity at 800°C is probably associated with the crystallographic transition[2,3] tetragonal (β) to cubic (γ) structure, occurring at about this temperature. When the temperature was lowered from 1060°C, a temperature hysteresis loop was developed in the region of 760–800°C; but the susceptibility seemed to be reversible at all other temperatures. Uranium is also known to have a crystal structure transition,[2] orthorhombic (α) to tetragonal (β) at 600°C. However, in the neighborhood of 600°C, only a small increase in susceptibility (within the range of experimental error) was observed.

* This work was supported in part by the ONR.
† Also at Catholic University of America.
[1] L. F. Bates and J. R. Mallard, Proc. Phys. Soc. (London) **63**, 520 (1950).
[2] A. S. Wilson and R. E. Rundle, Acta Cryst. **2**, 126 (1949).
[3] C. W. Tucker, Jr., Knolls Atomic Power Laboratory, Schenectady, New York, unpublished work referred to by Kasper, Decker, and Belanger, J. Appl. Phys. **22**, 361 (1951).

C2. Intensity of Magnetization of Thin Nickel Layers.* E. C. CRITTENDEN, JR., L. O. OLSEN, AND R. W. HOFFMAN, *Case Institute of Technology.*—The intensity of magnetization of nickel as a function of thickness is being investigated. The nickel is evaporated under a pressure of 1×10^{-5} mm or less at a constant rate of 70 angstroms per second onto fire-polished glass held at constant temperature. The change in electrical conductivity of a second monitor specimen is used to control the rate of deposition and to determine the thickness deposited on the specimen. A set of shutters exposes the specimen for a short period. The thicker monitor specimen avoids difficulty with the variation of resistivity with thickness. The magnetic data is obtained with an instrument previously described.[1] The specimens saturate at low fields as a result of the single domain structure. A decrease of intensity of magnetization to zero at a finite thickness is observed, as predicted by Klein and Smith.[2] For samples deposited at 75°C, ferromagnetic behavior ceases at about 20 angstroms. Work is continuing in an effort to minimize the effects of surface non-uniformities.

* Work is supported by the ONR.
[1] E. C. Crittenden, Jr., and R. I. Strough, Phys. Rev. **75**, 1630 (1949).
[2] M. J. Klein and R. S. Smith, Phys. Rev. **81**, 378 (1951).

C3. Atomic Moment and Magnetostriction in Ordered Iron-Aluminum Alloys. J. K. STANLEY, J. E. GOLDMAN, AND W. HASSEL,* *Westinghouse Research Laboratories.*—The atomic moment and saturation magnetostriction of polycrystalline iron-aluminum alloys in the range of 13 to 31 atomic percent aluminum have been measured in both the quenched and annealed condition. The quenched alloys were given a prolonged soak at a temperature above the critical ordering temperature before quenching; the annealed alloys were slowly cooled therefrom. Magnetization measurements were made

ballistically with the double balanced coil method in a field of 15,000 oersteds. Magnetostriction was measured using the resistance strain gauge technique with gauges mounted on the 15×3×0.035-cm samples in two directions in order to eliminate volume effects and increase the accuracy of the measurements of the longitudinal magnetostriction in the neighborhood of saturation. The atomic moment of the ordered samples as a function of composition can be represented by two straight lines with the break occurring at the Fe_3Al composition. The quenched samples do not show this sharp discontinuity and resemble more closely the curve of Fallot.[1] The magnetostriction is large and positive over the entire range and is a maximum at the composition Fe_3Al in both cases, but is greater for the ordered samples.

* Now at Carnegie Institute of Technology, Standard Oil of Indiana, and Naval Ordnance Test Station, Inyokern, respectively.
[1] M. Fallot, Ann. phys. 6, 361 (1936).

C4. Theory of the Magnetic Properties of Fe–Si and Fe–Al Alloys. J. E. GOLDMAN, *Carnegie Institute of Technology.*—The magnetic, metallurgical, and lattice properties of the Fe–Al and Fe–Si systems are very similar. Both have identical ordered structures at the composition Fe_3X, and in both cases the magnetic crystalline anisotropy changes sign at about 22 atomic percent Si and Al. However, in Fe–Al the magnetostriction increases,[1] whereas in Fe–Si it decreases and becomes negative at about 13 atomic percent silicon.[2] The behavior of the Fe–Si can be understood on the basis of Neel's theory in which the only ferromagnetic interaction in an iron lattice is the next-nearest neighbor interaction, since the nearest neighbors are too close for a strong exchange interaction. In ordered Fe_3Si, one-third of the iron atoms have only silicon atoms as next-nearest neighbors and will not be magnetic on an atomic dipole representation. The "magnetic" iron atoms now form a face-centered cubic "magnetic superlattice" which can be shown on the basis of the dipole interaction theory[3] to give a negative magnetrostriction of the proper order of magnitude. That the situation is different in the case of Fe_3Al will be discussed from the point of view of an exchange interaction through the $3p$ electrons in aluminum as is suspected to be the case in Heusler alloy.

[1] Stanley, Goldman, and Hassel, previous abstract.
[2] W. J. Carr, Dissertation, Carnegie Institute of Technology, 1950; W. J. Carr and R. Smoluchowski (to be published); J. E. Goldman, Proceedings of the International Conference on Magnetism, Grenoble, 1950.
[3] R. Becker, Z. Physik 62, 253 (1930); J. E. Goldman and R. Smoluchowski, Phys. Rev. 75, 140 (1949).

C5. Effect of Ordering on the Magnetic Anisotropy of Iron-Nickel Alloys. R. M. BOZORTH AND J. G. WALKER, *Bell Telephone Laboratories.*—Single crystals[1] of iron nickel alloys containing from 35 to 100 percent nickel were cut in the form of disks parallel to (100) planes. Measurements of the anisotropy constant, K, were made using the torsion magnetometer previously described.[2] Specimens (about 1 cm diameter, 1 mm thick) were cooled from above 600° to below 300°C at about 2°C/hr to promote atomic ordering, or were quenched from 600°C onto copper to maintain disorder. Anisotropy is dependent on heat treatment from about 50 to 85 percent Ni, the quenched alloys having the higher positive (or less negative) values of K, as observed by Grabbe.[3] Zero anisotropy occurs at 62 percent Ni for the ordered alloys, 71 percent Ni for the disordered alloys. The effect of ordering is greatest when the nickel content is somewhat below that corresponding to $FeNi_3$; at 73 atomic percent K is −3000 after quenching, −23000 after slow cooling.

[1] Walker, Williams, and Bozorth, Rev. Sci. Instr. 20, 947 (1949).
[2] H. J. Williams and R. M. Bozorth, Phys. Rev. 55, 673 (1939).
[3] E. M. Grabbe, Phys. Rev. 57, 728 (1940).

C6. Magnetic Anisotropy and Physical Structure of Alnico 5. Part I. R. D. HEIDENREICH AND E. A. NESBITT, *Bell Telephone Laboratories.*—It is concluded from electron metallographic results that the high coercive force and anisotropy of Alnico 5 are due to a very finely divided precipitate produced by the permanent magnet heat treatment. This precitate is a transition structure rich in cobalt and is face centered cubic with $a_0 = 10$A and appears as rods growing along the [100] directions of the matrix crystal when no magnetic field is applied during heat treatment. The size of the precipitate rods at optimum properties is approximately 75–100A by 400A long. The spacing between rows of rods is about 200A. The rods are not distinctly resolved in the electron images unless they are grown by aging at 800°C. Their orientation and structure is clearly evident in the electron diffraction patterns at all stages of growth. The precipitate responds to a magnetic field applied during heat treatment both by suppression of nuclei making an angle greater than about 70° with the field and by the forcing of the rods off the [100] direction into that of the field. The precipitate rods tend to scatter in direction about the field vector when the field is off the [100] but are aligned accurately when the field is along [100].

C7. Magnetic Anistotropy and Physical Structure of Alnico 5. Part II. E. A. NESBITT AND R. D. HEIDENREICH, *Bell Telephone Laboratories.*—As a result of measurements of magnetic anisotropy and coercive force on single crystals of Alnico 5 and the electron metallography of Part I, the following conclusions were obtained. When the alloy is heat-treated in a field, directional precipitation takes place largely in the field direction. The easy direction of magnetization is always the field direction; and magnetically the crystal has the twofold symmetry of the magnetic field. However, there is a strong tendency due to crystal forces for the precipitate to grow in [100] directions; and, therefore, the crystal has the highest anisotropy when the field and the [100] direction are parallel. The large increase in residual induction of Alnico 5 which results from the magnetic field heat-treatment is caused by the easy directions of the crystal changing from the [111] directions to a single easy direction parallel to the field. Domain rotations rather than boundary movements account for the coercive force of the alloy, since the dimensions of the individual particles are approximately 200 angstroms. The final physical picture of the alloy is one of single domains of precipitate material in parallel with single domains of matrix material, the observed coercive force being the resultant of this combination.

C8. Ultimate Strength Levels in Copper Wire. RICHARD LATORRE AND WALLER GEORGE, *Naval Research Laboratory.*—The resistance of OFHC wire to plastic extension at constant true strain rates has been measured using an extension of a technique previously described by the authors.[1] The results indicate the ultimate true stress to be essentially independent of strain rate over selected intervals and to rise rapidly from level to level over narrow strain-rate intervals. Three successively increasing levels of strength are observed at room temperature, at rates of straining from approximately 10^{-7} sec^{-1} to 1 sec^{-1}. The observed level differences are considered to be significant with respect to the magnitudes of experimental uncertainties, about ±3 percent. The position of the ultimate strength transition from the lowest level to the next higher can be shifted to higher strain rates by increasing the temperature of the specimen. In the region of this transition, the magnitude of the shift in strain rate with a 10°C temperature increase appears to be fitted by a relation between strain rate and temperature of the Ahrenious type.

[1] R. LaTorre and W. George, Phys. Rev. 75, 1309A (1949); 76, 470A (1949).

C9. Diffusion along Grain Boundaries. GLENN M. ROE, *Knolls Atomic Power Laboratory.*—Fisher[1] has presented a numerical calculation on the effect of a relatively high grain boundary diffusivity on the average concentration at a dis-

tance μ from an initial concentration discontinuity normal to the grain boundaries. He concludes that the log of the average concentration varies as the first power of μ. An analytical solution of the same problem shows that the log of the average concentration varies as (1) μ times a slowly varying function of μ for small distances, (2) $\mu^{4/3}$ for intermediate distances, and (3) eventually as μ^2 for large distances. The calculated curves will be compared with the measurements of Hoffman and Turnbull[2] on self-diffusion in silver.

[1] C. Fisher, J. Appl. Phys. **22**, 74 (1951).
[2] R. E. Hoffman and D. Turnbull (to be published in J. Appl. Phys.).

C10. Temperature Dependence of Internal Friction of Single Crystals. J. PITTENGER, *Carnegie Institute of Technology** (Introduced by J. E. Goldman).—The internal friction has been measured as a function of temperature for single crystals of Cu, Mg, and Al in the temperature range of 20 to 400°C and in frequency range of 4 to 30 kc and at various values of strain amplitude. Resonant rods were excited with a magnetic drive, and the decrement was measured by counting electronically the number of cycles after the drive is switched off. The Cu and Mg crystals both show a pronounced minimum in the decrement *vs* $1/T$ curve. In Mg this minimum occurs at about 60°C; in copper it is found at about 180°C and is considerably sharper. In Mg the minimum is broadened by the ability of this metal to anneal or "age" at room temperatures. In the case of the Al crystals the data indicates a slight rise in decrement near room temperature although the existence of a minimum in that region has not been established with certainty. The apparatus will be described, and an attempt made to interpret the data.

* Supported by the ONR.

C11. Rupture of Plastic Sheets as a Function of Size and Shape. H. L. SMITH, J. A. KIES, AND G. R. IRWIN, *Naval Research Laboratory.*—The role of stored elastic energy in the propagation of brittle fracture was investigated. Fracture strength was found to be a function of the dimensions of the test piece as well as of the material. This is in accordance with the predications of the modified Griffith theory as proposed by G. R. Irwin. Fractures were initiated in Plexiglas and cellulose acetate sheets by a bullet perforation while the specimen was under a tensile load. It was found that the initial stress required to cause complete fracture increased as the size of specimen decreased and as the ratio of width to length increased. As the initial stress was further increased, the specimen shattered or the crack split into branches. The crack length at which branching occurred was a linear function of an energy equivalent to that initially contained within an expanding geometrical figure in which similitude was maintained during the growth of the crack.

THURSDAY AFTERNOON AT 2:45

Knolls 585

(GEORGE BALDWIN presiding)

Nuclear Physics

D1. Initial Performance of the Purdue University Synchrotron.* R. O. HAXBY, H. J. HEIM, C. S. SPRAGUE, R. M. WHALEY, R. S. MATHEWS, P. C. MURRAY, C. A. TATRO, AND R. F. DONOVAN, *Purdue University.*—The Purdue synchrotron uses a ring-shaped magnet with a nominal vacuum tube radius of one meter. The machine is designed for pulsed operation with pulse rates up to 12 per second. The betatron principle is used to accelerate electrons up to 4 Mev. The betatron flux bars are designed so that injection of electrons and vacuum pumping may be done from inside the ring magnet. For synchrotron operation, a master oscillator-power amplifier system feeds a quarter-wave cavity which forms one section of the vacuum tube. This section is made of a low-loss ceramic, coated with silver, and striated to reduce eddy currents. The rest of the vacuum tube is made of ordinary porcelain. Successful operation as a betatron was achieved early this year while final tests were being made on the rf system. When the rf equipment was installed, a weak synchrotron beam was detected. The maximum energy attained so far is about 100 Mev.

* This work was supported in part by the ONR and AEC.

D2. Absorption and Scattering of γ-Rays in Water.* M. A. VAN DILLA AND G. J. HINE, *Massachusetts Institute of Technology.*—The transmission of the radium, Co^{60}, Au^{198}, and Hg^{203} γ-rays through water has been investigated under conditions which allow the separation of absorption and scattering effects. A point source and a small liquid-filled ionization chamber were placed in a steel water tank (3 feet diameter and 3½ feet high). When the water level in the tank was raised, an increase in ion current due to scattered γ-rays became apparent as the water level approached the source-chamber plane closer than 3 inches. A sharp drop in intensity was observed when the water entered the region between source and chamber (good geometry absorption), followed by an increase due to scattering as the water level rose further. Further experiments show the manner in which the relative intensity of primary and scattered γ-rays varies with the distance between source and chamber. A build-up factor is defined as the observed ion current with the water divided by the ion current in air times $\exp(-\sigma_a r)$. Close to the source ($r < 30$ cm) this function is slightly greater than unity owing to backscattered γ-rays. For larger distances it approaches zero, indicating multiple scattering processes and eventual photoelectric absorption of the scattered γ-rays. There is no indication of an equilibrium between the primary and secondary photons.

* Assisted by the joint program of the ONR and AEC.

D3. Measurements on the Relative Transmission of Beta-Particles through Geiger-Müller Counter Windows.* CHIA-HUA CHANG AND C. SHARP COOK, *Washington University.*—A method utilizing the electrostatic acceleration of beta-particles from the source of a thin lens spectrometer has been reported[1] at a previous meeting of the American Physical Society. A report of progress since that time will be made, and results obtained will be compared with results recently reported by Saxon.[2]

* Assisted by the joint program of the ONR and AEC.
[1] C. S. Cook and C. H. Chang, Phys. Rev. **79**, 244 (1950).
[2] D. Saxon, Phys. Rev. **81**, 639 (1951).

D4. The Relative Transmission of Electrons through Thin Zapon Foils.* PAUL H. OWEN AND C. SHARP COOK, *Washington University.*—Electrostatic acceleration of beta-par-

ticles[1] in a thin-lens spectrometer for the determination of their relative transmission through a G-M counter window has not been perfected for beta-particle kinetic energies below 25 kev. For studies of this low energy range, electrons have been accelerated from an electron gun, focused by a semicircular, uniform field, magnetic spectrometer and detected by a Faraday cage. A movable window assembly, placed immediately in front of the Faraday cage, has been constructed in such a way as to allow rapid insertion into or removal from the electron beam of a zapon foil. Such an arrangement has not been completely satisfactory, because of the collection of charge on the foil under certain conditions. The results will be discussed.

* Assisted by the joint program of the ONR and AEC.
[1] C. H. Chang and C. S. Cook, preceding abstract.

D5. Space-Charge-Limited and Space-Charge-Free Behavior of Diamond Crystal Counters. A. G. Chynoweth, *University of London, King's College.*—Applying alternate light flashes and electric field pulses to the crystal has enabled its behavior under a large variety of conditions to be investigated. The effect of field strength and illumination intensity on the growth and decay of the space charge field is described. From a simple picture of the electron trapping and releasing processes involved, it is predicted how the technique can be used to study the space-charge-free behavior of the counter. These predictions are verified experimentally. Preliminary studies of the effect of temperature on the counter suggest the possibility of permanently preventing the formation of space charge by keeping the temperature of the counter sufficiently high and also how information concerning the distribution of trap depths in the crystal and the lifetimes of trapped electrons could be obtained. For solid-state studies the technique has the advantage over luminescence methods in that radiationless transitions of electrons from trapping levels to ground states can be studied. Proportional response is obtained for beta-rays of energy 0.66 to 1.0 Mev, and the average energy required to liberate an electron from the lattice by the beta-rays is found to be approximately 7 ev.

D6. Response of Anthracene Scintillation Counters to High Energy Protons.* G. Guernsey, G. Mott, and B. K. Nelson, *University of Rochester.*—The resolution and pulse height variation with energy loss in anthracene have been studied for protons of energy 100–200 Mev. Protons of 200 Mev and less have been obtained by $N-P$ scattering in the external neutron beam of the U. and R. 130″ synchrocyclotron. Recoil protons have been detected by a scintillation counter telescope, the pulse height being analyzed in the last counter. The upper limit of the proton spectrum has been established as a reference point by range determinations. The lower energies have been obtained by either increasing the recoil angle or interposing copper absorbers. Preliminary results indicate that the resolution of the order of 10 percent width at half-maximum can be obtained. Data thus far obtained are consistent with proportionality between pulse height and the energy loss of protons in this range. The response to high energy protons is also being compared with that to deuterons and alpha-particles in approximately the same energy region.

* Supported by the AEC.

D7. Absolute Counting of Fast Neutrons with Anthracene Counters. W. G. Cross, *Chalk River Laboratory.*—High efficiency absolute counting of fast monoenergetic neutrons, possible with organic scintillation detectors, is complicated by the fact that the differential pulse height distribution is not rectangular (as the recoil proton energy spectrum is) but rises steeply at low energies. The pulse spectrum observed for 14-Mev neutrons (from the $T(d, n)$ α-reaction) has been explained quantitatively on the basis of (a) nonproportionality of anthracene's light output with proton energy, (b) alpha-particles from the $C^{13}(n, n)3\alpha$ and $C^{13}(n, \alpha)Be^{9}$ reactions, (c) wall losses in the crystal, and (d) small corrections for the statistical spread at the photomultiplier cathode. For crystals of various sizes, the neutron flux calculated from the part of the pulse distribution due to protons above 4 Mev, and hence above alpha-particle pulses, agrees within 5 percent with that derived from counting alpha-particles from the tritium target and assuming that they are emitted isotropically. For $D-D$ neutrons only (a) and (d) are appreciable, and the whole pulse spectrum is used to get the flux.

D8. Total Cross Sections of Light Nuclei for p, T Neutrons.* C. K. Bockelman,† H. H. Barschall, and D. W. Miller† *University of Wisconsin.*—Measurements of the energy dependence of total neutron cross sections of light nuclei were extended to higher energies by the use of the $T(p, n)$ reaction as a source of monoenergetic fast neutrons. Tritium was absorbed in a Zr film evaporated on a tungsten disk,[1] and was bombarded with protons from the electrostatic generator. Neutrons of energies up to 3.5 Mev were produced with a 20-kev energy spread. Narrow cross section peaks were observed for Be, C, and O. For Li, only a gradual rise in cross section was found. A comparison of measurements on normal B with those on enriched B^{10} gave the cross sections of B^{10} and B^{11}. For B^{10} only two broad maxima were observed, while the cross section of B^{11} shows five sharp peaks. In addition to these relatively narrow resonances, evidence was found for very broad levels in all the nuclei studied.

* Work supported by the AEC and the Wisconsin Alumni Research Foundation.
† AEC Predoctoral Fellow.
[1] A. B. Lillie and J. P. Conner, Rev. Sci. Instr. **22**, 210 (1951).

D9. Angular Distribution of Neutrons Scattered by Helium.* R. K. Adair, *University of Wisconsin.*—A proportional counter filled with helium was irradiated with monoenergetic fast neutrons produced by bombarding thin lithium targets and tritium-filled zirconium targets with protons from the electrostatic generator. Angular distributions of the neutrons scattered by helium were determined by measuring the distribution in energy of the pulses from the recoiling alpha-particles with a differential discriminator. Measurements were made for eleven different neutron energies from 400 kev to 2730 kev. The scattering of neutrons and protons from alpha-particles has been described[1] in terms of a potential leading to a $P_{3/2}-P_{1/2}$ doublet in He^{5}, split by about 5 Mev, a description which is consistent with the neutron-alpha total cross section and the proton-alpha differential cross sections. Using the same assumptions, the differential cross sections for the scattering of neutrons by alpha-particles was calculated and was found to be in qualitative agreement with the measured angular distributions.

* Work supported by the AEC and the Wisconsin Alumni Research Foundation.
[1] R. K. Adair, Phys. Rev. **82**, June 1, (1951).

D10. Recoils from High Energy Neutrons. C. E. Swartz, *University of Rochester.*—A helium-filled cloud chamber has been exposed to a collimated neutron beam from the Rochester 130″ cyclotron. Details of shielding and beam synchronization will be described. The helium recoils and disintegrations can be distinguished from background and oxygen events. The 2700 recoils are divided into three groups depending on the energy of the bombarding neutron. Angular distribution of each group shows that recoils from high energy neutrons are concentrated in angles nearly perpendicular to the beam.

FRIDAY MORNING AT 10:00

Knolls Auditorium

(M. H. HEBB presiding)

E1. The Behavior of Crystal Imperfections at High Temperatures. A. W. LAWSON, *University of Chicago.* (40 min.)

E2. Computing Metallic Cohesive Energy without the Use of Potential Functions. THOMAS KUHN, *Harvard University.* (30 min.)

E3. Crystal Growth. F. C. FRANK, *University of Bristol, England.* (40. min.)

FRIDAY MORNING AT 10:00

Knolls 441

(ARTHUR ROBERTS presiding)

Cosmic Rays and Nuclear Physics

F1. Distribution in "Size" of Cosmic-Ray Stars as a Function of Altitude and Surrounding Material. M. BIRNBAUM, F. W. O'DELL, M. M. SHAPIRO, AND B. STILLER, *Naval Research Laboratory.*—The frequency *versus* magnitude of nuclear explosions in emulsions exposed in the stratosphere was studied, using the multiplicity of "heavy" prongs (grain density >1.4 times minimum) as an index of star "size." From such distributions, together with data on hard-shower multiplicities, energy spectra are deduced. Ilford G.5 emulsions, 400μ thick, were flown at $\lambda = 57°$N at average atmospheric depths of 14 and 22 g/cm^2, surrounded by air and Pb. When the frequency of stars with prong number $\geq n$ is plotted against n, the results, like those at mountain altitudes,[1] can be represented by two straight lines which intersect at $n \simeq 7$. These lines decrease in steepness with rising altitude, as expected from the increasing mean energy of the star-producing particles. The stratosphere distribution in Pb differs inappreciably from that in air. Our "free air" curves are compared with Lord's,[2] at 15 g/cm^2, and with Bristol[3] data at 49 g/cm^2. The interpretation and application of such curves is discussed.

[1] E. P. George and A. C. Jason, Proc. Phys. Soc. (London) A, **62**, 243 (1949); N. Page, **63**, 250 (1950); G. Bernardini *et al.*, Phys. Rev. **79**, 952 (1950).
[2] J. J. Lord, Phys. Rev. **81**, 901 (1951); U. Camerini, *et al.*, Phil. Mag. **40**, 1073 (1949).

F2. Behavior in Pb Absorbers of the Nucleonic Component in the Stratosphere. MAURICE M. SHAPIRO, *Naval Research Laboratory,* AND ANDREW F. GABRYSH, *The Catholic University of America.*—The air-to-lead transition effect of the star-generating radiation in the stratosphere has been further studied with two[1] experimental arrangements, to investigate the effects of absorber geometry. In one flight (at mean pressure-altitude 2.3 cm Hg), ultrasensitive emulsions were placed vertically in a narrow aperture in Pb. The small-star frequency shows a maximum at $\simeq$28 g/cm^2. Stars with >6 prongs have a less pronounced effect. The slight initial drop previously reported for small stars is confirmed and explained. In another flight, at mean depth 2.5 cm Hg, rates of star production were measured above and below a massive Pb slab$\simeq$1 ft^2, and 2.15 cm thick.[2] The following ratios (below/above) were observed: for *all* stars, 1.74$\pm$0.16; for *small* ($\leq$6-fold) stars, 1.86$\pm$0.22; for *large* stars, 1.55$\pm$0.22. Our results showed no significant difference between vertical and horizontal plates above the lead. Dallaporta's secondary-neutron theory[3] is discussed, and an alternative hypothesis, i.e., that the transition effect at shallow depths is mainly due to *charged* secondaries (protons and/or pions) is tentatively proposed.

[1] In both the geometries differed from that in a parallel investigation by Shapiro, Birnbaum, O'Dell, and Stiller, Bull. Am. Phys. Soc. Vol. 26 No. 3, 10 (1951).
[2] Courtesy of Dr. G. Perlow, who sent this slab aloft for another experiment.
[3] Dallaporta, Merlin, and Puppi, Nuovo cimento **7**, 99 (1950).

F3. Directional Intensities of Cosmic Rays. H. W. BOEHMER AND J. E. COOLIDGE, *Pennsylvania State College.*—Measurements have been made of the directional intensities of cosmic radiation at Boulder, Colorado (lat. 40°N; long. 105° 16'W; alt. 5440 ft) using the dual counter telescope described in a previous publication.[1] The initial results presented here represent 20 days of observation in September and October of 1948. A total counting rate of 0.0135$\pm$0.00003 count/sec/steradian/cm^2 was observed for the vertical intensity; a hard component (>180 g/cm^2 of lead) of 0.00835$\pm$0.00004; a soft component (<90 g/cm^2 of lead) of 0.00429$\pm$0.00007. The variation of intensity with zenith angle was observed at 0°, 15°, 30°, 45°, 60°, and 75° and the total, soft, and hard components conformed to a simple cosine power function $I(\theta) = I(0)\cos\lambda\theta$ down to 60°. The 75° indications showed no such simple relation. The values of λ are 2.4$\pm$0.1, 1.77$\pm$0.01, and 1.90$\pm$0.04 for the soft, hard, and total components, respectively.

[1] H. W. Boehmer and J. E. Coolidge, Rev. Sci. Instr. **21**, 633–638 (1950).

F4. The Interaction of π-Mesons with Carbon Nuclei.* ANATOLE M. SHAPIRO. *Cornell University.*—π-mesons produced in targets placed in the Cornell synchrotron beam are focused by a double magnet system into a 12-in. cloud chamber. The mesons incident on the cloud chamber have an initial energy of 65$\pm$10 Mev. In an earlier experiment performed with this apparatus,[1] plates of several materials were placed in the chamber and the resulting interactions were studied. In the present experiment several improvements have been made and a more thorough investigation using carbon plates is in progress. To date 6180 traversals of $\frac{1}{4}$-in. carbon plates have been observed, and 28 stars of 0–3 prongs, 11 scatterings with angles greater than 75°, and 19 scatterings with angles between 20° and 75° have been found. After suitable corrections[1] this corresponds to 44 nuclear events and 13 diffraction scatterings between 20° and 75°. If the carbon nucleus were opaque to π-mesons with energy between 30 and 60 Mev, we would expect 57 nuclear events and 42 diffraction scatterings. These results indicate that carbon is only about (75$\pm$15) percent opaque. The cross sections for π^+ and π^- mesons are

equal within the present statistics. Further results will be presented.

* This work was performed under contract with the ONR.
[1] Camac, Corson, Littauer, Shapiro, Silverman, Wilson, and Woodward, Phys. Rev. 82, 335 (1951).

F5. A New System of Autoradiography. H. J. GOMBERG, *University of Michigan.*—A new system of autoradiography, suitable for highly accurate location of radioactive tracers in organic and inorganic materials, has been developed. To detect beta-particles from radioactive inclusions within the specimens, a one micron thick layer of sulfur sensitized silver bromide crystals is grown in a collodion film directly on the surface to be studied. The point at which the beta-particles leave the surface and enter the crystal layer can be located to within one micron. The formed layer of crystals is dense so that no particle can pass through it without interacting with the layer. From a statistical study of autoradiographs produced by calibrated iodine 131 sources, two beta-particle hits are necessary to render a grain developable. However, some beta-tracks have been observed, indicating higher sensitivity for specific beta-particle energies. Background fog has been kept low by temperature control during the formation of the crystals and chemical control of the constituents. Physical development rather than chemical development is used. Where direct chemical interactions between the surface being studied and the sensitized layer occurs, a thin inert protective layer must be used. Autoradiographs of tissue specimens and of metal alloys which can be enlarged 1500 diameters have been produced.

F6. Radio-Isotope Br^{76}. S. C. FULTZ* AND M. L. POOL, *Ohio State University.*—Selenium metal was bombarded with protons of 8.3-Mev energy. Besides established activities, an activity with half-life of 17.2 hr also was present. Decay curves for electromagnetically separated particles showed strong positron activity but no negatrons with this half-life. X-rays with this half-life were observed, and the ratio of x-rays to positrons is approximately 0.7. Absorption methods reveal that the positron spectrum appears to be complex, having end points at 1.096 and 1.645 g/cm^2 or 2.25 and 3.23 Mev, and the gamma-rays have averaged energies of 1.4 Mev and possibly another around 0.6 Mev. Comparison of the induced activities with isotopic percentages, using natural Se and Se enriched with Se^{78}, showed the 17.2-hr activity to be due to Br^{76}. The reaction is (p, n). Chemical separation confirmed that the activity is due to a Br isotope. It agrees somewhat with a 15-hr activity previously reported. An activity with a 76-day half-life also was observed. It was attributed to As^{73} obtained from Se^{76} by (p, α) reaction.

* Fellow, National Cancer Institute.

F7. On the $\gamma-\gamma$-Polarization-Polarization Correlation. J. E. MACDONALD AND D. L. FALKOFF, *University of Notre Dame.*—The theory[1] of the polarization-polarization ($P-P$) correlation of successive nuclear γ-rays showed that, unlike the directional correlation, this type of experiment could distinguish between the electric and magnetic multipole character of the γ-radiations. Later it was shown[2] that for many cases the simpler direction-polarization ($D-P$) experiment could yield the same information. However, there remained classes of $\gamma-\gamma$-sequences as e.g. magnetic dipole–electric quadrupole, electric quadrupole–magnetic dipole, magnetic dipole –magnetic dipole, for which the $D-P$ experiment could not distinguish between the several alternative schemes. We have further developed the $P-P$ theory and shown that it is possible in *all* cases to uniquely identify the electric or magnetic character of the γ-radiations provided the over-all counting efficiencies are different and known for the respective γ-rays. We have also shown that all the numerical coefficients occurring in the $P-P$ correlation function may be expressed in terms of the coefficients (calculated or observed) for the directional correlation, thus providing an internal consistency criterion for both experiments. This simplification also makes unnecessary the explicit calculation of any new combinations of matrix elements for the $P-P$ correlation.

[1] D. L. Falkoff, Phys. Rev. 73, 518 (1948).
[2] D. R. Hamilton, Phys. Rev. 74, 782 (1948).

F8. A Method of Measuring Conversion Coefficients.* THOMAS B. COOK, JR., AND S. K. HAYNES, *Vanderbilt University.*—The problem of determining conversion coefficients of isomeric transitions which are not accompanied by continuous beta-spectra involves numerous uncertainties because electron and gamma-intensities must be compared. The use of scintillation spectrometers makes possible the determination of conversion coefficients by measurements involving only electron-electron and gamma-gamma-intensity comparisons. An isotope is used for which α is known from comparison of conversion and beta-spectra and whose gamma-ray energy differs little from the energy of the gamma-ray whose conversion coefficient is being measured. By duplicating the geometry, absorbers used to remove the beta-rays, and source conditions for the two isotopes, one may assume that the distortions in the two sets of data are similar and may therefore be neglected in comparing the two sets of data. If the above conditions are satisfied, the calculation of the unknown conversion coefficient essentially involves a comparison of the areas under the two conversion lines, the heights of the Compton distributions produced by the two gamma-rays, and the known conversion coefficient. The measurement of α for the 390-kev transition in In^{113} by this method will be discussed.

* Supported by the Research Corporation and the AEC.

F9. Deuteron-Induced Reactions with a LiF Target.* FRANKLIN B. SHULL, *Washington University.*—Incomplete preliminary results have been obtained from magnetic analysis of charged particles from 10.3-Mev deuteron bombardment of LiF targets. Particles are observed at 90° from the incident beam and detected with photographic emulsions. Proton group from the $F^{19}(d, p)F^{20}$ reaction give tentative Q-values (in Mev) of 4.55, 3.86, 3.57, 2.35, 1.85, 1.43, 0.81, and 0.14. Two or more poorly-resolved groups give additional Q-values in the range 2.8 to 3.3 Mev. Four pronounced deuteron peaks correspond to Q-values of 0 and -0.48 Mev for $Li^7(d, d')Li^7$ and Q-values of 0 and -1.52 Mev for $F^{19}(d, d')F^{19}$. Additional unresolved deuteron groups seem to be present. At the time of writing this abstract, respectable numbers of tritons are being found which have approximately the energy expected if they are attributed to the $Li^7(d, t)Li^6$ and $F^{19}(d, t)F^{18}$ reactions. The triton analysis is slow and tedious, but it is hoped that definite results can be presented at the meeting.

* Supported by the joint program of the ONR and AEC.

F10. Neutrons from the Deuteron Bombardment of O^{16}.* FAY AJZENBERG, *University of Wisconsin.*—A thin tungsten oxide target was bombarded by 3.083-Mev deuterons from the Wisconsin electrostatic generator. The neutron spectrum was observed by means of Eastman NTA nuclear emulsions, 100 microns thick, mounted at 10 cm from the target, and at angles of 0°, 10°, 20°, 30°, and 90° to the beam. A total of 800 proton recoil tracks have been measured so far. These preliminary measurements indicate a level at 0.55 ± 0.02 Mev above the ground state of F^{17}. The intensities of the neutron groups as a function of angle, if interpreted on a stripping hypothesis,[1] favor $L=0$ deuterons producing the first excited state (and hence an $S_{1/2}$ state), but do not distinguish clearly between $L=1$ and $L=2$ deuterons for the ground-state transition. Mirror nuclei arguments predict that the ground state of

F^{17} should be the same as the ground state[2] of O^{17} and hence $D_{5/2}$. The present data are consistent with such an assignment.

* Supported by the AEC and the Wisconsin Alumni Research Foundation.
[1] S. T. Butler, Phys. Rev. **80**, 1095 (1950).
[2] F. Alder and F. C. Yu, Phys. Rev. **81**, 1067 (1951).

F11. Classification of Levels in N^{13}.* H. L. JACKSON† AND A. I. GALONSKY, *University of Wisconsin.*—Goldhaber and Williamson's data[1] for elastic proton scattering from C^{12} has been investigated by partial wave analysis, using Laubenstein's[2] technique. The analysis indicates that the first resonance (0.484-Mev bombarding energy) is due to an $S_{1/2}$ level in N^{13} with excitation energy $E_r=2.373$ Mev. The second resonance (1.73-Mev bombarding energy) results from a $P_{3/2}$ and a $D_{3/2}$ level with 3.503 and 3.550 Mev, respectively. The reduced widths of the $S_{1/2}$ and $D_{3/2}$ levels are comparable to the Wigner limit, but that of the $P_{3/2}$ level is much less. It is fairly certain that no other reasonable assignment explains the experimental data. Since the absolute cross section is in doubt to about ±30 percent, the interaction radius is somewhat arbitrary. Consequently, the numerical values of E_r and γ^2 may be slightly in error. However, to obtain a reasonable fit of the data, the interaction radius must be approximately $1.45(A^{\frac{1}{3}}+1^{\frac{1}{3}})\times10^{-13}$ cm. Below 1.0 Mev the experimental cross section is progressively less than that calculated. The discrepancy may result from a loss of detector efficiency at low energies.

* Work supported by AEC and Wisconsing Alumni Research Foundation.
† Kimberly-Clark Predoctoral Fellow.
[1] Goldhaber and Williamson, Phys. Rev. (to be published).
[2] R. A. Laubenstein, Ph.D. thesis, University of Wisconsin, 1950.

F12. The Systematics of Nuclear *Q*-Values. ALEX E. S. GREEN AND ROBERT B. MINOGUE, *The University of Cincinnati.*—The nuclear *Q*-values derived from nuclear energy surface may be computed simply and systematically if certain key functions of the mass number are known. The key functions associated with the semi-empirical nuclear energy surface and a far simpler modified set of key functions will be presented. A survey of experimental and computed neutron binding energies and alpha-decay energies will be presented. This survey reveals a serious breakdown of the semi-empirical surface for heavy elements. The significance of the breakdown and the nature of the true surface will be discussed.

FRIDAY AFTERNOON AT 2:00

Knolls Auditorium

(V. ROJANSKY presiding)

G1. Odd-Even Variations in Nuclear Resonances. H. HURWITZ, *Knolls Atomic Power Laboratory.* (20 min.)

G2. Photoelectric Disintegration of Nuclei. J. S. LEVINGER, *Cornell University.* (30 min.)

G3. Renormalization of Theories of Spin-Zero Particles. ABDUS SALAM AND P. T. MATTHEWS, *Institute for Advanced Study.* (30 min.)

FRIDAY AFTERNOON AT 2:00

Knolls 441

(L. APKER presiding)

Optical Properties of Solids; Thin Films; Electron Physics

H1. Infrared Properties of Tellurium.* J. J. LOFERSKI AND P. H. MILLER, JR., *University of Pennsylvania.*—The transmission of tellurium crystals (about 99.9 percent pure) in the infrared was observed, and the absorption edge was found to lie at 4.2 microns. A polished sample, 0.067 cm thick, transmits 25 percent of the incident energy in the range from 4.5 to 10 microns, in which range the transmission remains fairly constant. The same material exhibited a small photoconductivity at room temperature. For an incident energy of 10^{-4} watt and a wavelength of 2.0 microns, ΔI was $\sim3\times10^{-8}$ amp with a dark current of 15×10^{-8} amp. A signal which was three times the rms noise was still detectable at 4.0 microns. The effect of dilating the lattice by subjecting the samples to pressure and by doping them with considerable amounts of selenium will be discussed.

* Assisted by ONR.

H2. Energy Level Relationships in the Thallium Activated Potassium Chloride Phosphor. PETER D. JOHNSON AND FERD E. WILLIAMS, *General Electric Research Laboratory.*—Thallium activated potassium chloride exhibits[1] absorption bands at 1960A, 2060A, and 2460A and emission bands at 3050A and 4750A. Measurements of the intensities of the emission bands as a function of excitation wavelength and temperature elucidate the configurational relationships among the unexcited and excited states of the activator. The 4750A emission is favored by 1960A and 2060A excitation. The 3050A emission and 2460A excitation are similarly related, as indicated theoretically.[2] In addition, however, there is a tendency toward thermal equilibrium between the two emitting states which differ in energy by 0.02 ev. This effect results in the 4750A emission increasing at the expense of the 3050A emission at low temperatures. At high temperatures the decrease in efficiency of 3050A emission indicates an activation energy of 0.6 ev for radiationless de-excitation, in satisfactory agreement with 0.69 ev obtained from the intersection of the theoretical potential energy contours for the emitting and ground states. The quantitative analysis of these data, including the

identification of the excited states and the evaluation of the rate constants and transition probabilities, will be presented.

[1] R. Hilsch, Z. Physik **44**, 860 (1927); P. D. Johnson and F. E. Williams, J. Chem. Phys. **18**, 1477 (1950).
[2] F. E. Williams, Phys. Rev. **80**, 306 L (1950); J. Chem. Phys. **19**, 457 (1951).

H3. Theoretical Low Temperature Spectra of Luminescent Solids. FERD E. WILLIAMS, *General Electric Research Laboratory.*—A fundamental calculation of the absorption and emission spectra of thallium activated potassium chloride has been reported.[1] The quantum-mechanical zero point energies responsible for the broad spectral bands at low temperatures have been computed recognizing that the interaction with the lattice of the unexcited or excited activator is accurately in accord with the characteristics of a hormonic oscillator. The theoretical absorption spectrum,[2] evaluated from exact Hermite polynomial wave functions for the ground state and classical treatment of the excited state, has been confirmed experimentally.[3] The classical treatment is equivalent to the use of delta-functions. The use of Hermite polynomial wave functions for the final state is not feasible because vibrational quantum numbers between 35 and 65 are involved. Approximate wave functions have been investigated, and the importance to the spectrum determination of oscillations in extended wave functions has been demonstrated. The interpretation of the properties of luminescent centers from experimental low temperature absorption and emission spectra will be discussed in terms of principles derived from these calculations.

[1] F. E. Williams, Phys. Rev. **80**, 306 L (1950); J. Chem. Phys. **19**, 457 (1951).
[2] F. E. Williams, Phys. Rev. **82**, 281 L (1951).
[3] P. D. Johnson and F. J. Studer, Phys. Rev., to be published.

H4. Transparent Luminescent Films. F. J. STUDER, D. A. CUSANO, AND L. R. KOLLER, *General Electric Research Laboratory.*—A method has been found for depositing transparent luminescent coatings of various materials on glass, by means of vapor phase reactions at the heated glass surface. The best of these so far studied is manganese activated zinc sulfide which gives a yellow-orange luminescence. These coatings are produced by allowing a stream of zinc vapor, with a small amount of manganese chloride, to pass over a heated glass surface in an atmosphere of hydrogen sulfide. The thickness of the coatings is determined by the time the reaction is allowed to continue. These films respond to cathode rays only or to both cathode rays and ultraviolet, according to the conditions of preparation. The emission spectrum and the optical absorption coefficients of these films will be discussed. The penetration of electrons into these films has been studied by means of measurements of the voltage brightness relation under cathode-ray excitation at voltages up to 40 kv. The maximum depth of penetration is in fair agreement with the theoretical value. The shape of the curves indicates that the scattering of electrons in the films is large.

H5. Oxide Films on Sodium Surfaces. JAMES W. MOYER, *Knolls Atomic Power Laboratory.*—The rate of oxidation at a surface of sodium at room temperature has been found to depend markedly on the presence of small amounts of inert gas mixed with the oxygen. Using very pure oxygen, the rate is very low and a white layer of Na_2O is formed. With a small amount of nitrogen present, the rate is very high and colored films of oxide appear. The rate may be suddenly lowered in the latter case, however, by raising the oxygen pressure. Warming the sodium to about 90°C will restore the fast reaction rate. Some properties of the oxide films will be discussed as well as the mechanism for the oxidation.

H6. The Absorption of N_2 on W as a Function of Pressure, Temperature, and Time. J. A. BECKER AND C. D. HARTMAN, *Bell Telephone Laboratories.*—The amount of N_2 adsorbed on a clean 100 W surface held at a fixed temperature in N_2 gas for variable time, is determined by measuring the pressure rise when the W ribbon is flashed at 2300°K. The number of layers adsorbed, θ, is plotted *versus* time. For 600°K, and gas pressures less than 10^{-7} mm: θ increases linearly with time up to $\theta=0.6$; then $d\theta/dt$ decreases and approaches zero beyond $\theta=1$. The initial value of $d\theta/dt$ is proportional to the pressure. For pressures near 10^{-6} mm: θ reaches 1 in 8 seconds; then $d\theta/dt$ decreases rapidly and approaches zero when $\theta=1.7$. For pressures near 10^{-5} mm: $\theta=1$ in 4 seconds, $\theta=2$ in 60 seconds; then $d\theta/dt$ decreases rapidly toward zero. For 300°K, 3 to 4 layers can be adsorbed. From these data one can compute the probability, s, that a molecule which strikes the surface sticks to it. For $\theta<0.6$, s is about 0.3; then it decreases linearly to 0.02 near $\theta=1$; beyond this, s decreases to 0.0004 at $\theta=2$.

H7. A Mass Spectrometric Study of the Activation of Barium Oxide Cathodes.* PAUL M. STIER,† *Cornell University.*—A study of the activation of cathodes, prepared by decomposition of pure barium carbonate on platinum, has been carried out using a mass spectrometer whose ion source was similar to those of Dart[1] and Plumlee.[2] As the cathode temperature was raised, the intensity of ion peaks sensitive to cathode conditions were monitored cyclicly. The resulting CO^+ and CO_2^+ ion peaks were plotted as functions of time during cathode heating. Corrections were made for CO_2 dissociation by the ionizing electron beam, as determined by admitting CO_2 under the same operating conditions. Just prior (temperaturewise) to the carbonate breakdown and also during the rise of emission, significant quantities of CO were evolved by the cathodes. The lower temperature release is believed to be the result of outgassing from the porous $BaCO_3$ as well as partial oxidation of the binder residue. The CO evolved as the emission commences may be the result of reduction of BaO by residue carbon and amounts to nearly 10^{20} molecules/cc of BaO. Possible interpretation will be discussed.

* This paper is based on a thesis submitted in partial fulfillment of the requirements for the degree of Ph.D. in Physics at Cornell University, Ithaca, New York. It was supported in part by ONR.
† Now at the Oak Ridge National Laboratory, Oak Ridge, Tennessee.
[1] F. E. Dart, Phys. Rev. **78**, 761 (1950).
[2] R. N. Plumlee and L. P. Smith, J. Appl. Phys. **21**, 811 (1950).

H8. An Analysis of the Bioelectric Action Potentials Produced in the Lobes of Venus' Flytrap by Mechanical Stimulation. OTTO STUHLMAN, JR., *University of North Carolina.*—The slow electrical transients were subjected to dc amplification and photographically recorded from a Dumont oscillograph. Electrical contact with the epidermis of the leaf was established with nonpolarizable Ag—AgCl electrodes which terminated in microcontacts of asbestos fibers saturated with 0.7 percent KCl solution. Closure of the trap-like structure normally followed when any one or all of the spike-like trigger hairs on the inner surface of the trap were bent. This mechanical external stimulus was found to set up an electrical transient that traveled across the surface of the leaf at about 3.0 cm per second, depending on temperature and age of the leaf. The evidence tends to support the hypothesis that the complex negative action potential, about 0.05 volt at 25°C, originates at the point of mechanical stimulation and spreads as an electrical wave front over the surface of the leaf. The contour of the pulse was separable into two components: one attributed to the progressive depolarization of the cell structure, and the other to an accompanying electrolytic displacement causing the mechanical closure of the trap. The latter lagged or lead the former, depending on the relative positions of the electrodes on the surface of the leaf.

H9. Decay of Metastable Neon Atoms in the Afterglow of a Helium-Neon Discharge.* F. A. GRANT, *University of*

Maryland (Introduced by Raymond Makgan).—Using previously described techniques,[1] the decay of the population of $^3P_2$ metastable neon atoms has been measured in the afterglow of a helium-neon discharge. After the interruption of the electrical discharge, a beam of monochromatic radiation of wavelength 5945A was passed through the discharge tube, and the intensity of the transmitted radiation was measured with a photomultiplier tube. The absorption of the radiation is a measure of the population of $^3P_2$ neon atoms. Measurements have been made in the pressure range 0.1 to 2 mm of Hg using mixtures containing 5 percent to 100 percent neon.

* Supported by contract.
[1] F. A. Grant, Can. J. Research **A, 28**, 339–358 (1950).

H10. The Use of Probes to Study a Pulsed Mercury Arc Plasma.* B. T. McCLURE AND R. B. HOLT, *Harvard University.*—The short time response of conventional probes in mercury arc plasmas has been investigated. All evidence indicates that the probe response to plasma conditions attains an equilibrium value in less than a microsecond. Such probes have been used in order to observe changes in electron density, plasma potential, electron temperature, etc., in a plasma of an arc which is maintained at a low value of current and pulsed to a much higher value for 30 microseconds. Complete probe characteristics are taken by applying to the probe a 2-microsecond pulse which is adjustable in height and in phase relative to the arc pulse. The electron temperature increases gradually during the arc pulse and decreases abruptly following it. The electron density begins increasing toward the end of the 30-microsecond arc disturbance and returns to its equilibrium value some time later. Various other properties of the pulsed plasma have been noted and will be reported.

* Assisted by the ONR.

H11. Quantum Effects in the Interaction between Free Electrons and Radiofrequency Fields. CARL SHULMAN, *RCA Laboratories and Princeton University.*—The quantum nature of the exchange of energy between free electrons and electromagnetic fields implies a dispersion in energy exchange which the classical theory cannot predict. L. P. Smith[1] has shown that the standard deviation in the number of photons exchanged is proportional to the square root of the number of photons handled by an interacting electron, while the mean expected, or classical exchange, is proportional to the total number handled. This quantum dispersion was detected by observing the increase in the apparent temperature T of a high velocity beam which was allowed to interact with a strong longitudinal oscillating electric field at $\lambda = 1.25$ cm, such that the standard deviation arising from quantum processes was at least of order kT, while the mean exchange was held small by adjusting the exchange time to an integral number of cycles.

[1] L. P. Smith, Phys. Rev. **69**, 195 (1946).

FRIDAY EVENING AT 7:00

Hotel Van Curler

(J. H. VAN VLECK presiding)

Banquet of the American Physical Society

Cloud Physics. VINCENT J. SCHAEFER, *General Electric Company.*

SATURDAY MORNING AT 9:30

Union College, Chemistry Lecture Hall

(V. C. WILSON presiding)

I1. Principles of Optical Detection of Radiofrequency Resonance in Excited States and Ground States of Atoms and Ions. A. KASTLER, *Ecole Normale Superieure.* (20 min.)

I2. Optical and Radiofrequency Double Resonance. F. BITTER, *M.I.T.* (20 min.)

I3. Survey of Experimental Data on π-Mesons. ARTHUR ROBERTS, *University of Rochester.* (40 min.)

I4. Production of Neutral Mesons by Gamma-Rays. K. A. BRUECKNER, *Institute for Advanced Study.* (30 min.)

SATURDAY MORNING AT 10:00

Union College, Physics Lecture Hall

(R. N. HALL presiding)

Semi-Conductors Mostly

J1. The Specific Heat of Graphite from 13°K to 300°K. W. W. TYLER AND W. DESORBO, *Knolls Atomic Power Laboratory and General Electric Research Laboratory.*—The specific heat of high purity Acheson type graphite prepared by the National Carbon Company has been measured from 13°K to 300°K. Curves showing temperature dependence of C_p will be presented and compared with data of Nernst[1] (25.8–92.6°K), Magnus[2] (44.1–1100°K), and Jacobs and Parks[3] (93.3–

293.5°K). In the region 13–40°K the C_v data follows a $(T/\theta)^3$ dependence quite accurately in agreement with Gurney's theory.[4] The value of θ obtained is 608°K. The derived thermodynamic functions have been determined by graphical integration and tabulated at integral values of the temperature up to 300°K. $S^0_{298.16} = 1.371 \pm 0.005$ E.U. of which 0.004 E.U. is extrapolated from 13°K to 0°K assuming the third law and the T^3 dependence. Jacobs and Parks' value of 1.36 E.U. at 298.1°K had been obtained using graphical integration of their data from 90°K to 298.1°K and a T^3 extrapolation from 90°K to 0°K with the aid of Nernst's data.

[1] W. Nernst, Ann. Physik **36**, 395 (1911).
[2] A. Magnus, Ann. Physik **70**, 303 (1923).
[3] C. J. Jacobs and G. S. Parks, J. Am. Chem. Soc. **56**, 1513 (1934).
[4] R. W. Gurney, unpublished work.

J2. Resistivity of Heat-Treated Germanium between 11°K and 298°K. W. DeSorbo and W. C. Dunlap, Jr., *General Electric Research Laboratory.*—Two single crystals of germanium that had been made *P*-type by heat treatment have been studied in the temperature range between 11°K and 298°K. The samples were originally 5.3 and 5.8 ohm cm *N*-type, and were quenched in oil after having been heated in vacuum for one-half hour at 850°C. The resistivity reached a minimum at about 78°K, then rose by a factor of 1000 as the temperature was lowered to 11°K. The rise in resistivity between 78°K and 30°K was approximately exponential. An activation energy $\Delta\epsilon$ of about 0.12 ev was found from the relation $\rho = \rho_0 e^{\Delta\epsilon/kT}$. Below 30°K the resistivity change was equivalent to an activation energy of the order 0.003 ev. The activation energy 0.12 ev is considerably larger than values (~0.01) found by several authors[1,2] for impurity acceptors in germanium. We conclude that heat treatment introduces a different type of acceptor state into germanium, probably a lattice defect.

[1] G. L. Pearson and W. Shockley, Phys. Rev. **71**, 142 (1947).
[2] C. S. Hung and J. R. Gliessman, Phys. Rev. **79**, 726 (1950).

J3. Scattering by Ionized Impurities in Semiconductors. Harvey Brooks, *Harvard University.*—The fourier coefficients of the potential fluctuations in a semiconductor arising from a random distribution of ionized impurities have been obtained by two methods. The first is a modification of the Fermi-Thomas method for finite temperatures, introduced by Slater and James. The second is a Hartree self-consistent field method similar to that used by Bardeen in discussing the conductivity of the alkali metals. The two methods give the same results provided the density of impurities is substantially less than 10^{18} per cm^3 and the fluctuations are not larger than kT. The results were used to compute the electrical resistivity arising from impurity scattering. The formula agrees with that of Cornwell and Weisskopf except for the argument of the logarithmic factor, which is multiplied by $\gamma = (e^2/12\pi Kd)/(K^2/2md^2)$, where d is the mean distance between impurities. This factor is of order unity for practical cases but may be larger with both donors and acceptors present.

J4. Ionic and Electronic Conduction in Silver Sulfide. M. H. Hebb, *General Electric Research Laboratory.*—The mixed electronic and ionic conduction in silver sulfide is examined from the standpoint of Wagner's theory.[1] It is shown that the electric field in the experiments by Tubandt[2] is zero and that the ionic current there arises entirely from the gradient in chemical potential ζ. Published conductivity data together with free energies of formation are used to show that the electronic conductivity varies as $\exp B\zeta$. The coefficient B changes abruptly from e/kT for β-silver sulfide below 177°C to $e/2kT$ for the α-form above. This is attributed to the sudden freeing at the phase transition of electrons from excess silver atoms. Experiments in which ionic conduction was suppressed give potential distributions in excellent agreement with the theory.

[1] C. Wagner, Z. physik. Chem (B) **21**, 25 (1933).
[2] C. Tubandt, Handb. exp. Phys. XII/1 (1932).

J5. Electrical Conductivity of Compressed Semiconducting Powders, in Particular of Zinc Oxide. J. C. M. Brentano and Colman Goldberg,* *Northwestern University.*—The relation between conductance, time, and pressure was examined for compressed Al_2O_3 and ZnO powders. To determine the effect of moisture powders were heated in a desiccator to 130°C and handled under protective coatings. They gave the current-time dependencies previously observed.[1] After heating in high vacuum the current-time dependency disappeared, indicating removal of an otherwise stable surface film. For low pressures the conductance of ZnO increases with increased pressure. Above 2000 psi to 38000 psi it decreases, its logarithm decreasing approximately linearly with increasing pressure. The proportionality constant depends on the maximum pressure previously applied. This pressure effect is reversible. A slow time decay of conductance, extending over several hours, occurs after each sudden pressure change. This conductance behavior is determined by the contact areas of the particles increasing rapidly for small and slowly for large pressures, by the pressure dependency of activation energy (Bardeen) and by the lifting of electrons into the conduction band when lattice breaks occur. The theoretical treatment is given more fully by one of us (Goldberg) in his Doctoral dissertation (Northwestern, 1951).

* Milwaukee Gas Specialty Company Fellow.
[1] J. C. M. Brentano and D. H. Davis, Phys. Rev. **79**, 216 (1950).

J6. Effect of the Probe Metal in Locating a $p-n$ Barrier in Germanium. Frieda A. Stahl, *Sylvania Electric Products, Inc.*—In studying $p-n$ barriers in germanium, the inversion line determined by exploring with a narrow beam of light does not coincide with lines determined by probing with metal whiskers. Furthermore, the apparent location of the inversion depends upon the metal using in probing. Referred to the junction location found by a 0.1-mm light spot, all inversion locations determined by metals fall in a fixed order on the p-type side. The series thus far established, proceeding outward from this reference, is as follows: Al, phosphor bronze, W, Cu, Mo; other metals, including Ni, Pt, and Ta, are being studied. The distance between the reference junction location and the inversion location determined by a given metal appears to be proportional to the barrier width, within the limits of experimental error.

J7. The Effects of Pressure and Temperature on the Resistance of $p-n$ Junctions in Germanium.* Harry H. Hall, *University of New Hampshire,* J. Bardeen and G. L. Pearson, *Bell Telephone Laboratories.*—According to Shockley's theory,[1] the low voltage resistance, R_0 of a $p-n$ junction is proportional to $\exp(E_G/kT)$, where E_G is the energy gap. Measurements of the change with pressure of the characteristics of a junction in a single crystal of germanium indicate a change $\Delta R_0/R_0$ of 12.5 percent, corresponding to a change ΔE_G of about 3.1×10^{-3} ev, for a pressure change of 10,000 lb/in.[2] Analysis of measurements made at temperatures between 16.5°C and 20.5°C give values of E_G averaging about 0.72 ev. These values are in agreement with those obtained from the change in intrinsic resistivity with temperature and pressure.[2]

* Supported in part by the Bureau of Ordnance of the Navy.
[1] W. Shockley, Bell System Tech. J. **28**, 435 (1949).
[2] P. H. Miller and J. Taylor, Phys. Rev. **76**, 179 (1949) and Julius H. Taylor, Phys. Rev. **80**, 919 (1950).

J8. The Crystal Structure of Tetragonal Barium Titanate. Howard T. Evans, Jr., and Reina A. Hutner, *Philips Laboratories, Inc.*—A detailed crystal structure study of

tetragonal barium titanate has been carried out with diffraction intensities measured at room temperature. Integrated intensities have been measured on a single crystal 0.16×0.19 ×0.07 mm using a Weissenberg camera on which has been mounted a Geiger counter. 99 reflections ($h0l$) have been measured using MoKα radiation. The best fit of calculated and observed intensities is obtained with the atoms located in the space group $P4$ mm as follows: Ba(0, 0, 0); Ti($\frac{1}{2}$, $\frac{1}{2}$, $\frac{1}{2}$ +0.015); O_I($\frac{1}{2}$, $\frac{1}{2}$, −0.024); $2O_{II}$($\frac{1}{2}$, 0, $\frac{1}{2}$, −0.020), (0, $\frac{1}{2}$, $\frac{1}{2}$, −0.020). The Ti−O_I distances are 1.860 and 2.174A. A good approximation to the true structure consists of assuming the cubic oxygen lattice undistorted, and considering the barium and titanium ions displaced in the same direction along the z axis, the former by 0.10A, and the latter by 0.16A. Using this model, equations have been set up involving the spontaneous polarization, the local fields on each atom, the electronic polarizabilities of each atom, and the ionic polarization of the barium and titanium ions. From experimental and estimated values of these, the ionic charge of the titanium ion is determined to be about +0.4, if the barium charge is assumed to be +1.8.

J9. Kinetics of Solidification of Mercury Droplet Aggregates. DAVID TURNBULL, *General Electric Research Laboratory.*—Previous experiments[1] showed that the temperature coefficient of the solidification of stearate coated mercury droplets is in reasonable agreement with nucleation theory. However the isothermal rate constants for solidification could not be described satisfactorily in terms of the measured distribution of particle sizes. We have found that mercury droplets, ranging in diameter from 2 to 7 microns, when coated with a laurate film solidify at a conveniently measurable rate in the temperature range −117° to −120°C. Rates of solidification of the droplet aggregates were measured at various constant temperatures in the range −117 to −120°. The rates were described precisely in terms of the measured particle size distribution on the basis that the nucleation frequency, I, is proportional to the volume of the droplets. I is related to temperature, T, and the supercooling ΔT by the equation: $I = 10^{42.1} \exp[-8.0\times10^7/T(\Delta T)^2]$ cm^{-3} sec^{-1}. The measured factor $10^{42.1}$ is in fair agreement with the value 10^{46} predicted by nucleation theory.

[1] D. Turnbull, J. Chem. Phys. **18**, 768 (1950).

J10. A Direct Experimental Verification of Kelvin's Relation between Vapor Pressure and Droplet Curvature. VICTOR K. LA MER AND RUTH GRUEN, *Columbia University.*—Although Kelvin's relation (1871) predicting the increase in vapor pressure with increasing curvature is basic to colloid science; e.g. phenomena of capillarity, kinetics of phase transitions, production and stability of colloidal systems, etc., no unambiguous direct experimental confirmation has ever been obtained. Indirect tests on rate of evaporation in falling drop experiments (Woodland and Mack, J. Am. Chem. Soc. **55**, 3149 (1933)), are open to question due to the effect of surface film impurities. The quantitative acceptance of this fundamental law rests upon the thermodynamic cogency of the Gibbs-Poynting type of derivation, and the success of theories based upon it. Recently, we have extended the growth method of determining the radii of droplets in the sub-Tyndall region (see La Mer, Inn, and Wilson, J. Colloid Sci. **5**, 471 (1950), where 99 percent H_2SO_4 droplets are grown under controlled conditions over $H_2SO_4-H_2O$ master solutions) to D. O. P. (dioctyl phthalate) aerosols using toluene as the volatile growth producing component as well as oleic acid aerosols with chloroform as the volatile component. The large molecular volume of these solvents magnifies the Kelvin effect as compared to water. Excellent quantitative confirmation of the equation has been obtained by equilibrium methods.

SATURDAY MORNING AT 10:20

Union College, Electrical Engineering Lecture Hall

(J. H. VAN VLECK presiding)

Microwave Spectroscopy; Theoretical Physics

K1. A New Type of Hyperfine Structure in the NH_3 Microwave Spectrum. W. E. GOOD* AND D. K. COLES, *Westinghouse Research Laboratory*, G. R. GUNTHER-MOHR, A. L. SCHAWLOW, AND C. H. TOWNES, *Columbia University.*†—The $K=1$, $J=2$, 3, 4 and 5 lines of the inversion spectrum of $N^{14}H_3$ have been found to split into two slightly unequal components. The amount of splitting increases as J increases, representative values being 100 to 200 kc/sec. Satellites of these lines due to effects of the N^{14} quadrupole moment also split in approximately the same way. This new type of splitting is not primarily dependent on the nitrogen nucleus, since a similar splitting is observed in $N^{15}H_3$. In the cases examined closely, the weaker component of the double lines is on the low frequency side for odd J and on the high frequency side for even J, becoming more nearly equal to the stronger component for the larger values of J. No splitting of this type has been found for $K\neq1$. These observations are apparently satisfactorily explained as a new type of effect due to magnetic coupling between the protons and the molecular fields (see following abstract).

* Now at General Electric Research Laboratory.
† Work supported by the AEC.

K2. Theory of the Hyperfine Splitting of the Levels $K=1$ in NH_3. J. H. VAN VLECK, *Harvard University.*—A theoretical basis is developed for the doubling of the levels $K=1$ of ammonia observed experimentally as described in the preceding paper. The mechanism is one proposed to the writer by Professor Townes, and consists in the interaction of the spins of the protons with the off-diagonal elements of the orbital angular momentum, along with perturbations caused by molecular rotation. The K-degeneracy is lifted because the local fields at the various H nuclei differ from each other by 120° in orientation, and so do not have as much isotropy as the symmetrical top. The calculation is made by the Dirac vector model, and requires no group theory. Expressions for the splitting are complicated by the coupling of N^{14} or N^{15} to the NH_3 molecule. For large J, the splitting is approximate proportional to $2J+1$.

K3. Measurement of the Microwave Inverstion Spectrum of ND_3. R. G. NUCKOLLS, L. J. RUEGER, AND H. LYONS, *National Bureau of Standards.*—Measurement of the inversion spectrum of ND_3, previously reported[1] between 2094 and 2533 Mc, has been extended to below 1600 Mc. The main $K=J$ series of absorption lines has been identified and has its low

frequency limit at approximately 1600 Mc. This frequency is to be compared with the figure 2000 estimated by Weiss and Strandberg,[2] and 1600 estimated by Townes.[3] The apparent intensity distribution is shifted to higher J, K, values than for NH_3, as expected.

A newly designed Stark-modulation 10-ft coaxial absorption cell ($\frac{1}{4}$-in$\times\frac{5}{16}$-in. radii) was used with special wave guide transformer sections. Frequencies were read to 0.01 Mc, using a frequency multiplier system based upon the NBS 100-kc primary frequency standard, and are believed accurate to better than 0.1 Mc.

[1] Lyons, Rueger, Nuckolls, and Kessler, Phys. Rev. 81, 630 (1951).
[2] M. T. Weiss and M. W. P. Strandberg, Phys. Rev. 81, 286 (1951).
[3] C. H. Townes, private communication.

K4. Far Wing Absorption of Atmospheric Spectrum Lines. T. F. ROGERS, *Air Force Cambridge Research Laboratories.**—Certain measurements of microwave absorption lines during and immediately after the last war implied that the Van Vleck-Weisskopf equation predicts too low an absorption value, by a factor of about 5, in the line far wings. In consequence, the recent literature tends to conceive of a statistical rather than an impact, model for absorption in frequency regions remote from resonance, inasmuch as it predicts absorption values which decrease less rapidly away from resonance. Detailed consideration of recent experimental work, however, allows a reassessment of both the accuracy of the earlier measurement details and certain assumptions underlying parameter values then used in the impact equation. Absolute intensity measurement errors, multiple-line fine-structure influence, dipole moment value, and line-to-line variation in half-width values are possible sources of error. These, coupled with recent measurements over extremely wide frequency ranges, indicate that the assumed experimental-theoretical discrepancies are inconclusive, and that the Van Vleck-Weisskopf impact equation has not been shown to be invalid for atmospheric gases at pressures equal to or less than one atmosphere.

* Now at the Massachusetts Institute of Technology.

K5. Microwave Collision Diameters. J. WEBER, *U. S. Naval Ordnance Laboratory and University of Maryland.**—In the course of a microwave spectroscopy investigation of the isotopic exchange reaction betweeen ammonia and deuterium[1] the microwave collision diameters of several molecules were measured and compared with the microwave collision diameters of the corresponding isotopically substituted molecules. Results are presented and compared with what one might expect on the basis of collision broadening theory. The previously reported variation of collision diameter with mix ratio was not observed.

* Department of Electrical Engineering.
[1] J. Chem. Phys. (to be published).

K6. Radiation from Hyperfine Levels of Interstellar Hydrogen.* H. I. EWEN AND E. M. PURCELL, *Harvard University.*—The hyperfine transition in the ground state of atomic hydrogen ($\nu_H = 1420.405$ Mc/sec)[1] has been detected in galactic radiation. The hydrogen is apparently an extended source concentrated in the plane of the local galaxy. Measurements were made at a declination of $-5°$ with an antenna beam width of approximately 30°. The line as measured in the vicinity of the galactic center appears in emission with a temperature difference of $40°\pm5°$C with respect to the radiation field and with a width of approximately 80 kc. The line shows a doppler shift which can be explained by the earth's orbital motion and the motion of the solar system. Evidence that the source is extended is provided by the variation of doppler shift during the time of observation.

The apparatus, consisting essentially of a superheterodyne receiver and large horn type antenna, differs from a conventional radiometer by comparing the radiation temperature of the line with the background temperature in the same spectral region.

* Assisted by a grant from the Rumford Fund, American Academy of Arts and Sciences.
[1] A. G. Prodell and P. Kusch, Phys. Rev. 79, 1009 (1950).

K7. Interaction of Electronic States with the Rotation Spectrum.* B. V. GOKHALE, H. R. JOHNSON, M. W. P. STRANDBERG, *M.I.T.*—The rigid rotor idealization is used as a first approximation in the analysis of rotational spectra, but high resolution microwave spectroscopy has forced consideration of the interaction of vibration with rotation. In this paper, we treat the remaining interaction, that of the electronic states with rotation, theoretically, but with the result in terms of experimentally measurable quantities. The main results are two: A useful first approximation to the interaction for molecules made up of heavy nuclei is rigorously shown to be accomplished by replacing nuclear with atomic masses; the remaining fractional correction in the reciprocal moment of inertia tensor is the magnetic g gactor tensor in molecule fixed axes expressed in Bohr magneton units, $e/2mc$. As an example of the order of magnitude of this correction, we consider the molecule O=C=S. Changing from nuclear to atomic masses causes a decrease in the calculated O=C distance of 0.000158A and in the C=S of 0.000212A. Introduction of the measured $g_{bb}=g_{cc}=-0.025\pm0.002$ gives a further decrease in O=C of 0.000008A and in C=S of 0.000011A. These small quantities are frequently an order of magnitude larger than the estimated, experimental error due to the frequency measurement, although small compared to vibration interaction terms.

* This work has been supported in part by the Signal Corps, Air Materiel Command, and ONR.

K8. Diatomic Homonuclear Molecules in Magnetic Fields. NORMAN F. RAMSEY, *Harvard University.*—The hamiltonian of a $^1\Sigma$ diatomic homonuclear molecule in a magnetic field is discussed. Included in the hamiltonian are the effects of the nuclear and rotational magnetic moments interacting with the external magnetic field, magnetic shielding, molecular diamagnetism, the spin-spin magnetic interaction of the two nuclei, the interaction of the nuclear magnetic moments with the field due to the rotation of the molecule, the interaction of nuclear electric quadrupole moments, and nuclear polarizability. Perturbation theory expressions for the energy of H_2 and D_2 in the first rotational state are obtained in both strong and weak field limits. The secular equation is numerically solved for intermediate fields. Curves are given showing the theoretical dependence of the energy and the transition frequencies upon the field.

K9. A New Electric Field Design for the Molecular Beam Electric Resonance Method.* J. W. TRISCHKA, J. SWARTZ, AND R. LUCE, *Syracuse University.*—In the electric resonance method of molecular beam spectroscopy transitions are observed at radiofrequencies between the Stark levels of a single rotational state of a diatomic molecule.[1] One of the important factors contributing to broadening of the lines observed by this method is the inhomogeneity in the electric field used to produce the Stark splitting. Formerly fields uniform to 1 part in 2000 have been obtained between two condenser plates made of brass. In the present design two glass plates are coated with an almost opaque thickness of Al and separated by glass spacers. Optimum parallelism of the plates is obtained by observation of the Haidinger fringes produced when Na light is transmitted through the structure normal to the surfaces. With $\frac{1}{4}$-in. spacers and selected pieces of plate glass a field uniform to 1 part in 3500 was obtained. By making use of optical flats it should be possible to improve the uniformity by a factor of ten. Measurements on the spectra of CsF will be presented to show the effectiveness of the design.

* Supported in part by the ONR.
[1] H. K. Hughes, Phys. Rev. 72, 614 (1947).

K10. New Solutions for the Field Due to a Point Charge Moving with Uniform Velocity in a Straight Line. J. J. SMITH, *General Electric Company.*—The usual solution gives a field symmetrical with respect to the point charge. When u the velocity of the point charge equals c there should be no change in the field ahead of the charge for retarded solutions. New solutions found are given by

$$v=\frac{q}{\pi^2}\int dt_1\int_0^\infty \lambda d\lambda J_0(\lambda R)\int_0^\infty \cos\gamma[z-z_0+u(t_1-t_0)]\times\frac{\sin[c(t-t_1)(\lambda^2+\gamma^2)^{\frac{1}{2}}]d\gamma}{c(\lambda^2+\gamma^2)^{\frac{1}{2}}}.$$

If the limits for t_1 are from t_0 to t the retarded solutions for a point charge created at time $t_0<t$ is obtained. The advanced solution is obtained by a slight modification. In both cases the usual solution is obtained plus other terms. These new results do not become infinite except at the point charge itself even at the velocity of light. In the retarded case the field ahead of the charge is unchanged and a physical picture of the motion confirms the mathematics. In deriving the usual solution the limits with respect to t_1 are taken as $-\infty$ and $+\infty$ and this improper integral does not converge uniformly giving an incorrect result.

Author Index to Papers Presented at the Schenectady Meeting

Adair, R. K.—D9
Ajzenberg, Fay—F10
Baldwin, George—A2
Becker, J. A. and C. D. Hartman—H6
Birnbaum, M., F. W. O'Dell, M. M. Shapiro, and B. Stiller—F1
Bitter, F.—I2
Bockelman, C. K., H. H. Barschall, and D. W. Miller—D8
Boehmer, H. W. and J. E. Coolidge—F3
Bozorth, F. M. and J. G. Walker—C5
Brentano, J. C. M. and Colman Goldberg—J5
Brooks, Harvey—J3
Brueckner, K. A.—I4
Chang, Chia-hua and C. Sharp Cook—D3
Chynoweth, A. G.—D5
Cook, Thomas B., Jr. and S. K. Haynes—F8
Crittenden, E. C., Jr., L. O. Olsen, and R. W. Hoffman—C2
Cross, W. G.—D7
DeSorbo, W. and W. C. Dunlap, Jr.—J2
Evans, Howard T., Jr., and Reina A. Hutner—J8
Ewen, H. I. and E. M. Purcell—K6
Foster, J. S.—A3
Frank, F. C.—E3
Frank, N. H.—B3
Fultz, S. C. and M. L. Pool—F6
Gokhale, B. V., H. R. Johnson, and M. W. P. Strandberg—K7
Goldman, J. E.—C4
Gomberg, H. J.—F5
Good, W. E., D. K. Coles, G. R. Gunther-Mohr, A. L. Schawlow, and C. H. Townes—K1
Grant, F. A.—H9
Green, Alex E. S. and Robert B. Minogue—F12
Guernsey, G., G. Mott, and B. K. Nelson—D6
Hall, Harry H., J. Bardeen, and G. L. Pearson—J7
Haxby, R. O., H. J. Heim, C. S. Sprague, R. M. Whaley, R. S. Mathews, P. C. Murray, C. A. Tatro, and R. F. Donovan—D1
Hebb, M. H.—J4
Heidenreich, R. D. and E. A. Nesbitt—C6
Hurwitz, H.—G1
Jackson, H. L. and A. I. Galonsky—F11
Johnson, Peter D. and Ferd E. Williams—H2
Kastler, A.—I1
Kriessman, C. J., Jr., and T. R. McGuire—C1
Kuhn, Thomas—E2
La Mer, Victor K. and Ruth Gruen—J10
LaTorre, Richard and Waller George—C8
Lawson, A. W.—E1
Levinger, J. S.—G2
Loferski, J. J. and P. H. Miller, Jr.—H1
MacDonald, J. E. and D. L. Falkoff—F7
McClure, B. T. and R. B. Holt—H10
McEachron, K. B.—B1
Moyer, James W.—H5
Nesbitt, E. A. and R. D. Heidenreich—C7
Nottingham, W. B.—B2
Nuckolls, R. G., L. J. Rueger, and H. Lyons—K3
Owen, Paul H. and C. Sharp Cook—D4
Panofsky, W. K.—A4
Pittenger, J.—C10
Ramsey, Norman F.—K8
Roberts, Arthur—I3
Roe, Glenn M.—C9
Rogers, T. F.—K4
Salam, Abdus and P. T. Matthews—G3
Schaefer, V. J.—Friday evening
Shapiro, Anatole M.—F4
Shapiro, Maurice M. and Andrew F. Gabrysh—F2
Shull, Franklin B.—F9
Shulman, Carl—H11
Smith, H. L., J. A. Kies, and G. R. Irwin—C11
Smith, J. J.—K10
Stahl, Frieda A.—J6
Stanley, J. K., J. E. Goldman, and W. Hassel—C3
Stier, Paul M.—H7
Studer, F. J., D. A. Cusano, and L. R. Koller—H4
Stuhlman, Otto, Jr.—H8
Suits, C. G.—A1
Swartz, C. E.—D10
Trischka, J. W., J. Swartz, and R. Luce—K9
Turnbull, David—J9
Tyler, W. W. and W. DeSorbo—J1
Van Dilla, M. A. and G. J. Hine—D2
Van Vleck, J. H.—K2
Weber, J.—K5
Williams, Ferd E.—H3

Proceedings of the American Physical Society

Minutes of the Meeting at Vancouver, B. C., June 25–28, 1951

THE 308th meeting of the American Physical Society, being the 1951 summer meeting on the Pacific Coast, was held at Vancouver, British Columbia, on Monday, Tuesday, Wednesday, and Thursday, June 25–28, 1951. Two hundred persons registered; the ratio of registrants from the United States and Canada was about 5 to 3, and there were three registrants from Alaska and from England. All of the visitors were greatly impressed with both the many new buildings of the University of British Columbia and the beautiful surroundings of the Vancouver area. Special thanks goes to the local committee headed by Dr. G. M. Shrum of the University of British Columbia for the unusual arrangements which added greatly to the enjoyment of the meeting. These consisted of a tea party offered by the University at the Faculty Club on Monday afternoon, a ride on the ski lift to the top of Grouse Mountain followed by supper there on Tuesday evening, and a garden party on Wednesday afternoon at the home of Mr. and Mrs. F. Ronald Graham, friends of the University and distinguished residents of Vancouver. The hospitality of Mr. and Mrs. Graham and the opportunity to visit their beautiful home and estate adjoining the University campus were greatly appreciated.

The programme consisted of seventy-four contributed papers, five post-deadline papers, and eight invited papers, spread over three and one-half days of meetings. There was only one double session, and the meeting was outstanding for its leisurely quality. Among the many items of interest may be mentioned the invited paper of John H. Williams in which he described recent work by his colleagues at the University of Minnesota on the polarization of fast protons by scattering from helium, and the invited paper of R. G. Herb which described the historical development of the Van de Graaff electrostatic generator and recent work done with it at the University of Wisconsin. Listening between the lines, so to speak, the younger members of the Society could learn what has been known to workers with electrostatic generators for some time, namely, the great contributions that Dr. Herb has made in the development of this machine into a practical device for precision work in nuclear physics.

Errata Pertaining to Papers D8 and H13

D8, by Richard L. Moore. Instead of

$$\frac{E_0}{E_e}=\frac{3}{(a_i)^3}\left[\int_{x=1}^{x_0=\cdots}\right., \text{ etc.,}$$

read

$$\frac{E_0}{E_e}=\frac{3}{\langle(a_i)^3\rangle}\left[\int_{x=1}^{x_0=\cdots}\right., \text{ etc.}$$

H13, by Edward J. Althaus. Instead of the symbols V_0 and $V_\pm$ in lines 9 and 13, read V^0 and $V^\pm$.

PROGRAMME

MONDAY MORNING AT 10:00

Physics Building, Room 200

(A. M. CROOKER presiding)

Contributed Papers

A1. Ionization Currents and Dissociation in CF_3SF_5. MELVIN A. HARRISON AND RONALD GEBALLE, *University of Washington.*—Measurements of ionization currents in CF_3SF_5[1] have been made with plane-parallel electrodes at values of E/p from 150 to 230 volts/cm/mm. Semi-log plots of these currents against electrode separation at constant E/p do not exhibit the usual behavior. Instead they rise from an initial photoelectric value with a curvature concave downward, become linear for a distance, and eventually curve upward steeply. From slopes of the linear portions can be calculated values of α/p, Townsend's coefficient, which are of similar magnitude to those reported in other complex gases.[2] The initial rise can be attributed to dissociation which occurs in CF_3SF_5 to an unusual extent.[1] The discussion of Warren, Hopwood, and Craggs[3] supports this interpretation. Values of a dissociation coefficient, analagous to α/p, are found to be several times the latter. Ionization currents in O_2 at E/p below 50 volts/cm/mm exhibit a similar initial rise which is probably caused by attachment.[4]

[1] R. Geballe and F. S. Linn, J. Appl. Phys. **21**, 592 (1950).
[2] B. Hochberg and E. Sandberg, C. R. Acad. Sci., USSR **53**, 511 (1946).
[3] Warren, Hopwood, and Craggs, Proc. Roy. Soc. (London) **63**, 180 (1950).
[4] H. S. W. Massey, *Negative Ions* (Cambridge, 1950), second edition.

A2. Electric Field Studies Using Bentonite Suspensions. VIRGINIA P. PLATT AND RONALD GEBALLE, *University of Washington.*—The method suggested by Mueller[1] for studying electrostatic fields by utilizing the electro-optical properties of a monodisperse suspension of bentonite has been applied to two geometries. Photographs of isochromatic (lines of constant field magnitude) and isoclinic (lines of constant field direction) lines have been obtained for plane parallel electrodes as well as plane to plane on edge with various electrode separations and well conditions. For the latter electrode arrangement, off-axis fields have been measured. Checks against solutions of LaPlace's equation have been obtained for certain cases. It was found that very sharp isoclinics with complete elimination of the isochromatics could be obtained by diluting the suspension from 2 percent to 0.2 percent.

[1] Hans Mueller, J. Opt. Soc. Am. **31**, 286–291 (1941).

A3. The X-ray *K* Absorption Edges of Covalently Bonded Nickel, Iron, and Manganese. W. W. BEEMAN AND G. R. MITCHELL,* *University of Wisconsin.*—The *K* absorption edges of covalently bonded nickel in seven compounds are measured with a two-crystal spectrometer. Using Pauling's theory of the chemical bond, the shapes of the absorption edges of covalently bonded manganese,[1] iron,[2] and nickel, within approximately 20 ev of the absorption edge, are given a qualitative interpretation. It is found experimentally that prominent low energy absorption lines can be associated with $1s-4p$ transitions where the final $4p$ state is a nonbonding orbital of the metal atom.

* Now at U. S. Naval Ordnance Test Station.
[1] H. Hanson and W. W. Beeman, Phys. Rev. **76**, 118 (1949).
[2] Y. Yoshida, Sci. Pap. of the Inst. of Chem. and Phys. Res. **1015**, 272 (1941).

A4. A Theoretical Estimate of the Effect of Interstitial Atoms and Vacancies on the Elastic Coefficients of Simple Metals.* G. J. DIENES, *Atomic Energy Research Department, North American Aviation, Inc.* (Introduced by M. M. Mills).—Interstitial atoms and vacancies play an important role in the theory of solids and of radiation damage. It is difficult to separate and measure unambiguously these lattice disturbances in metals. It is suggested that measurements of changes in elastic constants may be appropriate in such investigations. An approximate theoretical treatment is given of the change in elastic constants of simple metals caused by the presence of a given small fraction of interstitial atoms and vacancies. The elastic coefficients are calculated from atomic interaction potentials using a simple exponential repulsive interaction for copper and a Morse potential function for sodium. In both cases, the presence of a small fraction of interstitials and vacancies results in large increases in the elastic coefficients, the change being proportional to the fraction of displaced atoms. Lattice vacancies alone were found to decrease the elastic coefficients, the change being essentially a bulk effect. Consequently, increases in the elastic coefficients measure primarily the fraction of interstitial atoms. It is concluded that the theoretically predicted effects should be easily observable experimentally provided thermal annealing is prevented. Changes in elastic constants, therefore, may serve as a useful tool for distinguishing between interstitial atoms and vacant lattice sites.

* This paper is based on work performed under Contract No. AT-11-1-GEN-8 for the AEC.

A5. Experimental Study of Initial Convection in Porous Media: Radioactive Instrumentation. L. E. SCHILBERG AND F. T. ROGERS, JR., *U. S. Naval Ordnance Test Station.*—The onset of convective flow in a water-sand mixture was determined simultaneously by three separate methods:[1] (a) visible motion of dye in the liquid; (b) a change in the heating rate; (c) a change in the counting rate of 0.01–0.1μc of P^{32} (as $H_3P^{32}O_4$ solution[2]) injected by a hypodermic syringe and micropipette. Screened and washed desert sand (of known flow-permeability) and tap water were contained in a 1000 ml beaker heated from below by a commercial type electric "hotplate." Thermocouples attached to a Brown "Electronik" thermograph measured temperatures at approximately 2 cm vertical intervals. Radioactive counting was accomplished by a medical-type, miniature G-M tube immersed in the sand and water mixture, attached to a scale-of-64 circuit, which recorded on a Brush recorder. Data which were obtained are discussed in the following abstract, and are there compared with present theory.

[1] F. T. Rogers, Jr., and L. E. Schilberg, J. Appl. Phys. **22**, 233 (1951).
[2] Furnished by ORNL under U.S.A.E.C. authorization No. 5849.

A6. Experimental Study of Initial Convection in Porous Media: Theory *vs* Experiment. F. T. ROGERS, JR., AND L. E. SCHILBERG, *U. S. Naval Ordnance Test Station.*—By means of the apparatus described in the preceding abstract, we have determined (mean, negative) critical thermal gradients, β_c, at the onset of convection in water in unconcolidated sands; twelve separate experiments were performed, under various conditions. For each experiment we obtained, in addition to such necessary data as flow-permeability, depth, and so on, a

heating-rate parameter, φ, defined by $T=\beta D(1-e^{-\varphi Z/D})/(1-e^{-\varphi})$, where T is temperature excess (at Z) over bottom temperature (at $Z=0$). We have also calculated β_c-values for each experiment by a recent form of the theory,[1] for comparison with experimental values. We wish to report that deviations of theoretical β_c's from observed β_e's, expressed as percents of experimental values, had, for the several methods of flow detection, the following respective average values: Visual, 150 percent, thermal, 36 percent; and radioisotopic, 11 percent.

[1] F. T. Rogers, Jr., and H. L. Morrison, Fourth Annual Heat Transfer and Fluid Dynamics Inst., Stanford University, June, 1951.

A7. Modifications to X-Ray Line Shapes due to Crystal Distortions. EUGENE P. COOPER,* *Naval Ordnance Test Station, Pasadena, California.*—In the study of the mechanism of cold-work, Warren and Averbach (*J. Appl. Phys.* **21**, 595, 1950) have used a fourier analysis of x-ray line shapes to yield the strain-distributions within cold-worked crystals (α-brass). Since the same type of x-ray line broadening has been observed for crystals (graphite), distorted by heavy particle irradiation, it is indicated that similar analytical methods might be used to study the mechanism of radiation damage. The limits of the fourier analysis method have been investigated; its validity becomes questionable in the limit of small crystal distortions. Since much smaller distortions are expected in radiation-damaged metallic crystals than in graphite, other analytical methods are necessary. Various "models" of radiation-damaged crystals have been studied; the comparison of the resulting x-ray line shapes with those of experiment may yield criteria for deciding the essential nature of radiation-damaged crystal structure, but sufficient experimental data are not yet available. The study indicates that the variation of average crystal planar spacing among the crystals of a powder sample is the most effective line-broadening distortion.

* The author did this work as consultant to North American Aviation.

A8. The Effect of Cyclotron Bombardment on Self-Diffusion in Silver.* A. B. MARTIN, R. D. JOHNSON, W. V. GOEDDEL, *Atomic Energy Research Department, North American Aviation, Inc.*—The radioactive tracer method has been used to measure the rate of self-diffusion in polycrystalline silver, and experiments have been performed to investigate the effect on this diffusion process of bombardment with 10-Mev protons from the Berkeley 60-inch cyclotron. Experimental techniques will be described and results will be presented for diffusion samples which were simultaneously irradiated in the cyclotron target box and annealed at 850°C, 800°C, and 750°C, and for control samples which were diffused at several temperatures in the range 900°C to 500°C.

* This paper is based on work performed under Contract No. AT-11-1-GEN-8 for the AEC.

A9. A Study of the Annealing Kinetics in Cold-Worked Copper.* DWAIN BOWEN, R. R. EGGLESTON, AND R. H. KROPSCHOT, *Atomic Energy Research Department, North American Aviation, Inc.*—The resoftening kinetics for cold work in copper have been studied using residual resistance as a measure of the degree of recovery. The specimens were quickly heated to the annealing temperature, held at temperature for a measured time and quenched for measurement. The assumption was made that the cold work could be characterized by a number of lattice defects n, and that these defects obeyed Matthiessen's rule. It was found that the resoftening was well represented by a single process of activation energy 24 kilocalories per mole. The difficulties that previous investigators have had in interpreting their data kinetically have been overcome by allowing reaction orders other than the first. In this case the annealing is well described by a third order reaction. $dn/dt=-vn^3e^{-E/RT}$. Some of the implications of the third-order reaction on the mechanism of resoftening, and on plastic deformation will be discussed.

* This paper is based on work performed under Contract No. AT-11-1-GEN-8 for the AEC.

A10. The Exclusion Principle and the Theory of Superconductivity.* WILLIAM BAND, *The State College of Washington.*—Consider a determinantal eigenfunction formed from any N one-particle free-electron wave function specified by a spectrum of N wave number k-vectors. We prove that the totality of such determinants formed from all conceivable spectra of N k-vectors in k-space forms a closed orthogonal set of determinantal eigenfunctions. Because of this closure theorem the antisymmetrical solution of any problem with N electrons satisfying the exclusion principle can be expressed as a linear combination of these basic determinants. It is then proved that first-order resonance energy due to lattice and phonon interaction with the assembly is proportional to the square root of the volume, $V^{\frac{1}{2}}$, for a given numerical density. The volume V over which the exclusion principle operates is restricted to a region in which the one-electron wave functions overlap. These domains may be identified at sufficiently low temperatures with the domains of phase-coherence among the zero-point Debye modes of vibration. Positive resonance energy favors coherence of the electron gas in one single assembly of maximum possible volume. Implications of this for the theory of superconductivity will be briefly discussed.

* Assisted by the ONR.

MONDAY AFTERNOON AT 2:00

Physics Building, Room 201

(GORDON F. HULL, JR. presiding)

Contributed Papers

B1. Beta-Decay of Para- and Orthotritium. B. A. JACOBSOHN, *University of Washington.*—It is possible in principle to distinguish between Gamow-Teller and Fermi selection rules by observing whether or not the nuclear spin can flip when an electron is emitted. An indirect way of observing this is to look for small interference effects in the decay of para- and orthotritium. Interactions leading to Fermi selection rules show no difference between the two. Those leading to Gamow-Teller rules show a difference between the beta-spectra of para- and equilibrium tritium which is most pronounced at low electron energies. When plotted against electron momentum, the percentage difference in the spectra resembles a damped sinusoidal function; the first three minima in the curve lie at -1.7 percent for 0.11-kv electrons, -0.6 percent for 0.68 kv and -0.3 percent for 1.7 kv, and the two intervening maxima are $+0.8$ percent and $+0.4$ percent. This is

probably much too small to be measured at present. The integrated effect on the number of He^3 nuclei produced cancels out almost completely because of the oscillation. The effect of the change in spacing and in the spring constant of the molecule because of low order rotations is shown to be negligible.

B2. The Gamma-Alpha-Reaction in Cu^{65}. R. N. H. HASLAM, L. A. SMITH, AND J. G. V. TAYLOR, *Betatron Group, University of Saskatchewan.*—Co^{61} has been produced by the (γ, α) reaction in Cu^{65} with the University of Saskatchewan betatron, and separated chemically from copper and nickel. Higher activities than previously reported have been obtained, allowing accurate determination of half-life and energy. The half-life is found to be 1.642 ± 0.003 hours, which is considerably lower than the literature values.[1-3] The β^- energy appears to be somewhat higher than the reported value of 1.3 Mev.[2] More accurate determinations will be carried out. Cross-section curves are being prepared. At corresponding energies the cross section is an order of magnitude greater than that reported by this laboratory[4] for $Rb^{77}(\gamma, \alpha)Br^{33}$.

[1] M. L. Perlman and G. Friedlander, Phys. Rev. **74**, 442 (1948).
[2] Parmley, Moyer, and Lilly, Phys. Rev. **75**, 619 (1949).
[3] H. H. Hopkins, Jr., and B. B. Cunningham, Phys. Rev. **73**, 1406 (1948).
[4] R. N. H. Haslam and H. M. Skarsgard, Phys. Rev. **81**, 479 (1951).

B3. Gamma-Neutron Cross Sections for N^{14} and O^{16}. R. J. HORSLEY, H. E. JOHNS, AND R. N. H. HASLAM, *Betatron Group, University of Saskatchewan.*—Activation curves for (γ, n) reactions in N^{14} and O^{16} have been obtained by irradiating NH_4NO_3 with x-rays from the University of Saskatchewan betatron. The two-minute oxygen activity was separated from the ten-minute nitrogen activity by an analysis of the decay curve. Cross-section curves will be presented. The nitrogen activity shows a slowly increasing initial portion from a threshold at 10.8 to a peak at 21.5 Mev.

B4. Two-Dimensional Pulse Height Presentation for Scintillation Spectrometry.* R. F. POST, *Stanford University.*—An oscillographic method has been devised for the presentation of the correlated pulse heights from coincident scintillation counts in two separate counters. The device described uses a cathode-ray tube[1] to present a cartesian plot of scintillation pulses as bright dots, the coordinates of which are proportional to the respective energies lost in the two crystals. Such a presentation, photographed, possesses features desirable for coincidence spectrometry. For example, the loci of events of constant *total* energy are diagonal lines. Utilizing this property of the plot, a two-crystal gamma-ray spectrometer[2] with high counting efficiency has been constructed. Presentation is accomplished by applying the count pulses to the x and y oscilloscope axes, respectively. A short pulse is applied to the intensifier grid, timed at the x-deflection maxima. Coincidences (within the intensifier pulse length) appear as bright dots (since dx/dt and $dy/dt \approx 0$). Near-coincidences appear as faint line segments ($dy/dt \neq 0$). The method is also being used in a pair-spectrometer to investigate pair-production by high energy electrons. Its utility for other experiments will be discussed.

* The work reported herein was performed under a con.ract between Stanford University and the ONR.
[1] H. Kallman and C. A. Ricardo, Rev. Sci. Instr. **21**, 48 (1950), seem to have been the first to use an oscilloscope for coincidence counting.
[2] R. Hofstadter and J. A. McIntyre, Phys. Rev. **78**, 619 (1950).

B5. Molded Noncrystalline Phosphors for Scintillation Counters. J. L. HORWOOD AND G. G. EICHHOLZ, *Radioactivity Division, Department of Mines and Technical Surveys, Ottawa.*—The scintillation properties of some noncrystalline phosphors have been investigated with gamma-rays from Co^{60} and RaC. The phosphors were prepared by moulding mixtures of polystyrene and anthracene, terphenyl, and other organic substances. Stable operating conditions were deduced from pulse height distribution curves for different compositions and counting volumes. The phosphors were compared with anthracene and sodium iodide crystals and liquid phosphors, and their emission spectra were obtained. No essential differences have been observed between dispersed systems and true solid solutions; however, no catalysts[1] were employed in preparing the samples. Some applications to measurements with large-area sources of low activity will be discussed.

[1] M. G. Schorr and F. L. Torney, Phys. Rev. **80**, 474 (1950).

B6. A High Resolution Coincidence Counting System.* N. S. SHIREN AND R. F. POST, *Stanford University.*—A coincidence system, having an intrinsic resolving time of 2×10^{-10} second, and developed for use with pulsed accelerators, will be described. The circuit is based on techniques originated by others.[1,2] Output pulses from two photomultiplier tubes are presented in the X and Y axes of a DuMont K-1032 cathode-ray tube. The beam spot is intensified by a pulse bracketing the accelerator pulse. The oscilloscope screen is masked except for a rectangular opening. Coincident pulses appear as loops originating from one corner of the rectangle. Diagonal spot positioning is used for pulse-height discrimination. The coincidences are observed by a 5819 photomultiplier. Single pulses cannot record as coincidences. Using thin stilbene crystals and pulsed 931A photomultipliers,[3] with delay line clipping, a resolving time of 7×10^{-10} second has been obtained, apparently limited by statistical effects in the crystals.[4] The system is being used in an investigation of pair production by high energy electrons from the Stanford 35-Mev electron linear accelerator.

*The work reported herein was performed under a contract between Stanford University and the ONR.
[1] H. Kallman and C. A. Ricardo, Rev. Sci. Instr. **21**, 48 (1950).
[2] R. Hofstadter and J. A. McIntyre, Rev. Sci. Instr. **21**, 52 (1950).
[3] R. F. Post and N. S. Shiren, Phys. Rev. **78**, 81 (1950).
[4] R. F. Post and L. I. Schiff, Phys. Rev. **80**, 1113 (1950).

B7. Total Cross Section of Copper for 30-Mev Photons. ARNE LUNDBY AND L. MARSHALL, *Institute for Nuclear Studies, The University of Chicago.*—Fifty-Mev bremsstrahlung from the University of Chicago betatron was collimated to 0.2-cm^2 area at 25 feet from the betatron target. It impinged on a 200-mg/cm^2 W radiator placed at the apex of a triangular pair spectrometer magnet. Electron and positron pairs produced by photons of 30 ± 3 Mev were detected by two scintillation counters placed to catch particles of equal energy. Pulses from the two counters were recorded in coincidence by a circuit of 2×10^{-9}-second resolution. The background count was found by inserting a delay of 4×10^{-8} second into one channel. Absorbers were put into the collimated bremsstrahlung beam at 20 feet from the target. In this way, the total cross section of copper for 30-Mev photons has been measured as $4.65 \pm 0.19 \times 10^{-24}$ cm^2. Measurements of cross sections of other elements and at other energies are in progress.

B8. Angular Correlation Functions for Large Values of Angular Momenta.* F. G. HESS, *University of British Columbia.* (Introduced by W. Opechowski).—Some angular correlation functions have been computed for the case that the first of the two successively emitted particles is a photon or an alpha-particle, and the second is a photon corresponding to a mixture of magnetic dipole and electric quadrupole. Explicit formulas, in terms of $\cos^2\theta$, have been obtained for an arbitrary value of the angular momentum L_1 carried off in the first transition on the assumption that the remaining angular momenta involved satisfy certain conditions, e.g., $J' = J + L_1$, $J = J'' + L_2$; $J' = L_1 - J$, $J = J'' + L_2$ (in Falkoff and Uhlenbeck's[1] notation).

* This work has been supported by the National Research Council of Canada.
[1] D. L. Falkoff and G.E . Uhlenbeck. Phys. Rev. **79**, 323 (1950).

B9. Energy Dependence of the Beta-Gamma-Angular Correlation in Sb^{124}. E. K. DARBY AND W. OPECHOWSKI, *University of British Columbia.**—Recently, Stevenson[1] briefly reported on his measurements of the energy dependence of the beta-gamma-correlation in Sb^{124}, in which he used a lens spectrometer. We have measured the same energy dependence using a twelve-channel kicksorter together with a thick crystal counter as a beta-detector.[2] The experimental curve representing the correlation coefficient (corresponding to coincidence counting rates at 90 and 180 degree) as a function of the energy seems to lie slightly higher than the values found by Stevenson, and to be not inconsistent with angular momenta assignments 1, 1, 0 (assuming the matrix element B_{ij} as dominant). We have also found that the integral correlation (beta-energy >1 Mev) is of the form $1-0.23\cos^2\theta$, in essential agreement with Beyster and Wiedenbeck.[3] This result was obtained using a thin crystal beta-counter, readings being taken at ten-degree intervals.

* This work has been supported by the National Research Council of Canada.
[1] D. T. Stevenson, Phys. Rev. **82**, 333A (1951).
[2] J. I. Hopkins, Rev. Sci. Instr. **22**, 29 (1951).
[3] J. R. Beyster and M. L. Wiedenbeck, Phys. Rev. **79**, 169 (1950).

B10. The Yield of the Reaction $C^{13}(p, \gamma)N^{13}(\beta^+)C^{13}$. J. D. SEAGRAVE, *Kellogg Radiation Laboratory, California Institute of Technology.**—The thick target yield of $C^{13}(p, \gamma)N^{13}$ has been studied from 0.45 to 2.5 Mev by observation of annihilation quanta associated with the positron decay of N^{13}. After bombardment by a fixed charge in a time short compared with the N^{13} half-life, the graphite targets were removed from vacuum, enclosed in aluminum, and placed directly over a NaI crystal and photomultiplier. The activity produced was counted with less than 1 percent random error. Only the two resonances previously reported were found. For the upper resonance[1] we find the values $E_R=1.70\pm0.008$ Mev, $\Gamma=70\pm5$ kev. The maximum thick target yield of the upper resonance is 1.45 ± 0.03 times that of the resonance at 0.45 Mev. No other resonances of intensity >2 percent appear below 2.1 Mev, or >15 percent between 2.1 and 2.5 Mev. A possible weak resonance near 2.3 Mev could not be confirmed. A measurement of the absolute yield was made with the aid of a single-channel differential analyzer, by comparison of the annihilation radiation from the N^{13} source with that from a Na^{22} source of known strength, with the result $7.7\pm0.7\times10^{-10}$ N^{13}/proton, at $E_p=1.00$ Mev, in agreement with a previous report.[2]

* Assisted by the joint program of the ONR and AEC.
[1] D. M. Van Patter, Phys. Rev. **76**, 1264 (1949).
[2] W. A. Fowler and C. C. Lauritsen, Phys. Rev. **76**, 314 (1949).

B11. Masses of Light Nuclei from Nuclear Disintegration Energies.* C. W. LI, WARD WHALING, W. A. FOWLER, AND C. C. LAURITSEN, *Kellogg Radiation Laboratory, California Institute of Technology.*—The recent accumulation of nuclear disintegration energy values makes it possible for the first time to derive the masses of light nuclei directly in terms of O^{16}, without recourse to mass spectrographic results. The masses are overdetermined by the experimental data, and some adjustment procedure must be used to determine unique mass values. The many cyclic conditions relating the overdetermined masses are used as a basis for this adjustment. Four fundamental mass differences have been calculated:

$$n-H^1 = 0.7824\pm0.001 \text{ Mev},$$
$$n_3+H^1-H^2 = 2.225\pm0.002 \text{ Mev},$$
$$2H-H^1-H^3 = 4.032\pm0.004 \text{ Mev},$$
$$2H^2-He^4 = 23.833\pm0.007 \text{ Mev}.$$

By means of these mass differences, the experimental Q-values have been adjusted by an approximate least-squares procedure to yield a numerically consistent set of adjusted Q-values and hence the values of masses. Several important atomic masses are, in amu,

$$n = 1.008\ 982\ (\pm3),$$
$$H^1 = 1.008\ 141\ (\pm3),$$
$$H^2 = 2.014\ 734\ (\pm6),$$
$$He^4 = 4.003\ 872\ (\pm15),$$
$$C^{12} = 12.003\ 803\ (\pm17).$$

Values for the 31 atomic masses from n' to F^{20} will be given. There are some discrepancies between these mass values and the most recent mass spectrographic results.

* Assisted by the joint program of the ONR and AEC.

Invited Paper

B12. The NRX Pile at Chalk River in Operation for Physics Research. W. B. LEWIS, *National Research Council, Chalk River.* (30 min.)

MONDAY AFTERNOON AT 2:00

Physics Building, Room 200

(F. A. JENKINS presiding)

Contributed Papers

C1. Ion Production by Resonance Irradiation of Hg Vapor in N_2. J. A. BERBERET AND K. C. CLARK, *University of Washington.*—Additional studies are reported on the mercury ions[1] formed in Hg vapor in the presence of N_2 by the core of the Hg resonance line $\lambda2537$. The ion current, which is proportional to the square of $\lambda2537$ intensity, is a volume effect. With extremely pure N_2 a saturation current of several hundred microamperes can be produced. In addition to the collection of ions, observations were made of the relative population of metastable Hg 6^3P_0 atoms by means of the reversal of $\lambda4047$, using various N_2 pressures up to 55 mm and the pulsed operation of either the $\lambda2537$ source or the collection voltage. By comparison of the decay rate of the ion current with that of the 6^3P_0 population, it is shown that the suggested ion formation processes involving only atoms[2] are improbable. Evidence is presented that collisions involving excited molecules of mercury[3] predominate in the ionization.

[1] W. Steubing, Physik. Z. **10**, 787 (1909). G. Giddings and G. Rouse, Proc. Natl. Acad. Sci. U. S. **12**, 447 (1926).
[2] F. Houtermans, Z. Physik. **41**, 619 (1927). F. Arnot and M. M'Even, Proc. Roy. Soc. (London) **A165**, 133 (1938).
[3] Lord Rayleigh, Proc. Roy. Soc. (London) **A114**, 620 (1927). S. Mrozowski, Revs. Modern Phys. **16**, 153 (1944).

C2. The Effect of a Magnetic Field upon the Lifetime of the Active Nitrogen Afterglow. W. R. KANE AND K. C. CLARK, *University of Washington.*—According to the theory of Mitra,[1,2] nitrogen ions, and not metastable atoms or molecules, are the carriers of energy in the Lewis-Rayleigh active nitrogen afterglow. As a test, a magnetic field was used to impede the diffusion of ions to the wall of a long glass tube of 4-inch diameter, in which decay occurred chiefly at the wall. The afterglow was produced by a disruptive electrodeless discharge, which was cut off just before the magnetic field was turned on. The decay of the afterglow intensity was recorded photographically by means of a 1P22 photomultiplier tube and oscilloscope. Decay times of the order of 0.07 second were observed at a pressure of 0.017 mm. A total of 95 runs was made, with the field alternately on and off. A field of 850 gauss was found to reduce the decay rate by 2.9±0.5 percent. This effect is approximately that redicted on the basis of kinetic theory and helps to substantiate the Mitra theory.

[1] S. K. Mitra, *Active Nitrogen—A New Theory* (Indian Assoc. Advancement Sci., Calcutta, 1945).
[2] S. K. Mitra, Phys. Rev. **74**, 1637 (1948).

C3. White Mountain Research Station. CHARLES L. D'OOGE, *U. S. Naval Ordnance Test Station* (Introduced by F. T. Rogers, Jr.).—In the autumn of 1948 a high altitude observatory was established at 10,600 feet in the White Mountains of California in response to suggestions of scientists in California. Two and one-half years of continuous operation have proved the accessibility and usefulness of the site. A description of the location, weather, and facilities is presented with a general comparison to other mountain stations in the country. Weather observations (including those for three winter seasons) show that the White Mountain Research Station enjoys the distinction of being the driest, most clement mountain station available. Temperatures for the period of operation have ranged from 75° to −19°F (with winter means of 17° to 28°F and a summer mean of about 45°F), relative humidity averages 50 percent, yearly precipitation averages about 11 inches, and the winter season's snowfall ranges from 138″ the first winter to 43″ the past winter. Clear and partly cloudy days outnumber cloudy days about three times. The location on a plateau area from 10,000 to 14,242 feet in elevation has proved ideal for investigations of cosmic radiation, solar and sky radiation, light of the night sky, sky brightness, and meteorological phenomena.

C4. Atmospheric Absorption of Solar Infrared Radiation. ROMUALD ANTHONY, *U. S. Naval Ordnance Test Station, Inyokern.*—Some observations of solar infrared radiation from 1.5μ to 20μ were made from Table Mountain, California. After correction for slit width and dispersion, the recorded deflections for given wavelengths between 7.4μ and 19μ were plotted to determine the absorption coefficient, α_ν, from the equation $I_\nu = I_{\nu 0} \exp(-\alpha_\nu e)$ as well as the shape of the curve. The coefficient α_ν was then plotted against frequency in cm^{-1}. In the region $\nu = 1150$ to 800 cm^{-1}, this curve was found to lie below the values obtained from Elsasser's[1] approximation. Comparison of $I_{\nu 0}$ in the above equation with the form of experimental curve of infrared solar radiation obtained at 37,000 feet altitude showed a marked difference.

[1] W. M. Elsasser, Phys. Rev. **53**, 768 (1938).

C5. On the (OI) Airglow in the Night Sky.* EDWARD V. ASHBURN AND DOROTHY DAVIS LOCANTHI, *U. S. Naval Ordnance Test Station, Inyokern.*—Photoelectric observations of the forbidden oxygen line at 5577A for one night are discussed. In general, each point in the sky has a pronounced maximum in intensity shortly after midnight. The sky was relatively brightest toward the southeast during midnight and relatively brightest toward the north after midnight. The height and movement of the apparent bright patches are discussed.

* The project was supported by a research grant from the ONR Project NR-082-045.

C6. Photoelectric Measurements of the Red and Green Auroral Lines. C. DAHLSTROM, D. HUNTEN, AND W. PETRIE, *University of Saskatchewan.*—Equipment consisting of a 1P21 photomultiplier tube, an ac amplifier, and an Esterline-Angus recorder have been used to measure the intensities of the forbidden OI lines at 5577, 6300, 6364 angstroms in auroral displays. The three radiations are fed into the photomultiplier through the use of interference filters, or, alternatively, a three-prism spectrograph. The results to date indicate that in steady displays the three energy levels involved are in a state of equilibrium, and an analysis of the intensities suggests that the excitation mechanism is not collisional in nature. Some other mechanism such as dissociative recombination must be operating.

C7. Spectrographic Survey of the Night Sky at College, Alaska.* L. HERMAN† AND H. LEINBACH, *University of Alaska.*—A spectroscopic survey of the night sky beginning in late November, 1950, reveals no time at which auroral phenomena is totally absent and that at times visual observation shows no evidence of the aurora. Characteristic auroral emissions are present at all times and can be photographed on moonlit and cloudy nights. Thus, auroral activity could be followed in all weather.

* The research reported in this paper has been made possible through the support and sponsorship extended by the Geophysical Research Directorate of the Air Force Cambridge Research Laboratories under contract AF 19(122)-431.
† On leave from the University of Paris.

C8. Absolute Absorption of O_2 in the Vacuum Ultraviolet. G. L. WEISSLER* AND PO LEE, *University of Southern California.*—Absorption coefficients of radiation between 300 and 1300A were measured in O_2, using photometric techniques with a constant intensity line emission source. Lambert's exponential law of absorption was shown to be obeyed for the O_2 pressures used. The coefficients near 1300A were less than 10 cm^{-1}. No strong continuous absorption was found in the region between 1300A and 740A. However, the bands in this range showed strong absorption, of the order of 500 cm^{-1} to 800 cm^{-1}. The strong continuous absorption below 740A had a maximum coefficient of $k = 900$ cm^{-1} at about 450A and showed still a $k = 530$ cm^{-1} at 303A. This continuum was interpreted as composed of the ionization continua of several Rydbert series converging to the excited states of the molecular ion, such as $O_2^+ b\ ^4\Sigma^- \leftarrow O_2 X\ ^3\Sigma_g^-$. An estimate of the integrated absorption coefficients was made and an approximate f-value of six was found in agreement with predictions from dispersion data. The k-values for 76 wavelengths will be presented.

* The aid of ONR is gratefully acknowledged.

C9. Isotope Shift in the Atomic Spectrum of Oxygen.* JOHN R. HOLMES AND LEE W. PARKER, *University of Southern California.*—Isotope shift has been measured in some of the visible and infrared lines of a mixture of O^{16} with about 20 percent O^{18} (kindly given by A. O. Nier). A mixture of about 5 mm of helium and 0.5 mm of oxygen was excited in an electrodeless quartz discharge tube immersed in liquid nitrogen. The oxygen lines emitted from this source were strong compared with the band background and intense enough to be conveniently photographed through a Fabry-Perot interferometer in series with a large prism spectrograph. The patterns were sufficiently sharp for the component due to O^{18} to be resolved clearly in several lines. Microdensitometer traces were taken of some lines, from which the isotope shift

was measured by fitting the positions of the peaks to a second degree interpolation equation, while for lines which were very close to adjacent lines the isotope shift was measured on a micrometer. The results are as follows:

Wavelength	Transition	Isotope shift
8820.45A	$3s'^1D_2^0-3p'^1F_3$	$+0.1088 \pm 0.001$ cm^{-1}
8221.84	$3s'^3D_3^0-3p'^3D_{3,2}$	$+0.0830 \pm 0.0015$
8232.99	$3s'^3D_1^0-3p'^3D_1$	$+0.08305 \pm 0.002$.

These lines occur in the displaced (^3D) system. In fifteen lines of the normal (^1S) system occurring as transitions between quintet levels no isotope shift was found.

* Work supported by the ONR.

C10. Electron Drift Velocities at Low X/p. W. N. ENGLISH,* *Chalk River Laboratory.*—Electron drift velocities have been measured as a function of electric field divided by pressure in the range 0.05 to 0.5 volt per cm per mm Hg. A plane parallel electron pulse chamber (with grid) was used, with collimated alpha-particle source mounted on the cathode. Electron drift velocity within 10 percent is obtained from the known length of alpha-track divided by the rise time of the pulse measured with a fast amplifier and oscilloscope. Data have been obtained for argon plus CO_2, 1 percent to 20 percent, and cp tank methane. Results in argon$-CO_2$ agree with Rossi and Staub. The methane gives the surprisingly high value of 8 cm/μsec at $X/p=0.5$, compared with 4.5 cm/μsec for the fastest argon$-CO_2$ mixture. Preliminary measurements in hydrogen agree with the published results of Bradbury and Nielson. A study of electron pulse amplitude *vs* X/p is also being made to obtain information on electron attachment to impurity atoms in free-electron gases.

* Now at Pacific Naval Laboratory, Esquimalt, B. C.

Invited Paper

C11. The Geophysical Institute, A Center for Research in the Arctic. WILLIAM S. WILSON, *University of Alaska.* (30 min.)

TUESDAY MORNING AT 9:00

Physics Building, Room 200

(S. E. MADDIGAN presiding)

Contributed Papers

D1. Mistuning Contributes to Tone Quality. EDWARD M. LITTLE, *University of Alaska.*—It is generally believed that the quality of a musical tone is determined by the strength of its harmonics. The quality is really not affected by the pitch vibrato on theater organs or the volume tremulant on concert and church organs. However, organists have known for hundreds of years that two ranks of pipes mistuned about .1 semitone with respect to each other—the celeste effect—add subtle warmth to the tone quality of chords, quite unlike the effect of vibrato or tremulo in which all tones vary synchronously. This explains why the quality of a chorus is much better than that of a quartet; the unavoidable differences in frequencies cause beats whose frequencies are roughly proportional to the frequencies of the notes, producing a delightful scintillation of tone quality, as all the notes of a chord beat at their own different rates. Experiments have been performed to find the optimum mistuning for each note of a diad. This may be demonstrated on a ukulele. This is to be extended to triads (chords), and also more than 2 notes beating. In the world's largest organ in the Wanamaker store, one celeste stop has 10 ranks of pipes!

D2. Emission of Electrical Influence. F. W. WARBURTON, *University of Redlands.*—Expansion of the coulomb electrical energy of two charges e' and e in terms of the time of propagation from e' to e together with a factor assumed to represent the manner in which e receives the emission from e', yields electric and magnetic potential energy, $W=ee'[1/r+(\mathbf{u}\cdot\mathbf{r})^2/2c^2r^3-\mathbf{g}\cdot\mathbf{r}/2c^2r+\cdots]$, where $\mathbf{u}$ is the relative velocity and $\mathbf{g}$ the relative acceleration of e' and e. The average negative gradient of this potential energy yields the reciprocal force discussed earlier.[1] This is one of the many formulas which correctly express the behavior of electric circuits and which have the advantage over standard theory of expressing the induced electric field of accelerated charges explicitly. Besides accounting for gyromagnetism by recognition of magnetic potential energy, and suggesting a stable electron, this energy formula provides description of energy transfer associated with accelerating an electron.

[1] F. W. Warburton, Phys. Rev. **69**, 40 (1946); **72**, 747 (1947).

D3. Phenomena Associated with the Flight of Ultra-Speed Pellets.* Part I: Ballistics. WILLIAM A. ALLEN, JOHN S. RINEHART, AND W. C. WHITE, *U. S. Naval Ordnance Test Station, Inyokern.*—Small metallic pellets have been fired at velocities up to 6 km/sec by means of modified shaped charges. Previous work in this field has been confined largely to observations of meteors and conventional shaped charges. Data obtained on ballistic phenomena verify the conventional drag force determinations extrapolated to large Mach numbers. Steel pellets at a velocity of 2.5 km/sec lose little mass in flight. Pellets composed of lighter metals, such as aluminum at a velocity of 5.0 km/sec, burn vigorously with the emission of much light and heat. It has been found that the motion of both non-burning and burning pellets can be represented within experimental error by the empirical equation, $v=v_0e^{-\alpha s}$, where v_0 is the initial velocity of the pellet, v is its velocity after it has traveled a distance s through the air and α is a constant.

* Work supported by Armament Branch, ONR.

D4. Phenomena Associated with the Flight of Ultra-Speed Pellets.* Part II: Spectral Character of Luminosity. W. C. WHITE, JOHN S. RINEHART, AND WILLIAM A. ALLEN, *U. S. Naval Ordnance Test Station, Inyokern.*—The spectroscopic character of the luminous trails generated by ultra-speed pellets has been investigated. A total of seven spectrograms have been measured and reduced. Three of these were of 5.0 km/sec aluminum pellets; two were of 5.9 km/sec magnesium pellets; one was of a 6.0 km/sec magnesium-aluminum-lithium pellet and one was of a titanium pellet whose velocity

was estimated at about 4.5 km/sec. The most pronounced features of the spectrograms are: (1) AlO bands in the aluminum spectra, (2) Mg lines and MgO bands in the magnesium spectra, (3) strong Li lines and a pronounced continuum in the magnesium-lithium-aluminum spectra and (4) TiO bands in the titanium spectra. Other features of the spectra are: (1) prominent Al I lines at λλ3944 and 2961 and a relatively weak continuum in the aluminum spectra, (2) a stronger continuum in the magnesium spectra and (3), relatively weak MgO bands in the Mg-Li spectra. The time resolved spectra show that the AlO persists in the excited state twice as long as the aluminum. The aluminum oxidizes almost completely leaving AlO in an excited state which continues to emit light after the aluminum is burned.

* Work supported by Armament Branch, ONR.

D5. Phenomena Associated with the Flight of Ultra-Speed Pellets.* Part III: General Character of Luminosity. JOHN S. RINEHART, WILLIAM A. ALLEN, AND W. C. WHITE, *U. S. Naval Ordnance Test Station, Inyokern.*—Ultra-speed pellets of the lighter metals such as aluminum and magnesium have intensely luminous trails associated with their flight through the air. A pronounced characteristic of the luminous trails is the *intermittent* manner in which the luminosity is generated. This effect has also been observed in meteors[1] and in studies of conventional shaped charges.[2] The brilliant flashes of light appear to be associated with the ablation and subsequent burning of material from the pellet. There is considerable evidence that the material is removed from the pellet in the form of small droplets. Luminous shock waves are also observed but this source of light contributes little to the total. Stereoscopic photographs indicate that the pellet may follow a more or less sinusoidal path or spiral through the air. Flashing seems to be associated with the maximum amplitude of the motion.

* Work supported by Armament Branch, ONR.
[1] W. W. Zimmerman and C. R. Hammond, Contr. Soc. Research Meteorites **2**, 2, 73 (1939); Harvard Coll. Obs. and Center of Analysis of M.I.T. Tech. Rept. **3**, 22 (1949).
[2] J. S. Rinehard, Rev. Sci. Instr. **21**, 939 (1950).

D6. Viscosity, Molecular Shape and Microwave Absorption in Solution. P. L. MCGEER, G. B. RATHMANN, A. J. CURTIS, AND C. P. SMYTH, *Princeton University.*—Measurements of dielectric constant and loss at wavelengths of 1, 3, and 10 cm over a temperature range from 4 to 60° have been carried out upon dilute solutions of polar molecules in *n*-heptane and a viscous paraffin oil. An almost thousand-fold variation in viscosity was achieved with the two solvents over the temperature range investigated. The change in relaxation time for the dipole orientation process over this viscosity range reached a maximum of only 15-fold for the long tetradecyl bromide molecule and was much smaller for the nearly spherical molecules of *t*-butyl chloride and methyl chloroform, which could rotate with little or no displacement of the surrounding solvent molecules. The relaxation times of the large and unsymmetrical molecules of α-chloronaphthalene and tetradecyl bromide are more affected by viscosity, because the orientation of their dipoles requires the displacement of the surrounding solvent molecules. A distribution of relaxation times was observed in these solutions, greater for the more viscous solvent. Possible reasons for the distribution would be orientation of the molecules by rotation about different axes, orientation of molecular segments, and thermal fluctuations.

D7. Studies of Thin Films by Electron Diffraction. N. R. MUKHERJEE AND OLIVER ROW, *Engineering Experiment Station, University of Washington* (Introduced by Professor C. L. Utterback).—Thin films of metals were prepared by evaporation on soluble plastic. Assuming that the entire sample was evaporated into a spherical space, the thickness of the film was calculated by inverse square law from the knowledge of the quantity of metal evaporated in each case. The substrate was dissolved and samples made out of free metallic films were studied with the electron diffraction camera. In all cases it is found that an optimum thickness exists at which a transmission diffraction pattern of any metal shows a greater number of rings, sharper rings and a better contrast between the rings and the background. The optimum thickness of the film appears to be an inverse function of density of the substance.

D8. Energy Loss of Shock Waves to Cloud Water Droplets. RICHARD L. MOORE,* *Sandia Corp. and Armed Forces Special Weapons Project.*—The break-up and subsequent evaporation of water droplets by a shock wave removes energy from the shock. At a certain radius (R_e) from the center of a spherical wave the radius (a_e) of the largest droplet remaining after passage of the shock front is just equal to the radius of the largest drop which can be evaporated by the shock. a_i is the initial radius of the droplet; $f(a_i)$ is the initial[1] frequency distribution of a_i. The assumptions involved will be stated and development will be made of the ratio of the energy lost outside R_e to that lost inside, which is:

$$\frac{E_0}{E_e}=\frac{3}{(a_i)^3}\left[\int_{x=1}^{x=1}x^2\left(\int_{a_i=0}^{a_ix^{-1}}(a_i)^3f(a_i)da_i\right.\right.$$
$$+\int_{a_ix^{-1}}^{a_ix^{2.9}}(a_i)^3\left(1-\left(1-\left(\frac{a^3}{a_i}\right)^2x^{-1}\right)^{\frac{1}{2}}\right)f(a_i)da_i$$
$$\left.\left.+\int_{a_ix^{2.9}}^{\infty}(a_i)^3(1-(1-x^{-0.9})^{\frac{1}{2}})f(a_i)da_i\right)dx\right].$$

The results** will be given as a function of the limits of $x=R/R_e$; of a_e; and of $f(a_i)$ in four types of clouds.

* Major, USAF.
[1] H. J. aufm Kampe, J. Meteorol. **7**, 54 (1950).
** Numerical evaluation of integrals completed by Test Data Division of Sandia Corporation.

D9. Analysis and Behavior of Some Magnetic Amplifier Circuits. HOWARD A. WILCOX, *Naval Ordnance Test Station, Inyokern.*—The magnetic amplifier is a set of saturable reactors in combination with an alternating power source whose function is to deliver either direct or alternating current to a load in the power circuit under the control of a small direct current in the control circuit. As such it becomes a direct coupled current amplifier capable of high gain, low drift, extreme ruggedness and reliability, and high over-all power efficiency. Many different magnetic amplifier circuits are known. Principles of approximate circuit analysis will be presented, together with the analyses of four basic magnetic amplifier circuits, namely the series and parallel connected circuits, with and without feedback. A detailed comparison between the analytical predictions and actual performances of the circuits will be given.

D10. Sources of Energy Degradation and Side Thrust in Laval Rocket Nozzles. A. B. C. ANDERSON AND H. W. WEDAA, *U. S. Naval Ordnance Test Station* (Introduced by F. T. Rogers, Jr.).—Results of an experimental survey of the effect of the placement of obstructions in the input side of a Laval nozzle on side-thrust and energy degradation are reported. Work was carried out using a 2-dimensional nozzle and nitrogen. Extremely small differential pressures between opposite sides of the nozzle were produced by the presence of huge unsymmetrical obstructions. Energy degradation in the gas flow, here, is measured by the departure of the experimentally observed pressure distribution from the theoretical, adiabatic; isentropic pressure distribution. Degradation due to wall friction is manifested, on the subsonic side, by a drop in the pressure distribution, on the supersonic side, by a rise in the pressure distribution with respect to the theoretical distribution. Physically, this degradation may be interpreted in terms

of the formation of a boundary layer. Results indicate that even a thick boundary layer on the subsonic side of the nozzle is squeezed to practically zero at the throat. A new boundary layer downstream of the throat appears to begin at the throat. Degradation due to the presence of the obstacles in the flow appears to be surprisingly small. Only when the flow channel created by the obstacle becomes smaller than the nozzle throat does the degradation become quite appreciable. This appears to be due to the creation of shock waves between the obstruction and the nozzle throat.

Invited Paper

D11. The Scattering of Light Nuclei. JOHN H. WILLIAMS, *University of Minnesota.* (30 min.)

TUESDAY AFTERNOON AT 2:00

Physics Building, Room 200

(G. M. SHRUM presiding)

Contributed Papers

E1. Li^7 Nuclear Electric Quadrupole Interaction in Crystalline $LiAl(SiO_3)_2$.* D. W. SMELLIE† AND H. E. PETCH,‡ *University of British Columbia* (Introduced by G. M. Volkoff).—Using an oscillating detector, the splitting of the nuclear magnetic resonance absorption line due to electric quadrupole coupling[1] has been observed for the Li^7 resonance in a single crystal of spodumene ($LiAl(SiO_3)_2$). The dependence of this splitting on the angle between the magnetic field and the *b*-axis has been measured in a plane perpendicular to the *c*-axis of the monoclinic structure. A discussion of the experimental results and their theoretical interpretation will be presented.

* Work supported by the National Research Council of Canada.
† Holder of a National Research Council Bursary.
‡ Holder of a Fellowship from the Research Council of Ontario.
[1] R. V. Pound, Phys. Rev. **79**, 685 (1950).

E2. Nuclear Spin of Selenium 77. SUMNER P. DAVIS AND F. A. JENKINS, *University of California, Berkeley.*—Previous evidence on the spin of Se^{77} is conflicting, hyperfine structure indicating $I>5/2$ and microwave spectra $I=1/2$. In order to decide the question, alternating intensities in the rotational structure of the ultraviolet bands of Se_2^{77} have been investigated. The source was a radiofrequency discharge in a small quartz tube containing a rare gas and a few milligrams of enriched selenium. This source is capable of yielding a band spectrum with as little as 2 μgm of the nonmetallic elements. High dispersion spectrograms have been obtained of 58.4 percent Se^{77}, and a detailed analysis of the 10.4 and 10.5 bands made. The Se_2^{77} bands show a pronounced intensity alternation, with the lines of odd *K* stronger. Overlapping by lines because of other species, principally $Se^{77}Se^{80}$, prevents an accurate measurement of the alternation ratio, but it appears to be large enough to exclude the higher value of *I*. Through the cooperation of the Oak Ridge laboratory, a sample containing 91.8 percent of Se^{77} is now available. By its use, it will probably be possible to give a definitive result at the time this paper is presented.

E3. The Neighboring Mirror Nuclei Ne^{11} and Na^{21}. GLEN E. SCHRANK AND J. REGINALD RICHARDSON, *University of California at Los Angeles.**—Ne^{19} and Na^{21} are neighboring mirror nuclei with a considerable difference in their *ft* values. A more detailed examination of their positron spectra and lifetimes seemed to be desirable. The presence of gamma-radiations[1] in the 1.5-Mev energy range from Na^{21} has been verified by the use of a NaI crystal gamma-ray spectrometer. The Ne^{19} isotope was produced by the (p, n) reaction on fluorine (BaF). The Na^{21} was produced by the (p, α) reaction on magnesium. The positron spectra were examined in a 180° beta-ray spectrometer and the upper limits were determined from Kurie plots. The results indicate an upper limit of 2.16 Mev for Ne^{19} and 2.50 Mev for Na^{21} with an uncertainty of one percent. There is evidence for the presence of a lower energy positron group in Na^{21}. The lifetimes obtained are 18.5 seconds for Ne^{19} and 22.8 seconds for Na^{21}. The difference in *ft* values for these two nuclei would therefore appear to be real, and not the result of experimental inaccuracies.

* This work was supported in part by the joint program of the ONR and AEC.
[1] E. Pollard and W. W. Watson, Phys. Rev. **58**, 12 (1940).

E4. The Radiations from K^{38}. DAVID GREEN AND J. REGINALD RICHARDSON, *University of California at Los Angeles.**—A large beta-ray spectrometer of the double lens type has been used to investigate the radiations from K^{38}. The isotope[1] under investigation was formed by the bombardment of KI with 18-Mev protons. The reaction involved is (p, pn). Because of the short lifetime for K^{38}, small crystals of KI are bombarded directly and then mounted on Nylon foils for measurement in the spectrometer. The purity of the activity is demonstrated by its measured time variation which gives a straight line when plotted in the usual way over a time corresponding to six half-lives. The half-life obtained is 7.7 minutes. The Kurie plot of the upper part of the positron spectrum yields an upper energy limit of 2.8 Mev. The gamma-radiation from this isotope is also being investigated.

* This work was supported in part by the joint program of the ONR and AEC.
[1] Ramsey, Meem, and Mitchell, Phys. Rev. **72**, 639 (1947).

E5. Use of the Rosenblum Spark Counter for Alpha-Counting. G. G. EICHHOLZ, *Radioactivity Division, Department of Mines and Technical Surveys, Ottawa.*—The properties of a simple spark counter of the Rosenblum type similar to that of Payne[1] and Connor[2] has been investigated. The system proved both rugged and reliable and for a collimated polonium source specific ionization curves were obtained which showed no more straggling than a shallow ionization chamber. The voltage characteristics of the counter differed somewhat from those of Connor. An interesting property of these counters is the effect of self-stabilization due to the corona discharge. Results of measurements on various radioactive powders will be discussed and the relative efficiency of these counters compared with other alpha-particle detectors.

[1] R. M. Payne, J. Sci. Instr. **26**, 321 (1949).
[2] R. D. Connor, Proc. Phys. Soc. (London) B. **64**, 30 (1951).

E6. Disintegration of 70-Day Ir^{193}. W. W. SCHOOP* AND R. D. HILL, *University of Illinois.*†—The internal conversion electron spectrum of long-lived Ir^{192} has been investigated previously by Levy,[1] Cork[2] and Hill and Meyerhof.[3] Using a 180° variable field spectrometer with a resolution of approximately 2 percent, we have identified gamma-ray lines of the following energies: 137, 208, 295, 308, 317, 469, 488, 592, 607, and 615 kev. In attempting to construct a level scheme of the gamma-ray emitting Pt^{193} nucleus, we have measured the intensities of the above transitions. From the electron spectrum, the relative total conversion electron intensities are, respectively: 7.5, 10, 35, 30, 100, 25, 2.0, 2.5, 2.5, 4.0. From the photo-electron spectrum, the gamma-ray intensities are, respectively: 45, 5, 35, 15, 100, 75, <10, <15, 20, 20. Although a number of energetically possible level schemes, which give rise to all gamma-rays, can be constructed, it is still impossible on the basis of the above intensity values to decide on a unique level scheme. Either a decomposition of the partial beta-ray spectra of Ir^{193} or an investigation of coincident transitions appears to be further required.

* Now at Boeing Airplane Company, Seattle, Washington.
† Assisted in part by the joint program of the ONR and AEC.
[1] P. W. Levy, Phys. Rev. **72**, 352 (1947).
[2] J. M. Cork, Phys. Rev. **72**, 581 (1947).
[3] R. D. Hill and W. E. Meyerhof, Phys. Rev. **73**, 812 (1948).

E7. The Solution of X-ray Activation Curves for Photonuclear Cross Sections. A. G. W. CAMERON AND L. KATZ, *University of Saskatchewan.*—Johns *et al.*[1] have recently published graphs of the Schiff bremsstrahlung intensity in the forward direction as functions of the photon and betatron energies, normalized to 100 roentgens measured in Lucite. They used these curves to calculate a number of (γ, n) cross-section curves from the corresponding x-ray activation curves. A modification of this method is proposed which is based on the photon differences between successive Schiff bremsstrahlung curves and the first derivative of an activation curve. It is required that the first and second derivatives be smooth; this requirement has been empirically justified. Tables of suitable computational functions have been prepared. The activation curves measured in this laboratory have been reanalyzed by this "photon difference" method, and the resulting curves were found in good agreement with those originally calculated. The new method avoids the necessity for arbitrary progressive smoothing of a cross section curve during computation, and effects a large reduction in the time required for such a calculation.

[1] Johns, Katz, Douglas, and Haslam, Phys. Rev. **80**, 1062 (1950).

E8. Photonuclear Cross Sections in Aluminum and Magnesium. L. KATZ AND A. G. W. CAMERON, *University of Saskatchewan.*—Activation curves for the reactions $Al^{27}(\gamma, n)Al^{26}$, $Mg^{24}(\gamma, n)Mg^{23}$, and $Mg^{26}(\gamma, p)Na^{25}$ have been measured using "swing" and "dropping" techniques for the rapid transfer of a sample from the betatron irradiation position to a counter. Absolute ordinates were determined by comparison to the known $Cu^{63}(\gamma, n)Cu^{62}$ activity at 22 Mev, and the corresponding cross sections were computed by the "photon difference" method.[1] The cross-section curves exhibited "resonance" peaks characteristic of photonuclear reactions. Preliminary values for the peak energies, peak cross sections, widths at half-maximum, and integrated cross sections of these curves are

$Al^{27}(\gamma, n)Al^{26}$	19.2 Mev	0.0082 barn	4.7 Mev	0.045 Mev-barn
$Mg^{24}(\gamma, n)Mg^{23}$	19.4	0.0111	5.8	0.064
$Mg^{26}(\gamma, p)Na^{25}$	22.6	0.0218	3.3	0.096

The (γ, p) cross section is larger than those of (γ, n) reactions in this part of the periodic table, and the peak is at a higher energy. This suggests that high energy photons interact primarily with nuclear protons. We hope to report also the cross section curve for the reaction $Mg^{25}(\gamma, p)Na^{24}$.

[1] See preceding abstract, E7.

E9. Photoneutron Cross Sections for the Reactions $Mo^{92}(\gamma, n)Mo^{91}$ and $Mo^{93}(\gamma, n)^{91}$. R. MONTALBETTI AND L. KATZ, *University of Saskatchewan.*—Samples of molybdenum were irradiated in the betatron x-ray beam and the resulting 15.5-min (isomeric state) and 65-sec (ground-state) activities in Mo^{91} studied. The threshold for the reaction leading to the isomeric state was found to be 13.2±0.2 Mev and that of the ground state 0.1±0.1 Mev lower. This casts some doubt on the decay energies of Mo^{91} and Mo^{91*} as published by Hanson *et al.*[1] Cross sections for each of the above reactions as a function of energy were obtained by analyzing the yield curves by the photon difference method.[2] They exhibited the usual "resonance" shape peaking at 18.7 Mev. Normalization against $Cu^{63}(\gamma, n)Cu^{62}$ activity at 23 Mev gave a peak cross section of 0.030 barn for $Mo^{92}(\gamma, n)Mo^{91}$ (65 sec) and 0.145 barn for $Mo^{92}(\gamma, n)Mo^{91*}$ (15.5 min). The integrated cross sections for these reactions are 0.18 Mev-barn and 0.87 Mev-barn respectively. The ratio of the 65-sec to the 15.5-min cross sections remained quite constant above 15.5 Mev. Below this energy the ratio increased rapidly, becoming very large as the threshold for the 15.5-min activity was approached.

[1] Hanson, Duffield, Knight, Diven, and Palevsky, Phys. Rev. **76** 578 (1948).
[2] Cameron and Katz, see accompanying abstract, E7.

E10. Mercury Isotopes Produced in Gold by High Energy Protons. J. H. MOON* AND A. L. THOMPSON, *McGill University.*—The internal proton beam of the 82-in. McGill synchrocyclotron has been used to bombard gold foils. The mercury isotopes produced were separated and investigated in a thin lens beta-ray spectrometer. The gold and platinum daughter activities were used to identify the mercury isotopes as Hg 196, 195, 193, 192, 191 which appeared successively as the proton energy was increased. No indication of Hg 194 was found. All the mercury isotopes investigated decayed by *K*-capture with the emission of many, highly internally-converted, low energy γ-rays. The following information was obtained:

Isotope	Hg 195	Hg 913	Hg 192	Hg 191	Au 191
Half-life	38.0 hr	14.5 and 29.0 hr	8.4 hr	12.4 hr	18.0 hr
Proton energy	35 Mev	55 Mev	65–80 Mev	70–80 Mev	···

Threshold energies are approximately 10 Mev below those given above which give abundant yields.

* Present address: Pacific Naval Laboratory, Esquimalt, B. C.

Invited Paper

E11. Research With the 37″ Cyclotron at UCLA. J. R. RICHARDSON, *University of California, Los Angeles.* (30 min.)

WEDNESDAY MORNING AT 9:00

Physics Building, Room 200

(H. GRAYSON-SMITH presiding)

Contributed Papers

F1. The Decay Scheme of Fe^{59}. K. C. MANN AND G. H. HANSON, *University of British Columbia.**—The beta- and gamma-radiations of Fe^{59} prepared by an (n, γ) process have been investigated, using a thin lens beta-ray spectrometer. In agreement with previous work,[1] two gamma-rays of approximately equal intensity were found with energies of 1.10 and 1.29 Mev, respectively. One beta-group of Mev maximum energy 0.45 Mev was found, but there was no evidence of the 0.26-Mev group previously reported.[1] A high energy (1.75 Mev) beta-group was present, but was identified as a P^{32} impurity. Neither gamma-transition showed any internal conversion. Coincidence measurements in this laboratory indicated that the gamma-rays are not in cascade. An expected 0.19-Mev gamma-ray was not detectable with the relatively high Geiger window cut-off energy and the uranium converter used, but work is continuing. The log (ft) value for the 0.45-Mev beta-transition was calculated to be 6.5, so that the transition is probably first forbidden, although the Fermi plot was straight. A tentative decay scheme is proposed.

* This work is supported by the National Research Council of Canada.
[1] M. Deutsch *et al.*, Phys. Rev. 62, 3 (1942).

F2. The Positron Spectrum from μ-Mesons. HARMON W. HUBBARD, *University of California, Berkeley.**—The electrostatically deflected proton beam from the 184-inch Berkeley cyclotron was used to produce a π^+ meson beam.[1] The beam is brought outside the "cove" shielding through a port by means of an electromagnet. A cloud chamber in a magnet producing a field of 8000 gauss is placed in the beam. Some of the mesons stop in carbon plates situated in the cloud chamber. The decay positrons, to which the stopped π^+ mesons give rise, are subjected to measurement. Examination of the tracks, which is now in progress, indicates the spectrum to have a maximum at about 35 Mev. A careful study is being made of the shape of the spectrum near the maximum positron energy, in view of its theoretical importance.[2]

* This work was performed under the auspices of the AEC.
[1] Richman, Skinner, Merritt, and Youtz, Phys. Rev. 80, 800 (1950).
[2] T. Tiomno and J. A. Wheeler, Revs. Modern Phys. 21, 144 (1949).

F3. Elastic Scattering of 31.8-Mev Protons from Helium. BRUCE CORK, *University of California, Berkeley.**—Measurements have been made of the elastic scattering of 31.8-Mev protons from helium at one atmosphere. The large solid angle geometry used for proton-proton scattering[1] was used to detect the forward scattered protons. Six different increments of angle have been observed from 17° to 62° in the center-of-mass system. A plot of the differential cross section and a comparison with Rutherford scattering will be given. It is planned to detect the forward scattered α-particles and thus obtain a more complete measurement of the differential cross section.

* This work was performed under the auspices of the AEC.
[1] Cork, Johnston, and Richman, Phys. Rev. 79, No. 1, 71–80 (1950).

F4. The Ratio of the Masses of the Positive π- and μ-Mesons. WILSON M. POWELL, *University of California, Berkeley.**—Photographs of the decay of π^+ mesons into μ^+ mesons were obtained in a cloud chamber with a magnetic field of 8200 gauss. If the meson beam is allowed to spray the top and bottom of the chamber, then occasionally very slow mesons scatter down or up into the gas of the chamber, and in a few cases π^+ mesons have been observed to come to rest before decaying. An error of 2.6 percent in the momentum of the μ^+ meson from a stopped π^+ meson gives a one percent error in the ratio of the masses. The same order of precision is possible if the π^+ meson is moving very slowly. By selecting only slowly moving π^+ mesons, individual measurements have a probable error of around three electron masses, and the value of the ratio of the masses agrees well within experimental error with that obtained by other methods.[1,2]

* This work was done under the auspices of the AEC.
[1] H. Bradner, U.C.R.L. 486 gives a summary.
[2] Smith, Barkas, Bishop, Bradner, and Gardner, Phys. Rev. 78, 86 (1950).

F5. $C^{14}-N^{14}$ β-Decay. W. FUTTERMAN, *University of Southern California* (Introduced by E. Gerjuoy).—Theoretical lifetimes and shapes of the $C^{14}-N^{14}$ β-decay spectrum have been calculated by well-known methods,[1] assuming the parities of the ground states of C^{14} and N^{14} are different.[2] This assumption, in conflict with the usual shell model assignments, makes the transition first forbidden. The calculated lifetimes for scalar, vector, tensor, and axial interactions: $\tau_{1S}=5.35\times10^{9}$ sec, $\tau_{1A}=8.19\times10^{9}$, with τ_{1V} and τ_{1T} too much smaller than the experimental value $\tau=2.16\times10^{11}$ to warrant further consideration. If the matrix of α is assumed ≈0, without attempt at explanation, then $\tau_{1V}=4.83\times10^{8}$, $\tau_{1T}=7.44\times10^{8}$. These theoretical lifetimes are consistent with observation, assuming about 10 percent $^1S_1$ in the ground state of N^{14}, a percentage consistent with the magnetic moment.[2] When the observed spectrum[3] is plotted on a corrected Fermi plot corresponding to any of these four lifetimes, the deviation from linearity is small but probably significant. Possible mechanisms which may reduce the value of the matrix element of α will be discussed.

[1] E. Greuling, Phys. Rev. 61, 568 (1942).
[2] E. Gerjuoy, Phys. Rev. 81, 62 (1951).
[3] S. D. Warshaw, Phys. Rev. 80, 111 (1950).

F6. Precision Analysis of Gamma-Ray Spectra from High Energy Proton Collisions with Nuclei. KENNETH M. CROWE, WOLFGANG K. H. PANOFSKY, ROBERT H. PHILLIPS, AND DARCY WALKER, *University of California, Berkeley.**—The gamma-ray spectra of the type measured by Bjorklund, Crandall, Moyer, and York[1] have been remeasured with the multiple channel[2] pair spectrometer previously described. The rate of data collection has been improved by the addition of a 196 coincidence pair computer. The results of these spectra, incorporation of the order of 10^5 pairs, are as follows: (1) The gamma-ray spectra from carbon and from wolfram are indistinguishable. This contradicts the results of earlier experiments which indicate that the difference in internal momenta between heavy and light elements materially affects the meson spectrum. (2) Comparison between 0° and 180° spectra makes an analysis of the spectrum into a pure π^0 effect impossible. It rather indicates that a mechanism other than bremsstrahlung and π^0 decay exists which contributes to the spectrum near 100 Mev. It is suggested that this mechanism might be production of π-mesons in one nucleon and reabsorption in another.

* This work was performed under the auspices of the AEC.
[1] Bjorklund, Crandall, Moyer, and York, Phys. Rev. 77, 213–218 (1950).
Aamodt, Hadley, and Panofsky, Phys. Rev. 81 565 (1951).

F7. Interpretation of (d, n) Angular Distributions.* W. HECKROTTE AND L. SCHECTER, *University of California, Berkeley.*—A continuation of the work[1] on the angular distribution of neutrons which result from bombardment by 20-Mev deuterons from the 60-inch cyclotron at Berkeley is in progress. Assignment of parities and possible spin values to the final states of the product nuclei has been extended to include the reactions $C^{12}(d, n)N^{13}$, $Co^{59}(d, n)Ni^{60}$, and $Au^{197}(d, n)^{198}$ on the basis of Butler's analysis.[2] For the $C^{13}(d, n)N^{14}$ reaction, the experimental method allows the detection of the neutrons which result from the formation of the ground state of N^{14}. On this basis, the assignment of odd parity and possible spin values of spin values of $\frac{1}{2}$, $\frac{3}{2}$ are made. This is in agreement with the shell model prediction of a $P_{\frac{1}{2}}$ state Similar information will be reported concerning the other reactions.

* This work was performed under the auspices of the AEC.
[1] Reported on at the Washington Meeting of the American Physical Society, April 26–28, 1951.
[2] S. T. Butler, Phys. Rev. **80**, 1095 (1950).

F8. A Search for an Excited He^4 Level.* J. BENVENISTE AND BRUCE CORK, *University of California, Berkeley.*—Evidence for the existence of an excited state of He^4 has been presented.[1] In this laboratory the proton linear accelerator has been used in a search for an excited level by the method of inelastic scattering of 31-Mev protons from He^4 nuclei. Laboratory angles of 30°, 45°, and 60° have been investigated by means of a telescope consisting of two gas counters in coincidence followed by an anticoincidence counter. A differential range analysis of the spectrum of scattered particles shows the elastically scattered protons and α-particles with good resolution. In addition, a third peak is observed which can, at present, here be explained as deuterons from the reaction $He^4(pd)He^3$. This peak has a differential cross section of approximately 8×10^{-27} cm² at 45° in the laboratory system. An upper limit for the differential cross section at 45° for the reaction $He^4(pp')He^{4*}$ (if it exists at all) is 3×10^{-27} cm². further investigations of particles scattered from He^4 are being made by differential energy analysis in a NaI(Ti) crystals.

* This work was performed under the auspices of the AEC.
[1] Argo, Gittings, Hemmendinger, Jarvis, and Taschek, Phys. Rev. **78**, 691 (1950).

F9. The Contribution of Protons to the Positive Excess of Cosmic Ray Particles at 3.4 Kilometers.* D. S. POTTER, GERALD GARRISON, CHARLES E. MILLER, WAYNE SANDSTROM, AND JAY TODD, JR., *Applied Physics Laboratory,† University of Washington.*—Momentum measurements were made of charged particles stopping in 15 and 30 cm of lead absorber placed under a magnetic cloud chamber. Event selection was accomplished by means of a suitable arrangement of coincidence and anticoincidence Geiger tubes. Such selection permits the separation of mesons from protons at momenta exceeding 500 Mev/c for the following two reasons: (1) the difference in the range-momentum relationships for protons and mesons in the momentum interval from 500 Mev/c to 1250 Mev/c, and (2) the nuclear interactions suffered by protons at momenta in excess of 1250 Mev/c. The proton intensities found from this spectrum are just sufficient to account for the difference between the positive and negative particle intensities for momenta less than 1000 Mev/c. At higher momenta, the proton intensity amounts to about half the difference. Thus, the positive excess at momenta less than 1000 Mev/c, obtained by this laboratory in an earlier investigation, can be completely accounted for by protons.

* Assisted by the joint program of the ONR and AEC.
† A Division of the Department of Physics.

F10. A Ten-Atmosphere Expansion Cloud Chamber with Thin Windows.* J. DEPANGHER, *University of California, Berkeley.*—The space available for the formation of tracks is a cylindrical volume of diameter 12 inches and height 2.5 inches. A $\frac{3}{4}$-inch thick Lucite cylinder backed by a $\frac{5}{16}$-inch thick perforated stainless steel cylinder make up the side wall. The perforation pattern is a compromise between strength and transparency, the latter being adequate for uniform illumination of the chamber interior as demonstrated by model tests. For photographing tracks from above, a Herculite glass cover plate is employed with diameter $13\frac{1}{2}$ inches and thickness $1\frac{1}{4}$ inches. Adiabatic expansion is achieved by a pantograph[1] operated Lucite piston and two expansion valves[2] which dump the gas into two expansion vessels. The entrance window is a box 16 inches long, closed at both ends by Be–Cu curved foils of 2 and 5 mil thickness. A second window is provided on the opposite side of the cloud chamber to minimize backscattering.

* This work was done under the auspices of the AEC.
[1] W. M. Powell, Rev. Sci. Instr. **20**, 403 (1949).
[2] The valves, though rectangular, are similar in principle to the valve described in the paper by R. P. Shutt and W. L. Whitmore, Rev. Sci. Instr. **21**, 643 (1950).

Invited Paper

F11. Energy Levels of Some Light Nuclei. R. G. HERB, *University of Wisconsin.* (30 min.)

WEDNESDAY AFTERNOON AT 2:00

Physics Building, Room 200

(C. C. LAURITSEN presiding)

Invited Papers

G1. Problems in the Understanding of the Semiconducting Properties of Germanium. W. H. BRATTAIN, *Bell Telephone Laboratories.* (30 min.)

G2. The Properties of $p-n$ Junctions in Germanium. G. L. PEARSON, *Bell Telephone Laboratories.* (30 min.)

G3. Physics Research in Europe. GORDON F. HULL, JR., *Office of Naval Research and Dartmouth College.* (30 min.)

THURSDAY MORNING AT 9:00

Physics Building, Room 200

(J. E. HENDERSON presiding)

Contributed Papers

H1. Meson Mass Ratio and Energetics of Meson Decay.* WALLACE BIRNBAUM, FRANCES M. SMITH, AND WALTER H. BARKAS, *University of California, Berkeley.*—The π/μ-meson mass ratio is being determined with new geometry, using similar range *vs* momentum relations as were employed in the measurement of the π-meson to proton mass ratio.[1] The π- and μ-mesons from the target were selected magnetically to enter the emulsion with approximately equal velocities. Two distinct range distributions corresponding to two distinct masses were found. The dispersion observed is in agreement with range straggling theory. Present statistics give the value for the π/μ-mass ratio as 1.317 ± 0.004. The absolute momentum, p_0, of the μ's from decay of π's stopping in the emulsion is also determined by comparison with μ's from the target which have momenta within a few percent of p_0. For this purpose, the absolute value of the magnetic field intensity of the 184-inch cyclotron has been mapped (using a nuclear flux meter) over the orbit of the mesons. Preliminary results give a value of 29.86 ± 0.06 Mev/C. From the above two basic results, and setting the mass of the "neutrino" involved in the $\pi-\mu$-decay equal to zero, we obtain: $\pi-\mu$-mass difference $=66.46\pm0.16M_0$, π-mass $=276.1\pm2.3M_0$, μ-mass $=209.6\pm2.4M_0$, as absolute values with no reference to the proton mass. The μ kinetic energy associated with $p_0=4.085\pm0.044$ Mev.

* This work was performed under the auspices of the AEC.

[1] Barkas, Smith, and Gardner, Phys. Rev. **82**, 102 (1951).

H2. Čerenkov Radiation from Protons and the Measurement of Proton Velocity and Kinetic Energy.* R. L. MATHER, *University of California, Berkeley.*—High velocity protons ($\beta=0.68$) from the electrically deflected external beam of the 184-inch cyclotron were sent through materials of high index of refraction, and light was detected photographically with the intensity and angular distribution characteristic of Čerenkov radiation as predicted by Frank and Tamm. By removing the effects of chromatic dispersion with a suitable prism, the angular intensity distribution was reduced to a bell-shaped distribution about the predicted angle with a standard deviation of around fourteen minutes of arc. The possibility that the angular distribution of Čerenkov radiation could be used as an absolute measure of the velocity of the proton, and hence its energy, has been exploited; and a device has been developed for this measurement. The resolution of the instrument is ±3.5 Mev, and the various effects which lower the resolution seem well understood. A nonconservative estimate of the accuracy with which the mean energy of the 340-Mev proton beam has been measured is ±0.8 Mev.

* This work was performed under the auspices of the AEC.

H3. An Analysis of the Self-Energy Problem for the Free Resting Electron. F. A. KAEMPFFER AND P. N. DAYKIN, *University of British Columbia.*—The self-energy of the free resting electron is calculated without the restriction that the radiation field of the electron be a purely retarded field. Both the one-electron theory and the hole theory of the positron are treated. It is shown that in the one-electron theory the normally quadratically divergent transverse part of the self-energy vanishes if the radiation field is assumed to be one-half retarded plus one-half advanced field, the remaining coulomb part of the self-energy being only linearly divergent. A similar theorem does not hold for the hole theory. A particular type of radiation field discussed by Stueckelberg leads to a vanishing self-energy in the one-electron theory. However, this does not solve the self-energy problem, as in this case radiation corrections for scattering will vanish as well.

H4. On the Feasibility of an Experiment to Observe the Exchange Effect in Positron-electron Scattering. J. R. H. DEMPSTER, *University of British Columbia.*—An estimate is made of the feasibility of a positron-electron scattering experiment to observe the exchange effect described by Bhabha on the basis of the hole theory of positrons. Such an experiment would be of particular interest, since it would afford a direct confirmation of the hole theory. The necessary calculations were carried out by Feynman's methods, with results in agreement (up to a factor 2) with those given by Bhabha. The results indicate that a successful experiment should be possible with careful technique. Suggestions are made regarding the best type of measurement at various energies.

H5. Nonlinear Meson Theories of Nuclear Forces. L. I. SCHIFF, *Stanford University.*—In earlier reports,[1] a qualitative account was given of nuclear saturation and the independent-nucleon model in terms of a nonlinear meson theory of nuclear forces. The nonlinearity was previously introduced into the free meson field, and was equivalent to a point contact repulsion between mesons. In place of this, the nonlinearity can be introduced into the coupling between mesons and nucleons, and then is equivalent to a suppression of meson emission and absorption by nucleons when mesons are already present. The latter formulation is in some respects simpler, since the source-free meson theory can be quantized in the usual way. Also, the classical field equation is readily solved outside the source region. Qualitatively, the two formulations are similar and lead to analogous predictions concerning physical phenomena. A quantitative comparison will be presented.

[1] L. I. Schiff, Phys. Rev. **80**, 137 (1950); Bull. Am. Phys. Soc. **26**, No. 3, 48 (1951), abstract WA5.

H6. Effect of Nuclear Symmetry on Dipole Transitions in Light Nuclei. L. E. H. TRAINOR, *University of Minnesota.*—The effect of nuclear symmetry on dipole transitions in light nuclei has been investigated using the independent particle model and Wigner's theory of the symmetric hamiltonian. On this model symmetry selection rules operate in addition to the usual selection rules to reduce the amount of nuclear dipole radiation. A detailed study has been made of the He^4 nucleus. The lowest excited state $^1P_1$ (completely symmetric) has zero-transition dipole moment to the ground $^1S_0$ state on this model, and the strong 21.6-Mev dipole transition observed[1,2] when protons are captured by tritium is due to the higher (symmetric on only three particles) $^1P_1$ level. Thus, the theory predicts an excited bound state of the He^4 nucleus. To explain the angular distribution of the gamma-rays, spin-orbit and tensory forces were introduced. Limitations of the model used, and extension of the symmetry selection rule to more general assumptions will be discussed.

[1] Argo, Gittings, Hemmendinger, Jarvis, and Taschek, Phys. Rev. **78**, 691 (1950).

[2] Jarvis, Hemmendinger, Argo, and Taschek, Phys. Rev. **79**, 929 (1950).

H7. Absorption of Extensive Showers by Water.* PAUL H. BARRETT,† *University of California, Berkeley.*—Decoherence curves were measured on the surface and under various depths (up to 10 m) of water at Lake Sabrina, California (2765 m elevation). Coincidence circuits were arranged to detect the presence of multiple cores in extensive showers. Results indicate that if multiple cores exist, they must have a lateral separation of less than 50 cm. Evidence is obtained that shows the photon distribution near the core to be more sharply peaked than the electron distribution. A theoretical calculation which assumes identical electron and photon distribution functions predicts the decoherence curves underwater to be obtained by a scale change from the decoherence curve with no absorber. The results of this calculation do not agree with experiment. The density and number spectra of extensive showers are calculated for this elevation.

* Assisted by the joint program of the ONR and AEC.
† AEC Predoctoral Fellow.

H8. Further Cloud Chamber Observation of *V*-Particles.* W. B. FRETTER, *University of California, Berkeley.*—Observation of *V*-particles has continued in a cloud chamber containing lead plates but without a magnetic field.[1] The total number observed to date is 36 uncharged and 8 charged particles. One of the uncharged particles disintegrates into a proton and a meson, the particles being identified only roughly by range, scattering, and ionization. Assuming a two-particle decay, some information can be obtained by considering the angular distribution of the product particles. It is not yet clear whether all events can be attributed to the decay of a particle slightly heavier than a proton, or whether another lighter *V*-particle may be involved. In some cases the presence of a third decay particle may be necessary, since the plane of the product particle does not line up with the original event. One picture shows evidence that one of the decay products of the charged *V*-particle is a neutron.

* Assisted by the joint program of the ONR and AEC.
[1] W. B. Fretter, Bull. Am. Phys. Soc. **26**, No. 1, 7 (1951).

H9. On the Mass of Neutral *V*-Particles.* R. B. LEIGHTON, A. J. SERIFF, AND C. D. ANDERSON, *California Institute of Technology.*—Measurements of the magnetic curvature and specific ionization of the two charged particles which result from the decay of neutral *V*-particles have shown that, at least in some cases, the masses of the particles differ markedly from one another, and seem to be approximately equal, respectively, to those of a proton and a meson. So far, in these cases, the particle of greater mass has carried a positive charge and the meson a negative charge, although mesons of positive charge have been observed where the mass of the second charged particle could not be estimated. On the assumption that the decay products are a proton and pi-meson, and that no neutral particles are produced, the above measurements lead to mass values which range from 2220 to 2265 electron masses for the *V*-particle, corresponding to a disintegration energy of 50 to 70 Mev. Other types of data, however, some of which have been previously reported,[1] indicate that the decay scheme is not necessarily that assumed above, so that (1) neutral *V*-particles may not have a single mass or (2) neutral particles may be present among the decay products. In the latter event, the mass value of the neutral *V*-particle calculated as above corresponds to a lower limit.

* Assisted by the joint program of the ONR and AEC.
[1] Seriff, Leighton, Hsiao, Gowan, and Anderson, Phys. Rev. **78**, 290 (1950). Armenteros, Barker, Butler, Cachon, and Chapman, Nature **167**, 501 (1951).

H10. The Directional Asymmetry of the Ratio of Positive to Negative Cosmic-Ray Mesons.* ROBERT V. PYLE, *University of California, Berkeley.*—The positive to negative ratio of cosmic-ray mesons in the 1-Bev to 2-Bev energy range is being measured as a function of zenith angle. At this latitude (Berkeley, 38°N) there should be no appreciable asymmetry due to the action of the earth's magnetic field on the primary radiation; all asymmetries are produced within the atmosphere. Separation of charge is effected in passage through 24 inches of iron magnetized to 18,800 gauss. The arrangement of the Geiger counters which detect the mesons is such that the scattering correction is negligible. Preliminary results indicate the positive to negative ratio is about 1.55 at 60° West zenith angle, 1.24 in the vertical direction, and 0.95 at 60°E. No variation with zenith angle is observed in the north-south plane. The results will be compared with theoretical predictions.

* Assisted by the joint program of the ONR and AEC.

H11. An Incomplete Cosmological Model.* GUY C. OMER, JR., *The University of Chicago.*—Astronomers are seriously questioning the previous estimations of extragalactic distances. Many difficult astronomical problems are involved which have not been solved. Since the scale of distances within the universe is open to so much suspicion, the problem of constructing cosmological models upon necessarily incomplete data is considered. The time-scale and the red-shift appear to demand a M_1 monotonically expanding model with a positive cosmological constant. The red-shift relation may impose an upper limit upon the inhomogeneity of the model. However, the curvature of space and the average density of matter appear at present to be indeterminant.

* This work was partially supported by the ONR.

H12. Conservation Laws in Feynman's Modified Electrodynamics. P. N. DAYKIN, *University of British Columbia.*—In Feynman's treatment of the electron self-energy problem, the divergence is eliminated by introducing a convergence factor into the integral over the virtual photon momentum space. Feynman[1] has remarked that his choice of convergence factor is inconsistent with the conservation of energy for the radiation field of an atom. This problem is examined in a more general way. The modification of the maxwell equations effected by the convergence factor is deduced. The equations satisfied by the modified field belong to the generalized electrodynamics described by Podolsky.[2] The modified energy-momentum tensor consistent with this electrodynamics is shown to satisfy the conservation law for the field with source.

[1] R. P. Feynman, Phys. Rev. **76**, 778 (1949).
[2] B. Podolsky, Phys. Rev. **62**, 68 (1942).

H13. Two Unstable *V* Mesons Observed in a Cloud Chamber at Sea Level.* EDWARD J. ALTHAUS,† *Washington University.*—In the course of observations[1] on μ-meson capture in Pb and C with a cloud chamber triggered by neutron-coincidences and without a magnetic field, two events out of 1215 pictures were observed that had characteristics similar to those of the *V* mesons first found by Rochester and Butler and subsequently by C. D. Anderson and others.[2] One of the events has been identified as a V_0, namely, one in which a fork occurs in the gas, apparently as the result of decay of a neutral particle of short life. Both legs are above minimum in ionization, and there is a star in a Pb plate which could be the origin of the neutral particle. The other appears to be a $V_\pm$ or a recoil-less deflection of a minimum density track in the gas, which has been interpreted as the decay of a charged particle heavier than a π-meson into a neutral and a charged particle. The particle subsequently passed through the Pb plate and stopped in a carbon plate. Other interpretations will be discussed.

* Supported by the ONR and AEC.
† Now at the University of Southern California.
[1] E. J. Althaus, Phys. Rev. **81**, 647A (1951).
[2] G. D. Rochester and C. C. Butler, Nature **160**, 855 (1947). Seriff, Leighton, Hsaio, Cowan, and Anderson, Phys. Rev. **78**, 290 (1950). V. D. Hopper and S. Biswas, Phys. Rev. **80**, 1099 (1950).

Author Index to Papers Presented at the Vancouver Meeting

Allen, William A., John S. Rinehart, and W. C. White—D3
Althaus, Edward J.—H13
Anderson, A. B. C. and H. W. Wedaa—D10
Anthony, Romuald—C4
Ashburn, Edward V. and Dorothy Davis Locanthi—C5
Band, William—A10
Barrett, Paul H.—H7
Beeman, W. W. and G. R. Mitchell—A3
Benveniste, J. and Bruce Cork—F8
Berberet, J. A. and K. C. Clark—C1
Birnbaum, Wallace, Frances M. Smith, and Walter H. Barkas —H1
Bowen, Dwain, R. R. Eggleston, and R. H. Kropschot—A9
Brattain, W. H.—G1
Cameron, A. G. W. and L. Katz—E7
Cooper, Eugene P.—A7
Cork, Bruce—F3
Crowe, Kenneth M., Wolfgang K. H. Panofsky, Robert H. Phillips, and Darcy Walker—F6
Dahlstrom, C., D. Hunten, and W. Petrie—C6
Darby, E. K. and W. Opechowski—B9
Davis, Sumner P. and F. A. Jenkins—E2
Daykin, P. N.—H12
Dempster, J. R. H.—H4
DePangher, J.—F10
Dienes, G. J.—A4
D'Ooge, Charles L.—C3
Eichholz, G. G.—E5
English, W. N.—C10
Fretter, W. B.—H8
Futterman, W.—F5
Green, David and J. Reginald Richardson—E4
Harrison, Melvin A. and Ronald Geballe—A1
Haslam, R. N. H., L. A. Smith, and J. G. V. Taylor—B2
Heckrotte, W. and L. Schecter—F7
Herb, R. G.—F11
Herman, L. and H. Leinbach—C7
Hess, F. G.—B8
Holmes, John R. and Lee W. Parker—C9
Horsley, R. J., H. E. Johns, and R. N. H. Haslam—B3
Horwood, J. L. and G. G. Eichholz—B5
Hubbard, Harmon W.—F2
Hull, Gordon F., Jr.—G3
Jacobsohn, B. A.—B1
Kaempffer, F. A. and P. N. Daykin—H3
Kane, W. R. and K. C. Clark—C2
Katz, L. and A. G. W. Cameron—E8
Leighton, R. B., A. J. Seriff, and C. D. Anderson—H9
Lewis, W. B.—B12
Li, C. W., Ward Whaling, W. A. Fowler, and C. C. Lauritsen —B11
Little, Edward M.—D1
Lundby, Arne and L. Marshall—B7
Mann, K. C. and G. H. Hanson—F1
Martin, A. B., R. D. Johnson, and W. V. Goeddel—A8
Mather, R. L.—H2
McGeer, P. L., G. B. Rathmann, A. J. Curtis, and C. P. Smyth—D6
Montalbetti, R. and L. Katz—E9
Moon, J. H. and A. L. Thompson—E10
Moore, Richard L.—D8
Mukherjee, N. R. and Oliver Row—D7
Omer, Guy C., Jr.—H11
Pearson, G. L.—G2
Platt, Virginia P. and Ronald Geballe—A2
Post, R. F.—B4
Potter, D. S., Gerald Garrison, Charles E. Miller, Wayne Sandstrom, and Jay Todd, Jr.—F9
Powell, Wilson M.—F4
Pyle, Robert V.—H10
Richardson, J. R.—E11
Rinehart, John S., William A. Allen, and W. C. White—D5
Rogers, F. T., Jr., and L. E. Schilberg—A6
Schiff, L. I.—H5
Schilberg, L. E. and F. T. Rogers, Jr.—A5
Schoof, W. W. and R. D. Hill—E6
Schrank, Glen E. and J. Reginald Richardson—E3
Seagrave, J. D.—B10
Shiren, N. S. and R. F. Post—B6
Smellie, D. W. and H. E. Petch—E1
Trainor, L. E. H.—H6
Warburton, F. W.—D2
Weissler, G. L. and Po Lee—C8
White, W. C., John S. Rinehart, and William A. Allen—D4
Wilcox, Howard A.—D9
Williams, John H.—D11
Wilson, William S.—C11